

Guide to Instruments and Methods of Observation

Volume III – Observing Systems

2021 edition

WEATHER · CLIMATE · WATER



WORLD
METEOROLOGICAL
ORGANIZATION

WMO-No. 8

Guide to Instruments and Methods of Observation

Volume III – Observing Systems

2021 edition



WORLD
METEOROLOGICAL
ORGANIZATION

WMO-No. 8

EDITORIAL NOTE

METEOTERM, the WMO terminology database, may be consulted at <https://public.wmo.int/en/meteoterm>.

Readers who copy hyperlinks by selecting them in the text should be aware that additional spaces may appear immediately following [http://](#), [https://](#), [ftp://](#), [mailto:](#), and after slashes (/), dashes (-), periods (.) and unbroken sequences of characters (letters and numbers). These spaces should be removed from the pasted URL. The correct URL is displayed when hovering over the link or when clicking on the link and then copying it from the browser.

WMO-No. 8

© World Meteorological Organization, 2021

The right of publication in print, electronic and any other form and in any language is reserved by WMO. Short extracts from WMO publications may be reproduced without authorization, provided that the complete source is clearly indicated. Editorial correspondence and requests to publish, reproduce or translate this publication in part or in whole should be addressed to:

Chair, Publications Board
World Meteorological Organization (WMO)
7 bis, avenue de la Paix
P.O. Box 2300
CH-1211 Geneva 2, Switzerland

Tel.: +41 (0) 22 730 84 03
Fax: +41 (0) 22 730 81 17
Email: publications@wmo.int

ISBN 978-92-63-10008-5

NOTE

The designations employed in WMO publications and the presentation of material in this publication do not imply the expression of any opinion whatsoever on the part of WMO concerning the legal status of any country, territory, city or area, or of its authorities, or concerning the delimitation of its frontiers or boundaries.

The mention of specific companies or products does not imply that they are endorsed or recommended by WMO in preference to others of a similar nature which are not mentioned or advertised.

CONTENTS

	<i>Page</i>
CHAPTER 1. MEASUREMENTS AT AUTOMATIC WEATHER STATIONS	1
1.1 General	1
1.1.1 Definition	1
1.1.2 Purpose	1
1.1.3 Meteorological requirements	2
1.1.4 System configuration	4
1.1.5 Types of automatic weather stations	4
1.1.6 Telecommunications	5
1.1.7 Networking	6
1.2 System configuration	6
1.2.1 Telecommunication networks	6
1.2.1.1 One-way communication	6
1.2.1.2 Two-way communication	6
1.2.1.3 Satellite transmission	6
1.2.1.4 Public switched telephone networks	7
1.2.1.5 Cellular networks	7
1.2.1.6 Remote connection to Internet or VPN	8
1.2.1.7 Other communication technologies	8
1.2.2 Central processing system	8
1.2.2.1 Collecting platform	9
1.2.2.2 Processing platform	9
1.2.3 Instruments	10
1.3 Automatic weather station hardware	11
1.3.1 Central processing unit	13
1.3.2 Sensing instrument interface	14
1.3.3 Cable connections and surge protection	15
1.3.4 Power supply	16
1.3.5 Enclosure protection	17
1.3.6 Installation structure	17
1.4 Automatic weather station software	17
1.4.1 Operating system	18
1.4.2 Application software	18
1.4.2.1 Initialization	18
1.4.2.2 Sampling and filtering	19
1.4.2.3 Raw data conversion	19
1.4.2.4 Manual entry of observations	20
1.4.2.5 Data reduction	20
1.4.2.6 Local data storage	21
1.4.2.7 Message coding	21
1.4.3 Remote diagnostics and maintenance	21
1.5 Quality control	22
1.6 Automatic weather station siting considerations	23
1.7 Maintenance	24
1.7.1 Service levels	25
1.7.2 Calibration and site inspection	26
1.7.3 Training	27
1.8 Consideration of system specifications and cost	27
Annex. Automatic Weather Stations – Low Cost	30
References and further reading	34
CHAPTER 2. MEASUREMENTS AND OBSERVATIONS AT AERONAUTICAL METEOROLOGICAL STATIONS	36
2.1 General	36
2.1.1 Definitions	36
2.1.2 Units	36
2.1.3 Requirements	36

	<i>Page</i>
2.1.4 Methods	38
2.2 Surface wind	38
2.2.1 General	38
2.2.2 Instruments and exposure	39
2.3 Visibility	40
2.3.1 Visibility for aeronautical purposes	41
2.3.2 Prevailing visibility	41
2.4 Runway visual range	41
2.4.1 General	41
2.4.2 Methods of observation	42
2.4.2.1 Measurement by observers	42
2.4.2.2 Measurement by video	42
2.4.2.3 Measurement by transmissometer	42
2.4.2.4 Measurement by forward-scatter or backscatter meters	43
2.4.3 Instruments and exposure	44
2.4.3.1 Transmissometers	44
2.4.3.2 Forward-scatter meters	45
2.4.3.3 Background luminance sensor	45
2.4.4 Instrument checks	45
2.4.5 Data display	46
2.4.6 Accuracy and reliability of runway visual range measurements	46
2.5 Present weather	46
2.6 Cloud	47
2.6.1 General	47
2.6.2 Observation methods	48
2.6.3 Accuracy of cloud-base height measurements	49
2.7 Air temperature	49
2.8 Dewpoint	49
2.9 Atmospheric pressure	50
2.9.1 General	50
2.9.2 Instruments and exposure	51
2.9.3 Accuracy of and corrections to pressure measurements	52
2.10 Other significant information at aerodromes	52
2.10.1 General	52
2.10.2 Slant visual range	52
2.10.3 Wind shear	52
2.10.4 Marked temperature inversions	53
2.11 Automated meteorological observing systems	53
2.12 Radar	54
2.13 Ice sensor	54
2.14 Lightning detection	54
2.15 Other relevant observations	55
References and further reading	56
CHAPTER 3. AIRCRAFT-BASED OBSERVATIONS	57
3.1 General	57
3.1.1 Definitions	57
3.1.2 Aircraft meteorological sensors	57
3.2 Pressure and Mach number	58
3.2.1 Pitot-static probe	58
3.2.2 Pressure altitude	59
3.2.2.1 Measurement uncertainty	61
3.2.3 Mach number	61
3.2.3.1 Measurement uncertainty	62
3.3 Air temperature	62
3.3.1 Total air temperature probe	62
3.3.1.1 Measurement uncertainty	63

	<i>Page</i>	
3.4	Wind speed and direction	63
3.4.1	Measurement uncertainty	64
3.5	Humidity	65
3.5.1	Measurement uncertainty	66
3.6	Turbulence	66
3.6.1	Turbulence from vertical acceleration	66
3.6.1.1	Measurement uncertainty	66
3.6.2	Derived equivalent vertical gust velocity	67
3.6.2.1	Measurement uncertainty	67
3.6.3	Eddy dissipation rate	67
3.6.3.1	Vertical accelerometer-based EDR	68
3.6.3.2	Vertical wind-based EDR	68
3.6.3.3	True airspeed-based EDR	69
3.6.3.4	Measurement uncertainty	69
3.6.3.5	Relationship between EDR and DEVG	69
3.7	Icing	70
3.7.1	Measurement uncertainty	70
3.8	Aircraft-based observing systems	70
3.8.1	Aircraft meteorological data relay	70
3.8.2	Tropospheric Airborne Meteorological Data Reporting	70
3.8.2.1	Overview	70
3.8.2.2	Relative humidity and temperature	71
3.8.2.3	TAMDAR icing detection	72
3.8.2.4	TAMDAR turbulence detection	73
3.9	Other systems and sources of aircraft-based observations	73
3.9.1	ICAO Automatic Dependent Surveillance	73
3.9.2	Automated Flight Information Reporting System	73
3.9.3	New and developing systems	74
3.9.3.1	Mode-S Enhanced Surveillance	74
3.9.3.2	Mode-S Meteorological Routine Air Report	74
3.9.3.3	Unmanned aerial vehicles	75
	References and further reading	76
 CHAPTER 4. MARINE OBSERVATION		78
4.1	General	78
4.2	Observations from ships	79
4.2.1	Operation of the WMO Voluntary Observing Ship Scheme	79
4.2.2	Voluntary Observing Ship observations	80
4.2.2.1	Elements observed	80
4.2.2.2	Equipment required	81
4.2.2.3	Automation of ship observations	81
4.2.2.4	Times of observation	82
4.2.2.5	Transmission of ship's observations	82
4.2.2.6	Wind	83
4.2.2.7	Atmospheric pressure, pressure tendency and characteristic of pressure tendency	86
4.2.2.8	Air temperature and humidity	88
4.2.2.9	Sea-surface temperature	89
4.2.2.10	Clouds and weather	91
4.2.2.11	Visibility	92
4.2.2.12	Precipitation	93
4.2.2.13	Ocean waves	94
4.2.2.14	Ice	99
4.2.2.15	Observations of special phenomena	103
4.3	Moored buoys	103
4.3.1	Atmospheric pressure	106
4.3.2	Wind measurements	106

	<i>Page</i>
4.3.3 Temperature	107
4.3.3.1 Air temperature	107
4.3.3.2 Water temperature	108
4.3.4 Ocean wave estimates	108
4.3.5 Non-directional ocean wave estimates	108
4.3.6 Directional ocean wave estimates	109
4.3.7 Water-column height for tsunami detection	109
4.3.8 Relative humidity	109
4.3.9 Ocean sensors	109
4.3.10 Surface ocean currents	110
4.3.11 Ocean current profiles	110
4.3.12 Salinity	110
4.3.13 Precipitation	110
4.3.14 Solar radiation measurements	111
4.3.15 Visibility	111
4.4 Light vessels	111
4.5 Towers and platforms	111
4.6 Drifting buoys	112
Annex 4.A. WMO/IOC Regional Marine Instrument Centres	115
Annex 4.B. Descriptions of precipitation for use by ship-borne observers of present weather	117
Annex 4.C. Recommended procedures for the reporting of swell by manually reporting ships	120
References and further reading	121
CHAPTER 5. SPECIAL PROFILING TECHNIQUES FOR THE BOUNDARY LAYER AND THE TROPOSPHERE	126
5.1 General	126
5.2 Surface-based remote-sensing techniques	126
5.2.1 Acoustic sounders (sodars)	126
5.2.2 Wind profiler radars	128
5.2.3 Radio acoustic sounding systems	130
5.2.4 Microwave radiometers	130
5.2.5 Laser radars (lidars)	132
5.2.6 Global navigation satellite system	133
5.2.6.1 Description of the global navigation satellite system	134
5.2.6.2 Tropospheric global navigation satellite system signal	135
5.2.6.3 Integrated water vapour	135
5.2.6.4 Measurement uncertainties	136
5.3 In situ measurements	136
5.3.1 Balloon tracking	136
5.3.2 Boundary layer radiosondes	136
5.3.3 Instrumented towers and masts	137
5.3.4 Instrumented tethered balloons	138
Annex. Ground-based remote-sensing of wind by heterodyne pulsed Doppler lidar	141
Attachment A. Continuous-wave doppler wind lidar	164
Attachment B. Retrieval of the wind vector	165
Attachment C. Applications	169
Attachment D. Typical application ranges and corresponding requirements	173
References and further reading	177

	<i>Page</i>
CHAPTER 6. ELECTROMAGNETIC METHODS OF LIGHTNING DETECTION	180
6.1 Introduction	180
6.2 Lightning discharge	180
6.2.1 Lightning types, processes and parameters	180
6.2.2 Lightning electromagnetic signatures	183
6.2.3 Glossary of terms	185
6.3 Principles of lightning location	187
6.3.1 General	187
6.3.2 Magnetic field direction finding	188
6.3.3 Time-of-arrival technique	189
6.3.4 Interferometry	190
6.4 Performance characteristics	191
6.5 Examples of modern lightning locating systems	192
6.5.1 Lightning Mapping Array, 60–66 MHz	193
6.5.2 United States National Lightning Detection Network, 400 Hz–400 kHz.	193
6.5.3 Lightning Detection Network, 1–200 kHz.	194
6.5.4 United State Precision Lightning Network, 1.5–400 kHz.	194
6.5.5 Earth Networks Total Lightning Network, 1 Hz–12 MHz.	195
6.5.6 World Wide Lightning Location Network, 6–18 kHz	195
6.5.7 Global Lightning Dataset, VLF	196
6.5.8 Arrival Time Difference network.	196
6.6 Utilization of lightning location systems by meteorological services	196
6.6.1 Storm recognition and alarms for severe weather	197
6.6.2 Nowcasting, forecasting and derived products	197
6.6.3 Lightning and climate	198
6.6.4 Verification of lightning-induced ground damage	198
References and further reading.	199
CHAPTER 7. RADAR MEASUREMENTS.	201
7.1 General.	201
7.1.1 The weather radar	201
7.1.2 Radar characteristics, terms and units	202
7.1.3 Radar accuracy requirements	202
7.2 Radar principles	203
7.2.1 Pulse radars	203
7.2.2 Propagation radar signals	207
7.2.3 Attenuation in the atmosphere.	208
7.2.4 Scattering by clouds and precipitation	209
7.2.5 Scattering in clear air	210
7.3 The radar equation for precipitation targets	210
7.4 Basic weather-radar system and data.	212
7.4.1 Reflectivity	212
7.4.2 Doppler velocity	213
7.4.3 Dual polarization	216
7.5 Signal and data processing	217
7.5.1 The Doppler spectrum.	217
7.5.2 Power parameter estimation.	217
7.5.3 Ground clutter and point targets	218
7.5.4 Overcoming the Doppler dilemma	220
7.6 Optimizing radar characteristics.	223
7.6.1 Selecting a radar	223
7.6.2 Wavelength and beam width	224
7.6.3 Transmitters and transmit power	225
7.6.4 Pulse length.	226
7.6.5 Pulse repetition frequency	226
7.6.6 The antenna subsystem	226
7.6.7 Illumination.	227

	<i>Page</i>
7.6.8 Typical weather radar characteristics	227
7.6.9 Radar volume scan strategy	229
7.6.10 Radar performance	229
7.7 Maintenance and calibration	230
7.7.1 Maintenance	230
7.7.2 Calibration	232
7.8 Radar installation	234
7.8.1 Optimum site selection	234
7.8.2 Data exchange, networking, database and processing	235
7.9 Sources of error	236
7.10 Overview of meteorological applications	243
7.10.1 General weather surveillance	243
7.10.2 Severe weather detection and warning	244
7.10.3 Nowcasting	249
7.10.4 Precipitation estimation	250
7.10.4.1 Vertical profile of reflectivity	251
7.10.4.2 The Z-R relation	253
7.10.4.3 Gauge adjustment	255
7.10.4.4 Dual-polarization precipitation techniques	255
7.10.5 Wind estimation/wind mapping	258
7.10.5.1 Wind profiling	258
7.10.5.2 Convective wind features	258
7.10.5.3 Wind mapping	259
7.10.6 Initiation and numerical weather prediction models	259
7.10.7 Humidity estimation	259
7.11 Meteorological products	259
Annex 7.A. Weather radar – system performance and operation	262
Attachment A. System performance parameter measurement	299
Attachment B. Sample radar specifications	337
Attachment C. Recording of measurement results	339
Attachment D. Recommended maintenance and calibration actions	342
Attachment E. Radar data exchange	345
Attachment F. Other radar systems	346
Annex 7.B. WMO guidance statement on weather radar/radio frequency shared spectrum use	351
Annex 7.C. Wmo guidance statement on weather radar/wind turbine siting	353
References and further reading	355
CHAPTER 8. BALLOON TECHNIQUES	361
8.1 Balloons	361
8.1.1 Main types of balloons	361
8.1.2 Balloon materials and properties	361
8.1.3 Balloon specifications	361
8.2 Balloon behaviour	362
8.2.1 Rate of ascent	362
8.2.2 Balloon performance	363
8.3 Handling balloons	364
8.3.1 Storage	364
8.3.2 Conditioning	364
8.3.3 Inflation	365
8.3.4 Launching	365

	<i>Page</i>	
8.4	Accessories for balloon ascents	366
8.4.1	Illumination for night ascents	366
8.4.2	Parachutes	366
8.5	Gases for inflation	366
8.5.1	General	366
8.5.2	Gas cylinders	367
8.5.3	Hydrogen generators	367
8.6	Use of hydrogen and safety precautions	368
8.6.1	General	368
8.6.2	Building design	369
8.6.3	Static charges	370
8.6.4	Protective clothing and first-aid facilities	371
	References and further reading	372
CHAPTER 9. URBAN OBSERVATIONS	373	
9.1	General	373
9.1.1	Definitions and concepts	373
9.1.1.1	Station rationale	373
9.1.1.2	Horizontal scales	374
9.1.1.3	Vertical scales	375
9.1.1.4	Source areas ("footprints")	376
9.1.1.5	Measurement approaches	377
9.1.1.6	Urban site description	377
9.2	Choosing a location and site for an urban station	378
9.2.1	Location	378
9.2.2	Siting	381
9.3	Instrument exposure	382
9.3.1	Modifications to standard practice	382
9.3.2	Temperature	382
9.3.2.1	Air temperature	382
9.3.2.2	Surface temperature	383
9.3.2.3	Soil and road temperature	383
9.3.3	Atmospheric pressure	384
9.3.4	Humidity	384
9.3.5	Wind speed and direction	384
9.3.5.1	Mean wind profile	384
9.3.5.2	Height of measurement and exposure	386
9.3.5.3	Wind sensor considerations	388
9.3.6	Precipitation	389
9.3.7	Radiation	390
9.3.7.1	Incoming fluxes	390
9.3.7.2	Outgoing and net fluxes	391
9.3.8	Sunshine duration	392
9.3.9	Visibility and meteorological optical range	392
9.3.10	Evaporation and other fluxes	393
9.3.11	Soil moisture	394
9.3.12	Present weather	394
9.3.13	Cloud	394
9.3.14	Atmospheric composition	395
9.3.15	Profiling techniques for the urban boundary layer	395
9.3.16	Satellite observations	395
9.4	Metadata	395
9.4.1	Local environment	396
9.4.2	Historical events	397
9.4.3	Observance of other WMO recommendations	398
9.5	Assessment of urban effects	398

	<i>Page</i>
9.6 Summary of key points for urban stations	398
9.6.1 Working principles	398
9.6.2 Site selection	398
9.6.3 Measurements	399
References and further reading	400
CHAPTER 10. ROAD METEOROLOGICAL MEASUREMENTS	402
10.1 General	402
10.1.1 Definition	402
10.1.2 Purpose	402
10.1.3 Road meteorological requirements	402
10.2 Establishment of a road meteorological station	403
10.2.1 Standardized representative measurements	403
10.2.2 Station metadata	403
10.3 Observed variables	404
10.3.1 Road meteorological measurements	404
10.3.1.1 Air temperature	404
10.3.1.2 Relative humidity	404
10.3.1.3 Wind speed and direction	404
10.3.1.4 Precipitation	405
10.3.1.5 Meteorological radiation	405
10.3.1.6 Visibility	406
10.3.1.7 Road-surface temperature	406
10.3.1.8 Road-pavement temperature	406
10.3.1.9 Road-surface condition and freezing temperature	406
10.3.1.10 Video surveillance	407
10.4 Choosing the road weather station equipment	407
10.4.1 The road environment	407
10.4.2 Remote-station processing capability	407
10.4.3 Network configuration and equipment options	407
10.4.4 Design for reliability	408
10.5 Message coding	409
10.5.1 Coding functions	409
10.5.2 WMO standard coding	409
10.6 Central control and data-acquisition computer	409
10.7 Communications considerations	409
10.8 Sensor signal processing and alarm generation	410
10.8.1 Signal processing algorithms	410
10.8.2 Alarm generation	410
10.9 Measurement quality control	411
10.9.1 Checking for spurious values	411
10.10 Road weather station maintenance	411
10.10.1 The road environment	411
10.10.2 Maintenance plans and documentation	412
10.10.3 Inspections and work programme	412
10.11 Training	412
References and further reading	413

CHAPTER 1. MEASUREMENTS AT AUTOMATIC WEATHER STATIONS

1.1 GENERAL

1.1.1 Definition

An automatic weather station (AWS) is defined as a “meteorological station at which observations are made and transmitted automatically” (WMO, 1992).

An AWS is now a common set of equipment found as part of a surface meteorological observing station. The majority of the sensing instruments are connected to an electronic data-acquisition system. A surface observing station with an AWS can be fully automatic or a mixed system, allowing the addition of visual observations by a human observer. The main functions of an AWS are the conversion of the measurements of meteorological elements into electrical signals via sensors, the processing and the transformation of these signals into meteorological data, and the recording and/or the transmission of the resulting information.

Such a combined system of instruments, interfaces and processing and transmission units is usually called an automated weather observing system (AWOS) or automated surface observing system (ASOS). It has become common practice to refer to such a system as an AWS, although it is not a “station” fully in line with the stated definition. Nevertheless, throughout this chapter, an AWS may refer to just such a system. Data loggers are sometimes used as the acquisition equipment of the system and they are considered to be a part of an AWS.

1.1.2 Purpose

Automatic weather stations are used for increasing the number and reliability of surface observations. This is achieved by:

- (a) Facilitating an increase in the density of observing networks by providing data from new sites where people are not available to take observations, and from sites that are difficult to access or inhospitable;
- (b) Supplying, for manned stations, data 24 hours a day;
- (c) Increasing the reliability of measurements by using digital measurement techniques;
- (d) Ensuring the homogeneity of networks by standardizing the measuring techniques;
- (e) Satisfying new observational needs and requirements;
- (f) Reducing human errors;
- (g) Lowering operational costs by reducing the number of observers;
- (h) Measuring and reporting with high frequency and/or continuously;
- (i) Compensating for the shortage in the number of observers;
- (j) Eliminating mercury from stations.

Concerning (j), the Minamata Convention on Mercury of the United Nations Environment Programme (UNEP) came into force globally in August 2017 and bans all production, import and export of observing instruments (thermometers, barometers, and so forth) containing mercury (UNEP, 2017). This agreement is a global treaty to eliminate the use of mercury to protect both human health and the environment from its adverse effects. As a result,

National Meteorological and Hydrological Services (NMHSs) must also transition away from mercury-based instruments. For most countries this will lead to the replacement of conventional instruments containing mercury with electronic ones (see Volume I, Chapter 1, 1.4.2).

While presenting many advantages there are drawbacks or complications that arise from the process of automation:

- (a) AWS networks decrease (sometimes to zero) the number of observers but increase the staff needed for the maintenance, inspections, system and software design and update, calibration of electronic instruments, and the like.
- (b) A more skilled workforce is required in the areas of telecommunications, information technology (IT) infrastructure, metrology and engineering.
- (c) Significant change may occur in the nature of some observations that may have an impact on climate monitoring; for example, the move from manual visual observations to automated measurements.
- (d) The quality of some observations may deteriorate due to key parts of the measurement process not being automated (for example, cleaning of the dome of solar irradiance instruments or evaporation pans).
- (e) For places where labour costs are low and technology expensive, the conversion to automation may not result in lowering of operational costs.

When considering conversion from manual to automated observations, careful consideration of the capability of staff, cost of infrastructure and maintenance and the various impacts on data quality and volume is advised.

1.1.3 **Meteorological requirements**

The general requirements, types, location and composition, frequency and timing of observations are described in WMO (2015*a*, 2015*b*).

The performance of today's electronics is no longer a limiting factor to achieve the accuracy requirements described in Volume I, Chapter 1, Annex 1.A of the present Guide. The measurement uncertainties associated with an AWS are mainly linked to the characteristics of the instruments themselves and their exposure.

The guidance provided in this chapter must be used in conjunction with the chapters on measurements of the various meteorological variables in Volume I and, in particular, with the chapters in Volume V on quality management (Chapter 1), sampling (Chapter 2) and data reduction (Chapter 3).

As for any observation network, the development and installation of AWSs should be the result of a definite, coordinated plan for providing users with data in the format required. To achieve this, negotiations should first be undertaken with the users to draw up a list of all functional requirements for the planned system (WMO, 2017*a*).

The *Guide to the Global Observing System* (WMO, 2010) gives a list of functional specifications for AWS concerning meteorological variables and associated Binary Universal Form for the Representation of Meteorological Data (BUFR) descriptors to be used (Appendix III.1), the basic set of variables to be reported by standard AWS for multiple users (Appendix III.2) and AWS metadata (Appendix III.3)

It is not sufficient to rely on equipment suppliers to determine operational requirements. The Commission for Instruments and Methods of Observation (CIMO) gives the following advice to Members of WMO and organizations taking meteorological measurements.

When considering the introduction of new AWS instrument systems, NMHSs should:

- (a) Introduce into service only those systems that are sufficiently well documented so as to provide adequate knowledge and understanding of their capabilities, characteristics and any algorithms used;¹
- (b) Retain or develop sufficient technical expertise to enable them to specify system requirements and to assess the appropriateness of the capabilities and characteristics of such systems and algorithms used therein;¹
- (c) Explore fully user requirements and engage users in system design of AWSs;
- (d) Engage users in validation and evaluation of the new automated systems;
- (e) Develop detailed guides and documentation on the systems to support all users;
- (f) Develop adequate programmes for preventive and corrective maintenance and calibration support of the AWSs and associated instruments;
- (g) Consult and cooperate with users, such as aeronautical authorities, throughout the process from AWS design to implementation and operational use.

With respect to the automation of traditional visual observations (present weather, visibility and clouds) NMHSs should understand that the observational characteristics of AWSs systems are different from the observation capability of a human observer:

- (a) The visibility measurement is representative of the instrument location (unless several visibility meters are installed), while a visual observation makes use a 360° field of view but is limited by the available visual landmarks. This means the automated measurement will have high precision for the specific location, but may not be representative of a wider area.
- (b) Cloud cover is usually derived from measurements of the cloud-base height from a ceilometer, combined or averaged over a given period of time (10, 30 or 60 minutes), while a human observer has a larger view of the sky, at least during day. The automated measurement represents a line through the sky in the direction of the upper winds. This may not correlate with the instantaneous whole-of-sky observation by a human.
- (c) A present-weather instrument is not currently able to identify the full range of present-weather codes that a human observer is able to report.

In essence, manual and automated observations of visibility, cloud cover and present weather are distinctly different. Therefore, the meteorological services should improve their definition of requirements with respect to:²

- (a) Areas of application for which data are no longer required;
- (b) Areas of application for which different or new data are needed;
- (c) Prioritizing the requirements for data to be provided by AWSs.

Where a proposed AWS has a role in providing data for climatological records (or where consistency of the measurands is important) it is important for the integrity, homogeneity and utility of the datasets that the following areas be considered for action:³

- (a) Ensure overlapping periods of comparable measurements between conventional and new automated instrumentation;

¹ Recommended by CIMO at its twelfth session (1998) through Recommendation 2 (CIMO-XII).

² Recommended by CIMO at its twelfth session (1998) through Recommendation 5 (CIMO-XII).

³ Recommended by CIMO at its twelfth session (1998) through Recommendation 3 (CIMO-XII).

- (b) Ensure proper documentation is available on differences between the old and the new site as well as on instrumentation changes (metadata).⁴

The overlap time⁸ is dependent on the different measured variables and on the climatic region. In tropical regions and islands, the overlap time could be shorter than in extratropical and mountainous regions. The following general guidelines are suggested for a sufficient operational overlap between existing and new automated systems:

- (a) Wind speed and direction: 12 months;
- (b) Temperature, humidity, sunshine, evaporation: 24 months;
- (c) Precipitation: 60 months.

A useful compromise would be an overlap period of 24 months (that is, two seasonal cycles).

1.1.4 **System configuration**

An AWS is usually not used as a stand-alone equipment. It is part of a system with three main elements:

- (a) The local AWS and the sensing instruments connected to it;
- (b) The local modem or interface used to connect the AWS to a telecommunication network;
- (c) A central processing system fed by the data transmitted by all the AWS making up the observing network. This central processing system is usually connected to the WMO Information System (WIS) or to an automatic message switching system (AMSS) linked to the WIS.

Therefore, an AWS cannot be considered independently of the environment (instruments, telecommunication and central processing system) that influences the role of the AWS, the distribution of the data processing, the quality control and the like.

1.1.5 **Types of automatic weather stations**

Automatic weather stations are used to satisfy several needs, ranging from a simple aid to the observer at manned stations to complete replacement of observers at fully automatic stations.

The proceedings of several international conferences on AWSs give very valuable information on the state of the art, the implementation of AWS networks, the migration from manual to automated measurements, technical aspects for communications and system design, and quality control and quality assurance (for example, see WMO, 2017b).

Offline AWSs, that is, stations recording data on site without any automatic transmission, are used less and less because data are not available in real time and they do not allow fast detection of possible failure of the equipment. Because of the wide offer of means of telecommunication now available, the use of real-time AWS can be recommended, even for climatological data.

Since observing stations can be very expensive, the stations' facilities can also be used to satisfy the common and specific needs and requirements of several applications, such as synoptic, aeronautical and agricultural meteorology, hydrology and climatology. They may also be used for special purposes, such as nuclear power safety, air and water quality, and road meteorology. They are, therefore, multi-purpose AWSs.

⁴ Note also WMO (2010), section 3.2.1.4.4(c) "one year of parallel measurements does not suffice; preference is given to at least two years, depending on the climatic region".

In practice, there exist several categories of AWS, though some equipment is able to cover several of these categories:

- (a) Light AWSs for the measurement of a few variables such as precipitation and/or air temperature, applicable for both for climatology and real-time use;
- (b) “Basic” AWSs for the measurement of “basic” meteorological measurements (typically air temperature, relative humidity, wind speed and direction, precipitation and, sometimes, atmospheric pressure);
- (c) “Extended” AWSs with the additional measurement of solar radiation, sunshine duration, soil temperature, evaporation and so forth;
- (d) AWSs with automation of visual observations: basic or extended AWSs with automatic observation of visibility, cloud-base height and present weather. Such stations are commonly named as AWOS or ASOS in some countries.

A wide range of low-cost AWS, including associated instruments, can be bought off the shelf, mainly used by hobby meteorologists or private companies. More information about low-cost AWSs can be found in the annex to the present chapter. To lower the price, the sensors are often integrated and third-party instruments are not available. The sensors and the electronics are not designed to be calibrated independently. Therefore the uncertainty of the measurements is greater than that obtained with “professional” equipment. It is difficult to estimate the uncertainty, due to a lack of documentation and the inability to open the equipment. Such equipment does not yet satisfy the CIMO requirements.

All-in-one AWSs are also available, designed by several suppliers of professional meteorological equipment. They include a set of embedded sensors with adapted electronics and software. Price, compactness and ease of installation are the advantages of these all-in-one AWSs, usually allowing the measurement of wind (with an ultrasonic instrument), air temperature and relative humidity within an embedded radiation screen, pressure and precipitation (by radar, detection of droplet hits, or with a more classical tipping bucket raingauge at the top of the instrument). But some instruments are difficult to calibrate, often poorly documented and all the parameters are measured at the same height, which is a strong weakness. If mounted at about 2 m, the wind measurement is very sensitive to the surface below; if mounted at 10 m to follow the recommendations concerning wind measurement, other parameters are also measured at 10 m, which does not comply with the CIMO siting recommendations.

1.1.6 Telecommunications

The available means of communications on the sites composing the observing network are a key factor in the design and the specification of an AWS system or network. Many technologies may be considered: public switched telephone network (PSTN), leased lines, cellular networks, satellite transmissions, optical fibres, access to Internet and use of a virtual private network (VPN) through these supports. The primary technical question before designing an observing network is to identify the available means of telecommunication. It is also important to consider the life cycle of the envisaged telecommunication medium, as rapid changes are possible in terms of coverage, price (generally decreasing), but also in terms of sustainability. Therefore, the AWS and network design should allow an easy change of the telecommunication modem or interface, both in terms of physical interface and software.

IT security has to be considered, especially if Internet is used as an interim media for the transmission of data and communication between systems. VPN and other techniques may be used, associated with the framework of machine to machine (M2M) communication.

The wide spread of telecommunication media and Internet may allow the application of the concept of the “Internet of things” (IoT) to individual “intelligent” meteorological instruments, thus eliminating the need for an AWS. This concept is not yet used for meteorological

instruments but will be available in the near future. With such connected instruments, the concept of an AWS could partly disappear on site, all the data acquisition and processing being implemented in the central system.

1.1.7 **Networking**

An AWS usually forms part of a network of meteorological stations, each transmitting processed data to a central network processing system by various data transmission means (see 1.1.6). As the tasks to be executed by this central system are strongly related, and often complementary to the tasks of the AWSs, the functional and technical requirements of both the central system and the AWSs have to be coordinated.

When planning the installation and operation of a network of AWSs, it is of the utmost importance to consider the various problems associated with maintenance and calibration facilities, their organization and the training and education of technical staff. Network density considerations are beyond the scope of the present Guide as they depend on the specific applications. However, the optimum siting and exposure of stations have an important influence on the performance of the stations and must be studied before they are installed.

1.2 **SYSTEM CONFIGURATION**

1.2.1 **Telecommunication networks**

1.2.1.1 ***One-way communication***

It is important to identify if the telecommunication media to be used with an AWS network is restricted to one-way (AWS towards the central system) or allows two-way communications. When limited to one-way communication it is not known on the AWS side if the data sent have been successfully received by the central system. Therefore, it is advisable to format the data messages with control codes allowing the receiver to check the integrity of the message. Correction codes may also be used to cope with possible transmission errors. If the volume of the message allows it, it can be a good practice to transmit several times the same measurement (in the same message or in consecutive messages) to manage errors and missed receptions.

1.2.1.2 ***Two-way communication***

When the telecommunication network allows it, the AWS can receive an acknowledgement from the central system for the correct reception of the transmitted messages. This guarantees the transmission of all new data since the last data are successfully received by the central system. The quantity of the data to be transmitted can be optimized, without the need to introduce the transmission of redundant data to deal with missing messages.

The AWS may also receive commands from the central system to change its configuration, the transmission intervals, retransmit old data, and so forth.

1.2.1.3 ***Satellite transmission***

Many satellite telecommunication systems are available, some of them being able to cover any part of the world.

Aside their main mission of imagery and sounding, nearly all the geostationary meteorological satellites have a data collection service (DCS), a transponder of messages from self-timed data collection platforms (DCP) towards the ground centre for the exploitation of the satellite data. A DCP is a one-way transmitter, associated with an antenna oriented towards a geostationary satellite, connected to an AWS. The messages have to be kept short (a few hundred bytes)

because of the low speed transmission of the channel (either 100 bauds for standard or 300, 1 200 or 4 800 bauds for high rate, depending on the satellite and DCS) and the limited time slot allocated to each station. As the transmission frequency is shared by several DCPs, each DCP must respect its allocated time slot and needs a precise clock, now easily achieved by using a local Global Positioning System (GPS) receiver. An AWS with a DCP typically transmits every hour, at a time slot and a frequency channel allocated by the satellite operator. The majority of the frequency channels are "regional" channels used by each single satellite, but "international" channels shared by all the geostationary meteorological satellites also exist, to be used by mobile platforms (buoys, ships), which can move seamlessly from the field of view of one satellite to another. A major advantage of DCSs is that DCP channels are available at no cost for meteorological, geophysical and hydrological messages, provided they are also made available through the WMO Global Telecommunication System (GTS) and discoverable in WIS. A disadvantage is that a specific transmission terminal (the DCP) is needed, with few manufacturers due to the quite low number of users and that normalized modern telecommunication protocols (Internet Protocol (IP), File Transfer Protocol (FTP), Hypertext Transfer Protocol (HTTP)) are not available at the DCP level.

Increasing numbers of commercial satellite telecommunication services exist, based either on geostationary telecommunication satellites or on low Earth orbit satellite constellations. Aside voice services, the operators offer data transmission services, generally using standard telecommunication protocols (IP based) and allowing M2M services. The required modems are not specific to meteorological applications but are adapted to many data-acquisition systems and therefore available at quite low prices. This allows the design of a system in which the AWS and the transmission modem are functionally separated, thus allowing an easy change of the telecommunication modem during the life cycle of the system, for example to use the services of a new (less expensive) telecommunication operator. Sometimes use of the telecommunication service has to be optimized to minimize the transmission cost, often linked to the quantity of data to be transmitted.

1.2.1.4 **Public switched telephone networks**

A PSTN is often available in developed countries in populated areas. It may be easily used for data transmission with a modem, allowing two-way communications with a central system. The connection may use either analogue signals (a modem generates standard modulation frequencies for binary codes) or numeric ones (Integrated Services Digital Network (ISDN)). The connection to a central system can be made in several ways:

- (a) A point-to-point connection, the central system having a modem or a pool of modems on a set of lines; a remote access service may be used, allowing IP-based protocols once the connection is established;
- (b) An access of the local AWS to an Internet service provider, thus allowing the use of an Internet link to connect to a central system; this eliminates the need for the central system to use a pool of modems. The use of Internet needs to consider security aspects, both on the side of the AWS and, in particular, on the side of the central system.

Many countries and telecommunication operators are announcing the end of PSTN (analogue and ISDN). The fixed networks of copper lines should not be abandoned, but can be used for IP-based communications, with asymmetric digital subscriber line (ADSL) connection or other techniques. Nevertheless, ADSL needs to be close enough to a switchboard, so the end of PSTN may reduce the availability of a connection through a fixed line for isolated locations.

1.2.1.5 **Cellular networks**

Cellular networks are developing increasingly, signalling the end of PSTN, and are now often the primary telecommunication offered. The required infrastructure is less expensive than a copper-based network of fixed lines. Several generations of data services exist, with an increasing flow rate (General Packet Radio Service, Edge, 3G, 4G, and so forth). Considering

the volume of meteorological observational data, a low rate is sufficient and it is preferred to have a better coverage rather than a higher flow rate. Many industrial modems are available, with low power consumption and being fully compatible with solar panels of a reasonable size. Technical specifications for operation under high and/or low temperature must be considered, since the modems are usually installed in the AWSs cabinet and therefore subject to local atmospheric conditions.

Standard IP-based protocols can be used (Transmission Control Protocol (TCP), FTP, HTTP, and the like). Operators also propose special services for M2M transmissions using dedicated VPN for the customer.

1.2.1.6 **Remote connection to Internet or VPN**

Satellite, PSTN, ISDN and cellular networks can be used for an IP connection to a central system, via Internet or a VPN. Any other Internet connection can also be used, such as optical fibres, Worldwide Interoperability for Microwave Access (WIMAX), TV cable, and the like.

1.2.1.7 **Other communication technologies**

Leased lines can be used when a permanent connection is needed between the AWS and a dedicated user (for example, an aeronautic user needing one-minute data in real time). Nevertheless, the offer of dedicated point-to-point lines is being replaced (by the operators) by IP-based connections, using the available transmission network.

In areas not covered by a PSTN or a cellular network, dedicated radio links may be used. But the allocation of a frequency band by the appropriate regulatory authorities may be difficult due to competition between radio-frequency band users. Specific radio bands reserved for data transmission are available, with a limitation of the power of the radio transmission, thus limiting the distance to a few hundred metres or a few kilometres. Such radio transmissions may be appropriate to connect a distant instrument to an AWS, for example at an aerodrome.

New technologies of low-power wide-area networks (LPWANs) are emerging. An LPWAN may be used to create a private wireless instrument network, but may also be a service or infrastructure offered by a third party, allowing the owners of instruments to deploy them in the field without investing in gateway technology. The volume of data that can be transmitted is limited to a few tens or hundreds of bytes, which may be compatible with hourly meteorological observations (depending on the design of the file of the meteorological data to be transmitted). The main advantages are: relatively long range (up to a few kilometres for reliable data transmission), very low power consumption of transmitters (durability up to five years with a single battery) and a low cost, both in terms of hardware and telecommunication service.

1.2.2 **Central processing system**

The majority of AWS are connected to a central system, which can be functionally separated into two parts:

- (a) A collecting platform, designed to collect data from the AWS;
- (b) A processing platform, receiving data from one or several collecting platforms and functioning as the interface towards the users of the observational data.

The collecting function and the data processing for supervising an AWS network are typical tasks of a supervisory control and data-acquisition (SCADA) system. SCADA are used in many industrial processes, factories, and any location where field devices (instruments) are needed to control and interact with a production process. The problematic of an observing network is similar in such systems: an observing network is composed of field devices (AWS plus instruments), communication infrastructure, and data collection and control (of the

observing network). Many commercial software packages used for collecting and monitoring meteorological observations are developed by SCADA editors. Systems developed by hydrometeorological equipment manufacturers may be specific to their own data-acquisition system (AWS) rather than being issued from a multi-purpose SCADA-type software, but they have the same functionalities.

1.2.2.1 **Collecting platform**

A surface observing system is often composed of several AWS networks, covering various needs and often set up during successive periods. Therefore, it is seldom the case that sets of equipment are homogeneous; different types of AWS, telecommunication media and protocols are mixed. Each generation of stations (AWS plus modem) is functionally linked to an associated collecting platform. For ease of use, it is possible to consider that each AWS type with a given telecommunication network is associated to a specific collecting platform. In case of multiple ways of telecommunication, a set of collecting platforms may exist. Depending on the software and hardware needed, these collecting platforms may be implemented in the same system or separately.

A collecting platform has a connection to the telecommunication network used. When modems have to be used (that is, for PSTN, ISDN, Global System for Mobile Communications (GSM) data, and the like) a pool of modems is managed. The modems can be physical equipment (one modem equals one equipment) or logical equivalents within a physical equipment, such as a remote access server (RAS). When the number of incoming lines is smaller than the number of AWSs from which data need to be collected, which is generally the case, the system must be designed to share the lines. If the AWS is initiating the connection, it has to follow a "telecommunication profile", including a calling schedule to share the lines with other stations. If the connection is initiated by the collecting platform, the AWSs can be called sequentially by the collecting platform. In any case, the collecting platform should check the operational status of each incoming line to detect problems, such as silent lines, error rate of communications on each line, and the like.

Increasingly, telecommunication networks are used as a gateway to the local area network of the network manager (using Internet or preferably VPN tunnels through Internet). The advantage in this case is that the collecting platform has no modems to handle, that means the physical interface to the telecommunication network is managed by the telecommunication operator. Standard IP-based protocol can be used, such as FTP transfers, emails, and so forth.

A collecting platform should monitor the communications with the AWS network by checking the actual connections compared to the expected ones. Silent AWSs should be identified. Supervision tools should be implemented to offer a global view of the network status (for example, green dots for AWSs awaited and received, red dots for AWSs awaited and not received), with detailed information for each station (such as the time stamp of the more recent data received) and each connecting line (if any).

If the telecommunication network allows two-way communications, the collecting platform is also used to configure the network and individual AWS, in particular in terms of transmission schedule, type of data to be collected, and the like.

Security protections should be installed to avoid unauthorized access to the system. These may include use of firewalls and control of the calling IP address or the calling phone number for authentication.

1.2.2.2 **Processing platform**

Data coming from one or several collecting platforms are sent to a processing platform. The primary function of this platform is to provide the measurement data to the end users. It is also

very important to use this platform to support the technical management of a network and to offer a technical supervision of the observing network. Various indicators may be used to help the network manager, such as:

- (a) Percentage of missing values for the whole network, for each station, over a one-hour period, a daily period, and the like;
- (b) Alarms for missing values, for each measured parameter (such as air temperature, wind speed and direction, and pressure);
- (c) Alarms for doubtful or erroneous values after application of quality-control checks;
- (d) Voltage of the battery and alarms of each AWS if voltage is too low (the voltage measurement may not be significant when the battery is being charged, for example, by solar panel; night measurements or minimum daily value have to be used);
- (e) Presence or absence of mains power (if present in the installation), in order to detect a failure such as the release of a circuit breaker, which could be hidden by a buffering battery;
- (f) When smart sensing instruments are used, they often deliver service parameters in addition to the desired meteorological variables. These service parameters are useful to detect or anticipate problems with the instrument (such as cleaning being required) and should generate alarms for the maintenance manager.

The typical operational functions of the processing platform are:

- (a) The quality control of the “raw” data: the quality-control algorithms may be partly split between the AWS itself and the central system.
- (b) The calculation of meteorological parameters from individual measurements, for example the calculation of dew-point temperature from measured air temperature and relative humidity. This calculation may be shared between the AWS and the central system.
- (c) When the data processing can be implemented either at the level of the AWS or the central server, it is recommended to choose a central implementation, where software development and updates are easier to implement. Nevertheless, some data processing by the AWS itself may be needed in case of a local use of the observation (for example, a local observer or an aerodrome), unless the telecommunication network used is considered as compatible and safe enough to download the local observation from the central system to the tower control. A local aeronautic usage is a special case that may need local data processing to supply the air traffic control (ATC) with local observation data, through aeronautical local reports.
- (d) The coding of standard messages to feed an AMSS, usually the source of data for the NMHS; standard messages in a format needed for the distribution on the GTS may also be formatted in the AMSS if not directly formatted in the central processing platform. For surface observations, alphanumeric messages (SYNOP) are replaced by self-described codes (table-driven code forms (TDCF)). BUFR templates have been designed for surface observations (WMO, 2015c).

1.2.3 Instruments

All modern sensing instruments are suited for use with an AWS. Instruments are described in Volume I of the present Guide. Some constraints for their use with an AWS are as follows:

- (a) They have to be robust and with minimal maintenance and cleaning required, as many sites have no local maintenance staff.

- (b) They should be easily interchangeable, with little or no change needed in the AWS configuration and calibration.
- (c) Their connection to an AWS should be fully documented in terms of cabling, power supply (range, power consumption with and without heating, warming-up time if the power supply is switched on and off to lower the power consumption, and so forth) and transfer function (relation between the electrical output and the meteorological parameters).

Instruments with an analogue output generally deliver only the meteorological variable measured. Those with a digital output deliver the meteorological variable that is measured, but also offer additional service parameters, useful to monitor the instrument's state and to optimize its maintenance. It is important that the service parameters are also taken into account by the system (AWS plus central system).

Radiometers (pyranometers, pyrhemometers, and the like) are a special case. The majority of these instruments use a thermopile that is often directly connected to the AWS. Therefore, the calibration factor of the thermopile has to be applied behind the sensors, either in the AWS itself or in the central system collecting the data. When a radiometer is changed on site (at least for a regular calibration) the associated calibration factor must be changed accordingly in the system. Experience shows that human-induced errors sometimes occur (for example, a change of the instrument or sensing element without updating the calibration factor at the same time). Some models of radiometers include a microprocessor to convert the analogue signals into numeric digital values within the instrument itself; the calibration factor is then included in the instrument and updated after calibration. Such an instrument is fully interchangeable, with no required update of a calibration factor in the system, which reduces possible human errors.

Wind measurements (mean values, gusts) need a high acquisition rate (see Volume I, Chapter 5, 5.8.2) and a calculation of mean values and gusts over larger periods (10 minutes for synoptic use, 2 minutes for local aeronautical use). The calculation can be carried out on the AWS itself, but many modern anemometers have an embedded calculation of the wind parameters. An advantage is the reduction of the data-acquisition rate at the level of the AWS, with a typical one-minute update of wind data, rather than a data sampling of several Hz. That said, the acquisition and archiving of raw wind data up to 1 Hz or higher might be desirable for certain applications, for example, incident and accident investigations for civil aviation.

It is highly recommended that barometers connected to an AWS have a digital output, to avoid additional uncertainty in the conversion of an analogue signal into pressure. Indeed, using a barometer with an analogue output requires a high-quality analogue-to-digital (A/D) converter (ADC) to achieve the recommended measurement uncertainty and performance requirements specified in Volume I, Chapter I, Annex 1.A of the present Guide.

It can be desirable to double (or even triple) some instruments. This approach can minimize the probability of missing values in case of instrument failure and/or introduce measurement redundancy in the system to detect possible instrument drift. The difference between two instruments indicates a drift of at least one of them; if three instruments are used, it becomes possible to identify automatically which instrument is drifting and choose to exclude its values. This procedure of using multiple sensing elements is used within some instruments. Several commercial models of barometers are available with one, two or three cells.

1.3 **AUTOMATIC WEATHER STATION HARDWARE**

Several designs of AWS exist:

- (a) A stand-alone equipment specifically designed for meteorological measurements. Depending on the manufacturer, it is designed to accept a given list of instruments. Therefore, it may be difficult to use or add new instruments that are not supported. Being

designed for meteorological measurements by the meteorological industry, there is good chance that all the needs may be fulfilled and therefore the restriction for adding new instruments may not be a problem.

- (b) An industrial data logger not specific to meteorological measurements. An advantage is a potential higher versatility, with analogue inputs, counters, and the like. Also, the cost may be lower than dedicated equipment. In some cases where meteorological instruments have stringent characteristics, such as the low output voltage of a radiometer using a thermopile, such data loggers may not be suitable. Wind measurement is also a special case if the data logger must derive wind parameters with a sampling rate of several Hz.
- (c) Some designs split the data acquisition between separate electronic boxes; some of them are associated with an instrument to digitize its analogue output, being as close to the instrument as possible. These interface boxes dialogue with a central processing unit.
- (d) In other designs, digital or smart instruments and analogue instruments digitized by an electronic interface are directly connected to a laptop, PC or industrial PC, installed either indoor or directly in the field. This allows use of the hardware and software of standard microcomputers. Nevertheless, cabling and surge protection should not be neglected.
- (e) When a human observer must interact with the AWS, for example to enter visual observation, a local PC is usually used, both to display the observations locally and to edit the visual observation. Such a computer may also deliver the observation data to local users, such as aeronautic users.

The layout of an AWS typically consists of the following:

- (a) On a standard observing area (see Volume I, Chapter 1 of the present Guide and WMO, 2010), a series of automated instruments sited at the recommended positions and interconnected to one or more data collection units using interfaces sited to avoid interference with one another and connected to a central processing unit (CPU) by means of shielded cables, fibre optics, or radio links;
- (b) A CPU for instrument data acquisition and conversion into a computer-readable format, proper processing of data by means of a microprocessor-based system in accordance with specified algorithms, the temporary storage of processed data and their transmission to remote users of meteorological information;
- (c) A modem or an interface to the telecommunication network used for the transmission of data towards a central system;
- (d) A stabilized power supply providing power to the various parts of the station;
- (e) For specific applications further additions to the station may include local terminals for the manual entry and editing of data, display devices and printers, and recorders.

It is good practice to design the system on a modular basis to adapt it to new instruments, new variables, changes in the telecommunication network, and so forth. Nevertheless, a high level of modularity may increase the cost of the equipment; therefore it is important to anticipate the possible future changes as much as possible in order to select a good compromise between modularity and a compact and standard design (across the whole network). Due to the short life cycle of many telecommunication networks, it is highly recommended to use an AWS with a modular telecommunication terminal.

For the maintenance of the AWS, the design should facilitate fieldwork for preventive and corrective maintenance (for example, a regular replacement is needed for instruments that need to be calibrated). Again, modularity is a solution or, alternatively, the possibility to easily replace the whole AWS if it is a stand-alone design. Connectors with a keyed position may be preferable to wires directly connected to a terminal strip.

Vital parts of an AWS often include components whose faulty operation or failure would seriously degrade or render useless the principal output. The inclusion of circuits to monitor automatically component status is an effective means of continuously controlling their performance during operation (“built-in test equipment”). For example, a power-failure detector that restarts the processor and continues the AWS function after a power failure; a “watchdog” timer to monitor the proper operation of microprocessors; and test circuits for monitoring the operation of station subsystems such as battery voltage and charger operation, aspirators (if temperature- and humidity-ventilated screens are used), ADCs, and heaters. Status information should be monitored as well, and transferred to the central server unit for automatic quality-control and maintenance purposes.

1.3.1 Central processing unit

The core of an AWS is its CPU. Its hardware configuration depends on the complexity and magnitude of the functions it has to perform. In general, the main functions of the CPU are the acquisition, processing, storage and transmission of data.

In the majority of existing AWSs, all these functions are carried out by one microprocessor-based system installed in a weather-proof enclosure as close to the instruments as possible, or at some local indoor location. If the unit is located near the instruments, on-site processing reduces the amount of data that must be transmitted and enables those data to be presented in a form suitable for direct connection to communication channels. In such cases, however, the CPU is vulnerable to power-supply failure and must be protected against the outdoor environment in which it must operate. If the unit can be located indoors, it can usually be connected to a mains power supply and operated as if it were located in a normal office environment. However, such a configuration results in an increased number of long signal cables and appropriate signal conditioners.

Depending on local circumstances and requirements, different units may also execute the different functions of the CPU. In such cases, each unit has its own microprocessor and relevant software. The units can be installed at different places in the station and can communicate with other units through well-established inter-processor data transfer links and procedures. They operate in a dependency relation, the data-processing unit being independent. An example is the installation of one or more data-acquisition units in the field close to the instruments that are connected to the data-processing or data-transmission unit of the CPU by means of one or more telephone lines using digital data transmission. Low-power wireless links may also be used, some frequency bands being dedicated to data transmission without a specific authorization procedure, assuming a low-power emission. These units can consist of one instrument (for example, an intelligent instrument such as a laser ceilometer), a number of similar instruments (for example, thermometers), or a number of different instruments, such as analogue instruments connected to a data logger in the field.

The data-processing hardware is the heart of the CPU. Its main functions are to act as the master control of the input/output of data to and from the CPU, and to carry out the proper processing of all incoming data by means of the relevant software.

The first AWS were equipped with 8-bit microprocessors and limited memory (32 to 64 kbytes). Systems using 16-, 32- or 64-bit microprocessors surrounded by a considerable amount of solid-state memory are now standard. These AWOSs provide more input/output facilities that operate at much higher processing speeds and are capable of performing complex computations. Together with this hardware, sophisticated software is applied. In addition to the random-access memories (RAM) for data, many systems have access to a read-only memory (ROM). Some of the range of ROMs include non-volatile programmable read-only memories (PROMs) for program storage. The CPU often uses non-volatile RAM (NVRAM) or electrically erasable programmable ROM (EEPROM, also known as flash memory). System configuration constants can be modified and the data stored safely during power failures. The AWS software may be downloaded from a local connection or even from the central system. The size of available memory currently is large enough to memorize tens or hundreds of days of observation data.

Real-time clock. The CPU of an AWS needs a 24-hour real-time clock powered by a battery, which ensures that the time is kept even during power outages. Ensuring the accuracy of actual AWS clocks requires special attention to ensure correct read-outs, sample intervals and time stamps. A clock stability better than one second over a 24-hour period is recommended and achievable. The real-time clock should also be synchronized either with the GPS signals or by a central reference clock, available through the telecommunication network (such as a time server over the Internet).

1.3.2 Sensing instrument interface

In general, the data-acquisition hardware is composed of:

- (a) Signal-conditioning hardware for preventing unwanted external sources of interference from influencing the raw instrument signals, for protecting the CPU electronics and for adapting signals to make them suitable for further data processing;
- (b) Data-acquisition electronics with analogue and digital input channels and ports, scanning equipment and data-conversion equipment to enter the signals into the CPU memory.

Low-pass filtering. Filters are used to separate desirable from undesirable signals. Undesirable signals are noise, alternating current line frequency pick-up, radio or television station interference and signal frequencies above half the sampling frequency. Generally, a low-pass filter is employed to control these unwanted sources of error, excluding that portion of the frequency spectrum where desirable signals do not exist. These filters may be realized either by analogue techniques (electronic) or digital filters.

Amplifiers. Analogue instrument signals can vary in amplitude over a wide range. The ADC, however, requires a high-level signal to perform best. In many cases, an amplifier module is used to boost possible low-level signals to the desirable amplitude. Amplifier modules are sometimes employed to standardize the voltage output of all instruments to a common voltage, for example 0–5 voltage direct current, in order to use a common high-performance ADC.

Resistances. Special modules are used to convert resistances, such as those of platinum thermometers, into an output voltage signal by providing the necessary output current. Temperature measurement is particularly susceptible to the method of conversion from resistance to temperature. Lower-quality systems may use a two- or three-wire approach, while the better designs use a four-wire method and switch the measurement direction. This allows for compensation for any lead resistance.

Data-acquisition function. The data-acquisition function consists of scanning the output of instruments or instrument-conditioning modules at a predetermined rate and translating the signals into a computer-readable format.

To accommodate the different types of meteorological instruments, the hardware for this function is composed of different types of input/output channels, covering the possible electrical output characteristics of sensors or signal-conditioning modules. The total number of channels of each type depends on the output characteristics of the instruments and is determined by the type of application.

Analogue inputs. The number of analogue channels depends on the basic design of the equipment. In general, a basic configuration can be extended by additional modules that provide more input channels. Analogue input channels are of particular significance as most of the commonly used meteorological instruments, such as temperature, radiometers and humidity instruments, deliver a voltage signal either directly or indirectly through the instrument-conditioning modules.

The data-acquisition tasks are the scanning of the channels and their A/D conversion. A scanner is simply a switch arrangement that allows many analogue input channels to be served by one

ADC. Software can control these switches to select any one channel for processing at a given time. In some AWS designs, a separate ADC is used for each channel. The ADC transforms the original analogue information into computer-readable data (digital, binary code). The A/D resolution is specified in terms of bits. An A/D resolution of 12 bits corresponds to approximately 0.025%, 14 bits to 0.006% and 16 bits to 0.0015% of the A/D full range of scale. In the first generation of AWSs, offset and gain of amplifiers and ADCs had to be adjusted by means of potentiometers. Modern electronics use fixed, stable and precise reference elements, which prevent any manual adjustments of the electronic chain.

Parallel digital input/output. The total number of individual channels is mostly grouped in blocks of 8 out of 16 bits with extension possibilities. They are used for individual bit or status sensing or for input of instruments with parallel digital output (for example, wind vanes with Gray code output).

Pulses and frequencies. The number of channels is generally limited because few instruments deliver such signals. Typical instruments are anemometers and (tipping-bucket) raingauges. Use is made of low- and high-speed counters accumulating the pulses in CPU memories. The counters should use analogue or digital filters to avoid unwanted pulses, such as electromagnetic spikes.

Serial digital ports. These are individual asynchronous serial input/output channels for data communication with intelligent instruments. The ports provide conventional inter-device communications over short (Recommended Standard 232 (RS-232), several metres) to long distances (using of a pair of modems or RS-422/485, several kilometres). Different instruments or measuring systems are sometimes connected to the same line and input port, each of the instruments being addressed sequentially by means of coded words. Unfortunately, there is no universal standardization of the dialogue protocol with the instruments, except protocols or formats defined by some manufacturers for their own equipment. SDI-12 (Serial Digital Interface at 1200 baud) is an asynchronous serial communication protocol for intelligent sensors that monitor environment data, which is supported by some instruments and AWSs.

Ethernet connection. Some instruments are quite autonomous and able to communicate either with the AWS or even with a central system (IoT) using IP-based protocols.

1.3.3 Cable connections and surge protection

Connections. Cables and a mechanical connecting system are necessary for connecting the instruments to the data-acquisition electronics. The cables may be connected directly to the data-acquisition system via a terminal strip, with screwed, soldered or self-locking connections. Packing glands are often used to cross the enclosure box of the AWS. Another solution is to use a pair of connectors, one of which is fixed on the enclosure box (and connected to the electronics). The advantage is the possibility to easily unlock an instrument and its cable for replacement. The type of connection and the location of possible connectors should be selected to facilitate the field operations, bearing in mind the expected periodicity of the instrument's replacement (for example, for regular calibration).

Instrument cables. Electrical signals from the instruments entering a data-acquisition system might include unwanted noise. Whether this noise is troublesome depends upon the signal-to-noise ratio and the specific application. Digital signals are relatively immune to noise because of their discrete (and high-level) nature. In contrast, analogue signals are directly influenced by disturbances at a relatively low level. The major noise-transfer mechanisms include capacitive and inductive coupling. A method of reducing errors due to capacitive coupling is to employ shielded cables. The additional use of a pair of wires that are entwined is effective in reducing electromagnetic coupling.

Surge protection. When an AWS could be subject to unintentional high-voltage inputs, the installation of a protection mechanism is indispensable to avoid possible destruction of the equipment. High-voltage input can be induced from magnetic fields, static electricity and

particularly from lightning. Protection modules against surge should be easily replaceable. They are often a one-shot protection, therefore their status should be easily testable, the best solution being a visual mark of their status. A basic rule for good surge protection is to ensure an equipotential bonding of the different electrical masses of the system, including the shield of the cables. Ground connections should be kept as short as possible to facilitate the path of high-voltage spikes through these connections rather than through the electronics. The ground of the AWS and its peripherals (including instruments) must be connected to the ground network of the site (if available). If not available, a local grounding electrode and associated buried grounding network must be installed to offer the best path to current surges.

Digital isolation. Electrical modules are used to acquire digital input signals while breaking the galvanic connection between the signal source and the measuring equipment. The modules (modems) not only isolate, but also convert the inputs into standard voltage levels that can be read by the data-acquisition equipment. The galvanic isolation allows avoidance of the use of copper lines to realize the equipotential bonding between distant points (copper wires and trenches over hundreds of metres are costly). Nevertheless, surge protection of a digital line remains necessary because high-frequency spikes are able to cross transformers, even with galvanic isolation.

1.3.4 **Power supply**

The design and capability of an AWS depend critically on the method used to power it. The most important characteristics of an AWS power supply are high stability and interference-free operation. For safety reasons, and because of the widespread use and common availability of 12 V batteries, consideration should be given to the use of 12 V direct current power supply. Where mains power is available, the batteries could be float charged from the mains supply. Such a system provides the advantage of automatic backup power in the event of a mains power failure. The capacity of the buffer batteries depends on the mean power consumption of the system (AWS plus instruments, including heating plus modem) and the accepted duration of mains power interruption.

Automatic weather stations deployed at remote sites where no mains power is available must rely on batteries nearly always sourced by solar cells or other power sources such as a diesel or wind- or water-driven generator. However, such low-power systems cannot, in general, support the more complex instruments required for cloud height and visibility measurements, which require large amounts of power. Furthermore, AWSs with auxiliary equipment such as heaters (for example, anemometers and raingauges) and aspirators can also consume considerable amount of power, thus restricting the installation of such AWSs to locations where mains power is available. If, because of the need for a versatile and comprehensive system, only the mains can supply sufficient power for full operation, provision should be made for support from a backup supply, for at least the system clock, the processor and any volatile memory that may contain recent data needed to restart the station automatically. It is also good practice to shut down the system when the voltage of the batteries falls below a fixed threshold to protect them, as such batteries will not support a deep discharge.

It is important the system be designed to measure and report the status of the power supply, for example battery voltage, charging current delivered by solar panels and presence or absence of the mains power. These status parameters should be transmitted to the central system to optimize the maintenance operations and to alert the maintenance staff of any problem. Mains power is protected by a circuit breaker, which may trip off in case of surge. On an isolated site, a staff displacement just to reactivate a circuit breaker may be very costly and time consuming, so it can be useful to install a circuit breaker with a possibility to reactivate it by remote command, unless the tripping off is linked to an electrical circuit default that needs to be repaired.

1.3.5 Enclosure protection

The electronics part of an AWS has to be protected from the outside atmosphere, unless it is installed within a building. A protective box is highly recommended. It should be large enough to allow easy access to the internal equipment, unless the system is designed for replacing the whole equipment, including protective box, in case of failure.

The protection against water and condensation should be assured by one of the two following techniques:

- (a) The protective box is completely sealed and not designed to be opened in the field. It should then include an internal bag of hygroscopic salts.
- (b) The protective box is aerated with gills that are additionally protected to prevent insects entering. The box should be designed to avoid the entry of water when opening its door.

The material should be chosen to avoid corrosion, especially if the site is close to the sea. A metallic box helps in protecting the electronics against surge.

1.3.6 Installation structure

When installed outside, the AWS box(es), the instruments and the terminal distribution of the mains power or the solar panels have to be installed on the supporting structure. The installation structure must not be neglected as it can be expensive. It is good practice to define standard accessories for the installation of an AWS and its components. Supporting structures may be proposed by the AWS's manufacturer. It is important to check that the instruments and other equipment are not interfering each other; in particular, the clearance rules described in the siting classification (see Volume I, Chapter 1, Annex 1.D of the present Guide) should be followed by the design of the supporting structure.

A concrete base may be necessary. An alternative may be the use of metallic ground screws, designed to support pylons, fences, and the like.

The need for a local earth electrode and buried earth network must be considered.

Depending on the location of the station and the surrounding risks (for example, animals and humans), fencing of the observing area may be necessary.

1.4 AUTOMATIC WEATHER STATION SOFTWARE

The three main AWS designs have different frameworks for the software:

- (a) A stand-alone AWS uses specific software developed by the AWS's manufacturer. Few or no modifications are possible by the end user except some configuration choices. But the AWS is often delivered ready to be used. Modifications to the AWS functionalities have to be implemented by the manufacturer.
- (b) An industrial data-logger is usually designed with a command language to allow users to configure the equipment according to their instruments and needs (of course, within the limits allowed by the data-logger design). The software configuration may be complicated and realized by the data-logger distributor, by a third-party integrator, or by the users themselves.
- (c) The software of a laptop or industrial PC with digital instruments directly connected to it is less dependent on the hardware and may enable use of more standard tools and languages. Some NMHSs develop their own software with this type of AWS configuration.

The software is a major part of the AWS. Unless great care is taken in the preliminary design and strong discipline maintained while coding, complex software readily becomes inflexible and difficult to maintain. Minor changes to the requirements, such as those often induced by the need for a new instrument, code changes, or changes in quality-control criteria, may often result in major and very expensive software revisions.

In general, a distinction can be made between application software consisting of algorithms for the proper processing of data in accordance with user specifications, and system software inherently related to the hardware configuration and comprising all software to develop and run application programs.

Discussion of the design of algorithms for synoptic AWSs can be found in WMO (1987) and for the processing of surface wind data in WMO (1991). Information on the algorithms used by Members is available in WMO (2003).

1.4.1 **Operating system**

The operating system of a stand-alone AWS or a data-logger is generally very specific to the hardware and based on an industrial real-time embedded operating system (so-called firmware), thus turning the CPU into a sort of black box. Sometimes the operating system is more classical, such as a Unix-based system. The user can execute only predetermined commands and, as a consequence, entirely depends on the manufacturer in the event of malfunctions or modifications.

When a laptop, PC or industrial PC is used as a CPU, its operating system is more standard, such as a Unix-based system or a Windows operating system. The full range of administration tools and communication layers are therefore available. However, such a system is more vulnerable to hacking and IT security protections have to be set and software updates and upgrades have to be applied regularly.

1.4.2 **Application software**

The processing functions that must be carried out by the CPU, the instrument interfaces, or a combination of both, depend to some extent on the type of AWS and on the purpose for which it is employed. Typically, some or all of the following operations are required: initialization, sampling of instrument output, conversion of instrument output to meteorological data, linearization, averaging, manual entry of observations, quality control, data reduction, message formatting and checking, and data storage, transmission and display. Quality control may be performed at different levels: immediately after sampling, after deriving meteorological variables, after the manual entry of data and message formatting, or in the central system (quality control is often split between the AWS itself and the central system). If there are no data quality control and message content checks, the AWS data are likely to contain undetected errors. While linearization may be inherent in the instrument or signal-conditioning module, it should always be carried out before the calculation of an average value.

The execution of the application software is governed by a schedule that controls when specific tasks must be executed. The overview of AWS application software in the following paragraphs is limited to some practical aspects related to AWSs.

1.4.2.1 **Initialization**

Initialization is the process that prepares all memories, sets all operational parameters and starts running the application software. To be able to start normal operations, the software first requires a number of specific parameters, such as those that are related to the station (station code (ID) number, altitude, latitude and longitude), date and time, physical location of the instrument in the data-acquisition section, and type and characteristics of instrument-conditioning modules. Conversion and linearization constants for instrument output conversion

into meteorological values, as well as absolute limits and rate of change limits for quality-control purposes and data buffering file location are also included. Depending on the station, all or part of these parameters may be locally input or modified by the user through interactive menus on a terminal. In the most recent generation of AWSs, initialization may be executed remotely, for instance by the central network processing system or by a remote personal computer. In addition to full initialization, a partial initialization should be programmed. This automatically restores normal operation without any loss of stored data following a temporary interruption caused by real-time clock setting, maintenance, calibration or power failure. The central system (typically a collecting platform) should be able to report the full set of initialization parameters of each AWS, for network and maintenance management.

1.4.2.2 ***Sampling and filtering***

Sampling is the process of obtaining a discrete sequence of measurements of a quantity. To digitally process meteorological instrument signals the question arises of how often the instrument outputs should be sampled. It is important to ensure that the sequence of samples adequately represents significant changes in the atmospheric variable being measured. A generally accepted rule of thumb is to sample at least once during the time constant of the instrument. However, as some meteorological variables have high-frequency components, proper filtering or smoothing should be accomplished first, by selecting instruments with a suitable time constant or by filtering and smoothing techniques in the signal-conditioning modules. More details are presented in Volume V, Chapter 2 of the present Guide.

Instruments needing a high-frequency sampling often have their own embedded microprocessor to calculate the relevant meteorological parameters, thus reducing the task of the AWS. A typical example is an anemometer with a recommended sampling frequency of several Hz.

The natural small-scale variability of the atmosphere; the introduction of noise into the measurement process by electronic devices and, in particular, the use of instruments with short time-constants; make averaging a most desirable process for reducing the uncertainty of reported data.

Volume I, Chapter 1, Annex 1.A of the present Guide recommends that “instantaneous” values of most of the meteorological variables be a one-minute average (except for wind and visibility).

1.4.2.3 ***Raw data conversion***

The conversion of raw instrument data consists of the transformation of the electrical output values of instruments or signal-conditioning modules into meteorological units. The process involves the application of conversion algorithms sometimes using constants and relations obtained during calibration procedures.

An important consideration is that some instruments are inherently non-linear; namely their outputs are not directly proportional to the measured atmospheric variables (for example, a resistance thermometer). Other measurements are influenced by external variables in a non-linear relationship (for example, some pressure and humidity instruments are influenced by the temperature). While some instruments may be linear or incorporate linearization circuits, the variables measured are not linearly related to the atmospheric variable of interest (for example, the extinction coefficient, but not visibility or transmittance, is the proper variable to be averaged to produce estimates of average visibility). Consequently, it is necessary to include corrections for non-linearity in the conversion algorithms, as far as this is not already done by signal-conditioning modules. Linearization is of particular importance when mean values must be calculated over a certain time. Indeed, when the instrument signal is not constant throughout the averaging period, the “average then linearize” sequence of operations can produce different results from the “linearize then average” sequence. The correct procedure is to average only linear variables. More details are presented in Volume V, Chapter 3 of the present Guide.

The knowledge of raw data values may be very valuable for maintenance staff; therefore, considerations must be given to the transmission of some raw data values towards the central system. A typical example is the use of analogue relative humidity instruments. If a 0–1 V output hygrometer is used, 0 V stands for 0% and 1 V for 100% of relative humidity, the maximum operational value. But such a hygrometer might output a raw value above 1 V, for example, 1.03 V. Obviously it is not an operational value of 103% of relative humidity, but it may be an instrument drift or a value inside the instrument tolerance limits. In the conversion to meteorological units, these 1.03 V should be limited to 100%, with a threshold limit (such as a value above 1.05 V is considered as an invalid value). But for the maintenance process, it is important to know that these 1.03 V have been reported by the hygrometer as it may be an indication of an instrument drift.

1.4.2.4 **Manual entry of observations**

For some applications, interactive terminal routines have to be developed to allow an observer to enter and edit visual or subjective observations for which no automatic instruments are provided at the station. These typically include present and past weather, visibility, cloud layers, state of the ground and other special weather phenomena. If some instruments for these parameters are installed in the system, they should be considered as an aid for the observer during the periods with human observation. That means that a terminal system (often a PC) used for manual entry should also display the measured parameters for the local human observer.

1.4.2.5 **Data reduction**

Besides instantaneous meteorological data directly obtained from the sampled data after appropriate conversion, other operational meteorological variables are to be derived and statistical quantities calculated. Most of them are based on stored instantaneous values, while, for others, data are obtained at a higher sampling rate, as, for instance, is the case for wind gust computations. For example, data reduction is the calculation of dew-point temperature from the original relative humidity and air temperature measurements, and the reduction of pressure to mean sea level. Statistical data include data extremes over one or more time periods (for example, temperature), total amounts over specific periods of time, from minutes to days (for example, rain), means over different time periods (for example, climatological data), and integrated values (for example, radiation). These variables or quantities can be computed at the level of the AWS, or in a central processing platform, from instantaneous data or extremes, and total amounts calculated over small periods (for example, one hour). A tendency of recent systems, when the telecommunication network allows it, is to collect centrally one-minute data (instantaneous values and meteorological variables calculated every minute; for example, wind parameters) and to process these data in a central processing platform. This allows a greater flexibility in the development and upgrade of the processing software, and simplifies the AWS software. One-minute data may greatly help the maintenance team to detect and identify possible measurement problems (see 1.2.2.1).

The algorithms used to derive values in the AWS are as important as the choice of instrument. Small and subtle changes can be introduced over time that can have significant impacts afterwards. A register of algorithms as well as software versions should be kept as a part of the metadata for the AWS. Where the algorithm is created in-house, it is wise to document the process and to develop data test sets so that changes to software can be consistently checked in the future.

CIMO is involved in a regular programme to survey and standardize algorithms for all variables. The results are published in WMO (2003). See also the corresponding chapters of Volume I of the present Guide for details on the meteorological variables.

1.4.2.6 **Local data storage**

Meteorological data are regularly transmitted to a central system under normal conditions. Nevertheless, a break in the telecommunication scheme may occur or data may be lost in the collecting process. Therefore, it is important that the local AWS has a local data storage and an associated procedure to access the data. Local data storage is no longer a problem with flash memory components. The AWS software generally manages the data in a circular memory over a given period, replacing old data by new. The size of data storage should be compatible with the accessibility of the observing site, up to several months for a very isolated site. It may be the same set of data that are normally transmitted to the collecting platform. If necessary, to reduce the memory size needed and/or to facilitate the procedure of recovery of data, hourly instantaneous variables and hourly statistical variables (extremes, totals) may also be stored locally.

The procedure to access the local data can be:

- (a) A transmission of old data when the telecommunication infrastructure becomes available again;
- (b) A local transfer of the data with a portable terminal locally connected to the AWS during a maintenance operation;
- (c) A local recuperation of a memory card (for example, a flash memory card) during a maintenance operation.

The recovery procedure must be accompanied by a mechanism of complementing the central database with the old recovered data.

1.4.2.7 **Message coding**

Functional requirements often stipulate the coding of meteorological messages in accordance with WMO (2011, 2015c). The implementation of message-coding algorithms should not be underestimated and may require noticeable efforts not only for their development but also for updating when formats are altered by international, regional and national regulations. The transition from alphanumeric codes (typically SYNOP) to TDCFs (BUFR or Character Form for the Representation and Exchange of Data (CREX)) facilitates the update of the content of observing messages.

The coding of standard messages is generally easier in a central processing platform, where more computing capacity and also more standard software tools are available (free BUFR coding software is available from several sources). Therefore, the majority of networks of AWSs are designed for a central coding in standard codes. The format of the messages between an AWS and the collecting platform varies. It should also be based on the principle of a table-driven code, allowing the upgrade of the transmitted variables without needing any changes in the transmission layers. In addition to the requested meteorological variables, additional service data should be coded and transmitted, such as service data from smart instruments, battery voltage, and raw data from some instruments (for example, the raw value output by a 0-1 V hygrometer, as described in 1.4.2.3). As such parameters are very specific to the AWS design and not listed in BUFR tables, it is an additional reason to code standard WMO messages at a central level.

1.4.3 **Remote diagnostics and maintenance**

Specific software routines are incorporated in the application software allowing field maintenance and calibration. Such activities generally involve running interactive programs for testing a particular instrument, AWS reconfiguration after the replacement of instruments or models, resetting of system parameters, telecommunication tests, entering new calibration constants, and so forth. In general, maintenance and calibration is conducted in an offline mode of operation, temporarily interrupting the normal station operation.

Some of these functions may also be available online via the data-collecting system. Any function allowing a distant diagnostic should be encouraged in the design of the system to reduce maintenance costs. In practice, transportation of maintenance staff to the measuring site is a huge percentage of the maintenance cost and any online possibility is welcomed (for example, transmission of service parameters, resetting a circuit breaker and downloading a new software version for the AWS or one of its components).

1.5 QUALITY CONTROL

The purpose of quality control at an AWS is to minimize automatically the number of inaccurate measurement data and the number of missing data by using appropriate hardware and software routines. Both purposes are served by ensuring that all calculated measurement data are derived from a reasonably large number of quality-controlled data samples. In this way, samples with large spurious errors can be isolated and excluded, while the computation can still proceed, not being contaminated by that sample.

Quality control ensures quality and consistency of data output. It is achieved through a carefully designed set of procedures focused on good maintenance practices, repair, calibration and data-quality checks.

In modern AWSs, the results of data quality-control procedures that reveal the reasons why a measurement is suspicious or erroneous and of hardware self-checks by built-in test equipment are stored in appropriate housekeeping buffers. The transmission of these results and the visual display of these status indicators form a very handy tool for continuous monitoring of the network and during field or remote maintenance. The transmission of housekeeping buffers, as an appendix to the routine observational message, as a separate bulletin, or as a clocked or on-request housekeeping message, from a network of AWSs to a central network processing system is highly recommended to support the maintenance of meteorological equipment.

Real-time procedures for the quality control of AWS data are highly advisable, and detailed recommendations exist in Appendix VI.2 of the *Guide to the Global Observing System* (WMO, 2010) and in Volume V, Chapter 1 of the present Guide. The following is a brief summary of the guidelines available in WMO (2010).

Intra-instrument checks. Each instrument sample is checked at the earliest practical point in the processing, taking into account instrument and signal-conditioning response functions, for a plausible value and a plausible rate of change. Some additional tests are possible, for example:

- (a) If barometers with two or three pressure cells are used, the difference between cells could generate an alarm if this difference is larger than a given threshold (for example, 0.3 hPa).
- (b) If relative humidity is measured by a hygrometer, the maximum daily value indicated by the instrument could be calculated (see 1.4.2.3). This parameter analysed over long periods may help to identify clues of a possible drift at the saturation point (100%).

Plausible value. A gross check that the measured value lies within the absolute limits of variability. These limits are related to the nature of the meteorological variable or phenomena, but depend also on the measuring range of selected instruments and data-acquisition hardware. Additional checks against limits that are functions of geographical area, season and time of year could be applied. The checks help to identify erroneous or suspicious values.

Plausible rate of change. Checks for a plausible rate of change from a preceding acceptable level. The test settings depend on the observed parameter and the atmospheric phenomena that could influence it. It also depends on the instrument characteristic (for example, time constant and persistency).

Minimum required variability of instantaneous values. Checks that the instrument is still reacting to atmospheric changes. A long period without significant change in the measured data is an indication of malfunction (for example, a cup and vane anemometer starting to jam). Variability and time response are dependent on the measured parameter and on the instrument's characteristic.

Maximum allowed variability of instantaneous values. Identical to the previous.

Number of valid samples in a period. This determines the validity of the average and its suitability for use in further calculations.

Inter-instrument checks. It is possible to make internal consistency checks of a measured variable against other measured variables, based on established physical and meteorological principles; for example, dew-point temperature cannot exceed ambient temperature; precipitation without clouds overhead or just after they have passed overhead is very unlikely; non-zero wind speed and zero wind direction variance strongly suggest a problem with wind-direction instruments.

Technical monitoring. Technical monitoring of all crucial AWS components.

Message checking. For AWSs equipped with software for directly coding and transmitting messages over the GTS, it is of vital importance to execute all the above checks very carefully. In addition, compliance with regulations concerning character, number, format, and so forth, should be controlled. Proper actions are to be considered when values are classified as suspicious.

For AWSs associated with a central collecting and processing system, the quality-control checks are split between the AWS software and the central software. If the raw data samples are not transmitted to the central system, only the checks using the raw data samples must be implemented inside the AWS. When one-minute data are transmitted centrally, the other quality-control checks should be implemented in the central processing system.

1.6 AUTOMATIC WEATHER STATION SITING CONSIDERATIONS

The proper siting of an AWS is a very difficult matter and much research remains to be done in this area. The general principle of siting is that a station should provide measurements that are and remain representative of the surrounding area, the size of which depends on the meteorological application. Existing guidelines for conventional stations are also valid for AWSs and are given in Volume I, Chapter 1, Annex 1.D of the present Guide, as well as in WMO (2010, 2014, 2017*b*).

The surrounding area and the obstacles close to the instruments should not decrease the representativeness of the measurements. The site classification defined in Volume I, Chapter 1, Annex 1.D of the present Guide should help in choosing a representative site: the ideal location should be a site of class 1 for all the measurements, but compromise is sometimes necessary because criteria and other influencing factors are not identical for all atmospheric parameters. The network designer should define the maximum classes allowed for selecting a measuring site and a derogation procedure in case of special difficulties to find a site following the criteria for selected classes. A split of the station, with delocalized instruments, might also be considered, an option made relatively easy by current available technology (see 1.2.1).

Some AWSs have to operate unattended for long periods at sites with difficult access, both on land and at sea. Construction costs can be high and extra costs can be necessary for servicing. They may have to operate from highly unreliable power supplies or from sites at which no permanent power supply is available. The availability of telecommunication facilities should be considered in the choice of the site. Security measures (against lightning, flooding, theft, vandalism, and so forth) are to be taken into account and the stations must be able to withstand severe meteorological conditions. The cost of providing systems capable of operating under

all foreseen circumstances is high and may be prohibitive. It is essential to obtain a thorough understanding of the working environment anticipated for the AWS before specifying or designing it. At an early stage of planning there should be a detailed analysis of the relative importance of the meteorological and technical requirements so that sites can be chosen and approved as suitable before significant installation investment is made.

1.7 MAINTENANCE

The cost of servicing a network of AWSs on land and, in particular, at sea can greatly exceed the cost of their purchase. It is, therefore, of central importance that AWSs are designed to have the greatest possible reliability and maintainability. Special protection against environmental factors is often justified, even when initial costs are high.

It is evident that any complex system requires maintenance support. Corrective maintenance is required for component failures. Hardware components may fail for many reasons; computer programs can also fail because of errors in design that can go undetected for a long time. To minimize corrective maintenance and to increase the performance of an AWS, well-organized preventive maintenance is recommended. Preventive maintenance is required for all system components, not only cleaning and lubricating mechanical parts. With the increasing reliability of the electronic components of an AWS, preventive maintenance, including services and instrument calibration, becomes the controlling factor in maintenance.

Adaptive maintenance is required to take into account the rapid changes in technology and the availability of spare parts after a few years of operation. Costs of reparation and components often rapidly increase after a system is no longer in active distribution, thus making it necessary to replace modules by new ones with different technology, because exact replacements (for example, when wishing to transfer programs and operating systems from one processor to another, to introduce modular changes for system reliability, to make connections with new telecommunication systems, and so forth) are seldom found. To reduce the costs for this type of maintenance, it is desirable to establish widely accepted standards on equipment and interfaces, as well as on software, and include them in AWS technical specifications.

The installation of a network of AWSs must not be seen as a one-shot investment. It is essential to organize maintenance according to a rational plan that details all the functions and to arrange them so that costs are minimized without adversely affecting performance. The modular structure of many modern AWSs allows maintenance to take place in the field or at regional and national centres.

Field maintenance. In general, it is not advisable to repair AWS instruments or other modules in the field because conditions might not favour effective work. It is recommended that corrective maintenance in the field is carried out by specialized technical personnel from a regional or national centre, depending on the size of the country. Simple preventive or corrective maintenance can be done by a local observer (when available) or a local design operator. The regular transmission of self-checking diagnostic information by the AWS is a very desirable practice to ensure rapid response to failures.

Regional centre. At a regional centre, technical personnel should be available to replace or repair modules and instruments requiring the detection and elimination of simple defects. The personnel should have good knowledge of the station hardware operation and must be trained in the execution of software maintenance routines. Such regional centres should be equipped with appropriate test equipment and sufficient spare modules and instruments to support the maintenance of the stations in their area. They also need the necessary access via a telecommunication network to the AWSs, the backbone network, and, possibly, the central servers. These centres need adequate transportation facilities for conducting fieldwork. Care should be taken to plan and visit periodically the remote sites to check for operational problems, vandalism, site conditions, changes, and so forth. Procedures for emergency visits to the different stations must be established, based on priorities defined at the station.

National centre. A national centre requires more highly skilled technical personnel capable of detecting and eliminating complex problems in instruments, modules and data-transmission means. The equipment necessary for checking and correcting all parts of an AWS should be available and the work should be performed in the centre. Any recurring defects should be referred to designers or suppliers in charge of correcting the design fault.

As software plays a very important role in each AWS and in the central network processing system, personnel with a profound knowledge of the AWS and central network system software are required. The necessary software development and test facilities should be available. Moreover, the national centre should be able to execute all tasks associated with adaptive maintenance.

With reference to the quality control of network data, it is of utmost importance to establish effective liaison procedures between the monitoring service and the appropriate maintenance and calibration service to facilitate rapid response to reports of fault or failure from the monitoring system.

For small countries, the tasks of the regional centres could be taken over by the national centre. Developing countries could consider establishing joint maintenance arrangements with neighbouring countries. A common international maintenance centre could be envisaged in order to keep maintenance costs reasonably low. However, such international cooperation would probably require the use of similar equipment. If the NMHS is unable to expand its staff or facilities, contractor services could be used to perform many of the supporting functions. Such support could, for example, be negotiated as a part of the system procurement. However, a maintenance contract should be extremely well prepared and the execution of the contract should be very carefully verified by the appropriate staff.

Suggestions for quality-management techniques are given in Volume V, Chapter 1.

1.7.1 **Service levels**

A service level for maintenance should define the maximum delay to diagnose a problem and a maximum delay to fix it. An example of such maximum delays, used by one NMHS, is given below:

- (a) Four hours on a very large aerodrome; this implies a local maintenance team is available 24 hours a day and spare parts are available locally.
- (b) Fifteen hours on an important aerodrome or synoptic station; fifteen hours stands for a rapid maintenance action on the day of the failure detection or the next morning if the failure occurs during the evening or night. This implies maintenance staff are available close to the site (for example, at less than 2-3 hours of driving), during working hours and with spare parts available locally, every day of the week.
- (c) Two or three days on other stations; this allows longer driving displacement and/or obtaining spare parts from a distant location (for example, a national centre) and staff availability only during working days.
- (d) Five days for lower-priority stations.

Service levels should be defined during the network definition, taking into account the users' needs, maintenance organization, distances between the maintenance centres and the observing stations, difficulties with transport arrangements and the cost of spare part stocks. The result will necessarily be a compromise between the users' expectations and the human and recurring costs. Different service levels may be defined for different stations.

1.7.2 Calibration and site inspection

Instruments, in particular AWS instruments with electrical outputs, drift in time and, consequently, regular inspection and calibration are needed. In principle, the calibration interval is determined by the drift specifications given by the manufacturer and the required uncertainty. WMO international instrument intercomparisons also provide some objective indications of instrument drifts and desirable calibration intervals. As signal conditioning modules and data-acquisition and transmission equipment also form a part of the measuring chain, their stability and correct operation also have to be controlled or calibrated periodically. The summary given below is limited to practical aspects related to AWSs. For more detailed information on calibration techniques and methods, see the different chapters of Volume I and to Volume V, Chapter 4 of the present Guide.

Initial calibration. Appropriate calibration facilities and instrumentation should be available prior to the procurement and installation of AWSs to enable verification of the specifications given by the manufacturer, testing of the overall performance of the station and inspection if transportation has affected the measuring characteristics of the equipment.

Field inspection. The periodic replacement or comparison of AWS instruments with travelling standards at the station is an absolute requirement to monitor the performance of the instruments. Travelling standards having similar filtering characteristics to the AWS measuring chain and with a digital read-out are preferred. In many countries, two travelling standards of the same type are used to prevent possible problems with change of accuracy due to transportation. To be able to detect small drifts, the travelling standards should have an uncertainty that is much lower than the relevant station instruments and should be installed during the comparison process in the same environmental conditions as the instruments for a sufficiently long time. As signal conditioning modules and data-acquisition equipment, such as the ADC, can also show performance drifts, appropriate electrical reference sources and multimeters should be used to locate anomalies. The period between inspection visits should be determined by the drift characteristics of the instruments. As experience with the instruments increases, deviation adjustment of the field inspection schedule can be justified.

Before and after field inspections, the travelling standards and reference sources must be compared with the working standards of the calibration laboratory. The maintenance service must be informed as soon as possible if uncertainty deviations are detected.

Field inspections should also be used to control the state of the observing site:

- (a) The site environment (obstacles such as trees, vegetation, buildings, and the like), to detect possible changes in the siting classification (see Volume I, Chapter I, Annex 1.D of the present Guide); photos are enormously useful for monitoring site changes;
- (b) The state of the vegetation in the instrument field and vegetation cutting if necessary;
- (c) The state of all infrastructure: fencing, supporting structures of the AWS and the instruments (for example, corrosion);
- (d) The state of the power supply system: cleaning of solar panels, periodic change of batteries;
- (e) The state of the surge protections;
- (f) The cleaning of instruments, as appropriate;
- (g) Any other task to be defined, as appropriate (according to the equipment user manual provided by the manufacturer).

The network manager should organize a regular field inspection every 6 to 12 months, depending on the instruments installed in the network, of the accessibility of the observing sites and of the maintenance organization.

Laboratory calibration. Those instruments that are at the end of their calibration interval, or show an uncertainty deviation beyond allowed limits during a field inspection, or instruments repaired by the maintenance service, should return to a calibration laboratory prior to their re-use. Instruments should be calibrated in a conditioned environment (environmental chambers) by means of appropriate working standards and well-defined procedures. These working standards should be compared and calibrated periodically with secondary standards and be traceable to international standards. Details on the strategy for traceability assurance are described in Volume I, Chapter 1, Annex 1.B of the present Guide.

1.7.3 Training

As an AWS is based on the application of technology that differs considerably from the equipment at conventional stations and networks, a comprehensive review of existing training programmes and of the skills of the necessary technical staff is obviously required. Any new training programme should be organized according to a plan that is geared to meeting user needs. It should especially cover the maintenance and calibration outlined above and should be adapted to the system. Requesting existing personnel to take on new functions, even if they have many years of experience with conventional stations, is not always possible and may create serious problems if they have no basic knowledge of electrical instruments, digital and microprocessor techniques or computers. It could be necessary to recruit new personnel who have such knowledge. Personnel competent in the different areas covered by AWSs should be present well before the installation of an AWS network (see WMO (1997) and Volume V, Chapter 5 of the present Guide).

It is essential that AWS equipment manufacturers provide very comprehensive operational and technical documentation together with operational and technical training courses. Generally, two sets of documentation are required from the manufacturer: user manuals for operational training and use of the system, and technical manuals with more complex documentation describing in great technical detail the operating characteristics of the system, down to subunit and even electronic component level and including maintenance and repair instructions. These manuals can be considered as the basic documentation for training programmes offered by the manufacturer and should be such that they can serve as references after the manufacturer's specialists are no longer available for assistance.

For some countries, it may be advisable to organize common training courses at a training centre that serves neighbouring countries. Such a training centre would work best if it is associated with a designated instrument centre and if the countries served have agreed on the use of similar standardized equipment.

1.8 CONSIDERATION OF SYSTEM SPECIFICATIONS AND COST

The installation of a new network of AWSs or the transition from manual to automatic stations is a difficult matter and should be managed as a project:

- (a) A project team with the necessary management skills should be set up.
- (b) Users' needs should be clearly established and translated into functional and technical specifications.
- (c) Future processes of procurement, sites selection, initial installation and maintenance during the whole lifetime of the system have to be identified and documented.
- (d) Explicit quality objectives should be defined:
 - (i) Target measurement uncertainty, understanding that it may be a compromise between state of the art and the affordable costs, with associated calibration periodicity;

- (ii) Target siting classification for observing sites and accepted compromises in case of difficulties to find class 1 sites (see Volume I, Part 1, Annex 1.D of the present Guide);
 - (iii) Target data availability, both in real-time and delayed;
 - (iv) Definition of an accepted service level (for example, maximum delay for fixing a problem on site);
 - (v) Identification of the life duration of the network;
 - (vi) Definition of the system redundancy (measurement, telecommunication, central unit system);
- (e) The available telecommunication networks have to be identified and selected.
 - (f) Existing equipment, to be reused or not, should be identified (instruments, central processing system, sites, site infrastructure, and so forth).
 - (g) The procurement laws to follow, the initial budget and the running costs should be identified.
 - (h) The specifications for the full system should be written and the procurement procedure (tender, in-house development, external or internal installation and maintenance, and the like) should be selected.
 - (i) The procurement process, the acceptance tests for the first equipment, the acceptance tests for the serial equipment should be defined and executed.
 - (j) The first installations on site and the link to the central system (collecting platform, processing platform) should be validated.
 - (k) The stations' and central supervision tools and methods, with appropriate indicators, should be deployed.
 - (l) Regular site inspection should be planned.
 - (m) The performances attained should be measured, compared to the target and then corrective and preventive action should be taken, accordingly.

It must be understood that AWSs have many advantages, but do not eliminate the need of a well-established organization for using and maintaining them.

The cost of a network of AWSs is split between many parts and the cost of the AWS itself is a small percentage of the total costs, which include:

- (a) Cost of the observing site itself: piece of land, fence, and possible trench for mains power or telecommunication lines;
- (b) Cost of the equipment: AWS, instruments, telecommunication modem or interface;
- (c) Cost of the on-site installation and installing structures;

- (d) Cost of the development and implementation of the central collecting and processing systems;
 - (e) The running expenditure for communications;
 - (f) The running cost for maintenance and calibration.
-

ANNEX. AUTOMATIC WEATHER STATIONS – LOW COST

1. INTRODUCTION

Historically the measurement of weather phenomena has been an activity performed by professional meteorological organizations, but in the last 10 years there has been a continually increasing number of lower-cost AWSs on the market (referred to here as “low-cost AWS(s)”). Low-cost AWSs range in price from as low as US\$ 50 up to, more typically, US\$ 7 000, and come in a variety of designs and configurations.

There are some common features of low-cost AWS, including:

- (a) Relatively low cost;
- (b) Low or very low power consumption;
- (c) Transmission of data in real time (with or without logging);
- (d) Often small and compact.

There are three main classes of low-cost AWS: compact; all-in-one; and stand-alone instruments (or IoT).

"Compact AWSs" consist of a mast, stand or pole with mounting arms for a variety of instruments and usually a cabinet to house a logger or processor, power supply and other modules (Figure 1.A.1). These AWSs are similar to professional metrological weather stations; they typically use individual instruments for each variable and the instruments are capable of being calibrated. The instruments can also be adjusted and replaced individually. The AWS may have some data-logging and data-transmission capability with the flexibility to tailor the message communications to fit into an existing data-reception system.

"All in one" generally refers to the instrument component of a low-cost AWS (Figure 1.A.2). The most common configuration of all-in-one AWSs includes temperature, relative humidity and pressure instruments with the capacity to add further instruments. Some may also have one or more additional measurements, such as: wind speed, wind direction, precipitation and solar radiation. There are also units that measure present weather variables such as hail and thunderstorms. Typically they are designed to be a single unit and mounted on a small post or mast. Some models include logging and battery storage that provide the entire system power supply, including transmission of limited volumes of data. However, more commonly these are additional items and costs.

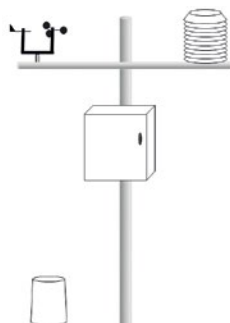


Figure 1.A.1. Example of a compact AWS

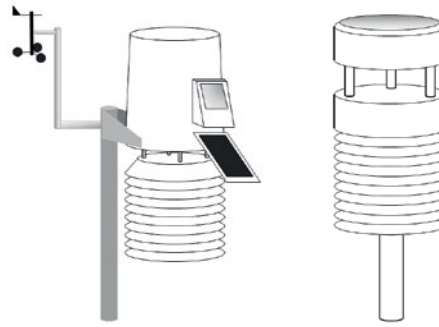


Figure 1.A.2. Examples of all-in-one AWS systems

"Stand-alone instruments" are a rapidly emerging technology, and these are commonly referred to as IoT devices. These systems use a network of individual intelligent instruments, transmitting information using low-power and low bandwidth via Wi-Fi, Bluetooth or Internet interfaces to centralized processing servers (WMO, 2012). There are also a growing number of add-ons to phones that measure weather parameters.

2. **ADVANTAGES AND DISADVANTAGES**

Depending on the intended use, each of these categories has its advantages and disadvantages.

All-in-one systems are simple to install and operate. However, the design tends to result in compromises in the quality of the information gathered. The instruments, all being in one small unit, may not all be exposed correctly, and some may compromise the measurements of others. Typically, they also have small radiation screens that can result in biased coupling of the instrument to the environment; for example, significant increases in the observed temperature during the day and moderate decreases during the night. This biased coupling also results in significant spikes in temperature. All-in-one systems also have the disadvantage that when a single instrument fails, often the entire unit needs repair or replacement. Calibration of these units is difficult, and for some variables this can only be performed by the manufacturer. Studies by the Royal Netherlands Meteorological Institute (Koninklijk Nederlands Meteorologisch Instituut, KNMI) (Vega, 2017) and Aston University (Bell et al., 2015) demonstrate that these instruments exhibit significant biases in their measurements. For example, the Aston University study showed hourly mean bias in the temperature of $+0.7\text{ }^{\circ}\text{C}$ in the summer and $+0.4\text{ }^{\circ}\text{C}$ in the winter. Additionally, the KNMI research demonstrated spikes of $1\text{ }^{\circ}\text{C}$ to $2\text{ }^{\circ}\text{C}$ in air temperature and gross underestimation of rainfall (62% losses).

Robustness is also a consideration with these all-in-one units. The units tend to be made of mass-produced plastic components that deteriorate with exposure to the elements. Their mounting systems also tend to be lightweight. As sold, the devices often include a rechargeable battery that is topped up by a small solar cell. Although this is adequate in warm climates, the battery often fails in sub-zero temperatures. The devices do not normally include the facility for the use of an external power supply.

Compact AWSs have the advantage that they can use commercial off-the-shelf instruments, offering the capability to change faulty instruments and allow for a better siting configuration. The masts and general infrastructure are lighter in weight and less robust than professional weather stations and more likely to fail during severe weather events. An advantage of many of the all-in-one and compact AWSs is that they are supplied with software for local data collection, distribution and display. Increasingly suppliers are providing cloud services where they collect and display data, and provide network statistics via a web browser interface and an API for interfacing to other data-processing systems. This has the advantage that information is available

from anywhere at any time and by many concurrent users. However, these software and data-management systems reduce the users' options to expand networks. Most of these AWS systems will not interface to other makes of compact and all-in-one AWSs.

The IoT systems offer the ability to optimize the siting and choice of individual instruments. However, the operation and management of these networks can become complicated. This distributed system technology is much newer and is not as proven as compact and all-in-one systems. Professional manufacturers of weather instruments have not started building instruments specifically for this market currently. As a result, many of the available instruments are at the lower-cost end of the market, produced by electronics integrators without extensive experience in meteorological measurement. Most of the manufactured devices are consumer grade, meaning the ongoing quality of data very quickly becomes unknown.

3. **SELECTION CONSIDERATIONS**

When choosing a low-cost AWS there is a large range of issues to consider to ensure the system is fit for purpose. One of the most significant considerations is defining the user requirements and then creating an appropriate specification for the AWS. Most manufacturers provide a specification for the sensor element, which relates to testing under laboratory conditions and without screens or other environmental interfaces. Additionally, there may be constraints on the way the instrument has been tested to achieve the specification. For example, the specification for relative humidity instruments is often for the instrument tested at a single temperature in the laboratory. It does not include considerations such as the effect of the full range of temperatures the instrument may experience in the field. Some instruments may include testing over a certain range of temperatures, but not over the full range of operational temperatures.

At the lower-cost end, there may be no manufacturer's acceptance testing or calibration and adjustment, the manufacturer instead relying on design and development specifications to represent all manufactured units. All this means that when selecting an AWS, significant care needs to be taken to ensure specifications from different manufacturers are genuinely comparable. For example, if the specified measurement uncertainty is small compared to other manufacturers, it may mean it is only applicable over a narrower range of conditions. Alternately, the specification may only be one standard deviation, not an uncertainty with a 95% confidence interval.

When considering systems such as an all-in-one units, the specifications will not typically include the effect of enclosures such as the screen on the instrument in the field. They are unlikely to include the impact of effects such as turbulence on wind measurements or precipitation, nor the impact of the instrument not being mounted at a standard height.

In the case of an all-in-one system, purchasers should look for AWSs with symmetrical design. This symmetry minimizes the impact of turbulence and shadowing on instruments. Some systems have a significant amount of electronics, which has the potential to affect temperature and humidity instrument readings. Consequently, it is advisable to choose instruments that have some separation between the electronics and the screen. Ideally, the screen should be at the bottom of the cylindrical system, thus minimizing heat transfer from other parts of the all-in-one system.

The materials used to construct the system are also important. Metal screens can have a significant effect on the measured temperature (Warne, 1998), as can the size and colour of the screen. Screens significantly smaller than 200 mm in diameter and 250 mm in height will result in poorer performance, exhibiting significant warming under insolation and some cooling overnight due to radiative cooling, compared to a standard siting (Warne, 1998). In general, the smaller the screen, the larger the impact. Even the colour of the screen, in the visible and infrared spectrum, is important: where possible, "white" should be used. Some manufacturers may provide a suitable screen but have large structures such as black or dark grey raingauges, which act as thermal masses and nearby radiation sources, affecting other sensors (Bell et al., 2015).

4. **OTHER MEANS OF LOWERING OPERATIONAL COST**

The use of compact, all-in-one or IoT technologies as a means of obtaining low-cost observations is not necessarily straightforward. Depending on the quality of data required and the cost of human resources these solutions may not represent value for money. All-in-one AWS instruments are more inclined to drift and fail, and thus require more servicing. For countries where the workforce is the most significant expense, this can result in maintenance costs (including calibration) that outstrip the upfront savings in capital investment. If, however, the intended use is to provide an increased density of observations in crowded environments, these systems may be the most economical solution. Using the manufacturer's stated drift characteristics, these systems may need to be replaced three to seven times in a ten-year period, and maintained or calibrated twice per year to keep them within their stated manufacturer's specification.

Compact AWS and IoT systems that use high-quality instruments reduce the maintenance burden. However, if the value the systems provide is their contribution to recording extreme weather events, then the savings in infrastructure investment may be wasted if the systems are lost or damaged during an extreme event. Currently, many of the IoT instruments are aimed at the amateur and home market, and as such are not suitable for use by NMHSs.

Low-cost AWSs may have their place in a tiered network and can provide significant value if their performance and operating limitations are understood. Alternately, substantial reductions in operational costs can be achieved in the operation of professional standard AWS networks by understanding the performance standards that a network achieves and the drivers of the cost to maintain the required standard. Substantial savings can be achieved through optimization of network operations. Analysis of before-and-after calibration checks, failures of systems in the field, root-cause analysis, and effective asset management provide the evidence needed to optimize the cost of operating a network. It is important for network managers to ask questions such as "Are our systems being over or under serviced?"; "Is the right preventive maintenance in place?"; "Are staff adequately trained?"; "Do we have the proper infrastructure in place for the environment in which the AWS is operating?". For countries where labour costs are high, then optimization of maintenance can bring more significant savings than the reduction in the quality and robustness of capital investment. In countries where the capital cost of investment is high and labour costs are relatively low, then there should be careful consideration of what should be automated.

The reasons for introducing low-cost AWSs into a professional meteorological network are varied. It may be to increase the density of observation points, create agility and flexibility with a network or to reduce the cost of operations. It is important to understand that just because these alternative systems have a lower upfront price tag, they may not be a "lower-cost" solution in the longer term. Issues concerning user requirements for data availability and quality; the cost of labour to maintain, operate and monitor; as well as the capital price of equipment need to be included in planning the overall network and its operation. Often the lower upfront price may be more costly.

REFERENCES AND FURTHER READING

- Bell, S., D. Cornford and L. Bastin, 2015: How good are citizen weather stations? Addressing a biased opinion. *Weather*, 70(3):75–84.
- Gifford, M.D., G.M. Pearson and K. Hegg, 2000: Operation of automated surface observing systems in harsh climatological environments. In: Papers Presented at the WMO Technical Conference on Meteorological and Environmental Instruments and Methods of Observation (TECO-2000) (WMO/TD-No. 1028). Beijing, 23–27 October 2000. Instruments and Observing Methods Report No. 74. Geneva.
- United Nations Environment Programme, 2017: Minamata Convention on Mercury, https://www.mercuryconvention.org/sites/default/files/documents/information_document/Minamata-Convention-booklet-Sep2019-EN.pdf.
- Vega, S., 2017: The Quality of Low-cost Weather Stations. Report by KNMI and The Hague University of Applied Sciences.
- Warne, J., 1998: A Preliminary Investigation of Temperature Screen Design and their Impacts on Temperature Measurements. Instrument Test Report 649. Melbourne, Bureau of Meteorology.
- , 2017: Desktop analysis of commercially available "All-in-One" and "Compact" weather stations – How well can we do it? In: Papers Presented at the WMO International Conference on Automatic Weather Stations (ICAWS-2017). WMO International Conference on Automatic Weather Stations (ICAWS-2017), "Automatic Weather Stations for environmental intelligence – the AWS in the 21st century". Offenbach am Main, Germany, 24–26 October 2017. Instruments and Observing Methods Report No. 127, https://library.wmo.int/index.php?lvl=notice_display&id=20023#.XOUzGa6Wapo.
- World Meteorological Organization, 1987: Some General Considerations and Specific Examples in the Design of Algorithms for Synoptic Automatic Weather Stations (D.T. Acheson) (WMO/TD-No. 230). Instruments and Observing Methods Report No. 19. Geneva.
- , 1991: Guidance on the Establishment of Algorithms for Use in Synoptic Automatic Weather Stations: Processing of Surface Wind Data (D.J. Painting) (WMO/TD-No. 452). Instruments and Observing Methods Report No. 47. Geneva.
- , 1992: *International Meteorological Vocabulary* (WMO-No. 182). Geneva.
- , 1993: *Guide on the Global Data-processing System* (WMO-No. 305). Geneva.
- , 1995: Papers Presented at the International Workshop on Experiences with Automatic Weather Stations on Operational Use within National Weather Services (WMO/TD-No. 670). Vienna, 15–17 May 1995. Austria, ZAMG.
- , 1997: Guidance on Automatic Weather Systems and their Implementation (WMO/TD-No. 862). Instruments and Observing Methods Report No. 65. Geneva.
- , 2003: Algorithms Used in Automatic Weather Stations: Evaluation of Questionnaire (M.D. Gifford) (WMO/TD-No. 1160). Instruments and Observing Methods Report No. 78. Geneva.
- , 2010 (updated in 2017): *Guide to the Global Observing System* (WMO-No. 488). Geneva.
- , 2014: *Guide to Meteorological Observing and Information Distribution Systems for Aviation Weather Services* (WMO-No. 731). Geneva.
- , 2015a (updated in 2018): *Technical Regulations* (WMO-No. 49), Volume I – General Meteorological Standards and Recommended Practices. Geneva.
- , 2015b (updated in 2017): *Manual on the WMO Integrated Global Observing System* (WMO-No. 1160). Geneva.
- , 2015c (updated in 2017): *Manual on Codes* (WMO-No. 306), Volume 1.2 – International Codes. Geneva.
- , 2017a: WMO Observing Systems Capability Analysis and Review Tool (OSCAR), <https://www.wmo-sat.info/oscar/>.

- , 2017b: Papers Presented at the WMO International Conference on Automatic Weather Stations (ICAWS-2017). WMO International Conference on Automatic Weather Stations (ICAWS-2017), “Automatic Weather Stations for environmental intelligence – the AWS in the 21st century”. Offenbach am Main, Germany, 24–26 October 2017. Instruments and Observing Methods Report No. 127, https://library.wmo.int/index.php?lvl=notice_display&id=20023#XOuzGa6Wapo.
- , 2017c: *Challenges in the Transition from Conventional to Automatic Meteorological Observing Networks for Long-term Climate Records* (WMO-No. 1202). Geneva.
-

CHAPTER 2. MEASUREMENTS AND OBSERVATIONS AT AERONAUTICAL METEOROLOGICAL STATIONS

2.1 GENERAL

2.1.1 Definitions

This chapter deals with the requirements for observations at aeronautical meteorological stations and the instruments and methods that are used. Synoptic observations measure at one location a representative value for a rather large area, but meteorological observations for aeronautical purposes are often made at several locations at the aerodrome and in the surrounding area, at more frequent intervals, to be representative of rather limited areas, such as the approach, touchdown and take-off areas.

The meteorological measurements to be taken are for the most part essentially the same as those taken for other applications, and described in other chapters in the present Guide. The exceptions are runway visual range (RVR), slant visual range and low-level wind shear which are unique to this application.

2.1.2 Units

The units for measuring and reporting meteorological quantities for aeronautical purposes are the same as for other applications, except that:

- (a) Surface wind speed may be measured and reported in metres per second or knots;¹ and wind direction² reported in degrees measured clockwise from geographic north³ (see 2.2.1);
- (b) Cloud-base height may be measured in metres or feet.

The choice of units is a matter for national practice, depending on the requirements of the aviation regulatory bodies.

2.1.3 Requirements

The formal requirements for aeronautical observations are stated in the *Technical Regulations*, Volume II (WMO, 2016). Detailed guidance on procedures and practices is found in WMO (2014). Useful guidance on observing and monitoring meteorological conditions is contained in WMO (2003). Special attention should be given to aeronautical meteorological stations established on offshore structures in support of helicopter operations (International Civil Aviation Organization (ICAO), 1996).

The requirements for uncertainty, resolution and range, and for currently achievable performance in meteorological measurements are given in Volume I, Chapter 1, and the operationally desirable accuracies of some measurements are provided in the *Technical Regulations*, Volume II, Part II, Attachment A.

¹ The unit of wind speed used is determined by national decision. However, the primary unit prescribed by the *Technical Regulations*, Volume II (WMO, 2016) for wind speed is the metre per second, with the knot permitted for use as a non-SI alternative unit (further information is given in ICAO, 2010).

² Direction from which surface wind is blowing.

³ Because wind direction reported to aircraft for landing or take-off purposes may be converted into degrees magnetic, the display at the air traffic service unit usually presents direction with respect to the magnetic north.

Despite the excellent performance of modern aircraft, weather factors still have a marked effect on their operation. The reliability and representativeness of aerodrome observations are very important in ensuring that landings and take-offs are made safely. The wind observation will determine the runway to be used, and the maximum take-off and landing weights. Temperature is also important and affects engine performance. Consequently, the load carried might have to be reduced, or the take-off would require a longer runway, particularly at airports in hot countries.

Routine observations are to be made at aeronautical meteorological stations, at times and frequencies determined by the Member country to meet the needs of national and international air navigation, giving due regard to regional air-navigation arrangements. Special and other non-routine observations are to be made on the same basis. Routine observations at aerodromes should be made at hourly or half-hourly intervals, during all or part of each day, or as necessitated by aircraft operations. Special observations must be made when specified changes occur between routine observations in respect of surface wind, visibility, RVR, present weather and/or cloud. These specified changes are set out in the *Technical Regulations*, Volume II, Part II, Appendix 3, 2.3.2. These observations, in the form of coded reports of the METAR or SPECI types, are exchanged internationally between aeronautical meteorological stations. Other types of reports are intended only for aeronautical operations, and should be prepared in a form defined jointly by the meteorological and airport authorities.

In view of the importance of meteorological observations for aircraft safety, it is essential that observers be correctly trained and have good eyesight. Observer training should include basic courses and regular refresher courses (for further information see the *Technical Regulations*, Volume I, Part II, 4, and WMO, 2012).

Siting, installation and the nature of meteorological systems are specified in the *Technical Regulations*, Volume II, Part I, 4, with technical specifications and detailed criteria in the *Technical Regulations*, Volume II, Part II, Appendix 3. These specifications are summarized below.

Special care is necessary in selecting appropriate sites for making observations, or for the installation of instruments at aeronautical meteorological stations, to ensure that the values are representative of the conditions at or near the aerodrome. In some instances, where information over a large area is required, it may be necessary to provide multiple installations for some instruments to ensure that values reported are representative of the entire area. For example, for long runways or for large aerodromes with several runways, where approach, touchdown and take-off areas may be as much as 2 to 5 km apart, the values of various parameters such as wind, cloud height, RVR, and so forth, measured at one end of a runway may be quite different from the conditions prevailing elsewhere on that runway, or over other areas of the runway complex of interest to aircraft operations.

At all aerodromes, the sites should be such that the measured values of the various meteorological parameters are representative of the aerodrome itself and/or the appropriate area of a particular runway or runway complex. At aerodromes where precision approach and landing operations are not in practice (non-instrument or non-precision approach runways), this criterion on representativeness is less restrictive than with precision approach runways (that is, with Category I, II or III runways (see WMO, 2014, and ICAO, 2011)).

In selecting locations for instruments at aerodromes, it is particularly important that, while the site and exposure of the instruments meet operational requirements, the instruments or their operation do not present hazards to air navigation; and that the presence or movement of aircraft at the aerodrome (taxiing, take-off runs, landing, parking, and the like) and the various aerodrome installations do not unduly influence the measured values.

The types of instruments to be used, their characteristics and the methods employed for the presentation and reporting of the measured values of the parameters are equally important. Meteorological instruments should be exposed, operated and maintained in accordance with the practices, procedures and specifications promulgated in the present Guide. Aeronautical meteorological stations shall be inspected at sufficiently frequent intervals to ensure that a high

standard of observations is maintained, that instruments and all their indicators are functioning correctly, and that the exposure of the instruments has not changed significantly (*Technical Regulations*, Volume II, Part I, 4.1.4).

Instrument design should permit remote indication, simultaneously at both the air traffic service (ATS) units and at the meteorological stations and offices, of the appropriate values of surface wind, temperature, dewpoint, atmospheric pressure, present weather, visibility, RVR (if the runways are equipped for take-offs and landings in fog) and cloud height, all of which should be representative of conditions in the touchdown and take-off areas concerned. Automatic instrumental systems for measuring the height of the cloud base and RVR are particularly useful at aeronautical stations.

At aerodromes where precision approaches and, in particular, where Category II, III A and III B operations are affected, and/or at aerodromes with high levels of traffic, it is preferable to use integrated automatic systems for acquisition, processing and dissemination/display in real time of the meteorological parameters affecting landing and take-off operations. These automatic systems should be capable of accepting the manual insertion of meteorological data that cannot be measured by automatic means (*Technical Regulations*, Volume II, Part I, 4.1.7). The requirements for automatic meteorological observing systems are specified in the *Technical Regulations*, Volume II, Part II, Appendix 3.

2.1.4 **Methods**

The methods for taking meteorological measurements at aerodromes are essentially the same as those for other meteorological applications and described in other chapters of the present Guide. This chapter describes some siting and sampling requirements, and some algorithms, which are particular to the aeronautical application.

2.2 **SURFACE WIND**

2.2.1 **General**

In aviation, measurements of airflow and low-level wind shear in the vicinity of the landing and take-off areas are of primary interest. The regulations are described in the *Technical Regulations*, Volume II, Part I, 4.1, with details in Part II, Appendix 3. At international aerodromes, ATS units, ATC towers, and approach control offices are normally equipped with wind-speed and wind-direction indicators, and air traffic controllers supply arriving and departing aircraft with readings from these indicators. To ensure compatibility, the indicators at the ATS units and the meteorological station should be connected to the same sensors.

The mean direction and speed of the wind are measured as well as gusts and specified significant variations of direction and speed. Wind reports disseminated beyond the aerodrome (*Technical Regulations*, Volume II, Part II, Appendix 3, 4.1.5) have the same content as those in synoptic observations (10 min means, and direction reported with respect to the geographic north),⁴ and the values transmitted should be representative of all runways. For local routine and special reports and for wind indicator displays in ATS units (*Technical Regulations*, Volume II, Part II, Appendix 3, 4.1.3.1), the averaging period is 2 min for both speed and direction, and the values should be representative of the runway in use. Although wind direction shall be reported with respect to the geographic north, expressed in “degrees true” (*Technical Regulations*, Volume II, Part I, 4.6.1 and Part II, Appendix 3, 4.1.5.1), it is still common practice that ATS personnel report the aircraft with respect to the magnetic north (“degree magnetic”). Gusts should be determined from 3 s running means. Volume I, Chapter 5, and Volume V, Chapter 2, of the

⁴ Usually referred to as the “true” north, with the unit “degree true”. The word “true” in “true north” or “degree true” should not be confused with the “true wind” (defined by WMO, 1992a). “True wind” is represented by the wind vector in relation to the Earth’s surface. For a moving object like an aircraft, it is the vector sum of the apparent wind (that is, the wind vector relative to the moving object) and the velocity of the object.

present Guide should be consulted on the precautions to be taken for sampling the anemometer output to measure the mean, gusts and variability of the wind speed and direction. Vector averaging is to be preferred to scalar averaging.

The wind measurements needed at aerodromes, such as mean value, extreme values, and so forth, should preferably be determined and displayed automatically, particularly when several sensors are used on different runways. When several sensors are required, the indicators shall be clearly marked to identify the runway and the section of runway monitored by each sensor.

2.2.2 Instruments and exposure

Wind-measuring instruments used at aeronautical stations are generally of the same type as those described in Volume I, Chapter 5 of the present Guide. The lag coefficients of direction and speed sensors should comply with the requirements of that chapter.

Sensors for direction and speed should be exposed approximately 10 m above the runway and should provide measurements that are representative of the conditions at the average lift-off and touchdown areas of the runway.

If wind sensors installed at aerodromes are to be representative of the conditions at take-off or landing areas, any disturbance or turbulence due to the proximity and passage of the aircraft themselves must be avoided (false gust indications due to landings and take-offs). For similar reasons, they must not be placed too close to buildings or hills or located in areas subject to microclimatic conditions (sea breeze, frequent storms, and the like). The preferred standard exposure of wind instruments is in open terrain, defined as an area where the distance between the anemometer and any obstruction is at least 10 times the height of the obstruction.

It is recommended that back-up or standby equipment should be provided in case of failure of the service instrument in order to avoid any interruption in the transmission of data to the ATS units. Where local conditions so warrant, one or more sets of sensors should be installed for each runway concerned. In such cases, the use of digital techniques is recommended since they enable data from a large number of sensors to be transmitted by one or two telephone cable pairs, and allow digital indicators to be used to display wind measurements using light-emitting diodes of different colours. The displays should show the "instantaneous" wind speed and direction (with a distance constant of 2 to 5 m), the average wind speed and direction over 2 or 10 min, and the minimum and maximum wind speeds. It is sometimes possible to select wind readings for different measurement points on the same indicator (thus reducing the number of indicators required).

When installing wind sensors at the aerodrome, particular attention must be paid to protecting them against atmospheric storm discharge (by the use of lightning conductors, earthing of the mast, and shielded or fibre optic cables); electronic data-processing equipment should also be protected.

In order to maintain the required accuracy, wind-measuring instruments should be kept in good order and regularly checked and recalibrated. Sensor performance must sometimes be checked in the wind tunnel, particularly for analogue systems. The use of digital techniques with the built-in testing of certain functions calls for fewer checks, but does not eliminate errors due to friction. Regular checks are to be made to detect defective components and deterioration of certain parts of the sensors.

The sources of error include friction, poor siting and problems with transmission or display equipment. Errors may also be caused by the design of the sensors themselves and are noticed particularly in light winds (rotation threshold too high, excessive inertia) or variable winds (over- or underestimation of wind speed or incorrect direction due to excessive or inadequate damping).

2.3 VISIBILITY

The definition of the meteorological optical range (MOR) and its estimation or instrumental measurement are discussed in Volume I, Chapter 9 of the present Guide. The measurement of visibility in aviation is a specific application of MOR. However, the term "MOR" is not yet commonly used in aviation and the term "visibility" has been retained in this chapter to describe operational requirements. For aviation purposes, it is common practice to report visual ranges like the RVR and "visibility for aeronautical purposes" (VIS-AERO). Note that the latter is used in reports and indicated as "visibility" only, which differs from the common definition of visibility (see Volume I, Chapter 9). Instruments used to measure MOR may also be used to measure RVR (see 2.4) and VIS-AERO (see 2.3.1). The *Technical Regulations*, Volume II, Part II, Appendix 3, 4.2 and 4.3 contain the formal descriptions for international aviation.

At international aerodromes, visibility observations made for reports disseminated beyond the aerodrome should be representative of conditions pertaining to the aerodrome and its immediate vicinity. Visibility observations made for reports for landing and take-off and disseminated only within the aerodrome should be representative of the touchdown zone of the runway, remembering that this area may be several kilometres from the observing station.

For aeronautical purposes, the measurement range for visibility is from 25 m to 10 km. Values greater than or equal to 10 km are indicated as 10 km. A sensor must therefore be able to measure values above 10 km or indicate if the measurement is greater than or equal to 10 km. The operationally desirable measurement uncertainty is 50 m up to 600 m, 10% between 600 m and 1 500 m and 20% above 1 500 m (*Technical Regulations*, Volume II, Part II, Attachment A). See Volume I, Chapters 1 and 9, for advice on the accuracy of measurements.

In view of the meteorological minima governing the operational decisions on whether an aircraft can or cannot land or take-off, precise, reliable information must be given whenever visibility passes through certain limits, namely whenever visibility drops below or increases beyond the limit values of 800, 1 500 or 3 000 and 5 000 m, in the case, for example, of the beginning, cessation or change in fog or precipitation (*Technical Regulations*, Volume II, Part II, Appendix 3, 2.3.3 (b)).

When there are significant directional variations in visibility, particularly when they affect take-off and landing areas, this additional information should be given with indications of the direction of observation, for example, "VIS 2000 M TO S".

When visibility is less than 800 m it shall be expressed in steps of 50 m in the form VIS 350M; when it is 800 m or more but less than 5 km in steps of 100 m; when it is 5 km or more but less than 10 km, in kilometre steps in the form VIS 7KM; and when it is 10 km or more, it shall be given as 10 km, except when the conditions for the use of CAVOK ("ceiling and visibility OK") apply (*Technical Regulations*, Volume II, Part II, Appendix 3, 4.2.4.1).

The methods described in Volume I, Chapter 9, apply. Meteorological visibility observations are to be made by an observer who has "normal" vision, viewing selected targets of specified characteristics at known distances from the meteorological station. These observations may also be made by using visibility-measuring instruments, such as transmissometers and scatter coefficient meters. The location of the observing sites should be such as to permit continuous viewing of the aerodrome, including all runways.

If a transmissometer is used for visibility measurements, a baseline length of 75 m is suitable for aeronautical operations. However, if the instrument is also to be used for measuring RVR, the baseline length should be chosen after taking into account the operational categories in force at the aerodrome.

2.3.1 **Visibility for aeronautical purposes**

The *Technical Regulations*, Volume II, Part I, 1.1 defines visibility. VIS-AERO is the greater of:

- (a) The greatest distance at which a black object of suitable dimensions, situated near the ground, can be seen and recognized when observed against a bright background;
- (b) The greatest distance at which lights in the vicinity of 1 000 cd can be seen and identified against an unlit background.

This VIS-AERO is in fact a “visual range” like RVR, involving subjective elements such as the virtual performance of a human eye and artificial lights. Nevertheless, the word “visibility” is commonly used without the addition “for aeronautical purposes” and confusion may arise with the official definition of “visibility” as defined by WMO (see Volume I, Chapter 9 of the present Guide), MOR (see 2.3). An optical range is purely based on the physical state of the atmosphere and not on human or artificial elements, and is therefore an objective variable. This visibility (for aeronautical purposes) shall be reported, as in METAR. Because an aeronautical meteorological station may be combined with a synoptic station, visibility in SYNOP reports will differ from visibility in METAR, although it is measured by the same equipment.

Visibility for aeronautical purposes can be measured and calculated similarly to RVR (see 2.4 for details), except that for the intensity of the light source, I , a constant value of 1 000 cd shall be used. Note that this value holds for lights usually used for the assessment of visibility, which are 10 times more intense than lights of moderate intensity (that is, 100 cd, see Volume I, Chapter 9).

2.3.2 **Prevailing visibility**

Prevailing visibility is defined as the greatest visibility value, observed in accordance with the definition of “visibility (for aeronautical purposes)”, which is reached within at least half the horizon circle or within at least half of the surface of the aerodrome. These areas could comprise contiguous or non-contiguous sectors. This value may be assessed by human observation and/or instrumented systems, but when instruments are installed, they are used to obtain the best estimate of the prevailing visibility (*Technical Regulations*, Volume II, Part I, 1.1). Prevailing visibility should be reported in METAR and SPECI code forms.

2.4 **RUNWAY VISUAL RANGE**

2.4.1 **General**

RVR is the range over which the pilot of an aircraft on the centre line of a runway can see the runway surface markings or the lights delineating the runway or identifying its centre line. It is discussed in the *Technical Regulations*, Volume II, Part I, 4.6.3 and Part II, Appendix 3, 4.3. Details on observing and reporting RVR are given in ICAO (2005). It is recommended that this measurement be taken during periods when horizontal visibility is less than 1 500 m.

A height of approximately 5 m is regarded as corresponding to the average eye-level of a pilot in an aircraft on the centre line of a runway. Note that for wide-bodied aircraft, the pilot’s eye-level may be at least 10 m. In practice, RVR cannot be measured directly from the position of a pilot looking at the runway centre line, but must be an assessment of what he or she would see from this position. Nevertheless, RVR should be assessed at a height of approximately 2.5 m above the runway for instrumented systems or approximately 5 m above the runway by a human observer (*Technical Regulations*, Volume II, Part II, Appendix 3, 4.3.1.1).

The RVR should be reported to the ATS units whenever there is a change in RVR, according to the reporting scale. The transmission of such reports should normally be completed within 15 s of termination of the observation. These reports are to be given in plain language.

2.4.2 **Methods of observation**

The RVR may be measured indirectly, by observers with or without supplementary equipment, by instrumental equipment such as the transmissometer or sensors measuring scattered light, or by video systems. At aerodromes, where precision approaches and, in particular, where Category I, II, III A and III B operations are executed, RVR measurements should be made continuously by using appropriate instruments, namely transmissometers or forward-scatter meters (*Technical Regulations*, Volume II, Part II, Appendix 3, 4.3.2.1 for Category II and III, and recommended for Category I in Appendix 3, 4.3.2.2).

The RVR can then be assessed for operational purposes using tables or, preferably, by automatic equipment with digital read-out of RVR. It should be computed separately for each runway in accordance with the *Technical Regulations*, Volume II, Part II, Appendix 3, 4.3.5.

2.4.2.1 **Measurement by observers**

The counting of runway lights visible in fog (or lights specially installed parallel to the runway for that purpose) by observers can provide a simple and convenient method of determining RVR (but for precision instrument landing, only if the instrumented system fails). The difficulty arising with this method is related to the resolution capability of the human eye which, beyond a certain distance (dependent on the observer), does not permit the runway lights to be distinguished and counted.

Since the observer's position when observing runway lights is not identical to that of the pilot, the use of conversion curves to determine the true RVR is essential. Specially designed marker boards, spaced out along the side of the runway, may also be used for RVR assessment during the day.

2.4.2.2 **Measurement by video**

To assess RVR using a video system, use is made of a video camera and receiver to observe markers at known distances consisting of either runway lights, special lights, or markers positioned alongside the runway. Such a system is also beneficial for detecting patchy or shallow fog, which cannot be detected by the instruments.

2.4.2.3 **Measurement by transmissometer**

The instrument most commonly used at present for making an assessment of RVR is the transmissometer, which measures the transmission factor along a finite path through the atmosphere (see Volume I, Chapter 9). RVR can be determined as follows:

- (a) RVR when runway lights are dominant (RVR based on illumination threshold): The RVR depends on the transmission factor of the air, on the intensity of the runway lights and on the observer's (and pilot's) threshold of illuminance, which itself depends on the background luminance. It can be computed from:

$$E_t = I R^{-2} T^{R/a} \quad (2.1)$$

where E_t is the visual threshold of illuminance of the observer (pilot), which depends on the background luminance L ; I is the effective intensity of centre-line or edge lights towards the observer (pilot); T is the transmission factor, measured by the transmissometer; R is the RVR; and a is the transmissometer baseline or optical light path. Note that for the illuminance E of the observer (pilot), it holds that $E = I/R^2$. The requirements for the light intensity characteristics of runway lights are given in ICAO (2013). In fact, it holds for both centre-line and edge light that the illumination of the observer (pilot) is angular dependent and as a consequence I depends on R . Therefore $I = I(R)$ and $E = E(I, R)$. The calculation of

R from equation 2.1 can be done only iteratively, which is relatively easy with the help of a simple calculator suitable for numerical mathematics. The value of E_t is determined with the help of a background luminance sensor (see 2.4.3.3);

- (b) Assessment of RVR by contrast (RVR based on contrast threshold): When markers other than lights are used to give guidance to pilots during landing and take-off, the RVR should be based upon the contrast of specific targets against the background. A contrast threshold of 0.05 should be used as a basis for computations. The formula is:

$$R = a \frac{\ln 0.05}{\ln T} \tag{2.2}$$

where R is RVR by contrast. Because the contrast threshold level is 0.05, RVR by contrast is identical to MOR, namely $R = MOR$. Note that RVR (based on illumination threshold) will always supersede RVR (based on contrast threshold), or $RVR \geq MOR$.

2.4.2.4 Measurement by forward-scatter or backscatter meters

Instruments for measuring the forward-scatter or backscatter coefficient (sometimes known as scatterometers) are discussed in Volume I, Chapter 9. Because of the physical principles of light scattering by aerosols, the measurement uncertainty of a forward-scatter meter (scatter-angle approximately 31°–32°) is smaller than with backscatter meters. Therefore, a forward-scatter meter is to be preferred. With these instruments the extinction coefficient σ can be determined, which is the principal variable to calculate RVR. Experience and studies with forward-scatter meters have demonstrated their capability to measure RVR for aeronautical applications (WMO, 1990, 1992b).

Since accuracy can vary from one instrument design to another, performance characteristics should be checked before selecting an instrument for assessing RVR. Therefore, the calibration of a forward-scatter meter has to be traceable and verifiable to a transmissometer standard, the accuracy of which has been verified over the intended operational range (*Technical Regulations*, Volume II, Part II, Appendix 3, 4.3.2).

A scatter meter determines, from the received scattered light, the extinction coefficient σ of the atmosphere at the position of the optical volume (see Volume I, Chapter 9). Because σ is a direct measure for the visibility, R can be determined relatively easily (from σ or MOR, where $MOR = -\ln 0.05/\sigma \approx 3/MOR$). The RVR can be determined as follows:

- (a) RVR when runway lights are dominant (RVR based on illumination threshold): RVR will be calculated in a similar way as with a transmissometer except that σ is used and not T . It can be computed from:

$$R = \frac{1}{\sigma} \left(\frac{I(R)}{E_t \cdot R^2} \right) \tag{2.3}$$

where R is the RVR; σ is the extinction coefficient (or $3/MOR$); E_t is the visual threshold of illuminance of the observer (pilot), which depends on the background luminance; and I is the effective intensity of centre-line or edge lights towards the observer (pilot). As with a transmissometer, R should be calculated iteratively;

- (b) Assessment of RVR by contrast (RVR based on contrast threshold): When markers other than lights are used to give guidance to pilots during landing and take-off, the RVR should be based upon the contrast of specific targets against the background. A contrast threshold of 0.05 should be used as a basis for computations. The formula is:

$$R = -\ln 0.05 / \sigma = MOR \tag{2.4}$$

where R is RVR by contrast. Note that RVR (based on illumination threshold) will always exceed RVR (based on contrast threshold), namely $RVR \geq MOR$.

2.4.3 Instruments and exposure

Instrumented systems may be based on transmissometers or forward-scatter meters to assess RVR. RVR observations should be carried out at a lateral distance of not more than 120 m from the runway centre line. The site for observations that are representative of the touchdown zone should be located approximately 300 m along the runway from the threshold. The sites for observations that are representative of the middle and far sections of the runway should be located at a distance of 1 000 to 1 500 m along the runway from the threshold and at a distance of approximately 300 m from the other end of the runway (*Technical Regulations, Volume II, Part II, Appendix 3, 4.3.1.2*). The exact position of these sites and, if necessary, additional sites (for long runways), should be determined after considering aeronautical, meteorological and climatological factors, such as swamps and other fog-prone areas. RVR should be observed at a height of approximately 2.5 m above the runway for instrumented systems or approximately 5 m above the runway by a human observer (*Technical Regulations, Volume II, Part II, Appendix 3, 4.3.1.1*).

The units providing air traffic and aeronautical information services for an aerodrome should be informed without delay of changes in the serviceability status of the RVR observing system.

A computer is usually used to compute the RVR at several measurement points and to display the measurements on-screen with the time of observation, the transmission factors, the luminance measured at one or more points on the aerodrome and the runway light intensity. The data are sent to display panels at the ATS and meteorological and other units concerned, or to printers for recording.

The runway light intensity should be entered automatically in the computer in accordance with the procedure described in the *Technical Regulations, Volume II, Part II, Appendix 3, 4.3.5* or as formally agreed upon between the ATS units and the local meteorological unit.

Analogue or digital graphic recorders (with time base) for transmission factors T and background luminance L may also be used. A graphic display of the RVR should also properly show the record of E_v and I (see equation 2.1).

2.4.3.1 Transmissometers

A description of transmissometers, their installation on site and their maintenance and sources of error is given in Volume I, Chapter 9 of the present Guide, with references to other literature.

A transmissometer system consists of a projector that directs a light of known intensity onto a photoelectric receiving device placed at a known distance from the projector. The variations in atmospheric transmission, due to fog or haze, and so on, are continuously measured and recorded. The instrument is calibrated to be direct-reading, giving the transmission factor in per cent.

The transmitter and receiver must be mounted at the same height on rigid, secure and durable stands, which, if possible, are not frangible and in such a way that shifting soil, frost, differential heating of towers, and so forth, do not adversely affect the alignment of the two units. The height of the optical path should not be less than 2.5 m above the level of the runway.

In one type of transmissometer, the transmitter and receiver are incorporated in the same unit (see Volume I, Chapter 9). In this case, a reflector (for example, mirror) is installed at the normal receiver location. The light travels out and is reflected back, with the baseline length being twice the distance between the transmitter/receiver and the reflector. The transmissometer may have a single or double base, depending on whether one or two receivers or retro-reflectors, positioned at different distances, are used.

The transmissometer baseline length, namely, the length of the optical path covered by the light beam between transmitter and receiver, determines the RVR measurement range. For an RVR between 50 and 1 500 m, the most commonly used baseline lengths are between 15 and 75 m.

However, for shorter transmissometer baseline lengths, a higher transmission factor measurement accuracy and better system linearity are necessary. If low RVRs must be measured for Category II and III landing requirements, a short base transmissometer should be selected. However, the maximum RVR that can be measured is then relatively low. A compromise must be found. Double-base transmissometers exist, offering a wider measurement range by the selection of one base or the other, but care must be taken when switching baselines to ensure that the RVR measurements remain consistent with each other.

Higher RVR values can be measured by using longer transmissometer baseline lengths, but greater luminous power is needed for transmission to compensate for light attenuation between the transmitter and receiver in dense fog, and a narrower reception angle is required to avoid scatter disturbance phenomena. The measurement of the weakest signals is also dependent on background noise in the measuring equipment.

Transmissometers are generally aligned parallel to the runway. However, direct (or reflected) sunlight should be avoided as this may cause damage. The optical axis should, therefore, be positioned in an approximate north-south direction horizontally (for latitudes below 50°). Otherwise, a system of baffles should be used.

2.4.3.2 **Forward-scatter meters**

Forward-scatter meters should be sited near the runway in a similar fashion to transmissometers. The positioning of forward-scatter meters requires fewer precautions than for transmissometers. Nevertheless, care should be taken to avoid direct or scattered sunlight which might influence (or damage) the receiver. In particular, sunlight may influence the receiver after scattering by snow cover, or lake or sea surface. Modern instruments compensate for contamination of the optical components.

2.4.3.3 **Background luminance sensor**

The threshold of illuminance E_t must be known when computing the RVR. A background luminance sensor should be placed at the end of the runway along which one or more transmissometers or scatter meters have been installed. One or more luminance sensors may be installed at the airport depending on the number of runways covered.

The background luminance sensor measures the luminance of the horizon or sky in the direction opposite the sun. The illuminance thresholds are introduced in the RVR computation either as a continuous or a step function (two to four steps). The curve for converting background luminance to illumination threshold is given in the *Technical Regulations, Volume II, Part II, Attachment D*, and in ICAO (2005). The recommended relation used for this curve is:

$$\log_{10} E_t = 0.05(\log_{10} L)^2 + 0.573 \log_{10} L - 6.667 \quad (2.5)$$

where L is the luminance of the horizon sky.

The background luminance sensor consists of a photodiode placed at the focal point of a lens with an angular aperture of approximately 10° to 20°, aligned in a north-south direction (to avoid direct sunlight) and at an angle of elevation of approximately 30° to 45° to the horizon.

2.4.4 **Instrument checks**

It is essential that regular periodic checks be made on all components of the transmissometer – or scatter meter – RVR system to ensure the proper operation and calibration of the system. In general, the literature provided by the companies manufacturing and developing such equipment will give detailed instructions for making such checks and will indicate the corrective action to be taken when specified instrumental tolerances are not met. For a transmissometer, when the visibility exceeds 10 to 15 km, it is simple to check that the equipment indicates a transmissivity of approximately 100% (see Volume I, Chapter 9 of the present Guide). For scatter

meters, "scatter plates" may be used, which emulate certain extinction values. However, the calibration of a forward-scatter meter should be traceable and verifiable to a transmissometer standard (see 2.4.2.4).

Correct maintenance and calibration are necessary in order to:

- (a) Prevent dirt from accumulating, on optical surfaces;
- (b) Check variations in the light intensity of the transmitter;
- (c) Avoid drift after calibration;
- (d) Check the alignment of transmitters and receivers.

Frequent maintenance is necessary at heavily polluted sites. Care is to be taken so that not all equipment is taken out of service at the same time during maintenance, and so that this interruption of service is not of long duration, particularly during periods when fog is forecast.

When fog persists for several consecutive days, the projector should be checked to ensure that its light intensity is steady and the equipment should be checked for drift. Checking optical settings is difficult, if not impossible, in very dense fog; it is therefore vital that instruments should be mechanically reliable and optically stable.

2.4.5 **Data display**

The RVR data display for the units concerned is updated according to the local agreements in force: every 15 to 60 s, and even every 2 min on some occasions. Changes in RVR should normally be transmitted within 15 s after termination of the observation.

2.4.6 **Accuracy and reliability of runway visual range measurements**

If scattered light sensors are used, as distinct from transmissometers, the equations for RVR are acceptable in the case of fine water droplets as fog, but not when visibility is reduced by other hydrometeors such as freezing fog, rain, snow or lithometeors (sandstorms). In which case, MOR and RVR measurements must be used with much caution since satisfactory relations for such cases have not yet been accepted.

Divergence between the RVR for a pilot and the measured value may reach 15% to 20%, with an assumed standard deviation of not more than 10%. In the case of observers, there are divergences in visual threshold and in observing conditions that, together, can cause differences in reported visual range amounting to 15% or 20%.

RVR measurements taken using transmissometers or scatter coefficient meters are representative of only a small volume of the atmosphere. In view of the considerable fluctuations of fog density in time, as well as in space, a mean value established over a large number of samples or measurements is essential. Rapid changes in RVR may give rise to difficulties for the ATS units when transmitting the information to aircraft. For these reasons, an averaging period of between 30 s and 1 min is recommended, computed as a mean or a sliding mean.

Operationally desirable accuracies of RVR measurement or observation are specified in the *Technical Regulations*, Volume II, Part II, Attachment A.

2.5 **PRESENT WEATHER**

The observation and reporting of present weather is discussed in Volume I, Chapter 14 of the present Guide, and the procedures are described in the *Technical Regulations*, Volume II, Part I,

4.6.4 with details in Part II, Appendix 3, 4.4. For aviation, emphasis is placed upon observing and reporting the onset, cessation, intensity and location of phenomena of significance to the safe operation of aircraft, for example, thunderstorms, freezing precipitation and elements that restrict flight visibility.

For take-off and landing, present weather information should be representative, as far as practicable, of the take-off and climb-out area, or the approach and landing area. For information disseminated beyond the aerodrome, the observations of present weather should be representative of the aerodrome and its immediate vicinity.

Most observations relating to present weather are made by visual means. Care should be taken to select observing sites that afford adequate views in all directions from the station. Instruments may be used to support the human observations, especially for measuring the intensity of precipitation.

Detectors used to identify the type of precipitation (rain, snow, drizzle, and the like) or visibility-reducing phenomena other than precipitation (fog, mist, smoke, dust, and the like) can assist the human observer and this can help if done by automation. They are based essentially on the measurement of the extinction coefficient or scintillation, and may also make use of relations between weather phenomena and other quantities, such as humidity. At present, there is no international agreement on the algorithms used for processing data to identify these phenomena. There is no vital need for this equipment in aeronautical meteorology while human observers are required to be present.

Descriptions of phenomena reported in present weather appear in Volume I, Chapter 14, as well as in WMO (1992*a*, 2011, 2017) and ICAO (2011).

Specifications for special reports regarding present weather are contained in the *Technical Regulations*, Volume II, Part II, Appendix 3, 4.4.2. The abbreviations and code figures used in METAR or SPECI plain language reports appear in the *Technical Regulations*, Volume II, Part II, Appendix 3, 4.4.2.3–4.4.2.9.

2.6 CLOUD

2.6.1 General

Observations and measurements of clouds are discussed in Volume I, Chapter 15 of the present Guide. For aviation applications (see the *Technical Regulations*, Volume II, Part I, 4.6.5 and Part II, Appendix 3, 4.5), cloud information (amount, base height, type) is required to be representative of the aerodrome and its immediate vicinity and, in reports for landing, of the approach area. Where cloud information is supplied to aircraft landing on precision approach runways, it should be representative of conditions at the instrument landing system middle marker site, or, at aerodromes where a middle marker beacon is not used, at a distance of 900 to 1 200 m from the landing threshold at the approach end of the runway (*Technical Regulations*, Volume II, Part II, Appendix 3, 4.5.1).

If the sky is obscured or not visible, the cloud-base height is replaced by a vertical visibility in the local routine (MET REPORT) and local special (SPECIAL) reports (*Technical Regulations*, Volume II, Part I, 4.5.1(i)) and in weather reports METAR and SPECI (WMO, 2011, FM 15/FM 16, paragraph 15.9). Vertical visibility is defined as the maximum distance at which an observer can see and identify an object on the same vertical as himself or herself, above or below. Vertical visibility can be derived from the optical extinction profile, determined by a LIDAR-based ceilometer. Assuming that the total extinction σ at altitude h can be derived from the backscatter

extinction coefficient σ_B at that altitude after appropriate calibration for the whole altitude range, and assuming that a contrast threshold of 5% is applicable similar to MOR, it should hold for the vertical visibility VV that:

$$\int_0^{VV} \sigma(h) \cdot dh = \ln \left(\frac{I(VV)}{I_0} \right) = \ln(0.05) = 3 \quad (2.6)$$

Because LIDAR-based ceilometers determine the local extinction coefficient for fixed intervals Δh , VV may be derived relatively easily from:

$$\sum_{i=1}^N \sigma_i \cdot \Delta h = 3, \text{ with } h_N = VV \quad (2.7)$$

Typical code words like CAVOK, SKC (sky clear), NCD (no clouds detected) and NSC (nil significant clouds) are used in reports when the state of the atmospheric or weather will not affect the operations of take-off and landing; replacing the quantitative information with simple acronyms is beneficial. Details on the use of these practices are given in the *Technical Regulations*, Volume II, Part II, Appendix 3, 2.2 and 4.5.4.3. For instance, CAVOK shall be used when cloud and present weather is better than the prescribed values or conditions, but if the specified conditions are met. Great care should be taken when using these abbreviations with automated measuring systems, which are not capable of measuring clouds or vertical visibility within the stated requirements.

The height of clouds bases shall be reported above aerodrome elevation. However, when a precision approach runway is in use which has a threshold elevation of 15 m or more below the aerodrome elevation, local arrangements shall be made in order that the height of the clouds reported to arriving aircraft shall refer to the threshold elevation.

2.6.2 Observation methods

The principal methods used for determining the height of the cloud base are:

- (a) Cloud-base searchlight;
- (b) Rotating-beam ceilometer;
- (c) Laser ceilometer;
- (d) Ceiling balloon;
- (e) Visual estimation;
- (f) Aircraft reports.

Cloud-base height should be obtained by measurement whenever possible. At busy or international aerodromes with precision approach systems, cloud-base measurements should be taken automatically so that this information and any changes can be available on a continuous basis.

The ceiling-balloon method is too slow and too prone to errors to be a routine method for measuring cloud-base height at aerodromes, and the visual method is also too prone to error, especially at night, to be used where the observations are critical. Aircraft reports of cloud-base height can provide the observer with useful supplementary information. Care should be taken when interpreting pilots' information due to the fact that the information may be several kilometres from the surface observation point.

2.6.3 Accuracy of cloud-base height measurements

The ragged, diffuse and fluctuating nature of many cloud bases limit the degree of accuracy with which cloud-base heights can be measured. Isolated or infrequent measurements, such as those obtainable by the use of cloud-base height balloons, may be unrepresentative of the cloud conditions as a whole. The best estimate requires the study of a quasi-continuous recording over a period of several minutes provided by one of the instruments mentioned above.

The accuracy of instrumental measurements indicated by manufacturers is usually obtained by using solid or artificial targets. Operational accuracy is, however, more difficult to achieve in view of the fuzzy nature of the cloud base.

2.7 AIR TEMPERATURE

A general discussion of instruments and methods of observation for air temperature may be found in Volume I, Chapter 2 of the present Guide. For air navigation purposes (see the *Technical Regulations*, Volume II, Part I, 4.1 and 4.5.1(j)), it is necessary to know the air temperature over the runway. Normally, data from well-sited, properly ventilated screens give sufficient approximations of the required values. Rapid fluctuations in air temperature (2 °C to 3 °C per half-hour) should be notified immediately to ATS units, principally in tropical and subtropical areas.

Temperature sensors should be exposed in such a way that they are not affected by moving or parked aircraft, and should yield values that are representative of general conditions over the runways. Thermometers with a time constant of 20 s should preferably be used to avoid excessively small fluctuations in temperature (average wind speed of 5 m s⁻¹), or, in cases of automatic measurements, an appropriate digital averaging or resistance/capacitance filtering should be applied. Remote indicating and recording systems are an advantage. Moreover, aerodromes with runways intended for Category II and III instrument approach and landing operations, require automated measuring equipment and displays at the automatic retrieval system site. Temperature measurements have become more integrated into automatic stations or data-acquisition systems, and are displayed in digital form. The displayed temperature should represent an average value over 1 to 10 min, obtained after linearization of the sensor output signal. The value obtained should be rounded off to the nearest whole degree for aeronautical use.

2.8 DEWPOINT

Atmospheric moisture at aeronautical stations is usually expressed in terms of the dewpoint temperature. The reading is rounded off to the nearest whole degree as in the case of air temperature. The procedures are described in the *Technical Regulations*, Volume II, Part I, 4.1 and 4.5.1(j). Observation methods are described in Volume I, Chapter 4 of the present Guide.

Modern humidity sensors allow the use of remote indicators and recorders. For manual observations the psychrometer is commonly used. A psychrometer of the ventilated type is to be preferred to meet the stated measurement uncertainty. The types of instruments commonly in use are as follows:

- (a) Capacitive sensors based on the measurement of a capacitor's capacitance, in which the value of the polymer dielectric varies as a function of the water vapour content of the ambient air. In practice, the measured capacitance is fairly linear with relative humidity. Dewpoint is calculated using the ambient air temperature (measured separately and at a very short distance) ($t_d = t_d(t, U)$). The appropriate formulae are given in Volume I, Chapter 4, Annex 4.B. To avoid condensation, which may last long after $U < 100\%$ and which might be trapped by the filter protecting the sensor, the sensor may be heated. For such a practice, the ambient air temperature should not be used, rather a temperature

value should be used that represents the heated air around the sensor. In practice, the appropriate procedure can only be achieved after careful calibration in well-designed climate chambers;

- (b) Dewpoint hygrometers, measuring the temperature at which a very light deposit of dew occurs on a mirror. The mirror is heated or cooled, most frequently by the Peltier effect, to obtain the point of equilibrium at which dew is deposited. The mirror is used with an associated photo-electronic dew-detection system. Although such systems deliver dewpoint temperature directly, pollution and deterioration of the mirror may cause significant biases. In particular, frost may destroy the mirror. At least every six months the mirror should be inspected, but only by skilled personnel. Great care should be taken when cleaning the mirror and the manufacturer's instructions should be followed precisely.

2.9 ATMOSPHERIC PRESSURE

2.9.1 General

A general discussion on the observations of atmospheric pressure may be found in Volume I, Chapter 3, and that for aviation purposes is found in the *Technical Regulations*, Volume II, Part I, 4.6.7. Pressure measurements for setting aircraft altimeters are essential at an aeronautical station. They are computed in tenths of hectopascals (0.1 hPa). They are referred to in the Q code as QFE and QNH, where:

- (a) QFE (field elevation pressure) is defined as the pressure value at an elevation corresponding to the official elevation of the aerodrome (*Technical Regulations*, Volume II, Part II, Appendix 3, 4.7.2). Aerodrome reference point, elevation and runway elevation are described in ICAO (2013);
- (b) QNH (atmospheric pressure at nautical height) is defined as the pressure value at which an aircraft altimeter is set so that it will indicate the official elevation of the aerodrome when the aircraft is on the ground at that location. QNH is calculated using the value for QFE and the pressure altitude relationship of the ICAO standard atmosphere. In fact, the ICAO standard atmosphere is a sub-range of the International Standard Atmosphere, which is documented by the ISO standard 2533 (ISO, 1975) and developed in liaison with the Committee on Space Research, ICAO and WMO. This standard atmosphere is a static atmosphere, with a fixed pressure and temperature at sea level and a fixed temperature gradient. Details of the standard atmosphere and its predefined constants are given in WMO (1966) and ICAO (1993). For the calculation of QNH from QFE, namely the reduction to mean sea level, this virtual atmosphere is used, and not the current true state of the atmosphere. As a consequence, QNH will differ from the reported atmospheric pressure reduced to sea level as described in Volume I, Chapter 3, 3.7 of the present Guide and for which the actual temperature is used. The calculation of QNH from QFE is based on a slide rule relationship (for stations below about 3 000 to 4 000 m):

$$QNH = A + B \times QFE \quad (2.8)$$

where *A* and *B* depend on the geopotential altitude of the station (for details, see WMO, 1966, Introduction to Table 3.10). To derive QNH, the following three-step procedure should be followed:

- (i) Determine the pressure altitude of the station from the QFE (the pressure altitude is calculated from QFE using the formulae of the standard atmosphere);
- (ii) Subtract (or add for stations below mean sea level) from this pressure altitude the elevation of the station with respect to mean sea level to give the pressure altitude at mean sea level (may be positive or negative);
- (iii) Derive from this pressure altitude the associated pressure value according to the standard atmosphere, which will be QNH.

An example of this procedure to derive QNH from QFE is shown in the figure below. The measured pressure and QNH and/or QFE values should be computed in tenths of a hectopascal. In local reports and reports disseminated beyond the aerodrome, QNH and QFE values should be included and the values should be rounded down to the nearest whole hectopascal. The ATS units, should be notified of rapid major changes in pressure.

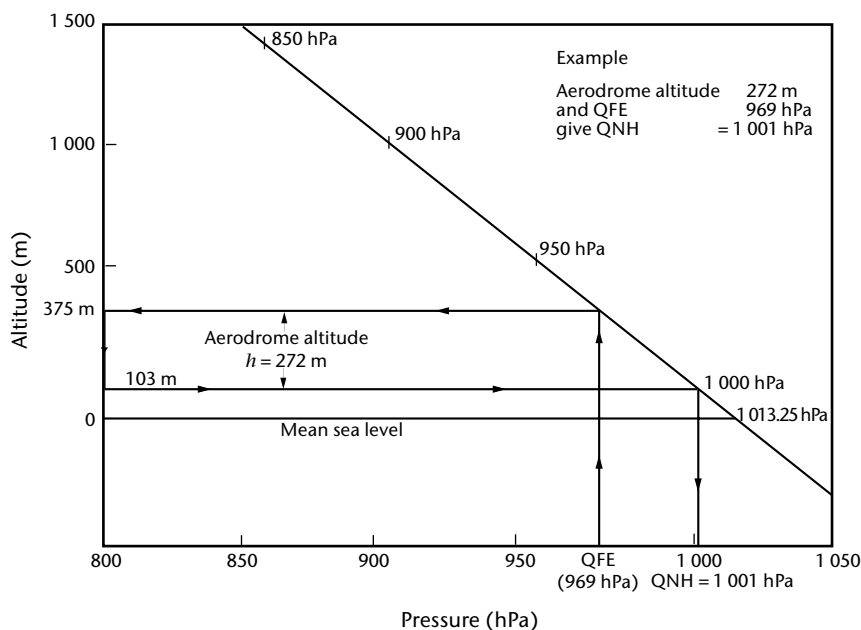
The curve represents the standard atmosphere (pressure altitude as a function of pressure).

2.9.2 Instruments and exposure

The instrumental equipment used at an aeronautical station for pressure measurement is identical to that at a synoptic station, except that greater use is often made of precision automatic digital barometers for convenience and speed of reading in routine observations. Aeronautical stations should be equipped with one or more well-calibrated barometers traceable to a standard reference. A regular schedule should be maintained for comparing the instruments against this standard instrument. Both manual and automated barometers are suitable, provided that temperature dependence, drift and hysteresis are sufficiently compensated. Details of suitable barometers are given in Volume I, Chapter 3 of the present Guide.

The exposure of barometers at an aeronautical station is the same as at a synoptic station. If barometers have to be exposed inside a building, sensors should be vented to the outside, using an appropriately located static-tube arrangement. Owing to wind impacts on a building, pressure differences inside and outside the building may be larger than 1 hPa. To prevent such bias, which may extend to about plus or minus 3 hPa with high wind speeds, the static-tube should be placed sufficiently far away from this building. Also, air conditioning may have impacts on pressure measurements, which will be avoided by using such a static tube.

Direct-reading instruments for obtaining QNH values are available and may be used in place of the ordinary aneroid or mercury barometer, which require reference to tables in order to obtain the QNH values. For such devices, correct values of A and B , which are a function of the station geopotential altitude (see equation 2.8), shall be entered. The readings given by these instruments must be compared periodically with QNH values calculated on the basis of measurements obtained using the mercury barometer.



The relation between QFE and QNH

2.9.3 **Accuracy of and corrections to pressure measurements**

Pressure values used for setting aircraft altimeters should have a measurement uncertainty to 0.5 hPa or better (*Technical Regulations*, Volume II, Part II, Attachment A). All applicable corrections should be applied to mercury barometer readings, and corrections established through regular comparisons between the mercury and aneroid instruments routinely used in observations must be applied to all values obtained from the latter instruments. Where aneroid altimeters are used in ATS tower positions, corrections different from those used in the observing station must be provided, for proper reduction to official aerodrome or runway level (*Technical Regulations*, Volume II, Part II, Appendix 3, 4.7).

The pressure values used for setting altimeters must refer to the official elevation for the aerodrome. For non-precision approach runways, the thresholds of which are 2 m or more below or above the aerodrome elevation, and for precision approach runways, the QFE, if required, should refer to the relevant threshold elevation.

2.10 **OTHER SIGNIFICANT INFORMATION AT AERODROMES**

2.10.1 **General**

Observations made at aeronautical stations should also include any available information on meteorological conditions in the approach and climb-out areas relating to the location of cumulonimbus or thunderstorms, moderate or severe turbulence, horizontal and/or vertical wind shear and significant variations in the wind along the flight path, hail, severe line squalls, moderate or severe icing, freezing precipitation, marked mountain waves, sandstorms, duststorms, blowing snow or funnel clouds (tornadoes or waterspouts), for example, SURFACE WIND 320/10 WIND AT 60M 360/25 IN APCH or MOD TURB AND ICE INC IN CLIMB OUT.

2.10.2 **Slant visual range**

Despite the development work carried out in various countries, no instrument for measuring the slant visual range has been made operational. The rapid technological development of all-weather landing systems has made it possible to reduce the set landing minima at aerodromes (Categories II, III A and III B) and has gradually resulted in this parameter being considered less important. No recommendation has been established for measuring this parameter.

2.10.3 **Wind shear**

Wind shear is a spatial change in wind speed and/or direction (including updraughts and downdraughts). Wind shear intensity may be classified into light, moderate, strong or violent according to its effect on aircraft. Low-level wind shear, that may affect landing and take-off operations, may exist as a vertical wind gradient in the lower layers of a thermally stable atmosphere, or it may be due to the effect of obstacles and frontal surfaces on wind flow, the effect of land and sea breezes, and to wind conditions in and around convection clouds, particularly storm clouds. Violent storms are by far the major cause of low-level wind shear, and a cause of fatal accidents for aircraft both on approach and landing, and during take-off.

The preparation and issuing of wind-shear warnings for climb-out and approach paths are described in the *Technical Regulations*, Volume II, Part II, Appendix 3, 4.8.1.4.

The measurement of vertical wind shear based on the information presented in Volume I, Chapter 5, may be determined directly by anemometers on tall masts, which must be at a certain distance from the airport. Remote-sensing systems include Doppler Radar, Lidar, Sodar and the wind profiler. The Lidar uses laser light, the Sodar is based on acoustic radiation, and the wind profiler radar employs electromagnetic radiation at a frequency of approximately 50 MHz, 400 MHz or 1 000 MHz.

Horizontal wind shear is usually detected by a system of anemometers over the entire aerodrome. This system is designated as a low-level wind shear alert system. Computer-processed algorithms enable a wind-shear warning to be given. This system is used particularly in tropical and subtropical regions where frequent, intense storm build-up occurs.

Global coverage of this subject is given in the *ICAO Manual on Low-level Wind Shear* (Doc. 9817), first edition, 2005.

Although wind shear may have a significant impact on aircraft operations, no recommendation or criteria has yet been established. Nevertheless, details on wind-shear warnings are given in ICAO (2011), Chapter 4.

2.10.4 **Marked temperature inversions**

Information on marked temperature inversions exceeding 10 °C between the surface and levels up to 300 m should be provided, if available. Data are usually obtained from balloon-borne radiosondes, remote-sensing, aircraft observations (for example, the WMO aircraft meteorological data relay (AMDAR) observing system) or by meteorological inference.

2.11 **AUTOMATED METEOROLOGICAL OBSERVING SYSTEMS**

Specially-designed instrument systems have become common practice at aeronautical stations for measuring, processing, remotely indicating and recording values of the various meteorological parameters representative of the approach, landing, take-off and general runway conditions at the airport (*Technical Regulations*, Volume II, Part I, 4.1).

These automated systems comprise the following:

- (a) An acquisition system for converting electrical analogue measurements (volts, milliamperes, resistance, capacitance) to digital values in the appropriate units, and for the direct introduction of digital data;
- (b) A data pre-processing unit (averaging of readings over a time period of 1 to 10 min depending on the parameter measured and minimum, maximum and average values for the various parameters);
- (c) A computer, used, for example, to prepare SYNOP, METAR and SPECI reports, and telecommunication software.

The observer should be able to include in these reports those parameters which are not measured by the automatic station; these may include present weather, past weather, cloud (type and amount) and, sometimes, visibility. For aviation purposes, these stations are, therefore, often only an aid for acquiring meteorological data and cannot operate without observers.

Instruments at the automatic station should be checked and inspected regularly. Quality checks are necessary and recommended in order to avoid major errors and equipment drift. Measurements taken by AWSs are dealt with in detail in the present volume, Chapter 1. Quality assurance and other management issues can be found in Volume V, Chapter 1. To guarantee the stated performance of the automated instruments, a detailed evaluation plan should be established with details on maintenance and calibration intervals, and with feedback procedures to improve the observing system.

Recommendations on reporting meteorological information from automatic observing systems are given in the *Technical Regulations*, Volume II, Part II, Appendix 3, 4.

2.12 **RADAR**

At aerodromes with heavy traffic, weather radars have become indispensable since they provide effective, permanent, real-time surveillance by producing additional observations to the usual meteorological observations for landings and take-offs. A radar can provide information over a wider area of up to 150 to 200 km. It is also an aid to short-range forecasting – within the hour or a few hours following the observation (possible aid in preparing the TREND report).

The echoes received are interpreted to identify the type of precipitation around the station: precipitation from stratus or convective clouds; isolated or line precipitation; or precipitation due to storms and, under certain conditions, detection of precipitation in the form of snow or hail. The image received enables the paths of squall lines or fronts to be followed and their development (intensification or weakening) to be monitored. If the radar is equipped with a Doppler system, the speed and direction of movement of these echoes can be computed.

The most widely used radars operate on wavelengths of 3, 5 or 10 cm. The choice depends on the region of the globe and the intended purpose, but the present general trend is towards the use of a 5 cm wavelength.

In certain regions, centralizing centres collect radar images from a series of radar stations in the country or region and assemble a composite image. Images are also exchanged between the various centres so that radar protection is provided over the largest possible area.

A general discussion on radar observations may be found in the present volume, Chapter 7.

2.13 **ICE SENSOR**

This type of instrument, described in Volume I, Chapter 14 of the present Guide, is installed at a number of aerodromes to provide information on runway conditions in winter. The temperature at the surface and a few centimetres below the runway, the presence of snow, water, clear ice or white ice and the presence of salts or de-icing products, if any, are measured or detected. These sensors, in the form of a compact unit, are placed at a certain number of points on the runways or taxiways with their number depending on the size of the aerodrome and the number of runways to be protected. Atmospheric sensors are also placed close to the runways for the measurement of air temperature and humidity, wind and precipitation.

A data-acquisition and data-processing system displays the parameters measured and their variations with time. Depending on the type of software used, warning systems alert the airport authority responsible for aerodrome operations to the presence of clear ice or forecasts of dangerous conditions for aircraft.

2.14 **LIGHTNING DETECTION**

Systems for locating thunderstorms based on the detection of the low-frequency electromagnetic radiation from lightning have been developed in recent years (see the present volume, Chapter 6). These systems measure the time taken for the signal to arrive and/or the direction from which it comes. Also, some systems analyse the characteristics of each radio impulse to identify cloud-to-ground lightning strokes. In certain regions, a number of these units are installed to measure and locate these phenomena in an area of 50 to 100 km around the aerodrome.

2.15 **OTHER RELEVANT OBSERVATIONS**

Additional information should be provided if the atmosphere is affected by dangerous pollution, for example, during volcanic eruptions. Information should also be provided to support rescue operations, especially at off-shore stations. If relevant for aircraft operations during take-off and landing, information on the state of the runway should be reported in METAR and SPECI, provided by the appropriate airport authority.

Volcanic ash should be reported (in SIGMET reports) as part of the supplementary information (*Technical Regulations, Volume II, Part II, Appendix 3, 4.8*). Details on observing volcanic ash, radioactive material and toxic chemical clouds are given in ICAO (2004, 2007).

In METAR and SPECI, information on sea-surface temperature and the state of the sea or the significant wave height should be included from aeronautical meteorological stations established on offshore structures in support of helicopter operations (*Technical Regulations, Volume II, Part II, Appendix 3, 4.8.1.5*).

REFERENCES AND FURTHER READING

- Committee on Low-Altitude Wind Shear and its Hazard to Aviation, 1983: *Low-Altitude Wind Shear and Its Hazard to Aviation*. National Academy Press, Washington, D.C. (available from <https://nap.nationalacademies.org/catalog/558/low-altitude-wind-shear-and-its-hazard-to-aviation>).
- International Civil Aviation Organization (ICAO), 1993: *Manual of the ICAO Standard Atmosphere: extended to 80 kilometres (262 500 feet)*. Third edition, Doc. 7488, Montreal.
- , 1996: *Manual on the Provision of Meteorological Service for International Helicopter Operations*. Doc. 9680, Montreal.
- , 2004: *Handbook on the International Airways Volcano Watch (IAVW)*. Second edition, Doc. 9766, Montreal.
- , 2005: *Manual of Runway Visual Range Observing and Reporting Practices*. Third edition, Doc. 9328, Montreal.
- , 2007: *Manual on Volcanic Ash, Radioactive Material and Toxic Chemical Clouds*. Second edition, Doc. 9691, Montreal.
- , 2010: *Units of Measurement to be Used in Air and Ground Operations*. ICAO Annex 5, Fifth edition, Montreal.
- , 2011: *Manual of Aeronautical Meteorological Practice*. Ninth edition, Doc. 8896, Montreal.
- , 2013: *Aerodromes*. ICAO Annex 14, Volume I, Sixth edition, Montreal.
- International Organization for Standardization, 1975: *Standard Atmosphere*. ISO-2355:1975. Geneva.
- World Meteorological Organization, 1966: *International Meteorological Tables* (S. Letestu, ed.) (1973 amendment). (WMO-No. 188, TP 94). Geneva.
- , 1990: *The First WMO Intercomparison of Visibility Measurements: Final Report (United Kingdom 1988/1989)* (D.J. Griggs, D.W. Jones, M. Ouldrige and W.R. Sparks). Instruments and Observing Methods Report No. 41 (WMO/TD-No. 401). Geneva.
- , 1992a: *International Meteorological Vocabulary* (WMO-No. 182). Geneva.
- , 1992b: *Visibility measuring instruments: Differences between scatterometers and transmissometers* (J.P. van der Meulen). Papers Presented at the WMO Technical Conference on Instruments and Methods of Observation (TECO-92). Instruments and Observing Methods Report No. 49 (WMO/TD-No. 462). Geneva.
- , 2003: *Guide to Practices for Meteorological Offices Serving Aviation* (WMO-No. 732). Geneva.
- , 2011: *Manual on Codes* (WMO-No. 306), Volume I.1. Geneva.
- , 2012: *Manual on the Implementation of Education and Training Standards in Meteorology and Hydrology* (WMO-No. 1083), Volume I. Geneva.
- , 2014: *Guide to Meteorological Observing and Information Distribution Systems for Aviation Weather Services* (WMO-No. 731). Geneva.
- , 2015 (Updated in 2018): *Technical Regulations* (WMO-No. 49), Volume I. Geneva.
- , 2016: *Technical Regulations* (WMO-No. 49), Volume II. Geneva.
- , 2017: *International Cloud Atlas - Manual on the Observation of Clouds and Other Meteors* (WMO-No. 407). Geneva.
-

CHAPTER 3. AIRCRAFT-BASED OBSERVATIONS

3.1 GENERAL

3.1.1 Definitions

This chapter describes the methods used for automatic meteorological measurements on modern commercial aircraft, known collectively as aircraft-based observations. The principles described here may be used for data processing on any adequately instrumented aircraft to define and develop aircraft-based observing systems.

The WMO AMDAR observing system is an aircraft-based observing system that is described in WMO (2017) so as to meet meteorological requirements for reporting meteorological data from an aircraft platform. The AMDAR system is operated by WMO Members in collaborative agreement with their partner airlines, and the resulting data are transmitted on WIS. Additional information is available in WMO (2017).

AMDAR and other aircraft-based observing systems are generally implemented on aircraft that are equipped with sophisticated navigation and other sensing systems. There are sensors for measuring airspeed, air temperature and air pressure. Other data relating to aircraft position, time of observation, acceleration and orientation are available from the aircraft navigation system. The aircraft also carry airborne computers for the flight management and navigation systems, by which navigation and meteorological data are computed continuously and are made available to the aircrew on the flight deck. In traditional aircraft-based observing systems, these data are further processed and fed automatically to the aircraft communication system for transmission to the ground, or, alternatively, a dedicated processing package can be used on the aircraft to access raw data from the aircraft systems and derive the meteorological variables independently.

In AMDAR systems, these facilities are used to compile and transmit meteorological reports in real time. Normally, the messages contain wind speed and direction (in the horizontal plane), air temperature, pressure altitude (altitude in the Standard Atmosphere related to a reference pressure level), time of observation, phase of flight and the aircraft position. If the aircraft is properly equipped, it may also report humidity or water vapour mixing ratio and a measure of turbulence.

The source data for meteorological observations require significant correction and complex processing to yield meteorological measurements that are representative of the free air-stream in the aircraft vicinity. A full description of all the processes involved is beyond the scope of the present Guide, but an outline of the principles is given here, with references for further reading.

3.1.2 Aircraft meteorological sensors

The basic sensors carried on modern commercial aircraft comprise the pitot-static probe and the total air temperature (TAT) probe. Data from these sensors, together with information from the aircraft navigation system, usually provided by one or a combination of radio navaid systems

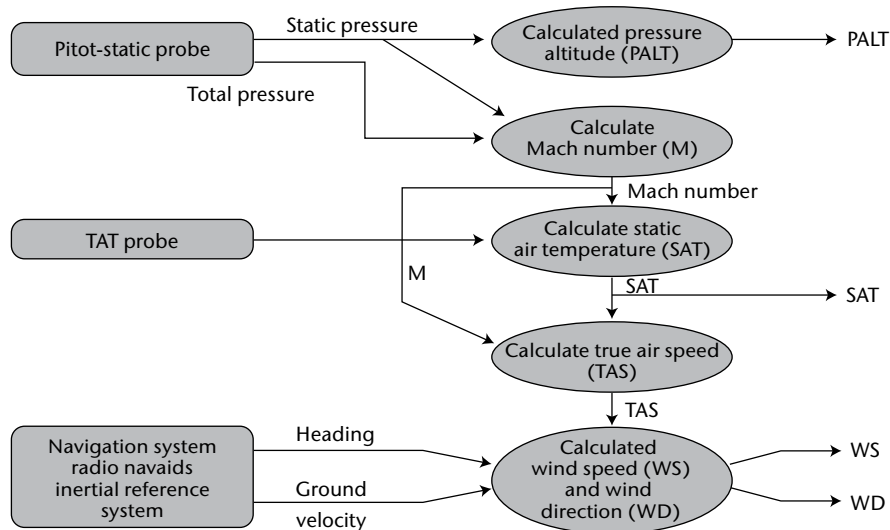


Figure 3.1. AMDAR sensor data processing

(GPS), distance-measuring equipment, very-high frequency (VHF) omni-directional radio range (VOR), an instrument landing system and in some cases an inertial navigation system, are processed to give the following meteorological elements:

- Pressure altitude H_p ¹ horizontal position and time (PALT in Figure 3.1);
- Static air temperature T_s (SAT in Figure 3.1);
- Wind speed $|V|$;
- Wind direction D_w .

On some aircraft, additional processing for measuring turbulence is available or additional sensors are available for measuring ice build-up on the front surfaces and/or for measuring relative humidity or water vapour mixing ratio r .

In order to appreciate the complexity of the processing system, the following description is structured according to the process flow in a typical operational system. It will be noted (Figure 3.1) that the computed variables are highly interdependent.

3.2 PRESSURE AND MACH NUMBER

3.2.1 Pitot-static probe

The pitot-static probe (Figure 3.2) is exposed in the free air-stream beyond the aircraft boundary layer and provides the total pressure (static pressure plus impact or dynamic pressure). Some of these probes can provide static pressure as well (that is, free air-stream pressure, ideally the undisturbed ambient pressure), but on most airliners normally in use for AMDAR, the static pressure is provided via orifices on the side of the aircraft body. The pressure values are measured by electronic transducers and passed to a central unit hosting the algorithms for the

¹ Pressure altitude is defined as a measure of height relative to the standard datum plane of 1 013.2 hPa. The variable flight level (FL) equals the pressure altitude for all levels. Pressure altitude and flight level may not be interchanged with indicated aircraft altitude, aircraft altitude, or aircraft height, for which other definitions apply. Because aircraft may fly at pressure levels above 1 013.2 hPa (that is, below the standard datum plane), pressure altitude (or flight level) may be negative.

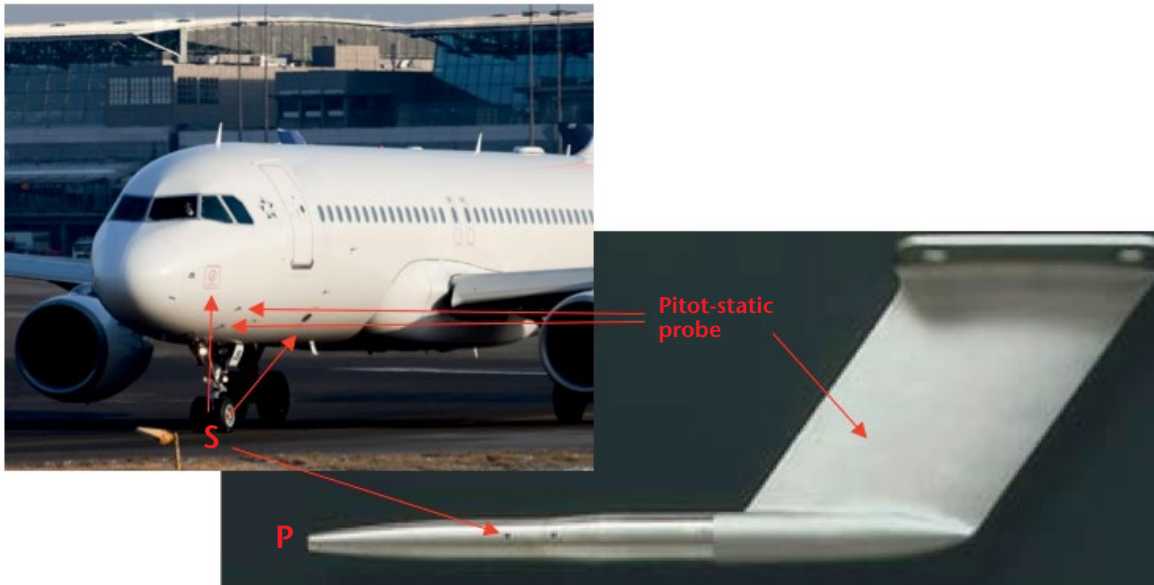


Figure 3.2. Typical configuration for the measurement of static pressure and pitot pressure on aircraft. Static pressure is taken (see the mark “S”) either at ports on both sides of the fuselage or at side ports of the pitot-static probe. Total pressure is taken at the forward-headed orifice of the pitot probes or the pitot-static probes (see the mark “P”) mounted on the fuselage a few metres behind the nose.

aerodynamic adjustments (correction for the built-in error) and finally to the air data computer (ADC). The ADC computes pressure altitude, static temperature and Mach number from these two measurements.

3.2.2 Pressure altitude

The static pressure measurement is not normally reported in AMDAR but is converted in the ADC to the equivalent altitude based on the International Standard Atmosphere (ISO, 2007). The Standard Atmosphere (see Figure 3.3) assumes a linear decrease in temperature with height of $6.5\text{ }^{\circ}\text{C}$ per km up to 11 km (36 089 ft),² and a mean sea-level temperature and pressure of $15\text{ }^{\circ}\text{C}$ and 1 013.25 hPa, respectively. From 11 km (36 089 ft) to 20 km (66 000 ft) the temperature is assumed constant at $-56.5\text{ }^{\circ}\text{C}$.

For pressure altitude H_p equal to or less than 11 km (36 089 ft), static pressure (p_s) is related to H_p by the following expression:

$$p_s = 1\,013.25 \cdot \left(1 - 6.8756 \cdot 10^{-6} \cdot H_p\right)^{5.2559} \quad (3.1)$$

with H_p in units of ft and p_s in units of hPa. For example, if H_p is 9 144 m (30 000 ft), $p_s = 300.9$ hPa.

The above expression (3.1) can be used to calculate the static pressure from the reported pressure altitude, provided that the on-board static pressure value was corrected only for aerodynamically-induced effects (built-in error) and the aircraft altimeter sub-scale (zero-reference) was set to ICAO standard mean sea-level pressure (1 013.25 hPa). Navigational procedures also provide for altimeter sub-scale settings at other reference levels. For example, the setting can be aerodrome pressure (field elevation pressure, QFE) or QNH (QFE value reduced to sea level by use of the Standard Atmosphere), which is a pressure reference on the

² It is general policy to use SI units. However, values for feet are also given for altitude in this chapter, respecting common practice in the aviation community. The SI base unit of length is the metre (m). One metre corresponds to 3.280 839 895 013 1 feet. Note that rounding errors may occur, so always check the results.

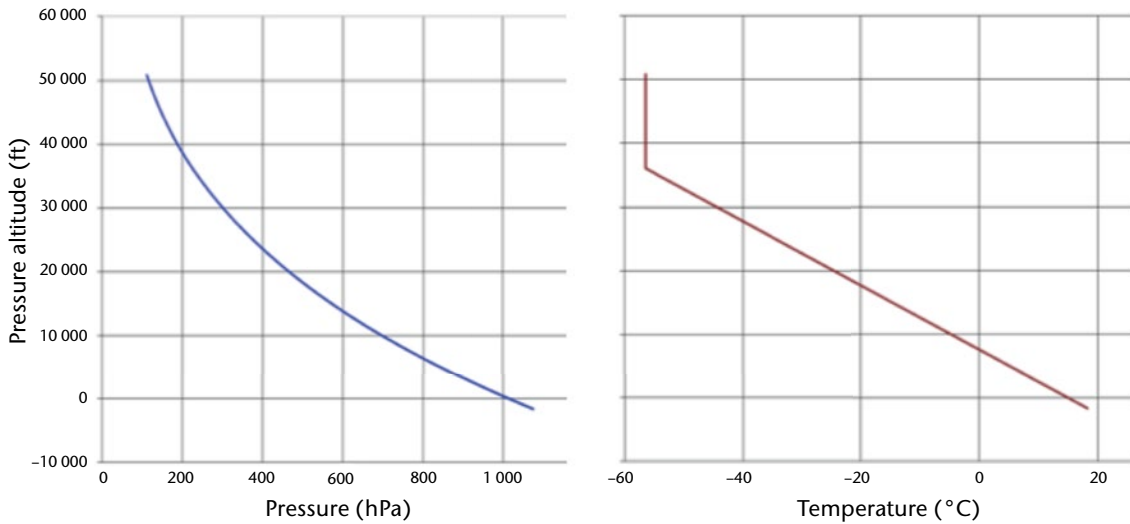


Figure 3.3. International Standard Atmosphere

standard atmosphere scale such that aerodrome height is indicated at touchdown on a specific airfield. The pressure altitude reported by the AMDAR on-board software should always be with respect to ICAO mean sea-level pressure only.

For use in the cockpit, the indicated altitude H_i (the pressure altitude above mean sea level (MSL)) is given by the pressure altitude (H_p) minus the altitude of the altimeter sub-scale reference on the standard atmosphere scale (H_r) plus the elevation of the reference pressure level above MSL (E_{Ref}). The general expression is:

$$H_i = H_p - H_r + E_{Ref} \quad (3.2)$$

$$H_r = \left[1 - \left(\frac{P_r}{1013.25} \right)^{0.19026} \right] \cdot 145442 \quad (3.3)$$

with H_r , H_i , and E_{Ref} in units of ft, and p_r in units of hPa; p_r is the altimeter sub-scale setting, such as:

QNH, then $E_{Ref} = 0$ m (0 ft) above MSL

or

QFE, then $E_{Ref} =$ field elevation above MSL

Note that $H_r = 0$ if $p_r = 1013.25$ hPa.

For example:

- (a) If the sub-scale setting is a QNH value of 1000.0 hPa and the indicated altitude is 2845 m (9335 ft), $H_p = 2845$ m + 110 m (9335 ft + 365 ft) = 2955 m (9699 ft) and $p_s = 705$ hPa;
- (b) If the sub-scale setting is a QFE value of 990 hPa, the aerodrome height is 84 m (276 ft) and the indicated altitude is 2761 m (9058 ft), $H_p = H_i + H_r$ (QFE) - $E_{Ref} = 2761$ m + 194 m - 84 m (9058 ft + 641 ft - 276 ft) = 2871 m (9423 ft) and the QNH value would be 1000 hPa.

However, for the purpose of AMDAR, the altitude parameter should be chosen which is solely based on the aerodynamically clean static pressure without any reference to QNH or QFE.

If H_p is greater than 11 km (36 089 ft), static pressure is given by:

$$p_s = 226.32 \cdot e^{\frac{36\,089 - H_p}{20\,806}}$$

or

$$H_p = 36\,089 - 20\,806 \cdot \ln\left(\frac{p_s}{226.32}\right)$$
(3.4)

with H_p in units of ft, and p_s in units of hPa. For example, if H_p is 40 000 ft, $p_s = 187.5$ hPa.

3.2.2.1 **Measurement uncertainty**

Sources of uncertainty include:

- (a) Calibration uncertainty;
- (b) Short-term random instrument error;
- (c) Calibration drift;
- (d) Exposure uncertainty or static source uncertainty (built-in).

Because aircraft safety separations are critical, these uncertainties are corrected for as much as possible in the ADC. Static source uncertainty, which is a function of probe location, Mach number and aircraft weight, is determined empirically during flight-testing. Uncertainty of pressure is inferred from reported heights.

A possible source of data latency with the AMDAR system is in the radio link between aircraft and ground. This link process is regulated by international standards, such as ARINC 620, AOSFRS (AMDAR Onboard Software Functional Requirements Specification) or AAA, which stands for ACMS (Aircraft Condition Monitoring System) Aircraft Communications Addressing and Reporting System (ACARS) AMDAR. In earlier versions of these standards, the pressure altitudes were reported in hundreds of feet, equivalent at cruise level to some 1.5 hPa. This represents roughly 0.1% of the full scale pressure measurement. With instrumental accuracy at best of the order of 1 hPa, the uncertainty in static pressure at cruise level derived from converting pressure altitude is approximately 2 hPa. At zero reference level, the resolution is equivalent to approximately 3.7 hPa, leading to an uncertainty of some 4 hPa. In recent versions of the AMDAR on-board software, the altitude is reported in tens of feet, in which case the uncertainty due to coding-related error is lower than the remainder of the measurement uncertainty. AMDAR-equipped aircraft meet the rules and requirements of reduced vertical separation minima as laid down by the approved authorities within air traffic management (ATM). The aircraft are required to maintain an altitude uncertainty of 50 m (160 ft), even in the altitude range of 9 144 m (30 000 ft) to 12 192 m (40 000 ft). Hence, the pressure uncertainty has to be within the range of ± 1.5 hPa and the quality control system of the airline must maintain this level of accuracy.

3.2.3 **Mach number**

Mach number (M , the true airspeed divided by the speed of sound in the free air) is an important element for aircraft operations. In AMDAR systems, it is used to correct air-temperature measurements and airspeed measurements. In dry air, the speed of sound is proportional to the square root of absolute (static) temperature T_s . Mach number only depends on two parameters:

- (a) The impact pressure q_c measured by the aircraft's pitot tubes; and
- (b) The static pressure p_s measured at specific locations on the side of the aircraft fuselage:

$$M^2 = \frac{2}{\kappa - 1} \left[\left(\frac{q_c + p_s}{p_s} \right)^{\frac{\kappa - 1}{\kappa}} - 1 \right]$$
(3.5)

where $q_c + p_s$ is the total pressure, and κ is the ratio of specific heats of dry air (C_p/C_v).

For further details, see the standard texts on aircraft aerodynamics such as Abbott and von Doenhoff (1959) and Dommasch et al. (1958).

3.2.3.1 **Measurement uncertainty**

The measurement uncertainty is determined almost entirely by the uncertainty of the fundamental measurements of pressure. In normal operation, the derived Mach number uncertainty should be lower than 0.2%.

3.3 **AIR TEMPERATURE**

3.3.1 **Total air temperature probe**

The TAT probe is exposed in the free air-stream and used to derive static (free air-stream) temperature. The accurate measurement of air temperature is fundamental to the other derived meteorological elements. For example, it is used in the calculation of true airspeed and thus has an impact on the calculation of the wind velocity components. The ADC corrects the temperature actually measured by the probe using the computed Mach number.

Most commercial aircraft are equipped with TAT probes of the immersion thermometer type. Figure 3.4 shows a typical example. The sensing element is a resistance thermometer. The housing is designed to divert cloud and precipitation hydrometeors from the sensing element, although it has been reported (Lawson and Cooper, 1990) that the sensing element becomes wet in cumulus clouds. However, the main reason for the aerodynamic particle separation is to protect the element against abrasive impacts.

The thermodynamically important part of the housing's design is to achieve, for the sampled air, a nearly complete adiabatic conversion of its kinetic energy into internal energy. The airspeed has

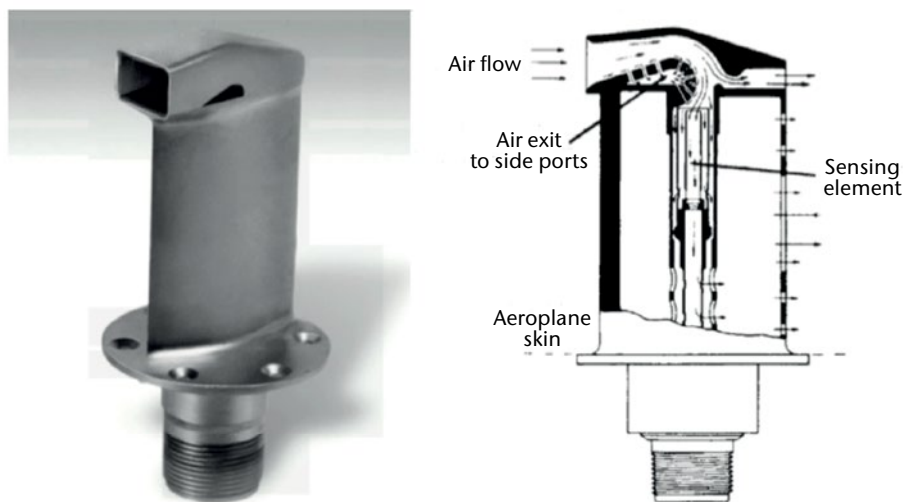


Figure 3.4. Typical example of an aircraft temperature sensor: a TAT probe (see Stickney et al., 1990). The internal aerodynamics is designed to make the flow stagnate before touching the sensor. The associated internal boundary layer is kept small enough and away from the sensor element to enable a pure adiabatic process. The flow's curvature serves for particle separation.

to be reduced to a leftover of a few m s^{-1} at the sensor. At this location, the air-stream getting in contact with the sensitive element must have been kept free of heat exchange with the internal walls. That is why all the different kinds of TAT housings are equipped/ designed with holes in the walls around the intake flow. These holes produce an aerodynamic sucking effect to curb the internal boundary layer. As a result, the heat exchange with the wall is kept sufficiently small to maintain accuracy of the measurements. Even if the housing's intake edge is heated for de-icing, the associated increase of the measured temperature is below 0.5 K at $M > 0.3$.

The temperature (T_r) measured by the probe is close to the theoretical value of T_t that would occur with perfect adiabatic compression of the free air-stream at an aerodynamically ideal stagnation point. The static air temperature T_s , which is the temperature of the free air-stream, is related to the measured temperature T_r by the expression (with T as absolute temperature):

$$\frac{T_r}{T_s} = 1 + \lambda \cdot \frac{\kappa - 1}{2} \cdot M^2 \quad (3.6)$$

where λ is the probe recovery factor. Modern TAT probes show typical values of the probe recovery factor around 0.98 for Mach numbers between 0.5 and 0.9. It primarily includes the effect of incomplete stagnation of air and, secondarily, that of a small frictional heat transfer to the flow to be sampled. The value of this coefficient is slightly smaller than 1. It depends on the housing's design but also on the Mach number. At cruise level at Mach 0.85, the probe temperature exceeds the ambient temperature by more than 30 K.

Further details about TAT probes can be found in Stickney et al. (1990).

3.3.1.1 **Measurement uncertainty**

The static temperature is a function of probe temperature and Mach number. As shown above, the Mach number is derived from total pressure and static pressure, themselves independent measurements from the pitot-static head. The uncertainty of measurement is therefore a function of three error sources in addition to calibration uncertainties and other effects (for example, probe de-icing).

The temperature uncertainty is approximately 0.4 K at Mach 0.8, reducing to 0.3 K at low Mach numbers. In the first version of the on-board software standard ARINC 620, the temperature had a resolution of 1 K. Since 1994, it has been specified to be coded in 0.1 K. If the sensor is wetted in cloud, it will be cooled by evaporation leading to additional uncertainties up to 3.0 K or so. At very low airspeed (for example prior to take-off) there may be insufficient airflow over the sensor to maintain the accuracy of measurement. Some aircraft employ aspirated sensors to overcome this problem. Normally the on-board software should be configured so that a data transfer does not begin before take-off. Despite the complexity of the data processing involved, operational experience suggests that mean temperature uncertainty at cruise height is approximately 1.0 K.

3.4 **WIND SPEED AND DIRECTION**

The measurement of the three-dimensional wind vector uses data from the aircraft navigation system (the complete combination or a subset of a radio navaid, inertial platform, magnetic compass and GPS system) and the airspeed system (ADC using pitot-static system plus TAT probe). Using these data, it is possible to calculate to a high degree of accuracy the velocity (v_g) of the aircraft, the ground speed with respect to the Earth and the aircraft velocity with respect to the air (v_a , true airspeed). The wind vector (v), therefore, is given by the vector triangle:

$$\vec{v} = \vec{v}_g - \vec{v}_a \quad (3.7)$$

The vectors \vec{v}_g and \vec{v}_a must be measured accurately since typical horizontal winds are small (some 10 m s^{-1}) compared with aircraft ground speed and true airspeed (200 to 300 m s^{-1}). In early AMDAR systems during long-range navigation the ground speed was derived solely from inertial navigation systems without any support of ground-based nav aids or GPS. Sometimes this may have reduced the accuracy of the ground-speed vector and the wind vector by some m s^{-1} .

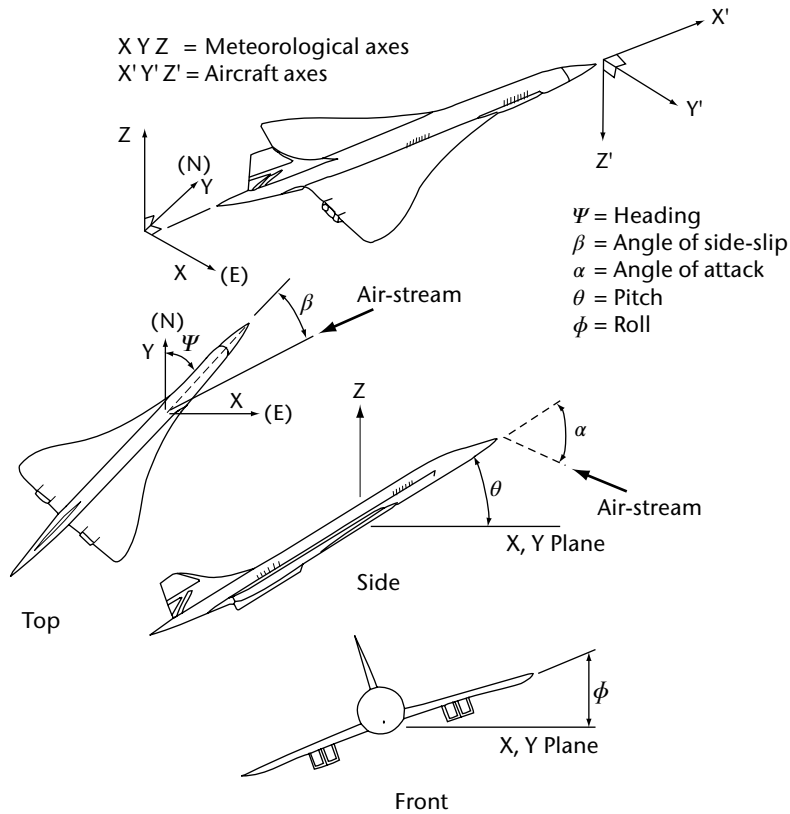


Figure 3.5. Angles between aircraft and the Earth's coordinate system as well as the air-stream

This has been improved with modern multi-sensor navigation systems in order to produce operational quality data (Meteorological Service of Canada, 2003). However, the three-dimensional solution of the vector (equation 3.7) needs the measurements of aircraft pitch, roll and yaw as well as the angle of attack and side-slip (Figure 3.5). In normal level flight, pitch and roll angle are very small and can be neglected. In the on-board system of a commercial aircraft, the wind vector triangle is only calculated in the X-Y plane of the Earth coordinate system and the angles of attack and side-slip are not measured.

The input data requirement reduces to true airspeed, heading and ground velocity. Heading and ground velocity are taken from the navigation system. True airspeed must be calculated from the Mach number and T_s . The components of the horizontal wind (u , v) are:

$$u = u_g - |\bar{v}_a| \sin \psi \quad (3.8)$$

$$v = v_g - |\bar{v}_a| \cos \psi \quad (3.9)$$

where $|\bar{v}_a|$ is the magnitude of the true airspeed; ψ is the heading relative to true north, positive clockwise; and u_g and v_g are the components of the ground speed.

3.4.1 Measurement uncertainty

True airspeed is a function of the Mach number and T_s (SAT in Figure 3.1):

$$|\bar{v}_a| = 38.867 \cdot M \cdot \sqrt{T_s} \quad (3.10)$$

$$|\bar{v}_a| = 38.867 \cdot M \cdot \sqrt{\frac{T_r}{1 + 0.194 \cdot M^2}} \quad (3.11)$$

Since uncertainties exist in both Mach number and T_s , the total uncertainty of the true airspeed's magnitude is given by:

$$\Delta|\bar{v}_a| = 38.867 \cdot \Delta M \cdot \sqrt{T_s} + \frac{19.433 \cdot M \cdot \Delta T_s}{\sqrt{T_s}} \quad (3.12)$$

with $|\bar{v}_a|$ in units of kt; T_s , T_r in units of K; ΔM is the uncertainty of the Mach number; and ΔT_s is the uncertainty of the static temperature.

Note from equation 3.5 that Mach uncertainty depends on the uncertainty of the pressure measurements. Unless gross temperature errors exist, the Mach number uncertainty can be the most significant. For example, with a Mach number uncertainty of 0.2% at cruise level, airspeed uncertainty is some 0.5 m s^{-1} (1 kt). Thus, with zero uncertainty from the navigation system, wind vector uncertainty of up to 0.5 m s^{-1} is to be expected. Note, however, that gross temperature errors will lead to gross wind errors.

Uncertainty in true airspeed combines with uncertainty from the inertial reference unit. The basic calculations assume perfect alignment of the aircraft with the air-stream (no angle of side-slip) and zero roll and perfect inertial platform alignment. At high roll angles, wind vector uncertainty, which is proportional to true airspeed, can be significant. Roll angles of 10 to 20 degrees imply that the actual angle of attack makes an angular deviation of the true airspeed by a couple of m s^{-1} . So, wind data are usually excluded or at least flagged when the roll angle is above a threshold (typically 3 to 5 degrees). At low wind speeds, vector uncertainty can lead to large errors in wind direction. Thus, a more useful indication, considering all of the above uncertainty sources and combining wind speed and direction uncertainty as vector uncertainty, would suggest a typical uncertainty of 2–3 m s^{-1} (4–6 kt). These estimates are in line with operational experience (see, for example, Nash (1994)).

3.5 HUMIDITY

Various sensor principles for the measurement of humidity are in use on research and operational commercial aircraft. The range of technologies covers capacitive-absorption, chilled mirrors and optical methods based on absorption or scattering. The instrument most widely used within AMDAR operations is one based on a tunable diode laser (May, 1998; Fleming, 2000, 2003) – the Water Vapor Sensing System (WVSS-II). The tunable diode laser absorption spectroscopy technology was originally designed by NASA's Jet Propulsion Laboratory for use on deep space missions, because it provides high accuracy and extreme stability of measurement over many years. WVSS-II is designed specifically for commercial aviation use in support of AMDAR, using a special relative narrowband absorption method at a suitable infrared line of the water vapour. The intensity of radiation at the detector is related to the emitted radiation by Beer's law such that:

$$I = I_0 \cdot e^{-k x \rho_w} \quad (3.13)$$

where I is the received signal; I_0 is the emitted signal; k is the mass attenuation coefficient; x is the path length; and ρ_w is the absolute humidity (density of water vapour) in the sensing volume. I_0 , k and x are known properties of the system. A local pressure and temperature measurement enables the system to take account of the density of dry air ρ_d . The absorption is scanned over a narrowband of wavelengths around the H_2O line at $1.37 \mu\text{m}$. The absolute humidity in the sampling volume is derived by use of the 2f method (May and Webster, 1993). The system's firmware finally converts the raw 2f signal together with coincident temperature and pressure measurements to the proper output parameter, the water vapour mass mixing ratio, m :

$$m = \frac{\rho_w}{\rho_d} \quad (3.14)$$

The sensor system is small enough for a manageable integration on commercial aircraft. Except for cases when phase transitions occur, m is conserved during the pressure and temperature

shift from outside into the sensor probe.³ The generated value of the mixing ratio is suitable for reporting without knowledge of local pressure and temperature values. This is also convenient in numerical atmospheric models using specific humidity, s (numerically almost indistinguishable from m) as the input variable. It has a simple relationship to the mass mixing ratio:

$$s = \frac{m}{1+m} \quad (3.15)$$

In instances when aircraft are flying through cloud particles or precipitation, or in conditions of real super-saturation, the mixing ratio as the measured parameter of WVSS-II may lead to a relative humidity of greater than 100% or a dewpoint ($T_d T_d$) being reported higher than the static (dry) temperature. This phenomenon is caused by either:

- (a) Partial evaporation of liquid or solid water particles in the sample air flow;
- (b) Existing super-saturation caused by a lack of condensation or sublimation nuclei, typically within the ice super-saturation region layers where enduring contrails are formed.

3.5.1 Measurement uncertainty

Up to 2012, some climate chamber assessments as well as flight tests of this spectrometric humidity measurement system have revealed two features of the instrument's performance: at measurement values above the detection limit of approximately 4 mg m^{-3} , the relative uncertainty is in the range of $\pm 10\%$. At an altitude of 200 hPa, the corresponding detection limit in the mixing ratio is 0.02 g kg^{-1} (or 30 ppmv). Comparison of this aircraft-based method with contemporary radiosondes (see, for example, Petersen et al. (2011, 2016)), shows that the sensor appears to meet WMO observational requirements across all specific humidity and relative humidity ranges, during both ascent and descent.

3.6 TURBULENCE

Turbulence, especially clear-air turbulence (turbulence in the absence of clouds), is an important and potentially dangerous phenomenon in aviation. Although for routine commercial operations flight paths are designed to avoid turbulence inevitably, aircraft will experience unexpected bumpiness and the departure from normal level flight can be measured by the aircraft instrumentation.

3.6.1 Turbulence from vertical acceleration

Vertical acceleration (normal to the aircraft horizontal reference plane) is measured in the inertial reference unit. The data output is referenced and scaled to the acceleration due to gravity and may be categorized as shown in the table. However, the severity of turbulence affecting an aircraft depends principally on airspeed, the mass of the aircraft, the altitude and the nature of the turbulence itself. Hence, reports of turbulence from an aircraft derived from peak acceleration according to the crude relationships given in the table are of limited application and are aircraft-specific because a given gust will have different effects on different aircraft.

3.6.1.1 Measurement uncertainty

There are two main sources of uncertainty in the aircraft instrumentation, namely the "zero", or reference, uncertainty and the output calibration (measurement) uncertainty. For most aircraft,

³ It should be noted that any changes to m during phase transitions can persist for some undefinable period of time depending on air flow being experienced by the sensor. This phenomenon is included in current extensive research into high altitude ice crystals, which is a hazard to aviation, by major stakeholders in the aviation industry.

Example of coding for the scale of turbulence, defined by peak acceleration

<i>Turbulence category</i>	<i>Peak acceleration^a</i>	<i>Code</i>
None	Less than 0.15 <i>g</i>	0
Light	0.15 <i>g</i> to, but not including, 0.5 <i>g</i>	1
Moderate	0.5 <i>g</i> to 1.0 <i>g</i>	2
Severe	Greater than 1.0 <i>g</i>	3

^a These accelerations, which may be positive or negative, are departures from the normal acceleration of gravity (1.0 *g*).

the reference value is nominally +1.0 *g*, but this can vary typically by 3%. This uncertainty can be virtually eliminated by correction when the aircraft is on the ground, leaving a residual (including measurement) uncertainty of approximately 3% of measurement (Sherman, 1985).

3.6.2 Derived equivalent vertical gust velocity

An alternative indicator of turbulence is the derived equivalent vertical gust velocity (DEVG), defined as the instantaneous vertical gust velocity, which, superimposed on a steady horizontal wind, would produce the measured acceleration of the aircraft. The effect of a gust on an aircraft depends on the mass and other characteristics, but these can be taken into account so that a gust velocity can be calculated which is independent of the aircraft. The DEVG (Sherman, 1985) is given by:

$$U_{de} = \frac{Am\Delta n}{V_c} \quad (3.16)$$

where U_{de} is the derived equivalent gust velocity; Δn is the modulus of the peak deviation of the aircraft vertical acceleration from 1.0 *g* in units of *g*; m is the total mass; V_c is the calibrated airspeed at the time of the occurrence of the acceleration peak; and A is a parameter that depends on the aircraft type, and weakly on the mass, the altitude and the Mach number.

3.6.2.1 Measurement uncertainty

Uncertainties in each of the elements contributing to U_{de} have been estimated. These are typically less than 3% maximum for each element in normal level flight and in the extreme could lead to a total uncertainty of 10% to 12%. Assuming a random distribution of errors, a typical uncertainty would be 3% or 4% of the final value of U_{de} . Aircraft manoeuvres can also lead to large vertical accelerations of an aircraft, and, conversely, active control techniques can dampen the acceleration due to gusts, leading to serious underestimation of vertical gust velocities.

3.6.3 Eddy dissipation rate

The eddy dissipation rate (EDR), ϵ , is a parameter that quantifies the turbulence intensity within a fluid. In the context of aircraft turbulence, it is standard practice to refer to $\epsilon^{1/3}$ as EDR. The advantage of EDR is that it is an aircraft-independent measure of the atmospheric turbulence intensity. There are several ways of estimating EDR (accelerometer-based versus wind-based), and they can be estimated, in principle, along any direction (though usually either vertical or longitudinal (along-track) is used). There are also different spectral models of turbulence that can be used for any of the algorithms:

$$F_v(f) = \frac{9\pi}{55V_t} \alpha \epsilon^{2/3} L^{5/3} \frac{(1 + \frac{32}{3}\pi^2 L^2 f^2 / V_t^2)}{(1 + 4\pi^2 L^2 f^2 / V_t^2)^{11/6}} \quad (3.17)$$

Equation 3.17 is the von Karman spectral model, where f is the frequency (Hz), V_t is the aircraft true airspeed (m s^{-1}), α is an empirical constant (taken here to be 1.6), and L is a length-scale parameter of the turbulence.

$$F_k(f) = \frac{24\pi}{55V_t} \alpha \varepsilon^{2/3} (2\pi f / V_t)^{-5/3} \quad (3.18)$$

Equation 3.18 is the Kolmogorov spectral model, which is just the high-frequency limit of equation 3.17. Both models attempt to describe the frequency power spectrum shape of wind data. The von Karman model better represents the larger scales, especially of the vertical velocity, though it is more complicated and includes the situation-dependent length scale L , in addition to EDR (squared). Research aircraft measurements have shown values of L from between 300 and 2 000 m (985 and 6 560 ft). For most of the algorithm implementations to date, a mid-range value of 669 m (2 195 ft) is used.

3.6.3.1 **Vertical accelerometer-based EDR**

This method, described in Cornman et al. (1995), is based on the vertical-acceleration parameter available from the inertial navigation system. For this method, the following relation (Cornman et al., 1995, equation 21) is used:

$$\varepsilon_w^{1/3} = \frac{\hat{\sigma}_{\ddot{z}}}{\left[0.7V_t^{2/3} I(f_l, f_h)\right]^{1/2}} \quad (3.19)$$

where $\hat{\sigma}_{\ddot{z}}$ is the variance of the bandpass filtered vertical acceleration, I is the integral of the aircraft response bandpass filtered function H , and:

$$I(f_l, f_h) = \int_{f_l}^{f_h} |H_{\ddot{z}w}(f)|^2 \hat{S}_w(f) df \quad (3.20)$$

where \hat{S}_w is the assumed Kolmogorov spectral model with $\varepsilon = 1$. The von Karman model could be substituted for the Kolmogorov. In the current implementation, f_l (stopband cut-off) and f_h (passband cut-off) are set to 0.1 Hz and 0.8 Hz, respectively. The purpose of the bandpass filter is to remove accelerations that are due to aircraft manoeuvres and wing bending mode frequencies rather than turbulence.

The aircraft response integral is evaluated for a range of flight conditions and stored in look-up tables, thus simplifying and reducing the on-board computation requirement. The algorithm calculates the running root-mean-square of the filtered signal over ten-second windows. At an 8 Hz sampling rate, this provides 480 EDR estimates per minute, from which the median and ninetieth percentile (referred to as the “peak”) of these estimates are used for downlink. The EDR measurement results are converted into reporting numbers by use of tables which are far more detailed than that given in 3.6.1. More information on reporting of EDR is provided in *AMDAR Onboard Software Functional Requirements Specification* (WMO, 2013).

3.6.3.2 **Vertical wind-based EDR**

This technique is briefly outlined in Cornman et al. (2004). The main idea is to compute the vertical winds directly, and then estimate the EDR from those calculations. This method has the advantage of not requiring the aircraft response function, which is difficult to obtain due to its proprietary nature.

$$w = V_T (\sin \alpha_b \cos \theta \cos \varphi - \cos \alpha_b \sin \theta) - \dot{Z} \quad (3.21)$$

The above equation is used to compute the vertical winds, where α_b is the body-axis angle of attack, θ is the pitch angle, φ is the roll angle, and \dot{Z} is the inertial vertical velocity. EDR is computed by:

$$\hat{\varepsilon}^{1/3} = \left[\frac{1}{k_h - k_l + 1} \sum_{k=k_l}^{k_h} \frac{S^w(k)}{\hat{S}_w(k)} \right]^{1/2} \quad (3.22)$$

where k_l and k_h are index bounds corresponding to frequency bounds of 0.5 and 3.5 Hz (respectively) for the current 8 Hz implementations, S^w is the power spectrum of w (equation 3.21) after time-series processing, and \hat{S}_w is the assumed von Karman spectral model with $\varepsilon = 1$, modified to account for various signal processing artefacts in S^w .

Nominally, the algorithm calculates EDR ($\varepsilon^{1/3}$) over ten-second windows, every five seconds. This provides 12 EDR estimates per minute, from which the actual mean and peak of these estimates are used for downlink. The mean and peak EDRs, along with quality-control metrics, are converted into reporting numbers by use of encoding (see 5.3.13.5 in ARINC, 2012). The reported precision of both the mean and peak EDR is 0.02, significantly higher than in the accelerometer-based method.

3.6.3.3 **True airspeed-based EDR**

This technique is similar to the vertical wind-based EDR (see 3.6.3.2) except that the spectral models are slightly different and true airspeed is used in place of w . The advantage of this method is that it is simpler to implement, requiring only one parameter. The disadvantage is that it estimates EDR mainly in the direction along the track, which has much less impact on the aircraft than from turbulence in the vertical direction.

3.6.3.4 **Measurement uncertainty**

As for DEVG, a large number of sources potentially contribute to EDR measurement uncertainty. Based on the analysis for DEVG, in the accelerometer-based method an uncertainty of some 5% to 10% can be expected for the mean, and somewhat larger for the peak. Based on simulations, similar performance is expected from the other EDR algorithms. A further complication arises over the choices of sampling interval and averaging time. Examination of typical time series of vertical acceleration data often indicates high variability of statistical properties over short distances. Variation of airspeed for a single aircraft alters the sampling distances.

3.6.3.5 **Relationship between EDR and DEVG**

Detailed field comparisons (Stickland, 1998) have been made between the accelerometer-based EDR and DEVG. These have shown a high correlation between peak EDR and DEVG for the same turbulence incidents. This result should be expected since the accelerometer-based EDR is directly proportional to the standard deviation of vertical acceleration over the measurement interval chosen. Hence, for a “normal” distribution, the extreme value will correlate closely with the peak vertical gust (proportional to the peak deviation of vertical acceleration). Clearly, this relationship will not apply to a singular event falling outside the assumed distribution, and the EDR filter cut-off at 0.8 Hz might well unduly attenuate very sharp gust events. For the vertical wind- and true airspeed-based methods, little filtering is applied, and it is not significantly susceptible to this last issue.

3.7 **ICING**

Several types of sensors may detect ice build-up on the flying surfaces. The following two types are in use:

- (a) A thin-film capacitive sensor attached to the airfoil;
- (b) A mechanical (vibrating-transducer) sensor exposed to the air-stream in a probe adjacent to the relevant flying surface.

3.7.1 **Measurement uncertainty**

The output of both sensors is essentially an “ice/no ice” signal, and uncertainty would be described by false-alarm rate. At present, no data are available on false-alarm rates for these sensors.

3.8 **AIRCRAFT-BASED OBSERVING SYSTEMS**

There are a number of operational aircraft-based observing systems in current operation. AMDAR is currently the major source of aircraft-based observations on WIS; however, additional observations derived from other aircraft-based observing systems contribute significantly and are expected to provide increased data volumes in the future.

A number of AMDAR-like systems either have or are being developed which will improve global coverage and increase the number of observations in the boundary layer and lower troposphere. Some emphasis is being placed on recruiting smaller regional and general aviation aircraft to install either conventional AMDAR systems or dedicated sensor and communication systems. These aircraft operate from smaller airports that are not normally covered by existing AMDAR-reporting aircraft from airlines participating in national and regional AMDAR programmes.

3.8.1 **Aircraft meteorological data relay**

The AMDAR observing system should be operated according to WMO specification and standards (WMO, 2017). AMDAR is currently based and relies almost exclusively upon ACARS. AMDAR systems report data in profile (ascent/descent) mode as well as during level flight at cruise altitude.

For additional information on the regulatory requirements for establishment and operation of an AMDAR programme and the provision of other aircraft-based observations, consult the *Manual on the WMO Integrated Global Observing System*, (WMO, 2015).

Current information on operational AMDAR programmes and additional resource and guidance material can be found at the WMO AMDAR website <https://public.wmo.int/en/programmes/global-observing-system/amdar-observing-system>.

3.8.2 **Tropospheric Airborne Meteorological Data Reporting**

3.8.2.1 **Overview**

Tropospheric Airborne Meteorological Data Reporting (TAMDAR) is a commercially developed, deployed and operated system that derives meteorological data from the predominantly aircraft-independent sensing and communications probe. Unlike in the WMO AMDAR observing system, in the TAMDAR system emphasis has been placed on equipping primarily regional carriers, as these flights tend to (a) fly into more remote and diverse locations, and (b) be of shorter

duration, thereby producing more daily vertical profiles and remaining in the boundary layer for longer periods. Although TAMDAR is fully functional and regularly operates above 12 192 m (40 000 ft), the aircraft that typically host the sensor often cruise below 7 620 m (25 000 ft).

TAMDAR collects measurements of relative humidity (RH), pressure, temperature, winds, icing and turbulence, along with the corresponding location, time and geometric altitude from a built-in GPS. These data are relayed via satellite in real time to a ground-based network operations centre, where in-line quality control procedures are performed prior to distribution. The overall humidity and temperature data quality is similar to that of radiosondes (Gao et al., 2012). The wind observations are derived in a similar fashion as typical AMDAR winds, using aircraft heading, true airspeed, and the ground track vector, which is provided by the internal GPS unit.

The TAMDAR sensor samples on a pressure-based interval on ascent and descent, and a time-based interval in cruise, which also varies with altitude from 3 min at lower altitudes to 7 min at higher altitudes. At present, on ascent and descent, the sensor reports every 10 hPa; however, this can be adjusted remotely in real time down to 1 hPa, ~10 m (~30 ft) depending on the rate of ascent and descent. During cruise, if any icing is detected, the sensor will send a custom report, so flights through icing conditions will generate far more observations than in clear skies.

3.8.2.2 *Relative humidity and temperature*

TAMDAR uses two capacitive sensing devices⁴ for redundancy to measure RH. The fundamental physical parameter that the TAMDAR capacitive sensor technology responds to is the density of H₂O molecules. RH is a derived parameter, which takes into account temperature and pressure. A custom hydrophobic membrane filter has been added to the devices, which significantly increases the reliability and accuracy by preventing direct wetting of the sensor element (see Mulally and Braid, 2009).

The reported RH value is a “consensus” value between the two devices that is determined by an algorithm in the ground processing system described in Anderson (2006). The system considers the value and quality of each sensor output. Typically, if both sensors are reporting similar values, the consensus value is simply the average of the two. If the sensors disagree by more than 5%, and one is determined to be faulty using methods described in Anderson (2006) and Gao et al. (2012), then the errant sensor's value is flagged and not used in the mean RH calculation.

Certain corrections must be applied to the actual RH that the sensor is reporting. The primary corrections are because of the Mach heating and the difference in air pressure between the ambient conditions and the conditions observed by the sensor. The RH for a parcel of air with a given water vapour concentration is a function of both temperature and pressure. There are four major factors that contribute to the uncertainty of the measurement of true RH as is done in TAMDAR:

- (a) The measurement uncertainty of the RH sensor itself (ΔRH);
- (b) The uncertainty of the TAMDAR probe temperature (T_{probe}) measurement – via a platinum resistance temperature device;
- (c) The measurement uncertainty of the calculated static air temperature (T_{static});
- (d) The measurement uncertainty of the ratio of the static pressure (P_{static}) to the RH sensor pressure (P_{probe}).

⁴ The current commercial version of TAMDAR has two devices whereas the new production prototype has three. As of March 2018, the prototype is only implemented in the Unmanned Ariel System (UAS) version of TAMDAR and not yet available on the commercial aircraft version.

The basic calculation necessary for static RH is described by:

$$\text{RH}_{\text{static}} = \text{RH}_{\text{probe}} \left(\frac{P_{\text{static}}}{P_{\text{probe}}} \right) \cdot \left(\frac{e_{s,\text{probe}}(T_{\text{probe}})}{e_{s,\text{static}}(T_{\text{static}})} \right) \quad (3.23)$$

where $\text{RH}_{\text{static}}$ is the atmospheric RH, RH_{probe} is the actual RH measurement from the RH sensor in the TAMDAR probe, P_{static} is the static air pressure, P_{probe} is the air pressure at the RH sensor in the probe, T_{probe} is the temperature in the probe sensing cavity, T_{static} is the static air temperature, $e_{s,\text{probe}}$ is the probe saturation vapour pressure relative to water, and $e_{s,\text{static}}$ is the static saturation vapour pressure relative to water. The saturation pressure ratio is strictly a function of T_{probe} and T_{static} as shown above. The calculation for the pressure ratio ($P_{\text{static}}/P_{\text{probe}}$) has been derived from data from extensive wind tunnel testing (see Braid et al., 2011; Smith et al., 2012).

The relationship between T_{probe} (essentially the recovered temperature) and T_{static} is:

$$T_{\text{probe}} = T_{\text{static}}(1 + \lambda \cdot M^2) \quad (3.24)$$

where M is the Mach number and λ is a constant approximately equal to 0.17. The actual RH sensor measurement is the true value plus a sensor uncertainty, ΔRH , thus:

$$\text{RH}_{\text{probe}} = \text{RH}_{\text{true}} + \Delta\text{RH} \quad (3.25)$$

Substituting equation 3.25 into equation 3.23 illustrates an issue that needs consideration when using the RH method. As the Mach number increases and the temperature decreases, the saturation pressure ratio ($e_{s,\text{probe}}/e_{s,\text{static}}$) in equation 3.23 increases rapidly, and, as a result, the effect of the sensor uncertainty, ΔRH , is amplified. The ground processing system estimates the error in the RH based on temperature and Mach. This is used along with the known accuracy of the RH sensor and the temperature accuracies to calculate an overall RH uncertainty, which is reported along with the RH.

The range of RH that will be experienced by the RH sensor is also reduced due to the Mach heating. At high speeds, the RH internal to the probe will generally be less than 10% due to the Mach heating of the air. This effect is addressed in TAMDAR by the calibration process. Each RH sensor is characterized over several RH and temperature conditions. Values are specifically chosen at conditions which are error prone, in particular cold, dry conditions. This calibration process results in an RH measurement capability that is useful even at high altitudes. It should be mentioned that one effect of Mach heating is beneficial. Since the response of the capacitive sensor slows down as temperature decreases, the Mach heating effect keeps the RH sensor significantly warmer than ambient, resulting in a response time much faster than otherwise.

3.8.2.3 TAMDAR icing detection

The TAMDAR sensor detects icing using two light-emitting diode (LED) and photo detector (PD) pairs, each having an associated analogue-to-digital converted (AtDC) voltage output value. When a TAMDAR sensor encounters conditions where icing is present, ice accumulates on the surface of the foil gap in the area between the LED/PD pairs. As the thickness of the ice increases, the infrared beams become obscured, dropping the AtDC values of the LED/PD pairs below half of the nominal unblocked value, which results in a positive icing indication within the TAMDAR sensor. Once the detection of ice is confirmed via algorithms that verify consistency of the event with current environmental conditions (that is, T), the TAMDAR probe heaters are automatically activated to remove the ice. The heating process continues until the AtDC values of the LED/PD pairs are greater than the threshold value.

All icing events experienced by TAMDAR are tracked in the data stream with the use of icing flags. These flags track the initiation of the icing event, the time at which the heaters were activated, the period of continued icing, the probe cool-down, and when icing is no longer present. When the de-icing heaters are on, the temperature measurement is affected, which impacts other data fields such as RH. The icing flags are therefore used to indicate that the data fields that are impacted by the heaters are invalid until the heaters turn off and the probe cools down.

3.8.2.4 **TAMDAR turbulence detection**

Turbulence is reported as an EDR and is based on true airspeed (TAS) samples which are calculated from the TAMDAR pitot and static port pressures and the TAMDAR temperature. The report includes the mean and peak EDR, and the time of peak for each one-minute period. The EDR turbulence algorithm is independent of aircraft configuration and flight condition. Thus, it does not depend on the type of aircraft or on load and flight capacity.

The TAMDAR methodology utilizes an estimate of the longitudinal wind via the TAS parameter to calculate EDR. TAMDAR can obtain TAS via two sources: (a) from the TAMDAR static and pitot pressure sensor measurements or (b) from the aircraft's ARINC 429 databus. Once the system takes a measurement of the differential pressure between the pitot and static pressure, the measure is then passed through a filter before TAS is calculated.

The MacCready method is used to estimate the EDR based on the expected $-5/3$ power spectra slope from the Kolmogorov model of the TAS signal. The filtering of the differential pressure sensor uses a low-pass Butterworth anti-alias filter, with fourth-order 5 Hz 3 decibel cut-off frequencies. Windowing is completed prior to fast Fourier transformation (FFT) to make the measurement more spectral (64 point FFT). An EDR is calculated every 3 s using a 6 s block of 10.67 Hz TAS data. EDR values can be averaged if desired for a smoother result; normally a 6 s average is used, but users have the ability to configure this averaging to match their needs. A quality assurance filter is also employed.

3.9 **OTHER SYSTEMS AND SOURCES OF AIRCRAFT-BASED OBSERVATIONS**

3.9.1 **ICAO Automatic Dependent Surveillance**

The development of global air navigation systems is closely linked to developments in communication systems. Thus, the Future Air Navigation System is coupled with the development of an Automatic Dependent Surveillance (ADS) system which itself is dependent on global satellite aircraft communication. The global aircraft communication system is migrating to an open network under the Aeronautical Telecommunication Network project (Wells et al., 1990). This will link the VHF and SATCOM Systems into a common open network.

The successful weather routing of commercial aircraft, especially to provide flight safety, minimize fuel consumption and airframe fatigue, and to ensure passenger comfort, demands greater accuracy in aviation weather forecasts. Hence, automatic reports of aircraft position for ADS allow for the inclusion of automated meteorological reports. The data to be included in these reports are essentially the same as those of current AMDAR systems including allowance for turbulence and humidity elements.

Data derived from the ICAO ADS contract (ADS-C) system are being transmitted on the GTS. These data are made available through the arrangement established with ICAO as set out in ICAO Annex 3 to the Convention on International Civil Aviation, *Meteorological Service for International Air Navigation*, Chapter 5 and Appendix 4. ICAO regulations stipulate that ATM centres are to transmit the ADS-C messages to the World Area Forecast Centres, which are then responsible for transmission of the data on the GTS (see *Procedures for Air Navigation Services – Air Traffic Management*, ICAO Doc. 4444, 4.11.4).

3.9.2 **Automated Flight Information Reporting System**

The Automated Flight Information Reporting System (AFIRS), like TAMDAR, is a commercially developed system installed on the aircraft to acquire and transmit aircraft data to the ground using Iridium-based satellite communication (SATCOM).

AFIRS capabilities include on-board interfacing allowing connection to numerous aircraft systems. These include event-triggered flight data recording and real-time aircraft health monitoring. With the use of these systems, AFIRS can collect weather data and format into a “flight following report” using the embedded logic application.

AFIRS collects measurements of temperature, wind direction and speed, and roll angle in addition to location, time and pressure altitude of the aircraft at time of measurement. As AFIRS data are collected from the existing onboard sensors, data will be consistent with data collected using the AMDAR methods.

Unlike AMDAR weather messages transmitted over ACARS, the AFIRS messages are usually transmitted as comma-separated values (csv) files and sent to the partner NMHSs by FTP.

3.9.3 **New and developing systems**

3.9.3.1 ***Mode-S Enhanced Surveillance***

Wind and temperature observations can also be inferred from surveillance data gathered for ATC purposes using a Mode-S(elective) Enhanced Surveillance (EHS) radar. This radar interrogates every aircraft for specific information at a frequency rate of 4 to 20 s, depending on the ATC purposes of the radar. In designated airspace, all aircraft are obliged to respond to the interrogation by the Mode-S EHS radar. The mandatory registers (BDS4,0, BDS5,0 and BDS6,0) contain information on aircraft identity, flight level, roll angle, magnetic heading, airspeed, Mach number and ground track. Position of the aircraft can be obtained either from the ATC radar or from the Automatic Dependent Surveillance Broadcast (ADS-B) data which are transmitted continuously by the aircraft.

The derivation of wind from Mode-S EHS is similar to AMDAR, except that the true heading has to be determined from the magnetic heading. Besides applying a magnetic variance table, additional aircraft-dependent corrections need to be applied. Heading corrections may change with time due to maintenance of the aircraft. At present these corrections are determined for every aircraft based on comparison with numerical weather prediction (NWP) data. Next to the heading correction, an airspeed correction can be applied also based on long-term comparison with NWP data (see de Haan, 2013). After corrections and quality control, the derived wind information is of similar quality as from AMDAR (de Haan, 2011, 2013).

The derivation of temperature from Mode-S EHS observations is done by combining the Mach number and the airspeed. The quality of the derived temperature is hampered by the reported resolution of the Mach number and airspeed, and is clearly of less quality than AMDAR temperature (de Haan, 2011, 2013).

Other meteorological parameters are being actively investigated, including geopotential height information from the pressure altitude and global navigation satellite system (GNSS) altitude information that can be interpreted as a mean-layer temperature (Stone and Kitchen, 2015).

3.9.3.2 ***Mode-S Meteorological Routine Air Report***

A Mode-S EHS radar can also interrogate non-mandatory registers which may contain meteorological information. An example is the Mode-S EHS BDS4,4 register, called Meteorological Routine Air Report. This register contains direct wind and temperature information which is very close to the AMDAR wind and temperature information (Stranjar, 2012). Since the register BDS4,4 is not mandatory, only a fraction (approximately 5%) of the aircraft respond to the request with valuable meteorological information.

Both the ADS and Mode S methods have been analysed within a study undertaken on behalf of EUMETNET (de Haan, 2015).

3.9.3.3 ***Unmanned aerial vehicles***

Over the last few years, rapid development of unmanned aerial vehicles (UAVs) and their many uses by various organizations has led to the inclusion of UAVs in strategic planning for ATM by governing bodies such as Single European Sky ATM Research, the Federal Aviation Administration and ICAO.

In parallel with these UAV developments, there has been an increased use of UAVs for research and development by several NMHSs and government bodies. Research includes boundary layer, storm genesis and environmental monitoring.

The next step to utilizing UAVs as aircraft weather reporting platforms is to develop further the research activities and implement “real-time” data communication infrastructure with NMHS UAV operations as well as encouraging private industry to allow the installation of weather sensors/payload within their UAV operations.

Available sensors for UAVs include temperature, wind direction and speed, and in some instances humidity. These sensors can be installed as part of an operational payload of a UAV and provide valuable boundary-layer information.

REFERENCES AND FURTHER READING

- Abbott, I.H. and A.E. von Doenhoff, 1959: *Theory of Wing Sections*. Dover Publications, Inc., Mineola, New York, 693 pp.
- AirDat, 2003: *TAMDAR – Tropospheric Airborne Meteorological Data Reporting Sensor and System Overview; AirDat Infrastructure and Global Capabilities*. Information document, AirDat LLC, Evergreen, Colorado.
- Anderson, A.K., 2006: *AirDat system for ensuring TAMDAR data quality*. Tenth Symposium on Integrated Observing and Assimilation Systems for the Atmosphere, Oceans, and Land Surface (IOAS-AOLS), American Meteorological Society, Atlanta, GA.
- ARINC, 2012: *620-7 Data Link Ground System Standard and Interface Specification*. Aeronautical Radio, Inc., Annapolis, Maryland.
- Benjamin, S.G., B.D. Jamison, W.R. Moninger, S.R. Sahm, B.E. Schwartz and T.W. Schlatter, 2010: Relative short-range forecast impact from aircraft, profiler, radiosonde, VAD, GPS-PW, METAR, and Mesonet observations via the RUC hourly assimilation cycle. *Monthly Weather Review*, 138:1319–1343.
- Braid, J., P. Van Wie and J. Rex, 2011: Using the TAMDAR sensor for in-flight ice detection and improved safety of flight. *SAE Technical Paper 2011-38-0051*, International Conference on Aircraft and Engine Icing and Ground Deicing, Society of Automotive Engineers.
- Cornman, L.B., G. Meymaris and M. Limber, 2004: *An update on the FAA Aviation Weather Research Program's in situ turbulence measurement and reporting system*. Eleventh Conference on Aviation, Range and Aerospace Meteorology, Hyannis, MA.
- Cornman, L.B., C.S. Morse and G. Cuning, 1995: Real-time estimation of atmospheric turbulence severity from in situ aircraft measurements. *Journal of Aircraft*, 32(1):171–177.
- Dommasch, D.O., S.S. Sherby and T.F. Connolly, 1958: *Airplane Aerodynamics*. New York, Pitman, 560 pp.
- Federal Aviation Administration: Unmanned Aircraft Systems. <https://www.faa.gov/uas/>.
- Fleming, R.J., 2000: Water vapor measurements from commercial aircraft: Progress and plans. *Preprints*. Fourth Symposium on Integrated Observing Systems, Long Beach, CA, American Meteorological Society, 30–33.
- , 2003: The WVSS-II and the UCAR air sampler: Purpose, design, status (personal communication). University Corporation for Atmospheric Research, Boulder, Colorado.
- Gao, F., X.Y. Zhang, N.A. Jacobs, X.-Y. Huang, X. Zhang and P.P. Childs, 2012: Estimation of TAMDAR observational error and assimilation experiments. *Weather and Forecasting*, 27:856–877.
- Haan, S. de, 2011: High-resolution wind and temperature observations from aircraft tracked by Mode-S air traffic control radar. *Journal of Geophysical Research*, 116(D10111).
- , 2013: *An Improved Correction Method for High Quality Wind and Temperature Observations Derived from Mode-S EHS*. KNMI Technical Report No. TR-338, De Bilt.
- Haan, S. de, J. Sondij, E. Stone, F. Besson, B. Strajnar, D. Lockett, S. Stringer, H. Vedel, J.A. Garcia-Moya Zapata and A. Hoff, 2015: *EUMETNET Aircraft Derived Data Feasibility Study Expert Team*. GIE EUMETNET.
- International Civil Aviation Organization, 2007: *Procedures for Air Navigation Services – Air Traffic Management*. Fifteenth edition, Doc 4444, Montreal.
- , 2013: *Meteorological Service for International Air Navigation*. ICAO Annex 3, Eighteenth edition, Amendment 76, Montreal.
- : UAS Tool Kit. <https://www.icao.int/safety/UA/UASToolkit/Pages/default.aspx>.
- International Organization for Standardization (ISO), 2007: *Standard Atmosphere*, ISO 2533:1975 (with two additions in 1985 and 1997, reviewed and confirmed in 2007). Geneva.
- Lawson, R.P. and W.A. Cooper, 1990: Performance of some airborne thermometers in clouds. *Journal of Atmospheric and Oceanic Technology*, 7:480–494.
- May, R.D., 1998: Open-path, near-infrared tuneable diode laser spectrometer for atmospheric measurements of H₂O. *Journal of Geophysical Research*, 103:19161–19172.
- May, R.D. and C.R. Webster, 1993: Data processing and calibration for tuneable diode laser harmonic absorption spectrometers. *Journal of Quantitative Spectroscopy and Radiative Transfer*, 49(4):335–347.
- Meteorological Service of Canada, 2003: *The Effect of Pitch and Roll Attitude on the Calculation of Wind* (G. Bruce). Aeromechanical Services Ltd., 1118-1c, Rev. 1.0.
- Moninger, W.R., S.G. Benjamin, B.D. Jamison, T.W. Schlatter, T.L. Smith and E.J. Szoke, 2010: Evaluation of regional aircraft observations using TAMDAR. *Weather and Forecasting*, 25:627–645.

- Mulally, D.J. and J.T. Braid, 2009: *The TAMDAR Sensor's Relative Humidity Performance on ERJ-145 Commercial Aircraft*. Thirteenth Symposium on Integrated Observing and Assimilation Systems for the Atmosphere, Oceans, and Land Surface (IOAS-AOLS), American Meteorological Society, Phoenix, AZ.
- Nash, J., 1994: Upper wind observing systems used for meteorological operations. *Annales Geophysicae*, 12:691–710.
- Petersen, R.A., L. Crouce, W. Feltz, E. Olson and D. Helms, 2011: *Validation Studies of WVSS-II Moisture Observations*. Fifteenth Symposium on Integrated Observing and Assimilation Systems for the Atmosphere, Oceans, and Land Surface (IOAS-AOLS), American Meteorological Society, Seattle, WA.
- Petersen, R.A., L. Crouce, R. Mamrosh, R. Baker and P. Pauley, 2016: On the impact and future benefits of AMDAR observations in operational forecasting. Part II: Water vapour observations. *Bulletin of the American Meteorological Society*, 97(11):2117–2133.
- Rodi, A.R. and P.A. Spyer-Duran, 1972: Analysis of time response of airborne temperature sensors. *Journal of Applied Meteorology*, 11:554–556.
- Sherman, D.J., 1985: *The Australian Implementation of AMDAR/ACARS and the Use of Derived Equivalent Gust Velocity as a Turbulence Indicator*. Structures Report No. 418, Department of Defence, Defence Science and Technology Organization, Aeronautical Research Laboratories, Melbourne, Victoria.
- Smith, W.L., P. Minnis, C. Fleeger, D. Spangenberg, R. Palikonda and L. Nguyen, 2012: Determining the flight icing threat to aircraft with single-layer cloud parameters derived from operational satellite data. *Journal of Applied Meteorology and Climatology*, 51:1794–1810.
- Stickland, J.J., 1998: *An Assessment of Two Algorithms for Automatic Measurement and Reporting of Turbulence from Commercial Public Transport Aircraft*. A report to the ICAO METLINK Study Group. Observations and Engineering Branch, Bureau of Meteorology, Melbourne.
- Stickney, T.M., M.W. Shedlov, D.I. Thompson, 1990: *Rosemount Total Temperature Sensors*. Technical Report 5755, Revision B, Rosemount Inc.
- Stone, E.K. and M. Kitchen, 2015: Introducing an approach for extracting temperature from aircraft GNSS and pressure altitude reports in ADS-B messages. *Journal of Atmospheric and Oceanic Technology*, 32(4):736–743.
- Strajnar, B., 2012: Validation of Mode-S Meteorological Routine Air Report aircraft observations. *Journal of Geophysical Research: Atmospheres*, 117(D23).
- Wells, V.E. et al., 1990: Migration of ACARS to the Aeronautical Telecommunication Network. *Proceedings of the Aeronautical Telecommunications Symposium on Data Link Integration*. Annapolis, Maryland.
- World Meteorological Organization, 2011 (updated in 2017): *Manual on Codes* (WMO-No. 306), Volume I.1. Geneva.
- , 2013: *AMDAR Onboard Software Functional Requirements Specification*. Instruments and Observing Methods Report No. 114. Geneva.
- , 2015 (updated in 2017): *Manual on the WMO Integrated Global Observing System* (WMO-No. 1160). Geneva.
- , 2017: *Guide to Aircraft-based Observations* (WMO-No. 1200). Geneva.
-

CHAPTER 4. MARINE OBSERVATION

4.1 GENERAL

Marine observations in the broadest definition cover any meteorological and related environmental observations at the air–sea interface, below the sea surface and in the air above the sea surface. Observations can be made using fixed or moving platforms, and be in situ or remote, using surface- or space-based techniques. In-situ measurements are essentially single-point observations intended to be representative of the surrounding sea area, as for synoptic meteorology. Remote-sensing techniques lead to large area or volume representation, which is particularly appropriate for observations of sea ice.

This chapter discusses observations at the air–sea interface made in situ, which include the usual surface parameters that are also measured over land and discussed in that context in [Volume I](#) of the present Guide. This chapter also considers other observations of importance to marine physics and physical oceanography, including: sea-surface temperature (SST); ocean waves; sea ice, icebergs and ice accretion; and salinity. Upper-air measurements are taken using techniques that are essentially the same over the sea and over land.

Detailed formal requirements for observations from sea stations are given in the [Manual on the WMO Integrated Global Observing System](#) (WMO-No. 1160). Advice on requirements and procedures is given in the [Guide to Marine Meteorological Services](#) (WMO-No. 471). In situ marine measurements or observations are made from a variety of platforms. They include ships recruited by WMO Members to participate in the Voluntary Observing Ship (VOS) Scheme, light vessels, moored buoys, drifting buoys, towers, oil and gas platforms and rigs, island automatic weather stations (AWS), and ship-borne AWS systems. The type of platform generally determines the range of elements measured and reported. Thus, ships of the VOS, using both automated and manual observation techniques, report the full range of observations required for synoptic meteorology. In contrast, moored buoys provide only automated observations, but of a wide range of variables which may include: surface air pressure, air temperature and humidity, wind speed and direction, wave height and period, and SST. The majority of drifting buoys report up to three parameters, namely position, atmospheric pressure at sea surface, and SST. A smaller fraction of the array measures sea-surface salinity, directional wave spectra, subsurface temperatures through the mixed layer, and wind speed and direction.

Observations from voluntary observing ships are most commonly compiled and transmitted to shore in a nationally or internationally agreed ship-to-shore transmission format, and then distributed internationally in appropriate WMO codes (for example, FM 94 BUFR). WMO codes are documented in the [Manual on Codes](#) (WMO-No. 306), [Volume I.1](#) and [Volume I.2](#); general information is found in [Volume I.2](#), Part B, and templates specific to particular types of marine observations are documented in [Volume I.2](#), Part C.¹ Further information can be found in the proceedings of a 2009 meeting on the ocean observing system (Hall et al., 2010), including information on VOS (Kent et al., 2010), research vessels (Smith et al., 2010), ship-based oceanographic measurements (Goni et al., 2010), profiling floats (Freeland et al., 2010), buoys (Meldrum et al., 2010; McPhaden et al., 2010; Send et al., 2010; Dohan et al., 2010; Keeley et al., 2010), and waves and sea-level (Swail et al., 2010a; Swail et al., 2010b; Merrifield et al., 2010). On the recommendation of the Joint WMO/Intergovernmental Oceanographic Commission (IOC) Technical Commission for Oceanography and Marine Meteorology (JCOMM), a network of WMO/IOC Regional Marine Instrument Centres (RMICs) has been set up to facilitate adherence of observational data and processed observational products to higher level standards for instruments and methods of observation, by providing (a) facilities for the calibration and maintenance of marine instruments and the monitoring of instrument

¹ The [Manual on Codes](#), Volume I.1 also presently describes the traditional alphanumeric codes (TAC) that have been used to circulate data for many years over GTS, principally in the VOS context referring to the FM 13 SHIP code. WMO, however, is in the process of fully discontinuing the TAC for GTS transmission. Therefore, the [Manual on Codes](#) may in the future be restructured to omit the first volume altogether.

performance; and (b) assistance for instrument intercomparisons, as well as appropriate training facilities complementing what the manufacturers are also providing. Their terms of reference and locations are given in [Annex 4.A](#).

The joint WMO/IOC International Forum of Users of Satellite Data Communications, known as the SATCOM Forum,² is an international body providing clear information about satellite communications to operational and scientific users and to liaise with the industry to advocate for appropriate new technical features, suitable pricing structures and remote data communication requirements for automatic environment observing systems coordinated through WMO and IOC and partner organizations.

4.2 OBSERVATIONS FROM SHIPS

This section contains detailed guidance and advice for taking measurements and making observations on ships. WMO's *Compendium of Lecture Notes in Marine Meteorology for Class III and Class IV Personnel* (WMO-No. 434) is another source. Details on surface observations to be carried out within the framework of the WMO VOS Scheme are provided in *Guide to the Global Observing System* (WMO-No. 488), Appendix III.4. Studies of the quality of observations from ships are given in *The Accuracy of Ship's Meteorological Observations: Results of the VSOP-NA* (WMO/TD-No. 455), WMO (1999), Kent et al. (1993; 2003), Taylor et al. (2003), Kent and Berry (2005), Ingleby (2010), and Kennedy et al. (2012). A discussion of good observing practice from the research community is presented by Bradley and Fairall (2006) and information on sensors used in the marine environment by Weller et al. (2008). In all instances, the safety of the crew member making the observations takes priority over performing, recording and disseminating the observations in whole or in part.

4.2.1 Operation of the WMO Voluntary Observing Ship Scheme

The VOS Scheme is operated by NMHSs under the guidance of the JCOMM Ship Observations Team (SOT) and in particular the SOT VOS Panel (VOSP). Full information on the VOS Scheme is given in *Guide to Marine Meteorological Services* (WMO-No. 471). VOS programme managers work with port meteorological officers (PMOs) and technicians who typically act as the link between the VOS operator and the ship. An essential first step in recruiting VOS is to obtain the permission of the owners and master of the vessel. When permission has been granted and the ship has been identified, PMOs and technicians should do the following:

- (a) Install calibrated instruments ensuring best exposure;
- (b) Install electronic logbook software;
- (c) Train observers on instrument care and operation;
- (d) Train observers in all aspects of observing practices;
- (e) Demonstrate use of electronic logbook software and compilation of the observation;
- (f) Record the required ship metadata as required for WMO (see the *Manual on the WMO Integrated Global Observing System* (WMO-No. 1160));
- (g) Demonstrate methods of report transmission for ships not equipped with an AWS (conventional ships);
- (h) Explain NMHS marine forecast products.

² <https://community.wmo.int/satcom-forum-introduction>.

Once a ship has been recruited, the PMO should ideally endeavour to visit it at least every three months (subject to shipping movements and staff resources; if not practicable, less frequent visits can be considered) to check the accuracy of the instruments, update electronic logbook software, and renew the supply of forms, documents and so on. AWSs and digital sensors may allow a longer checking period of one year. The PMO should take the opportunity to foster interest in meteorology and explain the mutual value to seafarers and meteorologists of accurate weather observations.

In some instances, a company operating a ship or platform takes observations/measurements for its own use and makes them available on the WMO GTS without much participation from a PMO. The installation, maintenance and training on the meteorological and oceanographic equipment may be done under contract. In cases where the vessel/station was not recruited by a PMO, efforts should be made to ensure that the relevant metadata are made available through the appropriate WMO channels.

4.2.2 **Voluntary Observing Ship observations**

4.2.2.1 ***Elements observed***

Ships participating in the VOS³ Scheme undertaking meteorological observations should ideally observe, at the times described in 4.2.2.4, the following elements:

- (a) Ship position (from ship's navigation system);
- (b) Ship course and speed (from ship's navigation system);
- (c) Wind speed and direction;
- (d) Atmospheric pressure;
- (e) Pressure tendency and its characteristics;
- (f) Air temperature;
- (g) Humidity;
- (h) SST;
- (i) Present and past weather, and weather phenomena;
- (j) Cloud amount, type and base height;
- (k) Precipitation;
- (l) Visibility;
- (m) Ocean wind waves and swell, including height, period and direction;
- (n) Sea-ice and/or ice accretion on board ship, when appropriate;
- (o) Special phenomena.

The observations listed above are measured, observed or visually estimated based on the capabilities of the measuring equipment on board the ship.

³ <https://old.wmo.int/wiswiki/tiki-index.php%3Fpage=SATCOM.html>.

Some specially equipped ships, for example research vessels, may make instrumentally measured observations and reports of precipitation, radiation, visibility, cloud parameters, wave parameters and others if applicable.

In general, instrumental observations requiring the use of a light at night should be ideally made after non-instrumental ones, so that the observer's eyes can adapt to the darkness without being impaired.

Where time, conditions or other factors limit the capacity to make all the observations, the highest priority for meteorological observations are items (a) through (f).

4.2.2.2 **Equipment required**

The following instruments are suitable for use on ships (chapters refer to [Volume I](#) of the present Guide):

- (a) A precision aneroid, dial aneroid or electronic digital barometer (see [Chapter 3](#));
- (b) A barograph, preferably open scale (desirable but not mandated) or a digital barometer that includes a barometric tendency trace (see [Chapter 3](#));
- (c) A liquid-in-glass⁴ or electrical resistance thermometer (see [Chapter 2](#));
- (d) A hygrometer or psychrometer (see [Chapter 4](#));
- (e) A sea-temperature thermometer and suitable receptacle for obtaining a sample of seawater, or a continuously immersed sensor (for example, an engine intake thermometer) or hull contact sensor with remote indicator.

The use of anemometers with suitable exposure as an alternative to the visual estimation of the wind speed (for example, using the Beaufort scale of wind force) is encouraged, provided that such instruments are routinely checked to ensure that they remain within acceptable tolerance determined by calibration. Additionally when using anemometers, observations of speed over ground, course over ground, and heading of the ship are needed to accurately calculate a true (Earth-referenced) wind (see [4.2.2.6.2](#)). Precipitation gauges are rarely provided for use on VOS.

The instruments used on ships should conform to the requirements laid down or recommended in other chapters of the present Guide, apart from the modifications described in the following sections of this chapter. Instruments supplied to ships should be regularly tested and inspected by (or on behalf of) the NMHSs concerned.

4.2.2.3 **Automation of ship observations**

Automatic weather stations or partially automated systems are increasingly being used on observing ships for both observation and data transmission purposes. Two basic modes of operation are used, as follows:

- (a) The observation is made automatically using AWS techniques, as described in the present volume, [Chapter 1](#). The position, course and speed of a ship are taken from its navigation system or computed independently using a satellite navigation system, usually GPS. The transmission of such observations can be either purely automatic or initiated manually according to the communications facilities;

⁴ Mercury-in-glass thermometers should not be used any more as the UNEP Minamata Convention on Mercury came into force globally in August 2017, and bans all production, import and export of mercury-based instruments (see, [Chapter 1, 1.4.2 in Volume I](#)).

- (b) The observations making up the marine report are a combination of automated and manual observations, namely automated observations augmented with visual observations entered by the observer before transmission (for example, adding visibility, weather codes, cloud amounts, types and base heights, wave heights, periods and directions, ice parameters and wind speed and direction where not measured using an anemometer).

4.2.2.4 **Times of observation**

When done manually, the observation of elements other than pressure should be made within 10 min preceding the standard time for the synoptic observation. Atmospheric pressure, however, should be read at the exact time or as close as possible to the standard time.

Surface observations on board ships are typically made as follows:

- (a) Synoptic observations from staffed ships are accepted at any time; however, they are traditionally made at main standard times: 0000, 0600, 1200 and 1800 UTC and/or at one or more of the intermediate standard times: 0300, 0900, 1500 and 2100 UTC;
- (b) Hourly or more frequent observations should be made when an automated system is used (augmented as frequently as possible with the additional visual elements);
- (c) Observations should be made more frequently whenever storm or stronger conditions threaten or prevail;
- (d) When sudden and dangerous weather developments are encountered, observations should be made for immediate transmission without regard to the standard times of observation (for example, within 300 nautical miles of a named tropical system);
- (e) Marine observations are just as valuable in coastal zones as in the open ocean and observations should be continued during the whole journey.

4.2.2.5 **Transmission of ship's observations**

Satellite communication systems are now in widespread use for disseminating ship observations. Details are given in Appendix III.4 of the *Guide to the Global Observing System* (WMO-No. 488). The following methods are most commonly used for conventional VOS:

- (a) Commercial satellite systems through the INMARSAT-C system that is carried by most ocean-going ships for compliance with the International Convention for the Safety of Life at Sea and Global Maritime Distress and Safety System requirements. Weather observations are normally sent to a suitable Land Earth Station (LES) via a special access code (SAC) 41 message, which allows the costs of the report to be borne by the NMHS. A list of the acceptable LESs for SAC messages is maintained on the WMO website at <https://community.wmo.int/list-inmarsat-land-earth-stations-accepting-special-access-codes>. INMARSAT-C has near-global coverage, except in very high latitudes which are not covered. However, other dedicated SACs are now being set up to allow ship-to-shore messages to be sent in a compressed format, thereby allowing NMHS to reduce the transmission costs of their national observing fleets.
- (b) Emails from the ship, regardless of the communication system, provides free transmission for the NMHS as the cost are born by the ship.

For AWSs:

- (a) Commercial satellite services such as Iridium are increasingly used for shipboard AWS systems. The Iridium Short Burst Data system using binary formatted messages can

significantly reduce transmission costs. Iridium has the advantage of providing global satellite coverage and can also improve data timeliness (for example, see Blouch and Billon, 2017).

- (b) The INMARSAT-C data reporting service is also used for sending compressed meteorological data from certain AWS systems on non-automated manually reporting observing ships, <https://community.wmo.int/list-inmarsat-land-earth-stations-accepting-special-access-codes>.
- (c) Service Argos: This system is primarily designed for location as well as data transmission and is limited by the number and the orbital characteristics of the polar-orbiting satellites carrying the Argos payload. The Argos system is used both for the communication and for the processing of ship observations onto the GTS (*Guide to Data Collection and Location Services using Service Argos*) but there can be several hours of delay, depending on the location of the observing station and the land receiving station. It is typically used for small drifting buoys, although it is increasingly being replaced by Iridium. A few autonomous shipboard AWS systems also use Argos for data transmission.
- (d) 3G/4G LTE-based technologies may also be used to relay data from VOSs when they are close to shore to a central receiver at port or directly to the synoptic data reception server. This technology enables the transfer of huge amounts of data as the bandwidth is comparatively higher and the cost of transmission is cheaper.
- (e) The International Data Collection System through the meteorological geosynchronous (GOES, METEOSAT, MTSAT) satellites. This system, funded mainly by NMHSs, allows for purely automatic data communication at predetermined time slots, once an hour. Data transmission is one way only and error rates can be significant. It is primarily used in connection with moored buoys but is also used for some shipboard AWS systems.

4.2.2.6 **Wind**

Observations of wind speed and direction may be made either by visual estimates or by anemometers. Winds should be measured only if using a well-maintained and recently calibrated instrument sited in a well-exposed location away from the influence of the superstructure, mast and spars. Reports of wind speed should be recorded in m s^{-1} , while for some purposes knots might still be used.

4.2.2.6.1 **Visual observations**

Visual estimates are based on the appearance of the sea surface. The wind speed is obtained by reference to the Beaufort scale (see table below). The Beaufort number obtained by estimation is converted into m s^{-1} or knots by the use of the wind speed equivalent columns of the Beaufort scale, so the wind speed is reported at a specific value in metres per second or knots according to the best estimate of the observer from within those equivalent ranges. National instructions may give guidance on preferred practice. The wind direction is determined by observing the orientation of the crests of wind waves (that is, wind-driven waves, and not swell) or the direction of streaks of foam which are blown in the direction of the wind. The specifications of the Beaufort scale numbers refer to the conditions in the open sea. In practice, wind directions made by visual methods are of good quality.

The wave height in itself is not always a reliable criterion since it depends not only on wind speed, but also on the fetch and duration of the wind, the depth of shallow waters, and the presence of swell running through a sea. The Beaufort scale, therefore, makes use of the relation between the state of the sea and the wind speed. This relation is, however, affected by several other factors which should, in principle, be taken into account in estimating wind speeds. These factors are the lag between the wind increasing and the sea rising, the smoothing or damping down of wind effects on the sea surface by heavy rain, and the effects of strong surface currents

(such as tidal currents) on the appearance of the sea. Sea criteria become less reliable in shallow water or when close inshore, owing to the effect of tidal currents and the shelter provided by the land. At these locations, or when the surface of the sea cannot be clearly seen (for example, at night), the Beaufort force of the relative wind on the ship may be estimated by noting wind effects on sound, on ship-borne objects such as flags, and on funnel smoke. In the latter case, the direction of the relative wind may also be estimated, for example, by observation of the funnel smoke. From these estimates, the speed and direction of the true wind can be computed (United Kingdom Meteorological Office, 1995).

4.2.2.6.2 Measurements with instruments

If instruments for measuring wind are installed on ships, the equipment should give both wind speed and direction and should be capable of minimizing roll effects (suitably designed cup anemometers and damped wind vanes are capable of rendering the effects of pitch and roll insignificant). The marine environment is harsh, so cup or propeller anemometers require regular maintenance and calibration in order to produce reliable wind data. Ultrasonic anemometers have no moving parts, require less maintenance, and are therefore increasingly being used on ships.

**Beaufort scale in operational use for WMO reports of estimated wind
referenced to 10 m above sea level**

Beaufort number (force)	Descriptive term	Mean equivalent wind speed		Wind speed equivalent range		Specifications for observations	Probable height of waves m	Probable maximum height of waves m
		knots	$m s^{-1}$	knots	$m s^{-1}$			
0	Calm	0	0	< 1	0–0.2	Sea like a mirror		
1	Light air	2	0.8	1–3	0.3–1.5	Ripples with the appearance of scales are formed, but without foam crests	0.1	0.1
2	Light breeze	5	2.4	4–6	1.6–3.3	Small wavelets; still short but more pronounced; crests have a glassy appearance and do not break	0.2	0.3
3	Gentle breeze	9	4.3	7–10	3.4–5.4	Large wavelets; crests begin to break; foam of glassy appearance; perhaps scattered white horses	0.6	1.0
4	Moderate breeze	13	6.7	11–16	5.5–7.9	Small waves, becoming longer; fairly frequent white horses	1.0	1.5
5	Fresh breeze	19	9.3	17–21	8.0–10.7	Moderate waves, taking a more pronounced long form; many white horses are formed (chance of some spray)	2.0	2.5
6	Strong breeze	24	12.3	22–27	10.8–13.8	Large waves begin to form; the white foam crests are more extensive everywhere (probably some spray)	3.0	4.0

Beaufort number (force)	Descriptive term	Mean equivalent wind speed		Wind speed equivalent range		Specifications for observations <i>On board ship (open sea)</i>	Probable height of waves <i>m</i>	Probable maximum height of waves <i>m</i>
		knots	$m\ s^{-1}$	knots	$m\ s^{-1}$			
7	Near gale	30	15.5	28–33	13.9–17.1	Sea heaps up and white foam from breaking waves begins to be blown in streaks along the direction of the wind	4.0	5.5
8	Gale	37	18.9	34–40	17.2–20.7	Moderately high waves of greater length; edges of crests begin to break into the spindrift; the foam is blown in well-marked streaks along the direction of the wind	5.5	7.5
9	Strong gale	44	22.6	41–47	20.8–24.4	High waves; dense streaks of foam along the direction of the wind; crests of waves begin to topple, tumble and roll over; spray may affect visibility	7.0	10.0
10	Storm	52	26.4	48–55	24.5–28.4	Very high waves with long overhanging crests; the resulting foam, in great patches, is blown in dense white streaks along the direction of the wind; on the whole, the surface of the sea takes a white appearance; the “tumbling” of the sea becomes heavy and shock-like; visibility affected	9.0	12.5
11	Violent storm	60	30.5	56–63	28.5–32.6	Exceptionally high waves (small and medium-sized ships might be for a time lost to view behind the waves); the sea is completely covered with long white patches of foam lying along the direction of the wind; everywhere the edges of the wave crests are blown into froth; visibility affected	11.5	16.0
12	Hurricane	64 and over	32.7 and over	64 and over	32.7 and over	The air is filled with foam and spray; sea completely white with driving spray; visibility very seriously affected	14 and over	–

Note that wave heights are indicated as a guide to show roughly what might be expected in the open sea. These wave heights should never be used for logging or reporting the state of the sea. In enclosed waters, or when near land, with an offshore wind, wave heights will be smaller and the waves steeper.

Source: OMI-CMI (1947)

It is difficult to obtain a good exposure for ship-borne wind instruments (Taylor et al., 2003; Yelland et al., 2001; Moat et al., 2005; Moat et al., 2006). The local effects produced by the superstructure, mast and spars should be minimized as much as possible by siting the instrument as far forward and as high as practicable. If fitted on a yardarm, it may be preferable that the speed and direction heads should form separate units, as a more even distribution of the weight on the yardarm can be obtained, and it may then be possible to fit the instruments farther outboard. Whether fitted on a yardarm or on a bracket fixed to the foremast, each unit should be mounted in position at a distance of at least 10 mast diameters away from the mast. If this is impracticable, a good technique is to fit two instruments, one on each side of the foremast, and always to use the one which is more freely exposed. The top of the foremast, if available, is generally thought to be the best site for an anemometer. Ultrasonic wind sensors are efficient and provide good accuracy when installed on the top of the main mast.

Various types of portable anemometers are on occasion used at sea (often to assist with ship berthing). Their main disadvantage is that they can hardly be given representative exposure, and, in practice, measurements taken with them show substantial scatter (Kent et al., 1993). Only an observer who understands the nature of the airflow over the ship in different circumstances would be able to choose the best place for making such observations and thus arrive at satisfactory results. This method may be useful if visual estimates of wind force are difficult or impossible, for example, with light winds at night.

When observations are taken from a moving ship, it is necessary to distinguish between the relative and the true wind; for all meteorological purposes the true wind must be reported. Relative wind should be transmitted if possible. The procedure for the calculation of true wind speed and direction from relative wind speed, relative wind direction, ship speed, course and heading is described in detail in Smith et al. (2003). It should be noted that the ship's course and the ship's heading may be significantly different particularly at low ship speeds or with large leeway. A simple vector diagram or a table may be used for computing the true wind from observations of the relative wind and ship speed and course (Bowditch, 2002). These additional elements are preferably obtained from a magnetic compass and the ship's speed information. They can also be obtained from the ship movement derived from a GPS receiver, but in that case the drift is not taken into account. In the past, this vector conversion was a frequent source of error in reported winds. However, increasing use of electronic logbook software that computes true wind will have reduced this source of error. For AWS, all of the required information is likely to be directly obtained from the anemometer and ship's navigation system.

The reported wind speed and direction will be the mean speed and direction measured over the 10 min period immediately preceding the observation. However, when the 10 min period includes a discontinuity in the wind characteristics, only data obtained after the discontinuity shall be used for reporting the mean values, and hence the period in these circumstances shall be correspondingly reduced.

The recording of ship metadata for WMO (see the [Manual on the WMO Integrated Global Observing System](#) (WMO-No. 1160)) is particularly important for wind observations (Yelland et al., 2001). Metadata should be provided to indicate the instrumentation used, how it is installed on board the ship (where on the ship and at what height), as well as details about the type of vessel (Kent et al., 2007). Metadata are used in particular to interpret the data correctly and increase data coherence (for example, bias correction) and permit traceability to standards.

4.2.2.7 ***Atmospheric pressure, pressure tendency and characteristic of pressure tendency***

4.2.2.7.1 **Methods of observation**

Pressure can be measured either by a precision aneroid, a dial aneroid or an electronic digital barometer. The barometer reading shall be taken as close to the observation time as possible. In a manual observation, the barometer will be read last and entered into the observation just prior to completion of the report. Automatic systems should have an averaging period of one minute (Chapter 1, Annex 1.A of [Volume I](#) of the present Guide). Most ships should report pressure to one decimal place.

With visual observation, the characteristic and amount of the pressure tendency in the past 3 h is usually obtained from a marine barograph, preferably an open-scale instrument graduated in divisions of 1 hPa. However, digital barometers that include an LCD display of the pressure tendency are increasingly being used.

With AWS, the characteristic and amount of the pressure tendency in the past 3 h are calculated automatically.

4.2.2.7.2 Instruments

All barometers should conform to the general requirements given in Chapter 3 of [Volume I](#), and should be supplied with a certificate giving the corrections (if any) that must be applied to the readings of each individual instrument. Barometers should be capable of being read to 0.1 hPa. The operational measurement uncertainty requirements and instrument performance are stated in Chapter 1, Annex 1.A of [Volume I](#). The required measurement uncertainty is better than 0.1 hPa (after reduction to sea level: <0.2 hPa). The achievable measurement uncertainty should never be worse than 0.3 hPa. Marine barographs should have a built-in damping device, for example, an oil bath containing the aneroid box or a dash pot connected to the lever mechanism, to prevent the wide trace produced by rapid pressure variations caused by gusty winds and movement of the ship. Both the barometer and barograph should also be vented to the outside with a static pressure head so that readings can be taken more accurately and are not affected by sealed bridges or conditions inside. If this is not possible, instructions should be given to ensure that the bridge wing doors are opened prior to taking an observation. This is especially important on ships with pressurized accommodation blocks or on vessels that are carrying hazardous cargoes where the wheelhouse may be hermetically sealed.

In general, many NMHSs set their barometers to “station level” pressure, and therefore the observations need to be corrected for the height of the barometer to give a sea-level pressure output. This height correction can be calculated automatically with electronic logbook software or by an AWS.

4.2.2.7.3 Exposure and management

Barometers and barographs should be mounted on shock-absorbing material in a position where they are least affected by concussion, vibration or movement of the ship. The best results are generally obtained from a position as close to the centre of flotation as possible. Barographs should be installed with the pen-arm oriented at a right angle to the centreline of the ship to minimize the risk of the arm swinging off the chart.

4.2.2.7.4 Corrections

Provision should be made for the application of the following corrections:

- (a) Instrument error (bias);
- (b) Reduction to sea level as appropriate;
- (c) Temperature (if applicable and appropriate tables are provided).

Barometers should be adequately compensated for temperature, otherwise the instruments should be provided with a temperature correction table and means should be provided for measuring the temperature. A table for reducing to sea-level pressure should be supplied when barometers are set to the station height, although this is not necessary for ships that use electronic logbooks or AWSs that are capable of automatically applying the height correction (Bowditch, 2002, Tables 29–34).

4.2.2.7.5 Sources of error

Errors are discussed in Chapter 3 of [Volume I](#) of the present Guide, but on ships in particular appreciable errors may be caused by the effect of the wind on the pressure in the compartment in which the barometer is placed. Where possible, these should be minimized by enclosing the instrument in a chamber connected to a static pressure head or by connecting the device directly to this static pressure head.

On non-automated barometers, the most frequent (human) errors are due to an absence of reduction to the sea level, a bad appreciation of the barometer height or a non-intentional double correction (correction applied on a barometer which already gives sea-level pressure).

4.2.2.7.6 Checking with standard instruments

Aneroid barometers and barographs should be checked, wherever possible, at approximately three-monthly intervals against the standard barometer of a PMO or a Transfer Standard barometer. However, as shipping movements can be highly dynamic this may not always be possible. A report of all comparisons should be logged by the PMO, and a label attached to the barometer showing the barometer check date and the correction to be applied. Standard barometers should be calibrated regularly.

Digital barometers have a much better stability and the length of time between calibrations may be as large as two years for some models.

4.2.2.8 *Air temperature and humidity*

Temperature (Chapter 2 of [Volume I](#) of the present Guide) and humidity (Chapter 4 of [Volume I](#)) observations used to be considered together as they were often measured by psychrometric methods with paired wet- and dry-bulb thermometers. With the increasing use of AWS, however, it is becoming more common for these parameters to be measured independently with a thermometer and separate hygrometer. Whichever method is used, the instruments should have effective ventilation of sufficient duration (to allow adaptation) and be well exposed in a stream of air, directly from the sea, which has not been in contact with, or passed over, the ship, and should be adequately shielded from radiation, precipitation and spray.

For visual observations, if a louvred screen is to be used, two should be provided, one secured on each side of the vessel, so that the observation can also be made from the windward side. In this way, thermometers in the hygrometer can be completely exposed to the air-stream and are uninfluenced by artificial sources of heat and water vapour. As an alternative, a single portable louvred screen can be used, which is hung on whichever side is windward to gain the same exposure. The muslin wick fitted to a wet-bulb thermometer in a louvred screen should be changed at least once each week, and more often in stormy weather.

Sling or aspirated psychrometers exposed on the windward side of the bridge have been found to be satisfactory. If manually operated psychrometers are used, the thermometers must be read as soon as possible after ventilation has stopped. Handheld hygrometers require several minutes to be acclimated to the open environment if they have been stored indoors before use. Acclimatization is reached when the readout of the instrument is stable for a period of up to one minute.

For the general management of psychrometers, the recommendations of Chapter 4 of [Volume I](#) should be followed. Distilled water should be used for the wet-bulb thermometer. If this is not readily available, water from the condenser will generally be more suitable than ordinary freshwater. Water polluted by traces of seawater should never be used because any traces of salt will affect the wet-bulb temperature significantly.

With AWS or a distant digital display, a manual reading of the instruments inside the screen is no longer necessary and a single screen typically can be installed far enough from the ship's

structure to provide good exposure. This means, however, that the filling of wet-bulb reservoirs becomes difficult, and consequently electronic temperature and RH sensors are typically used with AWS. These instruments require calibration on a regular basis.⁵ The AWS should report both air temperature and humidity as one-minute averages.

Humidity can be represented by several different variables, for example dew-point temperature, wet-bulb in combination with dry-bulb temperature or RH (Chapter 4 of [Volume I](#)) and should be recorded as the variable measured. Any conversion between humidity variables adds uncertainty and will be affected by any errors in other variables used and by truncation to fit transmission formats. For psychrometric measurements, both dry-bulb and wet-bulb temperature are reported with a resolution of 0.1 °C. The dewpoint should be calculated using standard tables issued nationally or using standard WMO formulae (Chapter 4, Annexes 4.A and 4.B of [Volume I](#)) and the psychrometric coefficient appropriate to the instrument being used. Dew-point temperature should also be reported to 0.1 °C resolution. Conversion of measurements of wet-bulb or dew-point temperature to RH recorded in whole per cent introduces significant uncertainty and should be avoided. When directly measuring RH (for example, using an AWS), RH should be reported with resolution of 1%.

4.2.2.9 ***Sea-surface temperature***

The routine measurement is to take the seawater temperature from near or just below the sea surface. More rarely the radiometric temperature of the surface skin of the ocean is measured.

The SST should be very carefully measured. This is because, among other things, it is used to obtain the difference with air temperature, which provides a measure of the stratification of temperature and humidity and of other characteristics of the lower layers of maritime air masses. The temperature of the seawater thermometer should be read to 0.1 °C.

It has not been possible to adopt a standard device for observing SSTs on account of the great diversity in ship size and speed and because of cost, ease of operation and maintenance considerations.

The SST may be observed by:

- (a) Taking a sample of the sea-surface water with a specially designed sea bucket;
- (b) Reading the temperature of the condenser intake water;
- (c) Exposing an electrical thermometer to sea-water temperature either directly or through the hull (for example, using an internally mounted hull contact sensor);
- (d) Using an infrared radiometer mounted on the ship to look down on the sea surface;
- (e) Using an expendable bathythermograph.

The principal methods used for many years have been (a) and (b). Studies of the difference in temperature provided by the two methods have been made ([Comparative Sea-surface Temperature Measurements](#) (WMO-No. 336)) in which it is reported that intake temperatures average 0.3 °C greater than those measured by sea-bucket samples. More recent studies suggest that this warm bias has reduced over time (Kent and Taylor, 2006). This study reported that the details of the intake temperature installation have a significant impact on the quality of observation. In recent years, as the speed and height of ships have increased, method (c), which gives the most consistent results, has been more widely used ([The Accuracy of Ship's Meteorological Observations: Results of the VSOP-NA](#) (WMO/TD-No. 455); Kent et al., 1993), however the location of the sensor on the hull is critical. It should not be mounted in locations where there are significant heat

⁵ The filters on humidity sensors should be replaced on a three-monthly basis. The complete sensor will probably require cleaning and recalibration in a laboratory every 12 months as a minimum.

sources such as the engine room. The use of radiometers is rarely encountered on VOS but may be used on some research vessels or on offshore platforms. Of all these methods, the condenser intake technique is the least desirable because of the great care needed to obtain good results.

4.2.2.9.1 Sea buckets

A sea bucket is lowered over the side of the ship to obtain a sample of seawater. The bucket is hauled back on board and a thermometer is then used to measure the temperature of the water. The sample should be taken from the leeward side of the ship, and well forward of all outlets. The thermometer should be read as soon as possible after it has attained the temperature of the water sample, ensuring that it is read out of the direct sunlight. When not in use, the bucket should be hung in the shade to drain.

A sea bucket should be designed to ensure that seawater can circulate through it during collection and that the heat exchange due to radiation and evaporation is minimized. The associated thermometer should have a quick response and be easy to read and should preferably be fixed permanently in the bucket. If the thermometer must be withdrawn for reading, it should have a small heat capacity and should be provided with a cistern around the bulb such that the temperature of the water withdrawn with it does not vary appreciably during the reading. The design of the bucket should be deemed adequate for its purpose by the organization recruiting the ship for observations.

Measurements from sea buckets of good design can be expected to agree well over an extensive range of conditions. However, sea buckets are less convenient to use than instruments attached to the ship and their use is sometimes restricted by weather conditions or by the size or speed of the ship.

4.2.2.9.2 Intake and tank thermometers

The thermometer provided within the intake pipe when the ship is built is normally not suitable for the measurement of SST to the required accuracy. Thus, the organization recruiting the ship should, with the permission of the shipping company concerned, install an appropriate thermometer. The thermometer should be mounted in a special tube providing adequate heat conductivity between the thermometer bulb and surrounding seawater, and positioned close to the water intake, although this may not always be practical.

When a direct-reading thermometer is installed in cramped conditions, the observer should be warned of the possibility of reading errors due to parallax. A distant-reading system with the display elsewhere (for example, in the engine room or on the bridge) overcomes this problem. The observer should also be aware that, for ships of deep draught, or when a marked temperature gradient exists within the sea-surface layer, intake temperature readings usually differ considerably from those close to the sea surface, and will vary according to the ship's load or ballast condition. Lastly, of course, the intake temperature should not be recorded when the ship is stationary, otherwise the cooling water is not circulating. It should be noted that the installation of retrofit intake, or hull contact SST sensor can often be time-consuming and complicated, often forcing PMOs or technicians to work in a difficult environment (interior of ships, with limited access, and the like).

The sea chest in the bottom of a ship is a cavity in which the intake pipes may terminate and which may be used to observe the intake temperature. It is a favoured position for the sensor of a distant-reading thermometer. The limitations already mentioned apply to such installations.

Although the majority of intake thermometers will only provide instantaneous temperature readouts, some ships may be equipped with temperature probes that can sample the measurements at a given frequency and average them over a period of time. In that case, and in order to provide for measurements that are more representative of the SST, a modal filtration algorithm may be used to exclude the extreme readings from the computed average.

4.2.2.9.3 Hull-attached thermometers

Hull-attached thermometers provide a very convenient and accurate means of measuring SST. They are necessarily distant-reading devices, the sensor being mounted either externally in direct contact with the sea using a “through-the-hull” connection, or internally (the “limpet” type) attached to the inside of the hull, except if the hull is a twin hull. Both types show very good mutual agreement, with the “through-the-hull” type showing a slightly quicker response. In case of internal sensor, magnetic probes are preferable than glued sensors for an easier installation and maintenance, but only for steel hulls.

The sensors must be located forward of all discharges at a depth of 1 to 2 m below the waterline. When large changes of draught can occur, more than one sensor may be needed. There can be considerable problems of fitting and wiring, which is best done when the ship is being built. For subsequent fitting, the limpet-type thermometer avoids the need for drydocking the ship.

4.2.2.9.4 Trailing thermometers

Several means have been devised for trailing the sensor of a distant-reading thermometer in the sea at a point from which a sea bucket would take its sample. The differences concern the way in which the connecting cable is brought on board and the arrangement for exposing the sensor to the sea. These devices provide readings that are in good agreement with those of an accurate sea bucket and can be used readily. However, since experience is limited, no information is available on their possible fouling by weeds, and so on. Thus, streaming and recovery may be necessary on each occasion as for a sea bucket. Trailing thermistors are rarely used by the VOS but are more common for research applications (Fairall et al., 1997; Bradley and Fairall, 2006; Weller et al., 2008).

4.2.2.9.5 Radiometers

Because of its temperature, any substance gives off heat energy as infrared radiation. The amount of energy and the wavelength of the radiation depend upon the temperature of the substance and its emissivity. Thus, radiometers which respond to infrared radiation can be used to measure the temperature of a substance. When directed at the sea surface, a radiometer measures the temperature of only the uppermost 1 mm or so, because the emissivity of water is near unity. This uppermost layer is often called the ocean skin. Large temperature gradients, with the coolest temperature at the top, may exist in the first few centimetres of the ocean, especially in relatively calm conditions.

Radiometers can be handheld (pointing forward and downward), mounted on the bow or on a boom extending over the water. Radiometer measurements represent the evaporative surface-skin temperature and are used on only a few ships (Barton et al., 2004; Donlon et al., 2008).

4.2.2.10 *Clouds and weather*

4.2.2.10.1 Amount of cloud and cloud type

Visual cloud observations should follow the same rules as those applicable to a land station (see Chapter 15 of [Volume I](#) of the present Guide and the [International Cloud Atlas](#) (WMO-No. 407). Detailed instructions should be provided by the PMO. Pictorial guides and coding information are available from many sources, such as the [International Cloud Atlas](#) (WMO-No. 407), as well as from publications of NMHSs. Most electronic logbook software include extensive pictures of clouds to assist with cloud type identification. Additionally, the template for reporting SHIP observations (Part C of the [Manual on Codes](#) (WMO-No. 306)) provides specific information on how to make and code VOS cloud reports.

The assessment of the total amount of cloud consists in estimating how much of the total sky area is covered with cloud and should be reported in per cent (%); however, oktas can still be used per national requirements. In BUFR FM 94 code (*Manual on Codes* (WMO-No. 306)) total cloud cover is given in percentage (113 indicating sky obscured by fog and/or other meteorological phenomena). The assessment of low cloud amount is performed in a similar way and reported in oktas for both ship-to-shore transmission and onward transmission in FM 94 BUFR. If no low cloud is present, the amount of medium cloud is reported instead. The type of low, middle and high cloud shall be determined as specified in the *International Cloud Atlas* (WMO-No. 407), or by identifying the appropriate cloud type from the photographs displayed in the electronic logbook software.

4.2.2.10.2 Cloud-base height

The cloud-base height is normally estimated by the VOS. In order to improve their ability to do this, observers should be encouraged to take every opportunity to check their estimates against known heights, for example, when a cloud base is seen to intercept a mountainous coast, although in such circumstances the cloud base may be lower at the mountain than out at sea.

Some specialized ships may have instruments installed to measure cloud-base height. The cloud-base searchlight is of limited value on a ship because of the short baseline. An instrument which does not require a baseline is to be preferred, such as a laser ceilometer (see Chapter 15 of *Volume I*). It should be installed so that it can be operated and read by the officer on watch on the navigation bridge.

4.2.2.10.3 Present and past weather

Present and past weather are primarily meant to serve as a qualitative description of weather events. Most VOS reports of present and past weather are made by visual and auditory observations and follow the same rules as those applicable to a land station (see Chapter 14 of *Volume I*). There are 100 categories of present weather for VOS manual observations (the first 100 codes in FM 94 BUFR code table 0 20 003). Past weather is reported in 10 categories (the first 10 codes in FM 94 BUFR code table 0 20 004 and 0 20 005). Two past weather categories should be reported which have been selected to give as complete a description of conditions over the reporting interval as possible. The *Manual on Codes* (WMO-No. 306) provides specific information on how to make and code VOS weather reports. For observers using electronic logbook software, further guidance is likely to be available from the software.

4.2.2.11 **Visibility**

At sea, the absence of suitable objects makes it impossible to estimate visibility as accurately as at land stations. On a large ship, it is possible to make use of objects aboard the ship (for example, the foremast) for estimation when the visibility is very low, but it should be recognized that these estimates may be in error since the ship may affect the air. For the higher ranges, the appearance of the land when near the coast is a useful guide, and, if fixes can be obtained, the distance of landmarks, just as when they are appearing or disappearing, may be measured from the chart. Similarly, in open sea, when other ships are sighted and their distances known, for example, by radar, the visibility may be estimated. In the absence of other objects, the appearance of the horizon, as observed from different levels, may be used as a basis for the estimation. Although abnormal refraction may introduce errors into such methods of estimation, these methods are the only ones available in some circumstances. At night, the appearance of navigation lights can give a useful indication of the visibility.

When the visibility is not uniform in all directions it should be estimated or measured in the direction of least visibility and a suitable entry should be made in the log (excluding reduction of visibility due to the ship's exhaust).

Information about visibility meters is given in Chapter 9 of [Volume I](#) of the present Guide. Only those types of visibility meters which can be used with a baseline or light path short enough to be practicable on a ship are suitable. This is the case of forward-scatter meters. Unfortunately, the heating effect of the ship, and its exhaust, may lead to unrepresentative measurements.

4.2.2.12 **Precipitation**

The VOS do not normally report information on precipitation within coded reports on weather types (see [4.2.2.10](#)). However, precipitation measurements can be reported from fixed stations or vessels equipped with a precipitation gauge. The measurement of precipitation at sea is discussed in [Precipitation Measurements at Sea](#) (WMO-No. 124) and WMO (1981) and in the context of observations from research vessels by Bradley and Fairall (2006) and Weller et al. (2008), who also describe newer measurement systems, such as optical raingauges, not typically used for routine observations. As an aid to observers on ships, descriptions of precipitation at sea, for use in reporting present weather, are given in [Annex 4.B](#).

The complete measurement comprises the determination of both the amount and the duration of precipitation. The amount of precipitation should be measured with a raingauge adapted for use aboard a ship.

It is difficult to obtain reliable measurements of precipitation on board a ship, owing to the aerodynamic effect of the superstructure of the ship, the influence of roll and pitch, the capture of spray, and the changes in ship position. The equipment used on ships for the measurement of precipitation should be constructed and exposed in such a manner that the first three effects mentioned above are avoided or minimized as far as possible. For a shipboard raingauge, placing the instrument as far forward and as high as practicable seems to be most effective. However, other exposures may be found in particular cases to provide for easier management (Bradley and Fairall, 2006).

Precipitation measurements from ships “on station” (for example, light vessels or research vessels holding a near stationary position) are particularly valuable because the effect of ship speed is eliminated and the data can, thus, be included in climatological analyses without reduction. However, any problems of platform motion and salt contamination must still be considered.

Gimbal-mounted raingauge

The most common instrument used on board ships for the measurement of precipitation is the gimbal-mounted raingauge. This arrangement is not very effective, especially during bad weather, as it is not able to keep the gauge horizontal at all times. An efficient gimbal arrangement is very complicated and expensive and is used only aboard special ships. Generally, when a raingauge is used, a fixed installation with a remote measurement arrangement seems to be a better option.

Conical marine raingauge

The conical marine raingauge is normally fixed high up on a mast. A plastic tube leads the water to a remotely placed collector on the deck, or in the wheelhouse. This can be a useful device for measuring precipitation, provided that the installation precautions are taken into account. The raingauge orifice should be fixed in a plane parallel to the ship’s deck.

Recording raingauge

Several types of recording raingauges have been developed for use at sea. In one type, the collector is installed in the open while the recorder is mounted indoors. The rainwater is channelled along a pipe from the collector to a reservoir near the recorder. A pen linked to a float in the reservoir records the change of water level therein on a chart on a rotating drum. The reservoir is emptied automatically by a siphon when the total collected corresponds to 20 mm of rainfall.

In the electrical contact type of raingauge, the connection between the gauge and the recorder is made by electrical means. The rainwater caught by the collector is stored temporarily in a reservoir. After an amount corresponding to 0.5 mm of rainfall has been received, the rising surface touches a needle to close an electric circuit. A motor then closes the inlet valve and simultaneously opens a drain valve. After the water has drained away, the valves revert to their original state and a single pulse is sent to the recorder. Errors occur when the motion of the ship or buoy causes the water level to fluctuate rather than to rise steadily. This limitation can be overcome by using a peristaltic pump. This device drains a fixed quantity of water (rather than all the water available) each time the contact is made and, therefore, is less sensitive to fluctuations in water level; there are also no valves to maintain.

A third type of recording raingauge is a specifically designed ship raingauge that uses a horizontal and a vertical omnidirectional collector to allow for rainfall measurements at high wind speeds (Hasse et al., 1998). By measuring the amount of water that is collected by the vertical collector surface, a correction for the wind effect is possible by using the wind speed measured simultaneously at the site of the instrument. Rainfall intensities and amounts are measured and calculated separately for the top and the side collectors and corrected rainfall values are obtained as a wind-speed-dependent weighted average.

Optical disdrometer

Because of the inherent wind- and turbulence-induced undercatch problems with conventional gauges on board ships and their inability to measure snow, considerable effort went into developing optical distribution droplet meters (disdrometers). A comprehensive overview on existing instruments and measurement principles is provided by Michaelides (2008).

One of the biggest advantages of optical disdrometers over conventional gauges is their capacity for measuring the precipitation rate through particle size distributions, which, in the case of rainfall, is commonly referred to as the drop size distribution. An optical disdrometer for shipboard operation preferably has a cylindrical measurement volume that is homogeneously illuminated (that is, by an infrared light diode). Hydrometeors that pass through this volume cause a light extinction proportional to their cross sectional area. Typically hydrometeors are counted and sorted into size bins during an integration time, thus allowing derivation of rain, snow and mixed-phase precipitation occurrence, intensity and accumulation (Klepp, 2015).

Precipitation radar

The observation of precipitation by radar requires the use of narrow radar beams and calibrating raingauges together with the addition of specialized equipment to monitor the state of the radar and to apply corrections. Radars provided on board ships for other purposes do not have these features and their use for the quantitative observation of precipitation is not normal practice.

4.2.2.13 **Ocean waves**

The main topics of this section are the definitions and behaviour of waves and the visual methods of observing them. Automated methods are briefly mentioned in 4.3 on moored buoys, although they are also applied on other types of platforms.

4.2.2.13.1 **Definitions and descriptions of waves**

Fetch. Distance along a large water surface trajectory over which a wind of almost uniform direction and speed blows.

Wind wave or wind sea. Waves raised by the wind blowing in the immediate neighbourhood of an observation site at the time of observation.

Swell. Any system of water waves which has left its generating area (or observed when the wind field that generated the waves no longer exists).

Wavelength. Horizontal distance between successive crests or troughs. It is equal to the wave period multiplied by the wave speed.

Wave height. Vertical distance between the trough and crest of a wave.

Wave period. Time between the passage of two successive wave crests past a fixed point. It is equal to the wavelength divided by the wave speed.

Wave speed. The distance travelled by a wave in a unit of time. It is equal to the wavelength divided by the wave period.

The observation should include the measurement or estimation of the following characteristics of the wave motion of the sea surface in respect of each distinguishable system of waves, namely sea and swell (principal and secondary):

- (a) Direction (from which the waves come) on the scale 01–36 as for wind direction (see Chapter 5 of [Volume I](#) of the present Guide);
- (b) Period in seconds;
- (c) Height.

The following methods of observing wave characteristics of separate wave systems should be used as a guide.

Wind-generated ocean waves occur in large systems which are defined in connection with the wind field that produced the waves and also with the relative position of the point of observation. Bearing in mind the distinction between sea and swell, the observer should differentiate between the recognizable wave systems on the basis of direction, appearance and period of the waves.

Figure 4.1 shows a typical record drawn by a wave-height recorder. It shows the height of the sea surface above a fixed point against time, namely it represents the up-and-down movement of a floating body on the sea surface as it is seen by the observer. It gives a representation of the sea surface in its normal appearance when it is stirred by the wind to form a wind wave.

Waves invariably travel in irregular groups with areas of slight wave development of two or more wavelengths between the groups. The irregularity is greater in the wind wave than in a swell. Furthermore, and this cannot be shown by a wave record, groups consisting of two or more well-formed waves in the sea can be seen to travel in directions which may differ as much as 20° or 30° from each other; as a result of interference of crossing waves, the crests of sea waves are rather short. Swell waves have a more regular appearance. These waves travel in a rather regular

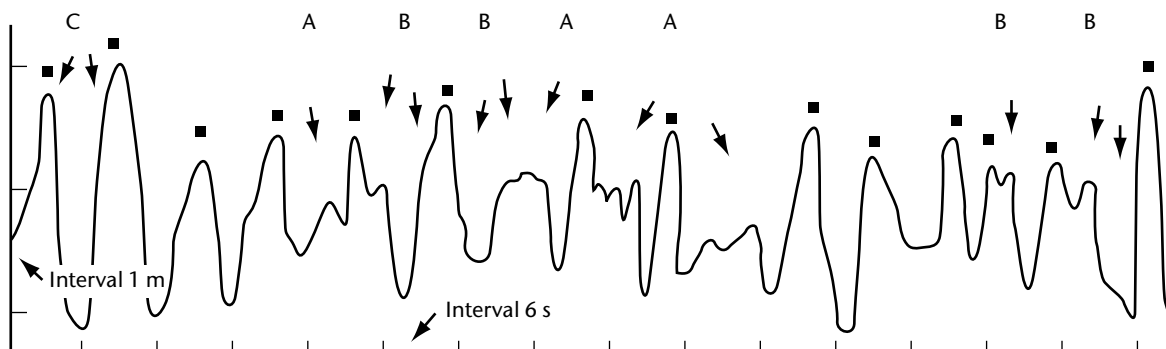


Figure 4.1. Typical sea and swell waves as shown by a wave-height recorder

succession and well-defined direction with generally long and smooth crests. Undisturbed typical swell waves may be observed in areas where there has been little or no wind over a period of several hours to a day or more. In most areas, sea and swell are intermixed.

4.2.2.13.2 Visual observations from ships

In trying to observe the wave characteristics of each of the recognizable wave systems (sea and swell) separately, the observer should be aware of the fact that the higher components of a wind wave resemble swell waves by their comparatively long crests and large periods. It may seem possible to split the assembly of waves of different heights, periods and directions (together forming the system of a wind wave) into two different waves systems and consider the smaller waves as wind waves and the larger waves as swell, but this may not be correct.

The distinction between wind waves and swell should be made on the basis of one of the following criteria:

Wave direction. If the mean direction of all waves of more or less similar characteristics (in particular, height and length) differs by 30° or more from the mean direction of waves of different appearance (in particular, height and/or length), the two sets of waves should be considered to belong to separate wave systems.

Appearance and period. When typical swell waves, characterized by their regular appearance and long crestedness, arrive approximately, namely within 20° , from the direction of the wind, they should be considered as a separate wave system if their period is at least 4 s greater than the period of the larger waves of the existing wind wave.

For measuring the mean period and height of a wave system, significant waves should be considered only; these are the higher waves in the centre of each group of well-formed waves (Figure 4.1). The flat and badly formed waves (A) in the area between the groups must be omitted from the record.

The mean period and the mean height of approximately 15 to 20 well-formed waves from the centres of the groups is actually required; of course, these waves cannot be consecutive. The smaller wave-like disturbances (B) which can be seen clearly to be forming under the action of the wind on top of the larger waves are also to be omitted from the record.

Occasionally, waves may be encountered which literally stand out above the normal waves (C). Such waves may occur singly or in a group of two or three. The observer should not concentrate on these maximum waves only; in order to arrive at a measure for the mean period and mean height of about 15 to 20 waves, he or she should also consider groups of well-formed waves of medium height. Consequently, the reported wave height will be smaller than the maximum height obtained by the observed waves. On average, the actual height of 1 out of about 10 waves will exceed the height to be reported. It is common practice to define the significant wave height measured by wave height recorders as the average height of the highest one third of the waves; it should approximate the wave height, which would be estimated by a manual observer.

The observer must bear in mind that only measurements or quite good estimates are to be recorded. Rough guesses have little value. The quality of the observations must have priority over their quantity. If only two, or even only one, of the three elements (direction, period and height) could be measured, or really well estimated, for example, at night, the report would still be of value.

The above considerations must be taken into account in all methods of observation described below. More details on waves are provided in the [Guide to Wave Analysis and Forecasting](#) (WMO-No. 702) and 4.3.4 to 4.3.6 of this chapter.

The direction from which the waves are coming is most easily found by sighting along the wave crests and then turning 90° to face the advancing waves. The observer is then facing the direction in which the waves are coming.

The recommended procedures for the reporting of swell by manually reporting ships are found in [Annex 4.C](#).

Wave period

If a stop-watch is available, only one observer is necessary; otherwise, two observers and a watch with a second hand are required. The observer notes some small object floating on the water at some distance from the ship: if nothing is available, a distinctive patch of foam can usually be found which remains identifiable for the few minutes required for the observations. The watch is started when the object appears at the crest of the wave. As the crest passes, the object disappears into the trough, then reappears on the next crest, and so forth. The time at which the object appears to be at the top of each crest is noted. The observations are continued for as long as possible; they will usually terminate when the object becomes too distant to identify, on account of the ship's motion. Obviously, the longest period of observation will be obtained by choosing an object initially on the bow as far off as it can be clearly seen.

Another method is to observe two or more distinct consecutive periods from an individual group while the watch is running continuously; with the passage of the last distinct crest of a group or the anticipated disappearance of the object, the watch is stopped, then restarted with the passage of the first distinct crest of a new group. The observer keeps count of the total number of periods until it reaches at least 15 or 20.

Observations can also be made by watching the pitch and roll of the ship's bow. The observer picks the point which is at the highest or lowest in the cycle and starts the timer from there. When it returns to the same point, the observer records the time. By repeating this process several times, a reliable observation can be determined. This also works during night-time observation for which the observer feels the rise and fall within his or her body.

With observations of a period less than 5 s and low wind velocity, the above observation may not be easily made, but such waves are less interesting than those with longer periods.

Wave height

With some experience, fairly reliable wave height estimates can be made. For estimating the height of waves having wavelengths much shorter than the ship, the observer should take up a position as low down in the ship as possible, preferably amidships where the pitching is least, and on the side of the ship from which the waves are coming. Use should be made of the intervals which occur every now and then, when the rolling of the ship temporarily ceases.

In cases of waves longer than the ship, the preceding method fails because the ship as a whole rises over the wave. Under these circumstances, the best results are obtained when the observer moves up or down in the ship until, when the ship is in the wave trough and upright, the oncoming waves appear just level with the horizon (Figure 4.2). The wave height is then equal

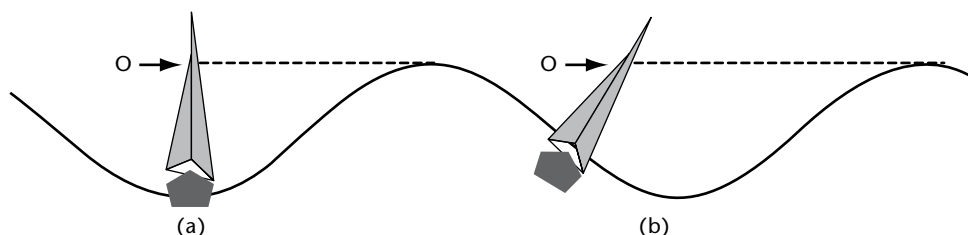


Figure 4.2. The effect of the ship's roll on the estimation of wave height

to the height of the observer above the level of the water beneath him or her (a). If the ship is rolling, care should be taken to ensure that the approaching wave is in line with the horizon at the instant when the ship is upright, otherwise the height estimate will be too large (b).

By far the most difficult case is that in which the wavelength exceeds the length of the ship, but the wave height is small. The best estimate of height can be obtained by going as near to the water as possible, but even then the observation can be only a rough estimate.

4.2.2.13.3 Waves in coastal waters

The following are additional definitions applying to sea surface in coastal waters:

Breaker. The collapse of a whole wave resulting from its running into very shallow water, of a depth of the order of twice the wave height.

Surf. The broken water between the shoreline and the outermost line of the breakers.

Breaking sea. The partial collapse of the crest of a wave caused by the action of the wind; steepening of waves due to their encountering a contrary current or tidal stream; or steepening of waves due to their running into shoal water not shallow enough to cause a breaker.

Wave observations made from a coastal station cannot be expected to be representative of conditions in the open sea. This is because the waves are affected by the depth of the water, by tidal influence and by reflection from objects such as steep rocks and jetties. In addition, the location may be sheltered by headlands or, less obviously, by shoals, both of which may affect the height and direction of travel. An extensive account of these phenomena is given in [The Accuracy of Ship's Meteorological Observations: Results of the VSOP-NA](#) (WMO/TD-No. 455).

When observations are to be made despite these difficulties, the waves should be chosen in the same way as at sea. If they are required for wave research, the exact mean depth of water at the time of observation and the time itself should both be stated.

4.2.2.13.4 Terminology for sea and swell waves

The following terminology is recommended for uses other than the inclusion in coded messages, such as supplying weather information and forecasts for shipping, publications, pilots, and so on:

For the length of swell waves:

Short	0–100 m
Average	100–200 m
Long	over 200 m

For the height of swell waves:

Low	0–2 m
Moderate	2–4 m
Heavy	over 4 m

For the height of sea waves:

Calm (glassy)	0 m
Calm (rippled)	0–0.1 m
Smooth (wavelets)	0.1–0.5 m
Slight	0.5–1.25 m

Moderate	1.25–2.5 m
Rough	2.5–4 m
Very rough	4–6 m
High	6–9 m
Very high	9–14 m
Phenomenal	over 14 m

In all cases, the exact bounding length or height is included in the lower category, namely a sea of 4 m is described as rough. When the state of the sea surface is so confused that none of the above descriptive terms can be considered appropriate, the term “confused” should be used.

4.2.2.14 **Ice**

Several forms of floating ice may be encountered at sea. The most common is that which results from the freezing of the sea surface, namely sea ice. The reporting of sea ice is discussed in [WMO Sea-ice Nomenclature](#) (WMO-No. 259).

The other forms are river ice and ice of land origin. River ice is encountered in harbours and estuaries where it is kept in motion by tidal streams and normally presents only a temporary hindrance to shipping. Ice of land origin in the form of icebergs is discussed separately below.

Both icebergs and sea ice can be dangerous to shipping and always have an effect on navigation. Sea ice also affects the normal processes of energy exchange between the sea and the air above it. The extent of sea-ice cover can vary significantly from year to year and has a great effect both on adjacent ocean areas and on the weather over large areas of the world. Its distribution is therefore of considerable interest to meteorologists and oceanographers. Broad-scale observations of the extent of sea-ice cover have been revolutionized by satellite photography, but observations from shore stations, ships and aircraft are still of great importance for detailed observations and for establishing the ground truth of satellite observations.

At present, observations of floating ice depend almost entirely on visual estimation. The only instrumental observations of floating ice are carried out by conventional radar and techniques such as passive microwave sensors or sideways-looking airborne radar. However, icebergs are poor reflectors of radar energy and cannot always be detected by this means.

4.2.2.14.1 **Observations of ice accretion**

Ice accretion can be extremely hazardous because of its effects on small ships, particularly on vessels of less than approximately 1 000 gross tonnage. Even on larger ships, it can cause radio and radar failures due to the icing of aeriels. Visibility from the bridge may also be affected. Problems have occurred due to icing on the deck cargoes of large container ships. Apart from its possible effect on stability, it may cause difficulty in unloading cargo at the port of destination when containers and their lashings are frozen solidly to the deck. Fishing vessels are particularly vulnerable to ice accretion. Further information is given in [The Accuracy of Ship's Meteorological Observations: Results of the VSOP-NA](#) (WMO/TD-No. 455), while a detailed consideration of the meteorological aspects appears in [The Meteorological Aspects of Ice Accretion on Ships](#) (WMO-No. 397).

There are two main types of icing at sea: icing from seawater and icing from freshwater. Icing from seawater may be due either to spray and seawater thrown up by the interaction between the ship or installation and the waves, or to spray blown from the crests of the waves, or both. Icing from freshwater may be due to freezing rain and/or drizzle, or occasionally when the occurrence of wet snow is followed by a drop in temperature, or it may be due to freezing fog. Both types may occur simultaneously.

The most important meteorological elements governing ice accretion at sea are wind speed and air temperature. The higher the wind speed relative to the ship and the lower the air temperature, the greater the rate of ice accretion. There appears to be no limiting air temperature below which the icing risk decreases.

Provision is made in the WMO code form for ships (*Manual on Codes* (WMO-No. 306), [Volume I.1](#) and [Volume I.2](#)), used for radio weather reports from ships at sea, for the inclusion of reports of ice accretion. This may be done either in code or in plain language. The coded form, in a single five-figure group, provides for reports of the cause of icing, the ice thickness and the rate of accretion. Plain-language reports must be preceded by the word ICING and are particularly encouraged for indicating features of the icing which are dangerous to vessels.

4.2.2.14.2 Formation and development of sea ice

Ice less than 30 cm thick

The first indication of ice formation is the appearance of small ice spicules or plates in the top few centimetres of the water. These spicules, known as frazil ice, form in large quantities and give the sea an oily appearance. As cooling continues the frazil ice coalesces to form grease ice, which has a matt appearance. Under near-freezing, but as yet ice-free, conditions, snow falling on the surface may result in the sea surface becoming covered by a layer of slush. These forms may be regrouped by the action of wind and waves to form shuga and all are classified as new ice. With further cooling, sheets of ice rind or nilas are formed, depending on the rate of cooling and on the salinity of the water. Ice rind is formed when water of low salinity freezes into a thin layer of brittle ice which is almost free of salt, whereas when water of high salinity freezes, especially if the process is rapid and the wind is very light, the ice has an elastic property which is characteristic of nilas. The latter form of ice is subdivided, according to its thickness, into dark and light nilas; the second, more advanced form reaches a maximum thickness of 10 cm.

The action of wind and waves may break up ice rind or nilas into pancake ice, which can later freeze and thicken into grey ice and grey-white ice, the latter attaining a thickness of up to 30 cm. These forms of ice are referred to collectively as young ice. In rough conditions this ice may be broken up into ice cakes or floes of various sizes.

Ice 30 cm to 2 m thick

The next stage of development is known as first-year ice and is subdivided into thin, medium and thick categories. Thin first-year ice has a thickness of 30 to 70 cm. Medium first-year ice has a range of thickness from 70 to 120 cm. In polar areas, thick first-year ice may attain a thickness of approximately 2 m at the end of the winter.

Old ice

Thick first-year ice may survive the summer melt season and is then classified as old ice. This category is subdivided into second-year ice or multi-year ice, depending on whether the floes have survived one or more summers. The thickness of old ice is normally in the range of 1.2 to 3 m or more before the onset of the melt season. Towards the end of the summer melt season, old ice may be considerably reduced in thickness. Old ice may often be recognized by a bluish surface, in contrast to the greenish tint of first-year ice.

Snow cover

During winter, ice is usually covered with snow which insulates it from the air above and tends to slow down its rate of growth. The thickness of the snow cover varies considerably from region to region as a result of differing climatic conditions. Its depth may also vary considerably within very short distances in response to variable winds and to ice topography.

Decay of sea ice

While the snow cover persists, almost 90% of the incoming radiation is reflected back into space. Eventually, however, the snow begins to melt as air temperatures rise above 0 °C in early summer, and the resulting freshwater forms puddles on the surface. These puddles absorb approximately 90% of the incoming radiation and rapidly enlarge as they melt the surrounding snow or ice. Eventually, the puddles penetrate to the bottom surface of the floes and are known as thaw holes. This slow decay process is characteristic of ice in the Arctic Ocean and seas where movement is restricted by the coastline or islands. Where ice is free to drift into warmer waters (for example, the Antarctic, East Greenland and the Labrador Sea), decay is accelerated in response to wave erosion as well as warmer air and sea temperatures.

Movement of sea ice

Sea ice is divided into two main types according to its mobility. One type is drift ice, which is continually in motion under the action of the wind and current; the other is fast ice, attached to the coast or islands, which does not move. When ice concentration is high, namely seven tenths or more, drift ice may be replaced by the term “pack ice”.

Wind stress in the drift ice causes the floes to move in an approximately downwind direction. The deflecting force due to the Earth's rotation (Coriolis force) causes the floes to deviate about 30° to the right of the surface wind direction in the northern hemisphere. Since the surface wind is itself deviated by a similar amount but in the opposite sense from the geostrophic wind (measured directly from isobars), the direction of movement of the ice floes, due to the wind drift alone, can be considered to be parallel to the isobars.

The rate of movement due to wind drift varies not only with the wind speed, but also with the concentration of the drift ice and the extent of deformation (see subsection below). In very open ice (1/10–3/10) there is much more freedom to respond to the wind than in close ice (7/10–8/10), where free space is limited. Two per cent of the wind speed is a reasonable average for the rate of ice drift caused by the wind in close ice, but much higher rates of ice drift may be encountered in open ice. Since it is afloat, a force is exerted on drift ice by currents that are present in the upper layers of the water, whether these are tidal in nature or have a more consistent direction due to other forces. It is usually very difficult to differentiate between wind- and current-induced ice drift, but in any case, where both are present, the resultant motion is always the vector sum of the two. Wind stress normally predominates, particularly in offshore areas.

Deformation of sea ice

Where the ice is subject to pressure, its surface becomes deformed. On new and young ice, this may result in rafting as one ice floe overrides its neighbour; in thicker ice, it leads to the formation of ridges and hummocks according to the pattern of the convergent forces causing the pressure. During the process of ridging and hummocking, when pieces of ice are piled up above the general ice level, large quantities of ice are also forced downward to support the weight of the ice in the ridge or hummock. The draught of a ridge can be three to five times as great as its height, and these deformations are major impediments to navigation. Freshly formed ridges are normally less difficult to navigate than older weathered and consolidated ridges.

4.2.2.14.3 Icebergs

Icebergs are large masses of floating ice derived from glaciers, including ice shelves. The depth of a berg under water, compared with its height above, varies widely with different shapes of bergs. The underwater mass of an Antarctic iceberg derived from a floating ice shelf is usually less than the underwater mass of icebergs derived from Greenland glaciers. A typical Antarctic tabular berg, of which the uppermost 10 to 20 m is composed of old snow, will show one part of its mass above the water to five parts below. However, the ratio for an Arctic berg, composed almost wholly of ice with much less snow, is typically 1:8.

Icebergs diminish in size in three different ways: by calving, melting and wave erosion. A berg is said to calve when a piece breaks off; this disturbs its equilibrium and as a result it may drift at a different angle or capsize. Large underwater projections, which may be difficult to observe, are a usual feature of icebergs. In cold water, melting takes place mainly on the water-line, while, in warm water, a berg melts mainly from below and calves frequently. It is particularly dangerous to approach a berg melting in warm water for it is unstable and may fragment or overturn at any time. There are likely to be many growlers and bergy bits around rapidly disintegrating icebergs, thus forming a particular hazard to navigation.

Bergs are poor reflectors of radar energy and cannot always be detected by this means. Their breakdown fragments (bergy bits and growlers) are even more difficult to detect with a ship's radar since they are often obscured by the background clutter from waves and swell. These smaller fragments are especially dangerous to shipping. Despite their low profile, they contain sufficient mass to damage a vessel which comes into contact with them at normal cruising speed. Some growlers consisting of pure ice hardly break the sea surface and are extremely difficult to detect.

4.2.2.14.4 Observations of sea ice and icebergs

The key to good ice observing lies in familiarity with the nomenclature and experience. [WMO Sea-ice Nomenclature](#) (WMO-No. 259), with its illustrations, is the best guide to the mariner for ice identification.

The four important features of sea ice which affect navigation are as follows:

- (a) Thickness: the stage of development (that is, new ice, young ice, first-year ice or old ice and their subdivisions);
- (b) Amount: concentration (estimated according to the tenths of the sea surface covered by ice);
- (c) The form of the ice, whether it is fast or drift ice and the size of the constituent floes;
- (d) Movement: particularly with regard to its effect on deformation.

Since icebergs represent such a hazard to navigation, particularly at night or in poor visibility, it is also important to report the number of icebergs in sight at the time of the observation, especially in waters where they are less frequently observed.

Sea ice can be reported in plain language or by the use of codes. WMO has adopted two sea-ice codes for international use. The simplest is the ICE group appended to the SHIP code format. The Ice Analysis (ICEAN) code has been developed for specialist use for the transmission of sea-ice analysis and prognoses.

There are two basic rules for observation from ships and shore stations:

- (a) Obtain a large field of view by making the observation from the highest convenient point above the sea surface (for example, the top of a lighthouse, the bridge or crow's nest of a ship);
- (b) Do not attempt to report sea-ice conditions beyond a radius of more than half the distance between the point of observation and the horizon.

WMO has developed a set of symbols for use on maps depicting actual or forecast sea-ice conditions. These symbols are intended for the international exchange of sea-ice information and for radio-facsimile transmission of ice data.

4.2.2.15 **Observations of special phenomena**

Marine observers can make reports of natural phenomena using either traditional or some electronic logbooks. However, such special observations cannot normally be circulated over the GTS owing to international format limitations. The observations can take the form of written descriptions, sketches or photographs, or a combination. A wide range of phenomena can be reported, including:

- (a) Astronomical phenomena (for example, eclipses, comets, zodiacal light, sunspots and novae);
- (b) Phenomena of the high atmosphere (for example, high-frequency radio fadeouts or blackouts, magnetic disturbances and storms, airglow, aurorae, meteors and fireballs, and noctilucent clouds);
- (c) Phenomena of the lower atmosphere (for example, abnormal refraction and mirages, glory or brocken spectres, coloured suns and moons, coronae, St Elmo's fire, crepuscular rays, dustfall, the green flash, halo phenomena, iridescent cloud, lightning, rainbows, scintillation, unusual sky colouration and waterspouts). Note that when describing waterspouts, the direction of rotation should always be given as if seen from above;
- (d) Sightings of marine mammals, birds, fish, invertebrates and mass plankton effects such as bioluminescence, red tides and discoloured water;
- (e) Other marine phenomena (for example, abnormal occurrences of compass deviations, changes in sea level or waves).

National publications, or information provided with electronic logbooks, provide information about the kinds of phenomena that are of interest and the information that is required for reporting particular types of phenomena.

4.3 **MOORED BUOYS**

Moored buoys come in a wide variety of configurations (for example, in terms of mooring design, sensor types, sampling schemes, mounting techniques and telemetry) serving a wide variety of operational and research applications and disciplines. This section, which does not reflect the wide variety of currently functioning systems, focuses on the requirements for marine meteorological measurements from operational metocean moored buoys. Information regarding other systems addressing the requirements for other applications and research can be found in other publications (for example, Bradley and Fairall, 2006) and websites:

- JCOMMOPS: <http://www.jcommops.org/>
- ATLAS tropical moored buoys: http://www.pmel.noaa.gov/tao/proj_over/mooring.shtml
- Ocean Climate Stations: <http://www.pmel.noaa.gov/OCS/>
- TRITON tropical western Pacific moored buoys: http://www.jamstec.go.jp/jamstec/TRITON/real_time/php/top.php
- Global Tropical Moored Buoy Array: <https://www.pmel.noaa.gov/gtmba/>
- OceanSITES reference moored buoys: <http://www.oceansites.org>
- Tsunami buoys: <http://www.ndbc.noaa.gov/dart/dart.shtml>
- Wave buoys: <https://community.wmo.int/activity-areas/Marine/WME>

More recent Indian Ocean m-TRITON moored buoys:

- <http://www.jamstec.go.jp/iorgc/iomics/index.html>

A typical metocean moored buoy is equipped with sensors to measure the following variables:

- Wind speed;
- Wind direction;
- Atmospheric pressure;
- SST;
- Wave height and period;
- Air temperature;
- Dew-point temperature or RH.

Additional elements measured by some moored buoys may include:

- Maximum wind gust;
- Wave spectra (directional or non-directional);
- Solar radiation (downward short-wave radiation);
- Surface current or current profiles;
- Surface salinity;
- Subsurface temperature and salinity down to 500 m or 750 m;
- Atmospheric visibility;
- Precipitation;
- Surface CO₂ concentration;
- Ocean surface pH;
- Photosynthetically active radiation;
- Fluorescence and turbidity;
- Water quality parameters.

For waves, the following variables are generally measured or estimated using the following definitions (see also 4.2.2.13 to complement these definitions):

Significant wave height. Estimate of the average height of the one-third highest waves;

Maximum wave height. The maximum single wave height which is observed in a certain time period;

Mean zero crossing wave period. The wave period corresponding to the number downward zero-crossing of the surface elevation. It can also be estimated from the second frequency moment of the wave energy spectrum;

Peak height. The wave height corresponding to the peak of the wave energy spectrum (the part of the spectrum with the highest wave energy);

Peak period. The wave period corresponding to the peak height of the wave energy spectrum;

Spectral wave period. The wave period corresponding to the mean frequency of the spectrum.

In addition to the meteorological and oceanographic measurements, it is necessary to monitor buoy locations to identify when they go adrift so that the appropriate authorities can be notified so that they do not provide a hazard to shipping. It is also useful to monitor various housekeeping and engineering parameters to aid data quality control and maintenance. Moored buoy technology has now matured to the extent that it is possible to maintain a buoy on station for as long as two years, even in the most severe conditions. Operational life is largely determined by the life of the sensors, with sensor exchanges often carried out at 12 to 24 month intervals. General practices to minimizing fouling in buoy systems include using copper tape and zinc oxide paste on instruments every 24 months.

The observations from moored buoys are now considered to be better quality than ship observations with regard to the accuracy and reliability of measurements (Wilkerson and Earle, 1990; Ingleby, 2010). Indeed, moored buoys are generally regarded as providing the highest quality observations of a wide range of marine meteorological variables and, in addition to their use by forecasters and assimilation into NWP models, the data are also used to provide information on the climatology of oceanic areas, “ground truth” reference data for satellite calibration/validation and estimates of surface fluxes (for example, Bourras, 2006).

Recently established moored buoy networks have a suite of subsurface measurements for better understanding of air–sea interaction.

Reliable performance is the key requirement for instruments used in offshore moored buoys for cyclone monitoring, as sensors that underperform can have a serious impact on societal protection, and in addition lead to costly repair and reinstalls. Recent developments in instrument selection and application practices based on the experiences of the global scientific community have improved their performances at sea (Venkatesan et al., 2015).

Typical measurement uncertainties obtained from operational metocean buoys are as follows:

Wind speed	1 m s ⁻¹ or 5% above 20 m s ⁻¹
Wind direction	10°
Air temperature	0.2 °C
Sea-level pressure	0.2 hPa
SST	0.2 °C
Dew-point temperature	0.5 °C
Significant wave height	10% or 0.2 m
Wave direction	10°
Wave period	1 s

The standard suite of sensors on operational metocean moored buoys measure wind speed, peak gust (for example, 3 to 5 second gust depending on national requirements), wind direction, barometric pressure, air temperature, water temperature, and significant wave height and peak (or average) wave period. Some buoys also measure (directional or non-directional) wave energy spectra.

4.3.1 **Atmospheric pressure**

Atmospheric pressure and its variability in both time and space are crucially important for NWP and for analysis and forecasting. Most buoys measure atmospheric pressure by means of digital barometers (see Chapter 3 of [Volume I](#) of the present Guide). The following pressure measurements are made:

- (a) Station pressure is the actual measurement made by the barometer on the moored buoy in hPa. In some cases two barometers may be used and their values averaged.
- (b) Sea-level pressure is the pressure reduced to sea level from the measurement height in units of hPa. For moored buoys deployed at sea this is very close to the station pressure. However, there can be a large difference between sea-level pressure and station pressure from buoys deployed in lakes at high elevations. The conversion to sea-level pressure is made using the procedures described in WBAN (United States Weather Bureau, 1963).

Many buoys that are deployed in regions subject to hurricanes or intense low-pressure systems have the capability of measuring supplemental one-minute average pressure data. These data are recorded after the hourly pressure data fall below a predetermined threshold (for example, 1 008 hPa in the tropics). The semi-diurnal pressure variation could be used for detection of cyclone. Air pressure exhibits two peaks and two low values in a day, and the highest and the lowest pressure values are almost repeated at the same time during the semi-diurnal oscillations. The reduction in semi-diurnal oscillation during a cyclone passage could be utilized in detecting a cyclone/low-pressure system. This method can improve the cyclone detection algorithm.

Supplemental pressure data are identified as follows:

- (a) The minimum one-minute barometric pressure in hPa from the primary (and secondary, if one is installed) barometer is the minimum one-minute mean barometric pressure for the entire hour;
- (b) The time is the minute within the hour that the minimum pressure occurred.

Wind can often cause dynamic changes of pressure which affects the reading of barometer. The inlet port of the barometer should be placed at location with minimal effect of wind. The barometric pressure is generally measured from the inlet port located at 3 m from the sea surface.

4.3.2 **Wind measurements**

Wind measurements are one of the most important measurements made from moored buoys. They are essential for the marine weather forecaster.

Definitions:

Wind direction. The direction from which the wind is blowing in degrees clockwise from true north. It is a unit vector average of the record of wind direction.

Wind speed. The scalar average of the wind speed over the sampling (usually a standard 10-min) period.

Wind speed maximum. The highest wind speed in the wind record. Gusts are determined from the highest running mean of the record over a short time interval (for example, 5 s).

The wind measurements are generally made by a propeller-vane or a cup anemometer and a wind vane. To avoid mechanical wear, ultrasonic wind speed and direction sensors with no moving parts are now commonly used on moored buoys where the wind direction measurement is normally associated with a compass bearing so the direction relative to the buoy can be

corrected to true. The wind sensor height will vary for different sized buoys so it is important that the sensor height (3 m above MSL) is reported in the BUFR (TM3-15-008) data exchanged on GTS so that users can derive the equivalent 10 m wind speed.

Four-blade, impeller-driven wind-vane sensors on meteorological moorings are typically used in some moored buoy networks. The final measurements are statistical estimates of the wind from time series of instantaneous wind samples taken at a minimum rate of 1 Hertz (Hz) over a particular length of time. The sampling rate is a function of the payload. Most moored buoys use an 8 min acquisition period. The standard wind measurements are produced each hour.

Some networks have their meteorological moored buoys perform statistical processing at the end of an acquisition period, and the output message is updated with the new statistics and six 10 min segments. Statistical processing includes the calculation of the mean for both direction and speed and the standard deviation of the speed. The hour's data do not represent data from minute 0 to min 59. Rather, these represent the latest, complete six 10 min segments before the end of the last acquisition. The 10 min segments are, however, bounded by minutes 0, 10, 20, and the like.

For the moored buoys of some networks the wind measurements are made at 3 m or 4 m, and wind speeds at 10 and 20 m above site elevation are derived from an algorithm (Liu et al., 1979) that uses the height of the anemometer, the wind speed, a constant RH of 85%, a constant sea-level pressure of 1 013.25 hPa, and the air and water temperature. If either the air or water temperature is unavailable, then the neutral stability is assumed, taking into account that neutral stability can introduce an error of up to 5%. If both are missing then neither 10 nor 20 m wind speeds are determined.

Some countries operating moored buoys have traditionally used a cup anemometer and a self-referencing wind vane to measure the speed and direction over a 10-min acquisition period prior to the top of each hour. However, during operation, saltwater permeates the seals and eventually failure of the instruments occurs when salt crystals form in the lubricant leading to mechanical failure of the moving parts. These have now been replaced with a new wind system utilizing a sonic anemometer and electronic compass. To further improve reliability, many moored buoys have dual wind systems to provide increased resilience in the event of anemometer failure (Turton and Pethica, 2010).

4.3.3 **Temperature**

Temperature is one of the basic meteorological measurements. Electronic thermistors are generally used to make all temperature measurements which are provided in degrees Celsius (°C). Temperature measurements can also be used for deriving sea-level pressure and standard-height wind speed from non-standard height atmospheric pressure and wind measurements, respectively.

4.3.3.1 ***Air temperature***

Air temperature measurements are generally very reliable; however, it is important to note that the physical position of temperature sensors can adversely affect measurements. Air temperature housings can lead to non-representative readings in low wind conditions (National Data Buoy Center (NDBC), 2003a). Air temperature is sampled at some rate during the sampling period (typically 1 Hz or 0.1 Hz). Air temperature is generally measured along with RH and the resolution is 0.1 °C. Some buoy operators also use high-resolution temperature sensors with resolution of the order of 0.000 1 °C. These are primarily used for underwater applications.

4.3.3.2 **Water temperature**

While there are generally few problems with water temperature measurements, it should be noted that the depth of water temperature sensors varies with buoy hull, and that the temperature probes on buoys are often attached to the inside of the hull. Since buoy hulls are highly thermally conducting, the temperatures measured may reflect the average temperature of the water around the submerged hull rather than the temperature of the water nearest the probe. In highly stratified water, especially during afternoon hours in calm wind conditions, the water temperature reported from a buoy may be 2 °C to 3 °C below the SST of the water. This value may also be biased due to biofouling. Most of the sensors for long-term underwater temperature measurement offer high resolution of the order of 0.000 1 °C. The temperature values indicated by other sensors such as current meters mounted at different locations can be compared for better estimation. The International Temperature Scale-90 is generally followed for water-temperature measurement.

4.3.4 **Ocean wave estimates**

Sea-state estimates are probably the most complex measurements made from moored buoys and are extremely important to marine forecasters, mariners, ocean engineers and scientists. On a buoy, all of the basic wave measurements are derived in some way from the time series of the buoy's motion. Complete details on wave measurements made by NDBC of the National Oceanic and Atmospheric Administration (NOAA) are provided in NDBC (2003a, 2003b, 2009).

Sea state is a description of the properties of sea-surface waves at a given time and place. This might be given in terms of the wave spectrum, or more simply in terms of the significant wave height and some measure of the wave period (AMS, 2000). Many moored buoys provide a measurement of the spectral variance density (Frigaard et al., 1997), which will be referred to as spectral wave density. Most buoys derive all non-directional wave parameters, heights and periods, steepness, and so on, from spectral wave densities. Furthermore, many buoys measure the spectral directional components defined by the mean wave direction, the spread, skewness and kurtosis defining the four Fourier coefficients (functionally related to each frequency) that centres disseminate through the WMO moored buoy BUFR Template TM 315008 (see the [Manual on Codes](#) (WMO-No. 306)).

4.3.5 **Non-directional ocean wave estimates**

Most buoys use accelerometers or motion sensors to measure buoy heave motion. The sensors are fixed to remain vertical relative to the hull or stabilized parallel to the earth vertical and the vast majority of ocean wave measurements are made in this way. Vertical stabilization, when used, is achieved through use of heave, pitch and roll sensors whose reference plane is mounted on a gravity-stabilized platform and provides for a natural period in the order of 40 s. This type of equipment is expensive and has a built-in mechanical system for keeping the accelerometer vertical as the buoy and sensor tilt.

Operational non-directional wave measurement systems report estimates of acceleration or displacement spectra. If not directly reported, displacement spectra are derived from acceleration spectra as part of the calculations involved in the shore-side processing of the wave data. From these spectra, average wave period, dominant wave period, significant wave height, and steepness are calculated. These non-directional wave parameters are defined as follows.

Average wave period, in seconds, can be computed in different ways. It can be such that it corresponds to the wave frequency that divides the wave spectrum into equal areas or it can be based on the second frequency moment of the non-directional spectral density. It can also be estimated using a zero crossing method.

Dominant wave period or peak wave period, in seconds, is the wave period corresponding to the centre frequency of the frequency band with the maximum non-directional spectral density.

Significant wave height, H_{m0} , is estimated from the variance of the wave displacement record obtained from the displacement spectrum according to following equation:

$$H_{m0} = 4 \left[\int_{f_l}^{f_u} S(f) df \right]^{\frac{1}{2}}$$

where $S(f)$ is the spectral density of displacement; df is the width of the frequency band; f_u is the upper frequency limit; and f_l is the lower frequency limit.

4.3.6 Directional ocean wave estimates

Directional wave measurement systems require, in addition to the measurement of vertical acceleration or heave (displacement), buoy azimuth, pitch and roll. These allow east-west slope and north-south slope to be computed. Most buoys use several different methods and sensor suites for the measurement of these angles.

It is recommended (Swail et al., 2010a; Swail et al., 2010b) that in order to serve the full range of users, directional spectral wave measuring systems should reliably estimate the so-called “First 5” standard. Technically, this refers to five defining variables at a particular wave frequency (or wave period). The first variable is the wave energy, which is related to the wave height, and the other four are the first four coefficients of the Fourier series that estimates the infinite series describing the directional distribution of that energy. At each frequency band, not only is the wave direction defined but also the spread (second moment), skewness (third moment) and kurtosis (the fourth moment). The skewness resolves how the directional distribution is concentrated (to the left or right of the mean) and the kurtosis defines the peakedness of the distribution. Obtaining these three additional parameters (spread, skewness and kurtosis) for each frequency band yields an improved representation of the wave field.

Wave measurements from moored buoys are also used to evaluate and validate wave measurements derived from high-frequency and X-band radar instruments and space-based instruments.

4.3.7 Water-column height for tsunami detection

Most buoy tsunameters report water level (actually water-column height) based on pressure and temperature measurements made at the sea floor and converted to a water-column height by multiplying the pressure by a constant 670 mm per pound per square inch absolute.

4.3.8 Relative humidity

Humidity sensors used by buoys employ a circuit that measures humidity through the change in capacitance of a thin polymer as it is exposed to variations in water vapour. A gas-permeable membrane protects the electronic parts from spray and particulate matter but allows air to enter the instrument housing. The sensor is temperature-sensitive and incorporates a temperature probe to provide a temperature correction in the calculation of RH.

4.3.9 Ocean sensors

To understand and predict the ocean, its properties must be monitored. Many buoys help to monitor the ocean by also measuring surface currents, ocean current profiles, near-surface temperature and water quality parameters. Included in the water quality parameters can be turbidity, redox potential (Eh), pH, chlorophyll-a, photosynthetically active radiation, “coloured dissolved organic matter” and dissolved oxygen. Buoy data are quality controlled in real time and where possible these data are distributed over WIS.

4.3.10 **Surface ocean currents**

Surface currents are collected to support commerce, safety of operation, search and rescue, oil spill response, and currents near harbour entrances that have an impact on ocean transportation. Surface currents measured from buoys are also used to validate surface currents derived from high-frequency radar instruments or satellite measurement. Most buoys acquire these measurements using buoy-mounted acoustic Doppler samplers. Sampling interval should be set in such a way as to eliminate the current due to wave orbital velocity.

4.3.11 **Ocean current profiles**

Ocean current profiles provide the motion of the ocean at different levels in the water column. This information is essential for assessing oil spill dispersal, search and rescue, stresses on offshore platforms, and validation for ocean models. These data are currently acquired from downward-looking, buoy- or cage-mounted systems. On offshore oil platforms, the current profiles may be downward looking from a number of levels in the water column, or upward-looking from a bottom-mounted system.

Most buoys use Acoustic Doppler Current Profiler (ADCP) technology as the primary sensor for collection of ocean current profile data. These sensors emit short-duration, high-frequency pulses of acoustic energy along narrow beams. Scatterers (assumed to be passive nekton and plankton) within the water column return the backscattered energy and the instruments resolve the along-beam Doppler frequency shifts into orthogonal earth coordinates to obtain ocean currents at various levels in the water column. ADCP is generally used independently or along with the buoy system to profile the required depth.

4.3.12 **Salinity**

Salinity is required to initialize ocean models that provide ocean forecasts and predict ocean circulations (which are largely density driven). Salinity is usually derived from measurements of the conductivity of seawater. Some instruments provide the salinity directly (through internal calculations) and others provide the conductivity, temperature and depth required to calculate the salinity. Salinity measurements are based on the practical salinity scale using the empirical relationship between the salinity and conductivity of seawater (although a new international thermodynamic equation of seawater-2010 (TEOS-10) was recently endorsed by IOC through its Assembly Resolution XXV-7). The salinity units are reported in practical salinity units. Measurement of conductivity is carried by two methods: (a) by using an inductive coil to sense the amount of conductive ions; (b) to take a known amount of seawater in a glass tube and measure the conductivity by measuring the change in resistance of a platinum electrode. Bio fouling of the instrument is a limiting factor for any attempt to provide an accurate salinity measurement from the moored buoy.

4.3.13 **Precipitation**

Precipitation measurements with large spatial coverage are critical for climate-related studies. Freshwater fluxes are indirect measures of local latent heating, which drives atmospheric circulation. For these reasons, siphon raingauges have been installed in the buoy systems. Precipitation is collected in a catchment funnel and drained into a measuring tube that has a capacitive transducer that provides the linear output. A self-siphon process empties the measuring tube once it is full. The sampling interval is 1 Hz for calculation of rain intensity. These sensors are slightly affected by the electromagnetic field generated by the transmission antennas and sufficient clearance space needs to be provided on moored buoys to overcome the interference.

4.3.14 **Solar radiation measurements**

Solar radiation is an important influence on physical, biological and chemical processes near the air–sea interface, and is therefore of interest to scientists and engineers. Solar radiation measurements taken at the surface have been used to calibrate visible range radiometers aboard satellites. The sensor is placed as high as possible on the platform to avoid shadows. Solar radiative flux is measured in watts per square metre and photosynthetically active radiation is measured in micromoles per square metre per second. Buoy systems are equipped with long-wave and short-wave radiation sensors with analogue and serial outputs

4.3.15 **Visibility**

Visibility sensors have been placed on some stations where visibility is a critical concern for safe navigation. The sensor measures the extinction of light across a small volume of air between an emitter and a collector. It is important to note that these are measurements at a single point, and that there are several similar but different definitions.

4.4 **LIGHT VESSELS**

In most respects, these platforms can be regarded as being similar to moored buoys as they are unmanned and rely on automated observing systems. Because of their larger dimensions and the feasibility of carrying a large instrument payload, it is more straightforward to deploy additional sensors, such as visibility sensors. In severe weather, such visibility sensors can be affected by sea spray generated by the vessel itself. Also, because light vessels are much larger than moored buoys, care has to be taken in the siting of wind sensors to avoid obstructions from the vessel structure, similar to that described earlier for VOS (see 4.2.2.6.2). However, in most conditions, performance is equal to that of instruments deployed on land-based AWSs.

Wave measurements have been made from light vessels in waters near the United Kingdom for many years, with records dating back to 1962. These measurements were originally made using shipborne wave recorder (SBWR) instruments mounted on the light vessels that used accelerometers and (water) pressure sensors to provide information on wave heights and periods. Since the 1990s, the wave measurements have been made using heave (“hippy”) sensors on the light vessels. However, it has long been suspected that the present wave measurements from the light vessels are less accurate than those from the UK Met Office’s moored buoys. This is because the present light vessel wave measurements are made using a heave sensor sited near the centre of the vessel that only measures the vertical displacement, whereas the earlier SBWR measurements were based on accelerometers to measure vessel heave and pressure sensors (below the waterline) to measure changes in the sea level relative to the vessel. Hence, the SBWR measurements took account of the inertia (that is, the light vessels are too large to accurately follow the rise and fall of each wave) of the vessel, while this is presently neglected. This results in the present heave-sensor-only measurements underestimating the significant wave height and overestimating the average wave period (Anderson et al., 2016).

4.5 **TOWERS AND PLATFORMS**

On towers (usually in relatively shallow waters close to shore) and on platforms in more remote areas, it is possible to operate standard AWSs, similar in design to land AWSs (see Chapter 1 of the present volume). Additional sensors are often deployed, for example, wave sensors and sensors for measuring mean water level above a reference point, ceilometers and visimeters. Fixed platforms can include large gravity based structures, and mobile jack-up rigs and semi-submersible rigs. Jack-up and semi-submersible rigs, and drill ships, could be considered stationary platforms as they are moored or dynamically positioned to remain in one place while

in operation. The majority of offshore platforms now carry automated weather stations that are operated by offshore industry companies and so fall into the category of “third-party data” that may (or may not) be made available via the WMO GTS.

On some platforms and rigs the automatically measured data can be supplemented by visual observations of cloud, visibility and weather, thus allowing full synoptic reporting. Visual observations from oil/gas platforms should be made according to the procedures recommended under 4.2. However, there are cases where different procedures apply. For example, a platform may include wave data from a nearby moored wave buoy, and SST from a nearby supply vessel.

Some manned fixed or stationary (offshore oil and gas) platforms may include measurements of wave parameters such as significant wave height and some measure of wave period in their weather report, using output from a nearby wave buoy or from an on-board wave radar.

Platforms and towers make convenient structures for mounting meteorological sensors. Installation and maintenance can be less complicated and more economical than for a moored buoy making data frequency and reliability better. Data quality is unaffected by ship or buoy motion and is less susceptible to errors from sensors damaged by wave action. Wave data, however, could be susceptible to the location of the fixed gauge location, such as a leg of a platform. Interaction of the physical structure and the incoming waves could generate interference or reflection patterns in the up- and down-wave conditions.

However, temperature and humidity sensors need very careful positioning as often there are heat and exhaust sources that will modify the local environment making values unrepresentative of environmental conditions. Wind measurements might be taken at heights in excess of 100 m above MSL and require correction to the equivalent 10 m surface wind (note that ideally it would be best to also have the actual observation and its height). In the case of towers close inshore, tide height can significantly alter the effective height of the wind sensor.

In conclusion, therefore, fixed towers and offshore platforms can provide a cost-effective source of supplementary data, removing the need to deploy moored buoys in those regions.

4.6 DRIFTING BUOYS

Drogued drifting buoys (Niiler, 2001; Maximenko et al., 2013; Centurioni, 2018) have been used for many years in oceanography, principally for the measurement of sea-surface currents. However, the development of reliable satellite tracking and data relay systems ([Guide to Data Collection and Location Services using Service Argos](#)) has led to a dramatic increase in the numbers of ocean drifting buoys deployed, and significant development has taken place in the sensor capabilities of drifters for meteorological and oceanographic purposes.

Nearly all of the Lagrangian surface drifting buoys (termed “drifter” hereafter) operating within the global surface drifter array report SST, geolocation and time of observations. Since the drifters are drogued to a depth of 15 m, the geolocation data and times are used to compute currents at that depth when the drogue is present.

The presence of the drogue is often determined with a strain-gauge sensor. Methods to recover near-surface ocean currents when the drogue is lost also exist. In 2018, over half of the drifters in the global array also measured sea-level atmospheric pressure, and a few drifters, deployed in support of special process studies and/or ocean–tropical cyclones interaction studies, measure sea-surface salinity (for example Centurioni et al., 2015; Hormann et al., 2015; Hormann et al., 2016), horizontal sea-level wind velocity and subsurface temperature, typically to a depth of 150 m. A subset of experimental undrogued drifters is also being deployed, and they are designed to measure the directional spectra of surface gravity waves. A modern description of drifting buoy systems is given in Centurioni (2018) as well as in UNESCO (1988). The WMO/IOC Data Buoy Cooperation Panel (DBCP) published the [Global Drifter Programme](#)

Barometer Drifter Design Reference. The reader should also refer to the annual reports and workshop proceedings of the DBCP, which are available from <https://community.wmo.int/mmop-publications-and-documents-0>.

The evolution of drifting buoy technology has been driven by the needs of oceanographic research, on the one hand, and operational meteorology, on the other. Thus, three main distinct types of buoys can be characterized as follows:

- (a) For oceanographic research, and especially for the World Ocean Circulation Experiment (Surface Velocity Programme (SVP), 1988–1993), a drifter with a drogue centred at 15 m depth and designed to measure near-surface currents in the upper-ocean mixed layer and equipped to measure SST with an accuracy ranging between ± 0.1 °C and ± 0.05 °C was developed and has been deployed in large numbers over the world's oceans;
- (b) For operational meteorology, a drifting buoy design has evolved based on those developed for the First Global Atmospheric Research Programme Global Experiment. These buoys primarily measure air pressure, SST and air temperature;
- (c) For polar applications, different ice floats have been designed to measure traditional atmospheric variables as well as ice and snow conditions (ice/snow temperature and temperature profiles in the ice, ice thickness, ice stress, water conditions below ice). By tracking the buoy position on the ice it is possible to estimate ice motion.

Efforts have been made to develop buoys that meet the combined requirements of oceanographic research and operational meteorology (Centurioni, 2018), which has resulted in the development of:

- (a) The SVP-B Drifter (see also Centurioni et al., 2016a) is a modification of the SVP Drifter described in point (a) of the preceding paragraph, with an air pressure sensor added. The barometer has a typical accuracy of ± 0.4 hPa;
- (b) The SVP-BW Drifter, which is essentially an SVP-B drifter with wind-measuring capability. Older wind drifters used a subsurface hydrophone and a surface vane to derive wind velocity estimates, but this technology has been entirely replaced with a sonic anemometer in the modern SVP-BW. The wind direction is measured with an internal compass with an accuracy of $\pm 2^\circ$;
- (c) The wind, pressure and temperature vertical profile buoy, or Autonomous Drifting Ocean Station (ADOS), which is a derivation of the SVP-BW Drifter with a subsurface thermistor chain replacing the drogue for the measurement of temperature profile to depths of 150 m;
- (d) The Salinity SVP (SVP-S) Drifter, which is an SVP or SVP-B Drifter with a conductivity sensor at a depth of approximately 0.45 m and an accuracy of the order of ± 0.0003 S m⁻¹. The accuracy of the surface temperature sensor for these drifters is of the order of ± 0.002 °C. Some experimental configurations have included additional conductivity/temperature sensors at additional depths (Dong et al., 2017);
- (e) The Directional Wave Spectra Drifter (Centurioni et al., 2016b; Centurioni et al. 2019), which is an undrogued drifter designed to measure directional wave spectra parameters using GPS technology. This experimental technology is becoming increasingly popular due to its high accuracy of directional spectra observations and low cost.

Drifting buoys are expendable devices, thus performance is a compromise between the requirements and the cost of manufacture and shipping. However, the performance of drifting buoy sensors is adequate for the purposes of synoptic meteorology and oceanography, as appropriate. Note that the quality of hydrophone-derived wind speed observations is questionable, resulting in their not being used by operational centres (Ingleby, 2010). The modern SVP-BW drifter technology that uses the sonic wind sensor is very promising and is currently being assessed.

The typical measurement uncertainties of operational systems are as follows:

Location	22 m ^a
SST	0.05 °C to 0.21 °C ^b
Air pressure	0.84 hPa ^c
Wind speed	3.5 m s ⁻¹ or 10% ^{bc}
Wind direction	18.5° ^c
Subsurface temperature	0.05 °C

Notes:

^a Accuracy of a GPS on a drifter in the ocean (see https://www.aoml.noaa.gov/phod/gdp/hourly_data.php).

^b Source: O'Carroll et al. (2008).

^c Source: *buoy monitoring statistics, European Centre for Medium-Range Weather Forecasts, January 2012.*

By 2018, data from drifting buoys are primarily transmitted through Iridium satellite. Examples of Iridium Short Burst Data formats have been proposed by Blouch et al. (2018).

Over the years drifting buoys have become the dominant source of in-situ surface air pressure and SST measurements over the global oceans. The pressure data are critical for global NWP (Centurioni et al., 2016b; Horányi et al. 2017), and the SST data now form a key part of the climate record and are also used to calibrate and validate satellite-derived SST products. There is presently a joint initiative between the DBCP, the GDP and the satellite community to evaluate drifters with higher accuracy SST sensors (to ± 0.05 °C or better) to determine whether, with reporting the time of measurement to ± 5 minutes and location to ± 5 km, which is now a standard feature of the Iridium/GPS drifters, they could lead to more accurate satellite SST products. The new European (EUMETSAT, COPERNICUS, EUMETNET) concept of SVP with Barometer and Reference Sensor for Temperature (SVP-BRST) was validated in 2018 (Poli et al., 2019). These buoys are used to deliver high-resolution SST in situ data to assist with the calibration and validation of the Sea and Land Surface Temperature Radiometer on Sentinel-3. Around 100 SVP-BRST buoys have been deployed.

ANNEX 4.A. WMO/IOC REGIONAL MARINE INSTRUMENT CENTRES

1. Considering the need for high-quality marine meteorology and oceanographic measurements from the world oceans to address the requirements of WMO and UNESCO/IOC programmes and co-sponsored programmes, the need for facilities for the regular calibration and maintenance of marine instruments and the monitoring of instrument performance, on a regional basis in order to address adherence of ocean observations and associated metadata to high-level standards for instruments and methods of observation, the need for documenting methods of measurements, for understanding biases introduced by each type of instrumentation, and for developing methods to correct such biases, in order to achieve delivery and use of coherent datasets, it has been recommended¹ that:

RMICs should have the following capabilities to carry out their corresponding functions:

Capabilities:

- (a) An RMIC must have, or have access to, the necessary facilities and laboratory equipment to perform the functions necessary for the calibration of meteorological and related oceanographic instruments deployed to address the common requirements of WMO and UNESCO/IOC marine-related programmes and co-sponsored programmes;²
- (b) An RMIC must maintain a set of meteorological and oceanographic standard instruments or references and establish the traceability of its own measurement standards and measuring instruments to the International System of Units (SI);
- (c) An RMIC must have qualified managerial and technical staff with the necessary experience to fulfil its functions;
- (d) An RMIC must develop its individual technical procedures for the calibration of meteorological and related oceanographic instruments using its own calibration equipment;
- (e) An RMIC must develop its individual quality assurance procedures;
- (f) An RMIC must participate in, or organize, inter-laboratory comparisons of standard calibration instruments and methods;
- (g) An RMIC must utilize the resources and capabilities of its region of interest according to the region's best interests, when appropriate;
- (h) An RMIC must apply international standards applicable for calibration laboratories, such as ISO/International Electrotechnical Commission (IEC) 17025, to the extent possible;
- (i) A recognized authority³ must assess an RMIC, at least every five years, to verify its capabilities and performance.

Corresponding functions:

- (a) An RMIC must assist Members/Member States of its region in calibrating their national meteorological standards and related oceanographic monitoring instruments according to the RMIC capabilities;

¹ Recommended by the Joint WMO/IOC Technical Commission for Oceanography and Marine Meteorology at its third session, held in 2009.

² Basically in-situ geophysical instruments deployed in the surface marine environment or subsurface.

³ JCOMM was the body that formally proposed new RMICs and proposed any authority to do evaluations

- (b) An RMIC must participate in, or organize, JCOMM and/or regional instrument intercomparisons, following relevant JCOMM recommendations;
- (c) An RMIC must make a positive contribution to Members/Member States regarding the quality of measurements;
- (d) An RMIC must advise Members/Member States on enquiries regarding instrument performance, maintenance and the availability of relevant guidance materials;
- (e) An RMIC must actively participate, or assist, in the organization of regional workshops on meteorological and related oceanographic instruments and measurements;
- (f) The RMIC must cooperate with other RMICs in the standardization of meteorological and related oceanographic measurements and sensors;
- (g) An RMIC must regularly inform Members/Member States and report, on an annual basis, to the JCOMM Management Committee on the services offered to Members/Member States and the activities carried out. JCOMM in turn should keep the Executive Councils of WMO and UNESCO/IOC informed on the status and activities of the RMICs, and propose changes, as required.

2. The mechanism for formal WMO and UNESCO/IOC designation of RMICs implies the following:

- (a) Governance for defining the functions and adoption of an RMIC is proposed by JCOMM and endorsed by the WMO and UNESCO/IOC Executive Councils;
- (b) A candidate RMIC is required to produce a statement of compliance, list capabilities of the proposed centre, state the suite of instrument expertise offered, state the formal commitment to voluntarily host the centre, and demonstrate capability to JCOMM;
- (c) The establishment of RMICs is initiated by JCOMM, and the designation process is coordinated by JCOMM and the WMO/IOC Secretariats according to the process endorsed by JCOMM and documented in JCOMM Technical Report No. 53;
- (d) Where more than one RMIC is established within a WMO and/or IOC Region, there should be coordination among the Centres.

3. The following centres have been designated as RMICs:

<i>Region</i>	<i>Centre</i>	<i>Location</i>
Asia-Pacific	National Center of Ocean Standards and Metrology	Tianjin, China
North America, Central America and the Caribbean	United States National Data Buoy Center	Stennis Space Center, Mississippi, United States of America

ANNEX 4.B. DESCRIPTIONS OF PRECIPITATION FOR USE BY SHIP-BORNE OBSERVERS OF PRESENT WEATHER

Precipitation occurs either in a more or less uniform manner (intermittent or continuous) or in showers.

All precipitation other than showers must be reported as intermittent or continuous.

Non-showery precipitation usually falls from stratiform clouds (mainly altostratus and nimbostratus). Showers fall from large convective clouds (mainly cumulonimbus or cumulus of moderate or strong vertical development) and are usually characterized by their abrupt beginning and ending and by variations in the intensity of the precipitation. Drops and solid particles in a shower are generally larger than those occurring in non-showery precipitation.

The drops of precipitation can be supercooled (that is, the temperature of the drops is below 0 °C). On impact with a surface, drops of supercooled rain form a mixture of water and ice having a temperature near 0 °C.

Forms of precipitation

The descriptions given below are compatible with the definitions given in the [International Cloud Atlas](#) (WMO-No. 407):

Drizzle. Fairly uniform precipitation of very fine drops of water very close to one another that fall from a cloud.

Drizzle drops usually have a diameter of less than 0.5 mm. The drops appear to almost float, and so make even slight movements of the air visible. Drizzle falls from a layer of stratus, usually low, sometimes touching the ground (fog). The amount of precipitation in the form of drizzle can be considerable (up to 1 mm h⁻¹), especially along coasts and in mountainous areas. The drops falling on the edge of a rain zone or during light rainfall may be as small as drizzle drops, owing to their partial evaporation. In this situation, raindrops are distinguished from drizzle drops in that they are more scattered.

Identification of the precipitating cloud as stratus also distinguishes rain from drizzle. For coding purposes, drizzle must be classified as slight, moderate or heavy, which are defined as follows:

- (a) *Slight drizzle:* Can be readily detected on the face of wheel-house windows, but produces very little runoff from deck, roofs, and so on;
- (b) *Moderate drizzle:* Causes windows, decks and superstructures to stream with moisture;
- (c) *Heavy drizzle:* Same as for moderate drizzle. It also reduces visibility to below 1 000 m.

Rain. Precipitation of drops of water that fall from a cloud. The number density and size distribution of raindrops vary considerably with the intensity and nature of the precipitation. Continuous rain usually falls from a more or less uniform layer or layers of thick stratiform cloud. For coding purposes, rain must be classified as slight, moderate or heavy. These terms are defined as follows:

- (a) *Slight rain:* May consist of scattered large drops or numerous smaller drops. The rate of accumulation on a deck is low and puddles form very slowly;
- (b) *Moderate rain:* Individual drops are not clearly identifiable. Rain spray is observable. Puddles form rapidly. Sounds from roofs range from swishing to a gentle roar;

- (c) *Heavy rain*: A downpour which makes a roaring noise on awnings and deckheads and forms a misty spray of fine droplets by splashing on deck surfaces.

Snow. Precipitation of ice crystals, singly or stuck together, that fall from a cloud. The form, size and concentration of snow crystals differ considerably according to the temperature and supersaturation at which they develop. A fall of snow usually includes various types of snow crystals and almost all types of crystal may be observed during a single fall of snow. Small droplets of frozen water are often attached to snow crystals. If present in great numbers, these can obscure the crystalline structure of the snow. At temperatures warmer than approximately $-5\text{ }^{\circ}\text{C}$, the crystals generally stick together to form snowflakes.

The intensity is coded as slight, moderate or heavy.

Showers. These are characterized by their abrupt beginning and end, and by the generally rapid and sometimes violent variations in the intensity of the precipitation. Drops and solid particles falling in a shower are generally larger than those falling in non-showery precipitation. Whether the precipitation (rain or snow) occurs as showers or not depends on the clouds in which it originates. Showers fall from large convection clouds and are defined as follows:

- (a) *Rain and snow showers*: Must be classified for coding purposes with regard to intensity as either slight, moderate or heavy. The description is the same as for slight, moderate or heavy rain or snow. It must be remembered, however, that the visibility in showery weather shows a much greater variability than for the same category of continuous rain;
- (b) *Violent showers*: Are exceptionally heavy or torrential rain showers. Such showers occur mostly in tropical regions.

Snow pellets. Precipitation of white and opaque ice particles that fall from a cloud. These particles are generally conical or rounded, and their diameter may be as large as 5 mm. Snow pellets are composed of a central nucleus covered with frozen cloud droplets. They form when a particle of ice, usually a crystal, collects cloud droplets, which rapidly freeze. Their density is generally low, less than 0.8 g cm^{-3} , due to air gaps between the nucleus and frozen droplets. Snow pellets are brittle and easily crushed. When they fall on hard ground, they bounce and often break. Showers of snow pellets fall from cumulus or cumulonimbus. The showers usually consist of snow pellets and snowflakes together, and normally occur when temperatures near the surface are close to $0\text{ }^{\circ}\text{C}$. Crystals can be observed that are not completely surrounded by droplets; this is the intermediate stage between a snow crystal and a snow pellet. For recording purposes, the intensity of snow pellets, when they occur alone, is determined according to the visibility in the same manner as for snow.

Hail. Precipitation of particles of ice (hailstones). These can be either transparent, or partly or completely opaque. They are usually spheroidal, conical or irregular in form, and generally 5–50 mm in diameter. The particles may fall from a cloud either separately or agglomerated in irregular lumps. Falls of hail always occur as showers. They are generally observed during heavy thunderstorms. For coding purposes, hail must be classified as either slight, moderate or heavy. The intensity is determined by the rate of accumulation of stones as follows:

- (a) *Slight hail*: Few stones falling, no appreciable accumulation on flat surfaces;
- (b) *Moderate hail*: Slow accumulation of stones. Fall sufficient to whiten the decks;
- (c) *Heavy hail*: Rapid accumulation of stones. Rarely experienced in temperate latitudes at sea.

Small hail. Precipitation of translucent ice particles that fall from a cloud. These particles are almost always spherical and sometimes have conical tips. Their diameter may approach and even exceed 5 mm. Small hail always occurs in showers from cumulonimbus. Small hail consists of snow pellets totally or partially encased in a layer of ice. Gaps within the snow pellets are filled with ice, or ice and water; a thin shell only may be frozen. The water

may come from cloud drops or partial melting of snow pellets. The density of small hail is relatively high; it ranges from 0.8 g cm^{-3} to, in rare examples, 0.99 g cm^{-3} . Usually, small hail is not easily crushable; when it falls on hard ground it bounces with an audible sound on impact. Small hail is an intermediate stage between the snow pellet and the hailstone. It differs from the snow pellet in its partially smooth surface and its higher density. It differs from the hailstone particularly in its smaller size.

Ice pellets. Precipitation of transparent ice particles that fall from a cloud. These particles are usually spheroidal or irregular, and rarely conical. Their diameter is less than 5 mm. Ice pellets originate as raindrops or snowflakes (less common) that generally fall from altostratus or nimbostratus. They fall into a subcloud layer of warm air where the snowflakes melt or partially melt, and then fall into a cold layer of air (below $0 \text{ }^{\circ}\text{C}$) where they freeze and reach the ground as frozen precipitation. Ice pellets of the form of frozen raindrops are transparent, the less common refrozen snowflakes are, in parts, transparent and, in parts, opaque, depending on whether the snowflake melted or only partially melted. Ice pellets are not easily crushable. When they fall on hard ground, they generally bounce with an audible sound on impact. Ice pellets may be partly liquid. Their density is usually close to, or above, that of ice (0.92 g cm^{-3}). The intensity of ice pellets is determined in the same manner as for hail.

Snow grains. Precipitation of very small opaque white particles of ice that fall from a cloud. These particles are fairly flat or elongated. Their diameter is generally less than 1 mm. Although frozen and occurring when the temperature is between approximately $0 \text{ }^{\circ}\text{C}$ and $-10 \text{ }^{\circ}\text{C}$, the other properties of this precipitation correspond to drizzle. When the grains hit hard ground they do not bounce. Snow grains fall mostly from stratus or from fog, and never in the form of a shower. Except in the mountains, snow grains usually fall in small quantities. As there is only one code specification that refers to snow grains, it is not necessary to classify intensity.

ANNEX 4.C. RECOMMENDED PROCEDURES FOR THE REPORTING OF SWELL BY MANUALLY REPORTING SHIPS

The recommended procedures for the reporting of swell by manually reporting ships, as agreed at the fifth session of the Ship Observations Team (SOT-V) in 2009 (WMO/IOC, 2009b), and implemented with the agreement of the Expert Team on Marine Climatology (ETMC; WMO/IOC, 2010), are given below:

- (a) When swell is not determined, meaning no observation has been attempted, the swell groups will be omitted from the observation;
 - (b) When no swell is observed owing to a calm sea, the direction of the main swell and the direction of the secondary swell will be reported as calm. The period and height of the main swell and secondary swell can then be omitted, because if a calm sea is reported it is inferred that these elements will also be calm, in which case they provide no additional information;
 - (c) When the swell direction is indeterminate, confused swell is reported. When the period and height of the swell are also confused, this will be included in the observation. The period and height of the secondary swell can be omitted;
 - (d) When the swell is confused but the period and height can be estimated, the swell direction is reported as confused, and the period and height of the primary swell is included in the report. The period and height of the secondary swell can be omitted;
 - (e) When only one swell is observed, the direction, period and height of this swell is reported. The period and height of the secondary swell can be omitted;
 - (f) When two swells are observed, both the swell direction and the period and height of each are included in the observation.
-

REFERENCES AND FURTHER READING

- American Meteorological Society. *Glossary of Meteorology*, 2nd ed.; American Meteorological Society, 2000. <https://glossary.ametsoc.org/wiki/Welcome>.
- Anderson, G.; Carse, F.; Turton J. et al. Quantification of Bias of Wave Measurements from Light Vessels. *Journal of Operational Oceanography* **2016**, 9 (2), 93–102. <https://doi.org/10.1080/1755876X.2016.1239242>.
- Barton, I. J.; Minnett, P. J.; Maillet, K. A. et al. The Miami2001 Infrared Radiometer Calibration and Intercomparison. Part II: Shipboard Results. *Journal of Atmospheric and Oceanic Technology* **2004**, 21 (2), 268–283. [https://doi.org/10.1175/1520-0426\(2004\)021<0268:TMIRCA>2.0.CO;2](https://doi.org/10.1175/1520-0426(2004)021<0268:TMIRCA>2.0.CO;2).
- Blouch, P.; Billon, C. E-SURFMAR Recommended Ship-to-shore Data Formats for Voluntary Observing Ships (VOS), 2017. <https://zenodo.org/record/1324186>.
- Blouch, P.; Billon, C.; Poli, P. 2018: E-SURFMAR Recommended Ship-to-shore Data Formats for Buoys. doi:10.5281/zenodo.1473443.
- Bourras, D. Comparison of Five Satellite-derived Latent Heat Flux Products to Moored Buoy Data. *Journal of Climate* **2006**, 19 (24), 6291–6313. <https://doi.org/10.1175/JCLI3977.1>.
- Bowditch, N. *The American Practical Navigator: An Epitome of Navigation*, 2002 Bicentennial edition, NIMA Pub. No. 9; National Imagery and Mapping Agency: Bethesda, USA, 2002.
- Bradley, F.; Fairall, C. *A Guide to Making Climate Quality Meteorological and Flux Measurements at Sea*, NOAA Technical Memorandum OAR PSD-311, NOAA/ESRL/PSD; National Oceanic and Atmospheric Administration: Boulder, USA, 2006.
- Centurioni, L. R. Drifter Technology and Impacts for Sea Surface Temperature, Sea-level Pressure, and Ocean Circulation Studies. In: *Observing the Oceans in Real Time*; Venkatesan, R.; Tandon, A.; D'Asaro E. et al., Eds.; Springer Oceanography: Cham, Switzerland, 2018.
- Centurioni, L.; Braasch, L.; Di Lauro, E. et al. A New Strategic Wave Measurement Station off Naples Port Main Breakwater. *Coastal Engineering Proceedings* **2016**. <https://doi.org/10.9753/icce.v35.waves.36>.
- Centurioni, L.; Horányi, A.; Cardinali, C. et al. A Global Ocean Observing System for Measuring Sea Level Atmospheric Pressure: Effects and Impacts on Numerical Weather Prediction. *Bulletin of the American Meteorological Society* **2017**, 98 (2), 231–238. <https://doi.org/10.1175/BAMS-D-15-00080.1>.
- Centurioni, L. R.; Hörmann, V.; Chao, Y. et al. Sea Surface Salinity Observations with Lagrangian Drifters in the Tropical North Atlantic During SPURS: Circulation, Fluxes, and Comparisons with Remotely Sensed Salinity from Aquarius. *Oceanography* **2015**, 28 (1), 96–105. <https://doi.org/10.5670/oceanog.2015.08>.
- Centurioni, L. R.; Turton, J.; Lumpkin, R. et al. Global In Situ Observations of Essential Climate and Ocean Variables at the Air–Sea Interface. *Frontiers in Marine Science* **2019**, 6 (419). <https://doi.org/10.3389/fmars.2019.00419>.
- Dohan, K.; Bonjean, F.; Centurioni, L. et al. Measuring the Global Ocean Surface Circulation with Satellite and In Situ Observations. In *Proceedings of OceanObs'09: Sustained Ocean Observations and Information for Society*, Venice, 21–25 September 2009; Hall, J.; Harrison D. E.; Stammer, D., Eds.; ESA Publication WPP-306, European Space Agency, 2010; Vol. 2. <https://doi.org/10.5270/OceanObs09.cwp.23>.
- Dong, S.; Volkov, D.; Goni, G. et al. 2017: Near-surface Salinity and Temperature Structure Observed with Dual-sensor Drifters in the Subtropical South Pacific. *Journal of Geophysical Research: Oceans* **2017**, 122 (7), 5952–5969. <http://dx.doi.org/10.1002/2017JC012894>.
- Donlon, C.; Robinson, I. S.; Wimmer, W. et al. An Infrared Sea Surface Temperature Autonomous Radiometer (ISAR) for Deployment aboard Volunteer Observing Ships (VOS). *Journal of Atmospheric and Oceanic Technology* **2008**, 25 (1), 93–113. <https://doi.org/10.1175/2007JTECH0505.1>.
- Fairall, C. W.; White, A. B.; Edson J. B. et al. Integrated Shipboard Measurements of the Marine Boundary Layer. *Journal of Atmospheric and Oceanic Technology* **1997**, 14 (3), 338–359. [https://doi.org/10.1175/1520-0426\(1997\)014<0338:ISMOTM>2.0.CO;2](https://doi.org/10.1175/1520-0426(1997)014<0338:ISMOTM>2.0.CO;2).
- Freeland, H.; Roemmich, D.; Garzoli, S. et al. Argo – A Decade of Progress. In *Proceedings of OceanObs'09: Sustained Ocean Observations and Information for Society*, Venice, 21–25 September 2009; Hall, J.; Harrison, D. E.; Stammer, D. Eds.; ESA Publication WPP-306, European Space Agency, 2010; Vol. 2.
- Frigaard, P. B.; Helm-Petersen, J.; Klopman, G. et al. IAHR List of Sea Parameters. In *Proceedings of the Twenty-seventh IAHR Congress*, San Francisco, 10–15 August 1997; 1997.

- Goni, G.; Roemmich, D.; Molinari, R. et al. The Ship of Opportunity Programme. In *Proceedings of OceanObs'09: Sustained Ocean Observations and Information for Society*, Venice, 21–25 September 2009; Hall, J.; Harrison D. E.; Stammer, D. Eds.; ESA Publication WPP-306, European Space Agency, 2010; Vol. 2.
- Hall, J.; Harrison, D. E.; Stammer, D., Eds. *Proceedings of OceanObs'09: Sustained Ocean Observations and Information for Society*, Venice, 21–25 September 2009; ESA Publication WPP-306, European Space Agency, 2010.
- Hasse, L.; Grossklaus, M.; Uhlig, K. et al. A Ship Rain Gauge for Use in High Wind Speeds. *Journal of Atmospheric and Oceanic Technology* **1998**, 15 (2), 380–386. [https://doi.org/10.1175/1520-0426\(1998\)015<0380:ASRGFU>2.0.CO;2](https://doi.org/10.1175/1520-0426(1998)015<0380:ASRGFU>2.0.CO;2).
- Horányi, A.; Cardinali, C.; Centurioni, L. The Global Numerical Weather Prediction Impact of Mean-sea-level Pressure Observations from Drifting Buoys. *Quarterly Journal of the Royal Meteorological Society* **2017**, 143 (703), 974–985. <https://doi.org/10.1002/qj.2981>.
- Hormann, V.; Centurioni, L. R.; Reverdin, G. Evaluation of Drifter Salinities in the Subtropical North Atlantic. *Journal of Atmospheric and Oceanic Technology* **2015**, 32 (1), 185–192. <https://doi.org/10.1175/JTECH-D-14-00179.1>.
- Hormann, V.; Centurioni, L. R.; Mahadevan, A. et al. Variability of Near-Surface Circulation and Sea Surface Salinity Observed from Lagrangian Drifters in the Northern Bay of Bengal During the Waning 2015 Southwest Monsoon. *Oceanography* **2016**, 29 (2), 124–133. <https://doi.org/10.5670/oceanog.2016.45>.
- Ingleby, B. Factors Affecting Ship and Buoy Data Quality: A Data Assimilation Perspective. *Journal of Atmospheric and Oceanic Technology* **2010**, 27, 1476–1489. <https://doi.org/10.1175/2010JTECHA1421.1>.
- Keeley, R.; Pazos M.; Bradshaw, B. Data Management System for Surface Drifters. In *Proceedings of OceanObs'09: Sustained Ocean Observations and Information for Society*, Venice, 21–25 September 2009; Hall, J.; Harrison, D. E.; Stammer, D., Eds.; ESA Publication WPP-306, European Space Agency, 2010; Vol. 2.
- Kennedy, J. J.; Smith R. O.; Rayner, N. A. Using AATSR Data to Assess the Quality of In Situ Sea-surface Temperature Observations for Climate Studies. *Remote Sensing of Environment* **2012**, 116, 79–92. <https://doi.org/10.1016/j.rse.2010.11.021>.
- Kent, E. C.; Ball, G.; Berry, D. et al. The Voluntary Observing Ship (VOS) Scheme. In *Proceedings of OceanObs'09: Sustained Ocean Observations and Information for Society*, Venice, 21–25 September 2009; Hall, J.; Harrison, D. E., Stammer, D., Eds.; ESA Publication WPP-306, European Space Agency, 2010, Vol. 2.
- Kent, E. C.; Berry, D. I. Quantifying Random Measurement Errors in Voluntary Observing Ships' Meteorological Observations. In *Advances in the Applications of Marine Climatology – The Dynamic Part of the WMO Guide to the Applications of Marine Climatology* (WMO/TD-No. 1081). WMO: Geneva, 2005.
- Kent, E. C.; Taylor, P. K. Toward Estimating Climatic Trends in SST, Part I: Methods of Measurement. *Journal of Atmospheric and Oceanic Technology* **2006**, 23 (3), 464–475. <https://doi.org/10.1175/JTECH1843.1>.
- Kent, E. C.; Taylor, P. K.; Josey, S. A. Improving Global Flux Climatology: The Role of Metadata. In *Advances in the Applications of Marine Climatology: The Dynamic Part of the WMO Guide to the Applications of Marine Meteorology* (WMO/TD-No. 1081). WMO/IOC: Geneva and Paris, 2003.
- Kent, E. C.; Taylor, P. K.; Truscott B. S. et al. The Accuracy of Voluntary Observing Ships' Meteorological Observations – Results of the VSOP-NA. *Journal of Atmospheric and Oceanic Technology* **1993**, 10 (4), 591–608. [https://doi.org/10.1175/1520-0426\(1993\)010<0591:TAOVOS>2.0.CO;2](https://doi.org/10.1175/1520-0426(1993)010<0591:TAOVOS>2.0.CO;2).
- Kent, E. C.; Woodruff, S. D.; Berry, D. I. Metadata from WMO Publication No. 47 and an Assessment of Voluntary Observing Ship Observation Heights in ICOADS. *Journal of Atmospheric and Oceanic Technology* **2007**, 24 (2), 214–234. <https://doi.org/10.1175/JTECH1949.1>.
- Klepp, C. The oceanic shipboard precipitation measurement network for surface validation – OceanRAIN. *Atmospheric Research*, Special issue on the Sixth Workshop of the International Precipitation Working Group **2015**, 163, 74–90. <https://doi.org/10.1016/j.atmosres.2014.12.014>.
- Laurindo, L. C.; Mariano, A.; Lumpkin, R. An Improved Surface Velocity Climatology for the Global Ocean from Drifter Observations. *Deep Sea Research Part I* **2017**, 124, 73–92. <http://dx.doi.org/10.1016/j.dsr.2017.04.009>.
- Liu, W. T.; Katsaros, K. B.; Businger, J. A. Bulk Parameterization of Air–Sea Exchanges of Heat and Water Vapor Including the Molecular Constraints at the Interface. *Journal of Atmospheric Sciences* **1979**, 36, 1722–1735. [https://doi.org/10.1175/1520-0469\(1979\)036<1722:BPOASE>2.0.CO;2](https://doi.org/10.1175/1520-0469(1979)036<1722:BPOASE>2.0.CO;2).

- Maximenko, N.; Lumpkin, R.; Centurioni, L. Chapter 12 – Ocean Surface Circulation. In *Ocean Circulation and Climate: A 21st Century Perspective*, 2nd ed.; International Geophysics Series Volume 103; Siedler, G.; Griffies, S. M.; Gould J. et al., Eds.; Academic Press, 2013.
- McPhaden, M. J.; Ando, K.; Bourlès, B. et al. 2010: The Global Tropical Moored Buoy Array. In *Proceedings of OceanObs'09: Sustained Ocean Observations and Information for Society*, Venice, 21–25 September 2009; Hall, J.; Harrison, D. E.; Stammer, D., Eds.; ESA Publication WPP-306, European Space Agency, 2010; Vol. 2.
- Meldrum, D.; Charpentier, E.; Fedak, M. et al. Data Buoy Observations: The Status Quo and Anticipated Developments over the Next Decade. In *Proceedings of OceanObs'09: Sustained Ocean Observations and Information for Society*, Venice, 21–25 September 2009; Hall, J.; Harrison, D. E.; Stammer, D., Eds.; ESA Publication WPP-306, European Space Agency, 2010; Vol. 2.
- Merrifield, M.; Aarup, T.; Allen, A. et al. The Global Sea Level Observing System (GLOSS). In *Proceedings of OceanObs'09: Sustained Ocean Observations and Information for Society*, Venice, 21–25 September 2009; Hall, J.; Harrison, D. E.; Stammer, D., Eds.; ESA Publication WPP-306, European Space Agency, 2010; Vol. 2.
- Michaelides, S. *Precipitation: Advances in Measurement, Estimation and Prediction*. Springer, 2008
- Moat, B. I., Yelland, M. J.; Molland A. F. Quantifying the Airflow Distortion over Merchant Ships, Part II: Application of the Model Results. *Journal of Atmospheric and Oceanic Technology* **2006**, 23 (3), 351–360. <https://doi.org/10.1175/JTECH1859.1>.
- Moat, B. I.; Yelland, M. J.; Pascal R. W. et al. An Overview of the Airflow Distortion at Anemometer Sites on Ships. *International Journal of Climatology* 2005, 25 (7), 997–1006. <https://doi.org/10.1002/joc.1177>.
- National Data Buoy Center. *Handbook of Automated Data Quality Control Checks and Procedures of the National Data Buoy Center*, NDBC Technical Document 03-02; National Data Buoy Center: Stennis Space Center, 2003a. <https://www.ndbc.noaa.gov/NDBCHandbookofAutomatedDataQualityControl2009.pdf>.
- National Data Buoy Center. *Nondirectional and Directional Wave Data Analysis Procedures*, NDBC Technical Document 03-01; National Data Buoy Center: Stennis Space Center, 2003b. <http://www.ndbc.noaa.gov/wavemeas.pdf>.
- National Data Buoy Center. *Handbook of Automated Data Quality Control Checks and Procedures*, NDBC Technical Document 09-02; National Data Buoy Center: Stennis Space Center, 2009. <http://www.ndbc.noaa.gov/NDBCHandbookofAutomatedDataQualityControl2009.pdf>.
- Niiler, P. P. The World Ocean Surface Circulation. In *Ocean Circulation and Climate: Observing and Modelling the Global Ocean*; Siedler, G.; Church J.; Gould, J., Eds.; Academic Press: San Francisco, 2001.
- O'Carroll, A. G.; Eyre, J. R.; Saunders, R. W. Three-way Error Analysis between AATSR, AMSR-E, and In Situ Sea Surface Temperature Observations. *Journal of Atmospheric and Oceanic Technology* **2008**, 25 (7), 1197–1207. <https://doi.org/10.1175/2007JTECHO542.1>.
- Organisation Météorologique Internationale – Comité Météorologique International (OMI-CMI). *Procès-Verbaux de la Session de Paris, 1946*, Publication No. 55; 105–106; La Concorde: Lausanne, 1947.
- Pazan, S. E.; Niiler, P. P. Recovery of Near-Surface Velocity from Undrogued Drifters. *Journal of Atmospheric and Oceanic Technology* **2001**, 18, 476–489. [https://doi.org/10.1175/1520-0426\(2001\)018<0476:RONSVF>2.0.CO;2](https://doi.org/10.1175/1520-0426(2001)018<0476:RONSVF>2.0.CO;2).
- Poli, P.; Lucas, M.; O'Carroll, A. et al. The Copernicus Surface Velocity Platform Drifter with Barometer and Reference Sensor for Temperature (SVP-BRST): Genesis, Design, and Initial Results. *Ocean Science* **2019**, 15, 199–214. <https://doi.org/10.5194/os-15-199-2019>.
- Send, U.; Weller, R. A.; Wallace, D. et al. OceansITES. In *Proceedings of OceanObs'09: Sustained Ocean Observations and Information for Society*, Venice, 21–25 September 2009; Hall, J.; Harrison D. E.; Stammer, D., Eds.; ESA Publication WPP-306, European Space Agency, 2010; Vol. 2.
- Smith, S. R.; Bourassa, M. A.; Bradley, E. et al. Automated Underway Oceanic and Atmospheric Measurements from Ships. In *Proceedings of OceanObs'09: Sustained Ocean Observations and Information for Society*, Venice, 21–25 September 2009; Hall, J.; Harrison D. E.; Stammer, D., Eds.; ESA Publication WPP-306, European Space Agency, 2010; Vol. 2.
- Smith, S. R.; Bourassa, M. A.; Sharp, R. J. Establishing more truth in true winds. In *Advances in the Applications of Marine Climatology: The Dynamic Part of the WMO Guide to the Applications of Marine Meteorology* (WMO/TD-No. 1081). WMO/IOC: Geneva and Paris, 2003.
- Swail, V.; Jensen, R. E.; Lee, B. et al. Wave Measurements, Needs and Developments for the Next Decade. *Proceedings of OceanObs'09: Sustained Ocean Observations and Information for Society*, Venice, 21–25 September 2009; Hall, J.; Harrison D. E.; Stammer, D., Eds.; ESA Publication WPP-306, European Space Agency, 2010a; Vol. 2.

- Swail, V.; Lee, B.; Soares, A. et al. Storm Surge. *Proceedings of OceanObs'09: Sustained Ocean Observations and Information for Society*, Venice, 21–25 September 2009; Hall, J.; Harrison D. E.; Stammer, D., Eds.; ESA Publication WPP-306, European Space Agency, 2010b; Vol. 2.
- Taylor, P. K.; Kent, E. C.; Yelland, M. J. et al. The Accuracy of Marine Surface Winds from Ships and Buoys. In *Advances in the Applications of Marine Climatology: The Dynamic Part of the WMO Guide to the Applications of Marine Meteorology* (WMO/TD-No. 1081). WMO/IOC: Geneva and Paris, 2003.
- Turton, J.; Pethica, C. Assessment of a New Anemometry System for the Met Office's Moored Buoy Network. *Journal of Atmospheric and Oceanic Technology* **2010**, *27*, 2031–2038. <https://doi.org/10.1175/2010JTECHA1475.1>.
- United Kingdom Meteorological Office. *Marine Observers Handbook*, 11th ed.; UK Met Office No. 1016, UK Met Office: London, 1995.
- United Nations Educational, Scientific and Cultural Organization (UNESCO). *Guide to Drifting Data Buoys*; WMO/IOC Manuals and Guides 20, 1988.
- United States Weather Bureau. *Manual of Barometry (WBAN)*, 1st ed; US Government Printing Office: Washington, DC, 1963; Vol. I. <http://babel.hathitrust.org/cgi/pt?id=uc1.31822010663441;seq=7;view=1up;num=i>.
- Venkatesan R.; Vengatesan, G.; Vedachalam, N. et al. Reliability Assessment and Integrity Management of Data Buoy Instruments Used for Monitoring the Indian Seas. *Applied Ocean Research* **2015**, *54*, 1–11. <https://doi.org/10.1016/j.apor.2015.10.004>.
- Weller, R. A.; Bradley, E. F.; Edson, J. B. et al. Sensors for Physical Fluxes at the Sea Surface: Energy, Heat, Water, Salt. *Ocean Science* **2008**, *4* (4), 247–263. <https://doi.org/10.5194/os-4-247-2008>.
- Wilkerson, J. C.; Earle, M. D. A study of Differences between Environmental Reports by Ships in the Voluntary Observing Programme and Measurements from NOAA Buoys. *Journal of Geophysical Research* **1990**, *95* (C3), 3373–3385.
- World Meteorological Organization (WMO). *International List of Selected, Supplementary and Auxiliary Ships* (WMO-No. 47). Geneva, 1955–. (Serial publication; recently annual. Editions prior to 1966 were entitled *International List of Selected and Supplementary Ships*; future editions will be known as *International List of Selected, VOSCLim, Supplementary and Auxiliary Ships*, <https://community.wmo.int/mmop-operational-information>.)
- World Meteorological Organization (WMO). *Precipitation Measurements at Sea* (WMO-No. 124). Geneva, 1962.
- World Meteorological Organization (WMO). *WMO Sea-ice Nomenclature* (WMO-No. 259). Geneva, 1970.
- World Meteorological Organization (WMO). *Comparative Sea-surface Temperature Measurements* (WMO-No. 336). Geneva, 1972.
- World Meteorological Organization (WMO). *The Meteorological Aspects of Ice Accretion on Ships* (WMO-No. 397). Geneva, 1974.
- World Meteorological Organization (WMO). *Precipitation Measurement at Sea*, Marine Meteorology and Related Oceanographic Activities Report No. 1. WMO: Geneva, 1981.
- World Meteorological Organization (WMO). *Wind Measurements Reduction to a Standard Level* (WMO/TD-No. 311). Geneva, 1989.
- World Meteorological Organization (WMO). *Compendium of Lecture Notes in Marine Meteorology for Class III and Class IV Personnel* (WMO-No. 434). Geneva, 1991.
- World Meteorological Organization (WMO). *The Accuracy of Ship's Meteorological Observations: Results of the VSOP-NA* (WMO/TD-No. 455). Geneva, 1991.
- World Meteorological Organization (WMO). *Guide to Wave Analysis and Forecasting* (WMO-No. 702). Geneva, 1998.
- World Meteorological Organization (WMO). The accuracy of meteorological observations from Voluntary Observing Ships: Present status and future requirements (Taylor, P. K.; Kent, E. C.). *Final Report of the First Session of the Commission for Marine Meteorology Working Group on Marine Observing Systems Subgroup on Voluntary Observing Ships* (Athens 1999), WMO TC CMM, 1999. <http://eprints.soton.ac.uk/347754/>.
- World Meteorological Organization (WMO). *Guide to the Global Observing System* (WMO-No. 488). Geneva, 2017.
- World Meteorological Organization (WMO). *Manual on Codes* (WMO-No. 306), Volume I.1. Geneva, 2019.
- World Meteorological Organization (WMO). *Manual on Codes* (WMO-No. 306), Volume I.2. Geneva, 2021.
- World Meteorological Organization (WMO). *International Cloud Atlas* (WMO-No. 407). Geneva, 2017.
- World Meteorological Organization (WMO). *Guide to Marine Meteorological Services* (WMO-No. 471). Geneva, 2018.
- World Meteorological Organization (WMO). *Manual on the WMO Integrated Global Observing System* (WMO-No. 1160). Geneva, 2021.

- World Meteorological Organization (WMO)/Intergovernmental Oceanographic Commission (IOC). *Guide to Data Collection and Location Services using Service Argos*, Data Buoy Cooperation Panel Technical Document No. 3. WMO and IOC: Geneva and Paris, 1995.
- World Meteorological Organization (WMO)/Intergovernmental Oceanographic Commission (IOC). *Guide to Moored Buoys and Other Ocean Data Acquisition Systems*, Data Buoy Cooperation Panel Technical Document No. 8. WMO and IOC: Geneva and Paris, 1996.
- World Meteorological Organization (WMO)/Intergovernmental Oceanographic Commission (IOC). *Global Drifter Programme Barometer Drifter Design Reference*, Data Buoy Cooperation Panel Report No. 4, Revision 2.2. WMO and IOC: Geneva and Paris 2009a.
- World Meteorological Organization (WMO)/Intergovernmental Oceanographic Commission (IOC). *Ship Observations Team Fifth Session*, JCOMM Meeting Report No. 63. WMO and IOC: Geneva and Paris, 2009b. http://sot.jcommops.org/vos/documents/sot5_report.pdf.
- World Meteorological Organization (WMO)/Intergovernmental Oceanographic Commission (IOC). *Third Session of the JCOMM Expert Team on Marine Climatology (Melbourne, Australia, 8–12 February 2010)*, JCOMM Meeting Report No. 70. WMO and IOC: Geneva and Paris, 2010.
- Yelland, M. J.; Moat, B. I.; Taylor, P. K. Air Flow Distortion over Merchant Ships, Progress Report to the Atmospheric Environment Service, Canada. 2001. <http://eprints.soton.ac.uk/67256>.
-

CHAPTER 5. SPECIAL PROFILING TECHNIQUES FOR THE BOUNDARY LAYER AND THE TROPOSPHERE

5.1 GENERAL

Special profiling techniques have been developed to obtain data at high temporal and spatial resolution which is needed for analysis, forecasting and research on the smaller meteorological scales and for various special applications. This chapter gives a general overview of current surface-based systems that can be used for these purposes. It is divided into two main parts: remote-sensing and in situ direct measuring techniques. Some of these techniques can be used for measurements over the whole troposphere, and others are used in the lower troposphere, in particular in the planetary boundary layer.

Remote-sensing techniques are based on the interaction of electromagnetic or acoustic energy with the atmosphere. The measuring instrument and the variable to be measured are spatially separated, as opposed to on-site (in situ) sensing. For atmospheric applications, the technique can be divided into passive and active techniques. Passive techniques make use of naturally occurring radiation in the atmosphere (microwave radiometers). Active systems (sodars, windprofilers, radio acoustic sounding systems (RASSs), lidars and GNSS) are characterized by the injection of specific artificial radiation into the atmosphere. These surface-based profiling techniques are described in 5.2. Other remote-sensing techniques relevant to this chapter are discussed in this volume, Chapter 7 (Radar measurements) and Volume IV (Space-based Observations).

Section 5.3 describes in situ techniques with instruments located on various platforms to obtain measurements directly in the boundary layer (balloons, boundary layer radiosondes, instrumented towers and masts, instrumented tethered balloons). Chapters 12 and 13 in Volume I describe the more widely used techniques using balloons to obtain profile measurements.

The literature on profiling techniques is substantial. For general discussions and comparisons see Derr (1972), WMO (1980), Martner et al. (1993) and the special issue of the *Journal of Atmospheric and Oceanic Technology* (Volume 11, No. 1, 1994; see <https://journals.ametsoc.org/view/journals/atot/11/1/atot.11.issue-1.xml>).

Users should take note of the detailed information that comes with specific commercial measurement systems. In particular, most include advice about site selection, safety, and the comparative advantages of specific signal-processing algorithms that can be turned on or off.

5.2 SURFACE-BASED REMOTE-SENSING TECHNIQUES

5.2.1 Acoustic sounders (sodars)

Sodars (sound detection and ranging) operate on the principle of the scattering of acoustic waves by the atmosphere. According to the theory of the scattering of sound, a sound pulse emitted into the atmosphere is scattered by refractive index variations caused by small-scale turbulent temperature and velocity fluctuations, which occur naturally in the air and are particularly associated with strong temperature and humidity gradients present in inversions. In the case of backscattering (180°), only temperature fluctuations with a scale of one half of the transmitting acoustic wavelength determine the returned echo, while, in other directions, the returned echo is caused by both temperature and velocity fluctuations, except at an angle of 90° , where there is no scattering.

Useful references to acoustic sounding include Brown and Hall (1978), Neff and Coulter (1986), Gaynor et al. (1990) and Singal (1990).

A number of different types of acoustic sounders have been developed, but the two most common types considered for operational use are the monostatic sodar and the monostatic Doppler sodar.

A monostatic sodar consists of a vertically pointed pulsed sound source and a collocated receiver. A small portion of each sound pulse is scattered back to the receiver by the thermal fluctuations which occur naturally in the air. The receiver measures the intensity of the returned sound. As in a conventional radar, the time delay between transmitting and receiving an echo is indicative of the target's range. In a bi-static sodar, the receiver is located some distance away from the sound source to receive signals caused by velocity fluctuations.

As well as measuring the intensity of the return signal, a monostatic Doppler sodar also analyses the frequency spectrum of the transmitted and received signals to determine the Doppler frequency shift between transmitted and backscattered sound. This difference arises because of the motion of the temperature fluctuations with the air, and provides a measure of the radial wind speed of the air. A Doppler sodar typically uses three beams, one directed vertically and two tilted from the vertical to determine wind components in three directions. The vertical and horizontal winds are calculated from these components. The vector wind may be displayed on a time-height plot at height intervals of approximately 30 to 50 m.

The maximum height that can be reached by acoustic sounders is dependent on system parameters, but also varies with the atmospheric conditions. Economical systems can routinely reach heights of 600 m or more with height resolutions of a few tens of metres.

A sodar might have the following characteristics:

<i>Parameter</i>	<i>Typical value</i>
Pulse frequency	1 500 Hz
Pulse duration	0.05 to 0.2 s
Pulse repetition period	2 to 5 s
Beam width	15°
Acoustic power	100 W

Monostatic sodars normally produce a time-height plot of the strength of the backscattered echo signal. Such plots contain a wealth of detail on the internal structure of the boundary layer and can, in principle, be used to monitor inversion heights, the depth of the mixing layer – changes in boundary stability – and the depth of fog. The correct interpretation of the plots, however, requires considerable skill and background knowledge, and preferably additional information from in situ measurements and for the general weather situation.

Monostatic Doppler sodar systems provide measurements of wind profiles as well as intensity information. Such systems are a cost-effective method of obtaining boundary layer winds and are particularly suited to the continuous monitoring of inversions and winds near industrial plants where pollution is a potential problem.

The main limitation of sodar systems, other than the restricted height coverage, is their sensitivity to interfering noise. This can arise from traffic or as a result of precipitation or strong winds. This limitation precludes their use as an all-weather system. Sodars produce sound, the nature and level of which is likely to cause annoyance in the near vicinity, and this may preclude their use in otherwise suitable environments.

Some systems rely upon absorbent foam to reduce the effect of external noise sources and to reduce any annoyance caused to humans. The physical condition of such foam deteriorates with time and must be periodically replaced in order to prevent deterioration in instrument performance.

5.2.2 **Wind profiler radars**

The term wind profiler is often used as an abbreviation for a whole class of Doppler radars that are specifically designed for determining vertical profiles of the wind. Unlike conventional weather radars, these instruments are able to make useful measurements even in the absence of precipitation and clouds. This clear air sensing capability is a truly unique feature of this radar. The use of wavelengths ranging from 0.2 to 7 m (corresponding to frequencies between about 1 300 and 40 MHz) makes it possible to detect echoes scattered from irregularities of the refractive index of air. If these have spatial scales of one half of the radar wavelength, then constructive interference occurs and makes the return strong enough to be detectable (Bragg condition). Note that no clear air scattering is observed if the half wavelength of the radar is smaller than the inner scale of turbulence, where refractive index irregularities vanish due to the dissipative effects of viscosity. In a first order approximation, the turbulent structures drift with the translational velocity of air, thus providing a direct measure of the wind.

Radar wind profilers not only receive electromagnetic waves backscattered at refractive index irregularities, but also echoes scattered from particles (mainly precipitation), airborne objects (birds, bats, airplanes) and even from the plasma in lightning channels. Also, echoes from the ground can be received through antenna side lobes. The relative contribution of these differing scattering processes is a function of radar wavelength.

There are two techniques for wind measurements by radar wind profilers, namely the Doppler method and the spaced-antenna method (Fukao et al., 2014), with most operational systems using the first method.

For the Doppler technique, the frequency shift, induced by the motion of the scattering matter along the line of sight of a particular beam direction, is measured and converted into a radial velocity. The horizontal and vertical wind components are obtained from sequentially made radial wind measurements in at least three linearly independent directions. The wind vector retrieval is based on further assumptions on the wind field structure. Horizontal homogeneity and stationarity of the mean wind field allows for a simple closed-form expression of this algorithm (see Teschke and Lehmann, 2017). Simple Doppler-beam-swinging configurations use a vertically pointing beam and about two to four oblique (about 15° off-vertical) beams. A higher number of off-vertical beams yield generally better results than the simple three-beam technique (Adachi et al., 2005). Other sampling configurations, such as velocity-azimuth display, are also possible.

The spaced-antenna technique uses a vertically pointing radar beam and at least three independent receiving vertically directed antennas. This allows for a correlation-based estimate of the wind speed based on the apparent motion of the backscattered interference or diffraction pattern on the ground. Corrections have to be made for temporal changes of the scattering structures to obtain an estimate of the horizontal wind. Spaced-antenna and Doppler techniques have comparative advantages and disadvantages, some of which are described in Dolman and Reid (2014).

The choice of operating frequency depends on the required altitude coverage and resolution but is strongly affected by regulatory constraints. In practice, most systems are built for the three frequency bands (approximately 50, 400 and 1 000 MHz) identified in the relevant regulatory decisions for spectrum allocation made by the World Radio Conference 1997 (Resolution 217). Obtaining the necessary frequency clearances (operating licences) can be an administrative problem and radio-frequency interference contaminations from other in-band radio services can lead to an additional challenge for the operation of a radar wind profiler. Typical characteristics are summarized in the table below.

<i>Profiler parameter</i>	<i>Stratosphere</i>	<i>Troposphere</i>	<i>Lower troposphere</i>	<i>Boundary layer</i>
Frequency (MHz)	50	400–500	400–500	1 000
Operating height range (km)	2–20	0.5–16	0.3–10	0.2–3
Vertical resolution (m)	150–500	150–500	150–300	50–300
Typical antenna size (m)	100×100	10×10	6×6	3×3

Radar wind profiler antennas typically employ a phase-array design with electronic beam steering, with the exception of a few mechanically steered dish-type antennas. The vertical resolution depends on the width of the transmitted pulse, and different pulse widths are typically used for specific low- and high-mode settings. Maximum height coverage is related to pulse width (through average power) so this choice trades range resolution for height coverage. Pulse-compression methods are also frequently used to improve height coverage without compromising range resolution. These are generally effective, but can potentially generate self-clutter (Wakasugi and Fukao, 1985).

The minimum usable height range depends on the antenna size, the pulse width, the recovery time of the radar receiver and the strength of possible near-range ground clutter returns. Because ground clutter is quite variable, this minimum range can change with time and site.

The strength of the received signal generally decreases with increasing height. This limits the height to which measurements can be taken. In contrast to the minimum range, the maximum range is a statistical quantity depending on both the characteristics of the radar hardware and the state of the atmosphere. It typically increases with the product of the mean transmitter power and the antenna aperture but is mainly subject to a physical (clear air scattering) limit given by the wavelength used. The maximum height varies considerably with the meteorological conditions and gaps in the coverage at lower heights may sometimes occur.

Care must be taken in siting profilers so as to minimize ground returns and to avoid possible in-band radio-frequency emissions of other radio services.

Large stratospheric profilers require large antenna arrays and high-power transmitters. It is therefore difficult to find suitable sites, and their minimum heights are not good enough for certain applications. They have the advantage of being able to routinely make wind measurements to about 20 km in height, and the measurements are not strongly affected by precipitation. Tropospheric profilers operating in the 400–500 MHz frequency band are likely the best compromise between height range covered and system size. Boundary layer profilers are less expensive and can use rather small antennas. Their vertical height range for clear air measurements is typically limited to the lower atmosphere, however the usable vertical range can increase significantly during precipitation, when scattering from hydrometeors becomes the dominant echoing mechanism.

The signal processing for Doppler wind profilers is similar to the processing employed in other Doppler radars. In contrast to weather radars, Doppler velocity resolution is typically better due to the longer dwell times, and the possibility of range and frequency aliasing can be fully avoided with a prudent sampling configuration. Since wind profilers are designed to receive the very weak returns from fluctuations of the refractive index, special algorithms for the filtering of ground and intermittent clutter echoes are mandatory. Intermittent clutter is comprised of unwanted echoes from aircraft, birds and insects. Migrating birds in particular can lead to grossly erroneous wind estimates if intermittent clutter suppression is not implemented (Bianco et al., 2013).

Radial wind measurements can be made with a resolution of a few seconds. As hydrometeors present a more efficient radar target than refractive index inhomogeneities for most profiler wavelengths, the measured radial velocity can be a weighted average of air velocity and the velocities of scattering particles. Practical experience has demonstrated that the horizontal wind vector can be estimated with sufficient accuracy from both clear-air and particle scattering, since the scattering particles usually follow the horizontal wind field almost instantaneously. Thus, the

horizontal wind can indeed be obtained in almost all weather conditions. Larger errors occur only if the implicit assumptions used in the wind estimation algorithm are violated. Note that the vertical wind can only be measured in a clear (particle-free) atmosphere.

Radar wind profilers are proven systems allowing for continuous, unattended operational measurements of the mean (upper-air) vertical wind profile directly above the site. The typical time resolution for a single wind profile ranges from about 10 to 60 minutes, depending on the instruments characteristics and configuration. The positive impact of such data in NWP has been successfully demonstrated (see, for example, Illingworth et al., 2015).

For further discussion see Gossard and Strauch (1983), Hogg et al. (1983), Weber et al. (1990), Weber and Wuertz (1990), WMO (1994), Wilczak et al. (1996), Muschinski et al. (2005), Hocking (2011), Doviak and Zrnić (2014), Fukao et al. (2014) and Hocking et al. (2016).

5.2.3 **Radio acoustic sounding systems**

A radio acoustic sounding system is used to measure the virtual temperature profile in the lower troposphere. The technique consists in tracking a short high-intensity acoustic pulse that is transmitted vertically into the atmosphere by means of a collocated microwave Doppler radar. The measuring technique is based on the fact that acoustic waves are longitudinal waves that create density variations of the ambient air. These variations cause corresponding variations in the local index of refraction of the atmosphere which, in turn, causes a backscattering of the electromagnetic energy emitted by the microwave Doppler radar as it propagates through the acoustic pulse. The microwave radar measures the propagation speed of these refractive index perturbations as they ascend at the local speed of sound. The acoustic wavelength is matched to one half of the microwave wavelength (the Bragg condition), so that the energy backscattered from several acoustic waves adds coherently at the receiver, thus greatly increasing the return signal strength. By measuring the acoustic pulse propagation speed, the virtual temperature can be calculated as this is proportional to the square of the pulse propagation speed minus the vertical air speed.

The extensive literature on this technique includes May et al. (1990), Lataitis (1992*a*, 1992*b*) and Angevine et al. (1994).

A variety of experimental techniques have been developed to sweep the acoustic frequency and then to obtain a virtual temperature profile. A number of RASSs have been developed by adding an acoustic source and suitable processing to existing wind profiler radars of the type mentioned above. For radar frequencies of 50, 400 and 1 000 MHz, acoustic frequencies of about 110, 900 and 2 000 Hz are required. At 2 000 Hz, acoustic attenuation generally limits the height coverage to 1 to 2 km. At 900 Hz, practical systems can reach 2 to 4 km. At 110 Hz, by using large 50 MHz profilers, maximum heights in the range of 4 to 8 km can be achieved under favourable conditions.

Comparisons with radiosondes show that, under good conditions, virtual temperatures can be measured to an accuracy of about 0.3 °C with height resolutions of 100 to 300 m. However, the measurements are likely to be compromised in strong winds and precipitation.

The RASS technique is a promising method of obtaining virtual temperature profiles. It has been used operationally, but has known biases. Further investigation is required before it can be used with confidence over a height range, resolution and accuracy that respond to user requirements.

5.2.4 **Microwave radiometers**

Thermal radiation from the atmosphere at microwave frequencies originates primarily from oxygen, water vapour, and liquid water and is dependent on their temperature and spatial distribution. For a gas such as oxygen, whose density as a function of height is well known, given the surface pressure, the radiation contains information primarily on the atmospheric temperature. Vertical temperature profiles of the lower atmosphere can be obtained by surface-

based passive microwave radiometers measuring the microwave thermal emission by oxygen in a spectral band near 60 GHz. Spectral measurements in the 22–30 GHz upper wing of the pressure broadened water vapour absorption band provide information on the integrated amount of water vapour and liquid water, and the vertical distribution of water vapour. In addition, spectral measurements in both bands, combined with infrared cloud-base temperature measurements, provide information on the integrated amount and the vertical distribution of liquid water. For further information, see Hogg et al. (1983), Westwater et al. (1990), Solheim et al. (1998), Ware et al. (2003) and Westwater et al. (2005).

Radiometers operating at different frequencies are maximally sensitive to temperature at particular ranges of atmospheric pressure. The sensitivity as a function of pressure follows a bell-shaped curve (the weighting function). The frequencies of the radiometers are chosen so that the peaks in the weighting functions are optimally spread over the heights of interest. Temperature profiles above the boundary layer are calculated by means of numerical inversion techniques using measured radiations and weighting functions. Space-based radiometry, described in Volume IV, precludes accurate temperature profiles from being obtained near the surface and in the boundary layer. This is because of the relatively broad width of the weighting function curves, radiation from the terrestrial surface and the fact that channels that are sensitive to the lower part of the atmosphere would also be sensitive to the skin temperature.

The principles of upward-looking radiometric temperature and humidity sounding from the terrestrial surface are well established. The temperature weighting functions of upward-looking profiling radiometers have narrow peaks near the surface that decrease with height. In addition, sensitivity to oxygen and water vapour emissions is not degraded by radiation from the terrestrial surface. This allows accurate temperature and humidity profile retrievals with relatively high resolution in the boundary layer and lower troposphere. On the other hand, the attenuation of microwave by the atmosphere, and the relatively broad width of the weighting function curves for channels sensitive to the upper part of the atmosphere, put a limit to the accuracy in retrieving temperature profiles above the boundary layer. Inversion techniques for upward-looking radiometers are based either on temperature and humidity climatology for the site that is typically derived from radiosounding, or based on variational techniques on modelling the relation between the measured radiation, vertical temperature and humidity profiles.

Surface-based radiometers usually have a reduced accuracy in retrieving temperature profiles when it rains or snows. It is due to the accumulation of water, snow (Woods et al., 2005) or ice (Fernández-González et al., 2014) over the radome, lack of scattering and emission/absorption effects of precipitation in the retrieval algorithm, and enhanced microwave attenuation in the atmosphere by precipitation. The first issue can be remedied by using a hydrophobic radome and forcing airflow over the radiometer surface to avoid accumulation of water, snow and ice (Chan, 2009) or making the observations at an off-zenith angle to stay away from the thin films of water (Xu et al., 2014). For the second issue, it can be handled by incorporating observations from radar and parameterization of rain microphysics in the retrieval (Chan and Lee, 2015).

Surface-based and space-based radiometers are highly complementary. Space-based measurements provide coarse temporal and spatial resolution in the upper troposphere, and surface-based measurements provide high temporal and spatial resolution in the boundary layer and lower troposphere. Retrieved profiles from surface-based radiometers can be assimilated into numerical weather models to improve short-term (1–12 h) forecasting by providing upper-air data in the interval between radiosonde soundings. Alternatively, raw brightness temperature from terrestrial radiometers can be assimilated directly into numerical weather models. This approach improves results by avoiding errors inherent in the profile retrieval process and also allows for flow-dependent considerations in the assimilation. A similar method, which assimilates raw satellite radiometer radiances directly into weather models, demonstrated improved results years ago and is now widely used.

The main advantages of surface-based radiometers are their ability to produce continuous measurements in time, and their ability to measure cloud liquid. Continuous upper-air temperature, humidity and cloud liquid measurements can be used to improve nowcasting and short-term precipitation forecasting. Changes in brightness temperature can also help to nowcast the onset of convective events (Chakraborty et al., 2016). These continuous

measurements can be also used to detect the development or time of arrival of well-defined temperature changes (for studies of gas emissions, air pollution, urban heat islands, severe weather forecasting and warnings (Kadygrov et al., 2003). Real-time radiometer data can also be used for alerting low-level wind-shear events for aviation use (Chan and Lee, 2013).

Profiling radiometer reliability and accuracy have been widely demonstrated during long-term arctic, mid-latitude and tropical operations (Güldner and Spänkuch, 2001; Liljegren et al., 2005). One result based on 13 months of operations (Gaffard and Hewison, 2003) shows that the root mean square (RMS) value of the difference between the temperature observed by the radiosonde and that retrieved by the microwave radiometer ranges from 0.5 K (near the surface) to 1.8 K (at a height of 5 km). A second result (Güldner and Spänkuch, 2001) is based on 18 months of operations during which radiometer retrievals with four radiosonde soundings were compared daily. This shows a similar RMS value from 0.6 K (near the surface) to 1.6 K (at a height of 7 km in summer and 4 km in winter). The RMS value of the water vapour profile is not more than 1 g m^{-3} in all altitudes (Gaffard and Hewison, 2003; Güldner and Spänkuch, 2001).

Terrestrial profiling radiometers demonstrate significant economic and practical benefits when lower tropospheric temperature, humidity and cloud liquid measurements with high temporal resolution are required, and where moderate vertical resolution is acceptable. Commercial profiling radiometer prices have dropped significantly over the past several years.

5.2.5 **Laser radars (lidars)**

Electromagnetic energy at optical and near-optical wavelengths (from ultraviolet through visible to infrared) generated by lasers is scattered by atmospheric gas molecules and suspended particles. Such scattering is sufficient to permit the application of the radar principle to make observations of the atmosphere by means of lidar (light detection and ranging). Optical scattering can generally be divided into inelastic and elastic. When the wavelength of the laser energy, scattered by atmospheric constituents, differs in wavelength from the incident laser wavelength, the process is called inelastic scattering. The most widely used inelastic scattering process used in experimental atmospheric lidar systems is Raman scattering, which results from an exchange of energy between incident photons and the molecular rotational and vibrational states of the scattering molecules. In elastic scattering processes, the incident and the scattered wavelengths are the same. This scattering may be Rayleigh or Mie scattering and depends on the species and size of particles with respect to the incident laser wavelength (see Chapter 7 of the present volume for further description of Rayleigh scattering). These major scattering processes can occur simultaneously in the atmosphere.

For further reference see Hinkley (1976), WMO (1982), Thomas (1991) and Syed and Browell (1994).

The majority of lidars are operated in a monostatic mode, whereby the receiver is collocated with the laser transmitter. A typical lidar system uses a pulsed laser to transmit pulses of coherent light into the atmosphere. The average power of the laser used varies from a few milliwatts to tens of watts. An optical telescope mounted adjacent to the laser is used to capture the backscattered energy. The light collected by the telescope is focused onto a photomultiplier or photoconductive diode. The received information is normally made available on a display for real-time monitoring and is transferred to a computer for more detailed analysis.

The strength of the return signal is dependent both on the amount of scattering from the target and on the two-way attenuation between the lidar and the target — this attenuation depends on the proportion of the beam's energy scattered from its path and on the absorption by atmospheric gases. The scattering and absorption processes are exploited in different lidars to provide a variety of measurements.

Lidars based on elastic scattering (called Rayleigh or Mie lidars, or simply lidars), are mostly used for studies on clouds and particulate matter. The measurement of cloud-base height by a lidar is very straightforward; the rapid increase in the signal that marks the backscattered return

from the cloud base can be readily distinguished; the height of the cloud base is determined by measuring the time taken for a laser pulse to travel from the transmitter to the cloud base and back to the receiver (see Volume I, Chapter 15).

Lidars are also used to detect the suspended particles present in relatively clear air and to map certain structural features such as thermal stability and the height of inversions. Natural atmospheric particulate levels are sufficiently high in the lower atmosphere to allow lidars to measure air velocities continuously in the absence of precipitation, like weather radars. For the measurement of atmospheric wind, the most commonly used methods include pulsed and continuous-wave coherent Doppler wind lidar, direct-detection Doppler wind lidar and resonance Doppler wind lidar. The annex discusses the requirements and performance test procedures for heterodyne pulsed Doppler lidar techniques.

Lidars can also be used to map and measure the concentration of anthropogenic particulates, such as those originating from industrial stacks. Lidar observations have made very extensive and well-documented contributions to the study of stratospheric aerosol particulate concentration, which is strongly influenced by major volcanic eruptions and is an important factor in the global radiation balance.

It is much more difficult to obtain quantitative data on clouds because of the variations in shape and distribution of droplets, water content, discrimination between water, ice and mixed phases, and the properties of suspended particles and aerosols. Indeed, such measurements require complex multiparameter research systems making several measurements simultaneously, using hypotheses concerning the optical properties of the medium, and complex mathematical data-reduction methods.

Differential absorption lidars (DIALs) work on the principle that the absorption coefficient of atmospheric gases varies greatly with wavelength. A DIAL system normally uses a laser that can be tuned between two closely spaced frequencies, one which is strongly absorbed by a particular gas, and one which is not. The differences in the measurements as a function of range can be used to estimate the concentration of the gas under study. This is a most promising remote-sensing technique for the measurement of atmospheric composition and has been successfully used to measure concentrations of water, sulphur dioxide, nitrogen dioxide and, in particular, ozone.

The application of Raman scattering is of particular interest because the scattered radiation is frequency shifted by an amount which depends on the molecular species (Stokes lines). The strength of the backscattered signal is related to the species concentration. Raman lidars do not require a particular wavelength or tuned laser; laser wavelengths can be selected in a spectral region free from atmospheric absorption. By measuring the Raman spectrum, spatially resolved measurements can be taken of preselected atmospheric constituents, which have been used to obtain tropospheric profiles of water vapour, molecular nitrogen and oxygen, and minor atmospheric constituents. The main disadvantages are the lack of sensitivity over long ranges owing to the small scattering cross-sections and the requirement for high-power lasers, which can lead to eye-safety problems in practical applications.

Lidar systems have provided a great deal of useful information for research studies but have had limited impact as operational tools. This is because they are relatively expensive and require very skilled staff in order to be developed, set up and operated. In addition, certain lidars are able to operate only under restricted conditions, such as in darkness or in the absence of precipitation.

5.2.6 Global navigation satellite system

The main purpose of GNSS is positioning, but since an atmospheric term influences the accuracy of the position estimate, meteorological content can be inferred from the estimated error. The time delay experienced by a signal originating from a satellite and measured by a receiver on Earth is related to the refractivity along the signal path, and thus also to the temperature and humidity along this path.

Meteorological information inferred from ground-based GNSS requires a surface network of GNSS receivers, a data connection and a processing facility. In general, a GNSS network of receivers is installed for land surveying purposes, and as a result close collaboration with national surveying institutes has been established in several countries. The collaboration is generally based on sharing sites and/or sharing information.

Additional information on processing techniques is available in WMO (2006b).

5.2.6.1 **Description of the global navigation satellite system**

The GNSS consists of three segments: the space, the ground and the user segment. The space segment comprises a number of satellites in orbit. Currently four systems are deployed or are being deployed: GPS (United States), GLONASS (Russian Federation), Galileo (European Union) and Compass (China). GNSS satellites transmit time coded signals in a number of carrier wave frequencies which differ for different satellite systems.

The principle of GNSS is the same for all four systems. On-board atomic clocks control all signal components in the satellites. The ground segment controls the satellites for orbit adjustment and provides the broadcast ephemerides, which are disseminated to the user segment via the navigation message of the GNSS signal. A GNSS antenna and receiver (surface-based or space-borne) form the user segment. The receiver compares the time coded signal from the GNSS satellites with its own internal clock, from which the receiver can compute the pseudo ranges (P) to each satellite in view. When at least four pseudo ranges are observed the receiver can compute its position and its clock error. The standard positioning technique using the time coded signals has an accuracy of about 3–5 m.

The GNSS main observables are pseudo range (P) and carrier phase (L). For example, the GPS signals are broadcast at two different frequencies: namely L1 (1 575.42 MHz) and L2 (1 227.60 MHz). Both frequencies transmit P and L observables. Thus, for a dual-frequency receiver, four observables are available per epoch. Equations 5.1 and 5.2 present both P and L expressed as a sum of all error contributions forming the GNSS measurement, that is:

$$P = \rho + c(dt_{\text{rec}} - dt_{\text{sat}}) + \delta_{\text{rel}} + L_{\text{atm}} + I + K + M + \delta_{\text{tide}} + \varepsilon_P \quad (5.1)$$

$$L = \rho + c(dt_{\text{rec}} - dt_{\text{sat}}) + \delta_{\text{rel}} + L_{\text{atm}} - I + N\omega_L + K + M + \delta_{\text{tide}} + \varepsilon_L \quad (5.2)$$

where c is the speed of light, ρ is the geometric distance between the satellite phase centre and the receiver phase centre, dt_{sat} is the satellite clock offset, dt_{rec} is the receiver clock offset, L_{atm} is the tropospheric delay, or slant total delay, due to the refractive nature of the atmosphere, I is the ionospheric delay along the ray path, δ_{rel} is the relativistic error, K is the receiver instrumental error, M is the multipath effect, δ_{tide} is the receiver position error due to polar tide, solid Earth tide and ocean loading, N is the ambiguity term (only relevant for carrier phase measurements, equation 5.2), ω_L is one wavelength contribution due to circular polarization of the signal and ε is the unmodelled noise error.

The observables have different uncertainty levels and different characteristics. In particular, phase measurements have a noise level of a few millimetres and are very accurate in comparison to pseudo range, which has an uncertainty of a few metres. Carrier phase is the primary and most important observable for low uncertainty parameter estimation, but pseudo-range observables are better suited for the observation and removal of specific receiver-related errors (multipath, and the like). Linear combination of the same kind of observable (P or L) measured at the two different frequencies is used to remove the first order of the ionosphere effect. Other techniques, such as double differencing, can remove the satellite and receiver clock error. However, this requires careful processing of the GNSS data.

5.2.6.2 Tropospheric global navigation satellite system signal

The atmospheric excess path is caused by refraction and bending of the signal due to gradients in refractive index n . According to Fermat's principle, this excess path is:

$$L_{\text{atm}} = \int_s n ds - D + \Delta S \approx \int_s (n-1) ds \quad (5.3)$$

where $D (= \int ds)$ is the geometric distance and ΔS the excess path due to bending; the latter can be neglected for elevations larger than 10 degrees. The refractivity N is defined as $N = 10^6 (n - 1)$ and, according to Smith and Weintraub (1953) and Thompson et al. (1986),

$$\begin{aligned} N &= k_1 \rho R_d + (k_2 R_v - k_1 R_d + R_v / T k_3) \rho_w \\ &= N_h + N_w \end{aligned} \quad (5.4)$$

for the neutral atmosphere. Here, ρ is air density (kg m^{-3}), ρ_w is water vapour density (kg m^{-3}), T is temperature (K) and $R_d = 287.05 \text{ J kg}^{-1} \text{ K}^{-1}$ and $R_v = 461.51 \text{ J kg}^{-1} \text{ K}^{-1}$ are the gas constants for dry air and water vapour. The empirical constants are $k_1 = 77.6 \text{ K hPa}^{-1}$, $k_2 = 70.4 \text{ K hPa}^{-1}$ and $k_3 = 373 \text{ 900 K}^2 \text{ hPa}^{-1}$ (Thayer, 1974). The first term in equation 5.4 is the hydrostatic refractivity, N_h , and the second term is called the wet refractivity, N_w .

Within a so-called network solution of GNSS data, the tropospheric delay is mapped to the zenith for all elevation and azimuth angles. In this way the number of unknowns is reduced and the position of the receiver can be estimated accurately. The mapped slant total delay to the zenith is called the zenith total delay (ZTD). When the precise position is estimated, an estimate of the atmospheric part of the signal can be retrieved. The ZTD can be considered as the sum of the zenith hydrostatic delay (ZHD) and the zenith wet delay (ZWD) (or, better, zenith non-hydrostatic delay). The integrals in the zenith direction of the hydrostatic and wet refractivity (expressed in metres) are:

$$\text{ZHD} = 10^{-6} \int_z N_h dz \quad (5.5)$$

$$\text{ZWD} = 10^{-6} \int_z N_w dz \quad (5.6)$$

5.2.6.3 Integrated water vapour

ZHD is related to the dry part of the atmosphere and, due to its stationary nature, can be estimated very accurately using the surface pressure measurements (p_s) and the location of the receiver (height h and latitude φ), using for example the Saastamoinen (1972) approximation, that is:

$$\text{ZHD}_{\text{saas}}(p_s, h, \varphi) = 2.2768 \cdot 10^{-5} p_s \left(1 - 2.66 \cdot 10^{-3} \cos(2\varphi) - 2.8 \cdot 10^{-7} h \right)^{-1} \quad (5.7)$$

The ZHD represents approximately 90% of the entire tropospheric path delay. On the other hand, the ZWD cannot be sufficiently well modelled by surface data acquisition due to the irregular distribution of water vapour in the atmosphere. The ZWD can be rewritten as (following Davis et al., 1985):

$$\text{ZWD} = 10^{-6} \left[k_2 R_v - k_1 R_d + k_3 R_v \left(\int_z \rho_w T^{-1} dz \right) \left(\int_z \rho_w dz \right)^{-1} \right] \int_z \rho_w dz \quad (5.8)$$

and by defining the weighted mean temperature as:

$$T_m = \left(\int_z \rho_w dz \right) \left(\int_z \rho_w T^{-1} dz \right)^{-1} \quad (5.9)$$

then:

$$\text{ZWD} = k'(T_m) \int_z \rho_w dz = k'(T_m) \text{IWV} \quad (5.10)$$

where IWV is the vertically integrated column of water vapour overlying the GPS receiver. Based on, for example, radiosonde observations, the weighted mean temperature can be estimated

by the surface temperature (T_s), that is $k'(T_m) \approx k(T_s)$ (Bevis et al., 1994). Thus, the IWV can be estimated using the estimated ZTD, surface pressure (p_s), antenna height (h) and latitude (φ) of the receiver:

$$\text{IWV} = k(T_s)^{-1} (\text{ZTD} - \text{ZHD}_{\text{saas}}(p_s, h, \varphi)) \quad (5.11)$$

The value of $k(T_s)$ is approximately 6.5 kg m^{-3} .

5.2.6.4 **Measurement uncertainties**

Since ZTD is estimated, its accuracy depends on the method used, the accuracy of a priori information used, the stability of the receiver position and many other things. For example, the accuracy of the position of the satellite orbits will in general be higher after approximately 14 days when the so-called final orbits are available. Therefore, a distinction has to be made between near-real-time and post-processed estimates of ZTD. The accuracy of IWV is obviously closely related to the accuracy of the ZTD estimate.

The measurement uncertainty of near-real-time estimates is about 10 mm. For post-processed estimates, this value is about 5 to 7 mm. The measurement uncertainty of IWV is dependent on the total amount of water vapour and is of the order of 5% to 10% (Elgered et al., 2004). The mean values have a clear seasonal signature: at mid latitudes very low values can be observed in winter (below 5 kg m^{-2}) and values of 40 kg m^{-2} can be seen during summer. In the tropics, values higher than 50 kg m^{-2} are not uncommon.

5.3 **IN SITU MEASUREMENTS**

5.3.1 **Balloon tracking**

Balloon tracking is frequently used to obtain boundary layer winds and is usually performed by optical theodolites or a tracking radar. Volume I, Chapter 13, gives a more general account of windfinding.

When making lower tropospheric soundings, it is desirable to use a slow rate of balloon ascent in order to give high vertical resolution. The reduced rate of ascent may be achieved either by means of a brake parachute or by a reduced free lift.

For radar tracking, a small radar reflector is suspended below the balloon. For lower tropospheric soundings, the radar should be able to provide data at ranges as short as 100 m, and ideally the launch point must be farther from the radar in a downwind direction than this minimum range.

A basic wind measurement can be taken using a single optical theodolite, but, in order to obtain reasonably accurate winds, a two-theodolite system is required. The baseline between the theodolites should exceed 1 km. In order to facilitate the sounding procedure and to ensure height accuracy, the theodolites should be equipped with computer interfaces so that the data can be logged and the necessary calculations performed in a timely manner. Under good conditions, wind profiles can be obtained up to an altitude of 3 000 m. However, the technique fails in adverse conditions such as precipitation, low cloud or fog.

It is, of course, possible to obtain additional wind data in the lower atmosphere using conventional radiosondes by taking more frequent tracking measurements in the first few minutes of a normal full sounding, for example, between 2 and 10 per minute.

5.3.2 **Boundary layer radiosondes**

Conventional radiosonde systems are described in detail in Volume I, Chapter 12. Special radiosondes have been designed specifically to make detailed observations of the boundary

layer and lower troposphere. They differ from conventional radiosondes in that the sensors have greater sensitivity and faster response rates. Such radiosondes are used to measure temperature, humidity and wind profiles in the layer from the surface to elevations of typically 3 to 5 km.

The vertical ascent rate of these radiosondes is usually arranged to be between 150 and 200 m min⁻¹, which is rather slower than conventional radiosondes. The slower rate of ascent allows more detailed vertical profiles to be produced. The rate of ascent is normally determined by selecting an appropriately sized balloon, but may be modified by the use of a trailing brake parachute.

Because these instruments are required only to reach a limited height, they can normally be carried by a pilot balloon. In other respects, the sounding procedures and data processing are similar to those employed by standard radiosondes.

For soundings to an altitude of no more than 2 000 m, the pressure sensor is sometimes dispensed with, which results in a simpler and less expensive radiosonde. Even simpler systems are available which measure temperature only.

The basic requirements for boundary layer radiosondes are as follows:¹

<i>Variable</i>	<i>Operating range</i>	<i>Resolution</i>
Pressure	1 050 to 500 hPa	±0.5 hPa
Temperature	+40 to -40 °C	±0.1 K
Humidity	100 to 20 (or 10)%	±2%
Wind speed	0.5 to 60 m s ⁻¹	±0.5 m s ⁻¹
Wind direction	0° to 360°	±5°

Measurements are typically taken at least every 30 s to give a vertical resolution of 50 to 100 m.

5.3.3 Instrumented towers and masts

Special instrumented towers and masts are used for many purposes, especially for the estimation of the diffusion of atmospheric pollution. A discussion is provided by Panofsky (1973).

For some purposes, the height of the tower must be up to 100 m, and for air-pollution monitoring and control projects it should exceed the height of the important sources of pollution by at least 50 m.

Measurements of temperature, humidity and wind should be made at several (at least two or three) levels, the lowest of which should be at the level of standard meteorological screen, close to the tower or mast. The number of measuring levels depends upon both the task and the height of the tower or mast. The use of just two levels provides no information on the shape of the vertical profile of meteorological variables and is, thus, very limiting. The number of measuring levels is usually greater for research projects than for routine use.

Usually, the data are processed and presented automatically together with differences between the levels that are provided to characterize the meteorological conditions. If the data are to be used directly by non-meteorological staff – such as those concerned with keeping concentrations of air pollutants within safe limits – they are often processed further by computer to provide derived data which are easily applied to the task in hand.

¹ These requirements for boundary layer profile measurements differ from those for surface measurements in Volume I, Chapter 1, Annex 1.A.

The sensors most commonly used for measurements on towers or masts are as follows:

- (a) Temperature: electrical resistance or thermocouple thermometers in screens, with or without aspiration;
- (b) Humidity: psychrometers, electrochemical or electromechanical sensors in screens;
- (c) Wind: cup and vane, propeller, sonic or hot-wire devices.

All sensors should have linear or linearized characteristics and their time constants should be small enough to ensure that the data gathered will adequately reflect local changes in the meteorological variables.

It is important that the structure of the tower or mast should not affect the sensors and their measurements appreciably. For open structures, booms – whether stationary or retractable – should be at least 2 m long, and preferably long enough to keep the sensors at least 10 tower diameters removed from the tower or mast. For solid structures, or where the required booms would not be practicable, a double system is required at each level, with booms on opposite sides of the tower or mast extending for at least three times the structure diameter. Measurements at a given time are then taken from the sensors exposed to the undisturbed wind.

Sometimes, in special situations, towers can be used to gather meteorological profile data without the direct mounting of fixed sensors; rather, a simplified method of sounding is used. A pulley is fastened at the highest possible point and a closed loop of rope extending to ground level is used to carry a radiosonde up and down the levels required by means of a hand- or motor-operated winch. The radiosonde, which is modified to include wind sensors, transmits its data to an appropriate receiving system at ground level. Much more vertical detail is possible than that provided by a boom installation, and the altitudes of significant features can be determined. However, sustained observation is possible at only a single level.

For an accurate definition of the extent of pollution dispersion in certain weather conditions, the tower height may be too limited. In such circumstances, unless a radiosonde station is within about 50 km, a special radiosonde is provided at the site of the tower or mast for making local soundings up to an altitude of about 3 000 m. In addition to their main purpose, the data obtained can be treated as complementary to those of the basic aerological network, and can also be used in more detailed investigations of local weather phenomena.

Tower measuring equipment requires periodical checking by highly qualified instrument maintenance staff who should pay special attention to the state and performance of sensors and recorders and the connecting cables, sockets and plugs exposed to outdoor weather conditions.

5.3.4 Instrumented tethered balloons

Typical applications of instrumented tethered balloons include the measurement of temperature, humidity and wind profiles (and their short-period changes) from the surface to an altitude of about 1 500 m, and longer-period investigation of the meteorological conditions at one or more selected levels. The sensors are suspended in one or more packages beneath the balloon, or clamped to the tethering cable. The sensor's response is normally telemetered to the ground either by radio, or by conductors incorporated into the tethering cable. The techniques are discussed by Thompson (1980).

Tethered-balloon systems tend to use either large (~600 m³) or small (~10 to 100 m³) balloons. The small balloons are normally used to obtain profiles, and the larger ones to obtain measurements at multiple levels. Tethered balloons should be designed for low drag and to ride steadily. They are usually inflated with helium. Larger balloons should be able to carry a load of up to 50 kg (in addition to the tethering cable) to an altitude of 1 500 m. The balloon should be capable of operation at wind speeds of up to 5 m s⁻¹ at the surface and 15 m s⁻¹ at altitudes within the operational range. The tethering cable of a large balloon should be able to withstand a force of 2 000 to 3 000 kg to avoid a breakaway (200 to 300 kg for smaller balloons).

Tethered-balloon flying is subject to national rules concerning aviation safety. For this reason and for the convenience of the operating staff, the use of balloons which have distinct colours and night-warning lights is highly recommended. An automatic device for the rapid deflation of the balloon is mandatory, while a metallized radar target suspended below the balloon is optional.

The main factors limiting tethered-balloon operation are strong wind speed aloft, turbulence near the surface and lightning risk.

The winch used to control the balloon may be operated electrically or by hand. At least two speeds (for example, 1 and 2 m s⁻¹) should be provided for the cable run. In addition, the winch should be equipped with a hand-brake, a cable-length counter and a tension gauge. The winch should be electrically earthed, whether electrically operated or not, as protection against atmospheric discharges.

The use of conductors to convey the sensor signals back to the ground is undesirable for a number of reasons. In general, it is preferable to use special radiosondes. Such radiosondes will have better resolution than those normally employed for free flights. The temperature and humidity sensors must have a horizontal shield to provide protection against solar radiation and rainfall, while allowing for adequate ventilation. Extra sensors are needed for wind speed and direction.

The basic requirements are the following:²

<i>Variable</i>	<i>Operating range</i>	<i>Resolution</i>
Pressure	1 050 to 850 hPa	±0.5 hPa
Temperature	40 to -20 °C	±0.1 K
Humidity	100 to 20 (or 10)%	±2%
Wind speed	0.5 to 15 m s ⁻¹	±0.5 m s ⁻¹
Wind direction	0° to 360°	±1°

For telemetry, one of the standard radiosonde frequencies may be used; the 400 MHz allocation is a frequent choice. The maximum weight, including the battery, should be within the load capability of the balloon; a limit of 5 kg is reasonable. The radiosonde should be suspended at least three balloon diameters below the balloon in a stable condition so that adequate shielding and ventilation are maintained.

A major problem encountered in the measurement of turbulent, rather than mean, quantities is the effect of cable vibration and balloon motion on the measurements. Special techniques have to be used for such measurements.

The ground-based equipment must include a receiver and recorder. The data are usually processed with the aid of a small computer.

Soundings can be performed during the ascent and descent of the balloon, either continuously or with pauses at selected levels. For the lower levels, height can be estimated from the length of the cable paid out, but at higher levels this method is no more than an approximation and an alternative is necessary. This takes the form of a calculation by means of the hydrostatic equation, using the observed distribution of pressure, temperature and humidity. Thus, the increment in geopotential metres from level n to level $n+1$ is given by:

$$29.27 T_v \ln(p_n / p_{n+1}) \quad (5.12)$$

² These requirements for boundary layer profile measurements differ from those for surface measurements in Volume I, Chapter 1, Annex 1.A.

where T_v is the mean of the virtual temperatures at levels n and $n+1$; and p_n and p_{n+1} are the two associated pressures. If conversion from geopotential to geometric height is required, this is readily done by using the Smithsonian meteorological tables; however, this is unlikely to be necessary. The height of the station barometer is taken as the datum for these calculations.

If the meteorological variables are observed using the level-by-level method, a few measuring cycles should be taken at each level, with the time required for stabilization being 2 to 3 min. In this way, the whole sounding sequence could take from a half to one whole hour. As for all radiosondes, a baseline check in a control screen should be made just before use, to establish the differences with a barometer and an aspirated psychrometer. A similar check should also be made just after the sounding is completed. Again, as for regular radiosonde ascents, the station-level data should be obtained not from the radiosonde data, but from conventional instruments in a standard station screen.

For the sounding data, pressure, temperature and humidity should be averaged at each level. For wind speed, the average should be calculated for a period of 100 or 120 s. If wind direction is not measured directly, it can be roughly estimated from the orientation of the balloon's longitudinal axis with respect to the north. The uncertainty of this method is $\pm 30^\circ$.

It should be stressed that operators must advise air traffic authorities of their plans and obtain permission for each sounding or series of soundings using tethered balloons.

ANNEX. GROUND-BASED REMOTE-SENSING OF WIND BY HETERODYNE PULSED DOPPLER LIDAR

(This annex presents the text of a common ISO/WMO standard. It is also published, with identical content, as ISO 28902-2:2017 (E)).

INTRODUCTION

Lidars (light detection and ranging), standing for atmospheric lidars in the scope of this annex, have proven to be valuable systems for remote-sensing of atmospheric pollutants, of various meteorological parameters such as clouds, aerosols, gases and (where Doppler technology is available) wind. The measurements can be carried out without direct contact and in any direction as electromagnetic radiation is used for sensing the targets. Lidar systems, therefore, supplement the conventional in situ measurement technology. They are suited for a large number of applications that cannot be adequately performed by using in situ or point measurement methods.

There are several methods by which lidar can be used to measure atmospheric wind. The four most commonly used methods are pulsed and continuous-wave coherent Doppler wind lidar, direct-detection Doppler wind lidar and resonance Doppler wind lidar (commonly used for mesospheric sodium layer measurements). For further reading, refer to references [1] and [2].

This annex¹ describes the use of heterodyne pulsed Doppler lidar systems. Some general information on continuous-wave Doppler lidar can be found in Attachment A. An International Standard on this method is in preparation.

1. SCOPE

This annex specifies the requirements and performance test procedures for heterodyne pulsed Doppler lidar techniques and presents their advantages and limitations. The term “Doppler lidar” used in this annex applies solely to heterodyne pulsed lidar systems retrieving wind measurements from the scattering of laser light onto aerosols in the atmosphere. Their performances and limits are described based on standard atmospheric conditions.

This annex describes the determination of the line-of-sight wind velocity (radial wind velocity).

Note: Derivation of wind vector from individual line-of-sight measurements is not described in this annex since it is highly specific to a particular wind lidar configuration. One example of the retrieval of the wind vector can be found in Attachment B.

This annex does not address the retrieval of the wind vector.

This annex may be used for the following application areas:

- (a) Meteorological briefing for, for example, aviation, airport safety, marine applications and oil platforms;
- (b) Wind power production, for example, site assessment and power curve determination;
- (c) Routine measurements of wind profiles at meteorological stations;

¹ Whereas this is referred to as an annex in the *Guide to Meteorological Instruments and Methods of Observation* (WMO-No. 8), it is referred to as a standard in the ISO document.

- (d) Air pollution dispersion monitoring;
- (e) Industrial risk management (direct data monitoring or by assimilation into micro-scale flow models);
- (f) Exchange processes (greenhouse gas emissions).

This annex addresses manufacturers of heterodyne pulsed Doppler wind lidars, as well as bodies testing and certifying their conformity. Also, this annex provides recommendations for the users to make adequate use of these instruments.

2. **NORMATIVE REFERENCES**

There are no normative references in this annex.

3. **TERMS AND DEFINITIONS**

For the purposes of this annex, the following terms and definitions apply.

Data availability. Ratio between the actual considered measurement data with a predefined data quality and the number of expected measurement data for a given measurement period;

Displayed range resolution. Constant spatial interval between the centres of two successive range gates;

Note: The displayed range resolution is also the size of a range gate on the display. It is determined by the range gate length and the overlap between successive gates.

Effective range resolution. Application-related variable describing an integrated range interval for which the target variable is delivered with a defined uncertainty;

Source: ISO 28902-1:2012, term 3.14

Effective temporal resolution. Application-related variable describing an integrated time interval for which the target variable is delivered with a defined uncertainty;

Source: ISO 28902-1:2012, term 3.12, modified

Extinction coefficient, α . Measure of the atmospheric opacity, expressed by the natural logarithm of the ratio of incident light intensity to transmitted light intensity, per unit light path length;

Source: ISO 28902-1:2012, term 3.10

Integration time. Time spent in order to derive the line-of-sight velocity;

Maximum acquisition range, R_{MaxA} . Maximum distance to which the lidar signal is recorded and processed;

Note: It depends on the number of acquisition points and the sampling frequency.

Maximum operational range, R_{MaxO} . Maximum distance to which a confident wind speed can be derived from the lidar signal;

Notes:

1. The maximum operational range is less than or equal to the maximum acquisition range.
2. The maximum operational range is defined along an axis corresponding to the application. It is measured vertically for vertical wind profiler. It is measured horizontally for scanning lidars able to measure in the full hemisphere.
3. The maximum operational range can be increased by increasing the measurement period and/or by downgrading the range resolution.
4. The maximum operational range depends on lidar parameters but also on atmospheric conditions.

Measurement period. Interval of time between the first and last measurements;

Minimum acquisition range, R_{MinA} . Minimum distance from which the lidar signal is recorded and processed;

Note: If the minimum acquisition range is not given, it is assumed to be zero. It can be different from zero, when the reception is blind during the pulse emission.

Minimum operational range, R_{MinO} . Minimum distance where a confident wind speed can be derived from the lidar signal;

Notes:

1. The minimum operational range is also called blind range.
2. In pulsed lidars, the minimum operational range is limited by the stray light in the lidar during pulse emission, by the depth of focus, or by the detector transmitter/receiver switch time. It can depend on pulse duration (T_p) and range gate width.

Physical range resolution. Width (FWHM) of the *range weighting function*;

Range gate. Width (FWHM) of the weighting function selecting the points in the time series for spectral processing and wind speed computation;

Notes:

1. The range gate is centred on the measurement distance.
2. The range gate is defined in number of bins or equivalent distance range gate.

Range resolution. Equipment-related variable describing the shortest range interval from which independent signal information can be obtained;

Source: ISO 28902-1:2012, term 3.13

Range weighting function. Weighting function of the radial wind speed along the line of sight;

Temporal resolution. Equipment-related variable describing the shortest time interval from which independent signal information can be obtained;

Source: ISO 28902-1:2012, term 3.11

Velocity bias. Maximum instrumental offset on the velocity measurement;

Note: The velocity bias has to be minimized with adequate calibration, for example, on a fixed target.

Velocity range. Range determined by the minimum measurable wind speed, the maximum measurable wind speed and the ability to measure the velocity sign, without ambiguity;

Note: Depending on the lidar application, velocity range can be defined on the radial wind velocity (scanning lidars) or on horizontal wind velocities (wind profilers).

Velocity resolution. Instrumental velocity standard deviation;

Note: The velocity resolution depends on the pulse duration, the carrier-to-noise ratio and integration time.

Wind shear. Variation of wind speed across a plane perpendicular to the wind direction.

4. FUNDAMENTALS OF HETERODYNE PULSED DOPPLER LIDAR

4.1 Overview

A pulsed Doppler lidar emits a laser pulse in a narrow laser beam (see Figure 5.A.1). As it propagates in the atmosphere, the laser radiation is scattered in all directions by aerosols and molecules. Part of the scattered radiation propagates back to the lidar; it is captured by a telescope, detected and analysed. Since the aerosols and molecules move with the atmosphere, a Doppler shift results in the frequency of the scattered laser light.

At the wavelengths (and thus frequencies) relevant to heterodyne (coherent) Doppler lidar, it is the aerosol signal that provides the principal target for measurement of the backscattered signal.

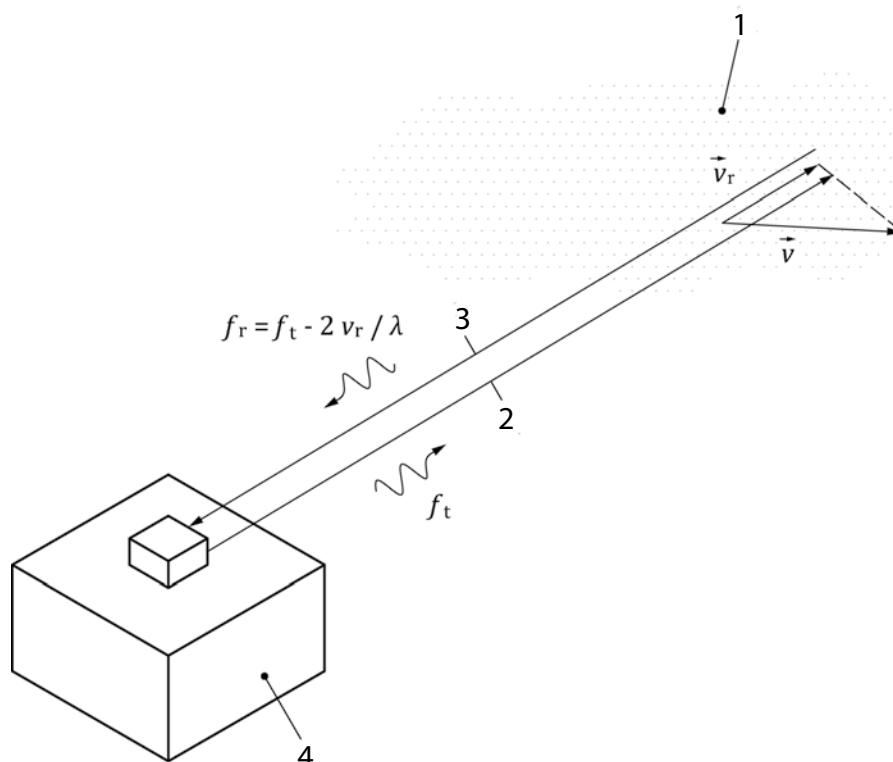
The analysis aims at measuring the difference, Δf , between the frequencies of the emitted laser pulse, f_t , and of the backscattered light, f_r . According to the Doppler's equation, this difference is proportional to the line-of-sight wind component, as shown in formula 5.A.1:

$$\Delta f = f_r - f_t = -2v_r / \lambda \quad (5.A.1)$$

where:

λ is the laser wavelength;

v_r is the line-of-sight wind component (component of the wind vector, \vec{v} , along the axis of laser beam, counted positive when the wind is blowing away from the lidar).



Key

- 1 Scattering particles moving with the wind
- 2 Optical path of the emitted laser pulse (laser beam)
- 3 Optical axis of the receiver
- 4 Lidar instrument

Figure 5.A.1. Measurement principle of a heterodyne Doppler lidar

The measurement is range resolved as the backscattered radiation, received at time t after the emission of the laser pulse, has travelled from the lidar to the aerosols at range x and back to the lidar at the speed of light, c . Formula 5.A.2 shows the linear relationship between range and time.

$$x = c \cdot \frac{t}{2} \tag{5.A.2}$$

4.2 Heterodyne detection

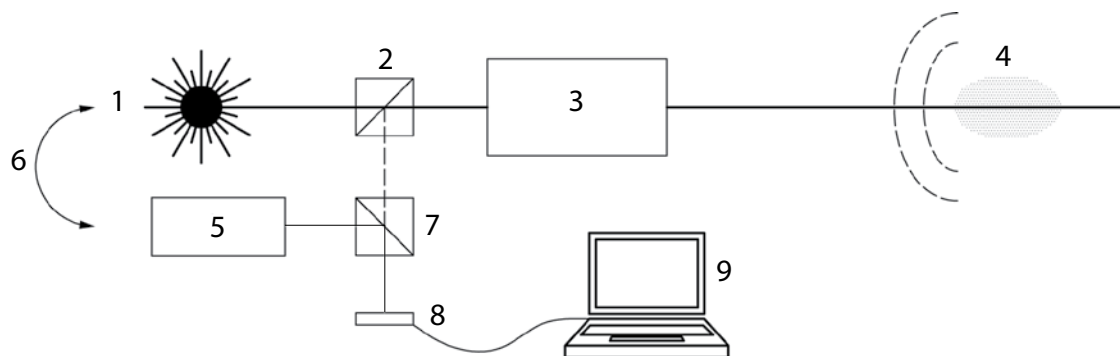
In a heterodyne lidar, the detection of the light captured by the receiving telescope (at frequency $f_r = f_t + \Delta f$) is described schematically in Figure 5.A.2. The received light is mixed with the beam of a highly stable, continuous-wave laser called the local oscillator. The sum of the two electromagnetic waves – backscattered and local oscillator – is converted into an electrical signal by a quadratic detector (producing an electrical current proportional to the power of the electromagnetic wave illuminating its sensitive surface). An analogue high-pass filter is then applied for eliminating the low-frequency components of the signal.

The result is a current, $i(t)$, beating at the radio frequency, $f_t + \Delta f - f_{lo}$:

$$i(t) = \underbrace{2 \cdot \frac{\eta \cdot e}{h \cdot f_t} \cdot K \cdot \xi(t) \cdot \sqrt{\gamma(t) \cdot P_r(t) \cdot P_{lo}}}_{i_{het}(t)} \cdot \cos[2\pi(\Delta f + f_t - f_{lo}) \cdot t + \varphi(t)] + n(t) \tag{5.A.3}$$

where:

- t is the time;
- h is the Planck constant;
- η is the detector quantum efficiency;
- e is the electrical charge of an electron;
- K is the instrumental constant taking into account transmission losses through the receiver;
- $\xi(t)$ is the random modulation of the signal amplitude by speckles effect (see 4.5.4);



- Key**
- 1 Pulsed laser
 - 2 Optical element separating the received and emitted lights
 - 3 Telescope (used for transmitting and receiving)
 - 4 Scatterers
 - 5 Local oscillator laser (continuous-wave laser)
 - 6 Frequency control loop (this device sets the difference, $f_t - f_{lo}$)
 - 7 Optical element aligning the beam of the local oscillator along the optical axis of the received light beam and mixing them together
 - 8 Quadratic detector
 - 9 Analogue-to-digital converter and digital signal processing unit

Figure 5.A.2. Principle of the heterodyne detection

$\gamma(t)$ is the heterodyne efficiency;

$P_r(t)$ is the power of the backscattered light;

P_{lo} is the power of the local oscillator;

f_{lo} is the frequency of the local oscillator;

$\varphi(t)$ is the random phase;

$n(t)$ is the white detection noise;

$i_{het}(t)$ is the heterodyne signal.

The heterodyne efficiency, $\gamma(t)$, is a measure for the quality of the optical mixing of the backscattered and the local oscillator wave fields on the surface of the detector. It cannot exceed 1. A good heterodyne efficiency requires a careful sizing and alignment of the local oscillator relative to the backscattered wave. Optimal mixing conditions are discussed in reference [3]. The heterodyne efficiency is not a purely instrumental function; it also depends on the refractive index turbulence (Cn^2) along the laser beam (see reference [4]). Under conditions of strong atmospheric turbulence, the effect on varying the refractive index degrades the heterodyne efficiency. This can happen when the lidar is operated close to the ground during a hot sunny day.

In formula 5.A.4, $P_r(t)$ is the instantaneous power of the backscattered light. It is given by the lidar equation (see reference [3]):

$$P_r(t) = A \cdot \int_0^{+\infty} x^{-2} \cdot G(x) \cdot g\left(t - \frac{2x}{c}\right) \cdot \beta(x) \cdot \tau^2(x) dx \quad (5.A.4)$$

with

$$\tau(x) = \exp\left[-\int_0^x \alpha(\zeta) d\zeta\right]$$

where:

x is the distance to the lidar;

A is the collecting surface of the receiving telescope;

$G(x)$ is the range-dependent sensitivity function ($0 \leq G(x) \leq 1$) taking into account, for example, the attenuation of the receiver efficiency at short range to avoid the saturation of the detector;

$g(t)$ is the envelope of the laser pulse power ($\int g(t) dt = E_0$, with E_0 as the energy of the laser pulse);

$\beta(x)$ is the backscatter coefficient of the probed atmospheric target;

$\tau(x)$ is the atmospheric transmission as a function of the extinction coefficient, α .

4.3 Spectral analysis

The retrieval of the radial velocity measurement from heterodyne signals requires a frequency analysis. This is done in the digital domain after analogue-to-digital conversion of the heterodyne signals. An overview of the processing is given in Figure 5.A.3. The frequency analysis is applied to a time window ($t, t + \Delta t$) and is repeated for a number, N , of lidar pulses. The window defines a range gate ($x, x + \Delta x$) with $x = c \cdot t / 2$ and $\Delta x = c \cdot \Delta t / 2$. N is linked to the integration time,

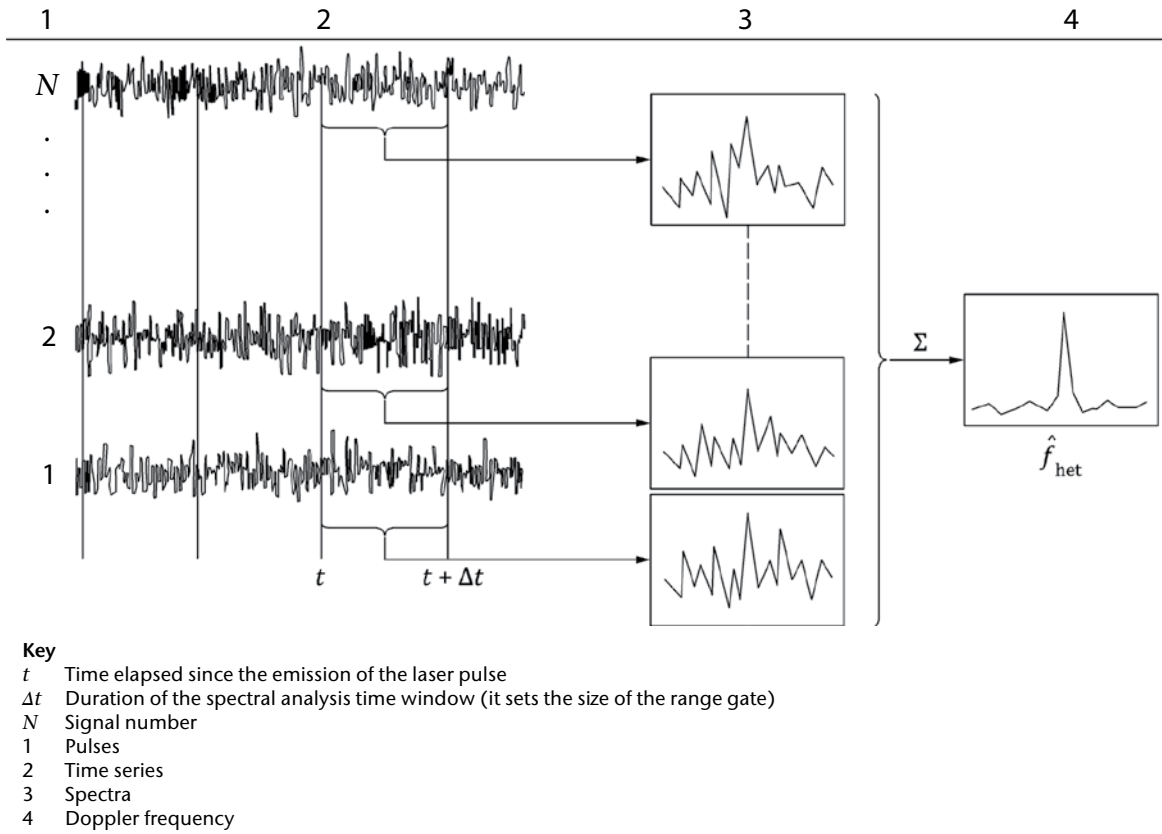


Figure 5.A.3. Diagram showing how the frequency analysis is conducted

$t_{int} = 1/f_{PRF}$ of the measurement (f_{PRF} is the pulse repetition frequency). The signal analysis consists in averaging the power density functions of the range gated signals. A frequency estimator is then used for estimating the central frequency of the signal peak. It is an estimate, \hat{f}_{het} , for the frequency, $f_{het} = \Delta f + f_t - f_{lo}$, of the heterodyne signal (see Figure 5.A.3).

Due to the analogue-to-digital conversion, the frequency interval resolved by the frequency analysis is limited to $(0, +F_s/2)$ or $(-F_s/2, +F_s/2)$ for complex valued signals. This limits the minimum and maximum values of \hat{f}_{het} and thus the interval of measurable radial velocities. As shown in reference [5], formula 5.A.5 estimates a range-gate average of the true wind radial velocity:

$$\hat{v}_r = -\frac{\lambda}{2} (\hat{f}_{het} - f_t + f_{lo}) \quad (5.A.5)$$

For instance, in the case the signal is real valued (no complex-demodulation), the frequency offset $f_t - f_{lo}$ is set to about $F_s / 4$, so $|\hat{v}_r| \leq \lambda F_s / 8$. Alternatively, a system specification requiring the possibility to measure radial winds up to v_{max} commands $F_s \geq 8v_{max} / \lambda$.

The averaging kernel is the convolution function between the pulse profile and the range-gate profile. Its length is a function of the pulse footprint in the atmosphere, Δr (see formula 5.A.6), of the range gate, Δx , and of the weighting factor, κ , where κ is the ratio between the gate full width at half maximum (FWHM) and Δx .

$$\Delta r = \frac{c \cdot T_p}{2} \quad (5.A.6)$$

where T_p is the FWHM duration of the laser pulse instantaneous intensity, $g(t)$.

The range resolution, ΔR , is defined as the FWHM of the averaging kernel. For a Gaussian pulse and an unweighted range gate, ΔR is calculated according to formula 5.A.7^[6]:

$$\Delta R = \frac{c}{2} \cdot \frac{\Delta t}{\operatorname{erf}\left(\frac{\sqrt{\pi} \cdot \Delta t}{2T_p}\right)} = \frac{\Delta x}{\operatorname{erf}\left(\frac{\sqrt{\pi} \cdot \Delta x}{2\Delta r}\right)} \quad (5.A.7)$$

For a Gaussian pulse and a Gaussian weighted range gate, ΔR is equal to formula 5.A.8:

$$\Delta R = \frac{c}{2} \cdot \sqrt{T_p^2 + (\kappa \cdot \Delta t)^2} = \sqrt{\Delta r^2 + (\kappa \cdot \Delta x)^2} \quad (5.A.8)$$

As shown in Figure 5.A.3, several signals are considered and range gated. The average spectrum is computed and a frequency estimator is applied.

Successive range gates can be partially overlapping (then successive radial velocity measurements are partially correlated), adjacent or disjoint (then there is a “hole” in the line-of-sight profile of the radial velocity).

Several possible frequency estimators are presented in reference [6] with a first analysis of their performances. Their performances are further discussed in reference [7]. Whatever the estimator, the probability density function of the estimates is the sum of a uniform distribution of “bad” estimates (gross errors) spread across the entire band $[-f_{\max}, f_{\max}]$ and a relatively narrow distribution of good estimates often modelled by a Gaussian distribution, as shown in formula 5.A.9:

$$p(\hat{f}_{\text{het}}) = \begin{cases} \frac{b}{2f_{\max}} + \frac{1-b}{\sqrt{2\pi}\sigma_f} \exp\left(-\frac{(\hat{f}_{\text{het}} - \bar{f}_{\text{het}})^2}{2\sigma_f^2}\right), & \text{for } \hat{f}_r \in [-f_{\max}, f_{\max}] \\ 0 & \text{otherwise} \end{cases} \quad (5.A.9)$$

In principle, the mean frequency, \bar{f}_{het} , can be different from the “true” heterodyne signal frequency, f_{het} . This can happen for instance when the frequency drifts during the laser pulse (chirp, see reference [8]). However, these conditions are rarely met and a good heterodyne Doppler lidar produces in practice unbiased measurements of Doppler shifts.

The parameter σ_f characterizes the frequency precision of the estimator. The corresponding radial velocity precision is $\sigma_v = \lambda \cdot \sigma_f / 2$. In a heterodyne system, it is typically of the order of several to several tens of centimetres per second. It degrades with the level of noise (power of $n(t)$ in formula 5.A.3) and improves with the number of accumulated signals, N . In practice the improvement is limited as the accumulation of a large number of signals results in a long integration time during which the natural variability (turbulence) of the wind increases.

Reference [9] discusses the presence of gross errors (also called outliers^[11]) and proposes a model for the parameter b as a function of the several instrument characteristics and the level of detection noise. An outlier happens when the signal processor detects a noise peak instead of a signal peak. The parameter b is a decreasing function of the carrier-to-noise ratio. Quality checks must be implemented in heterodyne lidar systems so gross errors are filtered out and ignored as missing data. The presence of gross errors sets the maximum range of the lidar.

4.4 Target variables

The aim of heterodyne Doppler wind lidar measurements is to characterize the wind field. In each range interval, the evaluation of the measured variable leads to the radial velocity; see formula 5.A.5.

There are additional target values like the variability of the radial velocity that are not discussed in this annex.

The target variables can be used as input to different retrieval methods to derive meteorological products like the wind vector at a point or on a line (profile), in an arbitrary plane or in space as a whole. This also includes the measurement of wind shears, aircraft wake vortices (see figure in Attachment C), updraft and downdraft regions of the wind. An additional aim of the Doppler wind lidar measurements is to determine kinematic properties and parameters of inhomogeneous wind fields such as divergence and rotation. See examples of applications in Attachment C.

4.5 Sources of noise and uncertainties

4.5.1 Local oscillator shot noise

The shot noise is denoted $n(t)$ in formula 5.A.3. Its variance is proportional to the local oscillator power, as shown in formula 5.A.10:

$$\langle n_{SN}^2 \rangle = 2eSP_0B \quad (5.A.10)$$

where:

S is the detector sensitivity, $S = \frac{\eta e}{hf_t}$, where η is the detector quantum efficiency;

B is the detection bandwidth.

It causes gross errors and limits the maximum range of the signal. If no other noise source prevails, the strength of the heterodyne signal relative to the level of noise is measured by the carrier-to-noise ratio (CNR), as shown in formula 5.A.11^[6]:

$$\text{CNR} = \frac{\eta \cdot K \cdot \gamma(t)}{h \cdot f_t \cdot B} P_r(t) \quad (5.A.11)$$

Note: Some authors sometimes call "signal-to-noise ratio" what is defined here as the CNR.

4.5.2 Detector noise

Additional technical sources of noise can affect the signal-to-noise ratio. As the shot noise, their spectral density is constant along the detection bandwidth (white noise).

- (a) Dark noise is created by the fluctuations of the detector dark current, i_D , as shown in formula 5.A.12:

$$\langle n_{DN}^2 \rangle = 2e i_D B \quad (5.A.12)$$

- (b) Thermal noise (Johnson/Nyquist noise) is the electronic noise generated by the thermal agitation of the electrons inside the load resistor, R_L , at temperature T , as shown in formula 5.A.13:

$$\langle n_{TN}^2 \rangle = \frac{4k_B T}{R_L} B \quad (5.A.13)$$

where: k_b is the Boltzmann constant.

4.5.3 Relative intensity noise

The relative intensity noise (dB/Hz) is the local oscillator power noise normalized to the average power level. The relative intensity noise (RIN) typically peaks at the relaxation oscillation frequency of the laser then falls off at higher frequencies until it converges to the shot noise level (pink noise). The RIN current increases with the square of the local oscillator power.

$$n_{RIN}^2 = (SP_0)^2 10^{0.1RIN} B \quad (5.A.14)$$

In a good lidar system, i_D , RIN, $1/R_L$ are low enough so that the local oscillator shot noise is the prevailing source of noise. In that case only, formula 5.A.14 is applicable.

4.5.4 **Speckles**

The heterodyne signal for a coherent Doppler wind lidar is the sum of many waves backscattered by individual aerosol particles. As the particles are randomly distributed along the beam in volumes much longer than the laser wavelength, the backscattered waves have a random phase when they reach the sensitive surface of the detector. They, thus, add randomly. As a result, the heterodyne signal has a random phase and amplitude. The phenomenon is called speckles (see reference [10]). It limits the precision of the frequency estimates.

4.5.5 **Laser frequency**

A precise measurement of the radial velocity requires an accurate knowledge of $f_r - f_{lo}$. Any uncertainty in this value results in a bias in \hat{f}_r . If the laser frequency, f_r , is not stable, it should either be measured or locked to f_{lo} .

4.6 **Range assignment**

The range assignment of Doppler measurements is based on the time elapsed since the emission of the laser pulse. This time must be measured with a good accuracy (the error, ϵ_t , must be smaller than or equal to $2\delta \cdot x / c$, where $\delta \cdot x$ is the required precision on the range assignment). This requires, in particular, that the time of the laser pulse emission is determined with at least this precision.

4.7 **Known limitations**

Doppler lidars rely on aerosol backscatter. Aerosols are mostly generated at ground and lifted up to higher altitudes by convection or turbulence. They are, therefore, in great quantities in the planetary boundary layer (typically 1 000 m thick during the day in tempered areas, 3 000 m in tropical regions), but in much lower concentrations above. It follows Doppler lidars hardly measure winds above the planetary boundary layer except in the presence of higher altitude aerosol layers like desert dusts or volcanic plumes.

Laser beams are strongly attenuated in fogs or in clouds. It follows the maximum range of Doppler lidars is strongly limited in fogs (a few hundreds of metres at best) and they cannot measure winds inside or beyond a cloud. They are able to penetrate into subvisible clouds as cirrus clouds. Therefore, wind information at high altitude (8 to 12 km) can be retrieved from crystal particle backscattering.

Doppler lidars detect cloud water droplets or ice crystals when they are present in the atmosphere. As they are efficient scatterers, they may dominate the return from the atmosphere, in case of heavy precipitation, for example, in which case the Doppler lidar measures the radial velocity of hydrometeors rather than the radial wind.

Rain downwashes the atmosphere, bringing aerosols to the ground. The range of a Doppler lidar is generally significantly reduced after a rain, before the aerosols are lifted again.

The presence of rainwater on the window of a Doppler lidar strongly attenuates its transmission. Unless a lidar is equipped with a wiper or a blower, its window should be wiped manually.

As explained in 4.2, the efficiency of heterodyne detection is degraded by the presence of refractive index turbulence along the beam. Refractive index turbulence is mostly present near the surface during sunny days. The maximum range of Doppler lidar looking horizontally close to the surface may thus be substantially degraded in such conditions.

5. SYSTEM SPECIFICATIONS AND TESTS

5.1 System specifications

5.1.1 Transmitter characteristics

5.1.1.1 Laser wavelength

The laser wavelength depends mainly on the technology used to build the laser source. Most of the existing techniques use near-infrared wavelengths between 1.5 and 2.1 μm , even though other wavelengths up to 10.6 μm may be used. The choice of the wavelength takes into account the expected power parameters but also the atmospheric transmission and the laser safety (see references [11] and [12]). In fact, the choice of the window between 1.5 and 2.1 μm is a compromise between technology and safety considerations ($> 1.4 \mu\text{m}$ to ensure eye safety).

5.1.1.2 Pulse duration

The laser pulse duration, T_p , is the FWHM of the laser pulse envelope, $g(t)$. T_p defines the atmosphere probed length, R_p , contributing to the instantaneous lidar signal, as shown in formula 5.A.15:

$$R_p = \frac{c \cdot T_p}{2} \quad (5.A.15)$$

As an example, a pulse duration of 200 ns corresponds to a probed length of approximately 30 m.

5.1.1.3 Velocity precision and range resolution versus pulse duration

There is a critical relationship between the pulse duration and two performance-related features. A long pulse duration of several hundreds of nanoseconds leads to a potentially narrow FWHM of the laser pulse spectrum (if “chirping” can be avoided), (see the Fourier transform of the overall pulse in the time domain). This can lead to a very accurate wind measurement even for a very low signal-to-noise ratio provided that outliers can be avoided (see 4.3). There is an adverse impact from high performance on range resolution. A pulse duration of 1 μs limits the effective range resolution to approximately 150 m (see formula 5.A.6).

5.1.1.4 Pulse repetition frequency

The pulse repetition frequency, f_{PRF} , is the laser pulse emission frequency. f_{PRF} determines the number of pulses sent and averaged per line of sight in the measurement time. It also determines the maximum unambiguous range where the information of two consecutive sent laser pulses will not overlap. The maximum unambiguous range, R_{MaxO} , corresponds to f_{PRF} as in formula 5.A.16:

$$R_{\text{MaxO}} = \frac{c}{2f_{\text{PRF}_{\text{max}}}} \quad (5.A.16)$$

For example, for a maximum operational range of 15 km, the maximum f_{PRF} is 10 kHz.

As for radars, however, specific types of modulation (carrier frequency, repetition frequency, and the like) can overcome the range ambiguity beyond R_{MaxO} .

5.1.2 **Transmitter/receiver characteristics**

The transmitter/receiver is defined at least by the parameters given in Table 5.A.1.

Table 5.A.1. Transmitter/receiver characteristics

<i>Transmitter/receiver characteristics</i>	<i>Remarks</i>
Aperture diameter	Physical size of the instrument's aperture that limits transmitted and received beams.
Laser beam diameter and truncation factor	For a Gaussian beam, the laser beam diameter is defined as the diameter measured at $1/e^2$ in power at the lidar aperture. The laser beam diameter defines the illuminance level and so the eye safety. The truncation factor is the ratio between the diameter measured at $1/e^2$ and the physical size of the instrument's aperture.
Focus point	Usually, pulsed lidars use collimated beams. For some applications, the beam can be partially focused at a given point to maximize the intensity on the beam laser within the measurement range. The intensity of the signal, and thus the velocity accuracy, will be optimized at this specific point.

In principle, pulsed systems are monostatic systems. For continuous-wave systems, bistatic set-ups are also available.

5.1.3 **Signal sampling parameters**

The sampling of the pulsed lidar signal in range is determined by the parameters given in Table 5.A.2.

Table 5.A.2. Signal sampling parameters

<i>Signal sampling parameters</i>	<i>Remarks</i>
Range gating	The range gate positions can be defined along the line of sight.
Range gate width	Given by the sampling points or the sampling frequency of the digitizer. Should be chosen close to the pulse length.
Number of range gates	For real-time processing, spectral estimation of all range gates must be computed in a time less than the integration time.
Radial window velocity measurement range	Wind velocities as low as 0.1 m/s can be measured with the aid of Doppler wind lidar systems. The measurement range is restricted towards the upper limit only by the technical design, mainly by the detection bandwidth. A radial wind velocity range of more than 70 m/s can be measured.
Resolution of the radial velocity	The wind velocity resolution is the minimum detectable difference of the wind velocity in a time and range interval. A resolution of 0.1 m/s or better can be achieved by averaging.

5.1.4 Pointing system characteristics

The pointing system characteristics are given in Table 5.A.3.

Table 5.A.3. Pointing system characteristics

<i>Pointing system characteristics</i>	<i>Remarks</i>
Azimuth range	When using a pointing device, a lidar has the capability to point its laser beam at various azimuth angles with a maximum angular capability of 2π . For endless steering equipment, a permanent steering along the vertical axis is allowed. Other scanning scenarios should be followed for non-endless rotation gear.
Elevation range	The pointing device can be equipped with a rotation capability around the horizontal axis. Potential 360° rotation can be addressed. Typical elevation angles are set from 0° to 180° in order to observe the semi-hemispherical part of the atmosphere above the lidar. Anyhow, a nadir pointing can be used for resting position of the equipment.
Angular velocity	The angular velocity is the speed at which a pointing device is rotating. A measurement can be performed during this rotation. In this case, the wind velocity information will be a mean of the various lines of sights in the probed area, between a starting angle and a stopping angle. Other scenarios of measurement can use a so-called step and stare strategy, with a fixed position during the measurement.
Angular acceleration	Defines how fast the angular velocity can change. To be defined for complex trajectories with fast changes in direction. Angle overshoots can be observed at high angular acceleration.
Pointing accuracy	The relative pointing accuracy is the standard deviation of the angular difference between the actual line-of-sight position (azimuth and elevation) and the position of the target (system of reference of the instrument). The absolute pointing accuracy needs prior calibration by angular sensors (pitch, roll, heading) (system of geographical reference).
Angular resolution	Minimum angle step that the line of sight can move. It can be limited by a motor reduction factor, position, encoder or mechanical friction.

5.2 Relationship between system characteristics and performance

5.2.1 Figure of merit

A figure of merit (FOM) helps to compare range performance of different lidars with different parameters. The example shown in Figure 5.A.4 allows the classification of pulsed lidar sensitivities, independently of atmospheric parameters. FOM is derived from the lidar equation (see formula 5.A.4) and is proportional to velocity spectrum, CNR, which is defined on the averaged spectral density as the Doppler peak intensity divided by the spectral noise standard deviation, assumed to be constant (white noise). N is the number of averaged pulses.

FOM is defined for a set of lidar parameters as in formula 5.A.17:

$$\text{FOM} = \eta_{\text{all}} \cdot E \cdot T_p \cdot D^2 \cdot \sqrt{t_i \cdot f_{\text{PRF}}} \quad (5.A.17)$$

where:

η_{all} is the overall efficiency, taking into account beam and image quality, overall transmission and truncation factor;

- E is the laser energy at the laser output (received energy is proportional to peak power and laser footprint);
- T_p is the pulse duration (this term comes from narrow bandwidth, inversely proportional to T_p);
- D is the collecting telescope diameter (for typical long-range applications, the optimum is 100 to 150 mm in size for near-infrared wavelengths);
- t_i is the integration time for one line of sight;
- f_{PRF} is the pulse repetition frequency.

The FOM is proportional to the square root of number N of accumulated spectra: $N = t_i \cdot f_{\text{PRF}}$.

When comparing two lidars at two different wavelengths, spectral dependence of atmospheric parameters should be considered. The FOM must be calculated with an integration time less than or equal to 1 s to avoid that wind or turbulence may fluctuate more than the Doppler spectral width.

A lidar may increase its FOM with a longer accumulation time within this 1 s time limit.

Considering state-of-the-art low aberration optical components, η_{all} can be estimated by the product of the emitting path transmission and the receiving path transmission.

It has to be noted that the FOM for a pulsed Doppler lidar may not be increased indefinitely by increasing the collecting area, D^2 , since phase distortion across the beam due to refractive index turbulence degrades the heterodyne efficiency^[3]. A practical limit is in the vicinity of a $D = 125$ mm usable diameter for long-range lidars.

Since the velocity spectrum CNR is inversely proportional to the squared range, the maximum operational range is approximately proportional to the square root of FOM, when atmospheric absorption can be neglected. When FOM is expressed in mJ ns m^2 , the maximum operational range, expressed in km, is almost the square root of FOM.

Table 5.A.4 computes the FOM for typical lidar figures and their corresponding typical measurement range.

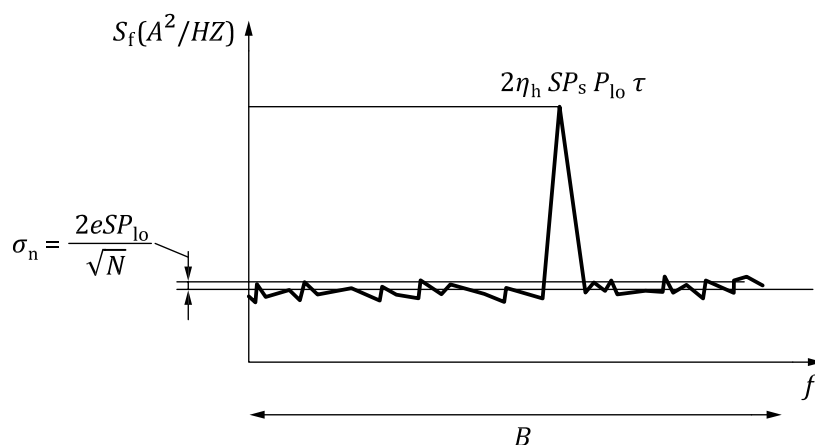


Figure 5.A.4. Example of an FOM

Table 5.A.4. FOM for typical lidar figures and their corresponding typical measurement range

η	E (mJ)	T_p (ns)	D (m)	f_{PRF} (Hz)	t_i (s)	FOM (mJ ns m ²)	Typical measurement range (km)
0.5	0.2	800	0.12	10 000	1	115	10
0.5	0.1	400	0.06	20 000	1	10	3
0.5	2	300	0.12	750	1	118	10

5.2.2 Time-bandwidth trade-offs

A good practice is to match the pulse duration with the desired range gate (see 4.6) so that the spatial resolution depends equally on these two parameters. With this assumption, spatial resolution is proportional to pulse duration. The shorter the pulse, the better the resolution. Velocity resolution is proportional to spectrum width and is larger when the spectrum is narrow. Because the spectrum width is inversely proportional to the pulse duration, range resolution and velocity resolution are also inversely proportional.

5.3 Precision and availability of measurements

5.3.1 Radial velocity measurement accuracy

Radial velocity measurement accuracy is defined (according to ISO 5725-1) in terms of:

- (a) Trueness (or bias) as the statistical mean difference between a large number of measurements and the true value;
- (b) Precision (or uncertainty) as the statistical standard deviation of a series of independent measurements. It does not relate to the true value.

Lidar data of good quality are obtained when the precision of the radial velocity measurements is higher than a target value (for example 1 m/s) with a predefined probability of occurrence (for example 95%).

An error value (1σ) of 0.5 m/s can be regarded as adequate for typical meteorological applications and for wind measurements to determine the statistics of dispersion categories for air pollution modelling^[13]. For wind energy applications, the requirements may be higher (0.2 m/s).

5.3.2 Data availability

Data availability is defined as the ratio of data with precision, P , to the total number of data during a measurement period.

The availability of measurement data, that is, the determinability of the wind profile, is a function mainly of the aerosol concentration and the clouds. Other filtering criteria may be applied, depending on the required data accuracy. For example, data that exhibit significantly non-uniform flow around the scan disc should be rejected.

5.3.3 Maximum operational range

Assuming the lidar line of sight remains within the planetary boundary layer (that is, no significant change of signal along the line of sight), Figure 5.A.5 shows a typical pulsed lidar data availability versus range plot.

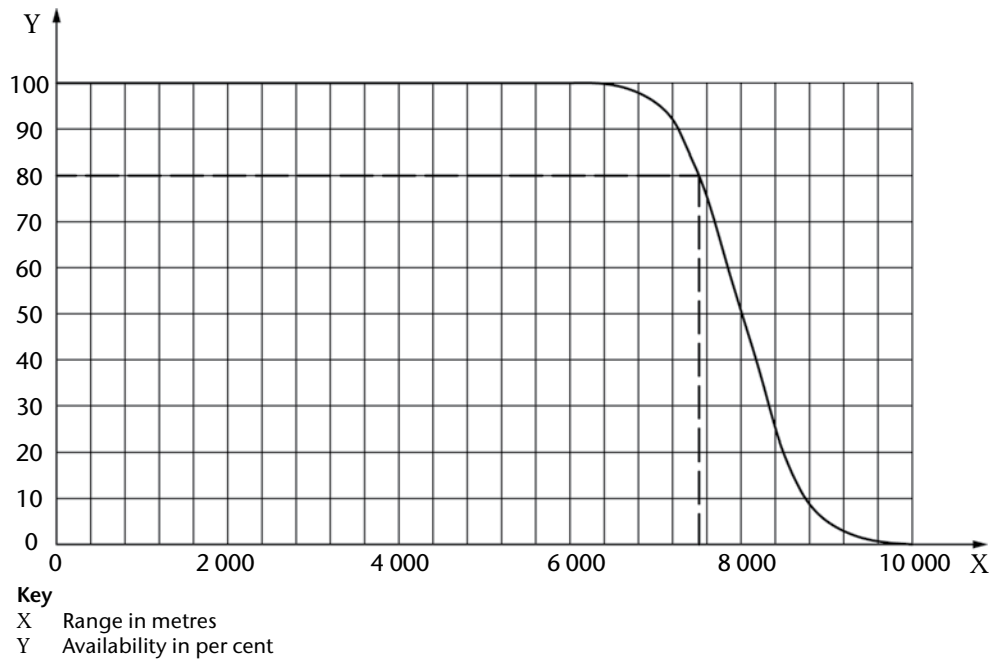


Figure 5.A.5. Example for maximum operational range

In this case, the range for 80% data availability (P_{80}) is 7 500 m.

The performance shown in this diagram is based on a standard atmosphere:

- (a) No clouds along the line of sight;
- (b) No precipitation;
- (c) Visibility over 10 km (clear air).

This performance will vary significantly with relevant local climatic and operational conditions. Data from greater ranges should be treated with caution, depending on the application.

Measurement range must be defined with a given availability criteria. A recent study about this link is described in reference [14].

For example, R_{50} corresponds to the maximum range with availability over 50%.

If the availability is not mentioned, the maximum operational range is supposed to be R_{80} , that is, the maximum distance where the availability is over 80%.

For a given availability, a change in velocity precision leads to a change in maximum operational range.

5.4 Testing procedures

5.4.1 General

In order to accurately assess for the accuracy of the target variables, the manufacturer should perform a set of validation tests for the range and velocity. Some can be performed under laboratory conditions. Certain other validation tests can only be performed by a comparison with other reference instruments, such as cup or sonic anemometers.

5.4.2 **Radial velocity measurement validation**

5.4.2.1 **General**

This section describes how the quality of radial velocity measurements can be checked and assessed.

5.4.2.2 **Hard target return**

This test consists in acquiring wind measurements with the beam directed to a stationary (unmoving) hard target (any building within lidar range) and checking the radial velocity measurement returned by the lidar is 0 m/s.

This test checks that the frequency difference, $f_t - f_{lo}$, between emitted laser pulses and the local oscillator is known or determined with a sufficient accuracy (see 4.5.3).

The range gate length should be close to the length of the laser pulse, and the distances of the range gates should be set so that the hard target is exactly at the centre of one range gate, otherwise, a velocity bias can occur in case of frequency drift within the pulse.

Hard target velocity measurements should be acquired during at least 10 min. The test is successful if the time sequence of hard target radial velocities is centred at about 0 m/s.

5.4.2.3 **Self-assessment of radial velocity precision**

In this test, the pulsed lidar beam is vertical and radial velocity measurements are acquired during at least 20 min at the rate of at least one profile of radial velocities every second. Let us denote by $v_r(x, k)$, $k = 1, \dots, K$ the time sequence of radial velocities measured at distance x . The test consists in forming the power spectrum of the time sequence, as shown in formula 5.A.18:

$$V(x, f) = \frac{1}{K} \left| \sum_{k=1}^K v_r(x, k) \exp(-2j\pi f k \delta t) \right|^2 \quad (5.A.18)$$

where δt is the constant time lag between successive $v_r(x, k)$ measurements.

On average, the power spectrum $V(x, f)$ should look like Figure 5.A.6. At low frequencies, the power spectrum is dominated by natural wind fluctuations and will follow a $f^{5/3}$ law. At high frequencies, the power spectrum is dominated by the flat level of measurement errors (white noise). The level of this flat part directly gives the variance of these measurements $\sigma_e^2(x)$.

Note: The test must be carried out at night when the natural variability of the wind is weak, that is, when the wind is considered to be calm. It may then happen that measurement errors are much larger than natural wind fluctuations so the $f^{5/3}$ part of the power spectrum is hidden.

Fully described in reference [15], this technique allows for the estimation of the measurement precision of the lidar without any ancillary data.

In Figure 5.A.6, the line is $V(f)$. At low frequencies, $V(f)$ should be proportional to $f^{5/3}$ (spectral behaviour of natural wind variability; see dashes). At high frequencies, the spectrum becomes flat (dash-dot line) at a level directly equal to the variance of measurement errors, $\sigma_e^2(x)$.

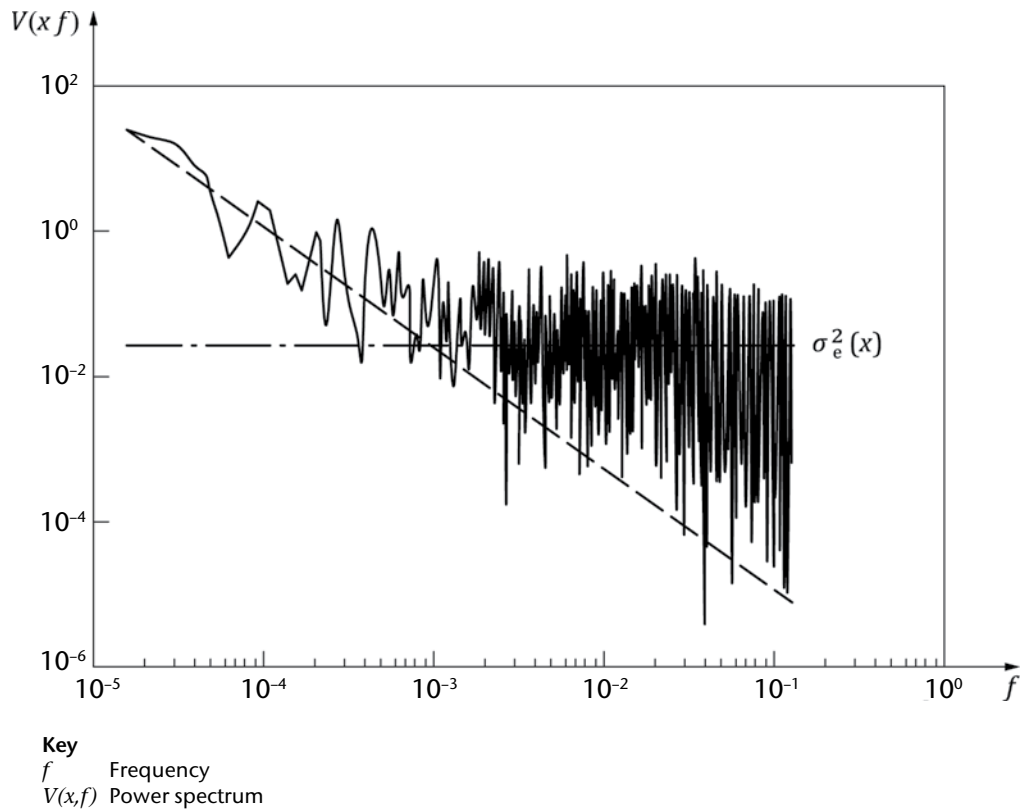


Figure 5.A.6. Power spectrum of radial velocity measurements

5.4.3 **Assessment of accuracy by intercomparison with other instrumentation**

5.4.3.1 **Sonic anemometer**

The last test consists of directing the lidar beam very close to a sonic anemometer on a mast or platform without vibration and comparing lidar radial velocities with the projection of the three-dimensional wind vectors acquired by the sonic anemometer on the beam direction.

Lidar and sonic anemometer data must be averaged over a minute.

The direction of the lidar beam must be determined with a good accuracy (of the order 1° or better) and as close as possible to the horizontal plane. The lidar beam must be at the height of the sonic anemometer (height difference of the order of 1 m or less).

The RMS of the differences between lidar and sonic anemometer data must be less than 0.1 m/s.

The mast will most likely cause wind flow perturbations downstream. Winds coming from directions such that the sonic anemometer is in the perturbed zone must be removed from the statistics.

5.4.3.2 **Performance test against masts**

The mast must be equipped with at least three-cup anemometers mounted horizontally.

5.4.3.3 Comparison with Doppler weather radars

The possibility for intercomparison between Doppler lidars and Doppler weather radars can be an option where the two systems are collocated. The details about this class of intercomparison are just becoming known as the deployment of systems integrating both sensors for all-weather remote-sensing of the wind field at airports, especially for wind shear detection, is just getting under way. Studies have recently been conducted^[16,17,18]. Both sensors should be collocated and should probe the same atmospheric volume in order to be certain of representative intercomparisons.

In addition to the siting requirement, it is very important that weather situations be selected in which the tracer targets of both sensors actually represent the flow of air. In conditions of dry weather, the Doppler lidar works best, while under such conditions of clear air, the radar measures only the returns due to scattering by insects. These scattered signals from insects provide no accurate indication of the actual air movement. Comparison with data from Doppler lidars typically shows differences of up to several metres per second. Therefore, echo classification in terms of radar targets has to be enabled in order to be able to reject insect returns. This means that the radar has to be capable of measuring at two orthogonal linear polarizations. During precipitation events, however, conditions are optimal for the radar, whereas the lidar may have significantly reduced range coverage. In weather situations with light rain or drizzle from stratiform cloud, both radar and lidar sensors are expected to obtain high-quality data. Such situations are thus best suited for this validation procedure. Appropriate filtering of radar data on the basis of target classification using dual-polarization moments needs to be conducted in order to get rid of any non-meteorological returns.

If these requirements are fulfilled, cross-comparison of Doppler weather radar and Doppler lidar can be performed on the basis of profiles of horizontal wind as obtained, for example, with velocity volume processing or velocity azimuth display methods. In this case, the scan geometry has to be considered. Ideally, the scan geometry for the radar and lidar should be the same with respect to elevation angles. Another option yet to be evaluated could be to compare the actual radial wind velocities on a range gate by range gate basis between the radar and lidar systems.

5.4.3.4 Comparison with radar wind profilers

Comparison with radar wind profilers may be performed if the two systems are collocated. The weather conditions under which both sensors work optimally are not exclusive of each other (sufficient aerosol tracers for lidar and sufficient turbulent eddies as targets for Bragg scattering for the wind profiler). Care must be taken that both sensors face optimal atmospheric conditions. Additionally, attention has to be paid to the scan mode used to derive the vertical wind profile so that the volume probed by the lidar matches the volume probed by the wind profiler.

5.4.4 *Maximum operational range validation*

In clear sky conditions, the atmosphere can be described by the visibility, V , the aerosol concentration and the aerosol type, where the last two can be properly described by the two optical lidar parameters extinction and backscatter coefficients. The visibility (see, for example, ISO 28902-1) and humidity are measured by standard ground-based meteorological local sensors, whereas the aerosol type and its size distribution are not. To simplify, atmosphere types can be sorted in a few categories associated with their lidar ratio. Lidar ratio values in the near infrared typically are limited in the range of 30 to 50 steradians. R_{MaxO} will not be too dependent on the aerosol variability on site except for conditions with local pollution sources.

Visibility is an important parameter for lidar range. The lidar equation (see formula 5.A.4) indicates that the received power is proportional to the backscatter coefficient and decreases exponentially with extinction, thus increases with visibility. Since $\alpha(x)$ and $\beta(x)$ are proportional, there is a maximum to the function $P_r(t)$ (see lidar equation in formula 5.A.4, and Figure 5.A.7), and so for R_{MaxO} .

To discard unfavourable visibility conditions for coherent Doppler wind lidars (fog and very clear), only haze and clear visibility conditions are selected for range measurements. Current lidars can work in precipitating conditions, but are subject to error in their determination of the vertical wind component; the horizontal component has been shown to be very accurate (see reference [18]).

Table 5.A.5. Plot numbers

Plot number	1	2	3	4	5
Typical FOM for 1 s integration time (m) ns m ²)	20	30	60	100	150

Because backscatter changes rapidly for high relative-humidity values, data corresponding to relative humidity > 70% should be filtered out the measurement dataset. So, precipitation conditions (rain, snow) are not considered.

Moreover, index turbulence, C_n^2 (depends on temperature and altitude), can modify R_{MaxO} by altering the beam wave front. Strong turbulent conditions must be removed from datasets (sunny days around noon), and experimental protocol must be followed up.

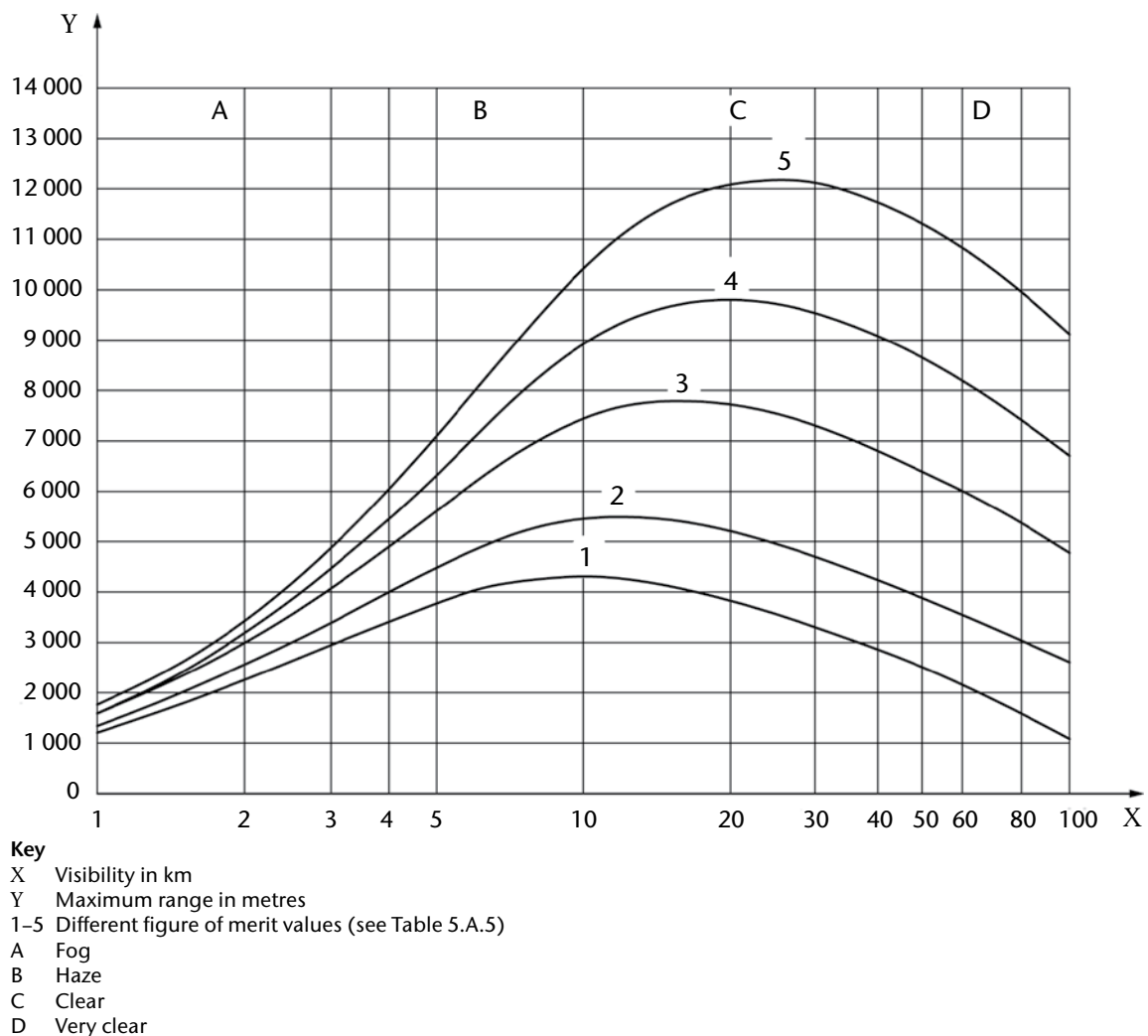


Figure 5.A.7. Dependency of the maximum operational range of the heterodyne Doppler signal to the visibility conditions

So the validation must be conducted under the following conditions:

- (a) The lidar is operated in operational conditions (vertical for profilers, low elevation for scanning lidars);
- (b) The full measurement range remains in the boundary layer;
- (c) $10 \text{ km} < \text{visibility} < 50 \text{ km}$ (at visible wavelength, dependency with wavelength is given in ISO 28902-1);
- (d) No precipitation;
- (e) No cloud on the line of sight;
- (f) $C_n^2 < 10^{-14} \text{ m}^{-2/3}$ (1 m above ground level).

Data not corresponding to these conditions should be filtered out for assessing the maximum operational range.

- (a) Context conditions are recorded simultaneously (temperature, C_n^2 , visibility, RH);
- (b) Datasets are created following the above-mentioned atmospheric conditions. 100 h of filtered data are required as a minimum for a good statistical dataset. It represents approximately four days of cumulated measurements with 1 s accumulation time. Depending on the atmospheric conditions, the evaluation period can last from four days and up to one month.

6. MEASUREMENT PLANNING AND INSTALLATION INSTRUCTIONS

6.1 Site requirements

The selection of the measurement site is essentially determined by the measurement task. Careful selection of the measurement site is necessary, in particular, for stationary systems or for the quasi-stationary use of mobile systems during long-term measurement campaigns. The following points must be taken into account when selecting the measurement site:

- (a) Unobstructed view: Unrestricted visibility can be limited by built-up areas, trees and buildings near the installation site of the lidar. If the view is limited by buildings, it is possible to avoid the limitation of the horizontal view by selecting a larger elevation angle. In the case of a velocity azimuth display scan, the measurement signals originating not from the free atmosphere but from obstacles must be excluded from the evaluation;
- (b) Electromagnetic radiation: Doppler wind lidar systems should be shielded properly against interferences by electromagnetic radiation (for example by radar, mobile radio or cellular phone networks).

Early inspection of the envisaged measurement site with the participation of experts (such as meteorologists) is recommended.

For optimal operational range retrieval, the lidar should be installed on a short grass-covered ground with no nearby structures, which would cause atmospheric turbulence affecting the lidar's operation and performance. The lidar should be installed at least at 3 m above the ground, especially when not located on a grass ground, like concrete, asphalt or a plain metallic platform, in order to avoid effects from turbulence nearby the optical output that will destroy the coherency of the atmosphere and thus drastically diminish the detection.

6.2 **Limiting conditions for general operation**

Interference factors regarding Doppler wind lidar measurements are:

- (a) Optically thick clouds;
- (b) Precipitation of any type (rain, hail, snow);
- (c) Blocking effects (such as from buildings).

6.3 **Maintenance and operational test**

6.3.1 **General**

To ensure the system functions as specified and to rule out deviations and technical errors such as maladjustments^[19], maintenance and operational tests must be performed in regular intervals. In addition to the information given here, typical application ranges and corresponding requirements can be found in Attachment D.

6.3.2 **Maintenance**

Maintenance such as regular cleaning of the optical components, calibration, and the like must be performed as a basic requirement of quality assurance. Maintenance procedures may be conducted by on-site personnel, using an automatic software detection of the decrease of the signal due to, for example, dust deposits, and making appropriate corrections to the data, or a combination of the two. Typical maintenance intervals are three months depending on the environmental conditions.

6.3.3 **Operational test**

Operational tests should be performed every 6 to 36 months. The tests depend on the individual system design. The manufacturer must specify the testing procedures and provide the necessary testing tools.

- (a) Output power and frequency of the laser source should be measured at the periodicity indicated by the manufacturer;
- (b) Signal output of the data-acquisition system reacting to a defined light pulse or defined target should be measured at the periodicity indicated by the manufacturer;
- (c) For scanning or steering systems, an alignment test using a calibrated instrument (for example a compass or inclination meter) should be performed.

6.3.4 **Uncertainty**

Table 5.A.6 compiles uncertainty contributions to the measurement variables and the line-of-sight wind velocity. The uncertainty contributions of the measurement variables influence the quality of the data produced by the system. The dominant uncertainties result from:

- (a) The initial calibration process of the system by the manufacturer;
- (b) The prevailing environmental conditions.

Table 5.A.6. Effects leading to uncertainty

<i>Measurement variables</i>	<i>Effects leading to uncertainty</i>
Signal-to-noise ratio	(a) Noise including detector noise (b) Speckle effect (when only a few pulses are averaged during the measurement time) (c) Laser power or pulse width fluctuations (d) Refractive index (temperature) turbulence (e) Lag angle at fast rotation speeds
Frequency shift, Δf	(a) Bias and fluctuations of emitted pulse frequency compared to local oscillator frequency (b) Pulse length (c) Signal-to-noise ratio (d) Number of averaged pulses (e) Quality of estimator
<i>Target variable</i>	<i>Uncertainty contribution</i>
Line-of-sight wind velocity (radial wind velocity)	(a) Wind turbulence (b) Wind gradient along the line of sight (c) Hard targets close to the range gate (d) Range ambiguities (e) Pointing accuracy

ATTACHMENT A. CONTINUOUS-WAVE DOPPLER WIND LIDAR

(informative)

As stated in this annex, there are several methods by which lidar can be used to measure atmospheric wind. The four most commonly used methods are pulsed and continuous-wave coherent Doppler wind lidar, direct-detection Doppler wind lidar and resonance Doppler wind lidar (most commonly used for mesospheric sodium layer measurements).

This annex describes the use of heterodyne (coherent) pulsed lidar systems. It should be noted that there is also ISO 28902-3 currently in preparation, which describes the use of continuous-wave coherent Doppler wind lidar for the measurement of atmospheric wind. ISO 28902-3 will specify the requirements and performance test procedures for continuous-wave Doppler lidar techniques and present their advantages and limitations. The term “continuous-wave Doppler lidar” or “continuous-wave Doppler wind lidar” is used in this annex to apply to continuous-wave lidar systems making measurements of wind characteristics from the scattering of laser light by aerosols in the atmosphere within the low-altitude boundary layer. A description is provided of typical measurement geometries, signal-processing options, performance requirements, and limits based on standard atmospheric conditions. The applications for continuous-wave lidar are, among others:

- (a) Wind energy;
- (b) Wind resource assessment;
- (c) Power curve verification;
- (d) Loss factor in the wind farm operation;
- (e) Wind hazards monitoring for aviation weather applications;
- (f) Wind shear;
- (g) Requirements for the detection of wake vortices behind aircraft.

ISO 28902-3 will address manufacturers of continuous-wave Doppler wind lidars, as well as those bodies concerned with testing and certifying their conformity. It will also provide recommendations for users to make adequate appropriate use of these instruments. A comprehensive bibliography of independent publications will be provided.

ATTACHMENT B. RETRIEVAL OF THE WIND VECTOR

(informative)

B.1 General

The wind is a three-dimensional vector quantity, with the wind field being generally a function of space and time. The measurement of the instantaneous wind at a particular position therefore always requires the determination of three vector components. A single Doppler lidar is only able to measure the component (or projection) of the wind vector along the line of sight of the laser beam. Three separated lidar systems would therefore be required to perform an exact local measurement at any fixed time. Under certain assumptions, it is possible to estimate the full wind vector from a single "monostatic" Doppler lidar. This process is called wind retrieval since the accuracy of the wind vector estimate depends on the validity of the assumptions regarding the wind field.

B.2 Coordinate system

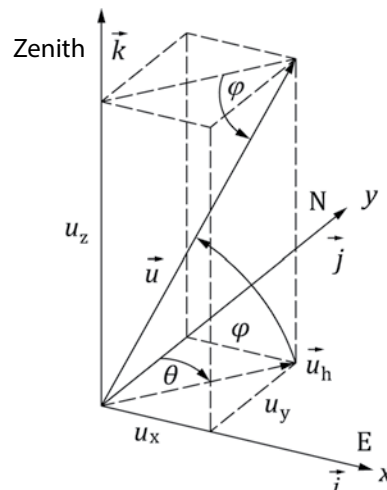
The figure below shows the wind vector $\vec{u}(\vec{r}, t)$ in the Cartesian coordinate system with the unit vectors $\vec{i}, \vec{j}, \vec{k}$. The components u_x, u_y, u_z are scalar functions of position, and time, $\vec{r} = \vec{r}(x, y, z, t)$, is the position or radius vector of an air parcel.

$$\vec{u} = \frac{d\vec{r}}{dt} = \begin{pmatrix} u_x \\ u_y \\ u_z \end{pmatrix} \quad (\text{B.1})$$

or

$$\vec{u} = (u_x \cdot \vec{i} + u_y \cdot \vec{j} + u_z \cdot \vec{k}) \quad (\text{B.2})$$

The coordinate system in the figure points to the east (E) with the positive x-direction (\vec{i}), to the north (N) with the positive y-direction (\vec{j}) and to the zenith with the positive z-direction (\vec{k}).



Coordinate system and wind vectors

With θ and ϕ , the components in Cartesian coordinates are:

$$\begin{aligned} u_x &= U \cdot \cos \phi \cdot \sin \theta \\ u_y &= U \cdot \cos \phi \cdot \cos \theta \\ u_z &= U \cdot \sin \phi \end{aligned} \quad (\text{B.3})$$

and the three-dimensional wind vector becomes:

$$\vec{u} = \begin{pmatrix} U \cdot \cos \phi \cdot \sin \theta \\ U \cdot \cos \phi \cdot \cos \theta \\ U \cdot \sin \phi \end{pmatrix} \quad (\text{B.4})$$

Example: Horizontal west wind: $\theta = 90^\circ$, $\phi = 0^\circ$

$$\Rightarrow u_x = U, u_y = u_z = 0 \Rightarrow \vec{u} = (U, 0, 0)$$

B.3 Horizontal wind vector

The horizontal wind vector, \vec{u}_h , and the horizontal projection of the three-dimensional wind vector, \vec{u} , in the figure becomes:

$$\vec{u}_h = \begin{pmatrix} u_x \\ u_y \end{pmatrix} = \begin{pmatrix} u_h \cdot \sin \theta \\ u_h \cdot \cos \theta \end{pmatrix} \quad (\text{B.5})$$

or, in component notation:

$$u_h = |\vec{u}_h| = U \cdot \cos \phi = \sqrt{u_x^2 + u_y^2} \quad (\text{B.6})$$

The value u_h is denoted as horizontal wind velocity or colloquially as wind velocity. According to the meteorological convention, the wind direction is defined as the direction opposite to the wind vector, \vec{u}_h . It is oriented clockwise from north via east, south and west (see figure above).

For the case of a lidar scanning in a disc at fixed elevation angle in uniform wind flow, the individual line-of-sight velocity points follow a cosine form as a function of azimuth angle. The peaks of the function correspond to the azimuth angle aligned parallel or anti-parallel to the wind direction. The function passes through zero when the azimuth angle is perpendicular to wind bearing since there is no component of velocity along the line of sight. The data are also conveniently displayed on a polar plot, which provides information at a glance on the speed, direction and vertical wind component. A standard least-squares fitting routine provides the best estimates of the values of the three unknown parameters (either u , v and w , or alternatively, horizontal speed, vertical speed and wind bearing).

B.4 Radial velocity

In lidar measurements, the component v_r of the local wind vector $\vec{u}(\vec{r}, t)$ in the beam direction of the laser, that is, the radial velocity at any arbitrary position \vec{r} , is the direct measurand determined from the Doppler frequency shift (see Figure 5.A.5). If the wind vector $\vec{u}(\vec{r})$ is written in a spherical coordinate system $(\vec{e}_r, \vec{e}_\theta, \vec{e}_\phi)$ instead of a Cartesian $(\vec{i}, \vec{j}, \vec{k})$ coordinate system, the radial velocity, v_r , is easily defined (compare formula B.2)^[20]:

$$\vec{u}(\vec{r}) = \vec{u}(r, \theta, \phi) = (u_r \cdot \vec{e}_r + u_\theta \cdot \vec{e}_\theta + u_\phi \cdot \vec{e}_\phi) \quad (\text{B.7})$$

where:

\vec{e}_r is the unit vector in the beam direction;

$\vec{e}_\theta, \vec{e}_\phi$ are the unit vectors in the azimuth and elevation direction;

u_r, u_θ, u_ϕ are the orthogonal wind vector components of the coordinate system carried along during the scanning operation.

The projection of the wind vector $\vec{u}(\vec{r})$ onto the beam direction, that is, the scalar product (\circ), can be derived with formula B.8:

$$\vec{u}(\vec{r}) \circ \vec{e}_r = u_r \equiv v_r \equiv -v_{\text{LOS}} \quad (\text{B.8})$$

v_{LOS} is equal by convention to the negative radial component v_r of the local wind vector at the position \vec{r} . The negative sign of v_{LOS} corresponds to the convention that in lidar systems the wind velocity is regarded as positive towards the laser.

With the known transformation relation between spherical and Cartesian coordinates^[19], v_r can be expressed by the Cartesian wind components u_x, u_y, u_z the result being:

$$v_{\text{LOS}} = -v_r = -(u_x \cdot \cos\phi \cdot \sin\theta + u_y \cdot \cos\phi \cdot \cos\theta + u_z \cdot \sin\phi) \quad (\text{B.9})$$

B.5 Retrieval of the wind vector

The atmosphere should be sensed at different angles in order to detect the (Cartesian) components u_x, u_y, u_z of the wind vector with the Doppler wind lidar.

Note: The wind components u_x, u_y, u_z are frequently also called u, v, w .

However, all wind components are usually subject to spatial and temporal fluctuations since the wind field in general cannot be regarded as homogeneous and stationary due to a variety of small-scale atmospheric processes like gravity waves, convection, turbulence or orographically induced flow effects. Homogeneity assumptions should therefore be made in order to retrieve an estimate of the wind vector from the radial components. The better this assumption holds, the more does the estimate represent the actual wind field. The problem has been extensively discussed in the literature and is explained in textbooks for both radar and lidar, see, for example, references [21] and [22].

Therefore, assuring that the wind field can be regarded as stationary over the measurement period and horizontally homogeneous over the sampled volume, that is, if the wind field is only a function of the vertical coordinate z , then the radial wind measurements for a fixed geometrical height are given by formula B.10, the simple matrix equation:

$$A \cdot u = v_r \quad (\text{B.10})$$

The rows of this ($n \times 3$) matrix A are comprised of the unit directional vectors describing the pointing of the n beams. The vector v_r is also of dimension n and contains the radial winds obtained in the n pointing directions. This is nothing more than a compact notation for the n scalar (inner) products as given in formula B.8. For $n = 3$, the inverse A^{-1} exists if A has rank 3 (for example, all row vectors are linearly independent) and the wind vector can be directly obtained through formula B.11:

$$u = A^{-1} \cdot v_r \quad (\text{B.11})$$

For $n > 3$ and $\text{rank}(A) = 3$, the linear system is overdetermined and has usually either one solution or no (exact solution) at all. However, an approximate solution can be found which minimizes . This least-square solution can be expressed by the Pseudoinverse $(A^T A)^{-1} \cdot A^T$ of matrix A as shown in formula B.12:

$$u = (A^T A)^{-1} \cdot A^T \cdot v_r \quad (\text{B.12})$$

A^T denotes the transpose of matrix A . Formula B.12 is sufficiently general and describes all possible scanning configurations with n discrete beam pointing directions. Care must be taken in the practical use of this formula to obtain numerically stable implementations.

The Doppler beam swinging technique or the velocity azimuth display scanning methods are two frequently used scan schemes for Doppler lidars.

In the case of the Doppler beam swinging technique, measurements are performed in at least three linearly independent directions. This method allows for a very fast scanning, but it may yield biased measurements if the wind field is non-homogeneous. The validity of the retrieval assumptions (homogeneity, stationarity) can be tested to some extent if more than three directions are used. An explicit example of the Doppler beam swinging method with $n = 3$ and $n = 4$ can be found in reference [23].

In the case of the velocity azimuth display scan, the beam direction azimuth is varied in a continuous scanning operation. The variation of the azimuth angle during the measurement series yields a set of different projections of the local wind vector onto these measurement directions. The elevation angle remains constant in the process. Originally, the velocity azimuth display method was proposed for a horizontally homogeneous wind field^[24]. Later discussions were extended to allow for an additional linear variation of the vector components^[25]. In the case of a homogeneous wind field, the result is a sinusoidal profile of the measured velocity v_{LOS} .

If the lidar is powerful enough to provide several azimuth scans at different elevations in reasonable time, these can be combined in order to compile a full volume scan. This makes it feasible to use a more elaborate model of the wind field that can be fitted to the vector of observations of v_r . That is, analogous to formula B.10, one can further expand the Taylor series incorporating also shearing of the wind, that is, the first spatial derivatives. For Doppler radars, this procedure is standard and is commonly known as velocity volume processing. It has been originally published in reference [26]. This analysis then leads to formula B.13 instead of formula B.10:

$$\begin{aligned}
 v_r = & \sin \theta \cdot \cos \phi \cdot u_0 + \cos \theta \cdot \cos \phi \cdot v_0 + \sin \phi \cdot w_0 \\
 & + r \cdot \sin^2 \theta \cdot \cos^2 \phi \cdot u'_x \\
 & + r \cdot \cos^2 \theta \cdot \cos^2 \phi \cdot v'_y \\
 & + r \cdot \cos \theta \cdot \sin \theta \cdot \cos^2 \phi \cdot (u'_y + v'_x) \\
 & + \sin \phi \cdot (r \cdot \sin \phi - z_0) \cdot w'_z \\
 & + \sin \theta \cdot \cos \phi \cdot (r \cdot \sin \phi - z_0) \cdot (u'_z + w'_x) \\
 & + \cos \theta \cdot \cos \phi \cdot (r \cdot \sin \phi - z_0) \cdot (v'_z + w'_y)
 \end{aligned} \tag{B.13}$$

It should be noted that this model does not allow to extract any information about horizontal vorticity since u'_y and v'_x only appear as a sum in formula B.13. This method has been applied to lidar data and compared with Doppler weather radar data in reference [16].

ATTACHMENT C. APPLICATIONS

(informative)

C.1 Wind energy

C.1.1 General

One of the main challenges in the wind energy market today is the optimal estimation of the future electrical output of a wind farm. Today, the procedure to estimate this is to have the best evaluation possible of the wind potential at a given site, the best evaluation of what a wind turbine can produce with the free wind that it receives and to properly evaluate the total production loss that can occur during the wind farm operation. Some of these losses can be due to the wakes, to the power performance loss of a wind turbine, downtime due to operation and maintenance of the wind farm and other parameters that can affect the global wind farm operation. Today, the ground-based coherent Doppler lidar is a suitable tool to be used during all the phases of the operation of a wind farm, from the development phase, to the commissioning, operation and repowering of old wind farms.

C.1.2 Wind resource assessment

Today the ground-based vertical-profiler lidar (both pulsed and continuous-wave types) is widely used in the wind energy market by all major developers in order to provide highly accurate wind speed data and reduce the horizontal and vertical uncertainty during the wind resource assessment campaign. Today ground-based coherent Doppler lidar can be used without any mast during the campaign and these data are considered as bankable. Considering the size of the wind turbine and the height that it can reach, the lidar allows a proper evaluation of the vertical wind profile that is critical for the design of a wind turbine. The vertical wind shear (change in wind speed along the vertical axis) and the vertical wind veer (change in wind direction along the vertical axis) are two key elements to be considered that can affect the annual energy production of a wind farm.

The wind farms are moving more and more offshore, and today the ground-based pulsed-scanning lidar can be used for wind resource assessment campaign scanning offshore from the shore. This allows to decrease the horizontal uncertainty in the wind resource assessment campaign at a much reduced cost than the standard offshore met mast. In addition to this, the correlation of the wind measured with the scanning lidar can be used to validate some wind models for the wind transition offshore to the shore.

C.1.3 Power curve verification

C.1.3.1 General

Today, the IEC standard 61400-12-1^[27] mentions that a met mast is to be used for the power curve verification of a wind turbine. Considering the maturity of the ground-based lidar for the wind resource assessment application, IEC 61400-12-1 is in the process of evolving and will be including the ground-based lidar vertical profiler for power curve verification.

The power curve verification standard is also including a new measurement method by applying the rotor equivalent power curve. In this case, the entire wind profile of the rotor diameter is considered and used, in order to estimate the total incoming wind along a plane rather than only the wind coming at hub height.

In addition to the vertical profiler, when a wind turbine cannot be reached within the $2.5D$ distance of the free wind of the wind turbine (where D is the rotor diameter), the scanning ground-based lidar can also be used to perform some power curve verification, by scanning from the ground to the front of the wind turbine.

C.1.3.2 Loss factor in the wind farm operation

When globally looking at a wind farm, there are some loss coefficients that wind farm developers apply to their annual electrical production output calculation, and the more accurate this information, the better the project and ease of financing.

The ground-based lidar is being used in a variety of programmes for the validation of the wake loss deficit coefficient. Major wind farm developers/owners have their own wind flow modelling tool to optimize the wind farm design and layout, and today the ground-based lidar is the appropriate tool used to validate their model, thanks to data generated by the lidar. In terms of optimization of the wind farm operation, the nacelle-based lidar is also widely used, for turbine control, yaw misalignment or nacelle anemometer calibration.

C.2 Wind hazards monitoring for aviation weather applications

C.2.1 General

According to the state of the art and the growth of the worldwide air traffic, several projects are going on worldwide in order to renew and optimize the regulations of air traffic management (ATM), such as the Single European Sky ATM Research project in Europe^[28] and the NextGen project in the United States of America. In the field of aviation weather, two major applications have been highlighted: the measurements of wind shears and wake vortices. For these two applications, coherent Doppler lidars are now considered as well adapted and powerful sensors to improve the wind observations in order to increase safety and optimize the air traffic.

C.2.2 Wind shear

Wind shears are defined as significant changes of head- or tail-winds along the takeoff path and the approach that can affect aircraft.^[29] These rapid changes in air speed cannot be balanced by acceleration or deceleration due to inertial effects. Thus, lift and drag, and therefore the resultant flight path, change. The effects of wind shear as mentioned above are particularly dangerous if they happen near the ground, that is, during takeoff or landing, where they can lead to severe accidents. This is why since the conference of Chicago, the International Civil Aviation Organization (ICAO) standards have taken care of the wind shear threats to civil air traffic by mentioning wind shears in Annex 3 to the Convention on International Civil Aviation – *Meteorological Service for International Air Navigation*^[29] and by providing the *ICAO Manual on Low-level Wind Shear* (Doc 9817)^[30]. The ICAO Annex 3 distinguishes two aspects of wind shears: the wind shear alerts and wind shear warnings.

- (a) Wind shear alerts consist in providing automatic alerts of wind shear intensity observed by ground-based remote sensors. The alerts are created once wind shears are above 15 kn (7.5 m/s) in terms of headwind/tailwind changes. As detailed in reference [30], the danger of wind shears is mainly due to the strong horizontal winds that induce strong headwind and tailwind changes for the aircraft;
- (b) Wind shear warnings must give concise information on the observed or expected existence of wind shears which could adversely affect aircraft. They are focusing below 500 m and along the takeoff path and approach. They are prepared by the meteorological office in charge of the met observations at a given airport. The wind shear warnings will be prepared “manually”, thanks to all the observations (ground-based, aircraft) and weather forecasts available.

According to the best practices, described in reference [30], coherent Doppler lidars are a good candidate technology for providing wind shear alerts and/or warnings since:

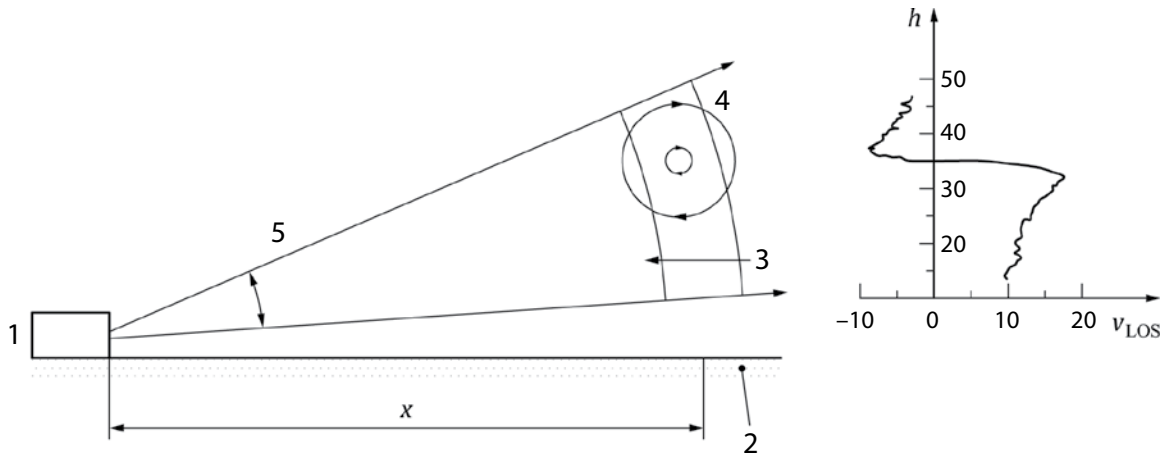
- (a) The areas of interest are the takeoff path and the approach that can be probed by a scanning coherent Doppler lidar with plan position indicator (typically with a 3° of elevation) or glide-path^[31] scans or lines of sights along the glide path;
- (b) The probing area for alerting wind shears is two extensions of 3 nautical miles of the runways, that is to say a measurement range of 7 km at least. Measurement range should be 7 km at least in appropriate atmospheric conditions (described in section 5);
- (c) The wind shear alerts are provided on the three boxes (of 1 nautical mile) that compose the extensions of each side of the runways, commonly called the "ARENA" (area noted for attention). To compute differences of headwind or tailwind, two points are needed at a minimum. This corresponds to a theoretical required resolution better than 1.852 km. But, in order to get accurate wind shear alerts and to be able to monitor all the types of wind shears and especially the smallest ones which are the microbursts (size > 1.5 km), a range resolution of 200 m is commonly used with lidars and radars;
- (d) ICAO documents mention the typical alert frequency suitable for the wind shears detection. In worldwide best practices, this frequency varies from 1 to 3 min;
- (e) Above all, it is important to notice that the configurations (such as accumulation time, scanning speed, alert frequency, probing area shape, probing range) of an equipment like a lidar dedicated to wind shear alerts or warnings should be adapted to the local requirements (typical local wind shear phenomena and the needs of users, such as the air traffic controllers).

Moreover, Doppler lidar systems compliant with requirements in Attachment D should be considered as a valuable supplement to Doppler weather radar observations, since they have complementary performance with respect to precipitation. Doppler lidars perform best in clear air conditions when Doppler radar receives only weak signals, and vice versa, when precipitation limits Doppler lidar observations, Doppler radar performs optimally. An example describing the set-up at Hong Kong International Airport including a Doppler lidar can be found in reference [31].

C.2.3 **Requirements for wake vortices detection behind aircraft**

There is strong interest of the ATC stakeholders for studying wake vortices because their strength (commonly characterized by their circulation) determines the minimum separation distance between aircraft in order to ensure safety. Wake vortices consist of two strong horizontal rotational flows that trail from each wingtip. They are generated by the lift of the aircraft which induces air flow from below the wings around the wingtips into the region above the wings. The wake vortices are very stable compared to turbulence and they can last up to 3 min with stable atmospheric conditions. Their circulation is determined by the aircraft weight and air speed and by the wingspan. Their size is about 20 m but they can be very dangerous especially in the takeoff and landing phases of flight.

That is why, since the 1960s, regulations have been created by ICAO to fix the separation distances between three categories. With the increase of worldwide air traffic and the development of super heavy aircraft, several projects aim at renewing the ATC regulations and especially the separation distances. Thus, plenty of wake vortices studies have been launched since the 1990s in using computational fluid dynamic models and coherent Doppler lidar technology in order to optimize the separation distances while ensuring safety^[32;33]. Scanning coherent Doppler lidars are particularly adapted to measure wake vortices since they allow to measure at high resolution below 10 m and at high frequency up to 5 s wake vortices generated by the aircraft below 500 m, for monitoring out-of-ground effects and in-ground effect wake

**Key**

- 1 Lidar
- 2 Runway
- 3 Crosswind
- 4 Vortex
- 5 Elevation scan

Measurement principle for determining aircraft wake vortices with Doppler wind lidar

vortex behaviour. Usually, wake vortices measurements are performed close to the runways with range height indicator scans with narrow angles of typically 10° to 40° to map vertically the motion of the wake vortices.

Lidar measurements can besides be post-processed to calculate wake vortices characteristics like the probability of detection, the localization of their cores and their circulation (strength)^[34,35].

C.2.4 **Siting constraints**

Since the Doppler lidar delivers only the radial wind speed, siting of the instrument is a crucial point, because runway-oriented wind has to have a significant projection onto the line of sight of the lidar. In general, the magnitude, and therefore the quality, of the runway-oriented wind component projected onto the line of sight deteriorates as $\cos^2 \theta$, θ being the angle between the line of sight and the runway^[6].

Another point is that, ideally, the 3° glide slope is to be scanned. This can be ideally done with one plan position indicator scan, if the lidar is located at the runway threshold. If more than one runway threshold is to be monitored with one instrument, following exactly the 3° glide is not possible, and the above-mentioned timing constraints usually do not allow scanning of more than one elevation. However, a 3° scan centred at the actual location of the lidar still outperforms an anemometer-based low-level wind shear alert system in terms of glide slope wind shear detection.

ATTACHMENT D. TYPICAL APPLICATION RANGES AND CORRESPONDING REQUIREMENTS

(informative)

Accordingly to the needs for the main applications (see table below), three accuracy classes for the wind velocity are being defined. These classes are related to a defined spatial and temporal resolution. The wind velocity accuracy must be ensured in all ranges of interest.

- (a) Class A: $x \leq 0.1$ m/s (for example, for wind energy purposes);
- (b) Class B: $0.1 < x \leq 0.5$ m/s (for example, for meteorological applications)^[13];
- (c) Class C: $0.5 < x \leq 1.0$ m/s (for example, for nowcasting)^[13].

Typical application ranges and corresponding requirements

<i>Application</i>	<i>Parameter to be provided</i>	<i>Reference</i>	<i>Typical probing range (m)</i>	<i>Range resolution (m)</i>	<i>Time resolution (min)</i>	<i>Velocity measurement accuracy (m/s)</i>	<i>Wind direction accuracy (°)</i>	<i>Minimum data availability (%)</i>
Radial velocity mapping	Line-of-sight radial velocity	Formula 5.A.5	200–10 000	25–100	1–10	0.5	Not applicable	50–99 ^a
Wind energy, e.g. site assessment, power curve, wind profile	Profile of the horizontal wind vector along the vertical axis	e.g. [36]	40–200	25	10	0.5	2	85
High-resolution numerical weather prediction	Profile of the horizontal wind vector along the vertical axis	[13]	> 50	25	10	0.5	2	80
Air pollution, e.g. dispersion modelling, risk management	Profile of the horizontal wind vector along the vertical axis	–	40–200	25	10	0.5	–	90
Aviation: wind shear	Radial wind along takeoff path, approach and runways	[29;36]	7 000–8 000 (5 500 + half the runway)	200	1	0.5	5	80
Aviation: vortex monitoring (ground-based systems)	Radial wind speed in perpendicular planes to the runway	–	Distance to runway + 300–500 on each side	25 (5 with overlap)	0.1	1	–	< 50
Met applications, e.g. nowcasting	Profile of the horizontal wind vector along the vertical axis	[13]	0–4 000	100	15	1	5	80

^a Depending on application

BIBLIOGRAPHY

- [1] Henderson, S.W., P. Gatt, D. Rees and R.M.N. Huffaker, 2005: Wind lidar. In: *Laser Remote Sensing* (T. Fujii and T. Fukuchi, eds.). 469–722, CRC Press, ISBN-10: 8247-4256-7.
- [2] Measures, R.M., 1992: *Laser Remote Sensing: Fundamentals and Applications*. Krieger Publishing, 524 pp., ISBN-10: 8946-4619-2.
- [3] Frehlich, R. and M. Kavaya, 1991: Coherent laser radar performance for general atmospheric refractive turbulence. *Appl. Opt.*, 30:5325–5352.
- [4] Belmonte, A., 2003: Analysing the efficiency of a practical heterodyne lidar in the turbulent atmosphere: telescope parameters. *Opt. Express.*, 11:2041–2046.
- [5] Frehlich, R., S. Hannon and S. Henderson, 1997: Coherent Doppler lidar measurements of winds in the weak signal regime. *Appl. Opt.*, 36:3491–3499.
- [6] Banakh, V.A. and I.N. Smalikho, 1997: Estimation of the turbulence eddy dissipation rate from the pulsed Doppler lidar data. *Atmos. Oceanic Opt.*, 10(12).
- [7] Frehlich, R., 1996: Simulation of coherent Doppler lidar performance in the weak signal regime. *J. Atmos. Ocean. Technol.*, 13:646–658.
- [8] Dabas, A., P. Drobinski and P. Flamant, 2000: Velocity biases of adaptive filters in heterodyne doppler lidar measurements. *J. Atmos. Ocean. Technol.*, 17:1189–1202.
- [9] Dabas, A., 1999: Semi empirical model for the reliability of a matched filter frequency estimator for Doppler lidar. *J. Atmos. Ocean. Technol.*, 16:19–28.
- [10] Goodman, J.W., 1975: Statistical properties of laser speckle patterns. In: *Laser Speckle* (J.C. Dainty, ed.). Springer.
- [11] American National Standards Institute (ANSI) Z136.1-2014: *American National Standard for Safe Use of Lasers*. ISBN: 978-1-940168-00-5.
- [12] IEC 60825-1:2014: *Safety of Laser Products – Part 1: Equipment Classification and Requirement*.
- [13] World Meteorological Organization: <http://www.wmo-sat.info/oscar/requirements>.
- [14] Boquet, M., P. Royer, J.P. Cariou, M. Machta and M. Valla, 2016: Simulation of doppler lidar measurement range and data availability. *J. Atmos. Ocean. Technol.*, paper accepted, DOI: 10.1175/JTECH-D-15-0057.1.
- [15] Frehlich, R., 2001: Estimation of velocity error for doppler lidar measurements. *J. Atmos. Ocean. Technol.*, 18:1628–1639.
- [16] Ernsdorf, T., B. Stiller, B.R. Beckmann, A. Weipert, S. Kauczok and R. Hannedes, 2014: Inter-comparison of X-band radar and lidar low-level wind measurement for air traffic control (ATC). Eighth Europ. Conf. on Radar in Meteorol. and Hydrol., Garmisch-Partenkirchen, Germany.
- [17] Hannedes, R., S. Kauczok and A. Weipert, 2014: Quality of clear-air radar radial velocity data: do insects matter? Eighth Europ. Conf. on Radar in Meteorol. and Hydrol., Garmisch-Partenkirchen, Germany.
- [18] Weipert, A., S. Kauczok, R. Hannedes, T. Ernsdorf and B. Stiller, 2014: Wind shear detection using radar and lidar at Frankfurt and Munich airports. Eighth Europ. Conf. on Radar in Meteorol. and Hydrol., Garmisch-Partenkirchen, Germany.
- [19] Jörgensen, H., T. Mikkelsen, J. Streicher, H. Herrmann, C. Werner and E. Lyck, 1997: Lidar calibration experiment. *Appl. Phys. B.*, 64:355–361.
- [20] Bronstein, I.N., K.A. Semendjajew, G. Musiol and H. Mühlig, 1993: *Taschenbuch der Mathematik*. Harri Deutsch.
- [21] Fukao, S. and K. Hamazu, 2013: *Radar for Meteorological and Atmospheric Observations*. Springer.
- [22] Banakh, V.A. and I.N. Smalikho, 2013: *Coherent Doppler Wind Lidars in a Turbulent Atmosphere*. Artech House.
- [23] Srinivaso, R.I., V.K. Anandan and R.R. Narasimha, 2008: Evaluation of DBS wind measurement technique in different beam configurations for a VHF wind profiler. *J. Atmos. Ocean. Technol.*, 25(12):2304–2312.
- [24] Lhermite, R.M., 1962: Note on wind variability with Doppler radar. *J. Atmos. Sci.*, 19(4):343–346.
- [25] Browning, K.A. and R. Wexler, 1968: The determination of kinematic properties of a wind field using Doppler radar. *J. Appl. Meteorol.*, 7(1):105–113.
- [26] Waldteufel, P. and H. Corbin, 1979: On the analysis of single Doppler radar data. *J. Appl. Meteor.*, 18:532–542.
- [27] IEC 61400-12-1:2005: *Wind Turbines – Part 12-1: Power Performance Measurements of Electricity Producing Wind Turbines*.
- [28] European ATM Master Plan, 2009: <https://www.atmmasterplan.eu/>.

- [29] International Civil Aviation Organization, 2007: *Meteorological Service for International Air Navigation*, Annex 3 to the Convention on International Civil Aviation.
- [30] International Civil Aviation Organization, 2005: *Manual on Low-level Wind Shear*, Doc 9817 AN/449.
- [31] Shun, C.M. and P.W. Chan, 2008: Applications of an infrared doppler lidar in detection of wind shear. *J. Atmos. Ocean. Technol.*, 25(5):637–655.
- [32] Wakenet-Eu: <https://wakenet-europe.eurocontrol.fr/>.
- [33] Lang, S. and W. Bryant, 2006: *Vortex Research in the USA (WakeNet-USA)*. Air Traffic Organization, Federal Aviation Administration.
- [34] Holzäpfel, F., T. Gerz, F. Köpp, E. Stumpf, M. Harris, R.I. Young and A. Dolfi-Bouteyre, 2003: Strategies for circulation evaluation of aircraft wake vortices measured by lidar. *J. Atmos. Ocean. Technol.*, 20(8):1183–1195.
- [35] Dolfi-Bouteyre, A., B. Augere, M. Valla, D. Goular, D. Fleury and G. Canat, 2009: 1,55 μm pulsed fibre lidar for wake vortex detection (axial or transverse). Wakenet-Eu Workshop.
- [36] Hasager, C.B., D. Stein, M. Courtney, A. Pena, T. Mikkelsen, M. Stickland and A. Oldroyd, 2013: Hub height ocean winds over the North Sea observed by the NORSEWIND lidar array: measuring techniques, quality control and data management. *Remote Sens.*, 5:4280–4303.
- [37] ISO 28902-1: *Air Quality – Environmental Meteorology – Part 1: Ground-based Remote Sensing of Visual Range by Lidar*.
- [38] ISO 28902-3: *Air Quality – Environmental Meteorology – Part 3: Ground-based Remote Sensing of Wind by Continuous-wave Doppler Lidar*.
-

REFERENCES AND FURTHER READING

- Adachi, A., T. Kobayashi, K.S. Gage, D.A. Carter, L.M. Hartten, W.L. Clark and M. Fukuda, 2005: Evaluation of three-beam and four-beam profiler wind measurement techniques using a five-beam wind profiler and collocated meteorological tower. *Journal of Atmospheric and Oceanic Technology*, 22:1167–1180.
- Angevine, W.M., W.L. Ecklund, D.A. Carter, K.S. Gage and K.P. Moran, 1994: Improved radio acoustic sounding techniques. *Journal of Atmospheric and Oceanic Technology*, 11(1):42–49.
- Bianco, L., D. Gattas and J.M. Wilczak, 2013: Implementation of a Gabor transform data quality-control algorithm for UHF wind profiling radars. *Journal of Atmospheric and Oceanic Technology*, 30(12):2697–2703.
- Bevis, M., S. Businger, S. Chiswell, T.A. Herring, R.A. Anthes, C. Rocken and R.H. Ware, 1994: GPS meteorology: Mapping zenith wet delays onto precipitable water. *Journal of Applied Meteorology*, 33:379–386.
- Brown, E.H. and F.F. Hall, 1978: Advances in atmospheric acoustics. *Reviews of Geophysics and Space Physics*, 16:47–109.
- Cadeddu, M.P., G.E. Peckham and C. Gaffard, 2002: The vertical resolution of ground-based microwave radiometers analysed through a multiresolution wavelet technique. *IEEE Transactions on Geoscience and Remote Sensing*, 40(3):531–540.
- Candlish, L.M., R.L. Raddatz, M.G. Asplin and D.G. Barber, 2012: Atmospheric temperature and absolute humidity profiles over the Beaufort Sea and Amundsen Gulf from a microwave radiometer. *Journal of Atmospheric and Oceanic Technology*, 29:1182–1201.
- Chan, P.W., 2009: Performance and application of a multi-wavelength, ground-based microwave radiometer in intense convective weather. *Meteorologische Zeitschrift*, 18:253–265.
- Chan, P.W. and Y.F. Lee, 2013: Application of brightness temperature data from a ground-based microwave radiometer to issue low-level windshear alert over Hong Kong International Airport. *Mausam* 64(3):457–466.
- Chan, W.S. and J.C.W. Lee, 2015: Vertical profile retrievals with warm-rain microphysics using the ground-based microwave radiometer operated by the Hong Kong Observatory. *Atmospheric Research*, 161–162:125–133.
- Chakraborty, R., S. Das and A. Maitra, 2016: Prediction of convective events using multi-frequency radiometric observations at Kolkata. *Atmospheric Research*, 169:24–31.
- Davis, J.L., T.A. Herring, I.I. Shapiro, A.E.E. Rogers and G. Elgered, 1985: Geodesy by radio interferometry: Effects of atmospheric modeling errors on estimates of baseline length. *Radio Science*, 20(6):1593–1607.
- Derr, V.E., 1972: *Remote Sensing of the Troposphere*. United States National Oceanic and Atmospheric Administration, WPL, Boulder, Colorado.
- Dolman, B. K. and I.M. Reid, 2014: Bias correction and overall performance of a VHF spaced antenna boundary layer profiler for operational weather forecasting. *Journal of Atmospheric and Solar-Terrestrial Physics*, 118:16–24.
- Doviak, R. J. and D.S. Zrnić, 2014: *Doppler Radar and Weather Observations*. Academic Press.
- Elgered, G., H.-P. Plag, S. Barlag and J. Nash, 2004: *COST716 Final Report*, European Union.
- Fernández-González, S., F. Valero, J.L. Sanchez, E. Gascón, L. López, E. García-Ortega, and A. Merino, 2014: Observation of a freezing drizzle episode: A case study. *Atmospheric Research*, 149:244–254.
- Fukao, S., K. Hamazu and R.J. Doviak, 2014: *Radar for Meteorological and Atmospheric Observations*. Springer Japan.
- Gaffard, C. and T. Hewison, 2003: Radiometrics MP3000 microwave radiometer trial report. *Technical Report –TR26*, Met Office, Workingham, Berkshire, UK.
- Gaynor, J.E., C.B. Baker and J.C. Kaimal, 1990: The international sodar intercomparison experiment. *Proceedings of the Fifth International Symposium on Acoustic Remote Sensing*. McGraw-Hill, New York, 67–74.
- Gossard, E.E. and R.G. Strauch, 1983: *Radar Observations of Clear Air and Clouds*. Elsevier, Scientific Publishing Co., Amsterdam.
- Güldner, J. and D. Spänkuch, 2001: Remote sensing of the thermodynamic state of the atmospheric boundary layer by ground-based microwave radiometry. *Journal of Atmospheric and Oceanic Technology*, 18:925–933.
- Hinkley, E.D., 1976: *Laser Monitoring of the Atmosphere: Topics in Applied Physics*. Volume 14, Springer Verlag, New York.

- Hocking, W.K., 2011: A review of mesosphere–stratosphere–troposphere (MST) radar developments and studies, circa 1997–2008. *Journal of Atmospheric and Solar-Terrestrial Physics*, 73(9):848–882.
- Hocking, W.K., J. Röttger, R.D. Palmer, T. Sato and P.B. Chilson (2016): *Atmospheric Radar: Application and Science of MST Radars in the Earth's Mesosphere, Stratosphere, Troposphere, and Weakly Ionized Regions*. Cambridge University Press.
- Hogg, D.C., M.T. Decker, F.O. Guiraud, K.B. Earnshaw, D.A. Merritt, K.P. Moran, W.B. Sweezy, R.G. Strauch, E.R. Westwater and C.G. Little, 1983: An automatic profiler of the temperature, wind and humidity in the troposphere. *Journal of Climate and Applied Meteorology*, 22:807–831.
- Illingworth, A. J., D. Cimini, C. Gaffard, M. Haefelin, V. Lehmann, U. Löhnert and D. Ruffieux, 2015: Exploiting existing ground-based remote sensing networks to improve high-resolution weather forecasts. *Bulletin of the American Meteorological Society*, 96(12):2107–2125.
- Kadygrov, E.N., E.A. Miller and A.V. Troitsky, 2013: Study of atmospheric boundary layer thermodynamics during total solar eclipses. *IEEE Transactions on Geoscience and Remote Sensing*, 51(9):4672–4677.
- Kadygrov, E.N. and D.R. Pick, 1998: The potential for temperature retrieval from an angular-scanning single-channel microwave radiometer and some comparisons with in situ observations. *Meteorological Applications*, 5:393–404.
- Kadygrov, E.N., G.N. Shur and A.S. Viazankin, 2003: Investigation of atmospheric boundary layer temperature, turbulence, and wind parameters on the basis of passive microwave remote sensing. *Radio Science*, 38(3):13.1–13.12.
- Lataitis, R.J., 1992a: Signal power for radio acoustic sounding of temperature: The effects of horizontal winds, turbulence and vertical temperature gradients. *Radio Science*, 27:369–385.
- , 1992b: *Theory and Application of a Radio-acoustic Sounding System*. NOAA Technical Memorandum ERL WPL-230.
- Liljegren, J.C., S.A. Boukabara, K. Cady-Pereira and S.A. Clough, 2005: The Effect of the half-width of the 22-GHz water vapor line on retrievals of temperature and water vapor profiles with a 12-channel radiometer. *IEEE Transactions on Geoscience and Remote Sensing*, 43(5):1102–1108.
- Madhulatha, A., M. Rajeevan, M.V. Ratnam, J. Bhate and C.V. Naidu, 2013: Nowcasting severe convective activity over southeast India using ground-based microwave radiometer observations. *Journal of Geophysical Research: Atmospheres*, 118(1):1–13.
- Martner, B.E., D.B. Wuertz, B.B. Stankov, R.G. Strauch, E.R. Westwater, K.S. Gage, W.L. Ecklund, C.L. Martin and W.F. Dabberdt, 1993: An evaluation of wind profiler, RASS and microwave radiometer performance. *Bulletin of the American Meteorological Society*, 74(4):599–613.
- May, P.T., R.G. Strauch, K.P. Moran and W.L. Ecklund, 1990: Temperature sounding by RASS, with wind profiler radars: A preliminary study. *IEEE Transactions on Geoscience and Remote Sensing*, 28(1):19–28.
- Muschinski, A., V. Lehmann, L. Justen and G. Teschke, 2005: Advanced radar wind profiling. *Meteorologische Zeitschrift*, 14(5):609–625.
- Navas-Guzman, F., O. Stahl and N. Kampfer, 2013: Study of cloud effect on the tropospheric temperature retrievals. In: *URSI Commission F Microwave Signatures 2013: Specialist Symposium on Microwave Remote Sensing of the Earth, Oceans, and Atmosphere*, October 2013, Finland, p.136.
- Neff, W.D. and R.L. Coulter, 1986: Acoustic remote sounding. In: *Probing the Atmospheric Boundary Layer* (Lenschow, D.H., ed.). American Meteorological Society, 201–236.
- Panofsky, H.A., 1973: Tower micrometeorology. In: *Workshop on Micrometeorology* (Haugen, D.A., ed.), Chapter 4, American Meteorological Society.
- Saastamoinen, J., 1972: Atmospheric correction for the troposphere and stratosphere in radio ranging of satellites. *Geophysical Monograph Series: The Use of Artificial Satellites for Geodesy*, 15:247–251.
- Singal, S.P., 1990: Current status of air quality related boundary layer meteorological studies using sodar. *Proceedings of the Fifth International Symposium on Acoustic Remote Sensing*, McGraw-Hill, New York, 453–476.
- Smith, E.K. and S. Weintraub, 1953: The constants in the equation for atmospheric refractive index at radio frequencies. *Proceedings of the IRE*, 41(8):1035–1037.
- Solheim, F., J.R. Godwin, E.R. Westwater, Y. Han, S.J. Keihm, K. Marsh, R. Ware, 1998: Radiometric profiling of temperature, water vapor, and cloud liquid water using various inversion methods. *Radio Science*, 33:393–404.
- Syed, I. and E.V. Browell, 1994: Recent Lidar technology developments and their influence on measurements of tropospheric water vapor. *Journal of Atmospheric and Oceanic Technology*, 11(1):76–84.
- Teschke, G. and V. Lehmann, 2017: Mean wind vector estimation using the velocity–azimuth–display (VAD) method: An explicit algebraic solution. *Atmospheric Measurement Techniques Discussions*, 10:3265–3271.

- Thayer, G.D., 1974: An improved equation for the radio refractive index of air. *Radio Science*, 9(10):803–807.
- Thomas, L., 1991: Lidar probing of the atmosphere. *Indian Journal of Radio and Space Physics*, 20:368–380.
- Thompson, A.R., J.M. Moran and G.W. Swenson, 1986: *Interferometry and Synthesis in Radio Astronomy*. John Wiley and Sons, New York.
- Thompson, N., 1980: Tethered balloons. In: *Air-sea Interaction: Instruments and Methods* (F. Dobson, L. Hasse and R. Davis, eds.) Chapter 31, Plenum Press, New York.
- Wakasugi, K. and S. Fukao, 1985: Sidelobe properties of a complementary code used in MST radar observations. *IEEE Transactions on Geoscience and Remote Sensing*, 23(1):57–59.
- Ware, R., R. Carpenter, J. Güldner, J. Liljegren, T. Nehrkorn, F. Solheim and F. Vandenberghe, 2003: A multi-channel radiometric profiler of temperature, humidity and cloud liquid. *Radio Science*, 38:8079–8092.
- Ware, R., D. Cimini, E. Campos, G. Giuliani, S. Albers, M. Nelson, S.E. Koch, P. Joe and S. Cober, 2013: Thermodynamic and liquid profiling during the 2010 Winter Olympics. *Atmospheric Research*, 132–133:278–290.
- Weber, B.L. and D.B. Wuertz, 1990: Comparison of rawinsonde and wind profiler radar measurements. *Journal of Atmospheric and Oceanic Technology*, 7(1):157–174.
- Weber, B.L., D.B. Wuertz, R.G. Strauch, D.A. Merritt, K.P. Moran, D.C. Law, D. van de Kamp, R.B. Chadwick, M.H. Ackley, M.F. Barth, N.L. Abshire, P.A. Miller and T.W. Schlatter, 1990: Preliminary evaluation of the first NOAA demonstration network wind profiler. *Journal of Atmospheric and Oceanic Technology*, 7(6):909–918.
- Westwater, E., S. Crewell, C. Mätzler and D. Cimini, 2005: Principles of surface-based microwave and millimetre wave radiometric remote sensing of the troposphere. *Quaderni Della Società Italiana di Elettromagnetismo*, 1(3).
- Westwater, E.R., Y. Han, V.G. Irisov, V. Leuskiy, E.N. Kadyrov and S.A. Viazankin, 1999: Remote sensing of boundary layer temperature profiles by a scanning 5-mm microwave radiometer and RASS: Comparison experiments. *Journal of Atmospheric and Oceanic Technology*, 16:805–818.
- Westwater, E.R., J.B. Snider and M.J. Falls, 1990: Ground-based radiometric observations of atmospheric emission and attenuation at 20.6, 31.65, and 90.0 GHz: A comparison of measurements and theory. *IEEE Transactions on Antennas and Propagation*, 38(10):1569–1580.
- Wilczak, J. M., E.E. Gossard, W.D. Neff and W.L. Eberhard, 1996: Ground-based remote sensing of the atmospheric boundary layer: 25 years of progress. In: *Boundary-Layer Meteorology 25th Anniversary Volume, 1970–1995*, 321–349. Dordrecht, Springer.
- Woods, C.P., M.T. Stoelinga, J.D. Locatelli and P.V. Hobbs, 2005: Microphysical processes and synergistic interaction between frontal and orographic forcing of precipitation during the 13 December 2001 IMPROVE-2 event over the Oregon Cascades. *Journal of Atmospheric Science*, 62(10):3493–3519.
- World Meteorological Organization, 1980: *Lower Tropospheric Data Compatibility: Low-level Intercomparison Experiment* (Boulder, United States, 1979). Instruments and Observing Methods Report No. 3. Geneva.
- , 1982: *Indirect Sensing: Meteorological Observations by Laser Indirect Sensing Techniques* (A.O. Van Gysegem). Instruments and Observing Methods Report No. 12. Geneva.
- , 1994: Comparison of windprofiler and rawinsonde measurements (J. Neisser, V. Görsdorf and H. Steinhagen). *Papers Presented at the WMO Technical Conference on Instruments and Methods of Observation (TECO-94)*. Instruments and Observing Methods Report No. 57 (WMO/TD-No. 588). Geneva.
- , 2006a: *Operational Aspects of Different Ground-Based Remote Sensing Observing Techniques for Vertical Profiling of Temperature, Wind, Humidity and Cloud Structure: A Review* (E.N. Kadyrov). Instruments and Observing Methods Report No. 89 (WMO/TD-No. 1309). Geneva.
- , 2006b: *National/Regional Operational Procedures of GPS Water Vapour Networks and Agreed International Procedures* (S. de Haan). Instruments and Observing Methods Report No. 92 (WMO/TD-No. 1340). Geneva.
- Xu, G., R. Ware, W. Zhang and G. Feng, 2014: Effect of the off-zenith observation on reducing the impact of precipitation on ground-based microwave radiometer measurement accuracy in Wuhan. *Atmospheric Research*, 140–141:85–94.

CHAPTER 6. ELECTROMAGNETIC METHODS OF LIGHTNING DETECTION

6.1 INTRODUCTION

There are many individual physical processes in cloud and ground lightning flashes. Each of these processes is associated with characteristic electric and magnetic fields. Lightning is known to emit significant electromagnetic energy in the radio-frequency range from below 1 Hz to near 300 MHz, with a peak in the frequency spectrum near 5 to 10 kHz for lightning at distances beyond 50 km or so. Further, electromagnetic radiation from lightning is detectable at even higher frequencies, for example, in the microwave (300 MHz to 300 GHz) and, obviously, in visible light (roughly 10^{14} to 10^{15} Hz). At frequencies higher than that of the spectrum peak, the spectral amplitude varies roughly inversely proportional to the frequency up to 10 MHz or so and inversely proportional to the square root of frequency from about 10 MHz to 10 GHz. Also, lightning is known to produce X-rays (up to 10^{20} Hz or more), although at ground level they are usually not detectable beyond a kilometre or so from the source. In general, any observable electromagnetic signal from a lightning source can be used to detect and locate the lightning process that produced it. In addition to electromagnetic radiation, lightning produces the acoustic radiation that can be also used for lightning location. The acoustic locating techniques, acoustic signal time of arrival and acoustic ray tracing are not further discussed here.

6.2 LIGHTNING DISCHARGE

Lightning can be defined as a transient, high-current (typically tens of kiloamperes) electric discharge in air whose length is measured in kilometres. As for any discharge in air, lightning channel is composed of ionized gas, that is, of plasma, whose peak temperature is typically 30 000 K, about five times higher than the temperature of the surface of the Sun. Lightning was present on Earth long before human life evolved, and it may even have played a crucial role in the evolution of life on our planet. The global lightning flash rate is some tens to a hundred per second or so. Each year, some 25 million cloud-to-ground lightning discharges (note that, on average, about three quarters of lightning discharges are confined to the cloud, that is, do not involve ground) occur in the United States alone, killing more people than tornadoes and hurricanes. Lightning initiates many forest fires, and over 30% of all electric power line failures are lightning related. Each commercial aircraft is struck by lightning on average once a year. A lightning strike to an unprotected object or system can be catastrophic.

6.2.1 Lightning types, processes and parameters

About 90% or more of global cloud-to-ground lightning is accounted for by negative (negative charge is effectively transported to the ground) downward (the initial process begins in the cloud and develops in a downward direction) lightning. Other types of cloud-to-ground lightning include positive downward, negative upward, and positive upward discharges. There are also bipolar lightning discharges sequentially transferring both positive and negative charges during the same flash. The basic elements of the negative downward lightning discharge are termed component strokes or just strokes. Each discharge (or flash) typically contains 3 to 5 strokes, the observed range being 1 to 26. Roughly half of all lightning discharges to Earth strike ground at more than one point, with the spatial separation between the channel terminations being up to many kilometres. The two major lightning processes comprising a stroke are termed the leader and the return stroke, which occur as a sequence with the leader preceding the return stroke. The following discussion considers lightning discharges in more detail. Rakov and Uman (2003) and references therein contain more details.

Two photographs of a negative cloud-to-ground discharge are shown in Figures 6.1(a) and 6.1(b). The image in Figure 6.1(a) was obtained using a stationary camera, while the image in Figure 6.1(b) was captured with a separate camera that was moved horizontally during the

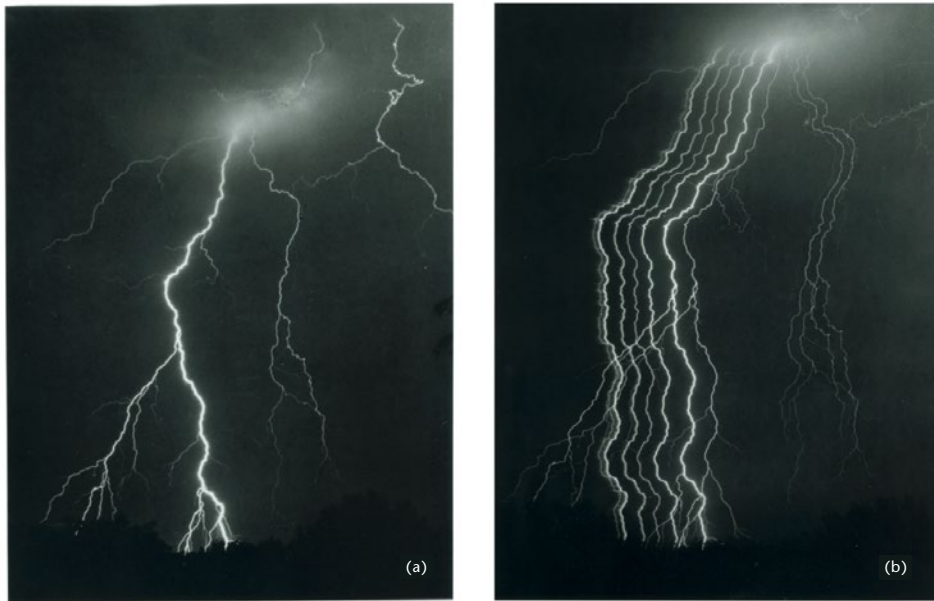


Figure 6.1. Lightning flash which appears to have at least 7 (perhaps as many as 10) separate ground strike points. Image (a) is a still photograph and image (b) a streaked photograph.

Some of the strike points are associated with the same stroke having separate branches touching ground, while others are associated with different strokes taking different paths to ground. Adapted from Hendry (1993)

time of the flash. As a result, the latter image is time resolved showing seven distinct luminous channels between the cloud and ground. The dark intervals between these channels are typically of the order of tens of milliseconds and explain why lightning often appears to the human eye to flicker. Each luminous channel corresponds to an individual stroke, the first stroke being on the far right (time advances from right to left). The first two strokes are branched, and the downward direction of branches indicates that this is a downward lightning flash.

Sketches of still and time-resolved images of the three-stroke lightning flash are shown in Figures 6.2(a) and 6.2(b), respectively. A sketch of the corresponding current at the channel base is shown in Figure 6.2(c). In Figure 6.2(b), time advances from left to right, and the timescale is not continuous. Each of the three strokes in Figure 6.2(b), represented by its luminosity as a function of height above ground and time, is composed of a downward-moving process, termed a leader, and an upward-moving process, termed a return stroke. The leader creates a conducting path between the cloud charge source region and ground and distributes negative charge from the cloud source region along this path. The return stroke traverses that path moving from ground towards the cloud charge source region and neutralizes the negative leader charge. Thus, both leader and return-stroke processes serve to effectively transport negative charge from the cloud to ground. As seen in Figure 6.2(b), the leader initiating the first return stroke differs from the leaders initiating the two subsequent strokes (all strokes other than the first are termed subsequent strokes). In particular, the first-stroke leader appears optically to be an intermittent process, hence the term “stepped leader”, while the tip of a subsequent-stroke leader appears to move continuously. The continuously moving subsequent-stroke leader tip appears on streak photographs as a downward-moving dart, hence the term “dart leader”. The apparent difference between the two types of leaders is related to the fact that the stepped leader develops in virgin air, while the dart leader follows the pre-conditioned path of the preceding stroke or strokes. Sometimes a subsequent leader exhibits stepping while propagating along a previously formed channel; in which case it is referred to as a dart-stepped leader. There are also so-called chaotic subsequent-stroke leaders. All types of leaders produce bursts of X-ray emission with energies typically up to 250 keV (twice the energy of a chest X-ray) (Dwyer, 2005).

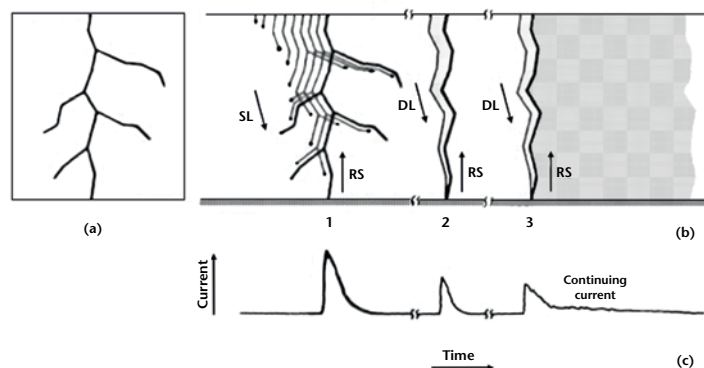


Figure 6.2. Drawing showing the luminosity of a three-stroke ground flash and the corresponding current at the channel base. Figure (a) is a still-camera image, (b) a streak-camera image, and (c) a channel-base current.

The electric potential difference between a downward-moving stepped-leader tip and ground is probably some tens of megavolts, comparable to or a considerable fraction of that between the cloud charge source and ground. The magnitude of the potential difference between two points, one at the cloud charge source and the other on ground, is the line integral of electric field intensity between those points. The upper and lower limits for the potential difference between the lower boundary of the main negative charge region and ground can be estimated by multiplying, respectively, the typical observed electric field in the cloud, 10^5 V/m, and the expected electric field at ground under a thundercloud immediately prior to the initiation of lightning, 10^4 V/m, by the height of the lower boundary of the negative charge centre above ground, 5 km or so. The resultant range is 50 to 500 MV.

When the descending stepped leader attaches to the ground, the first return stroke begins. The first return-stroke current measured at ground rises to an initial peak of about 30 kA in some microseconds and decays to half-peak value in some tens of microseconds. The return stroke effectively lowers to ground the several coulombs of charge originally deposited on the stepped-leader channel including all the branches, as well as any additional cloud charge that may enter the return-stroke channel.

Once the bottom of the dart-leader channel is connected to the ground, the second (or any subsequent) return-stroke wave is launched upward, which again serves to neutralize the leader charge. The subsequent return-stroke current at ground typically rises to a peak value of 10 to 15 kA in less than a microsecond and decays to half-peak value in a few tens of microseconds.

The high-current return-stroke wave rapidly heats the channel to a peak temperature near or above 30 000 K and creates a channel pressure of 1 MPa or more, resulting in channel expansion, intense optical radiation and an outward propagating shock wave that eventually becomes the thunder (sound wave) we hear at a distance.

The impulsive component of the current in a return stroke (usually subsequent) is often followed by a continuing current which has a magnitude of tens to hundreds of amperes and a duration of up to hundreds of milliseconds. Continuing currents with a duration in excess of 40 ms are traditionally termed long continuing currents. Between 30% and 50% of all negative cloud-to-ground flashes contain long continuing currents. Current pulses superimposed on continuing currents, as well as the corresponding enhancements in luminosity of the lightning channel, are referred to as M-components.

There is a special type of lightning that is thought to be the most intense natural producer of HF-VHF (3–300 MHz) radiation on Earth. It is referred to as compact intracloud discharge (CID). CIDs were first reported by Le Vine (1980) and received their name (Smith et al., 1999) due to their relatively small (hundreds of metres) spatial extent. They tend to occur at high altitudes (mostly above 10 km), appear to be associated with strong convection (however, even the strongest convection does not always produce CIDs), tend to produce less light than other

types of lightning discharges, and produce single bipolar electric field pulses (narrow bipolar pulses or NBPs) having typical full widths of 10 to 30 μs and amplitudes of the order of 10 V/m at 100 km, which is comparable to or higher than for return strokes in cloud-to-ground flashes. As an illustration of intensity of wideband electromagnetic signature of CIDs, 48 CIDs examined in detail by Nag et al. (2010) were recorded by 4 to 22 (11 on average) stations of the United States National Lightning Detection Network (NLDN), whose average baseline is 300–350 km.

6.2.2 Lightning electromagnetic signatures

Both cloud-to-ground and cloud lightning discharges involve a number of processes that produce characteristic electromagnetic field signatures. Salient characteristics of measured electric and magnetic fields generated by various lightning processes at distances ranging from tens to hundreds of kilometres are briefly reviewed below. The emphasis is put on those processes which produce substantial microsecond- and submicrosecond-scale field variations.

The table below summarizes essentially all identifiable lightning radiation field signatures as recorded at ground. Note that apparently there is no characteristic microsecond-scale field signature associated with lightning K- and M- processes. Besides return strokes (the first row) and CIDs (the last row), the pulses produced by lightning processes represented in the table occur in sequences with submillisecond-interpulse intervals. Leader pulses (second and third rows) are presumably emitted by the lower portion of the channel to ground just prior to the initiation of a return stroke, while both initial breakdown pulses (fourth and fifth rows) and regular pulse bursts (sixth row) are produced by lightning processes occurring inside the cloud. Characterization given below concerns both the overall pulse sequences and individual pulses.

Negative ground flashes

The typical microsecond-scale pulse structure of naturally occurring negative ground discharges, as observed at ground, includes an initial sequence of pulses (usually called initial or preliminary breakdown pulses) followed, typically some milliseconds to some tens of milliseconds later, by 3 to 5 relatively large return-stroke pulses spaced several tens of milliseconds apart. The duration of the initial sequence of pulses is typically a few milliseconds. Individual pulse waveforms characteristic of the preliminary breakdown in negative ground flashes are shown in Figure 6.3(a). The initial polarity of the preliminary breakdown pulses is usually the same as that of the following return-stroke pulse. The initial breakdown pulses can have amplitudes comparable to or even exceeding that of the corresponding return-stroke pulses. Just prior to the first return-stroke pulse and prior to some subsequent return-stroke pulses there are pulse sequences, in the former case associated with the stepped-leader process and in the latter case with dart-stepped (regular pulse train) or chaotic (irregular pulse train) leader processes. These pulse sequences have been observed to last for some tens of hundreds of microseconds, and the pulse amplitudes are one to two orders of magnitude smaller than the corresponding return-stroke pulse amplitude. The stepped-leader pulses are seen just prior to the return-stroke pulse in Figure 6.4(a), before $t = 0$. A rather irregular pulse train, indicative of chaotic leader, is seen prior to the subsequent return-stroke pulse (before $t = 0$) in Figure 6.4(b). Usually there is a relatively quiet millisecond-scale gap between the preliminary breakdown pulse sequence and the beginning of pronounced stepped-leader pulses. The intervals between the return-stroke pulses, and the interval of some tens of milliseconds following the last return-stroke pulse, contain regular pulse bursts of relatively small amplitude and some other, usually irregular, pulse activity. Pulse peaks in regular pulse bursts are approximately two orders of magnitude smaller than return-stroke initial field peaks in the same flash. As seen in the table, the regular pulse bursts are very similar in their characteristics to the pulse sequences associated with dart-stepped leaders. The geometric mean initial electric field peak normalized to 100 km for negative first strokes, about 6 V/m, is about a factor of two larger than for negative subsequent strokes, about 3 V/m. The geometric mean time interval between return-stroke pulses is 60 ms.

Characterization of microsecond-scale electric field pulses associated with various lightning processes (adapted from Rakov, 1999)

<i>Type of pulses</i>	<i>Dominant polarity (atmospheric electricity sign convention)</i>	<i>Typical total pulse duration (μs)</i>	<i>Typical time interval between pulses (μs)</i>	<i>Comments</i>
Return stroke in negative ground flashes	Positive	30–90 (zero-crossing time)	60×10^3	3–5 pulses per flash
Stepped leader in negative ground flashes	Positive	1–2	15–25	Within 200 μs just prior to a return stroke
Dart-stepped leader in negative ground flashes	Positive	1–2	6–8	Within 200 μs just prior to a return stroke
Initial breakdown in negative ground flashes	Positive	20–40	70–130	Some milliseconds to some tens of milliseconds before the first return stroke
Initial breakdown in cloud flashes	Negative	50–80	600–800	The largest pulses in a flash
Regular pulse burst in both cloud and negative ground flashes	Both polarities are about equally probable	1–2	5–7	Occur later in a flash; 20–40 pulses per burst
CID (narrow bipolar event)	Both polarities occur, with negative being more frequent	10–30	–	Typically not preceded or followed by any other lightning process within hundreds of milliseconds

Notes:

- a Polarity refers to the polarity of the initial half cycle in the case of bipolar pulses.
- b According to the atmospheric electricity sign convention, a downward-directed electric field vector is assumed to be positive.

Positive ground flashes

Positive flashes usually contain a single return stroke (although up to four strokes per flash have been observed) whose microsecond-scale electric and magnetic field waveforms are similar to those characteristic of negative first return strokes, except for the initial polarity. An example of positive return-stroke electric field waveform is given in Figure 6.4(c). Small pulses seen before $t = 0$ in Figure 6.4(c) are indicative of a stepped-leader process. As opposed to negative first strokes, these pulses are detected only in about one third of field waveforms. The mean initial electric field peak normalized to 100 km for positive first strokes is about a factor of two larger than for negative first strokes. Positive strokes to ground can be initiated in a way similar to how negative lightning flashes are initiated (see above) or they can be by-products of extensive cloud discharges.

Cloud flashes

The typical pulse structure that is observed in naturally occurring cloud discharges includes an initial sequence (or sequences) of pulses of relatively large amplitude, spaced some hundreds of microseconds apart and occurring within the first several to a few tens of milliseconds, followed by a number of regular pulse bursts of significantly smaller amplitude. Pulses within the burst

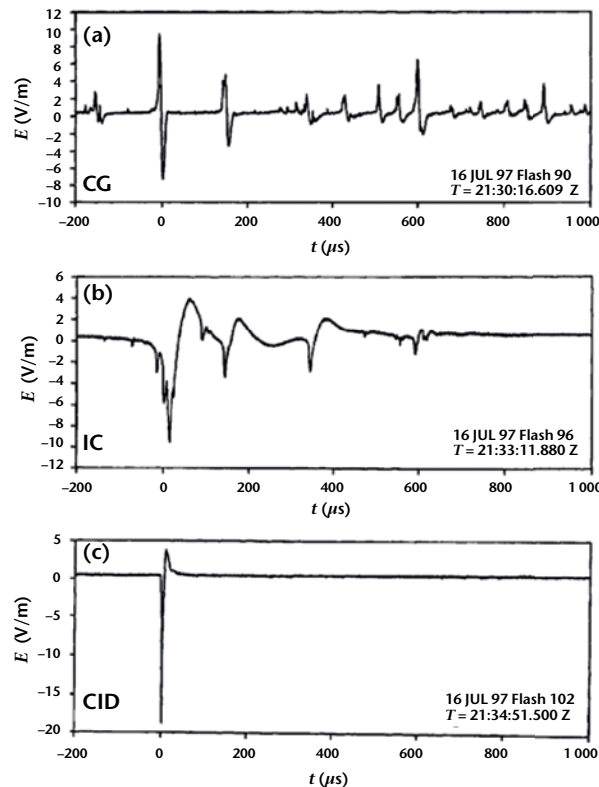


Figure 6.3. Examples of electric field (E) pulse waveforms characteristic of (a) the initial breakdown in negative ground (CG) flashes, (b) the initial breakdown in cloud (IC) flashes, and (c) compact intracloud discharges (CIDs). Positive electric field (atmospheric electricity sign convention) deflects upward. (Adapted from Rakov, 1999)

are several microseconds apart, with each burst lasting for some hundreds of microseconds. Individual pulse waveforms characteristic of the initial breakdown in cloud flashes are shown in Figure 6.3(b). The initial polarity of these pulses tends to be opposite to that of the initial breakdown pulses in negative ground flashes. There are also microsecond-scale pulses, with amplitudes appreciably lower than those of the initial breakdown pulses, which are dispersed, as opposed to clustering in bursts, throughout the flash. Some of these smaller and often irregular pulses are associated with step-like K changes (field signatures of K-processes). K changes typically occur in the late stage of the cloud flash and are separated by many tens of milliseconds.

Compact intracloud discharges

An example of electric field signature of CIDs (also called narrow bipolar events) is given in Figure 6.3(c). These pulses have peaks and peak time derivatives comparable to those of return strokes in ground flashes.

6.2.3 Glossary of terms

Atmospheric electricity sign convention. Electric field sign convention according to which a downward-directed field vector is defined as positive.

Bipolar lightning. Lightning discharges sequentially transferring both positive and negative charges to ground during the same flash.

Cloud flash. Flash that does not contact the ground.

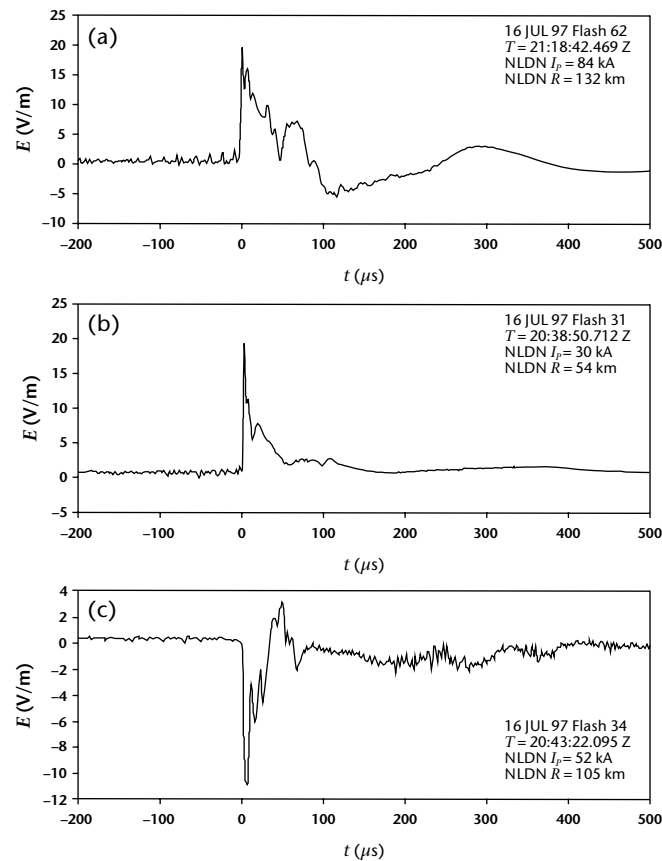


Figure 6.4. Examples of electric field pulse waveforms for (a) the negative first stroke, (b) the negative subsequent stroke, and (c) the positive first stroke. All three events have been detected by NLDN, and their NLDN-reported characteristics (estimated peak current I_p , and distance R) are given on the plots. See also caption of Figure 6.3. (Adapted from Rakov, 1999)

Cloud-to-ground (CG) flash, ground flash. Flash that contains at least one return stroke.

Cloud lightning. Lightning discharges that do not involve ground.

Compact intracloud discharge (CID). A small-spatial-scale (typically hundreds of metres) lightning discharge in the cloud that is thought to be the most intense natural producer of HF-VHF (3–300 MHz) radiation on Earth.

Continuing current. A steady current immediately following some return-stroke current pulses.

Discharge. Often used synonymously with “flash”.

Downward CG lightning. Lightning discharges to ground initiated by descending leaders from the cloud.

Event. Specific part of a flash, typically any isolated signal measured during a flash.

Flash, lightning flash. Complete neutralization process that involves many events (leaders, strokes, K-processes, continuing currents, and the like) within a time interval of typically about 1 s; refers to a cloud flash or a ground flash.

Ground flash density. The number of ground flashes per unit area per unit of time (usually per square kilometre per year).

K-processes. Transient processes occurring in a previously conditioned lightning channel that is not connected (or lost its connection) to ground. They can occur in both ground and cloud flashes.

Leader. Lightning process that creates a conducting path between the cloud charge source region and ground (in the case of downward CG lightning) and distributes charge from the cloud source region along this path.

Lightning or lightning flash. It can be defined as a transient, high-current (typically tens of kiloamperes) electric discharge in air whose length is typically measured in kilometres.

M-components. Transient processes occurring in a grounded lightning channel while it carries continuing current.

Negative lightning. Lightning discharges that effectively lower negative charge from the cloud to ground.

Positive lightning. Lightning discharges that effectively lower positive charge from the cloud to ground.

Return stroke, CG stroke, strike. Lightning process that traverses the previously created leader channel, moving from ground towards the cloud charge source region, and neutralizes the leader charge.

Rocket-triggered lightning. Lightning discharges artificially initiated from natural thunderclouds using the rocket-and-wire technique.

Sferic, or atmospheric. Signal from a lightning stroke that travels over long distances.

Strike, stroke. see "return stroke".

Thunderstorm cell. A unit of convection, typically some kilometres in diameter, characterized by relatively strong updraughts (>10 m/s). The lifetime of an ordinary cell is of the order of 1 h.

Upward CG lightning. Lightning discharges to ground initiated by ascending leaders from grounded objects.

6.3 PRINCIPLES OF LIGHTNING LOCATION

6.3.1 General

For the three most common multistation electromagnetic radio-frequency locating techniques – magnetic direction finding (MDF), time of arrival (TOA) and interferometry – the type of locating information obtained depends on the frequency f (or on the wavelength $\lambda = c/f$, where c is the speed of light) of the radiation detected (Rakov and Uman, 2003). For detected signals whose wavelengths are very short compared to the length of a radiating lightning channel, for example, the VHF range where $f = 30$ to 300 MHz and $\lambda = 10$ to 1 m, the whole lightning channel can, in principle, be imaged in two or three dimensions. For wavelengths that exceed or are a significant fraction of the lightning channel length, for example, the very low-frequency (VLF) range where $f = 3$ to 30 kHz and $\lambda = 100$ to 10 km and the low-frequency (LF) range where $f = 30$ to 300 kHz and $\lambda = 10$ to 1 km, generally only one or a few locations can be usefully obtained for each lightning channel. In the case of a single location for a CG return stroke, it is usually interpreted as some approximation to the ground strike point. The best electromagnetic channel imaging methods at VHF and the best ground-strike-point locating techniques at VLF and LF have accuracies (actually location errors or uncertainties) of the order of 100 m. On the other end of the accuracy scale, long-range VLF systems which operate in a narrow frequency band,

usually somewhere between 5 and 10 kHz, and detect lightning at distances up to thousands of kilometres have uncertainties in locating individual lightning flashes of the order of 10 km or more. These latter systems are often called thunderstorm locators.

For those electromagnetic locating techniques involving the measurement of field change amplitudes at multiple stations, the bandwidth of the measurement is not directly related to the locating accuracy. It is only necessary to have a measurement system that can faithfully reproduce the field changes of the process of interest. Hence, for example, from measuring the electrostatic field change in the frequency range from a fraction of a hertz to a few hertz at multiple stations, one can locate an average position for the charge source of a complete CG flash. And with a system bandwidth from a few hertz to a few kilohertz, so as to be able to resolve electrostatic field changes on a millisecond timescale, one can locate the charge sources for individual strokes in the flash as well as for continuing current. Lightning location using the return-stroke electric or magnetic radiation field peaks, similar to using the electrostatic field change, only requires that the system faithfully reproduces those peaks. The electric and magnetic field amplitude lightning locating techniques are not further discussed here.

Accurate lightning locating systems, whether they image the whole lightning channel or locate only the ground strike points or the cloud-charge centres, necessarily employ multiple sensors. Single station surface-based sensors, such as the lightning flash counters, detect the occurrence of lightning, but cannot be used to locate it on an individual flash basis. Nor are they designed to do so because of the wide range of amplitudes and wave shapes associated with individual events. Nevertheless, with single-station sensors one can assign groups of flashes to rough distance ranges if data are accumulated and averaged for some period of time. There are many relatively simple, commercially available single-station devices that purport to locate lightning. Most operate like AM radios, with the amplitude of the radio static being used to gauge the distance to the individual lightning flashes – a technique inherently characterized by large errors. In addition to field amplitude detectors, some commercial single-station devices employ optical detectors, magnetic direction finders and/or characteristics of lightning waveforms to allow estimates of the distance of CG return strokes from the sensor.

Single-station optical sensors on Earth-orbiting satellites detect the light scattered by the volume of cloud that produces the lightning and hence cannot locate to an accuracy better than about 10 km – about the diameter of a small cloud. Additionally, satellite-based sensors cannot distinguish between cloud and ground discharges. The next-generation series of Geostationary Operational Environmental Satellites (GOES-R) is planned to carry a Geostationary Lightning Mapper, which will monitor lightning continuously over a wide field of view. The launch of the first GOES-R series satellite is scheduled for 2015.

The following subsections discuss how individual sensors measuring various properties of the lightning electromagnetic radiation have been combined into systems to provide practical lightning locating. More details can be found in the reviews by Rakov and Uman (2003) and Cummins and Murphy (2009) and in the references therein.

6.3.2 **Magnetic field direction finding**

Two vertical and orthogonal loops with planes oriented north-south and east-west, each measuring the magnetic field from a given vertical radiator, can be used to obtain the direction to the source. This is because the output voltage of a given loop, by Faraday's law, is proportional to the cosine of the angle between the magnetic field vector and the normal vector to the plane of the loop. For a vertical radiator the magnetic field lines are circles that are coaxial with respect to the source. Hence, for example, the loop whose plane is oriented north-south receives a maximum signal if the source is north or south of the antenna, while the orthogonal east-west loop receives no signal. In general, the ratio of the two signals from the loops is proportional to the tangent of the angle between north and the source as viewed from the antenna.

Crossed-loop magnetic direction finders (DFs) used for lightning detection can be divided into two general types: narrowband (tuned) DFs and gated wideband DFs. In both cases the

direction-finding technique involves an implicit assumption that the radiated electric field is oriented vertically and the associated magnetic field is oriented horizontally and perpendicular to the propagation path.

Narrowband DFs have been used to detect distant lightning since the 1920s. They generally operate in a narrow frequency band with the centre frequency in the range of 5 to 10 kHz, where attenuation in the Earth-ionosphere waveguide is relatively low and where the lightning signal energy is relatively high. Before the development of weather radars in the 1940s, lightning locating systems were the primary means of identifying and mapping thunderstorms at medium and long ranges.

A major disadvantage of narrowband DFs is that for lightning at ranges less than about 200 km, those DFs have inherent azimuthal errors, called polarization errors, of the order of 10° . These errors are caused by the detection of magnetic field components from non-vertical channel sections, whose magnetic field lines form circles in a plane perpendicular to the non-vertical channel section, and also by ionospheric reflections – skywaves – whose magnetic fields are similarly improperly oriented for direction finding of the ground strike point.

To overcome the problem of large polarization errors at short ranges inherent in the operation of narrowband DFs, gated wideband DFs were developed in the early 1970s. Direction finding is accomplished by sampling (gating on) the north-south and east-west components of the initial peak of the return-stroke magnetic field, that peak being radiated from the bottom hundred metres or so of the channel in the first microseconds of the return stroke. Since the bottom of the channel tends to be straight and vertical, the magnetic field is essentially horizontal. Additionally, a gated DF does not record ionospheric reflections since those reflections arrive long after the initial peak magnetic field is sampled. The operating bandwidth of the gated wideband DF is typically from a few kilohertz to about 500 kHz. Interestingly, although an upper-frequency response of many megahertz is needed to assure accurate reproduction of the incoming radiation field peak, particularly if the propagation is over saltwater, practical DFs only need an upper-frequency response of a few hundred kilohertz in order to obtain an azimuthal error of about 1° . This is because the ratio of the peak signals in the two loops is insensitive to the identical distortion produced by the identical associated electronic circuits of the two loops. Similarly, with proper calibration and correction for propagation effects, practical DFs only need an upper-frequency response of a few hundred kilohertz in order to obtain a peak current estimation error of 15%–20%. Thus, the gated wideband DF can operate at frequencies below the AM radio band and below the frequencies of some aircraft navigational transmitters, either of which could otherwise cause unwanted directional noise.

Gated wideband DFs, as well as narrowband DFs, are susceptible to site errors. Site errors are a systematic function of direction but generally are time-invariant. These errors are caused by the presence of unwanted magnetic fields due to non-flat terrain and nearby conducting objects, such as underground and overhead power lines and structures, being excited to radiate by the incoming lightning fields. In order to eliminate site errors completely, the area surrounding a DF must be flat and uniform, and without significant conducting objects, including buried ones, nearby. These requirements are usually difficult to satisfy, so it is often easier to measure the DF site errors and to compensate for any that are found rather than to find a location characterized by tolerably small site errors. Once corrections are made, the residual errors have been reported (using independent optical data) to be usually less than 2° to 3° .

Since it is not known a priori whether a stroke to ground lowers positive or negative charge, there is a 180° ambiguity in stroke azimuth from the measurement of only the orthogonal magnetic fields. That ambiguity is resolved in all wideband DF systems by the measurement of the associated electric field whose polarity indicates the sign of the charge transferred to ground.

6.3.3 Time-of-arrival technique

A single time-of-arrival sensor provides the time at which some portion of the lightning electromagnetic field signal arrives at the sensing antenna. Time-of-arrival systems for locating lightning can be divided into three general types: (a) very short baseline (tens to hundreds of

metres), (b) short baseline (tens of kilometres), and (c) long baseline (hundreds to thousands of kilometres). Very short- and short-baseline systems generally operate at VHF, that is, at frequencies from 30 to about 300 MHz, while long-baseline systems generally operate at VLF and LF, 3 to 300 kHz. It is generally thought that VHF radiation is associated with air breakdown processes, while VLF signals are due to current flow in conducting lightning channels. Short-baseline systems are usually intended to provide images of lightning channels and to study the spatial and temporal development of discharges. Long-baseline systems are usually used to identify the ground strike point, cloud lightning events in predominantly vertical channels, or the average location of the flash.

A very short-baseline (tens to hundreds of metres) system is composed of two or more VHF time-of-arrival receivers whose spacing is such that the time difference between the arrival of an individual VHF pulse from lightning at those receivers is short compared to the time between pulses, which is some microseconds to hundreds of microseconds. The locus of all source points capable of producing a given time difference between two receivers is, in general, a hyperboloid, but if the receivers are very closely spaced, the hyperboloid degenerates, in the limit, into a plane on which the source is found. Two time differences from three very closely spaced receivers yield two planes whose intersection gives the direction to the source, that is, its azimuth and elevation. To find source location, as opposed to determining the direction to the source, two or more sets of three closely spaced receivers, the sets being separated by tens of kilometres or more, must be used. Each set of receivers is basically a TOA direction finder, and the intersection of two or more direction vectors yields the location.

Short-baseline TOA systems are typically networks of 5 to 15 stations that make use of time-of-arrival information for three-dimensional (3D) mapping of lightning channels. A portable version of such system has been developed by researchers at the New Mexico Institute of Mining and Technology. This system is presently referred to as the Lightning Mapping Array (LMA) and has recently become a major tool for both lightning research and operational applications. The short-baseline VHF TOA systems provide electromagnetic images of the developing channels of any type of lightning flash.

The first long-baseline (hundreds to thousands of kilometres) TOA systems operated at VLF/LF. For example, one of them employed a pair of receiving stations in Massachusetts with a bandwidth of 4 to 45 kHz and separated by over 100 km (the overall network was composed of four stations) to compare differences in the times of arrival of the signals at each station and hence determine directions to the causative lightning discharge in western Europe. The two-station system was basically a direction finder similar to the very short-baseline systems described above, but operating at lower frequencies and with a longer baseline. The resultant directions compared favourably with the locations reported by the UK Met Office's narrowband DF network which was operational at that time. Spherical geometry was used to account for propagation over the Earth's surface in finding the locus of points for a constant measured arrival time difference between receivers.

Another long-baseline TOA system, called the Lightning Position and Tracking System (LPATS), was developed in the 1980s. The LPATS, operating at LF/VLF, used electric field whip antennas at stations 200 to 400 km apart to determine locations via the measured differences between signal arrival times at the stations. In the frequency band used, return-stroke waveforms were generally the largest and hence most easily identified. In principle, responses from four stations (three time differences) are needed to produce a unique location since the hyperbolae on the Earth's surface from only two time differences can, in general, intersect at two different points. For CG lightning near or within the network, there is often only one solution, in which case the three-station approach suffices.

6.3.4 Interferometry

In addition to radiating isolated pulses, lightning also produces noise-like bursts of electromagnetic radiation lasting tens to hundreds of microseconds. These bursts are hard to locate using TOA techniques due to the difficulty in identifying the individual pulses. In the case of interferometry, no identification of individual pulses is needed, since the interferometer

measures phase difference between narrowband signals corresponding to these noise-like bursts received by two or more closely spaced sensors. The simplest lightning interferometer consists of two antennas some metres apart, each antenna being connected via a narrowband filter to a receiver. The antennas, filters and receivers are identical. The outputs of the two receivers are sent to a phase detector that produces a voltage that is proportional to the difference in phase between the two quasi-sinusoidal signals. The phase difference defines, as does the time difference in very short-baseline TOA systems, a plane on which the source is located, that is, one direction angle to the VHF source. To find the azimuth and elevation of a source, three receiving antennas with two orthogonal baselines are needed at minimum. To locate the source in three dimensions, two or more synchronized interferometers are needed, each effectively acting as a direction finder and separated by a distance of the order of 10 km or more. The principles of interferometric lightning location are described in detail by Lojou et al. (2008).

Most interferometric systems operate over very narrow frequency bands (a few hundred kilohertz to a few megahertz in the VHF/UHF bands), since this allows the system to have high sensitivity in a specific “quiet” band of operation. However, it also makes the system performance subject to local broadband interference, it may not provide the highest possible signal-to-noise ratio and it places a specific limitation in the spacing of the antenna array elements to avoid arrival-time (phase) ambiguity. There is a recent trend towards using broadband interferometry (Shao et al., 1996; Mardiana and Kawasaki, 2000; Morimoto et al., 2004). This trend is made possible by the advent of affordable broadband radio frequency and digital signal processing electronics.

6.4 PERFORMANCE CHARACTERISTICS

Generally, a modern VLF-medium frequency (MF) lightning locating system is expected to record (in separate categories) and locate over a certain area all CG strokes of either polarity, as well as cloud discharges. Also expected for each discharge is a measure of its intensity, usually in the form of peak current inferred from measured electric or magnetic fields. Accordingly, the system’s performance can be evaluated using the following characteristics:

- (a) CG flash detection efficiency;
- (b) CG stroke detection efficiency;
- (c) Cloud flash detection efficiency;
- (d) Percentage of misclassified events (particularly cloud discharges assigned to the positive or negative CG stroke category);
- (e) Location accuracy (or location error);
- (f) Peak current estimation error.

In general, the detection efficiency is the fraction (usually expressed in per cent) of the total events occurred that are detected by the system and is ideally equal to 100%. While the CG stroke detection efficiency can be readily defined (since these strokes involve a unique and observable feature – the luminous channel to ground – and the total number of occurred events can be determined), the cloud flash detection efficiency concept is rather uncertain. Indeed, there are many cloud discharge processes (some of them poorly understood) occurring on different spatial scales and timescales and apparently exhibiting no unique and readily observable features. As a result, the total number of occurred events is generally unknown. In practice, if all cloud discharge events are accepted as counts, the number of detected cloud discharges may be largely determined by the local noise level and the system’s signal transmission rate limit.

In defining the CG flash detection efficiency, which is probably the most important performance characteristic for lightning locating systems used for determining ground flash density, a flash is

considered to be detected if at least one stroke of the flash is detected. A similar approach could be applied to cloud flashes, although one would need to decide if a single count constitutes a flash and how to assign multiple counts to individual flashes.

The location error is the distance between the actual location and that reported by the system. In general, the location error consists of random and systematic components. The latter in some cases can be accounted for (for example, site errors in MDF systems).

The peak current estimation error is the difference between the actual peak current value and that reported by the system, and is usually expressed in per cent of the actual peak current. Peak currents are estimated by lightning locating systems using either an empirical or model-based field-to-current conversion equation. There are reasonable field-to-current conversion equations for CG strokes, but not for cloud discharge processes.

In order to evaluate the performance characteristics listed above, independent (ground-truth) data are needed. For example, discharges occurring at a precisely known location equipped with a current-measuring device (tall tower or lightning-triggering facility) can be used for estimating the location accuracy and peak current estimation error. Detection efficiencies and percentage of misclassified events are usually estimated based on time-resolved optical recordings. Sometimes lightning-related damage to various objects (buildings, trees, and the like) is used in estimating location errors, although identification of the causative lightning event in this approach is uncertain due to insufficient accuracy of timing information (usually not known within better than a minute). Less definitive evaluations of lightning locating systems' performance characteristics are possible via modelling or comparison with a more accurate system operating in the same area. As of today, only a limited number of ground-truth studies have been performed, particularly for first strokes in negative CG flashes, positive CG flashes and cloud discharges.

In some applications (for example, tracking of thunderstorm cells), the tracking ability may be more important than detection of individual lightning discharges. Performance of the systems intended primarily for such applications is often tested against radar or infrared satellite imagery, with a good correspondence between detected lightning and regions of high radar reflectivity or low cloud-top temperatures being viewed as the system's output validity criteria. For early warning, the ability to detect the first lightning is probably the most important performance characteristic.

It is not clear how to define the performance characteristics for VHF lightning channel imaging systems. Surely, they cannot locate all the VHF sources in the cloud. Limitations in sensitivity prevent these systems from regularly detecting and mapping positive leaders. Thus, the resultant VHF images are necessarily partial. Further, supplementary information about return strokes is usually needed to reliably distinguish between cloud and CG flashes, because the VHF radiation directly associated with subsequent return strokes is limited and difficult to detect. Also, no peak current estimates are possible. Nevertheless, VHF lightning channel imaging systems represent a very valuable tool for studying detailed lightning morphology and evolution, particularly inside the cloud, and are often used in testing other types of lightning locating systems.

6.5 EXAMPLES OF MODERN LIGHTNING LOCATING SYSTEMS

One VHF lightning channel imaging system (LMA), three VLF/LF (NLDN, LINET and the United States Precision Lightning Network (USPLN)), one ELF/VLF/LF/MF/HF (ENTLN), and three VLF (the World Wide Lightning Location Network (WWLLN), GLD360 and ATDnet) systems are briefly reviewed here as representative examples of modern lightning locating systems. The systems have been chosen because they are good examples of each type of system, but their inclusion should not be taken to imply that they are better than others or are recommended over the use of other systems not discussed here. Information about these and other systems can be found in Rakov and Uman (2003), Cummins and Murphy (2009), Betz et al. (2009) and references therein. There are more than 60 lightning locating networks worldwide that operate in the VLF/LF range.

Besides a general characterization of each system, the available information on its performance characteristics is given with emphasis on those based on formal ground-truth studies published in the peer-reviewed literature. Generally, the amount of such information for older systems is greater than for more recent ones.

6.5.1 **Lightning Mapping Array, 60–66 MHz**

LMA networks typically consist of 10–15 stations separated by 15–20 km and connected by wireless communication links to a central location (Thomas et al., 2004). Each station receives the lightning signals (from both cloud and CG flashes) in a locally unused television channel (usually TV channel 3, 60–66 MHz). A typical time resolution (the measurement time window) is 80–100 μs . A larger time window, typically 400 μs , is used for real-time processing and display.

The location accuracy of the New Mexico LMA has been investigated experimentally using a sounding balloon carrying a VHF transmitter, airplane tracks, and observations of distant storms (Thomas et al., 2004). Simple geometric models for estimating the location uncertainty of sources both over and outside the network have also been developed. The model results were found to be a good estimator of the observed errors. Sources over the network at altitudes ranging from 6 to 12 km were located with an uncertainty of 6–12 m rms in the horizontal and 20–30 m rms in the vertical, resulting in less than a 100-metre 3D error for most located sources. Outside the network the location uncertainties increase with distance.

6.5.2 **United States National Lightning Detection Network, 400 Hz–400 kHz**

The NLDN consists of more than 100 stations separated typically by 300–350 km and covering the contiguous United States (see Cummins and Murphy, 2009). A combination of TOA and MDF locating techniques is employed. Both cloud and CG lightning discharges are reported. Classification is accomplished by applying field waveform criteria. Peak currents are estimated from measured fields using an empirical formula based on rocket-triggered lightning data, with the field peaks being adjusted to account for propagation effects (stronger than the inverse proportionality distance dependence). Further information on the evolution of the NLDN, its enabling methodology and applications of NLDN data can be found in Rakov and Uman (2003, Chapter 17), Orville (2008), Cummins and Murphy (2009) and references therein.

CG stroke and flash detection efficiencies have been investigated, using video cameras, in southern Arizona, Oklahoma and Texas (Biagi et al., 2007). The stroke detection efficiency in southern Arizona was estimated to be 76% ($N = 3\,620$), and in Texas/Oklahoma it was 85% ($N = 885$). The corresponding flash detection efficiencies were 93% ($N = 1\,097$) and 92% ($N = 367$). Additionally, classification of lightning events as cloud or CG discharges was examined in this study, as well as in a similar study (but additionally using independent electric field waveform measurements) in the Colorado/Kansas/Nebraska region (Fleener et al., 2009).

CG stroke and flash detection efficiencies have been also investigated, using rocket-triggered lightning as the ground truth, in the Florida region (Jerauld et al., 2005; Nag et al., 2011). From the latest study (2004–2009), the CG stroke and flash detection efficiencies were found to be 76% ($N = 139$) and 92% ($N = 37$), respectively. Strokes in rocket-triggered flashes are similar to regular subsequent strokes (following previously formed channels) in natural lightning, and hence the 76% stroke detection efficiency is applicable only to regular negative subsequent strokes in natural lightning. The flash detection efficiency derived using rocket-triggered lightning is expected to be an underestimate of the true value for natural negative lightning flashes, since first strokes typically have larger peak currents than subsequent ones.

Nag and Rakov (2012) examined electric field waveforms produced by 45 positive flashes containing 53 strokes. Out of these 53 strokes, the NLDN located 51 (96%), of which 48 (91%) were correctly identified and 3 return strokes were misclassified as cloud discharges.

According to Cummins and Murphy (2009), the NLDN cloud flash detection efficiency (a flash was considered detected if at least one VLF/LF pulse produced by that flash was detected) is in

the range of 10% to 20%, depending on local differences in distances between stations. Nag et al. (2010) examined wideband electric fields, electric and magnetic field derivatives, and narrowband VHF (36 MHz) radiation bursts produced by 157 CIDs. The NLDN located 150 (96%) of those CIDs, and correctly identified 149 (95%) of them as cloud discharges.

Nag et al. (2011) estimated, from comparison of NLDN-reported locations with the precisely known locations of the rocket launchers which were taken as the accurate ground strike points, the median absolute location error to be 308 m, with the largest error being 4.2 km ($N = 105$). Peak current estimation errors have been estimated from comparison of NLDN-reported peak currents with directly measured currents at the triggered-lightning channel base. The median absolute value of current estimation error was 13% ($N = 96$). The current estimation errors never exceeded 129% in absolute value (60% if two outliers are excluded). These results are applicable only to regular negative subsequent strokes in natural lightning.

6.5.3 **Lightning Detection Network, 1–200 kHz**

The basic location method used in the Lightning Detection Network (LINET) is TOA, although the magnetic field sensors provide arrival-angle information that is employed as a plausibility check on computed locations. Height information derived from the arrival time at the nearest reporting sensor is employed to assist in classification of processes in cloud flashes and of in-cloud processes (for example, preliminary breakdown) in CG flashes on the one hand and CG strokes on the other (near-ground locations are assumed to be associated with CG strokes and elevated ones with all the other processes). It is stated that the reliable separation of return strokes and cloud pulses can be achieved as long as the closest sensor is within 100 km of the lightning discharge, which requires baselines of 200–250 km or less. Emphasis is placed on detection of low-amplitude signals of both cloud and CG lightning. Peak currents for processes in cloud flashes and for in-cloud processes (for example, preliminary breakdown) in CG flashes and CG strokes are estimated assuming direct proportionality between the peak current and peak magnetic (or electric) field and inverse distance dependence of field peak. More information about LINET can be found in Betz et al. (2009) and references therein.

Like for VHF channel imaging systems, it is not clear how to define the detection efficiency for LINET, which in a sense also maps the evolution of lightning channels, although with a considerably smaller number of located sources per flash. Additionally, in-cloud processes (for example, preliminary breakdown) in CG flashes are assigned to the cloud lightning category, which is apparently inconsistent with the traditional definitions of cloud flash as a lightning discharge without CG strokes and of CG flash as a lightning discharge that consists of both in-cloud processes and CG strokes. This is probably immaterial for a number of applications, such as cell tracking and detection of severe weather.

The random location error is claimed to be approximately 150 m, but the existence of systematic errors is acknowledged. Betz et al. (2009) showed an example of 58 located strokes apparently terminated on an instrumented tower with an average location error of less than ~100 m, after compensating systematic errors that caused a location bias of ~200 m.

Peak current estimation errors for LINET are unknown (no comparison with ground-truth data has been performed to date).

6.5.4 **United State Precision Lightning Network, 1.5–400 kHz**

The USPLN employs the VLF/LF TOA technique and consists of 100 electric field sensors covering the continental United States and other parts of North America. No formal performance testing studies regarding this system have been reported, but the operators of the system claim, apparently from the network simulation analysis, 95% stroke detection efficiency and 250-metre typical location error throughout most of North America (>80% detection efficiency and <1 km location error in key deployment areas elsewhere in the world). Differentiation between

cloud and CG processes is apparently accomplished by examining the frequency content and amplitude of the received signals. The field-to-current conversion procedure has not been formally described, nor is any information available about testing its validity.

6.5.5 **Earth Networks Total Lightning Network, 1 Hz–12 MHz**

The Earth Networks Total Lightning Network (ENTLN) sensors operate in a frequency range from 1 Hz to 12 MHz (spanning the ELF, VLF, LF, MF and HF ranges). The TOA method has been employed by this network of more than 700 sensors since 2013. Both cloud and CG lightning discharges are reported.

According to Heckman and Liu (2010), the whole electric field waveforms are transmitted from the sensor to the data-processing unit and used in both locating the lightning events and differentiating between cloud and CG processes. Strokes (or individual cloud events) are clustered into a flash if they are within 700 ms and 10 km of the first detected stroke (or cloud event). A flash that contains at least one return stroke is classified as a CG flash, otherwise it is classified as a cloud flash. In cell tracking and thunderstorm alert generation, only flashes (which are less likely than strokes to be missed by the system) are used.

No formal performance testing studies regarding this system have been reported in the peer-reviewed literature, but the operators of the system claim that performance testing studies conclude that ENTLN achieves 40%–50% cloud flash detection efficiency across much of the United States and up to 95% in the United States Midwest and East (Heckman and Liu, 2010). Maximizing the detection efficiency for cloud flashes appears to be the primary focus of this system. By extending the frequency range of detection into the MF and HF spectra, the ENTLN aims to detect and report weaker pulses at longer distances than other VLF/LF systems with similar baselines.

The field-to-current conversion procedure has not been formally described to date, nor is any information yet available about testing its validity.

6.5.6 **World Wide Lightning Location Network, 6–18 kHz**

The WWLLN utilizes a time-of-group-arrival (TOGA) method to locate lightning strikes. This method is based on the fact that lightning VLF signals (sferics) propagating in the Earth-ionosphere waveguide experience dispersion, in that the higher-frequency components arrive earlier than the lower-frequency components. The TOGA, a quantity that can be derived from the measured sferic waveform, is related to the distance travelled by the sferic. As of March 2012, the WWLLN employed 57 sensors located on all continents, although, according to Dowden et al. (2002), global coverage could be in principle provided by as few as 10 sensors. Distances between the sensors are of the order of thousands of kilometres. Presently, only those lightning events that triggered at least five sensors and that had residuals (uncertainties in the stroke timing) less than or equal to 30 μ s are regarded as located with acceptable accuracy.

In the latest study of WWLLN performance characteristics, Abarca et al. (2010) used NLDN data as the ground truth and found that the CG flash detection efficiency increased from about 3.9% in 2006–2007 to 10.3% in 2008–2009, as the number of sensors increased from 28 in 2006 to 38 in 2009. For events with NLDN-reported peak currents of 130 kA or higher, the detection efficiency was 35%. The average location error was estimated to be 4–5 km.

Interaction of lightning signals with the ionosphere spectrally distorts the received waveform, so that it is not straightforward to infer the peak current and even polarity of lightning. Nevertheless, Hutchins et al. (2012) developed a method to convert the stroke radiated power in the 6–18 kHz band to peak current. Errors involved in such conversion are presently unknown.

6.5.7 **Global Lightning Dataset, VLF**

The Global Lightning Dataset (GLD360), also referred to as the Global Lightning Detection Network, employs an unspecified number of VLF sensors strategically placed around the world. Locations are obtained using both TOA and MDF methods in conjunction with a lightning waveform recognition algorithm. The latter relies on a bank of canonical waveforms corresponding to propagation distances of the order of thousands of kilometres (Said et al., 2010).

According to the network operators, the expected CG flash detection efficiency is 60%–70% and the median location error is 5 to 10 km. Demetriades et al. (2010) evaluated the GLD360 performance characteristics using NLDN data as the ground truth and found that the CG flash detection efficiency was 86% to 92%, and the median location error was 10.8 km. From a similar study, but using the Brazilian lightning detection network, Naccarato et al. (2010) reported a CG flash detection efficiency of 16% and a mean location error of 12.5 km. Using synchronized electric field and high-speed video camera measurements of CG lightning in Belgium as ground truth, Poelman et al. (2013) found the CG flash and stroke detection efficiencies for the GLD360 to be 96% and 70%, respectively, with a median location error of 900 m. Using NLDN data as ground truth, Said et al. (2013) reported a CG flash detection efficiency of 57% and a median location accuracy of 2.5 km.

The GLD360 also reports the peak current and polarity. Relative to the NLDN, Said et al. (2013) found the arithmetic and geometric mean peak current magnitude error for the GLD360 to be 21% and 6%, respectively. GLD360 reported the same polarity for 96% of the matched strokes as the NLDN.

6.5.8 **Arrival Time Difference network**

The Arrival Time Difference network (ATDnet) long-range lightning location system (LLS) is the latest version of the UK Met Office VLF LLS that has been in place since 1987. The network currently consists of 10 sensors across Europe that contribute to the main network, with additional sensors within Europe and beyond for development and testing. The network is designed for lightning location in Europe, but is capable of regularly detecting lightning in Africa and South America. The sensors, referred to as outstations, detect VLF (sferic) signal waveforms and transmit waveform data to a central processor at the UK Met Office, where a waveform correlation technique is used to determine the arrival time differences of the waveforms across the network. These arrival time difference data are used to locate lightning.

Poelman et al. (2013) found the random location error of ATDnet to be on the order of 1 km, with a CG flash detection efficiency of 88%. The actual median location uncertainty of CG flashes across Europe is likely to be on the order of 2 to 5 km, although this requires verification in peer-reviewed literature. ATDnet does not currently provide information on stroke polarity, type (CG/IC) or power/peak current.

6.6 **UTILIZATION OF LIGHTNING LOCATION SYSTEMS BY METEOROLOGICAL SERVICES**

Lightning data have utility in different areas of importance to public and private meteorological service organizations. Typically, national meteorological agencies use LLS data to help accomplish their national duties to protect life and property, and commercial entities use lightning data to provide improved severe weather warnings, forecasts and guidance to clients for specialized applications including aviation, agriculture, energy and mass media.

6.6.1 Storm recognition and alarms for severe weather

One of the important duties of the meteorological services is to provide reliable warnings for severe weather conditions. As a rule, the best severe weather forecast skill and lowest false-alarm rates are achieved when several data sources are exploited, but since thunderstorms are typically accompanied by an increase of IC, LLS data alone can usually serve as a very clear indicator of the strength and extent of storm cells. This points to the importance of total lightning networks, such as those that detect in the LF/MF/HF ranges, since CG detection alone will not suffice for this application.

Although an alarm can be issued as soon as a stroke occurs in the vicinity of an instrumented area, a more reliable procedure involves the definition of a storm cell and tracking it as it moves inside or towards an area of interest. Some LLS allow for short-term extrapolation (nowcasting) of cell displacements on the order of 1 h or so. Monitoring the total flash rates and the rate changes makes it possible to identify lightning cells with the potential to produce severe weather. When a cell is identified and the total lightning rate exceeds a given threshold, an alert can be generated.

Except for certain storms generated along frontal boundaries, forecasting over longer durations with acceptable skill requires the use of NWP models. Finally, it may be pointed out that lightning, in combination with cell tracking, not only indicates the initiation of heavy thunderstorm activity but also signals the end of a threat in a given area.

Although storm reports from spotters on the ground or in the air are an invaluable source of information during severe weather, information derived from remote-sensing techniques (including lightning detection) is becoming more important all the time. One can now use radar reflectivity, cloud images, passive microwave brightness temperatures and lightning data (alone or in combination) to identify thunderstorm activity with high accuracy and reliability even in remote regions. Of all these techniques, global and/or local networks of LLS systems and stand-alone detectors on the ground or in aircraft are clearly the most definitive when it comes to identifying significant thunderstorm activity for the reasons discussed above. While the simple detection of a thunderstorm is feasible with any LLS, more complete measurements require advanced systems and techniques that are capable of providing early detection and identification of thunderstorm activity while at the same time reducing false alarms to an acceptable level.

6.6.2 Nowcasting, forecasting and derived products

Nowcasting is a widely used technique for very short-range weather forecasting. A nowcast starts with information about the current (weather) state of the atmosphere as expressed by one or more observed parameters, and then uses an estimate of their movement to predict their location and extent a short time in the future. Nowcast accuracy depends on the validity of the assumption that the weather associated with the observed parameter(s) will persist during that period without significant change. Of course, certain lightning parameters are indicative of the phase of a storm's life cycle and this may also be exploited for nowcasting. The above assumption is reasonable for short (~1 h) periods, but its validity diminishes with time. As a consequence, extrapolations over periods longer than about 1 h require the use of data assimilation and NWP techniques.

Qualitative evaluations of LLS data commonly involve the display of lightning data on maps (with or without other information) in real or near-real time. These products can be used for many purposes, such as localizing or limiting an area likely to be effected by a storm and aiding in the decision to issue an alarm. Beyond qualitative evaluation, high-quality LLS data are highly amenable to quantitative treatment including statistical evaluations of stroke rates to estimate storm intensity, which can greatly enhance their utility.

A number of projects are under way that are aimed at developing automated procedures for thunderstorm cell tracking and the evaluation of lightning parameters in these areas.

Refined interpretations, analysis and animations of results from cell tracking should greatly enhance the nowcasting potential of LLS data. The combination of cell tracking involving both lightning and radar represents another type of potentially useful derived product.

Finally, lightning data, as well as other observations such as radar reflectivity, can be used to generate model output statistics for objective forecasting (Glahn and Lowry, 1972; Knüpfper, 1996) that are appropriate for use in probabilistic post-processing techniques like those described for the hourly Rapid Refresh NWP model developed by the NOAA Earth System Research Laboratory (Weygandt et al., 2008).

6.6.3 **Lightning and climate**

Recent climate studies have noted the connection between lightning and climate change (Williams, 2005; Price, 2006, 2009). As surface and lower tropospheric temperatures rise, lightning rates are predicted to increase in the range of 10%–100% for every one degree of surface warming, depending on the model and assumptions used. There is also a clear relationship between temperature, water vapour and lightning activity; thunderstorms carry large amounts of water vapour into the upper troposphere and lower stratosphere, and this in turn influences the greenhouse effect on the Earth's climate. Further, lightning discharges produce nitrogen oxides that influence the production of the greenhouse gas ozone. It must be recognized, however, that even though the underlying mechanisms linking global climate change to lightning are well understood, different processes may dominate in unanticipated ways. For example, climate simulations by Grewe (2008) suggest that global warming can actually lead to the worldwide occurrence of fewer but more intense convective events. As such, lightning decreases in total flash frequency, but individual storms are predicted to produce more lightning.

In any case, lightning activity is one of the factors that should be taken into account in any detailed climate model or predictions of climate change. Consequently, it is important to monitor lightning activity at different scales over large areas and establish or extend the database of lightning events over long time periods. Relationships are also studied on short timescales, ranging from daily and diurnal variations, five-day waves, intra-seasonal, semi-annual and annual to longer periods. To achieve this goal, local high-precision LLS should be expanded, global LLS must be completed and standards for lightning detection must be introduced and implemented.

6.6.4 **Verification of lightning-induced ground damage**

An early motivation for the development of LLS was to have an objective way to verify the cause of lightning-induced damage in legal disputes, and most insurance companies use lightning data to verify or reject lightning damage claims. To be useful in this regard, LLS must exhibit both excellent detection efficiency and location accuracy at all thresholds. Location accuracy should be better than ~1 km so that a reliable correlation between lightning and damage can be demonstrated, and relatively weak strokes must be detected because even a 5 kA stroke can produce significant damage or over-voltage. Even higher location accuracy is needed for the power industry to determine if the interruption of a high-voltage transmission line could have been caused by a lightning stroke. Since heavy storms can produce high stroke rates and lightning flashes may be composed of many strokes with differing strike points, an accuracy of 100–200 m is desired for the establishment of a reliable spatial correlation. Of course, this requirement is relaxed when precise event timing of both the power failure and the strokes are available, and tools for automatic recognition of these incidents are now available commercially.

REFERENCES AND FURTHER READING

- Abarca, S.F., K.L. Corbosiero and T.J. Galarneau Jr., 2010: An evaluation of the Worldwide Lightning Location Network (WWLLN) using the National Lightning Detection Network (NLDN) as ground truth. *Journal of Geophysical Research: Atmospheres*, 115(D18).
- Betz, H.D., K. Schmidt and W.P. Oettinger, 2009: LINET – An international VLF/LF lightning detection network in Europe. In: *Lightning: Principles, Instruments and Applications* (H.D. Betz, U. Schumann and P. Laroche, eds.). Dordrecht, NL, Springer-Verlag.
- Biagi, C.J., K.L. Cummins, K.E. Kehoe and E.P. Krider, 2007: National Lightning Detection Network (NLDN) performance in southern Arizona, Texas and Oklahoma in 2003–2004. *Journal of Geophysical Research: Atmospheres*, 112(D5).
- Cummins, K.L. and M.J. Murphy, 2009: An overview of lightning locating systems: History, techniques, and data uses, with an in-depth look at the U.S. NLDN. *IEEE Transactions on Electromagnetic Compatibility*, 51(3):499–518.
- Demetriades, N.W.S., M.J. Murphy and J.A. Cramer, 2010: Validation of Vaisala's Global Lightning Dataset (GLD360) over the continental United States. *Preprints*, Twenty-ninth Conference on Hurricanes and Tropical Meteorology (10–14 May 2010), Tucson, AZ.
- Dowden, R.L., J.B. Brundell and C.J. Rodger, 2002: VLF lightning location by time of group arrival (TOGA) at multiple sites. *Journal of Atmospheric and Solar-Terrestrial Physics*, 64(7):817–830.
- Dwyer, J.R., 2005: A bolt out of the blue. *Scientific American*, 292(5):64–71.
- Fleenor, S.A., C.J. Biagi, K.L. Cummins, E.P. Krider and X.-M. Shao, 2009: Characteristics of cloud-to-ground lightning in warm-season thunderstorms in the Central Great Plains. *Atmospheric Research*, 91:333–352.
- Glahn, H.R., and D.A. Lowry, 1972: The use of model output statistics (MOS) in objective weather forecasting. *Journal of Applied Meteorology*, 11:1203–1211.
- Grewe, V., 2008: Impact of lightning on air chemistry and climate. In: *Lightning: Principles, Instruments and Applications* (H.D. Betz, U. Schumann and P. Laroche, eds.). Dordrecht, NL, Springer-Verlag.
- Heckman, S. and C. Liu, 2010: The application of total lightning detection and cell tracking for severe weather prediction. In: *Proceedings of the International Conference on Grounding and Earthing (GROUND'2010) and Fourth International Conference on Lightning Physics and Effects (LPE)* (November 2010), Salvador, Brazil.
- Hendry, J., 1993: Panning for lightning (including comments on the photos by M.A. Uman). *Weatherwise*, 45(6):19.
- Hutchins, M.L., R.H. Holzworth, C.J. Rodger and J.B. Brundell, 2012: Far-field power of lightning strokes as measured by the World Wide Lightning Location Network. *Journal of Atmospheric and Oceanic Technology*, 29:1102–1110.
- Jerauld, J., V.A. Rakov, M.A. Uman, K.J. Rambo, D.M. Jordan, K.L. Cummins and J.A. Cramer, 2005: An evaluation of the performance characteristics of the U.S. National Lightning Detection Network in Florida using rocket-triggered lightning. *Journal of Geophysical Research: Atmospheres*, 110(D19).
- Knüpfper, K., 1996: Methodical and predictability aspects of MOS systems. *Preprints of the Thirteenth Conference on Probability and Statistics in the Atmospheric Sciences* (21–23 February 1996), San Francisco, CA. American Meteorological Society, 190–197.
- Le Vine, D.M., 1980: Sources of the strongest RF radiation from lightning, *Journal of Geophysical Research: Oceans*, 85(C7):4091–4095.
- Lojou, J.-Y., M.J. Murphy, R.L. Holle and N.W.S. Demetriades, 2008: Nowcasting of thunderstorms using VHF measurements. In: *Lightning: Principles, Instruments and Applications* (H.D. Betz, U. Schumann and P. Laroche, eds.). Dordrecht, NL, Springer-Verlag.
- Mardiana, R. and Z-I. Kawasaki, 2000: Broadband radio interferometer utilizing a sequential triggering technique for locating fast-moving electromagnetic sources emitted from lightning. *IEEE Transactions on Instrumentation and Measurement*, 49(2):376–381.
- Morimoto, T., A. Hirata, Z. Kawasaki, T. Ushio, A. Matsumoto and J.H. Lee, 2004: An operational VHF broadband digital interferometer for lightning monitoring, *IEEJ Transactions on Fundamentals and Materials*, 124(12):1232–1238.
- Naccarato, K.P., O. Pinto Jr., S.A.M. Garcia, M. Murphy, N. Demetriades and J. Cramer, 2010: *Validation of the new GLD360 dataset in Brazil: First results*. Twenty-first International Lightning Detection Conference (19–22 July 2010), Orlando, Florida.

- Nag, A., S. Mallick, V.A. Rakov, J.S. Howard, C.J. Biagi, J.D. Hill, M.A. Uman, D.M. Jordan, K.J. Rambo, J.E. Jerauld, B.A. DeCarlo, K.L. Cummins and J.A. Cramer, 2011: Evaluation of U.S. National Lightning Detection Network performance characteristics using rocket-triggered lightning data acquired in 2004–2009. *Journal of Geophysical Research: Atmospheres*, 116(D2).
- Nag, A. and V.A. Rakov, 2012: Positive lightning: An overview, new observations, and inferences. *Journal of Geophysical Research: Atmospheres*, 117(D8).
- Nag, A., V.A. Rakov, D. Tsalikis and J.A. Cramer, 2010: On phenomenology of compact intracloud lightning discharges. *Journal of Geophysical Research: Atmospheres*, 115(D14).
- Orville, R.E., 2008: Development of the National Lightning Detection Network, *Bulletin of the American Meteorological Society*, 89(2):180–190.
- Poelman, D.R., W. Schulz and C. Vergeiner, 2013: Performance characteristics of distinct lightning detection networks covering Belgium. *Journal of Atmospheric and Oceanic Technology*, 30(5):942–951.
- Price, C., 2006: Global thunderstorm activity. In: *Sprites, Elves and Intense Lightning Discharges* (M. Fullekrug, E. Mareev and M. Rycroft, eds.). Springer, Amsterdam, 85–99.
- Price, C., 2009: Will a drier climate result in more lightning? *Atmospheric Research*, 91(2):479–484.
- Rakov, V.A., 1999: Lightning electric and magnetic fields. In: *Proceedings of the Thirteenth International Zurich Symposium on Electromagnetic Compatibility* (16–18 February 1999), Zurich, Switzerland.
- Rakov, V.A. and M.A. Uman, 2003: *Lightning: Physics and Effects*, Cambridge University Press.
- Said, R.K., M.B. Cohen and U.S. Inan, 2013: Highly intense lightning over the oceans: Estimated peak currents from global GLD360 observations. *Journal of Geophysical Research: Atmospheres*, 118(13) (available from <http://onlinelibrary.wiley.com/doi/10.1002/jgrd.50508/pdf>).
- Said, R.K., U.S. Inan and K.L. Cummins, 2010: Long-range lightning geolocation using a VLF radio atmospheric waveform bank. *Journal of Geophysical Research: Atmospheres*, 115(D23).
- Shao, X.M., D.N. Holden and P.R. Krehbiel, 1996: Broadband radio interferometry for lightning observation. *Geophysical Research Letters*, 23:1917–1920.
- Smith, D.A., X.M. Shao, D.N. Holden, C.T. Rhodes, M. Brook, P.R. Krehbiel, M. Stanley, W. Rison and R.J. Thomas, 1999: A distinct class of isolated intracloud discharges and their associated radio emissions. *Journal of Geophysical Research: Atmospheres*, 104(D4): 4189–4212.
- Thomas, R.J., P.R. Krehbiel, W. Rison, S.J. Hunyady, W.P. Winn, T. Hamlin and J. Harlin, 2004: Accuracy of the Lightning Mapping Array. *Journal of Geophysical Research: Atmospheres*, 109(D14).
- Weygandt, S.S., M. Hu, S.G. Benjamin, T.G. Smirnova, K.J. Brundage and J.M. Brown, 2008: *Assimilation of lightning data using a diabatic digital filter within the Rapid Update Cycle*. Twentieth International Lightning Detection Conference (21–23 April 2008), Tucson, AZ.
- Williams, E., 2005: Lightning and climate: A review. *Atmospheric Research*, 76:272–287.
-

CHAPTER 7. RADAR MEASUREMENTS

7.1 GENERAL

This chapter is a basic discussion of weather radars. It places particular emphasis on the technical and operational characteristics that must be considered when planning, developing and operating individual radars and radar networks in support of Meteorological and Hydrological Services. This is related to the use and application of weather-radar data. Radars used for vertical wind profiling are discussed in the present volume, Chapter 5.

7.1.1 The weather radar

Meteorological radars are primarily designed for detecting precipitation and associated weather phenomena. However, other objects, such as insects, birds, planes, sand and dust, ground clutter and even fluctuations in the refractive index in the atmosphere generated by local variations in temperature or humidity, can be detected by the weather radar.

This chapter deals with radars in common operational or near-operational use around the world. The meteorological radars having characteristics best suited for atmospheric observation and investigation transmit electromagnetic pulses in the 3–10 GHz frequency range (10–3 cm wavelength, respectively). Their system performance and operation are also described in more detail in Annex 7.A. Primarily, meteorological radars are designed for detecting and mapping areas of precipitation, measuring their intensity and motion, and their type. Radar echoes due to birds, insects or Bragg scattering (the turbulent fluctuations) can also produce radial wind data with Doppler radar. Their intensity patterns can reveal the location of atmospheric boundaries that are indicative of areas of low-level convergence where thunderstorms may initiate or develop.

Higher frequencies (35 and 94 GHz) are used to detect smaller hydrometeors, such as cloud, fog, drizzle, light snow and precipitation, and are becoming prevalent in the research community. These frequencies are generally not used in operational forecasting because of excessive attenuation of the radar signal by the intervening medium and their relatively short range, particularly in Doppler mode.

At lower frequencies (915–1 440 MHz, ~400–440 MHz and ~50 MHz), radars are capable of detecting variations in the refractive index of clear air, and are used for wind profiling. Although they may detect precipitation, their scanning capabilities are limited by the size and type of the antenna, and they generally point in the vertical or near-vertical.

The returned signal from the transmitted pulse encountering any target, called an echo, has an amplitude, a phase and a polarization. Amplitude is related to the size distribution and number of particles in the (pulse) volume illuminated by the radar beam. The amplitude is used to determine the reflectivity factor (Z), which is used to estimate the intensity of precipitation through the use of empirical relations. A primary application is to detect, map and estimate the precipitation at ground level instantaneously, nearly continuously, and over large areas.

Doppler radars have the capability of determining the phase difference between the transmitted and received pulse which is a measure of the mean radial velocity of the particles. This is the reflectivity weighted average of the radial components of the displacement velocities of the hydrometeors within the pulse volume. The Doppler spectrum width is a measurement of the spatial variability of the Doppler velocities and provides a measure of the variation in the radial velocity that is interpreted in terms of wind shear and turbulence. An important feature of Doppler is the ability to filter out echoes due to ground targets in the signal processing.

The current generation of radars has polarization capability. Operationally, pulses are transmitted simultaneously with horizontal and vertical polarizations. In the past, the pulses

were transmitted in sequence but required a high-power polarization switch that was prone to failure. Two receivers (physical or virtual) are used to measure the horizontal and vertical components of the returned signal. The main benefits are improved data quality through the ability to identify characteristics of the target (birds, bugs, precipitation and its type, clutter), hydrometeor classification and precipitation estimation. For forecast applications, the dual-polarization capability can identify hail and the rain–snow boundary. High precipitation rates affect the horizontal and vertical phase of the transmitted and received pulses, and this can be exploited for precipitation estimation even with partially blocked beams or attenuated signals. Dual polarization can be calibrated through self-consistent relationships between parameters.

Weather radars no longer operate in isolation. Given current telecommunication capabilities, data are exchanged, resulting in networks of weather radars. This has made it possible to extend their use in local applications (for example, severe weather warnings and nowcasting), regional (for example, data assimilation, precipitation estimation) and global applications (for example, climate change detection).

Modern weather radars should have characteristics optimized to produce the best data for operational requirements. They are the most complex of all the weather sensors used in operations and require special training and extensive knowledge of the instrument. The location of the radar is critical to meet the surveillance and detection requirements. There are a variety of configuration options to set up the radar, and components should be adequately installed and monitored for degradation and failure. Hence, a maintenance and support programme is needed to keep this instrument useful.

7.1.2 Radar characteristics, terms and units

The meteorological applications govern the selection of the characteristics of the radar (Tables 7.1, 7.2 and 7.3).

7.1.3 Radar accuracy requirements

Quantitative use of radar data in end-user applications relies on the accuracy and precision of the radar observations. Appropriately installed, calibrated and maintained modern radars are relatively stable and do not produce significant measurement errors due to the stability of the hardware. However, the maintenance and calibration of the radar is still a considerable challenge and requires highly qualified personnel. Measurement error still exists and requires engineering and scientific expertise to monitor, diagnose and mitigate the biases.

Table 7.1. Radar frequency bands

<i>Radar band</i>	<i>Frequency</i>	<i>Wavelength</i>	<i>Nominal</i>
UHF	300–1 000 MHz	1–0.3 m	70 cm
L	1 000–2 000 MHz	0.3–0.15 m	20 cm
S	2 000–4 000 MHz	15–7.5 cm	10 cm
C	4 000–8 000 MHz	7.5–3.75 cm	5 cm
X	8 000–12 500 MHz	3.75–2.4 cm	3 cm
K _u	12.5–18 GHz	2.4–1.66 cm	1.50 cm
K	18–26.5 GHz	1.66–1.13 cm	1.25 cm
K _a	26.5–40 GHz	1.13–0.75 cm	0.86 cm
W	94 GHz	0.30 cm	0.30 cm

Table 7.2. Some meteorological radar parameters and units

<i>Symbol</i>	<i>Parameter</i>	<i>Units</i>
Z_e	Equivalent or effective radar reflectivity factor	$\text{mm}^6 \text{m}^{-3}$ or dBZ
V_r	Mean radial velocity	m s^{-1}
σ_v	Spectrum width	m s^{-1}
Z_{DR}	Differential reflectivity	dB
K_{DP} , ϕ_{DP}	Specific differential phase, Differential phase	Degree km^{-1} , Degree
ρ_{HV}	Correlation coefficient	
LDR	Linear depolarization ratio	dB

Table 7.3. Physical radar parameters and units

<i>Symbol</i>	<i>Parameter</i>	<i>Units</i>
c	Speed of light	m s^{-1}
f	Transmitted frequency	Hz
f_d	Doppler frequency shift	Hz
P_r	Received power	mW or dBm
P_t	Transmitted power	kW
PRF	Pulse repetition frequency	Hz
T	Pulse repetition time(=1/PRF)	ms
Ω	Antenna rotation rate	Degree s^{-1} or rpm
λ	Transmitted wavelength	cm
φ	Azimuth angle	Degree
θ	Beam width between half power points	Degree
τ	Pulse width	μs
γ	Elevation angle	Degree

External physical factors, such as ground clutter effects, anomalous propagation, attenuation and propagation effects, beam effects, target composition, particularly with variations and changes in the vertical, rain rate-reflectivity relationship inadequacies and the meteorological situation, create artefacts in the data that must be removed during scientific data processing for use in quantitative applications. By considering only errors attributable to the radar system, the measurable radar parameters can be determined with an acceptable accuracy (Table 7.4).

7.2 RADAR PRINCIPLES

7.2.1 Pulse radars

The principles of radar and the observation of weather phenomena were established in the 1940s. Since then, great strides have been made in improving equipment, signal and data processing and data interpretation. The interested reader should consult some of the relevant texts for greater detail. Good references include Skolnik (1970, 1990) for engineering

Table 7.4. Accuracy requirements

<i>Parameter</i>	<i>Definition</i>	<i>Acceptable accuracy^a</i>
φ	Azimuth angle	0.1°
γ	Elevation angle	0.1°
V_r	Mean Doppler velocity	1.0 m s ⁻¹
Z	Reflectivity factor	1 dBZ
σ_v	Doppler spectrum width	1 m s ⁻¹
Z_{DR}	Differential reflectivity	0.2 dB
K_{DP}	Specific differential phase	< 0.5 degree km ⁻¹
ρ_{HV}	Cross-polar correlation	0.001

Note:

- a These figures are relative to a normal Gaussian spectrum with a standard deviation smaller than 4 m s⁻¹. Velocity accuracy deteriorates when the spectrum width grows, while reflectivity accuracy improves.

and equipment aspects; Battan (1973) for meteorological phenomena and applications; Atlas (1964, 1990), Sauvageot (1982) and WMO (1985) for a general review; Rinehart (2004) for a meteorologist's perspective; Doviak and Zrnić (1993) for Doppler radar principles and applications; and Bringi and Chandrasekar (2001) and Meischner (2003) for dual polarization. Considerable insight on radar quality, maintenance, hardware monitoring and calibration can be gleaned from the RADCAL 2000 (Joe, 2001), RADCAL 2013 (Chandrasekar and Baldini, 2013) and the RADMON 2010 (Joe, 2010) workshops. A brief summary of the principles follows.

Figure 7.1 shows a typical radar and radar site. The antenna (2–8.5 m) is inside the radome on top of the tower, which is of the order of 10–30 m or more in height. A tower is used to elevate the antenna above local obstructions. When determining the height of the tower, the growth of nearby trees should be taken into account. Too tall a tower will result in considerably more ground clutter due to the side of the main lobe and the side lobes. One of the buildings contains the radar electronics (transmitter/receiver and computers) and the other contains the uninterruptible power supply (UPS) and diesel generator. Radars are often located in rural locations and well-conditioned power is often not the norm. The UPS plays a critical role in removing power spikes and other anomalies in the power and is key to maintaining operations. The diesel or other kind of generator is capable of 2–3 days of operation but should be specified according to the needs. Note the lightning rod, on top of the radome, that is connected to grounding cables (not shown). This is critical as lightning can cause serious and long-term damage to the radar components. Power fluctuations due to lightning can exceed the capability of the UPS. Note also the red signal lights on top of the radome for warning aviators.

Electromagnetic waves at fixed preferred frequencies are transmitted from a directional antenna into the atmosphere in a rapid succession of short pulses. The pulse length and range processing determines the range resolution of the radar data. One emerging technology in operational radars is the use of low-power transmitters (solid state, travelling-wave tubes) that exploit a technique called pulse compression using a combination of long pulses at low power, frequency modulation and advanced signal-processing to achieve high-range resolution and high sensitivity that rival traditional pulse systems. Phased array antennas are an emerging technology that forms the beam by electronic phase shifting. They have the ability to point to different locations in an agile and non-sequential fashion. However, they all use a directional beam that can resolve targets in range, azimuth and elevation.



Figure 7.1. A typical weather radar within the Canadian network showing the major physical components of a radar system. The tower is about 30 m high, with a radome fitted with hazard lights and a lightning rod.

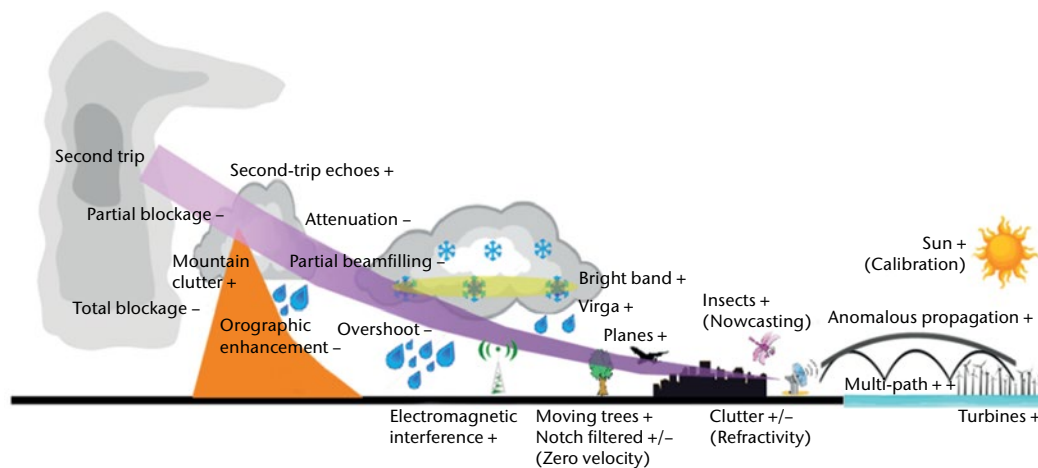


Figure 7.2. The weather radar can detect many things besides weather targets. This schematic illustrates many of these features. The + or – signs indicate whether the radar reflectivity is augmented or diminished by the feature. These artefacts need to be removed for quantitative applications.

Figure 7.2 shows a directional radar antenna emitting a pulsed-shaped beam of electromagnetic energy over the Earth's surface and illuminating various targets, including non-meteorological targets. Many of the physical limitations and constraints of the observation technique are immediately apparent from the figure. For example, (i) there is a limit to the minimum altitude that can be observed at far ranges due to the curvature of the Earth, (ii) there are non-meteorological targets, (iii) there are other emitters (Radio Local Area Networks, the Sun), (iv) there is anomalous propagation of the beam, (v) there is blockage and partial blockage due to mountains, (vi) there is precipitation of different types, and (vii) there are electromagnetic-precipitation interactions resulting in enhanced returns (bright band), and the like.

A parabolic reflector in the antenna system concentrates the electromagnetic energy in a conical-shaped beam that is highly directional. The width of the beam increases with range, for example, a nominal 1° beam spreads to 0.9, 1.7 and 3.5 km at ranges of 50, 100 and 200 km, respectively.

For a pulse radar, the short bursts of electromagnetic energy are absorbed and scattered by the illuminated meteorological and non-meteorological targets. Some of the scattered energy is reflected back to the radar antenna and receiver. Since the electromagnetic wave travels at the speed of light (that is, $2.99 \times 10^8 \text{ m s}^{-1}$), the range of the target can be determined by measuring the time between the transmission of the pulse and its return. Between the transmissions of successive pulses, the receiver listens for any return of the wave. The return signal from the target is commonly referred to as the radar echo. The time between consecutive pulses determines the maximum unambiguous range of the radar. Echoes can still be received from targets beyond this maximum range and are known as multiple-trip echoes.

For a pulse-compression radar with frequency modulation, the range to target is determined by the frequency within the long pulse. However, the maximum unambiguous range is still determined by the time between consecutive pulses. With the transmission of long pulses, the radar receiver is protected from the high power of the transmit pulse, and a long blind zone (10–30 km, depending on the pulse length) is created. In this type of radar, short pulses (with corresponding short blind zones, < 2 km) are transmitted to detect objects that are within this blind zone.

The radar range equation relates the power returned from the target to the radar characteristics. The power returned provides an estimate of the amount of precipitation in the resolution volume. This estimate depends on the assumption of the type of precipitation particles and their size distribution in the resolution volume.

The power measurements are determined by the total power backscattered by the target within a volume being sampled at any one instant in time. This volume is called the pulse volume or sample volume. The pulse volume dimensions (which determine the resolution of the radar) are dependent on the radar pulse length in space (h) and the antenna beam widths in the vertical (ϕ_b) and the horizontal (θ_b). The beam width, and therefore the pulse volume, increases with range. Since the power that arrives back at the radar is involved in a two-way path, the pulse-volume length is only one half the pulse length in space ($h/2$) and is invariant with range. The location of the pulse volume in space is determined by the position of the antenna in azimuth, the elevation, the range to the target and also by the non-linear propagation path of the radar beam away from the radar. For a pulse-compression radar, the pulse volume is primarily determined by the resolution of the frequency modulation and the capability of the receiving system to resolve changes in frequency.

Particles within the pulse volume are continuously shuffling relative to one another. This results in intensity fluctuations about the mean target intensity. Little significance can be attached to a single echo intensity measurement from a weather target. At least 25 to 30 pulses must be integrated to obtain a reasonable estimation of mean intensity, though this will depend on the level of data quality considered as acceptable (Smith, 1995). This was formerly carried out by an electronic integrator circuit but is now done in a digital signal processor. Further averaging of pulses in range, azimuth and time is often conducted to increase the sampling size and accuracy of the estimate at the expense of coarser spatial resolution. An important difference with non-meteorological radars is that the signal processing and the interpretation of the data are based on the premise that the backscatter is from a distributed target and not from a point target (such as an aeroplane). This requires processing for quantitative measurements (not just detection) and a different range dependency of the return power (different radar equation) compared to point target detection radars (such as for ATC).

Doppler radars have circuitry to measure the phase shift difference from successive pulses from the same radar pulse volume. The phase shift is proportional to the radar wavelength and therefore to the distance in the time between pulses. This phase shift is used to estimate the radial or Doppler velocity.

Dual-polarization radar can be of several types. The polarization can be circular and, though there have been very excellent research radars with this feature, it is not generally used in weather operations. Linear dual-polarization radars can send pulses at horizontal and vertical polarization in alternating or simultaneous fashion. In the former case, a fast high-power switch (switches every pulse) is required, but it has proved to be problematic and so few exist

in operations. The simultaneous transmit and receive (STAR mode) technique transmits equal powers in both the horizontal and vertical polarizations and the signal is received separately at horizontal and vertical polarizations. This has proved to be the solution for operations as the high-power, high failure fast switch is avoided. There are variations to these methods of creating the dual-polarization signal. The major advantage of the alternating dual-polarization mode is that it can measure the cross-polarization backscatter of the target (linear depolarization ratio (LDR)), and this is particularly useful for bright band detection. The major disadvantage of the STAR mode is this loss of LDR (as there is cross-polarization already in the transmitted pulse), a 3 dB loss of signal strength in both channels (due to power splitting), and cross-coupling artefacts, particularly in the ice phase of storms.

7.2.2 Propagation radar signals

Electromagnetic waves propagate in straight lines in a homogeneous medium. However, the atmosphere is vertically stratified and the rays change direction depending on the changes in the refractive index (which is a function of temperature and moisture). When the waves encounter precipitation and clouds, part of the energy is absorbed and part is scattered in all directions, including back to the radar site.

The amount of bending of electromagnetic waves can be predicted by using the vertical profile of temperature, moisture and pressure (Bean and Dutton, 1966). Under normal atmospheric conditions, the waves travel in a curve bending slightly earthward (Figure 7.3). The representation is drawn in physical space (the Earth is drawn with a radius of 6 371 km) and the figure shows that the beam bends downward, but still rises with range with respect to the Earth's surface. In a four-thirds (4/3) Earth model, where the Earth's surface is drawn with a radius of 8 975 km (4/3 x 6 371 km), the beams are straight lines (Figure 7.4).

This 4/3 model is most often used, but some radars (mountain top) use a 5/4 model. The height above the radar is given by the following equation:

$$h = \left[r^2 + (k_e a)^2 + 2rk_e a \sin \theta_e \right]^{1/2} - k_e a \quad (7.1)$$

where h is the height above the radar antenna, r is the range along the beam, a is the Earth's radius, e is the elevation angle above the horizon and $k_e a$ is the effective Earth radius.

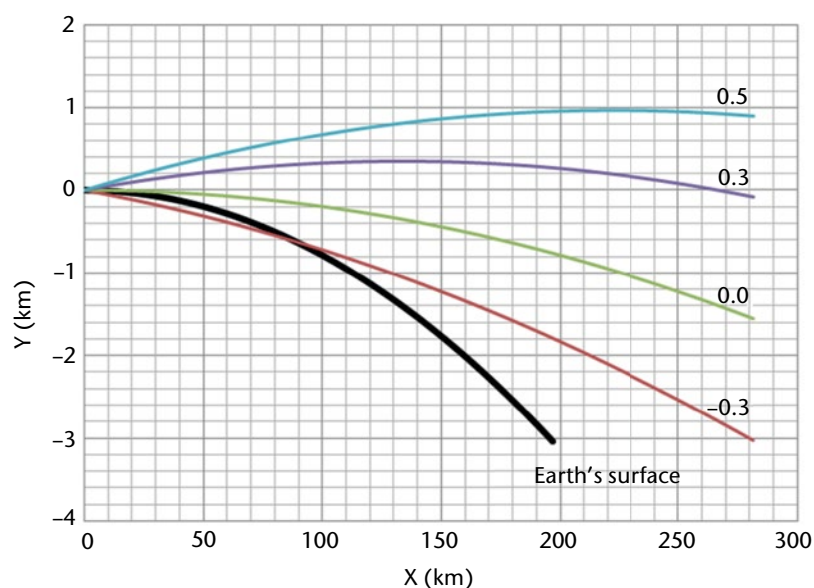


Figure 7.3. Schematic of beam height for selected elevation angles (-0.3, 0, 0.3 and 0.5) above the Earth's surface, for a standard index of refraction profile in the atmosphere plotted in physical space with an Earth curvature equivalent to the Earth radius

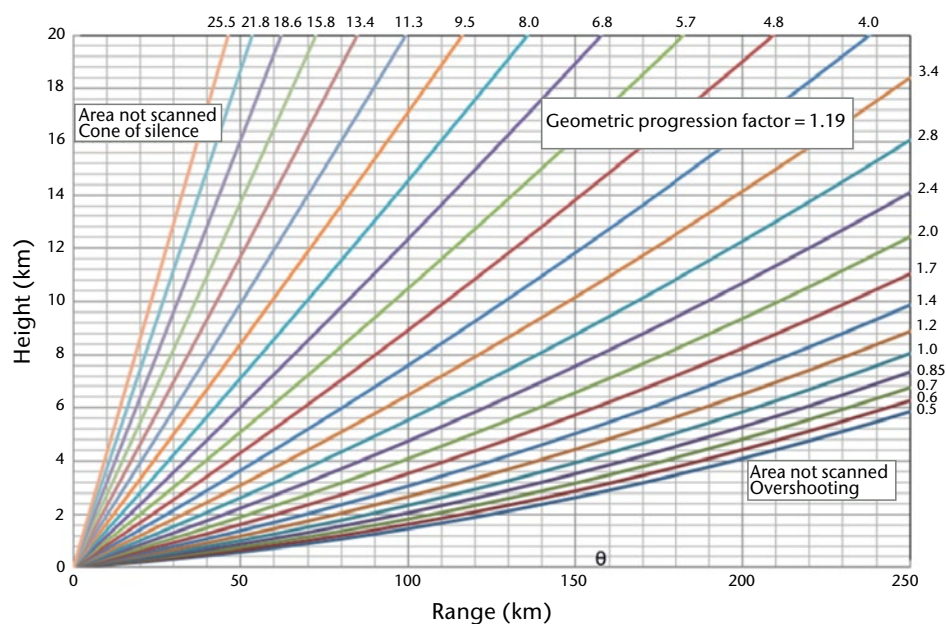


Figure 7.4. The beam height diagram is a useful tool for the interpretation of radar products. The beam height is plotted against a flat Earth, which is a more traditional presentation. The elevation angle sequence is one proposed by Marshall and Ballantyne (1978) to produce optimal horizontal products (CAPPs, echo tops).

The ray path can bend either upward (sub-refraction) or more earthward (super-refraction). In either case, the altitude of the beam will be in error using the standard atmosphere assumption. This is known as anomalous propagation. From a precipitation measurement standpoint, the greatest problem occurs under super-refractive or “ducting” conditions, where the ray can bend sufficiently to strike the Earth and cause ground echoes not normally encountered. The phenomenon occurs when the index of refraction decreases rapidly with height. This occurs when there is an increase in temperature and a decrease in moisture with height. These echoes must be eliminated when producing a precipitation map. The sub-refraction situation, where the beam doesn’t beam as much as normal or bends in the upward direction, is not evident to identify and thus is also a problem. In actual practice, the vertical profile of the index of refraction is not known, so that the precise location of the beam is not known.

Some “clear air” echoes are due to turbulent fluctuations in the refractive index. This is found in areas of turbulence, layers of enhanced stability, wind shear cells, or strong inversions (Bragg scattering). These echoes usually occur in patterns, mostly recognizable, but must be eliminated as precipitation fields (Gossard and Strauch, 1983).

7.2.3 Attenuation in the atmosphere

Microwaves are subject to attenuation owing to atmospheric gases, clouds and precipitation by absorption and scattering.

Attenuation by gases

Gases attenuate microwaves in the 3–10 cm bands. Absorption by atmospheric gases is due mainly to water vapour and oxygen molecules. Attenuation by water vapour is directly proportional to the pressure and absolute humidity and increases almost linearly with decreasing temperature. The concentration of oxygen, to altitudes of 20 km, is relatively uniform.

Table 7.5. One-way attenuation relationships

Wavelength (cm)	Relation (dB km ⁻¹)
10	0.000 343 $R^{0.97}$
5	0.00 18 $R^{1.05}$
3.2	0.01 $R^{1.21}$

Note: After Burrows and Attwood (1949).
One-way specific attenuations at 18 °C.
 R is in units of mm hr⁻¹.

Attenuation by gases varies slightly with the climate and the season. It is significant at weather-radar wavelengths over the longer ranges and can amount to 2 to 3 dB at the longer wavelengths and 3 to 4 dB at the shorter wavelengths, over a range of 200 km. Compensation can be quite easily accomplished automatically.

Attenuation by hydrometeors

Attenuation by hydrometeors can result from both absorption and scattering. It is the most significant source of attenuation. It is dependent on the shape, size, number and composition of the particles. This dependence has made attenuation very difficult to overcome in any quantitative way using radar observations alone, though great progress has been made using dual-polarization radar techniques.

Attenuation is dependent on wavelength. At 10 cm wavelengths, the attenuation exists but is rather small, while at 3 cm it is quite significant. At 5 cm, the attenuation may be acceptable for many climates, particularly in the high mid-latitudes. Wavelengths below 5 cm are not recommended for good precipitation measurement except for short-range applications (Table 7.5). Total attenuation of the signal can occur at 3 and 5 cm. Smaller wavelength radars are more sensitive to attenuation and attenuation correction, and quantitative precipitation estimation based on dual-polarization specific differential phase measurements has more impact on resulting data. These techniques are effective starting at lower precipitation rates for smaller wavelengths.

For precipitation estimates by radar, some general statements can be made with regard to the magnitude of attenuation. Attenuation is dependent on the water mass of the target, thus heavier rains attenuate more; clouds, with much smaller mass, attenuate less. Ice particles attenuate much less than liquid particles. Clouds and ice clouds cause little attenuation and can usually be ignored. Snow or ice particles (or hailstones) can grow much larger than raindrops. They become wet as they begin to melt and result in a large increase in reflectivity and, therefore, in attenuation properties. This can distort precipitation estimates.

7.2.4 Scattering by clouds and precipitation

The echo power detected is backscattered by the targets in the resolution volume (hydrometeors, ground, trees, and the like). The backscattering cross-section (σ_b) is defined as the area of an isotropic scatterer that would return to the emitting source by the same amount of power as the actual target. The backscattering cross-section of spherical particles was first determined by Mie (1908). Rayleigh found that if the ratio of the particle diameter to the wavelength was equal to or less than 0.06, a simpler expression could be used to determine the backscatter cross-section:

$$\sigma_b = \frac{\pi^5 |K|^2 D^6}{\lambda^4} \quad (7.2)$$

which is the justification for equation 7.3. $|K|^2$, the refractive index factor, is equal to 0.93 for liquid water and 0.197 for ice.

Table 7.6. Typical backscatter cross-sections for various targets

<i>Object</i>	$\sigma_b (m^2)$
Aircraft	10 to 1 000
Human	0.14 to 1.05
Weather balloon	0.01
Birds	0.001 to 0.01
Bees, dragonflies, moths	3×10^{-6} to 10^{-5}
2 mm water drop	1.8×10^{-10}

The radar power measurements are used to derive the scattering intensity of the target by using equation 7.2 in the form:

$$z = \frac{\bar{C}P_r r^2}{|K|^2} \quad (7.3)$$

The method and problems of interpreting the reflectivity factor in terms of precipitation rate (R) are discussed in 7.10.

7.2.5 Scattering in clear air

In regions without precipitating clouds, it has been found that echoes are mostly due to insects or to strong gradients of refractive index in the atmosphere (Bragg scatter). The echoes are of low intensity and are detected by most modern radars unless discarded via thresholding of the data. Equivalent Z_e values for clear air phenomena generally appear in the range of -55 to -5 dBZ, although these are not true Z parameters as the physical process generating the echoes is entirely different. For precipitation measurement, these echoes are “noise” in the signal. However, they can usually be associated with some meteorological phenomenon such as a sea breeze or thunderstorm outflows and therefore are useful to identify areas of potential convective initiation. Clear air echoes can also be associated with birds and insects in very low concentrations. Echo strengths of 5 to 35 dBZ are not unusual, especially during migrations (Table 7.6).

Although normal radar processing would interpret the signal in terms of Z , the scattering properties of the fluctuations of the index of refraction are quite different from that of hydrometeors. It is also known as Bragg scattering. The scattering is most often expressed in terms of the structure parameter of refractive index, Cn^2 . This is a measure of the mean-square fluctuations of the refractive index as a function of distance (Gossard and Strauch, 1983).

7.3 THE RADAR EQUATION FOR PRECIPITATION TARGETS

Meteorological targets consist of ice and/or water particles randomly distributed in space. The power backscattered from the target volume is dependent on the number, size, composition, relative position, shape and orientation of the scattering particles. The total power backscattered is the sum of the power backscattered by each of the scattering particles.

Using this target model and electromagnetic theory, Probert-Jones (1962) developed an equation relating the echo power received by the radar to the parameters of the radar and

the targets' range and scattering characteristics. It is generally accepted as being a reliable relationship to provide quantitative reflectivity measurements with good accuracy, bearing in mind the generally realistic assumptions made in the derivation:

$$\bar{P}_r = \frac{\pi^3}{1.024 \ln 2} \cdot \frac{P_t h G^2 \theta_b \phi_b}{\lambda^2} \cdot \frac{|K|^2 10^{-18} Z}{r^2} \quad (7.4)$$

where \bar{P}_r is the power received back at the radar, averaged over several pulses, in watts; P_t is the peak power of the pulse transmitted by the radar in watts; h is the pulse length in space, in metres ($h = c\tau/2$, where c is the speed of light and τ is the pulse duration); G is the gain of the antenna over an isotropic radiator; θ_b and ϕ_b are the horizontal and vertical beam widths, respectively, of the antenna radiation pattern at the -3 dB level of one-way transmission, in radians; λ is the wavelength of the transmitted wave, in metres; $|K|^2$ is the refractive index factor of the target; r is the slant range from the radar to the target, in metres; and Z is the radar reflectivity factor (usually taken as the equivalent reflectivity factor Z_e when the target characteristics are not well known), in $\text{mm}^6 \text{m}^{-3}$.

The second term in the equation contains the radar parameters, and in the third term the parameters depend on the range and characteristics of the target. The radar parameters are relatively fixed, and, if the transmitter is operated and maintained at a constant output (as it should be), the equation can be simplified to:

$$\bar{P}_r = \frac{C |K|^2 Z}{r^2} \quad (7.5)$$

where C is the radar constant.

There are a number of basic assumptions inherent in the development of the equation which have varying importance in the application and interpretation of the results. Although they are reasonably realistic, the conditions are not always met exactly and, under particular conditions, will affect the measurements (Aoyagi and Kodaira, 1995).

These assumptions are summarized as follows:

- (a) The scattering precipitation particles in the target volume are homogeneous dielectric spheres whose diameters are small compared to the wavelength, that is $D < 0.06 \lambda$ for strict application of Rayleigh scattering approximations;
- (b) The pulse volume is completely filled with randomly located precipitation particles;
- (c) The reflectivity factor Z is uniform throughout the sampled pulse volume and approximately constant during the sampling interval;
- (d) The particles are all water drops or all ice particles, that is, all particles have the same refractive index factor $|K|^2$, and the power scattering by the particles is isotropic;
- (e) Multiple scattering (among particles) is negligible;
- (f) There is no attenuation in the intervening medium between the radar and the target volume;
- (g) The radar uses linear polarizations (typically H or V);
- (h) The main lobe of the antenna radiation pattern is Gaussian in shape;
- (i) The gain of the antenna is known or can be calculated with sufficient accuracy;
- (j) The contribution of the side lobes to the received power is negligible;
- (k) Blockage of the transmitted signal by ground clutter in the beam is negligible;

- (l) The peak power transmitted (P_t) is the actual power transmitted at the antenna, that is, all waveguide losses, and so on, and attenuation in the radar dome, are considered;
- (m) The average power measured (P_r) is averaged over a sufficient number of pulses or independent samples to be representative of the average over the target pulse volume.

This simplified expression relates the echo power measured by the radar to the radar reflectivity factor Z , which is in turn related to the rainfall rate. These factors and their relationship are crucial for interpreting the power returned from the target and estimating precipitation amounts from radar measurements. Despite the many assumptions, the expression provides a reasonable estimate of the precipitation mass. This estimate can be improved by further consideration of factors in the assumptions.

7.4 BASIC WEATHER-RADAR SYSTEM AND DATA

The basic weather radar consists of the following:

- (a) An antenna to focus the transmitted microwaves into a narrow beam and receive the returning power;
- (b) A tower to elevate the antenna above immediate obstructions;
- (c) A transmitter to produce power at microwave frequency and a modulator to create the pulses and pulse rates;
- (d) A receiver to detect, amplify and convert the microwave signal into an LF signal;
- (e) A signal processor to extract the desired information from the received signal;
- (f) A system to control the radar and process the data into radar variables;
- (g) A data display to visualize the information in an intelligible form;
- (h) A recording system to archive the data for training, study and records.

A basic weather radar may be non-coherent (for example, a magnetron or power oscillator type transmitter), that is, the phase of successive transmitted pulses is random. Doppler measurements can be made if the phase of the transmitted pulse is measured and the return signal processed with reference to this phase. This is known as a coherent-on-receive Doppler radar. A coherent-on-transmit radar (for example, a klystron, power amplifier, solid state or travelling-wave tube type transmitter) transmits the same phase with each pulse. Power transmitted by a weather radar is typically several hundreds of kilowatts to a megawatt of peak power concentrated in a pulse of a microsecond in width, whereas the average power is typically a few hundred watts. Solid state or travelling-wave tube type transmitters send a pulse of much lower power but rely on long pulses to compensate.

7.4.1 Reflectivity

The backscattered power measured by a typical radar is of the order of 10^{-8} to 10^{-15} W, covering a range of about 70 dB from the strongest to the weakest targets detectable. Compared to the transmit power, this is over 20 orders of magnitude smaller. To measure the weakest and strongest signals simultaneously, receivers with large dynamic ranges (> 90 dB) are required and are now commonly available (Heiss et al., 1990; Keeler et al., 1995). In the past, logarithmic receivers with a dynamic range of 90 dB were used for reflectivity measurements. Linear receivers (that maintain phase linearity) are needed for Doppler measurements. In the past, these had limited dynamic range (40 to 50 dB), requiring automatic gain control.

The reflectivity factor is the most important parameter for radar interpretation. The factor derives from the Rayleigh scattering model and is defined theoretically as the sum of particle (drops) diameters to the sixth power in the sample volume:

$$Z = \sum_{\text{vol}} N(D) D^6 \quad (7.6)$$

where the unit of Z is $\text{mm}^6 \text{m}^{-3}$. In many cases, the number of particles and their composition and shape are not known and an equivalent or effective reflectivity factor Z_e is defined. For example, snow and ice particles must refer to an equivalent Z_e which represents Z , assuming the backscattering particles were all spherical drops of density ρ .

Rainfall rate is given by:

$$R = \sum_{\text{vol}} N(D) V_T \rho \pi / 6 D^3 \quad (7.7)$$

However, $N(D)$ is not known, and empirical relationships between Z and R have been developed; the most famous being the one commonly known as the Marshall-Palmer relationship:

$$Z = 200R^{1.6} \quad (7.8)$$

In order to cover the range of values, a common practice is to work in a logarithmic scale or dBZ units which are numerically defined as $\text{dBZ}_e = 10 \log_{10} Z_e$.

Volumetric observations of the atmosphere are normally made by scanning the antenna at a fixed elevation angle and subsequently incrementing the elevation angle in steps at each revolution. An important consideration is the resolution of the targets. Parabolic reflector and phased array (through phase shifting) antennas are used to focus the waves into a pencil shaped or Gaussian shaped beam. Larger reflectors create narrower beams, greater resolution and sensitivity at increasing costs. The beam width, often defined by the half power points, is one half that at the axis, is dependent on the wavelength, and may be approximated by:

$$\theta_e = \frac{70\lambda}{d} \quad (7.9)$$

where the units of θ_e are degrees; and d is the antenna diameter in the same units as λ . Good surveillance weather radars have beam widths of 0.5° to 1° . However, broader beams are useful for short-range applications.

The useful range of weather radars is dependent on the application and nature of the weather. Depending on the time interval between pulses (characterized by the pulse repetition frequency (PRF), say 300 s^{-1}), the maximum unambiguous range of the radar can be hundreds of kilometres (for example, 500 km). However, given the beam propagation and the curvature of the Earth, the beam, and therefore the pulse volume, is high and big (for example, at 250 km, a 1° beam width radar pointing at an elevation angle of 1° is 9 km high and 6 km wide, Figure 7.4). The beam may overshoot the weather, the pulse volume may not be filled and the sensitivity of the radar may not be sufficient to measure the precipitation intensity accurately. However, if echoes are observed, they will indicate very intense and hazardous thunderstorms or weather. Typical weather radars operate with a maximum range of the order of 250 to 600 km.

For good quantitative precipitation measurements, a 1° beam width radar has an effective range of about 80 km. The smaller the beam width of the radar, the greater the effective range (for example, a 0.65° beam has an effective range of about 120 km). At longer ranges, the data must be extrapolated to the ground. The beam spreads and under-filling results in under-reporting of the precipitation intensity. This is weather regime dependent, and the results discussed are for mid-latitudes.

7.4.2 Doppler velocity

The development of Doppler weather radars and their introduction to weather surveillance provided a new dimension to the observations (Heiss et al., 1990). Doppler radar provides a measure of the targets' velocity along a radial from the radar. So it provides a measurement of the velocity component of the wind in the direction either towards or away from the radar.

The typical speeds of meteorological targets are less than 50 m s^{-1} , except in the case of tornadoes/hurricanes. As discussed earlier, pulse-to-pulse phase changes are used to estimate the Doppler velocity. If the phase changes by more than $\pm 180^\circ$, the velocity estimate is ambiguous. To unambiguously and accurately measure the Doppler velocity of meteorological targets, the PRF must be high (smaller time interval between pulses) such that the maximum unambiguous range is reduced from that of a typical radar, measuring reflectivity only. At higher speeds, additional processing steps are required to retrieve the correct velocity. The maximum unambiguous Doppler velocity depends on the radar wavelength (λ) and the PRF, and can be expressed as:

$$V_{\max} = \pm \frac{\text{PRF} \cdot \lambda}{4} \quad (7.10)$$

The maximum unambiguous range can be expressed as:

$$r_{\max} = \frac{c}{\text{PRF} \cdot 2} \quad (7.11)$$

Thus, V_{\max} and r_{\max} are related by the equation:

$$V_{\max} r_{\max} = \pm \frac{\lambda c}{8} \quad (7.12)$$

These relationships show the limits imposed by the selection of the wavelength and PRF (see Figure 7.5). A high PRF is desirable to increase the unambiguous velocity; a low PRF is desirable to increase the radar range. Unfortunately, these limits fall within the desired measurement space of a weather radar, and compromises in the radar operating conditions are required. This is known as the Doppler dilemma and is further discussed in the signal and data processing section of this chapter. The maximum unambiguous velocity or range is often referred to as the Nyquist velocity or Nyquist range.

One of the significant consequences of the high PRFs is that there are often still detectable echoes beyond the Nyquist range. These echoes are referred to as second- (or multiple-) trip echoes since they are received from pulses transmitted previously. If the targets are strong enough, the power of these targets can still be received by the radar. However, the targets will be located

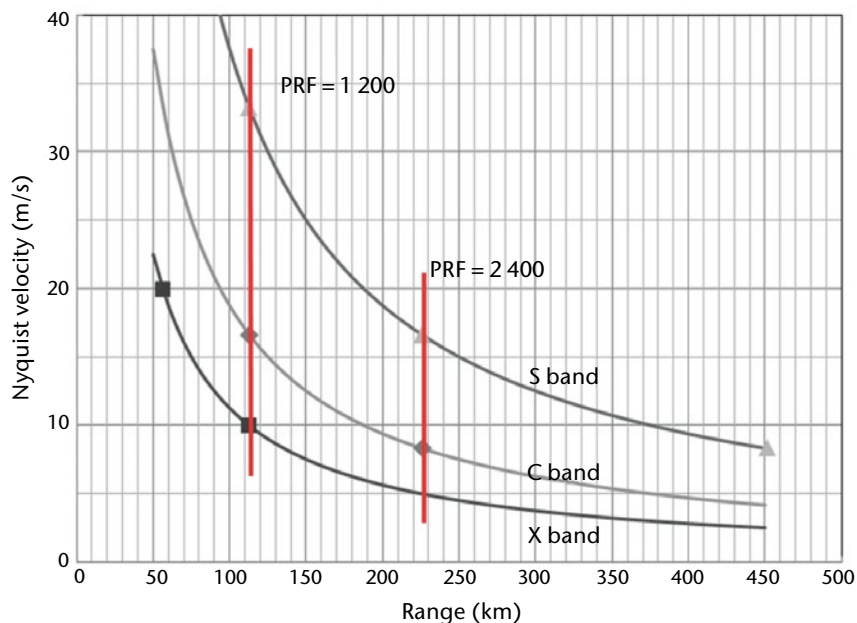


Figure 7.5. This illustrates the Doppler dilemma for the three common radar bands (X, C, S). The dilemma arises because one parameter, the PRF, which is the time between transmitted pulses, controls the maximum unambiguous velocity and the maximum unambiguous range in opposite ways. The markers and red lines indicate commonly used settings.

incorrectly in the first trip since the radar cannot determine whether the echo was a result of the current or previous pulse, given that the timing or range of the echo is based on the most recent transmitted pulse.

Some Doppler radars are fully coherent; their transmitters are oscillators and generate the same phase from pulse to pulse. These coherent radars typically employ klystrons, solid state or similar transmitters. Since these types of radars transmit the same phase for every pulse, the velocity of the second echoes will produce discernible mean radial velocities. This kind of radar cannot (without advanced processing) separate the range or the velocity of the multiple-trip echoes.

For coherent-on-receive Doppler radars, such as one with a magnetron amplifier transmitter, the phase from pulse to pulse is random. In this kind of radar, the phase of the most recently transmitted pulse is measured and the phases of all echoes are referenced to it. Therefore, the series of phases from the second-trip echo that referenced to the most recent phase will be random and will appear as noise in the Doppler spectrum. Figure 7.6 is a simulated example of a typical C band radar set-up. The sharp spike at zero velocity is due to stationary ground echoes and has a narrow power distribution. The broad peak on the right is the weather echo. It is broader than the ground clutter peak since it originates from a distribution of drops that are shuffling. Note that the tail of the weather contribution on the right is aliased and appears on the left edge of the graph. The signal fluctuates about the noise floor due to thermal noise in the system, and also about the weather spectrum due to the shuffling of the precipitation targets. A dynamic estimation of the noise power makes it possible to subtract the noise power from the overall power to produce a cleaner estimate of the first-trip power (Figure 7.7). This is an example showing (a) how stationary ground clutter can be filtered using a zero velocity notch filter, and (b) how second-trip echoes can be filtered using a noise type filter (signal quality index).

Two signal-processing systems of different complexity are used to process the Doppler parameters. The simpler pulse pair processing (PPP) system uses the comparison of successive pulses in the time domain to extract mean velocity and spectrum width. The second and more complex system uses FFT processing to produce a full spectrum of velocities in each sample volume. The PPP system is faster, less computationally intensive and better at low signal-to-noise ratios, but has poorer clutter rejection characteristics than the FFT system.

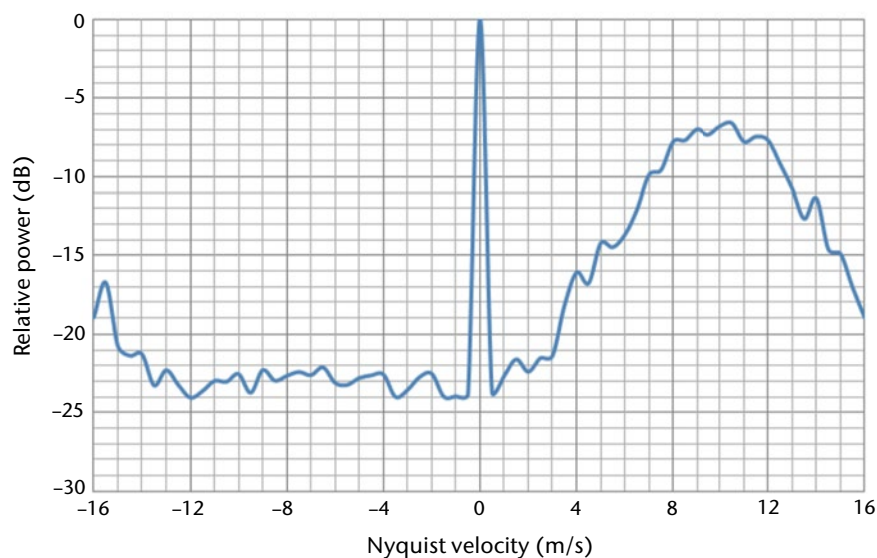


Figure 7.6. This Doppler spectrum shows the distribution of power within a single radar pulse volume as a function of the Doppler velocity.

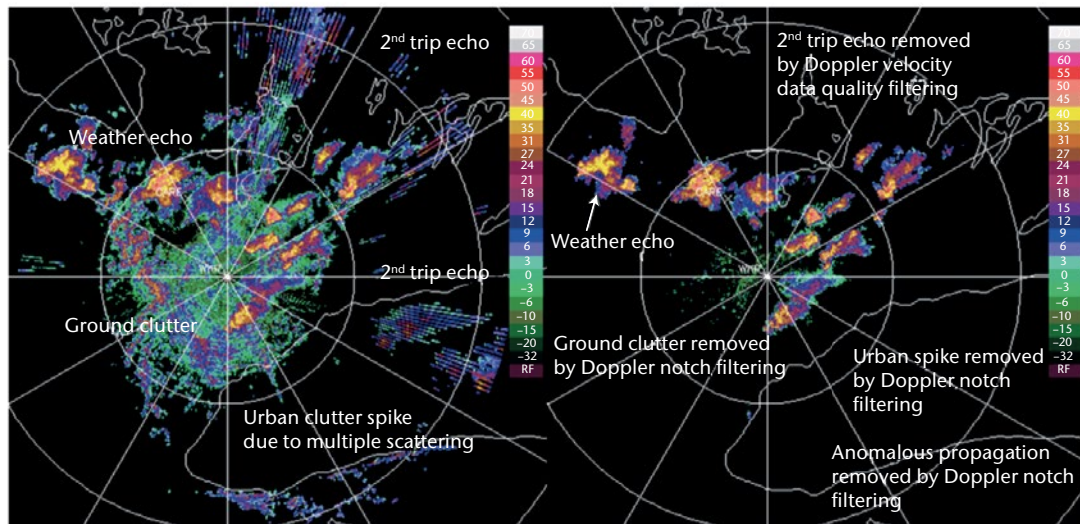


Figure 7.7. Modern Doppler radars can filter bad data or ground clutter in the signal-processing phase of the processing chain. The left image shows the raw data and the right image shows the filtering capability of Doppler signal and data processing. Polarization diversity capability for data quality is shown in Figure 7.29.

7.4.3 Dual polarization

There are several basic radar polarization techniques in current usage. One system transmits a circularly polarized wave, and the co-polar and orthogonal polarization powers are measured. Another system alternately or simultaneously transmits pulses with horizontal (H) then vertical (V) polarization utilizing a high-power switch. Simultaneous H and V radars do not require a fast switch. The complexity of unravelling the microphysical characteristics of the echo is still a challenge, and manufacturing a high-quality circular polarization system can be more costly. The linear polarization system is generally preferred since the retrieval of meteorological information is less calculation intensive, and conventional radars can be converted to dual polarization more easily. Except in a few situations, the high-power switch has proved to be problematic for alternating polarization, and as a result the STAR mode system is common in operational radars.

In general, the polarization technique is based on micro-differences in the scattering particles. Raindrops are elliptically shaped with the major axis in the horizontal plane when falling freely in the atmosphere. The oblateness of the drop is related to drop size. The power backscattered from an oblate spheroid is larger for a horizontally polarized wave than for a vertically polarized wave assuming Rayleigh scattering. This is also true for other targets such as insects, birds and ground clutter.

Table 7.2 describes the most common polarization diversity parameters. The differential reflectivity, called Z_{DR} , is defined as 10 times the logarithm of the ratio of the horizontally polarized reflectivity Z_H and the vertically polarized reflectivity Z_V . Comparisons of the equivalent reflectivity factor Z_e and the differential reflectivity Z_{DR} suggest that the precipitation may be separated as hail, rain, drizzle or snow (Seliga and Bringi, 1976).

As an electromagnetic wave propagates through a medium with oblate particles, the phase of the incident beam is altered due to attenuation differences (resulting in propagation speed differences) in the vertical and horizontal. The effect on the vertical and horizontal phase components depends on the oblateness and is embodied in an integral parameter termed the differential phase (φ_{DP}). If an appropriate range derivative can be computed, the specific differential phase (K_{DP}) can also be estimated. For heavy rainfall measurements, K_{DP} has certain advantages (Zrnić and Ryzhkov, 1995). English et al. (1991) demonstrated that the use of K_{DP} for rainfall estimation is much better than Z for rainfall rates greater than about 20 mm h^{-1} at the S band. Since this is a phase measurement and can be localized or specific to the range bin, this

parameter can be used to overcome issues of power calibration and partial beam blockage. With greater attenuation (shorter wavelengths), the effectiveness of this technique increases at lower reflectivities or precipitation rates.

The correlation of the vertical and horizontal time-series data provides a statistical measure of the dissimilarity of the H and V scattering cross-sections of the hydrometeors. It should be noted that this is a statistical measure, and so rain and snow, though on an individual particle basis appear to have quite different scattering characteristics, actually have high correlation in the statistical sense. Bebbington (1992) designed a parameter for a circularly polarized radar, termed the degree of polarization, which is insensitive to propagation effects (linear correlation is independent of propagation effects also). This parameter is similar to linear correlation for linearly polarized radars and appears to have value in target discrimination. For example, extremely low values are indicative of scatterers that are randomly oriented such as those caused by airborne grass or ground clutter (Holt et al., 1993).

7.5 SIGNAL AND DATA PROCESSING

7.5.1 The Doppler spectrum

The radar detects an electromagnetic wave returned from the target. This wave is a result of all the scatterers in the radar volume. Mathematically, a wave is characterized by an amplitude and phase or equivalently in complex numbers as the real or imaginary parts of a phasor. This is also called the in-phase or quadrature (I, Q) signals. The wave is measured several times and the results are a time series of I, Q samples. If a Fourier transform is applied to the data, then the magnitude of the Fourier transform coefficients constitutes the Doppler spectrum. The Doppler spectrum is a representation of the auto-correlation of the I, Q time series in frequency space (Wiener, 1964). The more time samples, the finer the resolution in the frequency domain. Processing in time domain is equivalent to that in the frequency domain. Figure 7.6 shows a typical Doppler spectrum and is useful to characterize the various aspects of the information within a single radar volume. The noise level (integrated over the entire spectrum) represents the minimum signal level or minimum detected signal of this range bin. The peak at zero frequency or zero velocity is the contribution of stationary echoes or ground clutter. The broader peak is due to the weather target. Note that the peak at zero velocity is broadened by the antenna motion, poor phase stability of the radar system and a fewer number of samples. The width of the ground clutter spectrum is generally smaller than the width of the weather spectrum and can, in most cases, be used to separate the ground from the weather echo. The area under the weather echo and above the noise level is the power of the weather echo. The area under the ground clutter spectrum is the power due to ground clutter.

7.5.2 Power parameter estimation

The hydrometeors are distributed within the pulse volume and shuffle relative to each other and produce a fluctuating signal. Averaging is required to reduce the variance of the measurements to within acceptable uncertainty. Generally, 30 independent pulses are required to estimate reflectivity (Doviak and Zrnić, 1993). This implies that the pulses need to be sampled at time intervals greater than the de-correlation time of the pulse volume, sampled in different locations in range or using some other technique (frequency shuffling).

Operationally, this is done in various ways depending on the application and processing philosophy. The antenna could slowly scan and the reflectivity could be estimated within one degree of azimuth and within one pulse volume, or it could rotate more quickly and range averaging could be employed in the signal or data processor. Additionally, poorer data quality could be acceptable and data smoothing could be applied at a later stage.

7.5.3 Ground clutter and point targets

Clutter can be the result of a variety of targets, including buildings, hills, mountains, aircraft and chaff, to name just a few. Good radar siting is the first line of defence against ground clutter effects. However, clutter is always present to some extent since the sides of the main beam and the side lobes interact with the nearby terrain (Figure 7.8). The radar beam is not perfectly conical but radiates in all directions, though the main power is along the bore sight. The beam width is often defined as the half power points (-3 dB of the power along the bore sight). This radiation pattern is determined by the geometry of the feed horn, the distance from the focal point, the parabolic dish and the struts holding the feed horn. The height of the first side lobe (marked) is more or less determined by these factors and often used as a measure of the quality of the antenna. Reducing or moving this side lobe in azimuth by shifting the feed horn results in either a broader main beam or power loss.

The intensity of ground clutter is inversely proportional to wavelength (Skolnik, 1970, 1990), whereas backscatter from rain is inversely proportional to the fourth power of wavelength. Therefore, shorter wavelength radars are less affected by ground clutter. Ground clutter echoes should be eliminated for precipitation estimation; however, clutter echo can be used for humidity measurements (Fabry, 2004). Point targets, like aircraft, can be eliminated, if they are isolated, by removing echoes that occupy a single radar resolution volume. Weather targets are distributed over several radar resolution volumes. Point targets can be eliminated during the data-processing phase. Point targets, like aircraft echoes, embedded within precipitation echoes may not be eliminated with this technique depending on their relative strength.

To remove ground clutter, a conceptually attractive idea is to use clutter maps. The patterns of radar echoes in non-precipitating conditions are used to generate a clutter map that is subtracted from the radar pattern collected in precipitating conditions. The problem with this technique is that the pattern of ground clutter changes over time. These changes are primarily due to changes in meteorological conditions; a prime example is anomalous propagation echoes that typically last several hours and then disappear. Micro-changes to the environment cause small fluctuations in the pattern of ground echoes which confound the use of clutter maps. Adaptive techniques (Joss and Lee, 1993) attempt to determine dynamically the clutter pattern to account for the short-term fluctuations, but they are not good enough to be used exclusively.

Doppler processing techniques attempt to remove the clutter from the weather echo from a signal-processing perspective. The basic assumption is that the clutter echo is narrow in spectral width and that the clutter is stationary. However, to meet these first criteria, a sufficient number

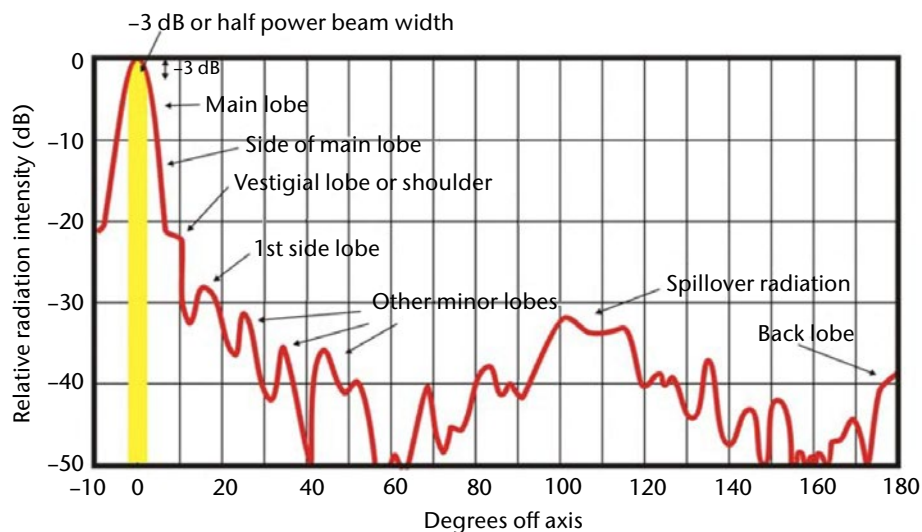


Figure 7.8. A generic antenna radiation pattern. Note that the antenna beam width is typically defined at the half power (50% or -3 dB) points. If the target is highly reflective, power is emitted and received on the side of the main lobe and the other side lobes.

of pulses must be acquired and processed in order to have sufficient spectral resolution to resolve the weather from the clutter echo. A relatively large Nyquist interval is also needed so that the weather echo can be resolved (see Figure 7.6). The spectral widths of ground clutter and weather echo are generally much less than 0.5 m s^{-1} and generally greater than 1 m s^{-1} , respectively. Therefore, Nyquist intervals of about 8 m s^{-1} are needed. Clutter is generally stationary and is identified as a narrow spike at zero velocity in the spectral representation (Figure 7.6). The spike has finite width because the ground echo targets, such as swaying trees, have some associated motion.

Time domain processing to remove the zero velocity component of a finite sequence is done with a high-pass digital filter. A width and depth of the digital filter to match the clutter must be assumed for the whole scanning domain, and mismatches are inevitable as the clutter varies (Zrnić and Hamidi, 1981). Adaptive spectral (Fourier transform) processing identifies the ground clutter echo, heuristically determines the clutter echo and removes the ground clutter power from the total power, thereby separating ground clutter from the weather echoes even if they are overlapped (Passarelli et al., 1981; Crozier et al., 1991; Figure 7.7). It can be difficult to separate the weather from the clutter echo when the weather echo is narrow (as in light snow situations) and the mean Doppler velocity is near zero. In this situation, too much weather echo can be removed. When the weather echo spectrum is narrow as in the case of snow or drizzle, the zero notch filter cannot distinguish the weather from the ground clutter. This is particularly true when the antenna spins fast, causing the ground echo spectrum to broaden, and when the mean radial velocity of the weather is near zero. Too much power is removed and results in an anomalous depression in reflectivity (Figure 7.9, left image). The arrow shows where the depressed echo corresponds to the zero line in the radial velocity image (Figure 7.9, right image). This is a minor drawback to Doppler notch filtering.

Improvements to the clutter echo identification include better techniques to identify the clutter echo (Gaussian model adaptive processing) and techniques to use texture of the data (variance of the reflectivity) associated with clutter before applying the clutter filters (Hubbert et al., 2009a; Hubbert et al., 2009b). Systems without Doppler could employ these texture techniques to remove ground clutter and anomalous propagation echoes.

An alternative approach, called micro-clutter removal, takes advantage of the observation that structures contributing to ground clutter are very small in scale (less than, for example, 100 m). Range sampling is carried out at a very fine resolution (less than 100 m) and clutter is identified using reflectivity and Doppler signal processing. Range averaging (to a final resolution of 1 km) is performed with clutter-free range bins. The philosophy is to detect and ignore range bins with clutter, rather than to correct for the clutter (Joss and Lee, 1993; Lee et al., 1995). This is

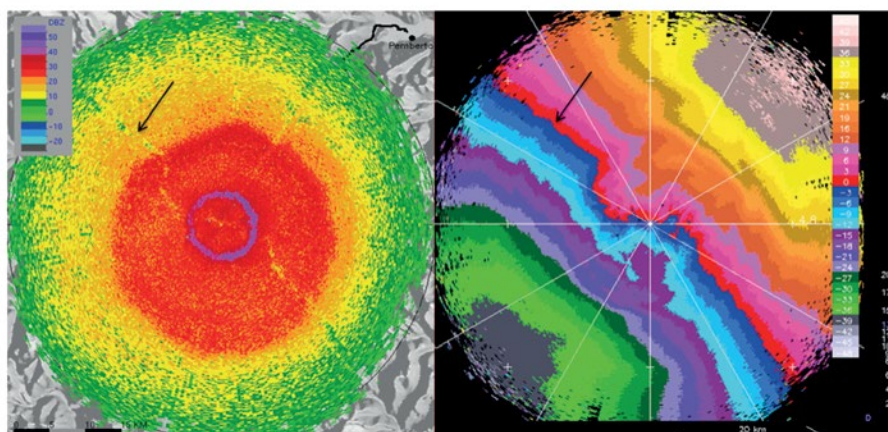


Figure 7.9. Doppler notch filtering can remove too much echo when the Doppler spectrum of the weather echo is narrow and near the zero Doppler velocity (see arrow). This problem is minor compared to other artefacts illustrated in Figure 7.2.

radically different from the previously discussed techniques and it remains to be seen whether the technique will be effective in all situations, in particular in anomalous propagation situations where the clutter is widespread.

Polarization radars can also identify ground clutter since the ground clutter has different polarimetric features as compared to precipitation. In addition, other kinds of clutter targets can be identified.

Clutter can be reduced by careful site selection (see below). Radars used for long-range surveillance, such as for tropical cyclones or in a widely scattered network, are usually placed on hilltops to extend the useful range, and are therefore likely to see many clutter echoes. A simple suppression technique is to scan automatically at several elevations, and to discard the data at the shorter ranges from the lower elevations, where most of the clutter exists. By processing the radar data into constant altitude plan position indicator (CAPPI) products, low elevation data are rejected automatically at short ranges (Marshall and Ballantyne, 1978). Figure 7.4 shows a geometric scan sequence proposed by Marshall and Ballantyne (1978) that is optimized to produce constant height products such as the CAPPI and echo top.

7.5.4 **Overcoming the Doppler dilemma**

The Nyquist interval and sampling govern the quality of the Doppler velocity estimates. The Nyquist interval ($\pm 180^\circ$) must be sufficiently large to span the spectrum of the weather echo. Typically, the weather echo usually has a 4–6 m s^{-1} width and so the Nyquist interval must be at least twice as wide. The tails of the spectrum may be aliased, but if the signal is strong the mean velocity can still be estimated.

In order to provide a statistically stable velocity estimate about 20–30 samples are required. These samples need to be correlated, so they need to be made quickly. Note that this is fewer than for reflectivity, and in theory, it is possible to recover velocity at lower signal-to-noise ratios (weaker signal strength) than reflectivity and in a shorter period of time.

To detect returns at various ranges from the radar, the echoes should be sampled periodically, usually about every 1 μs , to obtain information about every 150 m in range. This sampling can continue until it is time to transmit the next pulse (at about every 1 ms). A sample point in time (corresponding to a distance from the radar) is called a range gate. The interval between transmit pulses governs the maximum unambiguous range. The wavelength combined with the transmit interval governs the maximum unambiguous velocity. For weather-radar wavelengths and weather scenarios, these maxima are in conflict and this is called the Doppler dilemma, as increasing one results in reducing the other. This is shown in Figure 7.5. So, a fundamental problem with the use of any pulse Doppler radar is to mitigate the impacts of limited range and velocity.

Common techniques to mitigate the velocity limitation or to de-alias the velocities include multiple PRF techniques (Doviak and Zrnić, 1993; Crozier et al., 1991) or continuity techniques (Eilts and Smith, 1990). In the former, radial velocity estimates are collected at two or more different PRFs with different maximum unambiguous velocities and are combined to yield a new estimate of the radial velocity with an extended unambiguous velocity. For example, a C band radar using PRFs of 1 200 and 900 Hz has nominal unambiguous velocities of 16 and 12 m s^{-1} , respectively. The amount of aliasing can be deduced from the difference between the two velocity estimates to de-alias the velocity to an extended Nyquist velocity range of $\pm 48 \text{ m s}^{-1}$. Figure 7.10 shows how the dual-PRF technique is able to extend the unambiguous velocity. The top graph shows what the Doppler radar is able to measure as a function of true radial velocity (-48 to 48 m s^{-1}). In this example, the PRFs are in 4:3 ratio; other ratios such as 7:5 and 3:2 are possible. The bottom graph represents the unique difference in the measured Doppler velocities as a function of true radial velocity. From this difference, the fold number can be determined and the true velocity can be retrieved. The limit of the retrieval is determined by the unambiguous Nyquist velocities and their ratio. This limit is called the extended Nyquist velocity and is 48 m s^{-1} in this case. Figure 7.11 shows an example of the results of this technique.

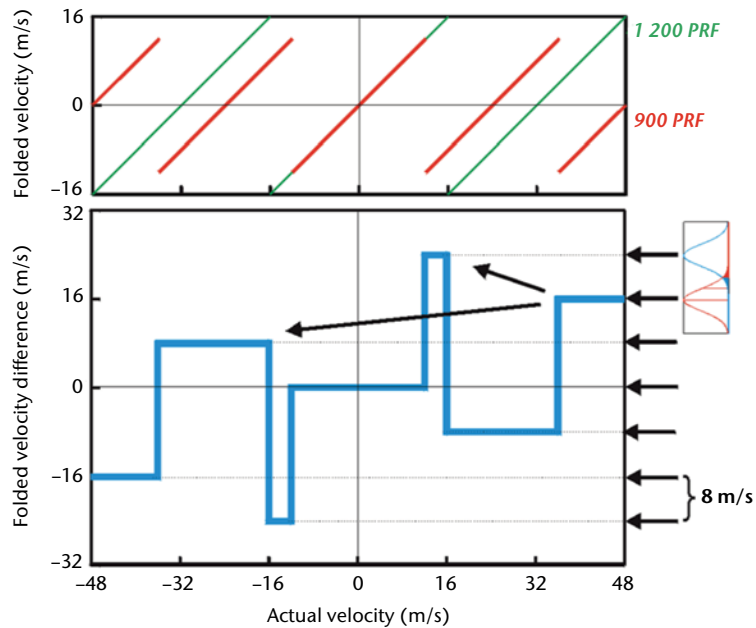


Figure 7.10. This is an example of a C band radar pulsing at 900 and 1 200 s^{-1} with unambiguous Nyquist velocities of 12 and 16 $m s^{-1}$, respectively. The technique relies on the difference between measured radial velocities (ordinate on the bottom image) to determine the fold number (abscissa on the bottom image) and then use that with the corresponding measured radial velocity to estimate the true radial velocity.

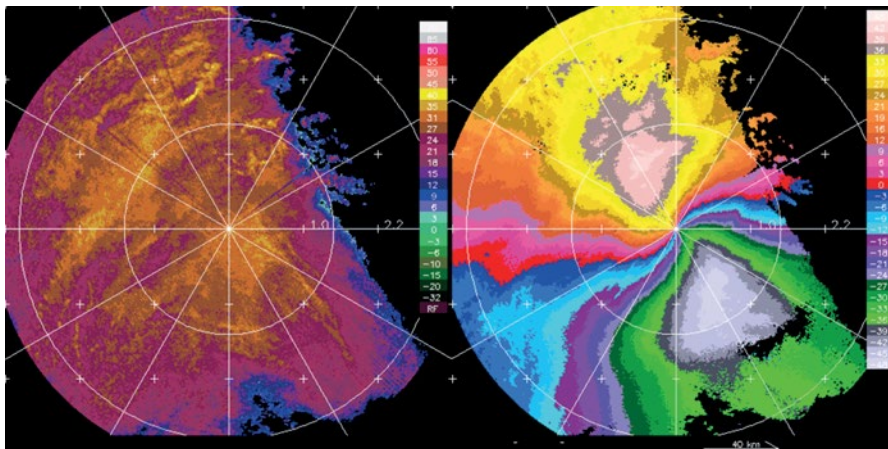


Figure 7.11. This figure illustrates the necessity and ability of a C band radar to extend the velocity out to at least 48 $m s^{-1}$. This is a case of a hurricane/extratropical transition passage and velocities are near 48 $m s^{-1}$. In this situation, the assumptions of the dual-PRF technique (the two measured estimates at different PRFs are from the same radial velocity) are satisfied and the result has little noise (right image, compare with Figure 7.20).

Combinations of PRF ratios commonly in use are 5:4, 4:3 or 3:2. The maximum unambiguous velocity commonly used is 16 $m s^{-1}$, though it is not a strict requirement. Lower velocities would result in larger maximum ranges. The difference in the use of the various ratios is that the variance in the mean velocity results in the uniform velocity assumption being violated and dual-PRF errors arising (Joe and May, 2003).

Continuity techniques rely on having sufficient echo to discern that there are aliased velocities and correcting them by assuming velocity continuity (no discontinuities of greater than $2V_{max}$).

Fold numbers are determined starting at the zero line, and whenever a discontinuity of a Nyquist interval is encountered, the fold number is increased or decreased and the Nyquist interval is added or subtracted.

The second fundamental problem is the range limitation imposed by the use of high PRFs (greater than about 1 000 Hz). Echoes beyond the maximum range will be aliased back into the primary range. For radars with coherent transmitters (for example, klystron or solid state), the echoes will appear within the primary range. For coherent-on-receive systems, the second-trip echoes will appear as noise (Joe et al., 1995; Passarelli et al., 1981; Figure 7.12). For the latter system, the noise is a result of the randomly transmitted phases. Doppler radars with their short Nyquist range are contaminated with second-trip echoes, regardless of whether they are coherent-on-receive (magnetron) or coherent-on-transmit (klystron) type. In Figure 7.12, from a C band magnetron radar, the second trip reveals itself as wedge-shaped echoes in reflectivity (black arrows) and this can be used to identify them. In the radial velocity field, the data are noisy (yellow arrows) and this can be used in the signal-processing stage to eliminate them as their Doppler spectrum is very broad, elevating the noise level. If these data were taken with a klystron radar, the radial velocity would appear as coherent data.

Phase coding techniques have been developed to distinguish the second-trip echoes for coherent Doppler radars. Processing can be done with respect to the current pulse for the first-trip echo and the previous pulse for the second-trip echo. This is called random phase processing. It is effective if the sensitivity of the radar is good (low) so that the second-trip echo can be detected above noise and if the phase stability is good (low) so that the phase or velocity can be recovered at long ranges. For coherent transmitters, a pseudo-random sequence can be generated. Better still is to modulate the phase in a known way to precisely separate the first from the second trip. Frush et al. (2002) developed this technique for klystron systems.

In a coherent-on-receive (for example, magnetron) system, the phase variation is implicitly random. In a coherent-on-transmit (for example, klystron) system, the phase variation is imposed by the modulator in a controlled fashion. An example is the SZ-2 phase modulation used in the United States WSR-88D system. The two examples in Figure 7.13 (a–d, e–h) are shown to illustrate the benefits and limitations of the random phase technique. Images 7.13(a) and 7.13(e) are taken with low PRF and represent the “truth”. Images 7.13(b) and 7.13(f) are retrieved from the random phase technique. The demarcation of the first–second trip boundary is indicated by the white arrow. The gap is because the receiver is turned off while the pulse is being transmitted. In images 7.13(a–d), a squall line has not reached the radar. The echoes near the radar are weak relative to those at far ranges and the technique works well as most of the second trip is recovered (compare 7.13(a) with 7.13(b)). In images 7.13(e–h), part of the precipitation system has reached the radar and so there are relatively strong echoes near the radar relative to those at far ranges. The technique works less well as there are significant amounts of the second trip that are not recovered (compare 7.13(e) with 7.13(f)). In this implementation of the technique, only single PRF data is possible and the Nyquist is 16 m s^{-1} (images 7.13(c) and 7.13(g)). The dual-PRF

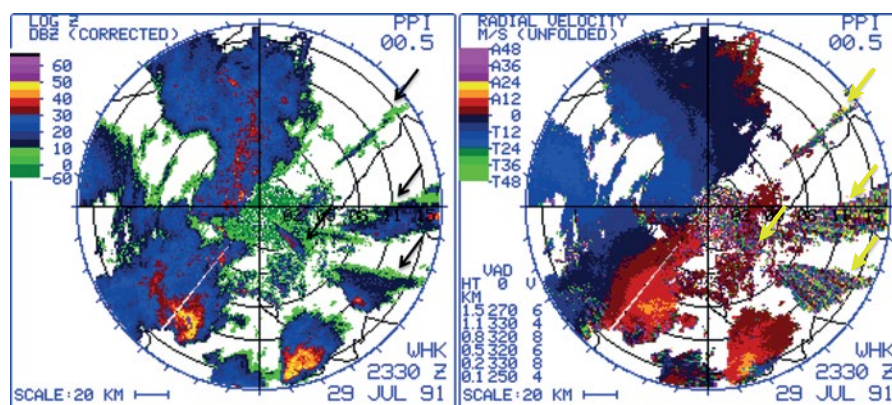


Figure 7.12. An example of second-trip echoes in reflectivity (left) and radial velocity (right) for a magnetron radar

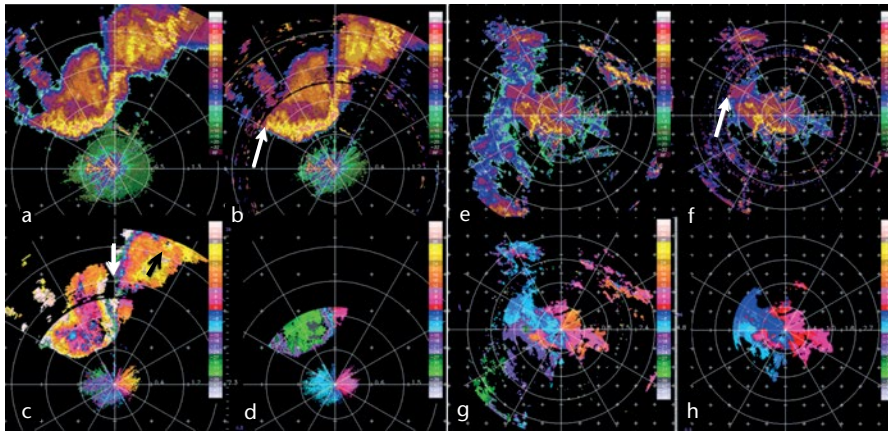


Figure 7.13. Examples of random phase range extension: the example on the left (a–d) shows a situation where the first-trip echo is weak and much of the second-trip echo is recoverable. In the example on the right (e–h), there is significant first-trip echo which precludes recovering the second-trip echo.

data with an extended Nyquist range of 48 m s^{-1} are shown in images 7.13(d) and 7.13(h). While aliased, the single PRF data can still be interpreted and effectively used by a well-trained analyst. For example, a “bookend vortex” can be observed in image 7.13(c) (white and black arrows). The corresponding reflectivity images are the inner (first trip) portions of images 7.13(b) and 7.13(f). An important aspect of random phase processing is that the first trip will have higher data quality as the impacts of the second-trip echo are filtered.

An earlier technique uses a surveillance scan with low PRF to determine the location of the reflectivity echo. Then when overlapping echoes are encountered in the shorter range Doppler mode, the echo power and velocity are assigned to the location with the greater power (Figure 7.14). This works if the power is significantly different ($> 5 \text{ dB}$). A long-range surveillance scan is used to locate the reflectivity echo. A short-range Doppler scan is used to measure the Doppler or radial velocity. The radial velocity is assigned to the reflectivity echo with the greatest power. If the powers are within 5 dB of each other, the technique does not work well and the radial velocity data are not recovered and are designated as range folded. They are marked as white in Figure 7.14. Some colour schemes are employed that mark these echoes as purple and so this is often called purple haze.

A combination of multiple PRF and phase diversity techniques can be used to mitigate both problems simultaneously (WMO, 2012; Yamauchi et al., 2013).

7.6 OPTIMIZING RADAR CHARACTERISTICS

7.6.1 Selecting a radar

A radar is a highly effective observation system. However, the application, the climatology, the local environment (blockage) and the network design determine the effectiveness of any particular radar or radar system. Everything about radar is a trade-off. No single radar can be designed to be the most effective for all applications. Characteristics can be selected to maximize the proficiency to best suit a few applications, such as tornado detection or snow squall detection, but not all applications (compared with long-range surveillance). Cost is a significant consideration. Much of the interdependence can be referenced to the radar range equation.

An important consideration is the radar network design and the application. Networks of X band radars are being proposed for a variety of local applications where the range requirement is of the order of 50 km or less and where low-level coverage is critical – as in low-level snow squall, tornado detection, microburst detection, complex terrain (mountainous), urban

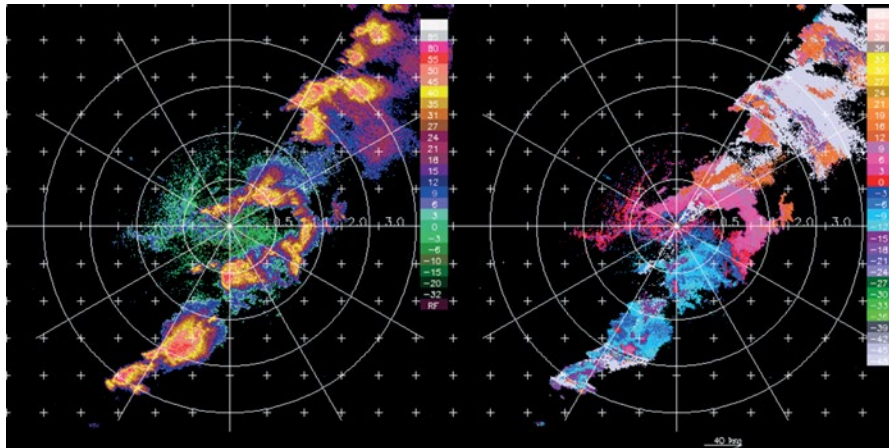


Figure 7.14. Without the advanced phase coded signal processing, multiple PRF techniques are used to recover the second trip. Low PRF scans with long-range capability are used to locate the reflectivity echo. High PRF but short-range scans are used to measure radial velocity. The radial velocity is assigned to the range bin with the highest power.

hydrology and perhaps wind turbine mitigation. The original intention of these networks was for adaptive sensing of the atmosphere for multiple applications – from weather to ATC. This is accomplished in conjunction with phased array antennas that have pointing agility and can scan in a cooperative fashion (McLaughlin et al., 2009). An innovation of this technology is the low requirements in terms of infrastructure of the phased array antenna that can be mounted on a side of a building or on an existing tower.

7.6.2 Wavelength and beam width

The larger the wavelength, the greater the cost of the radar system, particularly antenna costs for comparable beam widths (that is, resolution). This is due both to an increase in the amount of material and to the difficulty in meeting tolerances over a greater size. Within the bands of interest for weather radars (S, C and X), the sensitivity of the radar or its ability to detect a target is strongly dependent on the wavelength. However, this dependence is pragmatically mitigated by transmit power. It is also significantly related to antenna size, which impacts gain, beam width and beam filling. Smaller wavelength radars (35 GHz and 94 GHz) are becoming available for specialized applications, such as fog or cloud detection, or used from space-based platforms for cloud or precipitation measurements (for example, Tropical Rainfall Measuring Mission (TRMM); Global Precipitation Measurement (GPM); CloudSat; and Earth Clouds, Aerosols and Radiation Explorer (EarthCARE)).

Considerations of Doppler range within a radar network have a great impact on the wavelength chosen. For the same Nyquist velocity, an S band will have twice the Nyquist range compared to a C band radar and hence have a significant impact on unambiguous coverage. This may be mitigated with the velocity and range extension techniques discussed earlier.

Radar rays are attenuated most significantly in rain, less in snow and ice, and even less in clouds and atmospheric gases. In broad terms, attenuation at the S band is relatively small. The S band radar, despite its cost, is essential for penetrating the very high reflectivities in mid-latitude and subtropical severe storms with wet hail. X band radars can be subject to severe attenuation over short distances.

The great disadvantage is that smaller wavelengths have much larger attenuation. It remains to be seen whether the dual-polarization K_{DP} techniques can compensate for the attenuation until total attenuation occurs (which is very infrequent) and whether ignoring attenuation at S band is justified. If K_{DP} techniques prove to be superior for precipitation estimation than reflectivity techniques, the smaller wavelength is more sensitive to attenuation and so may be more effective.

The radar signal may be totally lost at C and X band, particularly if the radome is wet. While this may seem disastrous, the key question is whether the loss of signal (typically for tens of minutes for propagating storms) results in actual missed severe storm warnings or missed flash flooding. Experience indicates that warnings will have usually been already issued and the loss of one or two data points for hydrological purpose is not a devastating situation.

7.6.3 Transmitters and transmit power

Target detectability is directly related to the peak power output of the radar pulse. However, there are practical limits to the amount of power output that is dictated by power tube technology. Unlimited increases in power are not the most effective means of increasing the target detectability. For example, doubling the power only increases the system sensitivity by 3 dB. Technically, the maximum possible power output increases with wavelength and pulse width. Improvements in sampling, receiver sensitivity, antenna gain, pulse width or choice of wavelength may be better means of increasing detection capability.

Magnetrons and klystrons are common power sources. Magnetrons cost less but are power oscillators and so they are less stable in frequency. Many Doppler radars today are based on magnetrons, and with co-axial magnetrons and digital technology, the phase noise of these systems can be comparable to that of klystron systems. Smaller phase noise results in greater capability for clutter rejection (Figure 7.15). Phase noise of less than 0.5° is a minimum performance level of modern radars. At normal operating wavelengths, conventional radars should detect rainfall intensities of the order of 0.1 mm h^{-1} at 200 km and have peak power outputs of the order of 250 kW and 1 000 kW or greater in the C band and S band, respectively.

Solid state transmitters have recently been deployed operationally. They have the promise of reduced maintenance with the high reliability of solid state technology, excellent phase stability and electronic stability for dual-polarization measurements. Solid state transmitters are typically low power and require multiple long pulse lengths and pulse compression to attain the required sensitivities. They are a combination of pulse and frequency-modulated continuous wave radars. Range side lobes are an issue with pulse-compression modulation schemes and it remains to be seen whether they are significant in the weather application.

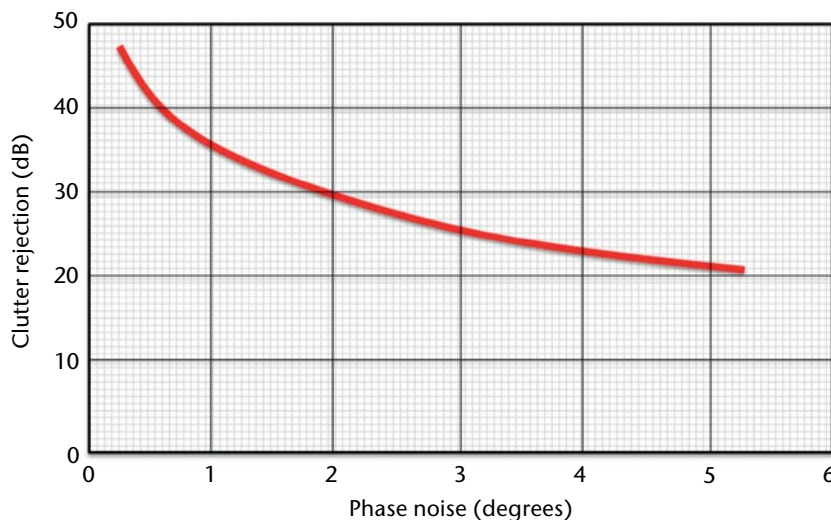


Figure 7.15. Coherency (phase noise) is a measure of the quality of a Doppler radar and is directly related to the ability to remove ground clutter and retrieve second-trip echoes using phase coding techniques.

7.6.4 **Pulse length**

The pulse length determines the target resolving power of the radar in range. The range resolution or the ability of the radar to distinguish between two discrete targets is proportional to the half pulse length in space. For most klystrons and magnetrons, the maximum ratio of pulse width to PRF is about 0.001. Common pulse lengths are in the range of 0.3 to 4 μs . A pulse length of 2 μs has a resolving power of 300 m, and a pulse of 0.5 μs can resolve 75 m.

Assuming that the pulse volume is filled with target, doubling the pulse length increases the radar sensitivity by 6 dB with receiver-matched filtering but decreases the resolution; decreasing the pulse length decreases the sensitivity while increasing the resolution. Shorter pulse lengths allow more independent samples of the target to be acquired in range and the potential for increased accuracy of estimate.

7.6.5 **Pulse repetition frequency**

The PRF should be as high as practical to obtain the maximum number of target measurements per unit time. A primary limitation of the PRF is the unwanted detection of second-trip echoes. Most reflectivity-only radars have unambiguous ranges beyond the useful range of weather observation by the radar. An important limit on weather target useful range is the substantial height of the beam above the Earth even at ranges of 250 km.

For Doppler radar systems, high PRFs ($\sim 1\ 200\ \text{s}^{-1}$) are used to increase the Doppler unambiguous velocity measurement limit. This results in the Doppler dilemma, where there is a trade-off between maximum range and maximum velocity. The PRF factor is not a significant cost consideration but has a strong bearing on system performance. Briefly, high PRFs are desirable to increase the number of samples measured, to increase the maximum unambiguous velocity that can be measured, and to allow higher permissible scan rates. Low PRFs ($\sim 300\ \text{s}^{-1}$) are desirable to increase the maximum unambiguous range that can be measured, and to provide a lower duty cycle.

7.6.6 **The antenna subsystem**

Weather radars normally use a horn fed antenna with a parabolic reflector to produce a focused narrow conical beam. Three important considerations are the beam width (angular resolution), the antenna gain and the side lobes. For common weather radars, the size of the antenna increases with wavelength for a fixed beam width and with the narrowness of the beam required. A common target for weather-radar antenna beam width is 1° , though there is inherently nothing special about this number.

Phased array antenna technologies are being explored in research and are now commercially available at X band at an affordable price. These antennas consist of phase controllable radiating elements that form the beam. Adaptable target specific or dependent scan strategies can be developed such that rapid scan or high-quality data requirements can be simultaneously satisfied in theory, but this is still to be demonstrated in operations. Ground clutter rejection may be superior as these systems do not scan but essentially momentarily stare at each radial and so the beam smearing of the ground clutter echo does not occur.

Antenna size and beam width

Weather radars normally have beam widths in the range of 0.5° to 2.0° . For a 0.5° and 1.0° beam at a C band wavelength, the antenna reflector diameter is at least 7.1 and 3.6 m, respectively; at S band it is 14.3 and 7.2 m. The cost of the antenna system and pedestal increases more than linearly with reflector size. There is also an engineering and cost limit. The tower must also be appropriately chosen to support the weight of the antenna.

The desirability of having a narrow beam to maximize the resolution and enhance the possibility of having the beam filled with target is particularly critical for the longer ranges. For a 0.5° beam, the azimuthal (and vertical) cross-beam widths at 50, 100 and 200 km range are 0.4, 0.9 and 1.7 km, respectively. For a 1.0° beam, the widths are 0.9, 1.7 and 3.5 km. Even with these relatively narrow beams, the beam width at the longer ranges is substantially large.

The gain of the antenna is also inversely proportional to the beam width and thus the narrower beams also enhance system sensitivity by a factor equal to differential gain. The estimates of reflectivity and precipitation require a nominal minimal number of target hits to provide an acceptable measurement accuracy. The beam must therefore have a reasonable dwell time on the target in a rotating scanning mode of operation. Thus, there are limits to the antenna rotation speed. Scanning cycles cannot be decreased without consequences. For meaningful measurements of distributed targets, the particles must have sufficient time to change their position before an independent estimate can be made. Systems generally scan at the speed range of about 0.5 to 6 rpm.

Most single polarization weather radars are linearly polarized, with the direction of the electric field vector transmitted being horizontal and sometimes vertical. Reasons for favouring horizontal polarization include: (a) sea and ground echoes are generally less with horizontal polarization; (b) lesser side lobes in the horizontal provide more accurate measurements in the vertical; and (c) there is greater backscatter from rain due to the drop ellipticity. However, at low elevation angles, better reflection of horizontally polarized waves from plane ground surfaces may produce an unwanted range-dependent effect.

Most if not all operational dual-polarization radar employ the STAR mode of transmission, with equal amount of power at two orthogonal linear polarizations (typically horizontal and vertical). This eliminates the need for a high-power, high failure polarization switch.

7.6.7 **Illumination**

Side lobes are an inherent property of any antenna. Side lobes also include the sides of the main lobe. The beam width is usually defined as the half power points of the main beam and there is power at angular distances away from the main beam. A major contributor to the side lobes is the feed horn and the struts supporting the feed horn. Side lobes may be mitigated by over-illuminating the dish; however, this results in a broader beam and less sensitivity.

In summary, a narrow beam width affects system sensitivity, detectability, horizontal and vertical resolution, effective range and measurement accuracy. The drawback of small beam width is mainly cost. For these reasons, the smallest affordable beam width has proven to improve greatly the utility of the radar (Crozier et al., 1991).

7.6.8 **Typical weather radar characteristics**

The characteristics of typical radars used in general weather applications are given in Table 7.7.

As discussed, the radar characteristics and parameters are interdependent. The technical limits on the radar components and the availability of manufactured components are important considerations in the design of radar systems.

The Z-only radars are non-coherent pulsed radars that have been in use for decades. The Doppler radars are de rigueur and add a new dimension to the observations. They provide estimates of radial velocity. Specialized Doppler radars have been developed for better detection of small-scale microbursts and tornadoes over very limited areas, such as for air-terminal protection. Dual-polarization radars are deployed and applications for data quality, target classification and quantitative precipitation estimation are finding their way into operations – including in hydrology, NWP, and climate change studies.

Table 7.7. Specifications of typical meteorological radars

Type	S	S	S	S	C	C	C	C	C	X
Frequency (GHz)	2 800–3 000	2 700–3 000	2 700–3 000	2 700–3 000	5 400–5 900	5 600–5 650	5 600–5 650	5 500–5 700	5 300–5 850	9 300–9 500
Wavelength (cm)	10.7	10.7	10.7	10.7	5.3	5.3	5.3	5.3	5.3	3
Peak power (kW) per channel	475	850	750	20	500	1 000	250	250	12	75
Pulse lengths (μ s)	1.57, 4.5	0.2–2.0	0.4–4.5	0.5–200	0.2–3.0	0.4–4.5	0.4–4.5		0.5–200	0.3–3.3
PRF (/s)	318–1 403, 318–452	200–2 400	250–2 000	100–20 000	200–2 400	200–2 400	250–2 000		100–20 000	250–3 000
Min dBZ at 50 km	–28.7	–15.5		–5.5	–17.5	–19.5		–15	–5	
MDS (dBm)	–113	–114	–114	–114	–114	–114	–114	–115	–114	–113
Receiver dynamic range (dB)		105	115	110	105	105	115	99	110	90
Antenna diameter (m)	8.53	8.5	8.5	8.5	4.2	4.2	4.2	4.5	4.2	2.4
Beam width (degrees)	1	0.95	1	0.95	0.95	0.95	1	1	0.95	1.05
Gain (dB)	45	45	44.5	45	45	45	44.5	45	45	44.5
Polarization	Horizontal	STAR	STAR	STAR	Dual linear	Dual linear	Dual linear	Dual linear	STAR	Dual linear
Max rotation rate (rpm)	6	10	6	6	10	10	8	6.7	6	6
Transmitter type	Klystron	Co-axial magnetron	Klystron	Solid state	Co-axial magnetron	Klystron	Klystron	Co-axial magnetron	Solid state	Co-axial magnetron
Clutter suppression	50	46	55	55	46	46	55	55	55	

7.6.9 Radar volume scan strategy

Most modern radars automatically perform a volume scan consisting of a number of full azimuth rotations of the antenna at several elevation angles. This is called the scan strategy and there are a variety of strategies for different purposes (Marshall and Ballantyne, 1978; Brown et al., 2005; Crum and Alberty, 1993; Germann et al., 2006a, Seltmann et al., 2013).

Long-range scans of 500 km or more (that result in limited Nyquist velocity) are needed for long-range surveillance. Rapid update of the order of 5 min is required to capture the evolving morphology of the convective thunderstorm. In aviation downburst applications, even shorter cycle times are required (Michelson et al., 1990). Research radars scan limited areas or sectors with 1 min or less cycle times (Wurman et al., 1996). Slow low-level scans with long pulse lengths are needed to maximize the capture of clear air echoes. Slow scanning will optimize the Doppler filtering of ground echoes. Multiple PRF techniques require the assumption of uniformity of radial velocity and can be implemented on a ray by ray or scan by scan basis.

Scans as low in elevation as possible are needed for optimizing the retrieval of quantitative precipitation estimates and also to optimize the detection of low-level and shallow weather. A geometric sequence of elevation angles are required to generate optimal CAPP1 or echo top products (Marshall and Ballantyne, 1978). The emerging X band phased array radar networks, such as that of the Collaborative Adaptive Sensing of the Atmosphere project or the Multifunction Phased Array Radar project, are revolutionizing the scan strategy concept as the electronic scanning can adapt to the weather or application (McLaughlin et al., 2009; Weber et al., 2007), or weaknesses may be mitigated with data from neighbouring radars.

The trade-off is the quality of the data. For example, slow scans for high spectral resolution for ground clutter mitigation or low data variance preclude scan strategies with very many elevation angles and hence result in poor vertical resolution. Data quality is a nebulous concept as it qualitatively refers to trade-offs in timeliness or temporal resolution (cycle time), spatial resolution (azimuth, range, elevation), data bias (velocity or reflectivity bias) and data variance. This is difficult to objectively optimize as the success metrics are quite diverse and setting the number of elevation angle sequence is not an exact science.

Of prime consideration is the nature of the weather and the location that requires the coverage. For example, the scan sequence for a radar located in a valley used for local and short-range application will or can be quite different from a radar that is used for long-range surveillance for land-falling hurricanes (Joe et al., 2014).

While it is attractive conceptually to set the elevation angle changes equal to the beam width, small changes in the elevation angle of even 0.1° degrees can produce significant views of the data, due to the stratified nature of the precipitation (snow, bright band, rain profiles) and the wind profile.

Raw polar data are stored in a three (range, azimuth, elevation) or multiple (radar parameter) dimensional array, commonly called the volume scan. This serves as the data source for further data processing and archiving. There can be several versions of raw data due to different data quality processing.

7.6.10 Radar performance

For more details on system performance of ground-based weather-radar systems measuring the atmosphere using frequencies between 2 GHz and 10 GHz, please see also Annex 7.A.

Minimum detectable signal

The minimum detectable signal (MDS) is a performance measure of the aggregate of the transmit power, antenna size, beam width or gain, pulse length, wavelength and other factors. This is often described in power units or system noise temperature. However, for a radar analyst,

Table 7.8. MDS of typical high-performance radars

<i>Radar</i>	<i>MDS at 50 km</i>
Z9110	-8.0 dBZ (few days in August) -10.0 dBZ (2 months)
Z9220	-1.0 dBZ
King City CONVOL (2 μ s)	-11.0 dBZ
King City DOPVOL (0.5 μ s)	-5.0 dBZ
Twin Lakes, OK	-7.5 dBZ
Lake Charles, LA	-8.5 dBZ

reflectivity at a fixed range provides a more intuitive measure of the performance of a radar. High sensitivity is highly desired in order to detect clear air echoes and light precipitation and to enhance the retrieval of second-trip echoes. Table 7.8 shows some MDS of typical high-performance radars.

Phase stability

Phase stability or phase jitter is a measure of the average change of phase from pulse to pulse. Some radar test software can provide this measurement using an acoustic delay line or from external targets. The advantage of the latter is that it tests the stability at different ranges or time delays and the entire processing change. Good phase stability ($< 0.5^\circ$) results in better velocity estimation, ground clutter rejection and better second-trip retrieval with magnetron systems.

Cross-polar correlation and *ZDR*

A measure of the quality of a dual-polarization radar is the cross-polar correlation (ρ_{HV}). If the radar is pointed at light rain or drizzle that is generally uniformly round, the correlation should be very close to 1.0. Good radars report values typically of 0.995 or better. This indicates that the dual polarization is very good and well configured.

If vertical scans are performed during stratiform conditions, the Z_{DR} values should be 0 and have no azimuthal dependence.

7.7 MAINTENANCE AND CALIBRATION

Radar is arguably the most complex of instruments that a meteorological service or service provider must service and maintain. It requires a very high level of training and skill development. Maintenance is critical to keeping the radar operating, and calibration is critical to the quality of the data. Both should follow the manufacturer's prescribed procedures. The following is an outline.

7.7.1 Maintenance

Modern radars, if properly installed and operated, should not be subject to frequent failures. Some manufacturers claim that their radars have a mean time between failures (MTBF) of the order of a year. However, these claims are often optimistic and the realization of the MTBF requires scheduled preventive maintenance. A routine maintenance plan and sufficient technical staff are necessary in order to minimize repair time. Mechanical and electronic failures are the most prevalent (Sireci et al., 2010; Figure 7.16).

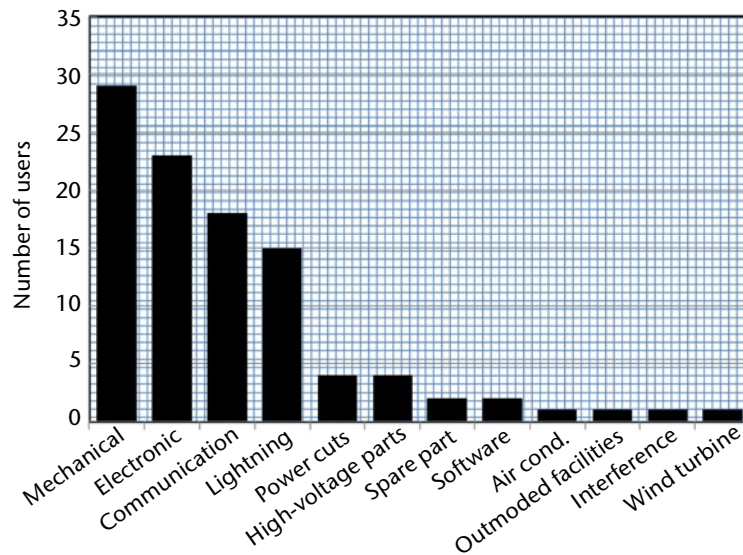


Figure 7.16. Results from the WMO weather radar survey showing the main failure modes of a radar (Sireci et al, 2010); figure courtesy of Oguzhan Sireci of the Turkish State Meteorological Service.

It should be noted that factors external to the radar can result in data not reaching the users. These include failures or poor quality of the main power, or there may be too many spikes or fluctuations in the power. The power grid may fail due to lightning or other reasons. Telecommunications may fail. Air conditioning systems may fail and result in the shutdown of sensitive electronic systems.

Preventive maintenance should include at least a quarterly check of all radar parts subject to wear, such as gears, motors, fans and infrastructures. The results of the checks should be written in a radar logbook by local maintenance staff and, when appropriate, sent to the central maintenance facility. When there are many radars, there might be a centralized logistic supply facility and a repair workshop. The latter receives failed parts from the radars, repairs them and passes them on to logistics for storage as stock parts, to be used as needed in the field. Basic record keeping is a must.

For corrective maintenance, the Service should be sufficiently equipped with the following:

- (a) Spare parts for all of the most sensitive and long lead item components, such as tubes, solid state components, boards, chassis, motors, gears, power supplies and so forth. Experience shows that it is desirable to have 30% of the initial radar investment in critical spare parts on the site. If there are many radars, this percentage may be lowered to about 20%, with a suitable distribution between central and local maintenance;
- (b) Test equipment, including the calibration equipment mentioned above. Typically, this would amount to approximately 15% of the radar value;
- (c) Well-trained personnel capable of identifying problems and making repairs rapidly and efficiently are critical.

Competent maintenance organization should result in radar availability 96% of the time on a yearly basis, with standard equipment. Better performances are possible at a higher cost.

Recommended minimum equipment for calibration and maintenance includes the following:

- (a) Microwave signal generator;
- (b) Microwave power meter;

- (c) MHz oscilloscope;
- (d) Microwave frequency meter;
- (e) Standard gain horns;
- (f) Intermediate frequency signal generator;
- (g) Microwave components, including loads, couplers, attenuators, connectors, cables, adapters, and so on;
- (h) Versatile microwave spectrum analyser at the central facility;
- (i) Standard electrical and mechanical tools and equipment.

7.7.2 Calibration

Ideally, the complete calibration of reflectivity uses an external target of known radar reflectivity factor, such as a metal-coated sphere. The concept is to check if the antenna and waveguides have their nominal characteristics. However, this method is very rarely used because of the practical difficulties in flying a sphere and multiple ground reflections, as well as the time and skill required (Brunkow, 2001).

A standard procedure is to use the sun as a calibration source for power and pointing accuracy. The sun is a microwave source and appears as a disk of about 0.5 degrees (Tapping, 2001). However, by maximizing the power, greater precision can be achieved. Beam propagation effects may affect low elevation angles and so higher angles are often used for solar calibration. Repeated measurements will statistically improve the precision of the results. It should be noted that antenna elevation pointing accuracy and precision may be a function of angle and so a variety of angles should be measured.

Routine electronic calibration generally ignores the antenna but includes the waveguide and transmitter receiver system. Typically, the following actions are prescribed:

- (a) Measurement of emitted power and waveform in the proper frequency band;
- (b) Verification of transmitted frequency and frequency spectrum, out-of-band power should be filtered;
- (c) Injection of a known microwave signal before the receiver stage, in order to check if the levels of reflectivity indicated by the radar are correctly related to the power of the input;
- (d) Measurement of the signal-to-noise ratio, which should be within the nominal range according to radar specifications.

If any of these calibration checks indicate any changes or biases, corrective adjustments need to be made.

Doppler calibration includes: the verification and adjustment of phase stability using fixed targets or artificial signals; the scaling of the real and imaginary parts of the complex video; and the testing of the signal processor with known artificially generated signals.

Levelling and elevation are best checked by tracking the position of the sun in receive-only mode and by using available sun location information; otherwise, mechanical levels on the antenna are needed. The presence or absence of echoes from fixed ground targets may also serve as a crude check of azimuthal antenna pointing and transmitter or receiver performance.

Although modern radars are usually equipped with very stable electronic components, calibrations must be performed often enough to guarantee the reliability and accuracy of the

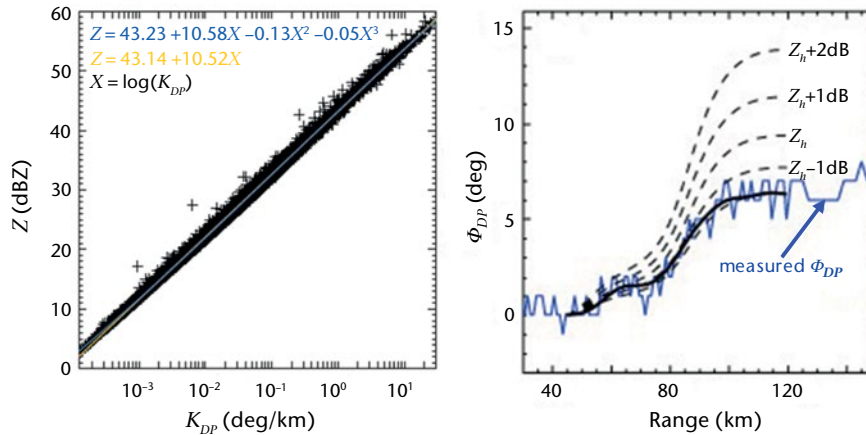


Figure 7.17. There is a close relationship between reflectivity and specific differential phase (Z and K_{DP}). The left figure shows the relationship from disdrometer measurements. The right figure shows one radial of data with significant differential phase. By adjusting the reflectivity and recomputing the differential phase, the radar can be calibrated in a self-consistent manner (figures courtesy of Isztar Zawadzki).

data. Calibration must be carried out either by qualified personnel, or by automatic techniques such as online diagnostic and test equipment. In the first case, which requires personnel, calibration should optimally be conducted at least every six months. Emerging systems may be designed to perform this automatically. Simple comparative checks on echo strength and location can be made frequently, using two or more overlapping radars viewing an appropriate target (Zhang et al., 2005).

Data techniques such as reflectivity accumulations, probability distributions of reflectivity as a function of range for the MDS, transmit–receive cell monitoring, and checking readback and command elevation angles can be used to monitor the health of the radar. Biases in radial velocity accumulations may reveal clutter filtering issues – generally under-filtering which results in biases in radial velocity towards zero (Joe, 2010).

Dual-polarization radars require two receivers that must be matched. Tolerances for all the components need to be tighter since small values are measured. Then, self-consistency and birdbath scans for Z_{DR} nulling can be used to check this. Self-consistency calibration refers to computing Z from K_{DP} using an empirical relationship derived from disdrometer measurements (Figure 7.17) and computed from theoretical formulae. Then, the reflectivity (calibration bias) is adjusted until the K_{DP} derived reflectivity matches the adjusted reflectivity. Given the quality (tightness of the scatter) of the Z – K_{DP} relationship, one could consider using K_{DP} as the dependent parameter for rainfall estimation. If the radar is pointed vertically (the antenna dish appears like a birdbath) in stratiform rain conditions, the Z_{DR} should be zero, and adjustments are needed if it is not. Monitoring the maximum reported ρ_{HV} will provide a check on the overall system performance – good radars should report 0.995 or better.

An innovative technique is the use of the TRMM or GPM space-borne radar for the calibration of ground-based weather radars. It is a single and stable downward-looking instrument that overflies the ground-based weather radars. Comparisons of echo top height, at a fixed and moderately low sensitivity, where attenuation is not significant, are used as the success metric for consistency in cross-radar calibration (Anagnostou et al., 2001).

7.8 RADAR INSTALLATION

7.8.1 Optimum site selection

Optimum site selection for installing a weather radar depends on the intended use. When there is a definite zone that requires storm warnings, the best compromise is usually to locate the equipment at a distance of between 20 and 50 km from the area of interest, and generally upwind of it according to the main storm track. It is recommended that the radar be installed slightly away from the main storm track in order to avoid measurement problems when the storms pass over the radar. At the same time, this should lead to good resolution over the area of interest and permit better advance warning of the coming storms (Leone et al., 1989).

In the case of a radar network intended primarily for synoptic applications, radars at mid-latitudes should be located at a distance of approximately 150 to 200 km from each other. The distance may be increased at latitudes closer to the Equator, if the radar echoes of interest frequently reach high altitudes. In all cases, narrow-beam radars will yield the best accuracy for precipitation measurements.

The adequacy and availability of digital elevation datasets such as GTOPO30 (<https://lta.cr.usgs.gov/GTOPO30>), SRTM30 and SRTM03 (<http://www2.jpl.nasa.gov/srtm/>) have resulted in software applications to help select a site. The basic product is a radar horizon plot where the elevation angle of the horizon, taking into account atmospheric beam propagation, is plotted against radar azimuth angle (Figure 7.18). In this figure, the range to terrain is colour coded as a function of azimuth and elevation angle. The colour indicates the range to which a radar beam (in this case, a 4/3 Earth model is assumed) will collect usable data. This is particularly useful in complex terrain where a radar located in the valley must provide coverage at low levels (in the valley) but with limited range as precipitation changes considerably from mountain crest to mountain valley. For example, the radar can see to 50 or 60 km along the 190° azimuth at elevations of 1° or 2°. This analysis cannot account for trees or artificial towers.

With this plot, the scan angles can be specified for optimal surveillance of the required critical areas. The datasets cannot take into account local blockage due to trees, buildings or towers.

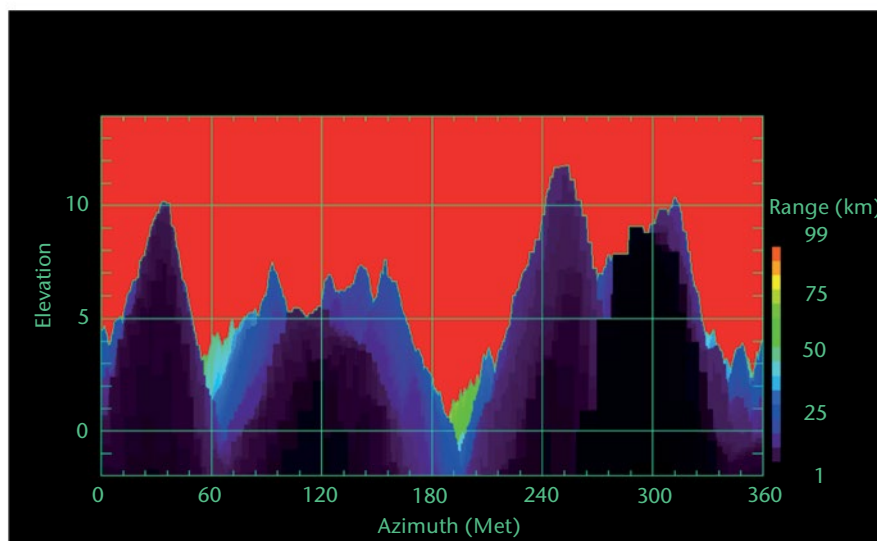


Figure 7.18. Global digital elevation model data are available and sufficiently accurate to be used to assess and help determine the siting of a weather radar. Given an azimuth and elevation, the image indicates the distance in which useful data can be collected.

The choice of radar site is influenced by many economic and technical factors as follows:

- (a) The existence of roads for reaching the radar;
- (b) The availability of power and telecommunication links. It is frequently necessary to add commercially available lightning protection devices;
- (c) The cost of land;
- (d) The proximity to a monitoring and maintenance facility;
- (e) Beam blockage obstacles must be avoided. No obstacle should be present at an angle greater than a half beam width above the horizon, or with a horizontal width greater than a half beam width;
- (f) Ground clutter must be avoided as much as possible. For a radar to be used for applications at relatively short range, it is sometimes possible to find, after a careful site inspection and examination of detailed topographic maps, a relatively flat area in a shallow depression, the edges of which would serve as a natural clutter fence for the antenna pattern side lobes with minimum blockage of the main beam. In all cases, the site survey should include a camera and optical theodolite check for potential obstacles. In certain cases, it is useful to employ a mobile radar system for confirming the suitability of the site. On some modern radars, software and hardware are available to greatly suppress ground clutter with minimum rejection of weather echoes (Heiss et al., 1990);
- (g) When the radar is required for long-range surveillance, as may be the case for tropical cyclones or other applications on the coast, it will usually be placed on a hilltop. It will see a great deal of clutter, which may not be so important at long ranges (see section 7.5.3 for clutter suppression);
- (h) Every survey on potential sites should include a careful check for electromagnetic interference, in order to avoid as much as possible interference with other communication systems such as television, microwave links or other radars. There should also be confirmation that microwave radiation does not constitute a health hazard to populations living near the proposed radar site (Skolnik, 1970, 1990; Leone et al., 1989).

7.8.2 Data exchange, networking, database and processing

Advancements in telecommunications and computer technology allow the transmission of radar data from a large number of sites to a central site for processing and visualization with common computer systems. Given current Internet, cell phone and even satellite data rates and costs, global data exchange of at least limited but useful and usable radar data is conceivable – though the details of telecommunication networks need to be investigated. It should be kept in mind that radars are often located at remote sites where advanced telecommunication systems are not available or the initial capital investments are needed to minimize operating and maintenance costs.

In some countries, multiple radar networks exist to address different applications – weather, aviation hazards at airports, hydrological resource management, ATC and even customs and immigration. Data exchange is conceivable given the caveat that the applications are very specific resulting in very specific data collection methodologies and perhaps even technologies. In some locales, this is operational but requires substantial effort to integrate and interpret.

WMO has existing standards for a few radar products. Anticipating the need for radar data for regional and global NWP, WMO has initiated a WMO radar data exchange project to define standards for raw radar data (Michelson et al., 2013). In addition, a WMO radar database has been created that attempts to provide basic metadata information about radars and radar networks on a global basis (Sireci et al., 2010).

Radar products are exchanged to generate multi-radar composite or mosaic products that are generally intended to represent surface precipitation over a vast area for long-range weather surveillance. This is common within but also between countries. The OPERA (European Operational Programme for the Exchange of Weather Radar Information) consortium is a centralized networking and processing multinational model (Dupuy et al., 2010). The BALTRAD consortium (<http://se.baltrad.eu/>) is another networking and processing model for handling heterogeneous radar networks that is open source with a peer-to-peer data exchange and processing software concept that allows individual members to receive or send data, and configure and process the software as they choose (Michelson et al., 2010). A particular challenge is the compositing of heterogeneous radars consisting of products derived from different geographical projection, spatial and temporal resolution and processing. This has led to the concept of exchanging the polar raw radar data to mitigate these issues. However, depending on the radar and the configuration, various processing steps have already been applied to the raw data to different degrees. These issues also apply to radar data exchange within a country as radars may be of different generations.

In terms of processing, there are many choices these days. Each manufacturer provides their own radar data processing and visualization systems usually with various features, such as networking capability included or for licence. There are also systems such as TITAN (Thunderstorm Identification, Tracking, Analysis and Nowcasting), which is a popular and freely available software used in many research and several meteorological services (Dixon and Wiener, 1993). It initially started as a tool for weather modification activities but has evolved to be multi-purpose. There are many sophisticated commercial systems that are radar system independent and that specialize in advance severe weather applications, such as Warning Decision Support System – Integrated Information (WDSS II) (Lakshmanan et al., 2007; <http://www.wdssii.org/>). One could build a radar system using tools provided by BALTRAD, or the NASA Radar Software Library (Wolff and Kelley, 2009). One could potentially negotiate or collaborate with an NMHS or a government agency for their system. Functionality varies from very basic decoders, to those generating basic products, to those with sophisticated data quality or automated severe storm detection and classification capability. The system to adopt should be based not only on the functionality, but also on the application and the available scientific and technical support and maintenance capacity.

7.9 SOURCES OF ERROR

Errors in the radar data need to be viewed within the context of the application. Precipitation estimation has often been the objective, and stringent data quality procedures need to be applied to remove and correct for the artefacts. There are different levels of data quality control. Hydrological applications require estimates even when the data are poor quality, whereas data assimilation is tolerant of missing data but not of poor data quality. Many of the issues of poor quality radar data are due to the external environment and not to the radar itself (Figure 7.2). It should be noted that these quantitative applications of weather radar are still in development, whereas the qualitative use of radar data for understanding and detecting severe storms is mature, which fully justifies the existence of radar networks.

The radar equation is developed with many assumptions. Whenever these assumptions are not satisfied, the reflectivity may be considered in error. For example, if the target is not uniform or completely filled or is mixed, the equation is not appropriate. Also, if the parameters in the equation, such as antenna gain, waveguide loss or pulse length, are incorrect then the radar constant will be in error and this will result in systematic biases in the conversion from power to reflectivity. In the following, various sources of error are discussed with respect to qualitative and quantitative applications.

Radar beam filling

In many cases, and especially at long ranges from the radar, the pulse width is large and the pulse volume is not completely filled with homogeneous precipitation, that is, it can be only

partially filled. This is particularly true with shallow weather systems (< 1 km in height, as in lake snowstorms), where the beam completely overshoots the precipitation and no precipitation echoes can be seen beyond about 50 km. At long ranges, the pulse volume is very large, and considerable smoothing naturally occurs as the radar beam is convolved with the target. In this situation, the beam is also very high above the Earth's surface and does not quantitatively reflect the surface precipitation very well. With taller systems (say 15 km), the radar will be able to detect these systems at long range (> 250 km) and has considerable value to the forecaster as these systems will be very intense. In general, the radar measurements may be quantitatively useful for ranges of less than about 80 km for a 1° beam width radar and about 110 km for a 0.65° beam width radar without additional adjustments to the data (see Figure 7.33).

Non-uniformity of the vertical distribution of precipitation

Related to radar beam filling is the non-uniformity of the precipitation intensity as a function of height. The first parameter of interest when taking radar measurements is usually precipitation at ground level. As with horizontal variability, the vertical variability or profile plays a significant role in the estimation of surface precipitation. Because of the effects of beam width, beam tilting and the Earth's curvature, radar measurements of precipitation at long ranges or equivalently in height are lower than at the surface (see 7.10.4.1).

Attenuation by intervening precipitation

Attenuation by rain may be significant, especially at the shorter radar wavelengths (5 and 3 cm). Attenuation by snow is less than that of rain but may still be significant over long path lengths. Contrary to common thought, attenuation at S band radar exists, but it is more difficult to identify. Dual-polarization techniques use the specific differential phase (K_{DP}) parameter, which is independent of attenuation and more effective at the shorter wavelengths. K_{DP} is a noisy parameter and the techniques are still being refined (see 7.10.4.4).

Beam blocking

Depending on the radar installation, the radar beam may be partly or completely occulted by the topography or obstacles located between the radar and the target. This results in underestimates of reflectivity and, hence, of rainfall rate. The K_{DP} is a local parameter; it is a measure of the differential attenuation (revealed in phase) within a radar volume, and so it is independent of beam blocking. In the case of narrow blockage, data interpolation may be sufficient for quantitative application. For qualitative usage, beam blockage is a nuisance that the analyst can overcome. When the beam is totally blocked, vertical adjustments using the profile of reflectivity may be used to a degree of success.

Attenuation due to a wet radome

Most radar antennas are protected from wind and rain by a radome, usually made of fibreglass. The radome is engineered to cause little loss in the radiated energy. For instance, the two-way loss due to this device can be easily kept to less than 1 dB at the C band, under normal conditions. However, under intense rainfall, the surface of the radome can become coated with a thin film of water or ice, resulting in a strong azimuth-dependent attenuation.

Combined with precipitation attenuation and at short wavelengths, the radar echoes may be totally suppressed. While this may seem disastrous, pragmatically, it occurs for a limited time (about 10 min), and for qualitative use, warnings will likely already have been issued. For data assimilation, dual-polarization data (K_{DP}) will be available that indicate that severe attenuation has occurred and data beyond will be unusable. For hydrological applications that operate on timescales of hours or days, short-term loss of data for flood forecasting is not significant. Depending on the weather regime, flash flooding prediction may be affected.

Electromagnetic interference

Electromagnetic interference from other radars or devices, such as Radio Local Area Networks (RLANs), is becoming increasingly significant, requiring substantial diligence to protect against it. Interference among adjacent radars is mitigated through the use of slightly different frequencies (but still in the same band) with appropriate filters on the transmitter and receiver. There may be occasional interference from airborne and ground-based C band radars using the same frequency.

Use of the electromagnetic spectrum is determined by agreement and managed through the International Telecommunication Union. At the World Radiocommunication Conference 2003, following demand for spectrum by the wireless community, the C band frequencies were opened up to the telecommunication industry on a regulated secondary non-interfering non-licensed basis to be shared with the meteorological community. In order to be non-interfering, the RLAN devices are supposed to implement Dynamic Frequency Selection, which is designed to vacate a C band channel if a weather radar is detected. However, the algorithms used to detect the weather radar are not sufficient to prevent interference before they vacate the channel. The Doppler spectra of RLAN signals appear as white noise and can be removed with adaptive noise techniques. However, they increase the noise level and reduce the sensitivity of the weather radar where the RLAN is detected. WMO has issued guidance statements relating to the co-use of the C band frequencies. Figure 7.19 shows some examples of this interference for sources at different ranges. Interference patterns like these are increasingly being observed. The image on the left shows a total reflectivity (no Doppler ground clutter filtering) plan position indicator (PPI) image at 0.42° elevation angle from a controlled study where the C band radar with an RLAN was specifically located at 6.4 km at about 40° azimuth. The RLAN is observed at 7° – 10° of azimuth. Nearer (or farther) positioning of the RLAN would result in broader (or narrower) patterns. In the experiment, an RLAN could be observed as far away as 16.7 km (maximum value in a vertical column within the volume scan). The image on the right is a “max reflectivity” product from the operational Ezeiza radar in Argentina and shows a pattern of perhaps 12 RLANs that are within 5 km of the radar. This is an extreme interference example. Also, if nearby, the interference can affect the three-dimensional radar data.

Extreme diligence is needed as these systems will be deployed massively and on a non-licensed basis where violations will be difficult to control. Cooperation and collaboration is expected, required and encouraged. Interference also occurs at S band due to wireless 4G technology and also other S band radars (ATC). WMO has prepared guidelines or statements on spectrum sharing with these new technologies (see Annex 7.B).

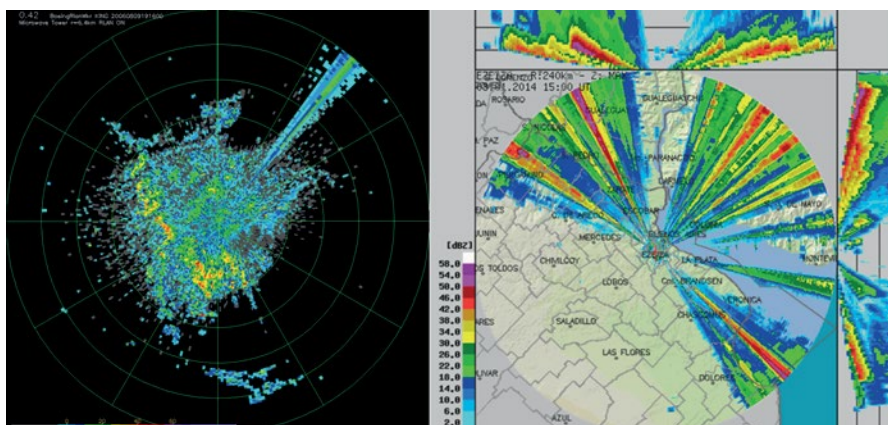


Figure 7.19. The image on the left demonstrates the type of expected interference from a Radio Local Area Network located 6.4 km away at 0.42° elevation angle. The image on the right is from an operational weather radar, courtesy of Claudia Campetella of the Servicio Meteorológico Nacional (Argentina).

Ground clutter

The contamination of rain echoes by ground clutter may cause very large errors in precipitation and wind estimation. Most modern radar antennas have standard side lobe performance that is difficult to improve as it is a geometric issue. Side lobes can be improved or moved to different angular locations, but moving the feed horn away from the focal point results in poorer antenna gain or beam width. The primary method to minimize ground clutter is a good choice of radar location. Ideally, the radar should be located in a slight depression or there should be trees to absorb and scatter the side lobes without blocking the main lobe. Signal and data suppression techniques have been extensively discussed.

Anomalous propagation

Anomalous propagation distorts the radar beam path and has the effect of increasing ground clutter by refracting the beam towards the ground. It may also cause the radar to detect storms located far beyond the usual range, making errors in their range determination because of range aliasing. Anomalous propagation is frequent in some regions, when the atmosphere is subject to strong decreases in humidity and/or increases in temperature with height. Clutter returns owing to anomalous propagation may be very misleading to untrained human observers. These echoes are eliminated in the same manner as ground clutter.

It should be noted that in general the location of the beam is not known since the atmospheric profile of the index of refraction is an idealization (Joe, 1999). Assimilation of radar volume data with the typical number of elevation angles (10–24) is problematic since the numerical weather prediction models now typically have 50–80 model levels. The lack of precise knowledge of the beam location and the mismatch between the number of radar data and model levels preclude the use of the data for assimilation beyond about 100 km.

Antenna accuracy

The antenna position may be known within 0.1° with a well-engineered system. However, positioning errors may arise due to a tilted antenna platform or instability in the feedback loop or mechanism due to wear and tear. This is particularly important at low elevation angles as small changes in elevation angle can result in large changes in coverage of shallow weather.

Electronics stability

Modern electronic systems are subject to small variations with time and have significantly improved since the early days of weather radar where receiver calibrations needed to be done daily. A well-engineered radar can be stable (< 1 dB variation) for months. The addition of a built-in test equipment monitoring system can activate an alarm or issue an e-mail when a fault is detected, and minimize the downtime for weather radars.

Variations in the Z – R relationship

To convert reflectivity to precipitation rate, an empirical relationship between Z and R is needed. The most famous and most frequent relationship used in operational radars is that of Marshall-Palmer (1948, actually reported in Marshall and Gunn, 1952). The uncertainty of this relationship was reported to be a factor of two. It also applies to snow. Reflectivity is a function of the drop size distribution, and different drop size distributions can produce the same Z . Hence, a variety of Z – R relationships have been formulated for different precipitation types – convective, stratiform and snow – with varying degrees of success (see 7.10.4.2). With dual-polarization radar, techniques have now been developed using the K_{DP} dual-polarization parameter. It remains to be seen whether vertical profile adjustment can rival the K_{DP} technique in partially blocked situations.

Radial velocity

The velocities measured by the Doppler radar are in the radial direction only, which can cause ambiguities. Automated interpretation is still an active area of research, but interpretations are possible in certain situations – large-scale synoptic flows and small-scale convective flows – with knowledgeable and well-trained analysts.

The velocities are reflectivity weighted estimates of the precipitation/target motion. If the radial components of the vertical motions are negligible (for example, low elevation angles), they can represent the precipitation motion which can often be interpreted as wind. However, care should be taken to not interpret the velocity as motion of the precipitation echo or system itself. In the example of a lenticular flow over a mountain peak, the echo motion (as indicated by reflectivity) may be stationary but the precipitation particles move through the feature and the echo will have non-zero Doppler. Insects and birds may bias the radial velocities. In general, the biases are relatively small (Wilson et al., 1994) if the birds or insects are not migrating. Ground clutter can also bias the radial velocities towards zero velocity (underestimation) if not enough of the ground echo is removed.

If the wind within a radar volume is not uniform and highly sheared, inaccurate estimates of the radial velocity will result. Consider the extreme case of a tornado that is totally or partially encompassed by radar volume. In the former case, a mean radial velocity of zero with very high spectral width is expected. In the latter case, a non-zero velocity may be expected if the Nyquist velocity is sufficiently high. If the Nyquist is relatively small, the mean velocity may be aliased several times and any velocity may be produced (Fabry et al., 2013). In addition, the weather spectrum may also be aliased, confounding retrieval of both the mean velocity and its spectral width. Dual-PRF techniques also fail in this instance as the uniformity assumption of the two dual-PRF estimates is violated. The antenna rotates as well and so this assumption can be violated in high shear areas, where the two velocity samples at the different PRFs are made at different azimuthal locations and where the velocity has large variance or spectral width. In the latter situation, the error in the technique is determined by this variance and the difference in the unambiguous Nyquist velocities (hence, the ratio of the PRFs). Correction techniques can alleviate the situation of high Doppler variance (Joe and May, 2003). Figure 7.20 shows a simulation. The top image shows a prescribed simulated field with a step in the velocity field. The middle figure shows what a C band Doppler radar would measure. The bottom figure shows the results of the mitigation technique.

Side lobe contamination

When strong reflectivity gradients are present, as in the case of thunderstorms with large wet hail, the side lobes can produce an echo while the main lobe is pointing at a significantly low or no reflectivity target. The side lobes are typically 25 dB or more lower (one way, or 50 dB two way) than the main beam (Figure 7.8). So if the side lobe is pointing at a target that is 60 dBZ in strength, as in the case of wet hail, and the main beam is pointing at a target that is 10 dBZ or lower, the radar will report an echo with reflectivity, radial velocity and dual-polarization characteristics assuming that the power originated in the main beam. Side lobe echoes appear as annular artefacts both in azimuth and elevation at constant range. This can appear as "wings" or "high echo top spikes" near areas of high reflectivities (left and right images in Figure 7.21, respectively). Multiple scattering effects appear as radial artefacts at constant azimuth but with increasing range. These are caused by high reflectivity zones plus reflection effects from a highly reflective surface (ground wetted by rain, for example) and are used as hail indicators in S band radars. Note that in the figure on the right there may have been azimuthal side lobe and/or three-body scattering but this would likely have been obscured by the stronger weather echoes. This is not evident within the thunderstorm area itself as the reflectivity will be dominated by the echo in the main lobe. However, it can be evident in the vertical and result in falsely high echo tops that have been called the hail spike and can be used to qualitatively diagnose hail in a thunderstorm (see Figure 7.21). This type of echo could also occur in the weak echo region that abuts the hail curtain of a thunderstorm, which can confound the interpretation of rotation signatures indicative of the presence of a mesocyclone.

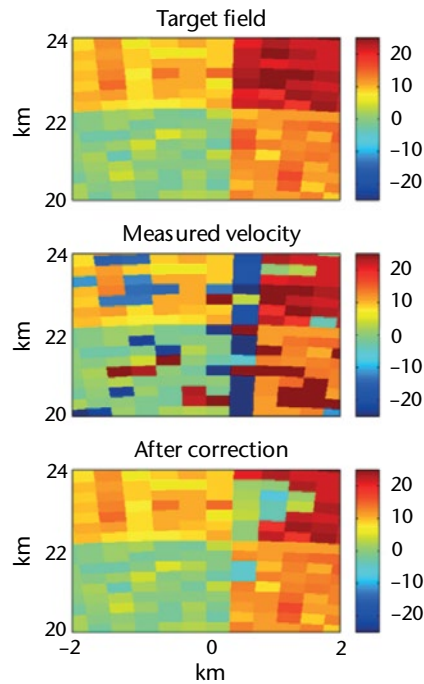


Figure 7.20. The dual-PRF technique assumes that the measurements are made from a volume with the same radial velocity. The images show the prescribed field, the measured and the corrected data. (Figure adapted from Joe and May, 2003)

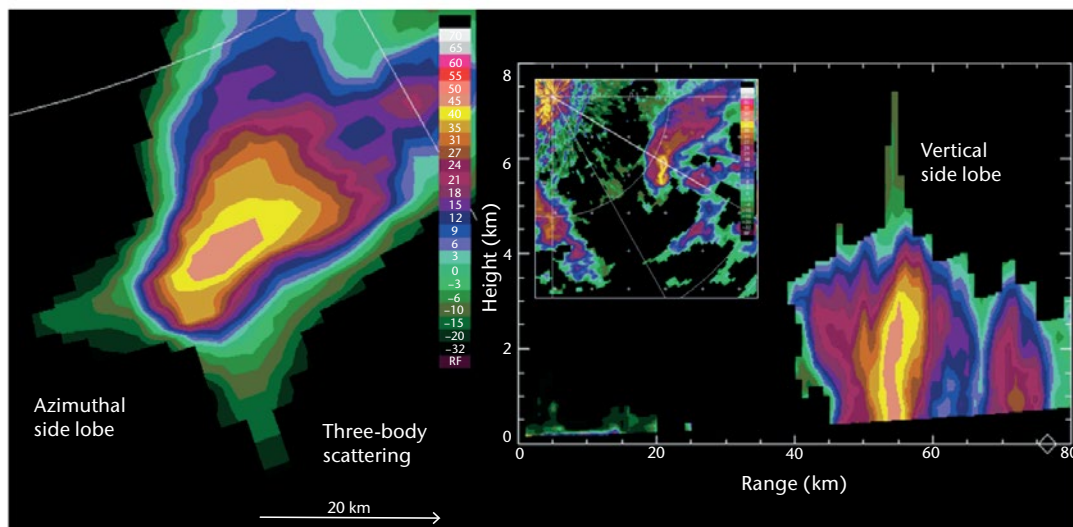


Figure 7.21. Side lobe and multiple scattering effects result in somewhat similar looking artefacts. Side lobe artefacts are at constant range, whereas multiple scattering is at constant azimuth.

Multiple scattering

The radar beam may be reflected multiple times due to the propagation conditions (see Figure 7.22). It may also be multiply scattered within a highly reflective thunderstorm (wet hail), to a wet underlying surface and back to the radar. This has been called three-body scattering and it results in an elongated echo in range beyond the strong reflectivity core (Zrnić et al., 2010).

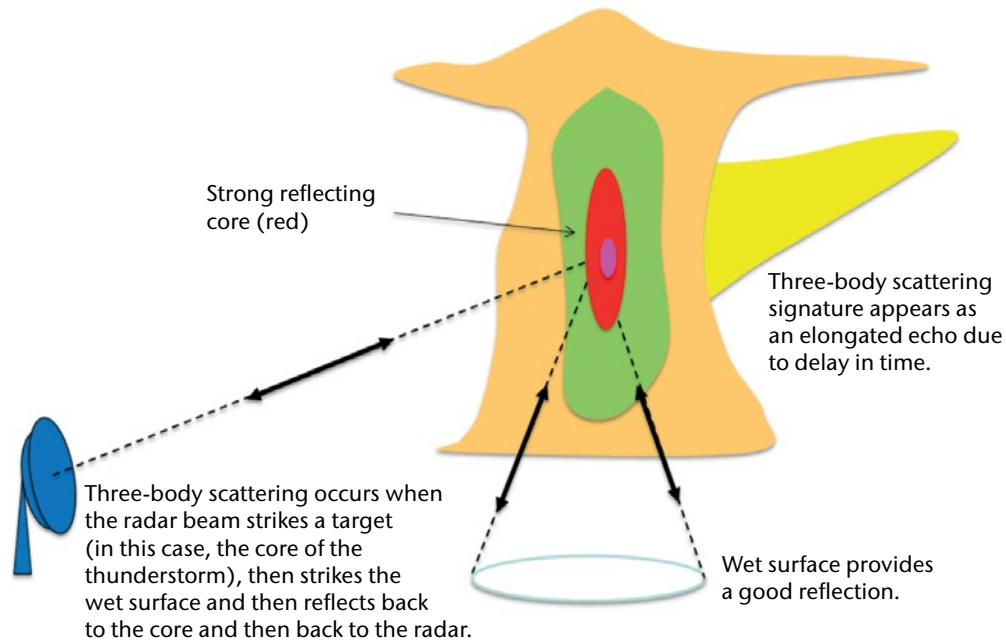


Figure 7.22. This schematic describes how three-body scattering occurs. The echo extending to the right (bright yellow) is an artefact due to the three-body scattering.

At S band radars, this is used as a hail signature, which is called the hail flare to distinguish it from the side lobe hail signature (Lemon, 1998). Multiple scattering is more prevalent as the wavelength decreases and the signature could occur in heavy rain at C or X band.

Second/multiple-trip echo

With the high PRFs used in Doppler radars, multiple-trip echoes may occur. This has already been discussed earlier and the differences between coherent-on-transmit and coherent-on-receive radars were highlighted. Figure 7.7 shows an example of second-trip echoes in reflectivity and radial velocity for a coherent-on-receive radar. In a coherent-on-transmit radar, the second-trip echo algorithm paints the overlapping echoes as range folded.

Wind turbines

An increasing issue is the proliferation of wind turbines and its impact on weather radar. Wind turbines are a source of natural power and sited in remote windy areas. These targets appear in the ground echo (and hence at the lower beams), but the turbine blades provide a moving target and hence generate a varying Doppler signature, and so are difficult to remove. In addition, the turbines are deployed in clusters of 100 or more, creating wind farms. Thus, significant areas will be affected. Figure 7.23 shows two different impacts of wind turbines. If the turbines are located close to the radar, they can create blocked sectors (left image). They may appear as somewhat isolated echoes (not shown). Multiple scattering may be observed (right image). In this example, the wind turbines are about 80–100 km from the radar. WMO has developed guidelines for mutual proximal operation.

Clutter maps may be one technique to remove the echoes. However, this removes the weather echo as well and therefore will require other mitigation strategies to infill the missing data (Figure 7.23). These may include interpolation from the sides or from above or with the use of gap filling data sources. As wind farms are proliferating, ongoing modification or adaptive strategies need to be developed to be able to maintain the data quality for weather applications. If the wind turbines are situated very near the radar, they can be an obstruction to the radar

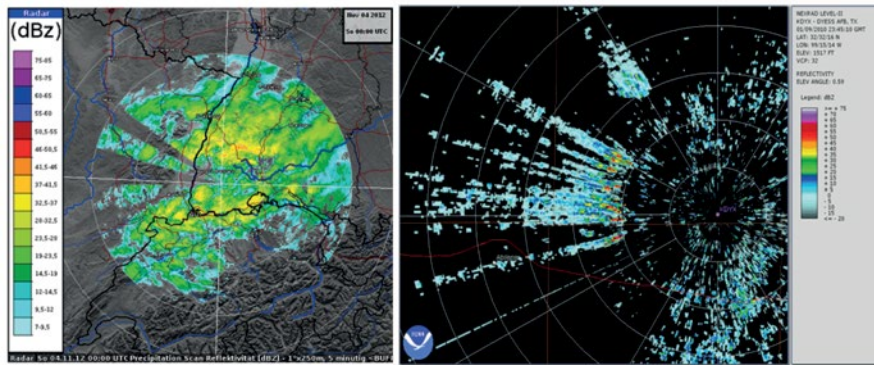


Figure 7.23. The image on the left (courtesy of Deutscher Wetterdienst) shows blocking (west of the radar) by wind turbines, and the image on the right shows interference and multiple scattering effects of the turbines (courtesy of the National Oceanic and Atmospheric Administration).

beam not only in the lower beams but also in the higher elevation beams through direct blockage and also due to multipath. WMO has developed guidelines regarding their deployment (see Annex 7.C).

7.10 OVERVIEW OF METEOROLOGICAL APPLICATIONS

Radar observations have been found most useful for the following:

- (a) Surveillance of synoptic and mesoscale weather systems;
- (b) Severe weather detection, tracking and warning, including severe wind hazard detection;
- (c) Nowcasting;
- (d) Estimation of precipitation intensity, echo classification;
- (e) Wind profiling and wind mapping;
- (f) Initiation of numerical weather prediction models;
- (g) Humidity estimation.

7.10.1 General weather surveillance

Radars can provide a nearly continuous monitoring of weather related to synoptic and mesoscale storms over a large area (say a range of 220 km and an area of 125 000 km²) if unimpeded by buildings, hills, mountains, and the like. Generally, only a single low-level sweep of the radar scanning at approximately 10–30 min is required. Owing to the Earth's curvature and the propagation of the radar beam, the maximum practical range for weather observation is about 250 to 350 km, as the radar will overshoot the weather at longer ranges. While radars have sufficient sensitivity to detect to farther ranges, the limit of modern radars is due to the beam height location. A radar with a 1° beam width antenna pointed at 0.5° elevation angle above the horizon is approximately 10 km above the Earth's surface at a range of 350 km. In addition, the beam width at that range is about 7 km wide. Shorter storms would not be detected or would be distorted in their representation. So storms must be substantial in size to be detected at that range. Pragmatically, scans of even 500 km or more are operationally used, particularly at the edges of radar networks. If echoes are detected, the forecaster will be provided with substantial information of a large and intense storm. Satellites and lightning detection networks may

provide information on the clouds and the electric activity that produce or are associated with the precipitation. Exchange of radar data to create a radar network is de rigueur and mandatory to create mosaic products for surveillance.

Another surveillance application is the detection of shallow weather (< 1 km), such as lake effect snow squalls, drizzle or even duststorms. Narrower beam widths provide better resolution and greater effectiveness at longer ranges as they can scan at lower elevation angles without additional ground clutter effects, can provide a filled beam to longer ranges and have greater sensitivity due to greater gain. Networks of low maintenance, low infrastructure and low cost X band radars are emerging which can fill this low-level scanning gap of large S and C band radars.

The cooperative exchange of weather-radar data among various operators is now important in radar applications. It can achieve broader views of large-scale precipitation systems, such as synoptic scale fronts and typhoons. Standard radar data formats would enable and facilitate the efficient development of inter-network products. A leading example is that done in the OPERA consortium.

Radar networks employing adaptive and collaborative scanning strategies are emerging (McLaughlin et al., 2009; Weber et al., 2007). Phased array radars with electronic steering capability are being developed that can scan in non-contiguous azimuthal and elevation directions to provide high temporal sampling of rapidly changing weather phenomena, such as tornadoes and downbursts, and even other targets such as aeroplanes. Adjacent radars may also fill low-level gaps in coverage due to beam propagation effects at long range and perhaps the "cone of silence" due to limited elevation scanning.

7.10.2 **Severe weather detection and warning**

A radar is the only realistic means of monitoring severe weather over a wide area (hundreds of kilometres of range) due to the temporal resolution (minute), spatial resolution (kilometres) and detected weather elements (reflectivity from precipitation). Radar echo intensities, area and patterns are used to identify areas of severe weather, including thunderstorms with probable hail and damaging winds. Doppler radars can identify and provide a measurement of intense winds associated with gust fronts, downbursts and tornadoes to add an additional dimension (Lemon, 1978). Dual-polarization radars have the capability to separate echoes due to different types of scatterers and can distinguish hail from heavy rain and rain from snow (Zrnić et al., 2001). The nominal range of coverage of a single radar is about 250 km, which is sufficient for local short-range forecasting of about 1–2 h lead time and warning. Radar networks extend the coverage and lead time (Germann et al., 2006b). Effective warnings require effective interpretation performed by alert and well-trained personnel.

Technique for thunderstorm warning by radar

The technique for using radar for the provision of warnings is attributed to Lemon (1978), who outlined the reflectivity features to identify for the provision of severe thunderstorm warnings that include tornadoes, strong wind, heavy rain, flash flooding and hail. Since then, Doppler and dual-polarization features as well as additional reflectivity features have been added to the list of criteria. Figure 7.24 lists (on the left) and provides an example (on the right) of the severe weather features (Lemon, 1978; Lemon et al., 1978). These features include strong reflectivities aloft, high echo tops, weak echo regions aloft indicative of strong updraughts, strong low-level reflectivity gradients and low-level hook patterns. A set of the multi-panel images (shown on the right in Figure 7.24) is called a cell view and is automatically created once a cell has been identified in radar data-processing software. The sub-images are derived radar products that a severe weather analyst would use to decide on the storm severity, its stage in the life cycle and whether to issue a warning. Given the location of various features of the thunderstorm (for example, location of the echo top, location of the storm centroid or location of the bounded weak echo region), cross-section lines can be configured and vertical cross-sections can be automatically created.

1. Large cell with strong elevated reflectivity (MAX R > 45 dBZ)
2. Tall (high echo top)
3. Weak echo region
4. Hook/kidney beam shape
5. Echo top over the updraught/low-level reflectivity gradient
6. Rotation mesocyclones
7. Downdraughts
8. Hail

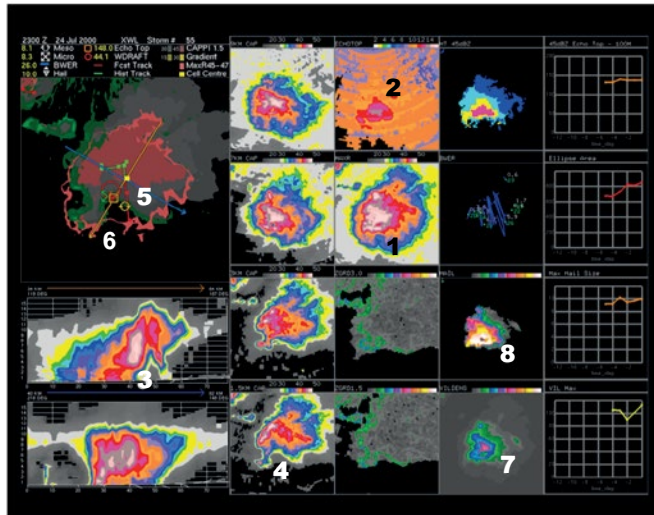


Figure 7.24. The severe storm features are listed on the left (Lemon, 1978). The cell-view product is an image centred on the automatically detected thunderstorm cell and shows relevant products for decision-making (number in cell view matches the list number).

The temporal and three-dimensional spatial relationship is important to diagnose the life cycle phase of the storm for anticipating its evolution and hence for its warnings. This is a challenging problem and not every thunderstorm produces weather reaching the severity threshold for warnings (see Table 7.9). The original technique, that is still used today, was applied by examining various radar products and interrogating the data in various ways (Figure 7.24).

The application of Doppler radar to real-time detection and tracking of severe thunderstorms began in the early 1970s. Donaldson (1970) was probably the first to identify a vortex flow feature in a severe thunderstorm. Quasi-operational experiments have demonstrated that a very high percentage of these single-Doppler vortex signatures are accompanied by damaging hail, strong straight wind or tornadoes (Ray et al., 1980; JDOP, 1979). This vortex is known as a mesocyclone, which is a vertical column of rising rotating air typically 2 to 10 km in diameter. The mesocyclone signature is a small anomalous Doppler velocity pattern and is first observed in the mid-levels of a storm that descends to cloud base and may be coincident with the presence of severe weather (Markowski, 2002; Burgess, 1976; Burgess and Lemon, 1990; Figure 7.25). Mesocyclonic rotation in severe storms indicates a strong and long-lived storm deserving of a severe weather warning. This is identified as small quasi-circular areas of away and towards radial velocities aligned approximately at constant range in an azimuthal direction, as can be seen in Figure 7.25. It should be noted that storm motion should be removed to easily see the away/towards couplet. In the northern hemisphere, the rotation is generally (but not always) counter-clockwise and vice versa in the southern hemisphere. This behaviour has led to improved severe

Table 7.9. Thunderstorm characteristics for different warning thresholds

Thresholds	Rank weight	Rank (0–8)	Bounded weak echo region count	Mesoscale shear (m/s/km)	Hail size (cm)	Downdraught (m/s)	VIL density (kg m ² /km)	Max Z (dBZ)	45 dBZ echo top height (km)
Minimum	1	0–2	5–11	4	0.5	10	2.2	30	5.5
Weak	2	3–4	12–17	6	1.3	15	3.0	45	8.5
Moderate	3	5–6	18–21	8	2.3	20	3.5	50	10.5
Severe	4	7+	22–26	10	5.0	25	4.0	60	12.5

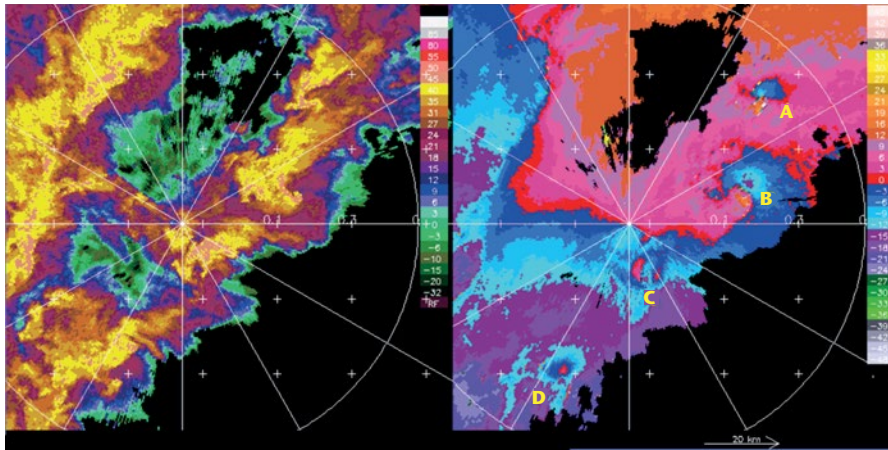


Figure 7.25. Multiple mesocyclones (A–D) are observed along a squall line and are identified as couplets of relative away and towards velocities at constant range. Symmetric velocity signatures observed in the storm are not evident or have been removed.

storm and tornado warning lead times of 20 min or longer during quasi-operational experiments in Oklahoma (JDOP, 1979). During these experiments, roughly 50% of all mesocyclones produced verified tornadoes; also, all storms with violent tornadoes formed in environments with strong shear and possessed strong mesocyclones (Burgess and Lemon, 1990).

A tornado is approximately 200–500 m in diameter. This is often at the resolution of the radar data and so difficult to consistently detect unless a high zoom magnification is employed. When detected, it is observed as a large difference in radial velocity in adjacent radar data volumes and called the tornado vortex signature, and this is embedded within the mesocyclone (Figure 7.26). In some cases, the tornado vortex signature has been detected aloft nearly half an hour or more before a tornado touched the ground. Several years of experience with the tornado vortex signature have demonstrated its great utility for determining tornado location, usually within ± 1 km. It is estimated that 50% to 70% of the tornadoes east of the Rocky Mountain high plains in the United States can be detected (Brown and Lemon, 1976). Large Doppler spectrum widths (second moment) have been identified with tornado location. However, large values of spectrum width have also been well correlated with large values during storm turbulence. In the reflectivity image (Figure 7.26, left image), a classic hook echo is observed and is indicative of precipitation associated with a strong downdraught in the rear of the strong thunderstorm.

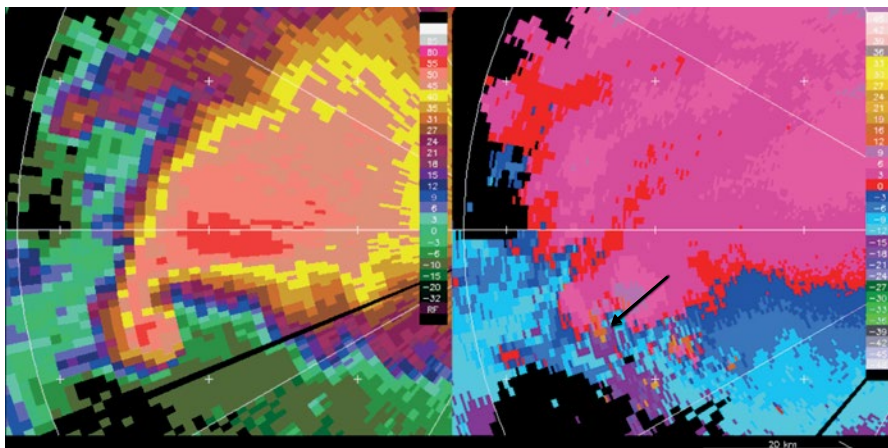


Figure 7.26. A tornado vortex signature is identified as an away/towards couplet on adjacent range bins (see arrow on right image), embedded within a mesocyclone. The image on the left shows a classic hook echo.

Divergence calculated from the radial velocity data appears to be a good measure of the total divergence. Estimations of storm-summit radial divergence match those of the echo top height, which is an updraught strength indicator. Quasi-operational Doppler experiments have shown that an increase in divergence magnitude is likely to be the earliest indicator that a storm is becoming severe. Moreover, large divergence values near the storm top were found to be a useful hail indicator. Low-level divergence signatures of downbursts have been routinely made with terminal Doppler weather radars for the protection of aircraft during take-off and landing. These radars are specially built for limited area surveillance and repeated rapid scanning of the airspace around the airport terminals. The microburst has a life cycle of between 10 to 20 min, which requires specialized radar systems for effective detection (see Figure 7.27). This is an example of a wet downdraught and has a strong associated reflectivity. Dry downdraughts may not be identifiable in the radar data if the precipitation evaporates and if there are no other targets for the radar to detect. In this case, a highly sensitive radar is required or a Doppler lidar or anemometer network. In this application, the radar computer system automatically provides warnings to the ATC tower (Michelson et al., 1990). Mesoscale winds (40–50 km in scale) are difficult to interpret with Doppler radar as the orientation of the flows confounds the assumption of uniformity. Assumptions have to be made of the wind direction based on research studies and conceptual models of the airflow within these systems (Smull and Houze, 1987). Fortunately, in some cases, the flows and the reflectivity structure are distinctive and strong winds can be identified and warnings provided. Figure 7.28 shows a system moving to the east, and hence the full strength of the straight line winds (also known as a derecho) is evident in the away (orange) radial velocities (marked A). In this case, the away velocities are moving into towards velocities. This is also shown in the bowing of the reflectivity echo (left image). At other azimuths, the radial wind is not perpendicular to the system motion (marked B) and the analyst must take this into account.

The best method for measuring winds inside precipitation is the multiple Doppler method, which has been deployed since the mid-1970s for scientific research field programmes of limited duration. However, real-time operational use of dual- or triple-Doppler analyses is not anticipated because of the need of relatively closely spaced radars (~40 km). An exception may be the limited area requirements of airports, where a network of X band radars may be useful (McLaughlin et al., 2009; Wurman et al., 1995).

Many techniques have been proposed for identifying hail with 10 cm conventional radar, such as the presence of 50 dBZ echo at 3 or 8 km heights (Dennis et al., 1970; Lemon et al., 1978). Empirical but limited studies have shown the ability to predict hail size (Treloar, 1998; Joe et al., 2004; Witt et al., 1998). Federer et al. (1978) found that the height of the 45 dBZ contour must exceed the height of the zero degree level by more than 1.4 km for hail to be likely. An extension

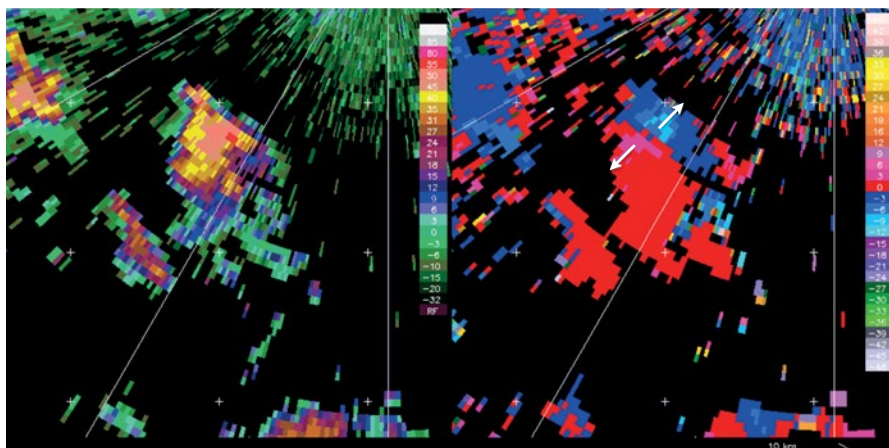


Figure 7.27. A downburst (micro or macro) is observed as a couplet of away and towards radial velocities aligned along a radial (see arrows on the right image). This is a rapidly evolving feature of thunderstorms, and can emanate from very ordinary and small thunderstorms.

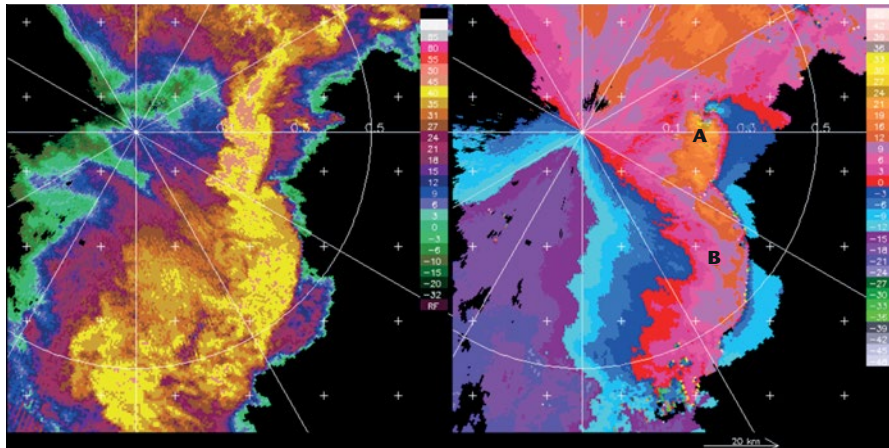


Figure 7.28. Another signature of strong intense hazardous winds can be observed as a linear or curvilinear feature in the reflectivity (left) or radial velocity data (right).

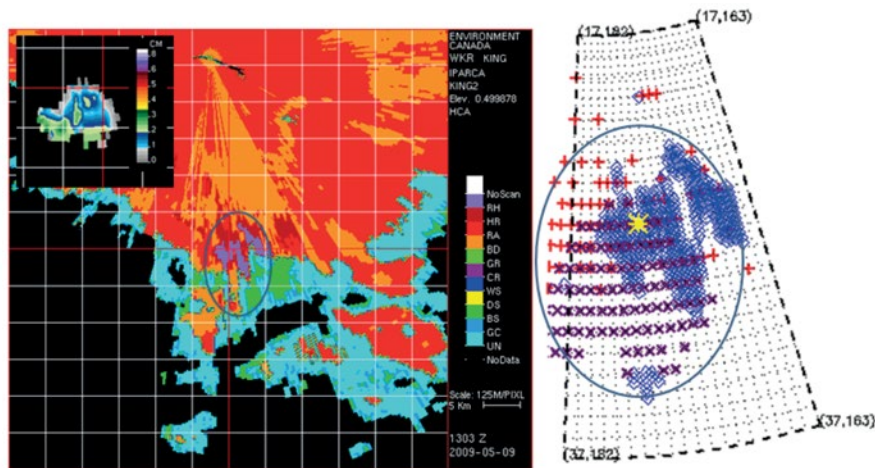


Figure 7.29. The inset figure is a reflectivity-based hail size product and the large image is a polarization diversity product to identify precipitation type, including hail. The image on the right provides detailed analysis of this example. Figure is courtesy of Sudesh Boodoo of Environment Canada.

of this method has been verified at the Royal Netherlands Meteorological Institute and is being used operationally (Holleman et al., 2000; Holleman, 2001). A different approach towards improved hail detection involves the application of dual-wavelength radars – usually X and S bands (Eccles and Atlas, 1973). The physics of what the radar sees at these various wavelengths is crucial for understanding the strengths and limitations of these techniques (hydrometeor cross-section changes or intensity distribution).

Studies of polarization diversity show some promise of improved hail detection and heavy rainfall estimation based upon differential reflectivity (Z_{DR}) as measured by a dual-polarization Doppler radar (Seliga and Bringi, 1976; Figure 7.29). The image on the left shows a classification of the radar echo using dual-polarization signatures of a hail situation. Fuzzy logic techniques are commonly used to combine various dual-polarization parameters such as Z , Z_{DR} , ρ_{HV} and K_{DP} to identify the nature of the radar echo. In this case, the classification scheme is indicated in the left image and includes (from top to bottom): hail, heavy rain, rain, big drops, graupel, ice crystals, wet snow, dry snow, biological scatters and ground clutter. The inset image is a hail size estimate based on combining vertically integrated liquid (VIL), MAX reflectivity and freezing level (Treloar, 1998; Joe et al, 2004). A maximum hail size of 3.2 cm is indicated. The image on the right compares, in detail, the dual-polarization hail detection using data at two different resolutions (plus signs for 1 km resolution and diamond symbols for 250 m resolution) and slightly different

times compared to the older reflectivity only technique (crosses). The blue ellipse corresponds to the blue ellipse in the left image. All three algorithms verified with the 3+ cm hail reported at the airport (yellow mark, middle of the red grid lines).

Recent advances include the automated detection and classification of thunderstorms through advanced processing techniques (Lakshmanan et al., 2007; Joe et al., 2002; Joe et al., 2012). Thunderstorms evolve on a temporal scale of minutes and precipitation initiates aloft. So, radar features both aloft and near the surface are used for identification of severe weather. Hence, the radar should scan in multiple elevation angles with a cycle time of the order of 5 min.

Doppler radars are particularly useful for monitoring tropical cyclones and providing data on their eye, eye wall and spiral-band dynamic evolution, as well as the location and intensity of hurricane-force winds (Ruggiero and Donaldson, 1987; Baynton, 1979).

7.10.3 Nowcasting

A strict definition of nowcasting is that it is a prediction in the 0–2 h timescale and, traditionally, it refers to automated linear extrapolation of the current situation as revealed by observations. The original nowcasting system was based on doing a cross-correlation analysis of two radar images (CAPPI) for the echo motion (Bellon and Austin, 1978). The motion analysis was done in nine sectors of the image and used to extrapolate the echoes up to 90 min into the future. Points were identified for the nowcasts and a meteogram was created that indicated the most likely and probable values (Figure 7.30). The figure on the left is a single image of weather, presented as a CAPPI, that is moving to the north-east. The figure on the right shows the nowcast (the most likely, left column, and the most probable reflectivity, right column) for various points. Only two points are indicated in this example for clarity of presentation. This is a meteogram presented as an image (current time is at the top, and future time increments are presented downward in 10 min steps). An inherent assumption in this nowcast is that the precipitation system persists for the next 90 min. This illustrates the specificity characteristic of nowcasts and their precision in terms of time, space and weather element. The skill of this nowcast is very high for the first 20–30 min and it is used as a call to action or warning service. No evolution is assumed.

Using continental composite of radar data and a scaling approach to filter out the high-frequency or small-scale reflectivity patterns, nowcasts of the large-scale patterns have skill out to six or more hours that exceeds the skill of the numerical weather prediction models at this time. This is compared to the 2 to 3 h for the smaller scales. However, the skill levels are not capable of providing the precision needed for call-to-action type warning services.

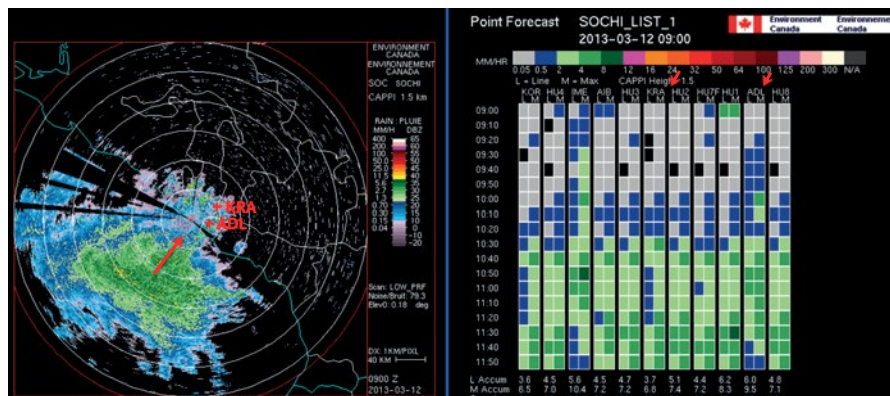


Figure 7.30. An example of a cross-correlation nowcast; the weather is moving from the south-west (left image) and the meteogram on the right shows the most likely and most probable precipitation intensities at different locations (only Kerang (KRA) and Adelaide (ADL) are shown on the left, which are the sixth and tenth sites on the right image).

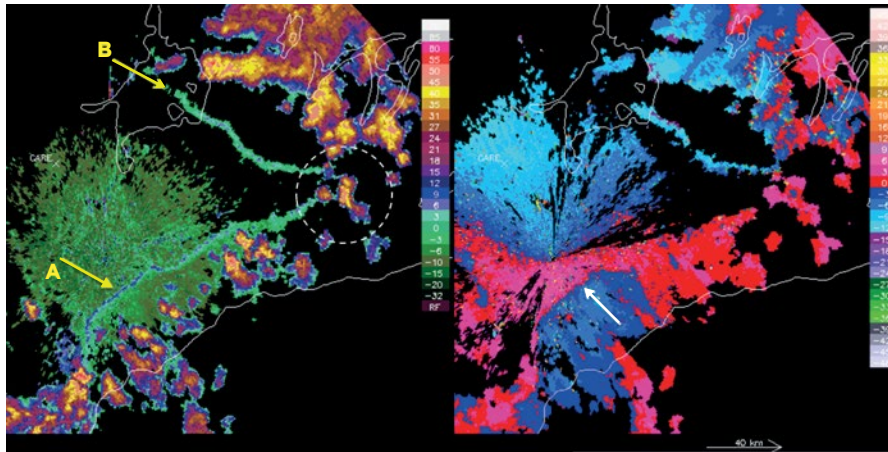


Figure 7.31. Modern radars are sensitive enough to see lake breeze and thunderstorm outflows (A, B, respectively, left image). The intersection is a location of enhanced lift and therefore a location of potential convective initiation (see the storm forming within the dashed white circle).

Doppler radar studies of the role of boundary layer convergence lines in new thunderstorm formations support earlier satellite cloud-arc studies. There are indications that mesoscale boundary-layer convergence lines (including intersecting gust fronts from prior convection) play a major role in determining where and when storms will form. Wilson and Schreiber (1986) have documented and explained several cases of tornado genesis by non-precipitation induced wind shear lines, as observed by Doppler radar (Mueller and Carbone, 1987).

An important nowcasting application is the analysis of the radar fields for the initiation of convection. Recent scientific studies have shown that airmass thunderstorms, which were previously thought to be random and unpredictable, actually form on small-scale atmospheric boundaries (Wilson et al., 1998). These boundaries can be detected in both the reflectivity and radial velocity fields in the clear air echoes as line features or convergence lines (Figure 7.31). The boundaries are formed by a variety of mechanisms including lake breezes (A), thunderstorm outflows (B), drainage flows from mountain valleys, dry lines and others. Enhanced lift occurring at the intersection of these boundaries can initiate thunderstorms. Note the distinctive convergence signature in the radial velocity image (white arrow, right image).

The source of the clear air echoes can be turbulent fluctuations or insects. Polarization radar studies indicate that insects are the primary source of these radar returns. Extensions to the traditional nowcasting systems include the prediction of convective initiation and dissipation, modelling the life cycle of thunderstorms, and using numerical weather prediction models in the analysis (Wilson et al., 1998; Sun et al., 2013). In addition to the radar data, associated model fields, such as temperature and humidity, are also extrapolated (Crook and Sun, 2002; Sun et al., 2013). Increasing the cycle time (rapid update to 1 h or better), reducing the spin up and improving the physics of high-resolution models are improvements that are anticipated (Sun et al., 2013). Another emerging nowcasting application is the development of ensemble precipitation nowcasts where the small scales are both filtered and re-created using a family of statistically consistent estimates (Seed, 2003).

7.10.4 Precipitation estimation

Radars have a long history in estimating the distribution, the intensity and thereby the amount of precipitation with a good resolution in time and space. Most studies have been associated with rainfall, but snow measurements can also be taken with appropriate allowances for target composition. The retrieval of precipitation intensity is mainly based on empirical relationships from the returned power or reflectivity (Marshall and Palmer, 1948; Marshall and Gunn, 1952; Wilson and Brandes, 1979; Chandrasekar et al., 2003). Dual-polarization radars use additional information based on the shift in the phase of the attenuated propagating wave and on the

differential scatter due to the large non-spherical particles. Comprehensive hail studies are rare due to difficulty in gathering ground truth information. Readers should consult reviews by Joss and Waldvogel (1990), and Smith (1990) for a comprehensive discussion of the problems and pitfalls, and the effectiveness and accuracy. Emerging radar processing systems are able to remove ground clutter (including anomalous propagation) in a variety of ways, and mitigate the vertical profile of reflectivity problem by adjustment with gauges or disdrometers in quasi-real-time.

7.10.4.1 **Vertical profile of reflectivity**

At long ranges, errors caused by the inability to observe the precipitation close to the ground and the lack of beam filling are usually dominant. Because of growth or evaporation of precipitation, air motion and change of phase (ice and water in the melting layer, or bright band), highly variable vertical reflectivity profiles are observed, both within a given storm and from storm to storm. In convective rainfall, experience shows that there is less difficulty with the vertical profile problem. However, in stratiform rain or snow, the vertical profile becomes more important. With increasing range, the beam becomes wider and higher above the ground. Therefore, the differences between estimates of rainfall by radar and the rain measured at the ground also increase. Reflectivity usually decreases with height; therefore, rain is underestimated by radar for stratiform or snow conditions. Figure 7.32 shows three idealized vertical profiles of reflectivity for different weather situations. They are shown at zero range. These profiles are increasingly smoothed with range due to the broadening of the beam. The beam propagation effect also occurs, and the lower part of the profile no longer contributes to the measured value. At long ranges, for low-level storms, and especially when low antenna elevations are blocked by obstacles such as mountains, the underestimate may be severe. This type of error often tends to dominate all others. This is easily overlooked when observing storms at close ranges only, or when analysing storms that are all located at roughly the same range. The effective range for quantitative precipitation estimation is about 80 km for a 1° beam width radar (Figure 7.33) and longer for smaller beam width radars (120 km for 0.65° beam width radar) without adjustment.

In shallow weather that is prevalent in winter conditions, the beam smoothing effect (illustrated in Figure 7.32) reduces the reflectivity with range. This results in accumulations (radar reflectivity

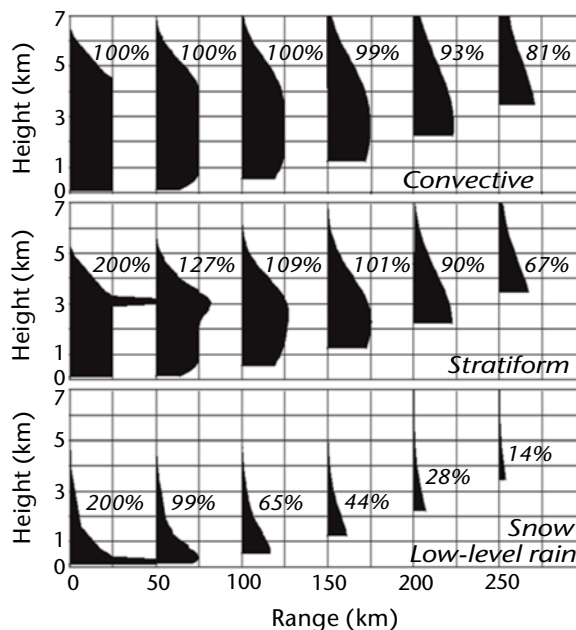


Figure 7.32. Beam smoothing and beam propagation modify the appearance of the vertical profile of reflectivity with range. Three situations are depicted with the maximum reflectivity in the column as a percentage of the surface precipitation taking into account the bright band (adapted from Joss and Waldvogel, 1990).

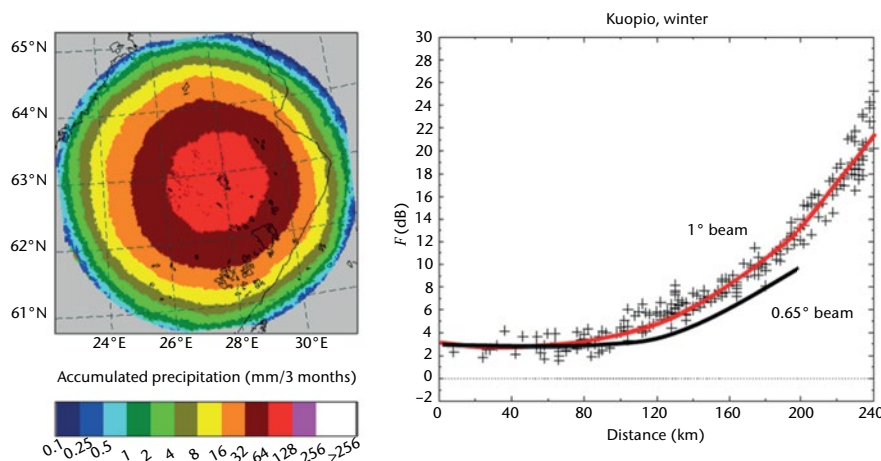


Figure 7.33. This shows an accumulation of radar-derived precipitation over a winter season. The annular pattern is primarily due to the lack of beam filling at long ranges for shallow winter weather systems. The right image shows how this is reflected as a range bias with the radar–gauge comparisons (figure courtesy of Daniel Michelson of the Swedish Meteorological and Hydrological Institute using data from the Finnish Meteorological Institute).

or derived precipitation rate) that take on an annular pattern shown in the left image of Figure 7.33. Non-uniform filling of the radar volume with range also contributes to the rapid reduction in the reflectivity. Comparisons with values measured with gauges over a season are shown on the right (ratio of the radar versus in situ gauge measurements), illustrating this degradation in measured precipitation amounts. In this particular location, with this 1° beam width radar and this weather regime (Finland in winter), the effective range (the flat part of the curve) is about 80 km for direct precipitation estimates. Since the effect is geometric, a smaller beam width would extend this effective range. This is illustrated for a 0.65° beam width, where the effective range is extended to about 110–120 km.

No one method of compensating for the effects of the vertical reflectivity profile in real time is widely accepted. However, three compensation methods can be identified:

- (a) Range-dependent correction: The effect of the vertical profile is associated with the combination of increasing height of the beam axis and spreading of the beam with range. Consequently, a climatological mean range-dependent factor can be applied to obtain a first-order correction. Different factors may be appropriate for different storm categories, for example, convective versus stratiform;
- (b) Spatially varying adjustment: In situations where the precipitation characteristics vary systematically over the surveillance area, or where the radar coverage is non-uniform because of topography or local obstructions, corrections varying with both azimuth and range may be useful. If sufficient background information is available, mean adjustment factors can be incorporated in suitable look-up tables. Otherwise, the corrections have to be deduced from the reflectivity data themselves or from comparisons with gauge data;
- (c) Full vertical profiles: The vertical profiles in storms vary with location and time, and the lowest level visible to the radar usually varies because of irregularities in the radar horizon. Consequently, a point-by-point correction process using a representative vertical profile for each zone of concern may be needed to obtain the best results. Representative profiles can be obtained from the radar volume scan data themselves, from climatological summaries or from storm models. This is the most complex approach but can be implemented with modern data systems (Joss and Lee, 1993).

Figure 7.34 shows an example of the latter method of correcting for the vertical profile of reflectivity with range effect, which is now routinely used on a radar network basis. The figure on

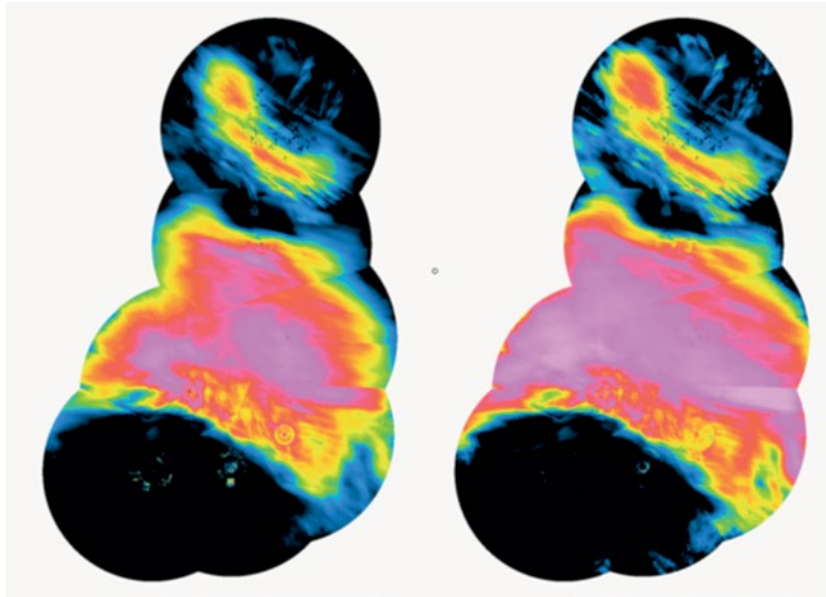


Figure 7.34. This shows the case of an east-west stationary front. The image on the left shows the fall off with range (see Figure 7.33). The image on the right shows the range adjustment made to the data (figure courtesy of Jarmo Koistinen, Finnish Meteorological Institute).

the left shows a 24 h accumulation of radar-derived precipitation rate during a stationary front passage. The pattern would be expected to be broadly uniform. The figure on the right is created with an adjustment for the vertical profile effect at long ranges, and hence the accumulations at the edges are enhanced. The difference in the images also illustrates the benefits of a network approach to generating precipitation products, as the vertical profile effect of the individual radars is not so evident in the interior of the network.

Improvements in digital radar data processing and real-time integration with gauge networks have led to the development of new quantitative, radar-based products for hydrometeorological applications. A number of European countries and Japan are using such radar products with numerical models for operational flood forecasting and control (Berenguer et al., 2012; Cluckie and Owens, 1987). The synthesis of radar data with raingauge data provides a powerful nowcasting product for monitoring rainfall. Radar-AMeDAS Precipitation Analysis is one of the products provided in Japan (Makihara, 2000). Echo intensity obtained from a radar network is converted into precipitation rate using a $Z-R$ relationship, and 1 h precipitation amount is estimated from the precipitation rate. The estimated amounts are then calibrated using raingauge precipitation amounts to provide a map of 1 h precipitation amount with high accuracy.

7.10.4.2 **The $Z-R$ relation**

In ideal conditions (close to the radar, no artefacts), precipitation is usually estimated by using the $Z-R$ relation:

$$Z = A R^b \quad (7.13)$$

where A and b are constants. The relationship is not unique and many empirical relations have been developed for various climates or localities and storm types. Nominal and typical values for the index and exponent are $A = 200$, $b = 1.60$ (Marshall and Palmer, 1948; Marshall and Gunn, 1952). This can be applied to an accuracy of a factor of two for both rain and snow. The equation is developed under a number of assumptions that may not always be completely valid. Nevertheless, history and experience have shown that the relationship in most instances provides a good estimate of precipitation at the ground unless there are obvious anomalies (Figure 7.35). A survey of the $Z-R$ relationships in worldwide use indicated that the Marshall-

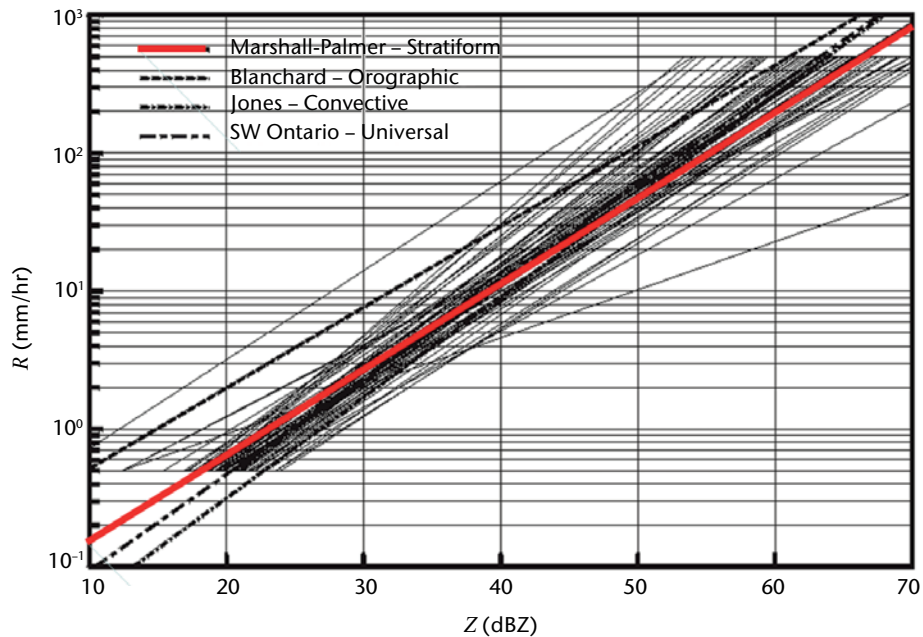


Figure 7.35. A plot of a plethora of Z - R relationships from Battan (1973)

Palmer relationship is used in 80% of the operational weather radars – a remarkable achievement considering the very few data points used to form the original relationship (Sireci et al., 2010). The red line in Figure 7.35 represents the original Marshall-Palmer relationship (reported in Marshall and Gunn, 1952, and Marshall and Palmer, 1948). Attempts at improvements have been made throughout the years and the black lines represent these other relationships (Battan, 1973). It is remarkable that the original relationship, made with few measurements and in a specific weather regime, has stood the test of time.

There are some generalities that can be stated. At 5 and 10 cm wavelengths, the Rayleigh approximation is valid for most practical purposes unless hailstones are present ($Z > 57$ dBZ is often taken as the boundary between rain and hail). Large concentrations of ice mixed with liquid can cause anomalies, particularly near the melting level. By taking into account the refractive index factor for ice (that is, $|K|^2 = 0.208$) and by choosing an appropriate relation between the reflectivity factor and precipitation rate (Z against R), precipitation amounts can be estimated reasonably well in snow conditions (the value of 0.208, instead of 0.197 for ice, accounts for the change in particle diameter for water and ice particles of equal mass). However, snowfall gauge measurements are problematic and there are few comprehensive studies of radar-snowfall relationships.

The rainfall rate (R) is a product of the mass content and the fall velocity in a radar volume. It is roughly proportional to the fourth power of the particle diameters. Therefore, there is no unique relationship between radar reflectivity and the precipitation rate since the relationship depends on the particle size distribution. Thus, the natural variability in drop size distributions is an important source of uncertainty in radar precipitation measurements when other factors are taken into account.

Empirical Z - R relations and the variations from storm to storm and within individual storms have been the subject of many studies over the past 40 years, particularly for storm event studies. A Z - R relation can be obtained by calculating values of Z and R from measured drop size distributions produced by an instrument known as a disdrometer. An alternative is to compare Z measured aloft by the radar (in which case it is called the equivalent radar reflectivity factor and labelled Z_e) with R measured at the ground. The latter approach attempts to reflect any differences between the precipitation aloft and that which reaches the ground. It may also include errors in the radar calibration, so that the result is not strictly a Z - R relationship.

Disdrometers are now being deployed in operational networks for determining the Z - R relationship for climatology, storm studies and real-time adjustment, and are very sensitive and can detect very light precipitation.

The possibility of accounting for part of the variability of the Z - R relation by stratifying storms according to rain type (such as convective, non-cellular, orographic) has received a good deal of attention. Although variations in the drop size distribution are certainly important, their relative importance is frequently overemphasized. After some averaging over time and/or space, the errors associated with these variations will rarely exceed a factor of two in rain rate. They are the main sources of the variations in well-defined experiments at near ranges.

7.10.4.3 **Gauge adjustment**

There is general agreement that comparisons with gauges should be made routinely as a check on radar performance, and that appropriate adjustments should be made if a radar bias is clearly indicated. However, this needs to be done judiciously as tuning the adjustment for one situation may create problems in other situations. In situations where radar estimates are far from the mark due to radar calibration or other problems, such adjustments can bring about significant improvements.

Ground level precipitation estimates from radar systems are made for areas of typically 1–4 km² spatial resolution and successively for 5–15 min periods using low elevation (elevation angles of < 1°) plan position indicator scans, constant altitude PPI synthetic products or even more sophisticated products. The radar estimates have been found to compare with spot precipitation gauge measurements within a factor of two. The gauge samples an extremely small area (100 cm², 200 cm²), while the radar integrates over a volume, on a much larger scale (1–4 km²). This difference accounts for a considerable amount of the discrepancy. There are indications that the gauge accuracy may, for some purposes, be far inferior to what is commonly assumed, especially if the estimates come from a relatively small number of raingauges (Neff, 1977). An important consideration is the success metric. Seasonal averages may be acceptable in some applications and a single Z - R relationship may be sufficient. However, for flash flood warnings, real-time adjustments may be required.

Note that these adjustments do not automatically ensure improvements in radar estimates, and sometimes the adjusted estimates are poorer than the original ones. This is especially true for convective rainfall where the vertical extent of echo mitigates the difficulties associated with the vertical profile, and the gauge data are suspect because of unrepresentative sampling. Also, the spatial decorrelation distance may be small, and the gauge–radar comparison becomes increasingly inaccurate with distance from the gauge. A general guideline is that the adjustments will produce consistent improvements only when the systematic differences (that is, the bias) between the gauge and radar rainfall estimates are larger than the standard deviation of the random scatter of the gauge versus radar comparisons. This guideline makes it possible to judge whether gauge data should be used to make adjustments and leads to the idea that the available data should be tested before any adjustment is actually applied. Various methods for accomplishing this have been explored, but at this time there is no widely accepted approach.

7.10.4.4 **Dual-polarization precipitation techniques**

Various techniques for using polarization diversity radar to improve rainfall measurements have been proposed. In particular, it has been suggested that the difference between reflectivities measured at horizontal and vertical polarization (Z_{DR}) or the phase shift (ϕ_{DP} or K_{DP}) can provide useful information about drop size distributions (Seliga and Bringi, 1976). These methods depend on the hydrodynamic distortions of the shapes of large raindrops, with more intense rainfalls with larger drops giving a stronger polarization signature. The attenuation must be first corrected and again dual-polarization techniques are applicable here. There is still considerable research on whether this technique has promise for operational use for precipitation

measurement (English et al., 1991). At long wavelengths, the rain rate thresholds where K_{DP} techniques are effective are higher (for example, at S band it is about 20 mm h^{-1} , and at X band it is about 4 mm h^{-1}).

At close ranges (with high spatial resolution), polarization diversity radars may give valuable information about precipitation particle distributions and other parameters pertinent to cloud physics. At longer ranges, it is impossible to be sure that the radar beam is filled with a homogeneous distribution of hydrometeors. Consequently, the empirical relationship of the polarimetric signature to the drop size distribution increases uncertainty. Of course, knowing more about $Z-R$ will help, but, even if multi-parameter techniques worked perfectly well, the error caused by $Z-R$ could be reduced only from 33% to 17%, as shown by Ulbrich and Atlas (1984). For short-range hydrological applications, the corrections for other biases (already discussed) are usually much greater, perhaps by an order of magnitude or more.

Dual-polarization radars can overcome attenuation, partial beam filling and partially blocked beams. Figure 7.36 shows a C band radar where the polarization technique is used to correct for attenuation. The dual-polarization parameters are sensitive to the size and shape of the large particles, and the smaller the wavelength, the more sensitive the radar. In this example, a precipitation system that caused localized flooding was observed by a C band radar and an S band radar. The C band (King City with a 0.65° beam) was about 40 km from the flooding and the S band (Buffalo with a 1° beam) was about 100 km away. Images (a) and (b) show one instance of the low-level radar reflectivity from both radars. The red grid lines are reference lines. The location of the raingauge is about 7 km to the south-west. The C band radar data are attenuated compared to the S band data (image (b) is more intense than image (a)). During the event, the C band radar experienced a wet radome which also strongly attenuated the signal. Images (c) and (d) are accumulations based on their respective dual-polarization-derived precipitation products from over the 8 h period of the event (see also Figure 7.37). The resolution difference is evident, but the accumulation patterns are very similar. This illustrates the great potential for a dual-polarized C band radar to overcome significant attenuation. Interestingly, the dual-polarization precipitation estimate from the S band radar was actually lower and closer to the raingauge value (not shown) than using the traditional $Z-R$ relationship, as the particle classification of hail versus rain was used to prevent the overestimation.

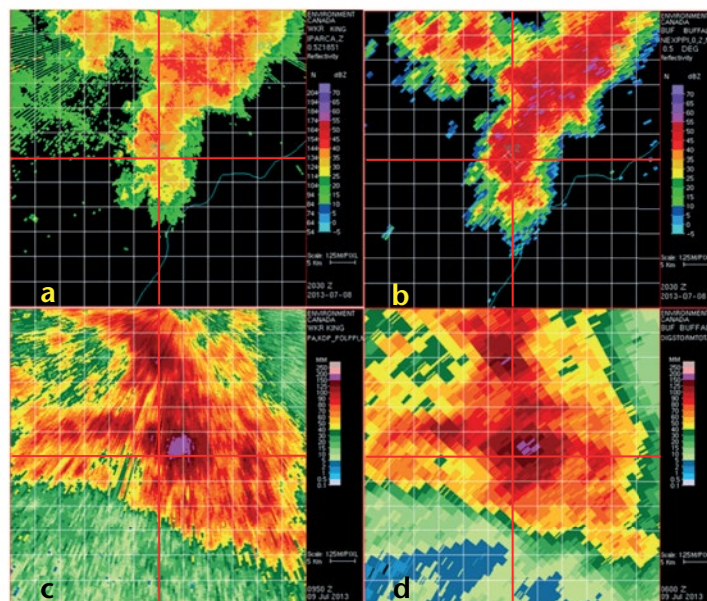


Figure 7.36. The top figures show attenuation of a C band dual-polarization radar (a) compared to an S band radar (b) at one instant. The bottom figures are precipitation accumulations over the period of the event and show remarkable similarities after correction using polarization diversity capability (see also Figure 7.37; figure courtesy of Sudesh Boodoo of Environment Canada).

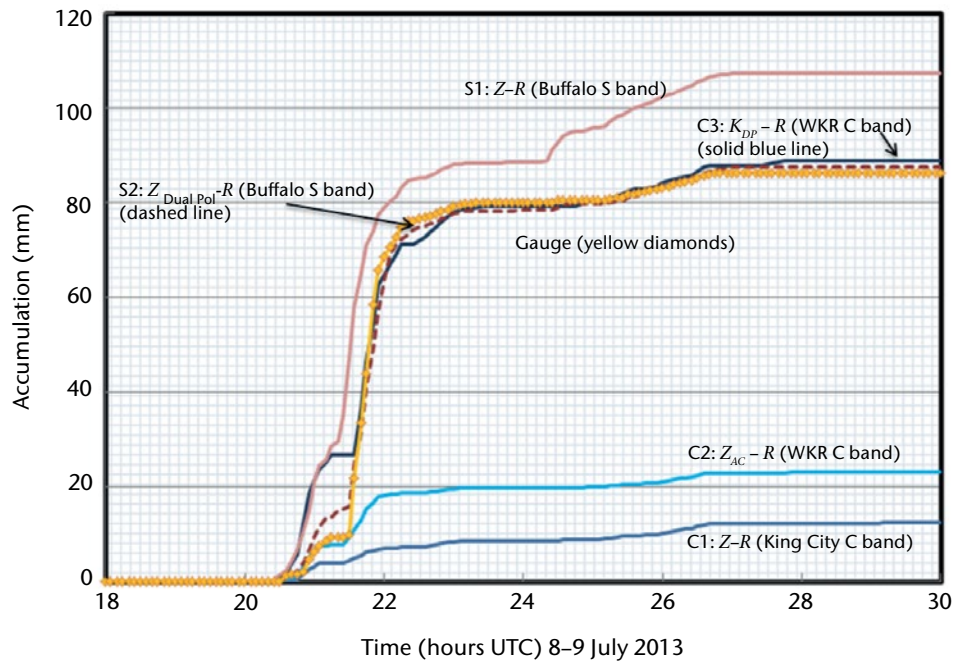


Figure 7.37. A meteogram of accumulated rain from a gauge (yellow line with symbols) and three C band (C1, C2, C3) and two S band (S1, S2) estimates of the precipitation accumulation using a variety of polarization diversity techniques for one gauge site; point is about 7 km south-west of the centre (see also Figure 7.36; figure courtesy of Sudesh Boodoo of Environment Canada).

Figure 7.37 shows the comparison of various rainfall estimates from C and S band radars and a raingauge. The bottom (C1) and top (S1) lines are accumulations based on traditional simple reflectivity converted to rain rate ($Z = 300 R^{1.4}$) from the King City C band (40 km from the gauge site) and the Buffalo S band (100 km from the gauge site) radars. Both radars are well calibrated and only Doppler ground clutter rejection has been applied to the data. The $Z_{AC}-R$ line (C2) is a Z_{DR} -only attenuation corrected reflectivity converted to rain rate and accumulated. The dashed (S2) and dark blue (C3) lines are the precipitation estimates using a mix of dual-polarization techniques from the S band radar (S2) and from the $K_{DP}-R$ technique from the C band radar (C3), respectively. The improved Buffalo S band results are attributed to removing the hail bias using the dual-polarization particle classification technique. The specific differential phase (K_{DP}) technique, which is insensitive to attenuation, partial beam blockage and partial beam filling, improves the King City C band estimates. This illustrates the impact of dual polarization on the quantitative use of both S and C band radars. It also illustrates the larger impact of dual polarization on C band radars.

Rain/snow/hail discrimination and other target classification

With conventional or reflectivity-only radars, the pattern and intensity of the echo were used to roughly estimate the nature of the target. In summer, reflectivities less than about 12 dBZ were considered to be non-precipitating echoes, light rain was up to about 30 dBZ and heavy rain up to about 50 dBZ or so. Reflectivities above 57 dBZ were considered to be hail. Snow is not generally separable with these kinds of radars in the horizontal. In the vertical, the bright band (a region of enhanced reflectivity due to large wet snow aggregates) delineated snow aloft from rain below. Dual-polarization radars characterize the target using reflectivity information from orthogonal channels, their cross-polar signal and changes in propagation phase. Surface temperature and humidity and soundings from numerical weather prediction models are also used. Fuzzy logic techniques use independent estimates from a variety of dual-polarization parameters to classify the echo type into a variety of categories including: ground clutter, rain, snow, hail, biological scatters and even big and small drops (Figure 7.29).

Aeroplanes were identified as isolated point anomalies and ground echoes were identified as stationary or permanent echoes at short range around the radar. The reflectivities of aeroplanes and ground echoes can vary greatly because small changes in aspect angle result in substantial changes in backscatter.

Doppler radars can identify non-moving targets, such as ground clutter and anomalous propagation echoes, even in the presence of weather phenomena. These ground targets can be effectively filtered out in signal processing to produce "corrected (for ground clutter) reflectivity". Most if not all modern radars have Doppler and thus have this capability. Before Doppler radars, a variety of techniques were used to remove ground clutter including: (i) CAPPI, (ii) ground clutter maps, and (iii) the statistical fluctuation of the reflectivity statistics.

7.10.5 **Wind estimation/wind mapping**

Doppler velocities are radial velocities, and a family of true velocities can create the same radial velocity. Hence, radial velocities alone are ambiguous and require simplifying assumptions to interpret. On typical colour displays, velocities between $\pm V_{\max}$ are generally assigned warm/cool colours to indicate away/towards motions. Velocities extending beyond the Nyquist (unambiguous or extended) velocity enter the scale of colours at the opposite end. This process may be repeated if the velocities are aliased more than one Nyquist interval.

7.10.5.1 **Wind profiling**

Doppler radar can be used to derive vertical profiles of synoptic scale horizontal winds. When the radar's antenna is tilted above the horizontal, increasing range implies increasing height. A profile of wind with height can be obtained by sinusoidal curve-fitting to the observed data (termed velocity azimuth display (VAD) after Lhermitte and Atlas, 1961) if the wind is assumed to be relatively uniform or linear over the area of the scan. The winds at zero radial velocity bins are perpendicular to the radar beam axis. The colour display may be used to easily interpret VAD data obtained from large-scale precipitation systems. Typical elevated conical scan patterns in widespread precipitation reveal an S-shaped zero radial velocity contour as the mean wind veers with height (Wood and Brown, 1986). On other occasions, closed contours representing jets are evident. See Figure 7.12 for a sample of synoptic Doppler wind fields.

If uniformity can be assumed, then divergence estimates can also be obtained using the VAD technique by fitting a curve with a constant term to the equation. This technique cannot be accurately applied during periods of convective precipitation around the radar as the uniformity assumption is not satisfied. Doppler radars have successfully obtained VAD wind profiles and divergence estimates in the optically clear boundary layer during all but the coldest months, up to heights of 3 to 5 km above ground level. The VAD technique seems well suited for winds from precipitation systems associated with extratropical and tropical cyclones. In the radar's clear-air mode, a time series of measurements of divergence and derived vertical velocity is particularly useful in nowcasting the probability of deep convection.

7.10.5.2 **Convective wind features**

In the case of convection, small-scale wind features are due to divergence, convergence and rotation as observed in gust fronts, downbursts, mesocyclones, and the like. These appear as small anomalies of one kilometre to tens of kilometres in scale embedded in mean flows of hundred kilometre scales. Taking into account assumptions about the flow, and in combination with conceptual models and an understanding of the thunderstorm or mesoscale convective system wind flows, colour displays of single-Doppler radial velocity patterns can aid in the real-time interpretation and diagnosis of thunderstorm severity (Burgess and Lemon, 1990). Lemon (1978) listed the features and diagnostic procedure to identify severe thunderstorms (see 7.10.2). Convective wind features confound the interpretation of radial velocity fields in particular when there are mesoscale flows on the scale of 40 to 100 km and three-dimensional regimes, as in complex mountainous terrain.

7.10.5.3 **Wind mapping**

Since the mid-1970s, experiments have been made for measuring three-dimensional wind fields using multiple Doppler arrays. Measurements taken at a given location inside a precipitation area may be combined, by using a proper geometrical transformation, in order to obtain the three wind components. Such estimations are also possible with only two radars, using the continuity equation. Kinematic analysis of a wind field is described in Browning and Wexler (1968). However, for accurate velocity estimation, the radars must be relatively close together (40–80 km) and the target area must be in two lobes perpendicular to the radar baselines. Operationally, it is unusual to find radars situated so close to one another.

7.10.6 **Initiation and numerical weather prediction models**

A variety of radar data and products are used for data assimilation in some numerical weather prediction centres. Not all models use the same products. Precipitation is a derived parameter in numerical weather prediction models, and so it is difficult to directly assimilate precipitation or reflectivity fields. Winds are direct model variables and radial velocities may be assimilated with less contrivance. These include VAD wind profiles, composited radar-derived surface precipitation fields in global models and, in some cases, three-dimensional reflectivity and radial velocity fields for local area or small-scale models in polar coordinates. López (2011) has demonstrated the value of assimilating the United States Stage IV surface precipitation product on the weather in Europe and Asia. These and other applications (typhoon tracking) are prime drivers for the global weather radar data exchange initiative.

7.10.7 **Humidity estimation**

An emerging innovation is the retrieval of humidity from beam propagation differences of echoes from the omnipresent ground targets (Fabry, 2004). This innovation is counter-intuitive to the siting of weather radars since they are sited to minimize ground clutter. Index of refraction fluctuations cause beam propagation path length changes which can be detected as changes in the phase of the signal or the Doppler shift. By comparing the shift in dry versus moist conditions and accounting for range ambiguities, the path length change can be estimated and then related to the index of refraction change using Snell's law. The index of refraction is dependent on temperature, pressure and humidity but primarily on the latter, and hence the humidity can be retrieved very near the radar. Several research radars have this capability and some operational systems (in France and the UK) are prototyping this for operational deployment.

7.11 **METEOROLOGICAL PRODUCTS**

The radar data can be processed to provide a variety of meteorological products to support various applications. The quality of these products depends on the type of radar, the scan strategy, its signal-processing characteristics and the associated radar control and data analysis/production system. These products include grids of raw or derived radar parameters, vertical wind profiles, location and characteristics of analysed thunderstorm cells, their historical tracks, nowcasts, and the like. Polar coordinate data are converted to two- or three-dimensional Cartesian coordinates using interpolation techniques onto grids with different geographical projections. Several of the products listed below are illustrated in Figure 7.24. A list of typical radar products is presented in Table 7.10.

The following is a list of common generated products:

- (a) The PPI: A polar format display of a variable, obtained from a single full antenna rotation at one selected elevation. It is the classic radar display, used for weather surveillance. This is the most basic of products. Note that it is made at constant elevation angle, and so increasing range means that the data are taken at increasing height. Any parameter can be displayed in this format.

Table 7.10. List of typical radar products

PPI of basic parameters (low level)	Cell identification and tracking
Maximum reflectivity in a column	Mesocyclone, tornado vortex signature
Echo top	Downburst, microburst
Derived thunderstorm severity products	Gust front, convergence
Surface precipitation rate	Nowcast
Surface accumulation products	Hail probability, size
Basin products	Bounded weak echo region
Hydrometeor classification – hail, rain, snow, etc.	VAD wind profiles
Arbitrary cross-sections of various parameters	Mosaics of multiple radar

- (b) The CAPPI: A horizontal cross-section display of a variable at a specified altitude, produced by interpolation from the volume data. It is used for surveillance and for identification of severe storms. It is also useful for monitoring the weather at specific flight levels for air traffic applications. One of the rationales for the CAPPI is that by judicious selection of the altitude, a near clutter-free product can be produced in the absence of the Doppler zero velocity notch filter.
- (c) The pseudo range–height indicator (RHI): A display of a variable obtained from a volume scan where the data from the same azimuth are extracted and collated to provide vertical information on the structure of the weather. Classically, this was done with an antenna doing a physical vertical sweep, typically from 0° to 90°, at one azimuth. Manual intervention was required to select the azimuth and decide when to do the scan. The advantage of this classic technique is that the density of information is much higher. Typically, very fine elevation angle changes (~0.1°) can be used. The quality of the pseudo RHI technique depends on the scan strategy, but it has the great advantage of flexibility. It is used for identifying severe storms, hail and the bright band.
- (d) Vertical cross-section: A display of a variable above a user-defined surface vector (not necessarily through the radar). It is produced by interpolation from the volume data.
- (e) The column maximum: A display, in horizontal plane, of the maximum value of a variable (usually reflectivity) above each point of the area being observed. This is useful to identify the maximum reflectivity in a storm to assess its severity or to estimate the maximum precipitation that could be expected. In some cases, due to radar siting issues, where the low levels could not be observed (mountainous terrain), this was used to estimate surface precipitation. Sometimes, there is a minimum altitude threshold to the data, so that the high reflectivities in the bright band do not overly influence the use of this product. A variation is to limit the altitude of the data to quickly provide insight into the vertical structure of the storm.
- (f) Vertically integrated liquid: An indicator of the intensity of severe storms. It can be displayed, in horizontal plane, for any specified layer of the atmosphere. As this is dominated by the highest reflectivities, it is very similar to the maximum reflectivity product in pattern but in different units.
- (g) Echo tops: A display, in horizontal plane, of the height of the highest occurrence of a selectable reflectivity contour, obtained by searching in the volume data. It is an indicator of the strength of the updraught and therefore an indicator of severe weather and hail.
- (h) Often the reflectivity products are converted to precipitation products by an empirical relationship between Z and R . These precipitation products are aggregated into accumulation products of varying time duration.

- (i) Modern computing systems have significant processing capabilities. Techniques or algorithms have been developed to search the three-dimensional data to locate and quantify the characteristics of contiguous areas of high reflectivity which are related to severe weather thunderstorms for the analyst (Figure 7.24).

In addition to these standard or basic displays, other products can be generated to meet the particular requirements of various users (hydrology, nowcasting or aviation):

- (a) Precipitation accumulation: An estimate of the precipitation accumulated over time at each point in the area observed;
- (b) Precipitation sub-catchment totals: Area-integrated accumulated precipitation;
- (c) VAD: An estimate of the vertical profile of wind above the radar. It is computed from a single antenna rotation at a fixed elevation angle;
- (d) Velocity volume processing, which uses three-dimensional volume data;
- (e) Storm tracking: A product from complex software to determine the tracks of storm cells and predict future locations of storm centroids;
- (f) Wind shear: An estimate of the radial and tangential wind shear at a height specified by the user;
- (g) Divergence profile: An estimation of divergence from the radial velocity data given some assumptions;
- (h) Mesocyclone: A product from sophisticated pattern-recognition software that identifies rotation signatures within the three-dimensional base velocity data that are on the scale of the parent mesocyclonic circulation often associated with tornadoes;
- (i) Tornado vortex signature: A product from sophisticated pattern-recognition software that identifies gate-to-gate shear signatures within the three-dimensional base velocity data that are on the scale of tornadic vortex circulations;
- (j) Particle type: The echo is classified according to precipitation type and derived from dual-polarization data.

In addition, radar network processing results in a radar mosaic. The products mentioned above apply on a network basis; in fact, this is standard practice. Considerations for radar products include: (i) projections are used for visualization of the data; (ii) for areas of overlapping radar coverage, various algorithms are used – based either on the nearest radar, the maximum value or a sophisticated estimation of data quality. If the overlap is significant, a neighbouring radar may fill the void in the "cone of silence". The development of networked radar products needs also to consider intra-network and inter-network homogenization of the data. This includes temporal and spatial harmonization, mutual calibration of the radar data, and examination of the radar sensitivities which can result in discontinuities in the network products.

ANNEX 7.A. WEATHER RADAR – SYSTEM PERFORMANCE AND OPERATION

(This annex presents the text of a common ISO/WMO standard. It is also published, with identical content, as ISO 19926-1:2018(E)).

INTRODUCTION

The rapid development of weather radar occurred just before and during the Second World War. Initially, radar was demonstrated at long (10 m to 50 m) wavelengths, but quickly moved to shorter wavelengths (3 cm and 10 cm) with the requirement for, and development of, compact and high power transmitters. C-band (5 cm) wavelengths were available in the late 1950s. The first operational Doppler radars appeared in the mid-1980s, with demonstration of the technology's application in operations and the availability of high-speed, affordable processors and efficient software codes. The adoption of dual-polarization capability for operational radars followed in the mid- to-late 1990s.

Radars provide localized, highly detailed, timely and three-dimensional sensing and observing capability that no other meteorological monitoring system can provide. They are able to measure variations in precipitation rates at a resolution of a few square kilometres or better and at time cycles of the order of a few minutes. They provide the capability to monitor rapidly evolving weather events, which is critical for the provision of early warnings of severe and hazardous weather. This includes heavy rain, hail, strong winds (for example, tornadoes and tropical cyclones) and wind shear; the conditions that have the highest impact on society of all the weather elements. Doppler and dual-polarization radars are able to resolve the high variability of wind and precipitation types, and even see insects or clear air turbulence used to predict the onset of thunderstorms and for measuring vertical wind profiles. Dual polarization is also used for quality assurance and to improve precipitation estimates.

With high speed telecommunications and data processing, radar systems are now networked to better monitor large-scale weather phenomena, such as tropical cyclones and major extra-tropical storms (both in summer and winter). The data derived from the networking of radars can provide longer lead times (from 60 min to 90 min to several hours) for early warnings. Numerical weather prediction systems have also now advanced and the assimilation of continental-scale radar-derived precipitation data into global models can significantly improve the 4-day to 5-day precipitation forecasts of neighbouring areas and continents.

The provision of homogeneous, high-quality data starts with the installation and use of appropriate radar technology for the local weather environment and conditions. The wavelength of the radar, the beam width of the antenna, the type and power of the transmitter, the sensitivity of the receiver and the waveform all have significant impacts on the resolution and quality of radar data. Weather radars have traditionally been specified and configured to meet local requirements for weather monitoring and surveillance and to cater for local geography and other factors, leading to globally diversity in technology and in sampling strategies. These all impact on different data quality metrics, such as availability, timeliness and accuracy. These metrics also rely on the operation and maintenance of the radar systems through adherence to prescribed and standardized procedures and practices. This requires the establishment of standards, technical specification best practices and guidelines for network design, site selection, calibration, system and equipment maintenance, sampling and data processing, and distribution.

The purpose of this document is wide and addresses organizations in all countries using weather radar, with particular emphasis on countries that do not have a long tradition of weather radar operation and usage. It provides:

- Support to manufacturers to maintain a comparable and high level of competitive weather radar systems;
- Aid for tendering authorities to take into account state of the art of system performance as well as merely component definitions in their documents and, thus, to help to compare different incoming bids;
- Provision of a valid documentation on the potential and limitations of weather radar systems, thus supporting capacity building worldwide;
- Advice on the general requirements for siting, operation, maintenance and calibration tasks to keep radar systems on a high level of data quality and availability;
- A description of the required range of tasks for operating and maintaining weather radar systems in order to let managers allocate enough financial resources and staff capacity for this purpose.

Further information, such as the fundamentals of weather radar measurement, can be found in [1].

1. SCOPE

This document specifies system performance of ground-based weather radar systems measuring the atmosphere using frequencies between 2 GHz and 10 GHz. These systems are suitable for the area-wide detection of precipitation and other meteorological targets at different altitudes. This document also describes ways to verify the different aspects of system performance, including infrastructure.

This document is applicable to linear polarization parabolic radar systems, dual-polarization and single-polarization radars. It does not apply to fan beam radars (narrow in azimuth (AZ) and broad in elevation (EL)), including marine and aeronautical surveillance radars, which are used for, but are not primarily designed for, weather applications. Phased array radars with electronically formed and steered beams, including multi-beam, with non-circular off-bore sight patterns, are new and insufficient performance information is available.

This document does not describe weather radar technology and its applications. Weather radar systems can be used for applications such as quantitative precipitation estimation (QPE), the classification of hydrometeors (for example, hail), the estimation of wind speeds and the detection and surveillance of severe meteorological phenomena (for example, microburst, tornado). Some of these applications have particular requirements for the positioning of the radar system or need specific measurement strategies. However, the procedures for calibration and maintenance described in this document apply here as well.

This document addresses manufacturers and radar operators.

2. NORMATIVE REFERENCES

There are no normative references in this document.

3. TERMS AND DEFINITIONS

No terms and definitions are listed in this document.

ISO and IEC maintain terminological databases for use in standardization at the following addresses:

- ISO Online browsing platform: available at <https://www.iso.org/obp>
- IEC Electropedia: available at <http://www.electropedia.org/>

4. ABBREVIATED TERMS

ADC	analogue–digital converter
AZ	azimuth
BITE	built-in test equipment
BPF	band-pass filter
CW	continuous wave
EL	elevation
H/V	horizontal/vertical
HPBW	half power beam width
ITU-R	International Telecommunication Union, Radiocommunication Sector
LDR	linear depolarization ratio
LNA	low noise amplifier
MTBF	mean time between failures
NF	number of failures
NMHS	National Meteorological and Hydrological Service
PRT	pulse repetition time
QPE	quantitative precipitation estimation
RF	radio frequency
SG	signal generator
SNR	signal-to-noise-ratio
STALO	stable local oscillator
STAR	simultaneous transmit and receive
TR	transmit/receive
TWT	travelling wave tube
UPS	uninterrupted power supply

5. **BASICS**

5.1 **Frequency bands**

A weather radar is a system that is designed to measure hydrometeors in a large area, using a remote-sensing technology based on microwaves. The microwaves of S-, C- and X-bands are used in many cases and the scale and observation characteristics of the system are different depending on the characteristics of each frequency (wavelength). S-band systems are large and their observation range is wide, while X-band systems are compact and their observation range is narrow. The useful range of S-band and C-band radars are typically limited by the Earth's curvature (≥ 300 km), whereas at X-band the limit is normally attenuation dependent (50 km to 100 km). See [1] for more details. Table 7.A.1 shows the typical items for each frequency band.

It is necessary to select the frequency band according to the range of observation and the scale of system at the location.

Table 7.A.1. Typical specification for different frequency bands of weather radar

Frequency band	Frequency range ^a	Antenna diameter ^{b,c}	Rain attenuation (two-way) at 30 mm/h ^d
S	2 700 GHz to 3 000 GHz	8.5 m	0.02 dB/km
C	5 250 GHz to 5 900 GHz	4.2 m	0.13 dB/km
X	9 300 GHz to 9 800 GHz	2.4 m	1.22 dB/km

^a Operating frequency range differs from each country.

^b For more information on frequency band and antenna size, refer to [1], Chapter 7.6.8.

^c Typical values for a 1° HPBW.

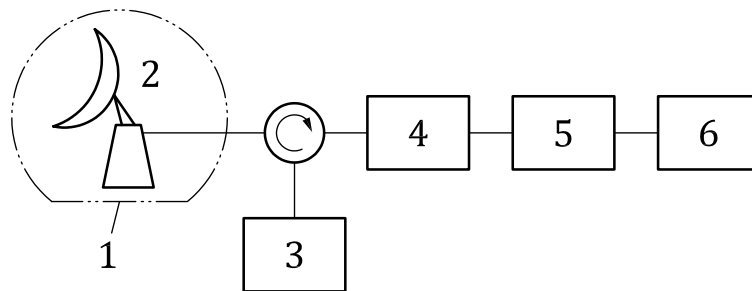
^d For attenuation due to rain, refer to [1], Chapter 7.2.3.

5.2 **System configuration**

5.2.1 **Overview of radar system component units**

Figure 7.A.1 shows the basic configuration of a radar system. Antenna mounted receivers (and in some cases transmitters) are also becoming common recently.

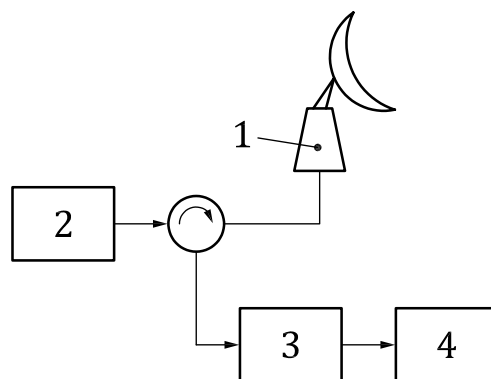
The weather radar system is divided into a single polarization type, which is in most cases horizontal polarization (see Figure 7.A.2), and a dual-polarization type, where both



Key:

- | | |
|---------------|--------------------|
| 1 Radome | 4 Receiver |
| 2 Antenna | 5 Signal processor |
| 3 Transmitter | 6 Data processor |

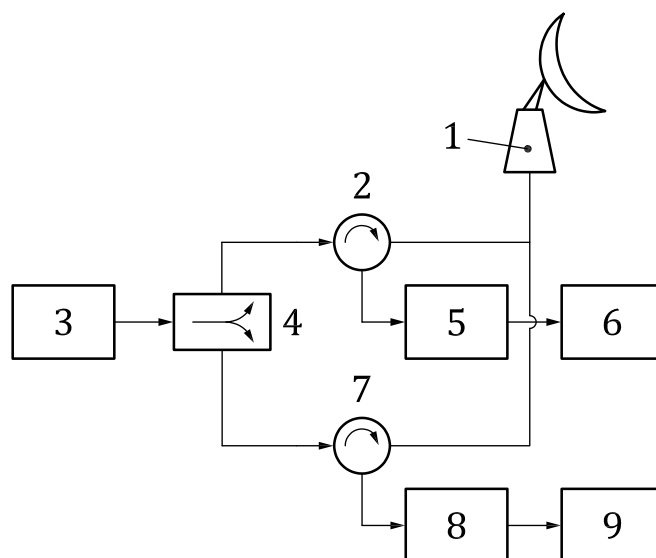
Figure 7.A.1. Configuration and diagram of radar system



Key :

- | | | | |
|---|-------------|---|------------|
| 1 | Antenna | 3 | TR limiter |
| 2 | Transmitter | 4 | Receiver |

Figure 7.A.2. System diagram of a single polarization type

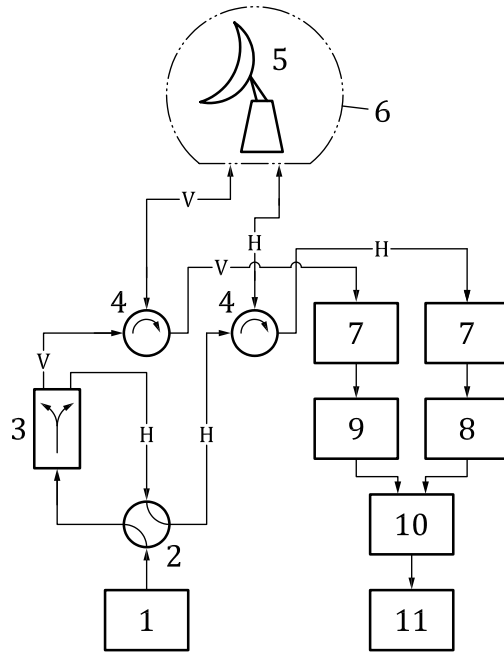


Key:

- | | | | |
|---|-------------------------------------|---|-----------------------------------|
| 1 | Antenna | 6 | Receiver (H channel) |
| 2 | Horizontal polarization (H) channel | 7 | Vertical polarization (V) channel |
| 3 | Transmitter | 8 | TR limiter |
| 4 | 3 dB power splitter | 9 | Receiver (V channel) |
| 5 | TR limiter | | |

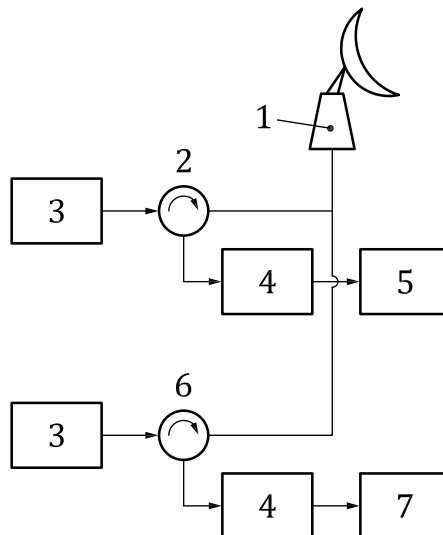
Figure 7.A.3. System diagram of a dual-polarization distribution transmitter type

horizontal and vertical polarizations of the emitted and received microwaves are used. The dual-polarization type is further divided into a dual-polarization distribution transmitter type (see Figures 7.A.3 and 7.A.4), which distributes single transmitter output, and a dual-polarization independent transmitter type, which has two independent systems of transmitter (see Figure 7.A.5).



- Key:
- | | |
|----------------------------|--|
| 1 Transmitter | 7 TR limiter |
| 2 Polarization mode switch | 8 Horizontal polarization receiver channel |
| 3 3 dB power splitter | 9 Vertical polarization receiver channel |
| 4 Circulator | 10 Signal processor |
| 5 Antenna | 11 Data processor |
| 6 Radome | |

Figure 7.A.4. System diagram of a dual-polarization distribution transmitter type plus additional linear depolarization ratio mode



- Key:
- | | |
|---------------------------------------|-------------------------------------|
| 1 Antenna | 5 Receiver (H channel) |
| 2 Horizontal polarization (H) channel | 6 Vertical polarization (V) channel |
| 3 Transmitter | 7 Receiver (V channel) |
| 4 TR limiter | |

Figure 7.A.5. System diagram of a dual-polarization independent transmitter type

5.2.2 **Dual-polarization transmit modes**

5.2.2.1 **General**

Depending on the transmitter system (see types dual polarization distribution transmitter or independent transmitter, illustrated above) different transmit modes are available.

5.2.2.2 **Simultaneous transmit and receive, or hybrid mode**

In simultaneous transmit and receive (STAR) mode, a linear horizontal and a vertical polarized wave is transmitted simultaneously and each wave is received by the respective receiver chain. The advantages of this technique are that it can be used with a single transmitter (distributed transmitter type), no expensive second transmitter is required and a simple power splitter in the transmit path is sufficient. The disadvantage is that, in the case of a depolarizing medium (for example, melting layer, wet or melting hail), a cross-talk between horizontal and vertical waves occurs and contamination of radar products (for example, differential reflectivity Z_{dr}) will occur.

5.2.2.3 **Alternate H/V mode**

In the alternate H/V mode, horizontal and vertical polarized waves are transmitted alternatively from pulse to pulse. Two receivers will receive the co-polar and the cross-polar signal for each pulse. The advantage of the alternate H/V mode is that both the co-polar and cross-polar components of the scatter matrix can be measured. If the radar is of the distributed transmitter type, a polarization switch is required instead of the power splitter. Fast high-power switches are currently expensive and brittle. For that reason, the alternate H/V mode is normally only used for research radars, which are not operated continuously. In cases where the radar uses two independent transmitters, the alternate H/V mode can be simulated by transmitting alternately every second pulse per transmitter.

5.2.2.4 **Linear depolarizing ratio mode**

The LDR mode is a special mode enabling radars to build in the distribution transmitter type configuration (see Figure 7.A.4) to measure the LDR. LDR is the ratio between cross-polar and co-polar reflectivities. LDR is a good indicator for melting layer or wet or melting hail and ground clutter. To enable LDR mode, a bypass around the power splitter is necessary. This bypass will send the transmit power only to the horizontal feed. On receipt, the horizontal polarization receiver measures the co-polar signal and the vertical polarization receiver measures the cross-polar signal. Typically, a slow switch (switching time approximately 1 s to 3 s) is used and the change between STAR and LDR modes will be performed after only one plan position indicator (PPI) scan. With the exception of LDR, no other dual-polarization product can be measured.

5.2.3 **Description of components**

5.2.3.1 **Antenna**

A directional antenna is used to concentrate energy into a narrow beam. A parabolic reflector type is generally used. The size of the antenna to obtain the same beam width is different depending on the frequency used. If the wavelength is shorter, the same beam width is realized by a parabolic antenna with a smaller diameter. Generally, a single antenna has the dual purpose of transmission and reception. In addition, the antenna is divided into single polarization type (one feed horn) and dual-polarization type (a feed horn capable of separating two orthogonal polarizations).

Phased array antenna is an emerging technology for weather radars, where the antenna is a panel of several solid-state emitters. See Attachment F for more details.

5.2.3.2 Radome

A radome is used to cover the antenna and to protect it from rain, wind, ice and snow. The radome is formed as a spherical or dome type by combining a multiple number of panels. The radome is of a variety of types depending on the size and the purpose of the observation of antenna.

The radome for dual polarization is devised to show a behaviour as uniform as possible for both horizontal and vertical polarized waves crossing the radome. This can be achieved by proper design of the panel shapes, for example, by using geodesic or quasi-random geometry of these panels.

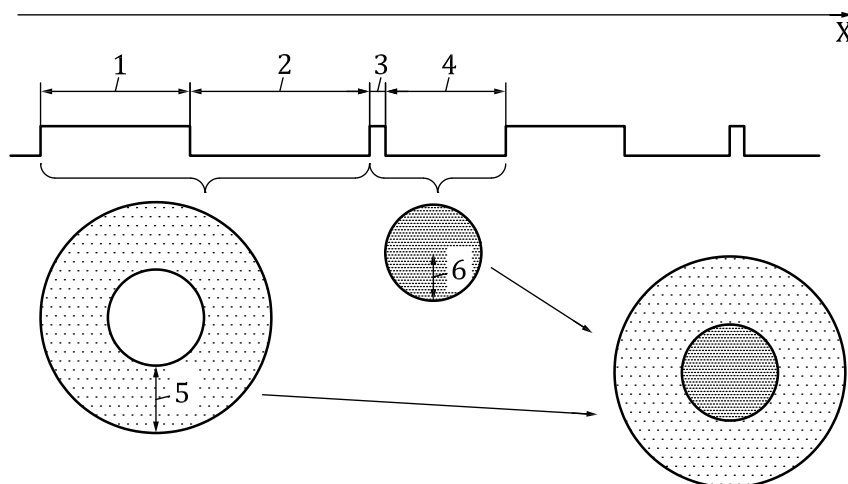
The radome will introduce some losses. See A.3.9.2 for estimation of losses of a dry radome. It has to be noted that water, snow or ice on the radome can lead to strong losses (several dB).

5.2.3.3 Transmitter

5.2.3.3.1 General aspects

A transmitter is a device to generate transmission radio waves. It generates a stable high-power microwave pulse and radiates radio waves into the air via antenna. There are two types of transmission devices: electron tube (magnetron, klystron, travelling wave tube (TWT), etc.) and semiconductor (solid-state). For TWT and solid-state transmitters, the pulse-compression technology is applied to obtain fine resolution and to increase the signal-to-noise ratio (SNR).

In pulse-compression radars, a long and short pulse are usually transmitted alternately, since, while transmitting a long pulse, a blind range is generated and this needs to be covered. A long and short pulse transmission example is illustrated in Figure 7.A.6.



- Key:
- | | |
|----------------------------|------------------------------------|
| 1 Long pulse transmission | 5 Observation range by long pulse |
| 2 Long pulse reception | 6 Observation range by short pulse |
| 3 Short pulse transmission | X Time |
| 4 Short pulse reception | |

Figure 7.A.6. An example of long/short pulse transmission

5.2.3.3.2 *Transmitter duty cycle*

In a pulsed radar system, the transmitter radio frequency (RF) power is on for only a small portion of the time. The rest of the time is spent receiving echoes from the atmosphere. The portion of time when the transmit power is on is called the transmitter “duty cycle”. The duty cycle together with the peak power determine the average power or energy radiated into the atmosphere.

In a weather radar transmitter using a tube transmitter (magnetron or klystron), the duty cycle is typically in the order of 1%. This leads to a typical average power of a few hundred W. In TWT transmitters, the peak power is typically lower and longer pulses similar to solid-state transmitters are used. The peak power of the tube transmitters ranges from tens of kW to MW, depending on the application and frequency of the radar.

In a weather radar transmitter using a solid state (semiconductor) transmitter, the duty cycle is typically in the order of 10%, leading again to a similar average power of a few hundred W (some tube transmitters, for example, TWT transmitters, also rely on low-peak power and a high-duty cycle similar to the solid-state transmitters).

5.2.3.3.3 *System pulse width range*

In electron tube devices, short pulses with high-peak power are typically used. The pulse width is in the order of 1 μ s (ranging from 0.3 μ s to 5 μ s in magnetron and klystron transmitters).

The pulse width of a solid-state transmitter is typically in the order of 100 μ s (ranging from 20 μ s to 200 μ s) corresponding to a range of 15 km. A pulse-compression technique is used to achieve similar range resolution as with the short pulses from a tube transmitter. Often, there is also a separate short pulse covering the close distances, which are masked by the long transmit pulse (see Figure 7.A.6).

5.2.3.3.4 *Pulse repetition frequency*

The pulse repetition frequency, f_{PRF} , or the time interval between triggering radar transmit pulses, the pulse repetition time (PRT), is a parameter that can be defined by the radar operator. However, there are several constraints for the selection of the f_{PRF} . High f_{PRF} will reduce the unambiguous maximum range, r_{max} , of a radar. Radar echoes from distances beyond r_{max} will be displayed as second-trip echoes. r_{max} is shown by formula (7.A.1):

$$r_{\text{max}} = \frac{c}{2f_{\text{PRF}}} \quad (7.A.1)$$

where c is the speed of light.

EXAMPLE For a maximum range of 250 km, f_{PRF} is not higher than 600 Hz.

On the other hand, high f_{PRF} is necessary for a broad unambiguous Doppler velocity range, v_a (often called “Nyquist interval”), as shown by formula (7.A.2):

$$v_a = f_{\text{PRF}} \frac{\lambda}{4} \quad (7.A.2)$$

where λ is the wavelength of the pulse emitted by the radar.

For a C-band radar at a f_{PRF} of 600 Hz, v_a would be in the order of 8 m/s, which is too low for the observation of most meteorological phenomena.

With modern signal processing, several techniques exist to overcome these physical constraints. Dual- f_{PRF} or staggered-PRT techniques allow for the extension of the Nyquist interval by a factor of two to three, or even more. Various second-trip recovery techniques allow for the elimination or recovery of second-trip echoes.

The f_{PRF} of transmitters is limited by the duty-cycle, see 5.2.3.3.2.

Typical ranges of f_{PRF} for X-, C- and S-band radars are 300 Hz to 2 000 Hz. The higher f_{PRF} are needed for X-band radars, to compensate for the wavelength impact on v_a in formula (7.A.2). This leads to low r_{max} in formula (7.A.1) and so for X-band radars second-trip echoes removal is often mandatory.

5.2.3.4 Receiver

The receiver is the device to amplify and detect the radio wave, which is returned to the antenna, and to extract amplitude information and phase information from the received signal. The receiver is protected from the transmitted power by a circulator and/or a TR limiter.

Pulse-compression radars apply frequency modulation at long pulse transmission, and, with pulse-compression processing in the receiver, achieve the same SNR and range resolution in the range sampled by the modulated pulse as a radar with tube transmitter. The SNR of the range sampled by the short pulse is lower than that of the range sampled by a tube transmitter radar.

The combination of short and long pulses increases the effective dynamic range from close to far range similar to that of sensitivity time control (STC).

Note: STC is used to attenuate strong signals at close ranges. Is not necessary for receiver systems with a large dynamic range.

5.2.3.5 Signal processor

A signal processor processes the digitized amplitude information and phase information data from the receiver and calculates a variety of key variables necessary for observation, such as rainfall intensity and rainfall moving radial velocity.

Typical output data for a dual-polarization radar are shown as follows:

- Reflectivity factor (Z);
- Differential reflectivity (Z_{dr});
- Doppler velocity (V);
- Spectrum width (W);
- Differential phase (Φ_{dp});
- Correlation coefficient between Z_{h} and Z_{v} (ρ_{hv}).

5.2.3.6 Data processor

A data processor generates the weather products according to the purpose of the radar system, based on a variety of key variables, which are extracted by the signal processor.

6. SYSTEM PERFORMANCE AND MEASUREMENT PARAMETERS

6.1 General aspects

System performance indicates the performance of a weather radar system as a whole, rather than the performance of each unit comprising the radar.

System performance criteria are determined so that evaluation by these criteria can be applied to different types of weather radars, bringing a good user benefit as it makes it easy for users to write system specifications. On the other hand, adopting a standard set of criteria will lead to fair competition among manufacturers, as it will exclude radars with insufficient system performance from the global markets. For this purpose, criteria must be measurable in a common way for all the weather radars before they are shipped from factory.

Sensitivity, spatial resolution, accuracy of Doppler velocity and accuracy of dual-polarization measurement are chosen as top criteria showing the system performance of weather radar most distinctively; these are called "fundamental parameters".

Additionally, parameters are chosen that are not included in the fundamental parameters, but that are also very important in defining system performance; these are called "other key parameters". Summaries are given in Tables 7.A.2 and 7.A.3. Explanations of the fundamental parameters are given in 6.2, while 6.3 explains other key parameters. Methods for measuring these values are given in Attachment A. An example on how to record them is given in Attachment C.

Table 7.A.2. Fundamental parameters

<i>Parameter category</i>	<i>Purpose</i>	<i>Value</i>
Sensitivity	Determines how far or how weak the radar echo is that the radar can detect	Reflectivity sensitivity A dBz at B km The smaller A is for a distance B , the weaker the echoes that the radar can observe or conversely, the farther the radar can observe the same echo
Spatial resolution	Determines the detail to which the radar can distinguish	Beam resolution (in degrees), range resolution (in m) The smaller the value is, the higher the detail that the radar can observe
Precision of Doppler velocity	Determines the ability to remove ground clutter using Doppler filtering technique	Phase stability (in degrees) The smaller the value is, the greater the ability to remove ground echoes
Accuracy of dual-polarization measurement	Determines the ability to observe weather echo types accurately with polarimetric parameters	Cross polarization isolation (in dB) Reported as a negative value, the smaller the value, the better the system is able to separate the horizontal from the vertical signal

Table 7.A.3. Other key parameters

<i>Parameter category</i>	<i>Purpose</i>	<i>Value</i>
Antenna side lobe	Determines the faithfulness of the radar values due to strong off-axis echoes	Gain difference (in dB) relative to the maximum gain at the centre of the main lobe Reported as a negative number, the lower the value, the less spurious energy observed by the radar
Range side lobe	Relevant for pulse-compression radars, determines the faithfulness of the radar values due to strong, out of resolution volume, but radially aligned echoes	Gain (in dB) relative to peak power of the pulse Reported as a negative number, the lower the value, the less energy from out of resolution volume echoes observed by the radar
Maximum rotation speed	Determines how fast the radar antenna can rotate	Maximum rotation speed (in rpm or degrees/s) The bigger the value is, the faster radar can scan
Acceleration	Defines how quickly the antenna can change its speed	Acceleration (in degrees/s ²)
Antenna pointing accuracy	Determines the precision of the angular location of the data	Antenna pointing accuracy (in degrees) The smaller the value is, the more accurate and more precise
Beam direction co-alignment	Determines how well the horizontal and vertical beams are aligned	Alignment (in degrees) The smaller the value is, the better aligned
Beam width matching	Determines how well the horizontal and vertical beam widths match	Matching (in degrees) The smaller the value is, the better match
Dynamic range	Determines the breadth of values that the radar can measure	Dynamic range (in dB) The bigger the value is, the broader range of signals that the radar can detect
Unwanted emissions	Determines the purity of the transmitted spectrum of the radar	A dB at B MHz The smaller the value, the purer and cleaner the transmitted spectrum

6.2 Fundamental parameters

6.2.1 Sensitivity

6.2.1.1 Definition

Sensitivity is defined as how far or how weak a radar echo is that the radar can detect. Setting A dBz as reflectivity of rainfall and B km as maximum distance to observe A , sensitivity A dBz at B km is calculated as shown by formula (7.A.3):

$$A = 10\log(C_0 C_{1F}) + 20\log(B) \quad (7.A.3)$$

where:

C_0 is a parameter determined regardless of system performance;

C_{1F} is a parameter specific to each weather radar system, system loss included.

Note: A pulse-compression radar has two constants C_{1F} , one for the short pulse and one for the long pulse.

A setting B , C_0 , C_{1F} and A is calculated. The smaller A is for a distance B , the smaller echoes radar can observe. Parameters that define C_0 and C_{1F} in Table 7.A.4 (for example, λ , SNR , S_{min} , P_t) are described in the following subsections.

6.2.1.2 Derivation from radar formula

The sensitivity related to rainfall target is a measurement to see how far the rainfall target is observable.

If the received power scattered from the rainfall target is P_r and the radar reflectivity factor of rainfall target is Z , P_r is expressed as formula (7.A.4):

$$P_r = \frac{C \cdot Z}{r^2} \quad (7.A.4)$$

with formula (7.A.5) (see, for example, [2]):

$$C = \frac{P_t G_t G_r h \theta_H \theta_V \pi^3}{2^{10} (\log_e 2) \lambda^2} \left| \frac{\epsilon - 1}{\epsilon + 2} \right|^2 \quad (7.A.5)$$

and formula (7.A.6):

$$Z = \int N_D D^6 dD \quad (7.A.6)$$

where:

P_t is the transmit power, in W;

G_t, G_r is the antenna gain (transmit, receive);

h is the spatial pulse length defined as $c \cdot \tau$, in m;

θ_H is the antenna beam width of horizontal plane, in rad;

θ_V is the antenna beam width of vertical plane, in rad;

λ is the wavelength, in m;

ϵ is the complex permittivity of precipitation particle;

D is the raindrop diameter, in m;

- N_D is the number of raindrops in unit volume, in $1/m^3$;
- r is the range to scatter, in m;
- C is the radar constant, in W/m [2].

Note: For practical applications, system losses are considered (see 6.2.1.4).

When P_r is at the minimum power level that can be detected, it can be expressed as S_{min} (see A.3.6). Substituting this S_{min} into formula (7.A.4) obtains the minimum radar reflectivity factor, Z_{min} , at any arbitrary distance r , as shown by formula (7.A.7):

$$Z_{min}(r) = \frac{S_{min}}{C} r^2 \tag{7.A.7}$$

where $Z_{min}(r)$ is the sensitivity index of weather radar.

If the items from the right side of formula (7.A.7), which need not be measured for each radar unit, are placed as C_0 and, if the items that are specific to the radar device and need to be measured are placed as C_1 , formula (7.A.7) is expressed as formula (7.A.8):

$$Z_{min}(r) = C_0 C_1 r^2 \tag{7.A.8}$$

C_0 includes the following items from the right side of formula (7.A.7), as shown by formula (7.A.9):

$$C_0 = \frac{2^{10} (\log_e 2) \lambda^2}{\pi^3 \left| \frac{\epsilon - 1}{\epsilon + 2} \right|^2} \tag{7.A.9}$$

Similarly, as C_1 has $P_t, G_t, G_r, h, \theta_H, \theta_V$ and S_{min} in formula (7.A.7), it is expressed as formula (7.A.10):

$$C_1 = \frac{S_{min}}{P_t G_t G_r h \theta_H \theta_V} \tag{7.A.10}$$

The value of C_0 is related to wavelength and temperature. Typical values of C_0 for each frequency band of S, C and X in 20 °C are shown in Table 7.A.4. The wavelength of S-band is 0.1 m, the wavelength of C-band is 0.057 m and the wavelength of X-band is 0.032 m.

Table 7.A.4. Typical value of C_0 (temperature 20 °C)

Items	S-band	C-band	X-band
λ (m)	0.1	0.057	0.032
$\left \frac{\epsilon - 1}{\epsilon + 2} \right ^2$	0.928	0.928	0.927
C_0	0.246 7	0.080 1	0.025 3

As the wavelength λ is normally set by the transmission frequency f_0 (MHz), it is calculated as shown by formula (7.A.11) using the speed of light as 3×10^8 m/s:

$$\lambda = \frac{300}{f_0} \tag{7.A.11}$$

6.2.1.3 Basic calculation

The unit (mm^6/m^3) is used for the unit of radar reflectivity factor Z and is normally expressed in decibels relative to Z as dBz. The common logarithm on both sides of formula (7.A.8) is obtained considering this and is multiplied by 10 as shown by formula (7.A.12):

$$10\log[Z_{\min}(r)] = 10\log(C_0) + 10\log(C_1) + 20\log(r) + 180 \quad (7.A.12)$$

$10\log(C_1)$ is expanded from formula (7.A.10) as shown by formula (7.A.13):

$$\begin{aligned} 10\log(C_1) &= 10\log(S_{\min}) - 10\log(P_t) - 10\log(G_t) - \\ &10\log(G_r) - 10\log(h) - 10\log(\theta_H) - 10\log(\theta_V) \end{aligned} \quad (7.A.13)$$

The units used for the items to be measured are:

- Minimum detectable signal: $10\log(S_{\min})$, in dBm
- Transmit power: $10\log(P_t)$, in dBm
- Antenna gain: $10\log(G_t)$, $10\log(G_r)$, in dB
- Spatial pulse length: h , in m

The spatial pulse length is the value of the pulse width τ (in s) multiplied by the speed of light. As the pulse width is normally measured in the unit of μs , the spatial pulse length is obtained as shown by formula (7.A.14):

$$h = 300\tau_{(\mu\text{s})} \quad (7.A.14)$$

- $\theta_{H/V}$ in rad

As the beam width is measured by degrees, it is converted into radian as shown by formula (7.A.15):

$$\theta_{H/V} = \frac{\pi}{180 \cdot \theta_{H/V(\text{deg})}} \quad (7.A.15)$$

6.2.1.4 System loss and attenuation of radio wave

The radio wave is attenuated (power loss) during transmission in the actual operation. Therefore, it is necessary to consider the power loss caused by the radar component, such as waveguide, and the attenuation caused when the radio wave propagates in space (due to air and rainfall). These loss and attenuation lead to deterioration of the radar sensitivity index Z_{\min} (increase). If the power loss generated by the radar component is F , F is included in C_1 because this element is specific to the radar device and should be measured. Refer to A.3.9 for system loss to be measured.

This is calculated as C_{1F} and is obtained from formula (7.A.13) as shown by formula (7.A.16):

$$\begin{aligned} 10\log(C_{1F}) &= 10\log(S_{\min}) - 10\log(P_t) - 10\log(G_t) - 10\log(G_r) - \\ &10\log(h) - 10\log(\theta_H) - 10\log(\theta_V) + 10\log(F) \end{aligned} \quad (7.A.16)$$

In addition, giving the attenuation by atmosphere, water and vapour as L , L is the function of the propagation range, r , and the rainfall intensity, R , and is expressed by formula (7.A.17):

$$L(r, R) = 2 \int_0^r (k_a + k_r R^\alpha) dr \quad (7.A.17)$$

where:

- k_a is the specific attenuation due to air, in dB/km;
- k_r, α is the specific attenuation due to rain k_r , in dB/km;
- R is the rainfall intensity, in mm/h;
- r is the range, in km.

If the rainfall intensity along the propagation path R is constant (R_0), only the distance is variable in formula (7.A.17) and is expressed as shown by formula (7.A.18):

$$L(r) = 2(k_a + k_r R_0^\alpha) r \quad (7.A.18)$$

to simplify the evaluation of sensitivity index during rainfall.

As the values of k_a , k_r , and α are different depending on the frequency used, set typical values for them according to each frequency band, as shown in Table 7.A.5 for evaluation.

Table 7.A.5. Specific attenuation due to air and rain (one-way, R in mm/h)

Frequency band	Specific attenuation due to air ^a	Specific attenuation due to rain ^b	
	k_a (dB/km)	k_r (dB/km)	α
S	0.005 89	0.000 343	0.97
C	0.007 07	0.001 8	1.05
X	0.008 835	0.01	1.21

^a See Reference [3].

^b See Reference [1], Table 9.5, one-way specific attenuations at 18 °C.

Lastly, it is insufficient to use S_{\min} as it is. Usually a proper value of SNR (in dB) should be added. This value is to be decided by users. In case users cannot decide, 1 dB is used.

Based on the above, formula (7.A.12) is practically expressed as shown by formula (7.A.19):

$$10\log[Z_{\min}(r)] = 10\log(C_0) + 10\log(C_{1F}) + 20\log(r) + L(r) + SNR + 180 \quad (7.A.19)$$

6.2.1.5 Pulse-compression gain

In pulse-compression radars, pulse-compression gain, G_c , and pulse width, τ_c , after pulse-compression processing are used for sensitivity index calculation of formulae (7.A.13) and (7.A.14), as shown by formulae (7.A.20) and (7.A.21):

$$P_t = P'_t G_c \quad (7.A.20)$$

$$10\log(P_t) = 10\log(P'_t) + 10\log(G_c) \quad (7.A.21)$$

Where P'_t is the original transmit peak power multiplied by pulse-compression gain G_c , G_c becomes $10\log(bT)$ theoretically (where b is the frequency modulation width and T is the transmission pulse width). h of formula (7.A.14) is calculated using τ_c .

Note: Pulse-compression gain only applies to the long pulse.

6.2.2 **Spatial resolution**

6.2.2.1 **Definition**

Spatial resolution describes the detail that the radar is capable of distinguishing.

As shown in Figure 7.A.7, it represents a sampling volume of the radar surrounded by $h/2$ (where h is spatial pulse length) and beam width. The smaller the sampling volume is, the higher the detail that the radar can observe.

Spatial resolution is decomposed into beam resolution and range resolution.

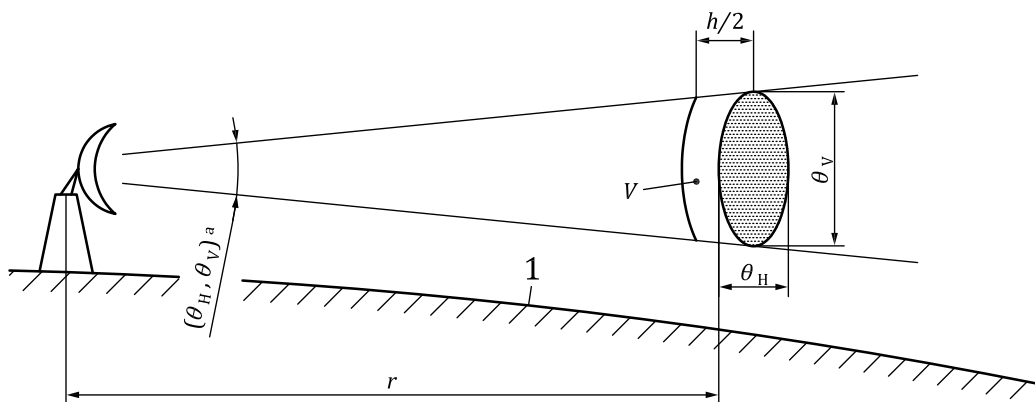
This system performance is evaluated in accordance with Table 7.A.6.

Table 7.A.6. System performance parameters

Category	Parameter	Evaluation
Beam resolution	θ_H : Antenna HPBW of horizontal plane (in rad) θ_V : Antenna HPBW of vertical plane (in rad)	The smaller, the better
Range resolution	ΔR_{pc} : For pulse-compression radar (in m) ΔR_{np} : For non-pulse compression radar (in m)	The smaller, the better

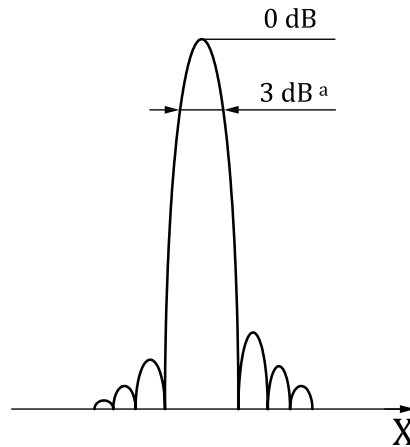
6.2.2.2 **Beam resolution**

Beam resolution is determined from measurement of antenna main lobe. Main lobe is measured by half width (at 3 dB down point, see Figure 7.A.8) and shows how narrow the beam is around the centre of emission. Fine beam resolution is obtained when the main lobe half width is smaller. It should be noted that beam resolution is limited by the worst value between the transmit beam main lobe and the receiver's processing unit of angle.



- Key:
- 1 Surface of the ground
 - V Target volume
 - H Pulse length
 - a Beam width
 - R Range

Figure 7.A.7. Spatial resolution



Key:

- X Horizontal/vertical angle
^a Down point: beam width

Figure 7.A.8. Beam resolution

6.2.2.3 Range resolution

Range resolution is related to transmit pulse length, but is constrained by bottlenecks through the entire system, including receiver's characteristics, such as bandwidth and sampling interval. These must be taken into account to calculate range resolution rather than simply using the spatial length of transmit pulse.

Since a received signal is obtained as a discrete value for every sampling interval in the case of a digital receiver system, the pulse width at the 3 dB down point of the received power waveform is not monitored directly in the same way as the transmit pulse width measurement.

Regarding this, pulse-compression and non-pulse-compression radars should be treated differently.

For non-pulse-compression radar, range resolution should be estimated using a combination of bottleneck factors that limit resolution performance, namely, transmit pulse half power width, sampling time interval and receiver bandwidth.

Range resolution is estimated as shown by formula (7.A.22):

$$\Delta R_{\text{rrp}} = \max(L_1, L_2, L_3) \quad (7.A.22)$$

using resolution values L_1 , L_2 and L_3 calculated from bottleneck factors, corresponding to transmit pulse half width, sampling time interval and receiver bandwidth, respectively.

As for the transmit pulse half width, L_1 is calculated with the measured transmit pulse half width τ_t , as shown by formula (7.A.23):

$$L_1 = \frac{c}{2} \tau_t \quad (7.A.23)$$

where τ_t is the transmit pulse half power width.

The sampling time interval of the received signal is the processing time interval, t_s , in the final stage of the signal processor. Using a time interval t_s , L_2 is obtained as shown by formula (7.A.24):

$$L_2 = \frac{c}{2} t_s \quad (7.A.24)$$

Finally, from the receiver's bandwidth (3 dB down point from the peak), L_3 is calculated as shown by formula (7.A.25):

$$L_3 = \frac{c}{2} \frac{1}{\Delta f} \quad (7.A.25)$$

where Δf is the bandwidth of the receiver's band-pass filter (BPF) measured at the 3 dB down point from the peak.

In pulse-compression radar, waveform shaping by raised cosine is conducted on the transmit wave to prevent the spectrum from widening. On the other hand, a windowing function is applied to the received wave to suppress the range side lobe. With this waveform shaping, Gaussian approximation fits well the waveform after pulse compression. Figure 7.A.9 shows an example sampling pattern of the received signals.

Since the sampling interval is generally not sufficiently small compared to pulse width, pulse width is estimated from the three sampling levels of the received signals corresponding to a transmit pulse peak and both sides of the 3 dB down point of the pulse peak.

The received pulse waveform $y(x)$ is shown by formula (7.A.26):

$$y(x) = A \cdot e^{-\frac{(x-\mu)^2}{2\sigma^2}} \quad (7.A.26)$$

where:

- x is time as the abscissa axis;
- A is the maximum amplitude;
- μ is the average value;
- σ^2 is variance.

Pulse width is estimated by calculating A , μ and σ^2 with three measured values of (x_1, y_1) , (x_2, y_2) and (x_3, y_3) , which are sampled from the received pulse waveform. To increase the precision of pulse width estimation, y_2 should be nearly the peak value and y_1 and y_3 should be lower than and nearest to the 3 dB down point from y_2 .

The natural logarithm on both sides of formula (7.A.26) becomes formula (7.A.27):

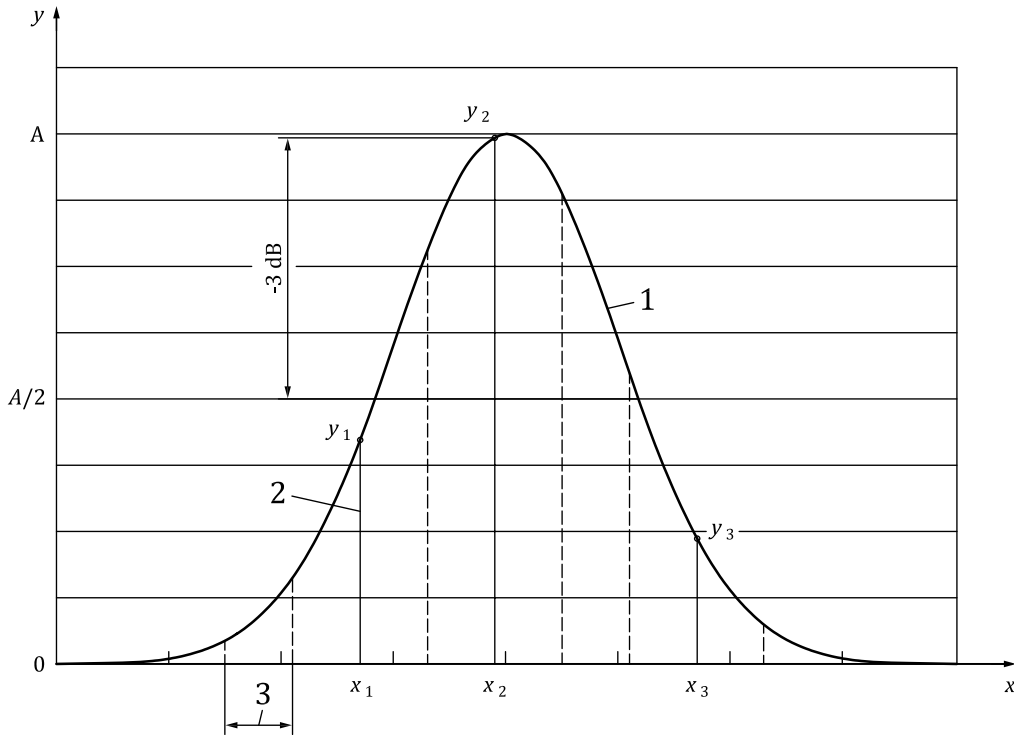
$$\ln[y(x)] = \ln(A) - \frac{(x-\mu)^2}{2\sigma^2} \quad (7.A.27)$$

The average value, μ , the variance, σ^2 , and the maximum amplitude, A , are obtained by substituting three measured values into formula (7.A.27) and solving simultaneous formulae (7.A.28)–(7.A.30):

$$\mu = \frac{\ln\left(\frac{y_3}{y_2}\right)(x_1^2 - x_2^2) - \ln\left(\frac{y_2}{y_1}\right)(x_2^2 - x_3^2)}{2\ln\left(\frac{y_3}{y_2}\right)(x_1 - x_2) - \ln\left(\frac{y_2}{y_1}\right)(x_2 - x_3)} \quad (7.A.28)$$

$$\sigma^2 = \frac{(x_1^2 - x_2^2) - 2\mu(x_1 - x_2)}{2\ln\left(\frac{y_2}{y_1}\right)} \quad (7.A.29)$$

$$A = y_1 e^{\left[\frac{(x_1 - \mu)^2}{2\sigma^2}\right]} \quad (7.A.30)$$



- Key:
- 1 Received pulse waveform after pulse compression
 - 2 Sampling pulse
 - 3 Sampling interval

Figure 7.A.9. Received signal sampling waveform

When pulse width is defined as the width of the 3 dB down point from the maximum amplitude, A , pulse width, τ_{pc} , is given as shown by formula (7.A.31):

$$\tau_{pc} = 2(x_3 - \mu) \sqrt{\frac{3}{10\log(A) - 10\log(y_3)}} \quad (7.A.31)$$

Range resolution of pulse-compression radar, ΔR_{pc} , is calculated using the estimated τ_{pc} above as shown by formula (7.A.32):

$$\Delta R_{pc} = \frac{c}{2} \tau_{pc} \quad (7.A.32)$$

6.2.3 Phase stability

The radar system's Doppler velocity precision depends on the phase stability of transmit frequency and the stability of pulse repetition frequency. Phase noise degrades the radar system's Doppler observation capabilities and therefore affects ground echo clutter rejection and the estimation of the dual-polarization data. The stable local oscillator (STALO) is usually considered the most dominant factor of phase instability [4] in systems with amplifiers (klystron, solid-state). Ideally, an oscillator generates a single frequency, but, in fact, instability is caused by random fluctuations of phase around the carrier. Phase noise is measured in units of dBc/Hz as the spectral power density of each 1Hz bandwidth, away from the carrier and referenced to the carrier frequency power.

Having $L(f)$ as spectral density (expressed as antilogarithm) of 1 Hz bandwidth caused by random fluctuations, let θ_{ps} be defined as phase stability within a specified range (a, b) in units of degrees, which is calculated as shown by formula (7.A.33):

$$\theta_{ps} = \frac{180}{\pi} \sqrt{2 \int_a^b L(f) df} \quad (7.A.33)$$

where $\sqrt{2}$ means that phase stability should be calculated as double-side band.

As integral range, (a, b) must be set to (100 Hz, 1 MHz) for the calculation, considering typical f_{PRF} values for S-/C-/X-band. Regarding frequency differences Δn , increase of phase noise when the frequency of the oscillator is multiplied by N is expressed as shown by formula (7.A.34):

$$\Delta n = 20 \log_{10} N = 10 \log_{10} N^2 \quad (7.A.34)$$

Since phase noise in terms of root mean square (RMS) is the square root of an integral value as antilogarithm, there is a proportional relationship between the oscillation frequency and phase noise in units of degree.

The above method intends to estimate the phase noise resulting from the STALO only. In magnetron radars, a sample of every transmitted pulse is taken, and phase information from this sample is used in the receiver to measure the Doppler shift from successive pulses. This is called "coherent-on-receive". In these systems, additional sources of phase noise must be considered. A method that determines the phase stability of the full radar system is the use of an optical delay line. The delay line will generate the delay needed for the Doppler measurement. Other options, such as surface or bulk acoustic wave delay lines, suffer from high insertion losses reducing the SNR. Moreover, the inherent delays are too short for long-range measurements.

The optical delay line consists of an RF-to-optical and an optical-to-RF converter with a fibre optic reel in between. The RF-to-optical transmitter consists of a continuous wave (CW) laser diode, which is usually amplitude modulated with the microwave signal. The optical-to-RF receiver converts the optical signal that has travelled through the fibre optic reel back into an RF signal with the same characteristics but with reduced amplitude. The length of the reel determines the delay of the received transmit pulse.

Using the existing signal-processing hardware, the comparison of the transmit signal phase (transmit sample) with the received echo phase will show the inherent phase noise of the system. The system coherence will also be calculated by the signal-processing unit of the radar receiver. This method cannot only be used for magnetron radars but also provides an integral phase noise measurement for klystron or solid-state systems.

6.2.4 Accuracy of dual-polarization measurement

6.2.4.1 Dual polarization

The accuracy requirements for dual-polarization radars are higher than for conventional radars using single polarization only. Dual-polarization products are based on differences between two polarizations and offsets between the two channels can produce large errors in retrieved quantities, for example, estimated rain rate. For example, it is assumed that reflectivity factor can be estimated with an accuracy of about 1 dB, whereas, for differential reflectivity (Z_{dr}), the difference in reflectivity factor on linear horizontal and vertical polarization, an accuracy of at least 0.2 dB is required [5].

6.2.4.2 **Cross polarization and port isolation**

Cross polarization is the characteristic of an antenna to separate the horizontal from the vertical signal. The parameter is typically determined by the antenna manufacturer on a far field test stand.

Port isolation describes the capability of the radar system to separate the horizontal from the vertical signals after reception by the antenna system. This parameter can be determined easily for single radar components, such as the rotary joints or the waveguide switch. However, to estimate the integral port isolation for all contributing components is technically very complex. Since in current radar systems the port isolation is several orders of magnitude lower than the cross polarization, this parameter is of lower relevance in the system performance context.

6.3 **Other key parameters**

6.3.1 ***Side lobe***

Regarding side lobes, suppression level of antenna side lobe and range side lobe should be measured. The former determines the faithfulness of the radar values due to strong off-axis echoes. The latter is relevant for pulse-compression radars and determines the faithfulness of the radar values due to strong, out-of-resolution volume but radially aligned echoes.

6.3.2 ***Beam direction co-alignment***

This parameter is defined as the difference in degree between the peaks of the horizontal and the vertical co-polarized antenna diagrams. It is a measure to compare the beam direction of the horizontal and the vertical beam.

6.3.3 ***Beam width matching***

This parameter is defined as the difference in degrees between the horizontal and vertical co-polarized antenna diagrams at a given level (-3 dB, -10 dB). It is a measure to compare the symmetry of the radiated volume by the horizontal and the vertical beams.

6.3.4 ***Maximum rotation speed***

This parameter is related to how fast the antenna can rotate. The bigger the value is, the faster radar can perform scanning.

6.3.5 ***Acceleration***

This parameter defines how quickly the antenna can change its speed. As measuring absolute acceleration properly in units of degrees/s² is complicated, this document defines as an alternative the time the antenna takes to stop completely in both AZ/EL directions when in full motion.

The acceleration value alone does not completely describe how fast and precisely the antenna can change EL and AZ position. This is called "step response time", which is not further discussed in this document. This parameter defines the time needed to step the antenna from one position to another within a given accuracy window to allow for settling. An important application is the stepping from one EL to the next during a volume scan.

6.3.6 **Antenna pointing accuracy**

Antenna pointing accuracy addresses different aspects:

- The ability of the positioner unit to steer the antenna dish with a defined precision to a given AZ and EL angle in relation to a mechanical reference point on the positioner unit;
- The ability of the system to point to the same given position repeatedly over a long time (months, years);
- The precise alignment of the internal (hardware) AZ/EL reference to the local geographical orientation to relate the measured data to a position on the Earth;
- The alignment of the beam in both polarizations (if applicable) to the focus point of the antenna.

There are many influences on the pointing accuracy, such as the type of positioning system (gears, belt), the mechanical installation at the site (levelling), the structure of the tower (steel, concrete), the north alignment, and the assembly of the dish and feed horn.

The geographical alignment of the antenna and its stability over a long period of time can be verified and monitored with software tools from radar manufacturers, which use the electromagnetic signal of the sun as a position reference. Prerequisites for this kind of measurement are the availability of the precise geographical position of the radar system and the correct time, since both will be used to estimate the reference position of the sun. Details on the recommended frequency of antenna pointing checks with the sun are given in Attachment D.

Because of difficulties of obtaining absolute pointing accuracy inside a factory, a feasible way is to measure pointing accuracy in terms of repeatability in a factory, followed by sun checking on site. Repeatability checks the antenna capabilities to point to the same direction after continuous movement.

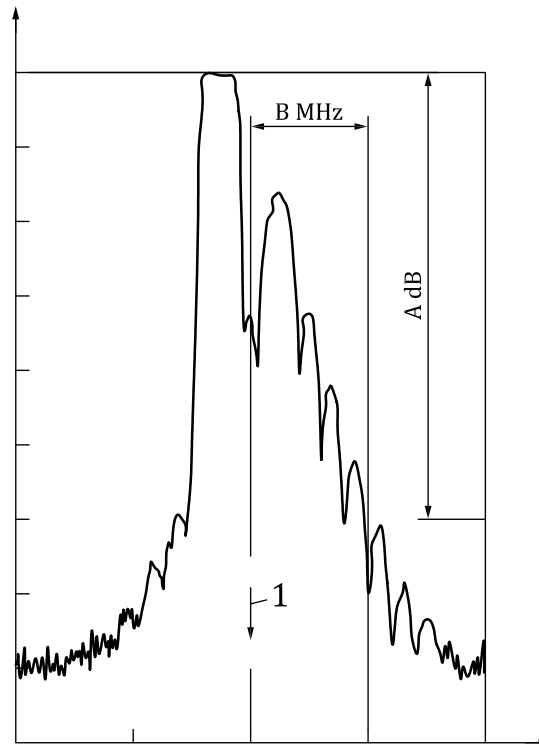
6.3.7 **Dynamic range**

Dynamic range, LV_d , is the ratio of the maximum to minimum signal strength that the radar receiver can measure. It is the difference, in dB, of the receiver output between the minimum detectable signal (S_{min}) and the point at which the receiver amplifier saturates. Saturation can also occur in the digital domain due to overflow. Measurement or calculation of S_{min} is described in A.3.6. Defining the maximum signal can be done by using the compression point of a receiver. The 1 dB compression point is very common for the characterization of receivers. It is the point where the receiver gain is reduced by 1 dB due to compression. When the amplifier is operating in the linear region, an increase of input signal by 3 dB will result in an increase of output signal by 3 dB.

For the measurement, it is recommended to use an external and highly stable signal generator (SG). The output power range of the SG must span the expected dynamic range of the receiver. The dynamic range should be measured over the complete receiver chain from the input of the receiver, which is usually at the waveguide to coaxial transition. This includes analogue and digital signal processing. The complete receiver chain includes the low noise front end, downconverters, filters, analogue–digital converter (ADC) and digital signal processing.

6.3.8 **Unwanted emissions**

The level of unwanted emissions describes the purity of the transmitted spectrum of the radar (see Figure 7.A.10). The expression A dB at B MHz shows A dB is decreased from the peak spectrum value at a point B MHz away from the central frequency. The greater the value A , the more radars can operate in the same band due to narrow frequency bandwidth.



Key:
1 Centre frequency

Figure 7.A.10. Unwanted emissions

Limits for unwanted emissions are specified by several national and international standards, for example, CEPT ERC Rec (02)05 (2012), CEPT ERC Rec 74-01E (2011), ITU-R SM.329-12 and ITU-R SM.1541-6.

7. CALIBRATION, MONITORING AND MAINTENANCE

7.1 General aspects

The terms “calibration”, “maintenance” and “monitoring” are related to each other and often it is not easy to distinguish clearly between them. During calibration (see 7.2) the performance of the radar system is characterized in order to provide radar data with high accuracy, that is, estimate reflectivity with an accuracy better than 1 dB. Maintenance (see 7.4) is performed to replace broken parts of a radar (see 7.4.3), preventive maintenance (see 7.4.2) will ensure the performance of the radar and will extend the time between failures. After replacing parts of the radar, a calibration is often necessary. Monitoring (see 7.3) describes a process that ensures high data quality of the radar. Often during monitoring, decisions on intermediate maintenance or calibration are made.

Calibration and maintenance are performed at regular intervals, as described below. In most cases, maintenance of radar hardware has to be performed on site, software maintenance could be done from remote, whereas calibration can be performed on site (for example, if hardware settings have to be adjusted or special equipment is involved) or from remote (for example, if calibration constants are adjusted). Monitoring should be performed at least on a daily basis; therefore, monitoring will be from remote for unmanned sites. Monitoring is performed during normal operation; no interruption of radar operation is necessary.

The calibration and maintenance of any radar should follow the manufacturer's prescribed procedures. An outline is given in subsections 7.2 to 7.5.

7.2 **Calibration**

7.2.1 **General**

Regular calibration is crucial for a good system performance.

7.2.2 **Types of calibration**

Ideally, the complete calibration of reflectivity uses an external target of known radar reflectivity factor, such as a metal-coated sphere. The concept is to check if the antenna and waveguides have their nominal characteristics. However, this method is very rarely used because of the practical difficulties in flying a sphere and multiple ground reflections. Antenna parameters can also be verified by sun flux measurements. Routine calibration ignores the antenna, but includes the waveguide and transmitter receiver system. Typically, the following actions are prescribed:

- Measurement of emitted power and waveform in the proper frequency band;
- Measurement of transmission and receiver losses;
- Verification of transmitted frequency and frequency spectrum;
- Injection of a known microwave signal before the receiver stage, in order to assign a reference power to a given ADC count;
- Measurement of the SNR ratio, which should be within the nominal range according to radar specifications.

If any of these calibration checks indicate any changes or biases, corrective adjustments must be made. Doppler calibration includes: the verification and adjustment of phase stability using fixed targets or artificial signals; the scaling of the real and imaginary parts of the complex video; and the testing of the signal processor with known artificially generated signals.

Although modern radars are usually equipped with very stable electronic components, calibrations must be performed often enough to guarantee the reliability and accuracy of the data. Calibration must be carried out either by qualified personnel or by automatic techniques, such as online diagnostic and test equipment. In the first case, which requires personnel, calibration should optimally be conducted at least once per year; in the second, it may be performed daily or even semi-continuously. Simple comparative checks on echo strength and location can be made frequently, using two or more overlapping radars viewing an appropriate target.

Radar systems must be calibrated regularly to ensure constantly high measurement accuracy. This involves the calibration of various parameters at different time intervals. The radar constant, C , should be measured with an accuracy of ± 1 dB. The error in the radar reflectivity factors is larger, since, in addition to the radar constants, this includes further parameters (for example, atmospheric attenuation). The table in Attachment D summarizes the parameters to be measured, the methods used in practice and the required calibration frequency.

7.2.3 **Items, procedures and intervals of calibration**

The frequencies suggested in Attachment D are indicative values only. Users should follow the manufacturer's instructions.

7.3 **Monitoring**

7.3.1 **General**

Monitoring describes procedures to monitor the state, functionality and data quality of a radar system. It should be done on a regular basis, at least daily, based on the instructions and recommended procedures given by the manufacturer. For unmanned radar sites, monitoring is performed from remote central offices. Inconsistencies discovered during monitoring can lead to intermediate maintenance or calibration or other actions described by the manufacturer.

Monitoring of the radar system has a considerable influence on radar data quality and therefore radar data application, such as QPE and data assimilation. The monitoring of data quality will be included in the planned ISO 19926-2.

Depending on the radar hardware and software, various parameters of the system can be monitored automatically or manually. Automatic monitoring will involve the release of text messages to service personnel. Manual monitoring is done on a regular basis by service personnel for technical performance or by a meteorologist for radar products, such as reflectivity, rain rate or Doppler velocity (for radar data exchange, see Attachment E). A simple monitoring of the functionality of a weather radar would comprise frequent checks of uncorrected radar images and verification of the strength and location of ground clutter targets. Sudden changes would indicate failures of the receiver or transmitter or a pointing direction adjustment of the antenna. Even a simple comparison of radar-derived rain rate to a nearby rain gauge could give indications of the functionality of a weather radar. Regarding polarimetric radar, monitoring the maximum p_{HV} in light stratiform rain during the normal operation of the radar gives a good indication of the overall quality and condition of the system.

Several items described in 7.2 and 7.3 can be considered as monitoring. Especially, those items recommended for daily or even more frequent checks can be considered as monitoring, as long as automatic procedures would raise an alarm as soon as parameters deviate from predefined values. Calibration checks with the sun (see 7.3.3) can monitor the receiver stability and pointing accuracy in case the data evaluation is performed in real time and transmitted to the remote central office. A built-in test equipment (BITE) can monitor a large number of technical parameters and will raise alarms in case the parameters are outside predefined boundaries. BITE can also monitor external devices, such as air conditioning or uninterrupted power supplies. BITE alarms should be sent automatically as text messages to service personnel.

In addition, radome attenuation up to several dB must be considered in situations where heavy rain or snowfall leads to water, ice or melting ice cover on the radome. Ageing of the radome can increase the time until water or ice cover runs off. This can be improved by hydrophobic coating of the radome. Fissures in the radome can lead to water sucking of the radome and thus increased losses. A regular cleaning and inspection of the surface of the radome is recommended.

7.3.2 **Stability of radar system**

With the benefit of today's modern radar technology (for example, low noise amplifiers (LNAs), fast and accurate ADCs) and with careful and regular calibration, it is possible to achieve high system stability: intrinsic uncertainties associated with the radar system itself are smaller than the uncertainties associated with the intrinsic variability of reflectivity of the radar target.

For quantitative radar applications, high stability and accurate calibration are mandatory. Monitoring the stability of only the receiver chain or transmitter chain (one-way) is simpler than monitoring the stability of the entire radar system (two-way).

To monitor the stability of the receiver chain, a reference power signal (instead of the received power coming from the antenna), is injected into the LNA input of the receiver and exactly that value (\pm a given uncertainty) is used for linking the given analogue-to-digital unit value

at the output of the digital receiver to the reference power value. No measurement is made of the power backscattered by a given object at a given distance. It is simply known that a given power on a logarithmic scale (dBm) corresponds to a given log-transformed analogue-to-digital unit. In the case of an antenna-mounted receiver, an effective solution uses a noise source as the reference signal, taking advantage of its high temperature stability [6].

Monitoring the entire system's stability requires the assessment of losses (receive and transmit chains including waveguide, rotary joint, couplers, cables, radome, etc.), antenna gain and the accuracy of the antenna pointing angle. Assuring the stability of the entire system requires the calibration of the radar system against some known reference target (for example, a metal sphere, a corner reflector with certified radar cross section) at various distances from the sensor itself. However, passive scatterers, such as large spheres or corner reflectors, are difficult to deal with, especially in heavily cluttered mountainous terrain.

There are two ways to overcome this difficulty:

- Total system stability (two-way) is occasionally [7] [8] or continuously [9] [10] checked using active calibrators;
- The problem is split into two simpler, complementary parts:
- An external receiver is used as a one-way passive calibrator for checking the transmit chain (for example, see [7] and [11]);
- The sun is used for calibrating [12] and checking [13] [14] the receive chain.

Results from the latter method were derived using data acquired in 2008 [13] [14] during a period of quiet solar flux activity. More recently, it has been shown this method is also practicable during more active solar periods [15] [16]. The use of the sun is optimal in terms of cost/benefit. Solar monitoring can be carried out continuously.

In the event that regular monitoring indicates change in stability, the user should consult the manufacturer's instructions for guidance on corrective action.

7.3.3 ***Monitoring receiver stability and electrical pointing using the sun***

7.3.3.1 **General remarks**

The sun is a known source of microwave energy, and it can be used to check and monitor several aspects of a weather radar operation. These checks can be performed as separate tasks between the operational scans or during the radar maintenance; sun observations during normal operational scans can also be used.

Refer to system manuals for detailed instructions on how tests are performed for individual radars.

7.3.3.2 **Antenna pointing accuracy**

The position of the sun at any given time is well known. The microwave signal from the sun can be used to verify and calibrate the pointing accuracy of the radar antenna in both AZ and EL. Typically, this is done by performing a sector scan around the sun and calculating the offset in both AZ and EL using the known position of the sun and the angle information from the radar antenna control. For EL offset, the refraction at low EL angles has to be taken into account. Most weather radar systems have an automated procedure for this. In addition, methods for calculating the offsets using the sun "hits" during normal operational scans have been developed.

The use of solar radiation to monitor the antenna pointing accuracy implicitly requires that the time in the radar control system is accurately synchronized.

Sector scans around the sun can also provide an estimate on the antenna gain and beam width.

7.3.3.3 Receiver stability

The condition of the radar receiver chain can also be monitored using the microwave signal from the sun. It has to be noted, however, that the solar flux fluctuates a lot over time. Reference values for the solar flux can be retrieved from solar observatories.

In the case of dual-polarization radars, the sun signal can be seen in both receiver channels. The horizontal and vertical signals should have the same magnitude but be uncorrelated (ρ_{HV} close to 0) since the sun is an unpolarized source.

7.4 Maintenance

7.4.1 General aspects

Radar maintenance, which is essential to ensure correct and ongoing radar operation, requires highly skilled human resources and significant financial resources for staff travel, test equipment and appropriate spares.

Radar maintenance also requires the availability of detailed, manufacturer-provided maintenance manuals and documentation.

Modern radars, if properly installed and operated, should not be subject to frequent failures. Some manufacturers claim that their radars have an overall mean time between (major) failures (MTBF) of the order of one year. However, these claims are often optimistic and the realization of the MTBF requires scheduled preventive maintenance. A routine maintenance plan and sufficient technical staff are necessary to minimize repair time.

Competent maintenance organization should result in radar availability 96% of the time on a yearly basis, with standard equipment. Better performances are possible at a higher cost.

To avoid maintenance-related shutdowns during critical weather conditions, this is coordinated in advance with the weather forecast. Normally, maintenance lasts only a few hours.

7.4.2 Preventive maintenance

Preventive maintenance should include at least a monthly check of all radar parts subject to wear, such as gears, motors, fans and infrastructures. The results of the checks should be written in a radar logbook by local maintenance staff and, when appropriate, sent to the central maintenance facility. When there are many radars, there might be a centralized logistic supply and a repair workshop. The latter receives failed parts from the radars, repairs them and passes them on to logistics for storage as stock parts to be used as needed in the field.

7.4.3 Corrective maintenance

For corrective maintenance, the service should be sufficiently equipped with the following:

- Spare parts for all of the most sensitive components, such as tubes, solid-state components, boards, chassis, motors, gears, power supplies, and the like. Experience shows that it is

desirable to have up to 30% of the initial radar investment in critical spare parts on the site. If there are many radars, this percentage can be lowered, with a suitable distribution between central and local maintenance.

- Test equipment, including the calibration equipment mentioned above. Typically, this would amount to up to 15% of the radar purchase price.
- Well-trained personnel capable of identifying problems and making repairs rapidly and efficiently.

7.4.4 **Maintenance options**

Weather radar systems must at least be equipped with the following maintenance options:

- Remote access;
- On/off switch (reset);
- Test with reference signals;
- Software/firmware upgrades;
- Antenna pointing adjustment;
- Fault and status diagnosis.

Some maintenance tasks can be performed remotely (a reliable connection is required), others require an on-site visit.

7.4.5 **Maintenance items and intervals**

Maintenance methods and procedures vary with radar manufacturer. Nevertheless, manufacturers often use similar maintenance items and measuring instruments.

First and foremost, this involves regular, repeated checking of the parameter calibrations provided by the manufacturer. Parameters deviating from the reference value must be recalibrated.

Test results, such as transmitted power or dynamic range, should be within tolerance to maintain high-quality data. However, it is difficult to define clearly these tolerance values because they depend on the purpose of the observation and the system configuration.

Recommended minimum equipment for calibration and maintenance includes the following:

- Microwave SG;
- Microwave power meter and/or power sensor;
- MHz oscilloscope;
- Microwave frequency counter and/or spectrum analyser;
- Microwave components, including loads, couplers, attenuators, connectors, cables, adapters, etc.;
- Standard electrical and mechanical tools and equipment;
- Diode detector and 3 dB attenuator for pulse width measurements.

An example of each item with the corresponding maintenance intervals for the radar system is shown in Attachment D. Since some of those devices are used to calibrate the radar, they must be calibrated at regular intervals.

Maintenance encompasses not only the radar system itself, but also other technical units vital for its operation (for example, ventilation, UPS and air conditioning). Their maintenance interval may differ from that of the radar system itself. The hardware associated with the software used in control systems, the service and the product generation also undergo regular checks. These must take place every two years. In addition, maintaining the inventory of suitable spare parts at the radar site and in a central warehouse are also important contributors to continuous availability.

7.5 Life-cycle management

7.5.1 Spare-parts strategy

The high data availability requirement of a weather radar requires 24/7 operation without long breaks because of time-consuming maintenance or failures in the system. To ensure high availability, it is good policy to store critical spare parts at the radar site or at the operator's warehouse, where they can be quickly deployed in case of a failure. These spare parts can include, for example, the critical parts of the radar transmitter, receiver, antenna drive system, electric power and communication interfaces.

Refer to the manufacturer's documentation for a detailed list of recommended spare parts.

Less critical spare parts can be ordered on demand from the manufacturer. Many manufacturers offer service contracts or express spare part services to ensure swift delivery of the factory spares.

The manufacturer must be able to deliver a complete list of all the spare parts in the system with delivery times.

7.5.2 System availability

System availability should be defined as the percentage that the system operates satisfactorily over a certain period of the time including time used for scheduled preventive maintenance and corrective maintenance, and is defined by formula (7.A.35):

$$\text{System availability} = \frac{(MTBF \cdot NF)}{(MTBF + MSRT) \cdot NF + TTPM} \cdot 100\% \quad (7.A.35)$$

where:

- NF* is the total number of failures during the system operating period; "failure" is defined as loss of functionality whereby the system is unable to fulfil the system requirements; therefore, even if a functional failure occurs on a certain unit, as long as the system fulfils the system requirements because of such a redundancy, it does not correspond to a failure;
- MTBF* is the mean time between failure; defined as the total measured operating time divided by the total *NF* of the system;
- MSRT* is the mean service restoration time;
- TTPM* is the total time for preventive maintenance; defined as the total time of scheduled preventive maintenance time during the system operating period.

The *MSRT* is defined by formula (7.A.36):

$$MSRT = MTTR + MRT \quad (7.A.36)$$

where:

- MTTR* is the mean time to repair; defined as the total measured repair time divided by the total *NF* of the system provided that the necessary replacement parts are available on site;
- MRT* is the mean response time, defined as the mean time required, starting from the incident of failure, for a technician to be ready to commence a repair action; if required, because spare parts are not in the radar site, the time for transportation from the central warehouse or manufacturer should be included in the *MRT*; holding suitable spare parts and keeping an inventory of them are also important for high availability.

A conceptual image of each parameter is shown in Figure 7.A.11.

7.5.3 **Life-cycle costs**

A Doppler radar is a complex tool that is able to detect an object and determine its position and the radial component of its velocity at a given time. A Doppler weather radar is a very complex but unique tool that is able to obtain a real-time overview on the current precipitation fields. It clearly shows where and when something is happening. However, to describe precisely what is happening and to quantify accurately the precipitation rate is far more difficult. With this basis, it is not surprising that the general recommendation of this document regarding required personnel is that the ratio between full-time equivalent (FTE) of radar engineers/scientists and the number of radars in the network must be larger than 1. Weather radar life-cycle costs also include spare parts costs and basic operation maintenance costs.

8. **STAFF, COMPETENCIES AND TRAINING**

The selection, design, operation, maintenance and use of a weather radar network requires a broad understanding of the technology, its limitations and the application requirements.

The design of the radar network and the selection of the radar technology requires trade-off studies and that the wide variety of user applications are taken into account. The users of the radar data and products require knowledge of end-user applications and mesoscale meteorology. As experience and knowledge of the radar capabilities evolve, there could be additional developments for sustainable and enhanced weather services.

Radar utilizes high power transmitters, very sensitive receivers, sophisticated signal processing, heavy rotating pedestals and antennas, and self-monitoring tools. The radar site is most often located as a stand-alone remote facility with heating/cooling equipment, shelters,

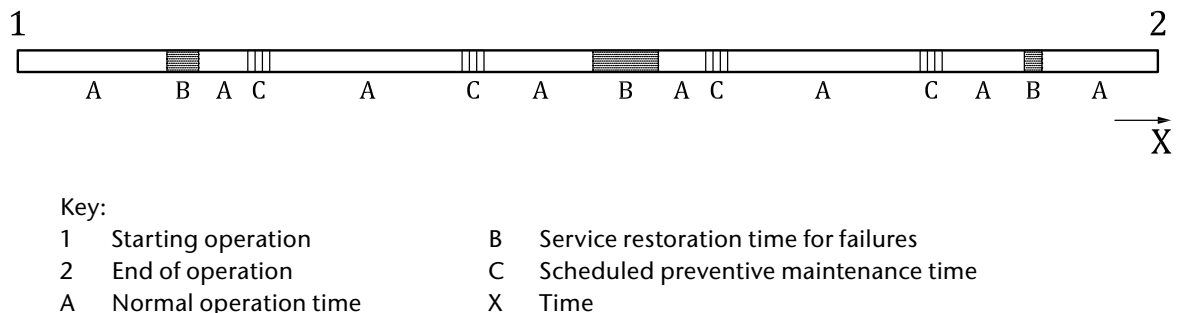


Figure 7.A.11. Example of calculation of system availability criteria

telecommunications, auxiliary power facilities and site maintenance issues. The radar requires calibration and maintenance to produce reliable measurements. Small changes in calibration and interpretation can significantly impact the outcomes. Quality management requires monitoring and recording system changes.

Hence, there are a wide range of competencies to operate and use a radar and radar network, including scientific, meteorological, technical and logistical skills. These competencies are shown in Table 7.A.7.

Operators of radars also support other monitoring technologies. WMO is developing comprehensive competencies over a range of such technologies.

Table 7.A.7. Staff, competencies and training

<i>Name</i>	<i>Description</i>
Project leadership and management	<p>The organization must “own” the project. Understanding of the overall goals, and the ability to lead and manage the end-to-end project is critical.</p> <p>The overall approach, the negotiations for and management of funds, and the leadership of people and contracts is required. Many competencies can be provided in creative ways (for example, by teams, external consultants or others), but project ownership must reside within the organization.</p> <p>Education/experience: leadership and project management skills.</p>
Scientific and meteorological	<p>Strategic planning is required to specify the service and the service level, and to design the radar network and its applications. This is needed at the beginning of the project and could be provided by consultants working closely with the NMHS.</p> <p>Specific competencies:</p> <ul style="list-style-type: none"> - Understanding of the organization’s strategic plan and envisioned service and service levels; - Understanding of weather (climatology of precipitation intensity, height of relevant weather systems, characteristics of severe weather) in the coverage area; - Basic understanding of user or application requirements (bias, accuracy, data quality); - Basic understanding of radar technologies (attenuation, beam width, scan strategy, ground clutter mitigation) and trade-offs. <p>Education/experience (of the team):</p> <ul style="list-style-type: none"> - Meso-meteorological and hydrological knowledge (mesoscale meteorology, distributed watershed); - Understanding of the application of radar technology; - Understanding of the strategic direction of NMHS; - Able to perform requirements analysis; - Scientific knowledge of radar limitations.
Scientific and engineering	<p>Technical support is required to convert the user specifications into technical specifications and for technical and process planning. This can be a team of people or provided through consultants working with NMHS and system designers.</p> <p>Specific competencies:</p> <ul style="list-style-type: none"> - Understanding of radar technology and trade-offs; - Understanding of the impact on service and application levels; - Understanding of organizational competencies (project management, technical capacity); - Understanding of safety, licensing and construction practices. <p>Education/experience:</p> <ul style="list-style-type: none"> - Industrial, electro-mechanical engineering for planning; - Radar hardware knowledge; - Organizational knowledge; - Quality management design principles knowledge.

<i>Name</i>	<i>Description</i>
Technical – support and maintenance	<p>Ongoing maintenance, calibration and support is required. It may be contracted out, but this could be fraught with problems (for example, competency with radar can be difficult to find).</p> <p>Specific competencies:</p> <ul style="list-style-type: none"> - General knowledge and practice of occupational safety procedures when working with high-power systems and heavy machinery; - General understanding of electronics (need to operate voltmeters, SGs, oscilloscopes, spectrum analysers); - Comfortable working with computers, setting up networks, backing up data and computers; - General knowledge of site maintenance (road repair, diesel and UPS power systems, air conditioners, heating systems); - Basic knowledge of high-power systems, heavy machinery, electronic components at line replacement unit level, telecommunications; - Diagnostic and analytical skills; - Understanding of quality management culture; - Basic knowledge of radar applications. <p>Education/experience:</p> <ul style="list-style-type: none"> - Advanced technical skills with high-power electrical RF systems, electronic and computer systems, and heavy mechanical systems; - Knowledge of auxiliary power systems and general site maintenance.
Quality management	<p>Roles are to manage radar equipment quality, the radar network operations and maintenance, including engineering (maintenance, testing, sparring planning) and scientific (hardware diagnostic support) support, metadata management, archiving, radar and processing system monitoring and updating.</p> <p>Education/experience (team and a variety of skills needed):</p> <ul style="list-style-type: none"> - Basic technical skills to monitor and diagnose operational systems, and report system changes; - Computer technology skills for archiving and retrieving metadata and data; - Computer software and system installation skills for updating radar processing and hardware systems.
Meteorological and/or application developer and research	<p>Role is to optimize the use of radar data and integrate it into forecast systems, and training end users. This includes quality management of the radar system. This can be a wide-ranging group of people (“local guru”) and could be developed over time.</p> <p>Specific competencies:</p> <ul style="list-style-type: none"> - Training and products, which may initially be done by radar manufacturer software; - Experience with technology resulting in continual capacity building, which is best done in-house; - Maturity with technology resulting in increased or enhanced requirements, which can require changes in the radar or product generation configuration or in data sharing; - Broad knowledge of radar applications, including knowledge of cloud physics, meso-scale meteorology, precipitation measurements and hydrological application; - Application development, which is open ended and could be from commercial services, data exchange, software applications for radar, integrated observing systems, forecasting, and product improvement and enhancement. <p>Education/experience: knowledge of end-user application and scientific/software application development, including integration into forecast or other application systems.</p>

9. SITING AND INSTALLATION

9.1 General aspects

The planned ISO 19926-2 will provide information on effects that reduce the quality of precipitation measurement by radar and their detection, as well as relevant countermeasures, such as post-processing of radar data.

9.2 Selection and preparation of a radar site

The choice of the site for a radar system depends on the planned application.

In the case of a radar network intended primarily for synoptic applications, radars at mid-latitudes should be located at a distance of approximately 150 km to 200 km from each other. If the radar network is used for quantitative rainfall measurements, where it is paramount to use radar beams at low height, that distance should not exceed 100 km. The distance can be increased at latitudes closer to the equator, if the radar echoes of interest frequently reach high altitudes. In all cases, narrow-beam radars will yield the best accuracy for precipitation measurements.

When there is a definite zone that requires storm warnings, the best compromise is usually to locate the equipment at a distance of between 20 km and 50 km from the area of interest and generally upwind of it according to the main storm track. It is recommended that the radar be installed slightly away from the main storm track in order to avoid measurement problems when storms pass over the radar. At the same time, this should lead to good resolution over the area of interest and permit better advance warning of incoming storms [17].

Radar sites on high mountains are of little benefit for detecting precipitation near the ground. Measurements with negative EL produce strong ground echoes, hence they make sense only in exceptional cases. In mountainous regions, therefore, it is mostly impossible to achieve a trade-off between good visibility range and near-ground measurements. Here, the auxiliary positioning of smaller systems in large mountain valleys can play a valuable supplementary role.

The choice of radar site is also influenced by many economic and technical factors, including the following:

- The existence of roads for reaching the radar.
- The availability of power and telecommunication links. It is frequently necessary to add commercially available lightning protection devices. The installation of lightning rods should be carefully designed, as the antenna performance (in particular, the side lobes attenuation) can be seriously impacted when the radar beam intercepts such rods.
- The cost of land.
- The proximity to a monitoring and maintenance facility.
- The existence of as few obstacles as possible for the radar beam to maximize the radar visibility and minimize the amount of ground clutter and beam blockage. No obstacle should be present at an angle greater than a half beam width above the horizon, or with a horizontal width greater than a half beam width. This applies to the immediate vicinity and also for longer distances. In the case of small-scale applications, special attention should be paid to avoiding ground echoes in the target area. In large-scale applications, in contrast, unrestricted visibility is the top priority. Simulation software can be used to assess the quality of a candidate radar site with respect to ground clutter and blockage. The input of such software is a detailed terrain EL model (including, if possible, anthropic obstacles) and the characteristics of the antenna and the radar pulse: height above ground of the feed horn, pulse frequency, antenna gain, 3 dB beam width, pulse power and antenna EL.

- The obstacles environment of a radar site is subject to evolution, for example, new buildings or trees growing. The radar operator often has legal means to limit future increases in the amount of obstacles and their sizes, and should use them to their full extent.
- For a radar to be used for applications at relatively short range, it is sometimes possible to find, after a careful site inspection and examination of detailed topographic maps, a relatively flat area in a shallow depression, the edges of which would serve as a natural clutter fence for the antenna pattern side lobes with minimum blockage of the main beam. In all cases, the site survey should include a camera and optical theodolite check for potential obstacles. In certain cases, it is useful to employ a mobile radar system for confirming the suitability of the site [18].
- When the radar is required for long-range surveillance, as can be the case for tropical cyclones or other applications on the coast, it will usually be placed on a hilltop. It will see a great deal of clutter, which may not be so important at long-range surveillance.

Every survey on potential sites should include a careful check for electromagnetic interference to avoid, as much as possible, interference with other communication systems, such as television, microwave links or other radars. There should also be confirmation that microwave radiation does not constitute a health hazard to populations living near the proposed radar site [17][19]. In most cases, there are legal regulations about these topics to be followed. To avoid interferences, emission and/or reception filters may have to be installed on the waveguide, as they introduce an additional attenuation for the signal.

It can even be necessary to operate the radar without emission in a particular angular sector (“sector blanking”) so as to not exceed the legal exposure to microwaves. The sector blanking function of the radar must be monitored by a dedicated safety control system. The safety control system would interrupt the transmitter if it unintentionally tries to transmit into the sector.

9.3 **Supporting infrastructure**

Supporting infrastructure for a weather radar site can include:

- A radar tower (which might need to be constructed);
- An electrical power supply;
- Data transmission facilities (approximately 8 Mbps for a dual-polarization radar);
- A controlled environment in the operators’ room (humidity and temperature);
- A UPS (size, required available support time and a generator);
- Accessibility (where unmanned operation is required, the equipment must be of higher quality).

A radar tower of significant height can be necessary to overcome too much beam blockage and ground clutter in the close vicinity of the radar. Horizontality of the radar plane reference should be maintained even in the case of strong winds.

A continuous power supply is needed for a radar for which the data are expected to be available at all times. If the radar site is isolated, it may not be enough to rely on the power grid. An electric generator with a UPS is then necessary.

Air conditioning in the electronic cabinet room is necessary most of the time to keep within the safe temperature and humidity limits of the electronics. It is often necessary to extend it to the radome interior to avoid, for example, the development of mould.

Telecommunications and computer technology allow the transmission of radar data (usually) to a central data hub. Here, data from many radars and from other data sources, such as satellites, are collected and integrated. The operation of each radar must be remotely monitored so that remote control actions or on-site actions can be determined from the distance.

Transmission can take place through fibre optic links, or other high-speed ground-based lines, radio or microwave links, and satellite communication channels. It should be kept in mind that radars are often located at remote sites where not all telecommunication systems are available.

9.4 Coverage

The physical surveillance range of any weather radar is practically limited to about 450 km because even summer storms beyond this range are usually below the horizon. In fact, without beam blockage and with standard refractivity, the horizon's altitude at 450 km is 12 km. Thus, only the tops of strong convective storms are detected.

For qualitative continuous monitoring of most of weather-related phenomena, the typical maximum range is 230 km, for which the lowest altitude that the radar can observe without beam blockage is about 3 km. Furthermore, a pencil beam antenna with 1° HPBW provides at 230 km an angular resolution of 4 km. Hence, quantitative estimates are impossible at such ranges.

Consequently, QPE is typically restricted to a maximum range of about 90 (150) km for HPBW = 1° (0.6°). Without beam blockage, the lowest altitude that the radar can observe with the angle of EL set to 0° at a range of 90 (150) km is 500 (1 300) m.

The situation becomes much more difficult in mountainous terrain, where weather echoes can only be detected at high altitudes because of beam shielding by reliefs. In this case, terrain blockage combined with the shallow depth of precipitation during cold seasons and low melting levels causes inadequate radar coverage to support QPE at the 60 km to 90 km range. This raises the question of how to tackle the emerging need for improved low-altitude coverage. Cost, radiation safety and aesthetic issues encourage the use of short-range radars equipped with small antennas and low-power transmitters that could be installed on either low-cost towers or existing infrastructures. Low-cost, low-power, short-range X-band radars can be a valid solution for complementing long-range radars. In this case, the typical maximum range is of the order of 50 km.

Radars can provide a nearly continuous monitoring of weather related to synoptic and mesoscale storms over a large area (for example, a range of 220 km, area 125 000 km²) if unimpeded by hills. Owing to ground clutter at short ranges, the Earth's curvature and the widening of the radar beam, quantitative precipitation detection more than 100 km away from the radar is possible only to a limited extent and the maximum practical range for weather observation is about 200 km.

Over large unpopulated areas, other means of observation are often not available or possible. In regions where very heavy and extensive precipitation is common, an S-band radar is recommended. In other areas, such as mid-latitudes, C-band radars can be effective at a much lower cost. X-band radars suffer from attenuation and can only be used at short distances.

9.5 Visibility and interferences

Unrestricted radar visibility should be ensured at all radar sites. This applies to the immediate vicinity and also for longer distances.

In the case of small-scale applications, special attention should be paid to avoiding ground echoes in the target area. In large-scale applications, in contrast, unrestricted visibility is the top priority.

Ground echoes (ground clutter) are reflections of the radar beam off of natural topography (for example, mountains, trees) and/or obstacles (for example, buildings, wind farms) located in proximity to a weather radar. Side lobes give rise to ground echoes.

Topographical maps can be used as a start to find an appropriate site for a weather radar. A site where the side lobes could be removed by natural terrain or trees is ideal. A site survey should include a camera and optical theodolite check for local obstacles, such as towers or tall trees. In extreme cases, it is useful to employ a mobile radar system for confirming the suitability of the site. An electromagnetic interference surveillance must be conducted.

ATTACHMENT A. SYSTEM PERFORMANCE PARAMETER MEASUREMENT

(normative)

A.1 General

Three measurement diagrams are available depending on the configuration described in 5.2.1. As a typical configuration, this attachment shows parameter measurement methods of the dual-polarization independent transmitter type.

A.2 Standard specification format

Based on section 6, Table A.1 lists important weather radar performance parameters and their corresponding thresholds. Since some of the parameters are dependent on the radar wavelength, separate thresholds are given for X-, C- and S-bands where necessary. Furthermore, each parameter threshold is given for three categories representing the different levels of technical precision available at the time of publication. Level “threshold” represents minimum requirements for a quantitative weather radar system. Level “common” refers to typical requirements for weather radars. Level “achievable” requires high-end hardware as well as high-end design and manufacturing to comply with the thresholds. Consequently, the latter systems are significantly more expensive than radars systems of the “common” level.

Since Table A.1 focuses on quantitative weather radars, there can be other applications that do not require all parameters to be of the level “threshold” or better. It is recommended to measure the parameters given in Table A.1 with a resolution better than 1/10 of the target value.

The table in Attachment B lists examples of common specifications of weather radar in the current market (as of 2016).

Table A.1. Standard specification format

System performance requirements for weather radar		Category		
Fundamental parameters	Criteria	Achievable	Common	Threshold
Sensitivity	Reflectivity sensitivity must be A dBz or less at a distance up to B km, where max unambiguous velocity of more than ± 48 m/s is attained with 2-stagger f_{PRF} of either 2:3 or 3:4 or 4:5			
	For S-band	< 10; 240	< 18; 240	< 23; 240
	For C-band	< 5; 120	< 13; 120	< 18; 120
	For X-band	< 0; 60	< 8; 60	< 13; 60
Spatial resolution	Beam resolution must be θ_H and θ_V (in degrees) or less	< 0.55 ^a	< 1	< 2
	Range resolution must be RR (in m) or less	≤ 75	≤ 150	$\leq 1\ 000$
	Antenna side lobe must be ΔV_{pa} (in dB) or less	< -27	< -23	< -20
	Range side lobe must be ΔV_{pr} (in dB) or less for pulse-compression radar	< -70	< -50	< -30

<i>System performance requirements for weather radar</i>		<i>Category</i>		
Phase stability	Phase stability must be θ_{ps} (in degrees) or less			
	For S-band	< 0.1	< 0.3	< 1
	For C-band	< 0.2	< 0.6	< 2
	For X-band	< 0.4	< 1.2	< 4
Accuracy of dual-polarization measurement	Cross polarization ratio must be XPD_{sys} (in dB) or less	< -35	< -30	< -20
<i>Other key parameters</i>	<i>Criteria</i>	<i>Achievable</i>	<i>Common</i>	<i>Threshold</i>
Maximum rotation speed	Antenna maximum rotation speed must be R_{max} (in rpm) or more	≥ 10	≥ 6	≥ 2
Acceleration	As EL antenna acceleration, EL drive time from 0 to 90 degrees, and 90 to 0 degrees must be less than t_{aEL} (in sec)	< 10	< 20	< 40
	As AZ antenna acceleration, time from maximum speed to complete stop must be less than t_{aAZ} (in sec)	< 3	< 5	< 10
Antenna pointing accuracy	Antenna pointing accuracy must be θ_{ps} (in degrees) or less	< 0.05	< 0.1	< 0.2
Dynamic range	Dynamic range must be LV_d (in dB) or more	> 120	> 100	> 80
Unwanted emissions	The level of unwanted emissions must be A dB or less at B MHz away from the central frequency f_0 (in MHz)	No values given ^b		

^a Except for S-band.

^b Depending on national regulations.

A.3 Fundamental parameter measurement

A.3.1 General

System performance parameters shown in Table A.2 are sorted by the components of radar. For some items, there are differences of measurement between pulse-compression radar and non-pulse-compression radar.

Table A.2. System performance parameters

<i>Component</i>	<i>Measurement parameter</i>	<i>Parameter category</i>	<i>Applicability</i>	<i>Remarks</i>	<i>Section</i>
Transmitter	Peak transmit power (P_t)	Sensitivity	Common		A.3.3
	Transmit pulse width (τ)	Sensitivity	Common	Also related to range resolution	A.3.2

<i>Component</i>	<i>Measurement parameter</i>	<i>Parameter category</i>	<i>Applicability</i>	<i>Remarks</i>	<i>Section</i>
Antenna	Gain (Gt, Gr)	Sensitivity	Common		A.3.4
	Beam width ($\theta_{H/V}$)	Sensitivity and Spatial resolution	Common		A.3.4
	Cross polarization ratio (<i>XPD</i>)	Accuracy of dual-polarization measurement	Common	To be measured along with "isolation" in the receiver category	A.3.5
Receiver	Minimum detectable signal (<i>S</i> _{min})	Sensitivity	Different for pulse-compression and non-pulse-compression radar		A.3.6
	Pulse-compression gain	Sensitivity	Pulse compression radar		A.3.7
	Range resolution (non-pulse-compression radar)	Spatial resolution	Non-pulse compression radar		A.3.8.2
	Range resolution (pulse-compression radar) Equal to received pulse width (τ)	Sensitivity and Spatial resolution	Pulse compression radar		A.3.8.3
	H/V isolation	Accuracy of dual polarization measurement	Common	Related to "cross polarization ratio (<i>XPD</i>)" in the antenna category	A.3.5
System loss	Transmit path	Sensitivity	Common		A.3.9
	Receive path		Common		A.3.9
	Matched filter losses		Different for pulse-compression and non-pulse-compression radar		A.3.9.4
	Radome transmission loss		Common		A.3.9

A.3.2 **Transmit pulse half power width**

A.3.2.1 **Measurement diagram**

The test equipment must be protected as the sampled transmitter power can be fairly high.

A.3.2.2 **Measurement device**

The measurement device is given in Table A.3.

Table A.3. Measurement device of transmit pulse half power width

No.	Name of device	Remarks
1	Oscilloscope	
2	Detector	
3	Attenuator	3 dB attenuator

A.3.2.3 **Measurement method**

Connect a detector and oscilloscope to the transmit output monitoring point as shown in Figure A.1. First, measure a coarse peak as P_p , as shown in Figure A.2. Then, record 10% P_p , where P_p becomes 10%. From the middle point between two 10% P_p , draw a line upward. The cross point is set as P_p' .

Then, measure the point where P_p' becomes 50% using step attenuators. At this amplitude, draw a line in the time axis to get pulse width τ .

Alternately, pulse width can be measured using a peak power sensor/meter instead of oscilloscope/step attenuators.

A.3.3 **Peak transmit power, P_t**

A.3.3.1 **Measurement diagram**

The measurement diagrams are given in Figures A.3 and A.4.

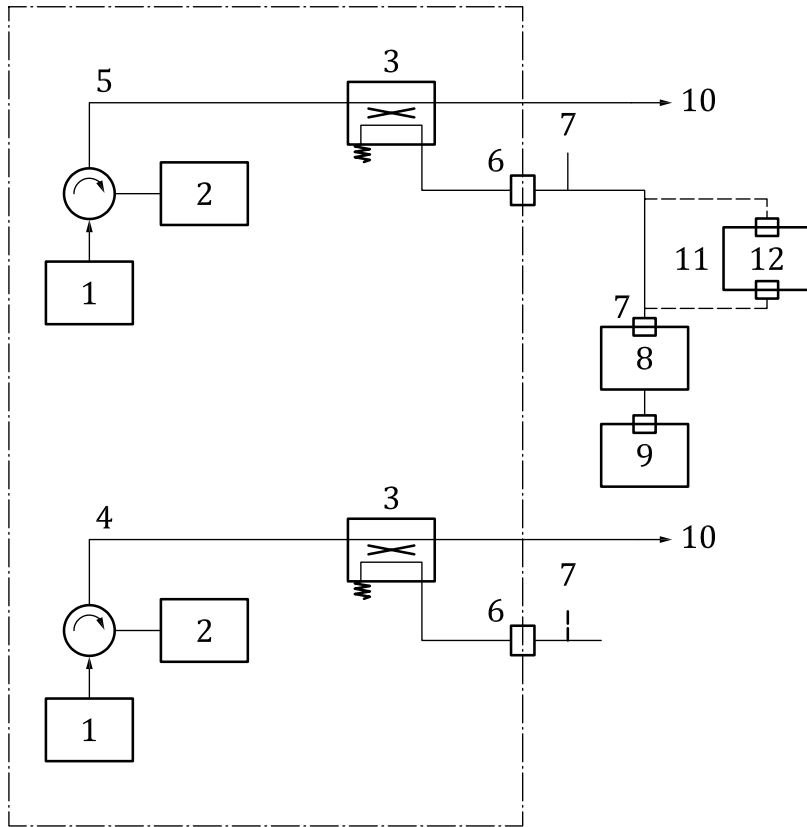
The test equipment must be protected as the sampled transmitter power can be fairly high.

A.3.3.2 **Measurement device**

The measurement device is given in Table A.4.

Table A.4. Measurement device of cable loss

No.	Name of device	Remarks
1	Power meter	
2	Signal generator	
3	Measurement cable	



- Key:
- | | |
|---|-------------------------|
| 1 Transmitter | 7 Cable for measurement |
| 2 Dummy load | 8 Detector |
| 3 Directional coupler | 9 Oscilloscope |
| 4 Vertical polarization (V) channel | 10 To antenna pedestal |
| 5 Horizontal polarization (H) channel | 11 Insert |
| 6 Monitoring point for transmitter output | 12 3 dB attenuator |

Figure A.1. Measurement diagram of transmit pulse half power width (τ) (dual-polarization independent transmitter type)

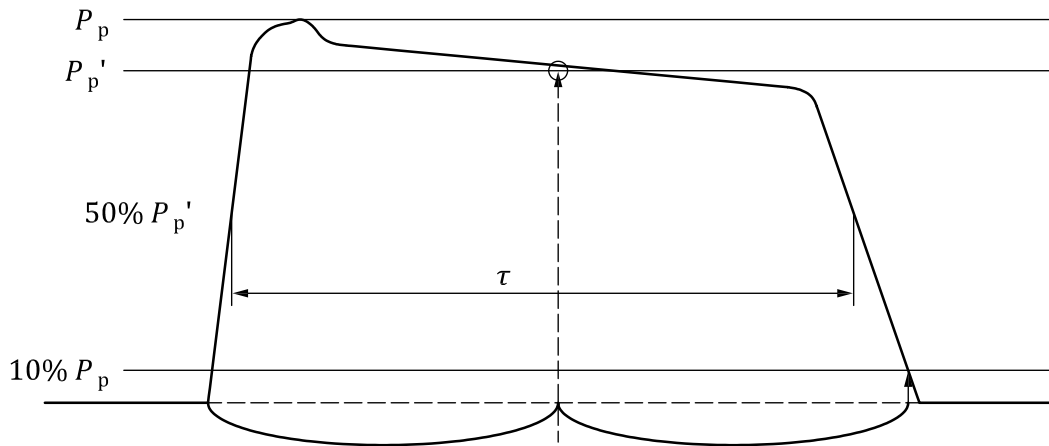
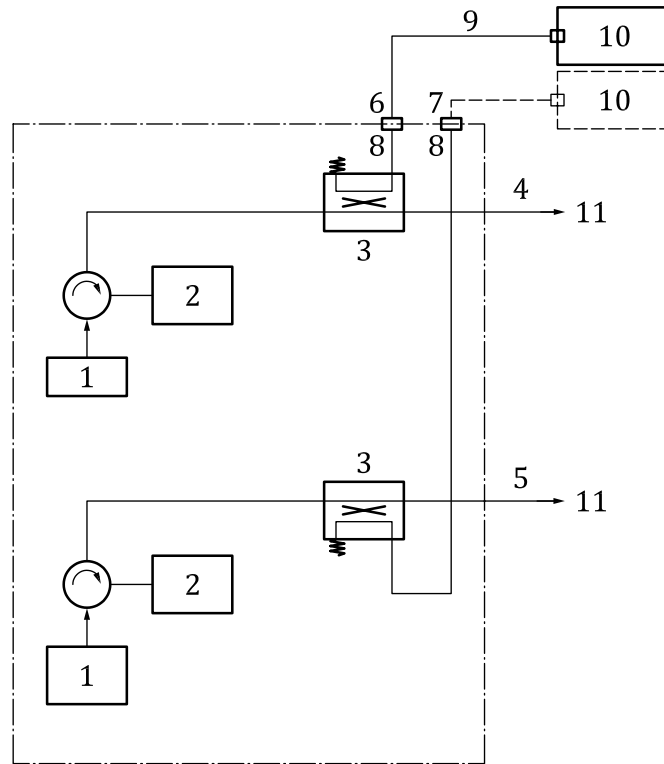


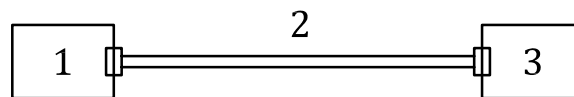
Figure A.2. Pulse width definition



Key:

- | | |
|---------------------------------------|---|
| 1 Transmitter | 7 V channel |
| 2 Dummy load | 8 Monitoring point for transmitter output |
| 3 Directional coupler | 9 Cable for measurement |
| 4 Horizontal polarization (H) channel | 10 Power meter |
| 5 Vertical polarization (V) channel | 11 To antenna pedestal |
| 6 H channel | |

Figure A.3. Measurement diagram of Pt (dual-polarization independent transmitter type)



Key :

- | |
|-------------------------|
| 1 SG |
| 2 Cable for measurement |
| 3 Power meter |

Figure A.4. Measurement diagram of cable loss

A.3.3.3 Measurement method

A.3.3.3.1 General

The forward port of the transmitter coupler must be used for the measurement of the peak transmit power. Usually it is located very close behind the transmitter output and it is the first coupler in a radar system waveguide run. It is important to know the coupling ratio of the couplers. If possible, the power meter should be directly connected to the transmitter coupler without an additional cable. The transmitter power measurements must be performed with all available pulse length settings. The corresponding fPRF must be chosen in order to obtain the same duty cycle for each pulse length setting.

A.3.3.3.2 *Cable loss measurement*

If the power meter cannot be directly connected to the transmitter coupler and a cable has to be added, the loss of the cable must be measured and added to the peak power measurement. Otherwise, the power meter must be connected directly to the coupler.

Measure the cable loss L_c to be used for P_t measurement in advance.

Set the frequency of the SG to the transmission frequency f_0 of the radar equipment with sufficient output level P_{SG} (for example, 0 dBm). Connect one end of the cable to the SG and the other end to the power meter, as shown in Figure A.4.

The reading of the power meter shows the attenuation L_c of the cable with negative numbers.

A.3.3.3.3 *Measurement of P_t*

Fast peak power sensors are typically less accurate in terms of absolute power than slow average power sensors. A peak power sensor is used to determine a coarse peak power and accurate pulse width (refer to A.3.2). On the other hand, average transmit power is measured by an average power meter. Then, peak power is finally determined using these values.

Connect the power meter directly or with the cable to the transmitter coupler and set the transmitter in the transmission mode. Depending on the transmitter type, measure the average power using the methods shown in Figures A.1 to A.4. Determine the loss L_t (including the degree of coupling of the directional coupler) from the transmission output to the transmitter coupler. If the reading of the power meter is P'_m (in dBm), the transmit power P_A is obtained by formula (A.1):

$$P_A = P'_m + L_t + L_c \quad (\text{A.1})$$

To convert the average power P_A to transmit peak power P_t , use the transmitter duty cycle, which is dictated by the pulse width (τ) and pulse repetition frequency (f_{PRF}). f_{PRF} is measured with the diagram shown in Figure A.1 (a frequency counter can be used instead of an oscilloscope).

The transmit power to be used as the calibration value is calculated by formula (A.2):

$$P_t = \frac{P_A}{\tau \cdot f_{PRF}} \quad (\text{A.2})$$

Refer to A.3.2 for pulse width measurement.

A.3.4 *Antenna gain, beam width*

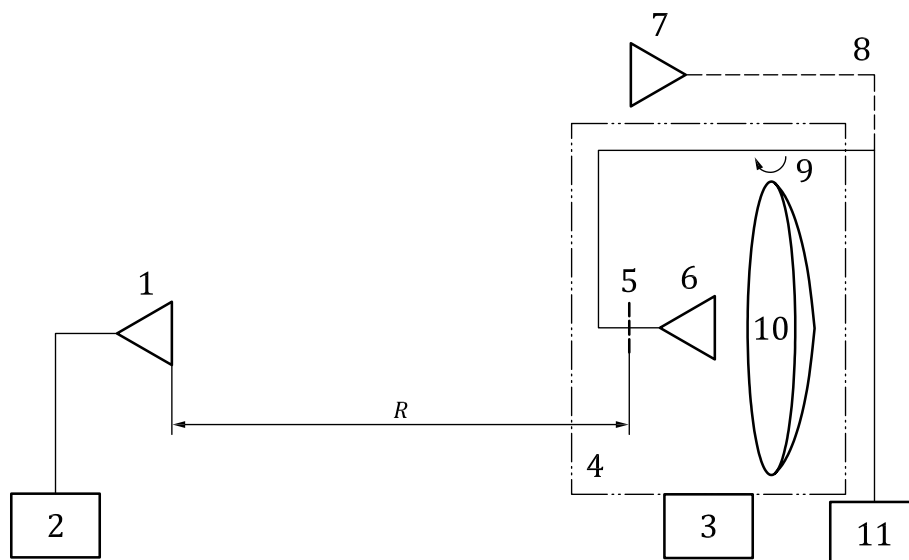
A.3.4.1 *General*

There are three methods for accurate antenna characterization, which differ significantly: the far-field range method, the compact range method and the near-field measurement method. In this subsection, only the far-field range method is described.

A.3.4.2 *Measurement diagram*

The measurement diagram is given in Figure A.5.

The distance R from an antenna to be measured to a transmission antenna should be basically far-field, namely $R > 2D^2/\lambda$ (where D is the antenna diameter and λ is the wavelength), but if a performance equal to or better than the case of far-field can be proven, near-field measurement is also acceptable.



- Key :
- | | | | |
|---|------------------------|----|--|
| 1 | Transmission antenna | 7 | Standard horn antenna |
| 2 | SG | 8 | Replaced by the antenna for gain measurement |
| 3 | Rotating platform | 9 | Az rotation for G_0 measurement |
| 4 | Antenna to be measured | 10 | Reflector |
| 5 | Measuring point | 11 | Receiver |
| 6 | Feed horn | | |

Figure A.5. Measurement diagram of antenna gain

A.3.4.3 Measurement device

The measurement device is given in Table A.5.

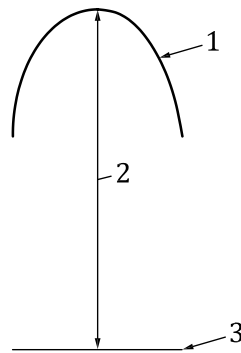
Table A.5. Measurement device of antenna gain

No.	Name of device	Remarks
1	Receiver	
2	Pattern recorder	
3	Standard horn antenna	
4	Signal generator	
5	Transmission antenna	
6	Mixer	

A.3.4.4 Measurement method

A.3.4.4.1 Antenna gain

Receive the output of the SG, which is radiated from the transmission antenna installed at a sufficiently remote distance, as shown by the measurement diagram in Figure A.5, with the measured antenna placed on the rotating table, and record the received signal level into the pattern recorder through the receiver. If the pattern recorder records the received signal level in dB scale, the result of the gain pattern (G_1) of the measured antenna is drawn as shown in Figure A.6. Then, replace the feed horn by the standard horn and fix it in the direction of transmission antenna. In the same way, record the received signal level into the pattern recorder.



Key :

- 1 Gain pattern of antenna to be measured (G_1)
- 2 Gain difference ΔG (read out from pattern recorder)
- 3 Gain of standard horn antenna G_s (basis)

Figure A.6. Example of antenna pattern chart

After this, compare G_1 and G_s and read the maximum level difference (gain difference ΔG) from the record of the pattern recorder.

The gain G_s of the standard horn, which is measured in advance, is added to ΔG to obtain the antenna gain $G(G_t G_r)$.

This can be calculated as indicated by formula (A.3) (in dBi):

$$G = \Delta G + G_s \quad (\text{A.3})$$

Measure the values of H and V polarization in the case of a dual-polarization type. If the frequency used for measurement is specified, measure the level at that specified frequency. If the frequency range is specified, measure the level at the upper/lower limits as well as the mean value.

Measure the loss of the connection waveguide (component of the antenna) in advance and subtract it to obtain the antenna gain.

A.3.4.4.2 **Antenna beam width, $\theta_{H/V}$**

Similar to the antenna gain, receive the output of the SG, which is radiated from the transmission antenna installed at a sufficiently remote distance, with the measured antenna placed on the rotating table and, at the same time, measure the reception output in the rotating direction using the reference antenna.

Read the value at the 3 dB down point of beam width from the chart of received gain pattern that was recorded by the pattern recorder (see Figure A.7).

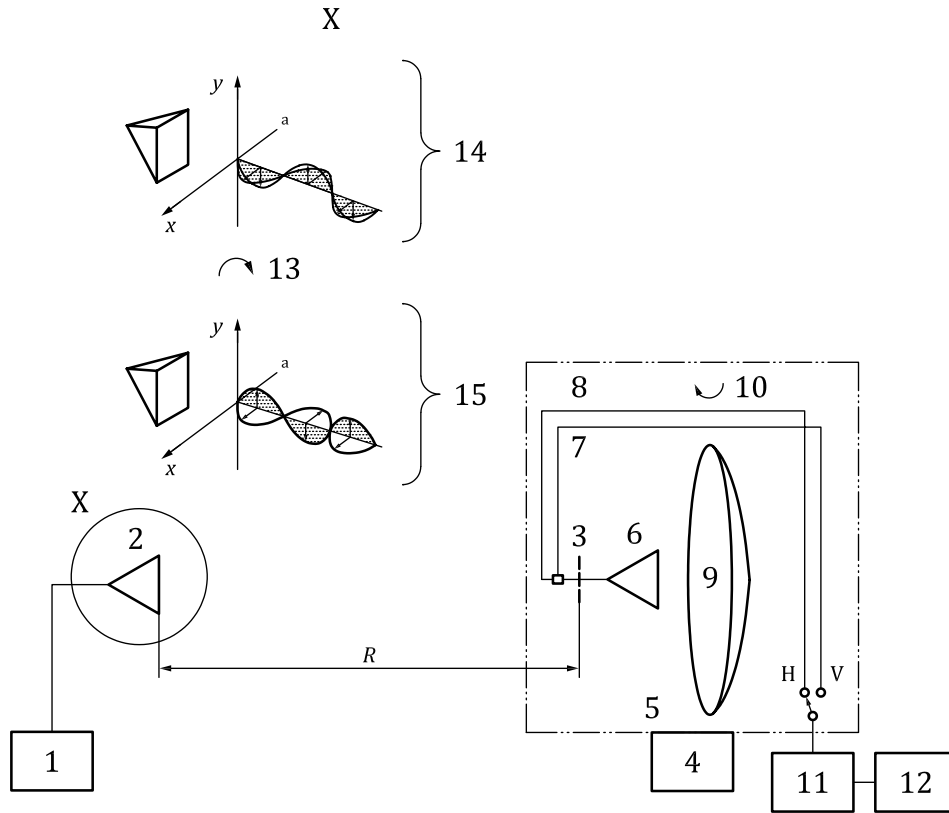
A.3.5 **Cross polarization isolation**

A.3.5.1 **Measurement diagram**

The measurement diagrams are given in Figures A.7 and A.8.

A.3.5.2 **Measurement device**

Refer to A.3.4.



Key:

- | | |
|--------------------------|--|
| 1 SG | 9 Reflector |
| 2 Transmission antenna | 10 Az rotation for directivity measurement |
| 3 Measuring point | 11 Receiver |
| 4 Rotating platform | 12 Pattern recorder |
| 5 Antenna to be measured | 13 90 degrees turn of antenna |
| 6 Feed horn | 14 Horizontal polarization wave |
| 7 V-port | 15 Vertical polarization wave |
| 8 H-port | |

Figure A.7. Measurement diagram of antenna cross polarization ratio

A.3.5.3 Measurement method

Referring to 6.2.4, the accuracy of dual-polarization, cross polarization isolation is measured. Isolation for the receiver is included since poor isolation at the receiver degrades system performance, even if cross polarization ratio at the antenna is high.

As in Figure A.8, the cross polarization ratio at the antenna measures a ratio of the peak value of a co-polar transmitted signal, received by cross-polar receiver, to the peak value of the received co-polar signal. Cross polarization ratios for H/V polarization are expressed as formulae (A.4) and (A.5):

$$XPD_h = Peak_{cross,h} - Peak_{co,h} \tag{A.4}$$

$$XPD_v = Peak_{cross,v} - Peak_{co,v} \tag{A.5}$$

where:

- $Peak_{co}$ is the peak value of a co-polar signal with suffix h or v representing horizontal and vertical polarization waves;
- $Peak_{cross}$ is the maximum value of a cross-polar signal within the angular range of the 3 dB beam width, with suffix h or v representing horizontal and vertical polarization waves.

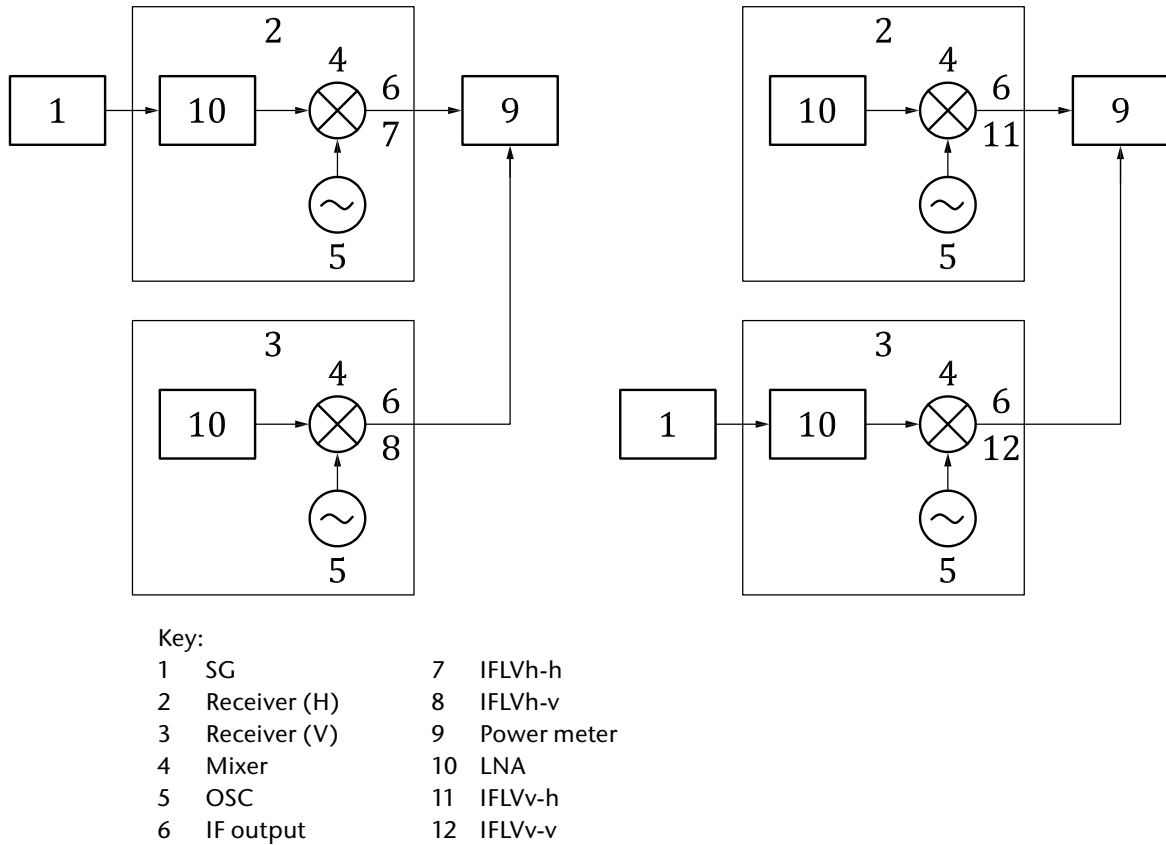
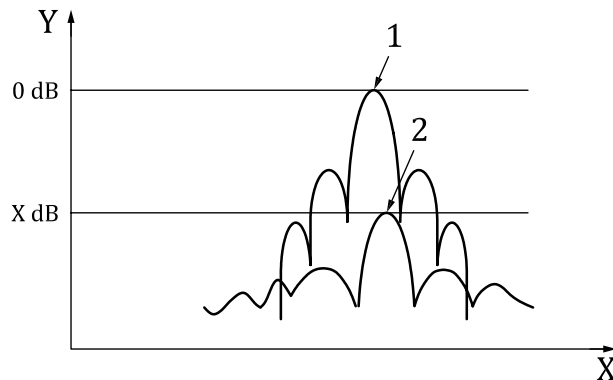


Figure A.8. Measurement of H/V isolation

H-pol: To find $Peak_{co}$ and $Peak_{cross}$, plot the distribution of co-polar and cross-polar signals in the horizontal plane of the receiving antenna on a sheet of paper (as in Figure A.9). Then, rotate the receiving antenna by 90° and plot the distribution of co-polar and cross-polar signals in the vertical plane of the receiving antenna on a sheet of paper.

V-pol: To change the polarization directions from horizontal to vertical, rotate the transmission antenna by 90° .

Following this, isolation at the receiver is measured (see Figure A.8). Connect the SG to LNA (H). Set the frequency of the SG to centre frequency f_0 used by the radar. Record the signal level of



Key:

1 $Peak_{co}$	X Degree
2 $Peak_{cross}$	Y Signal power

Figure A.9. Measurement of antenna cross-polarization ratio

the H-port and V-port, $IFLV_{h-h}$ and $IFLV_{h-v}$, respectively, at f_0 with the power meter and take its difference, $IFLV_{diff-h} = IFLV_{h-v} - IFLV_{h-h}$, as the isolation level for the H-port. Then, connect the SG to LNA (V). Set the frequency of the SG to f_0 . Record the signal level of the V-port and H-port, $IFLV_{v-v}$ and $IFLV_{v-h}$, respectively, and take its difference, $IFLV_{diff-v} = IFLV_{v-h} - IFLV_{v-v}$, as the isolation level for the V-port. Instead of a power meter, the calibrated digital receiver can be used.

Cross-polarization ratio at the antenna and isolation at the receiver are combined to express the H/V isolation of the system through the antenna to the receiver, $XPD_{sys}(h)$, $XPD_{sys}(v)$, as shown by formulae (A.6) and (A.7) (in dB):

$$XPD_{sys}(h) = \max(XPD_h, LV_{diff-h}) \quad (A.6)$$

$$XPD_{sys}(v) = \max(XPD_v, LV_{diff-v}) \quad (A.7)$$

A.3.6 **Minimum detectable signal, S_{min}**

A.3.6.1 **Theoretical estimation**

The minimum detectable signal, S_{min} , can be calculated by formula (A.8) (in dBm):

$$S_{min} = 10 \log(kTB) + NF + 30 \quad (A.8)$$

where:

- k is the Boltzmann constant (1.38×10^{-23} W/Hz/K);
- T is the temperature, in K;
- B is the bandwidth of receiver, in Hz;
- NF is the noise figure, in dB;
- 30 is a constant for dBw to dBm.

B and NF are measured by the method shown in A.3.6.2. The temperature T is the physical temperature of the receiver. It should not deviate too much from 290 K to avoid measurement errors – see, for example, [19].

The S_{min} can now be calculated for any given SNR . For example, for $SNR = 0$ dB, the S_{min} equals the noise power. Refer to 6.2.1 for SNR , which in this document derives sensitivity.

Measurement methods are different for pulse-compression and non-pulse-compression radars.

A.3.6.2 **Non-pulse-compression radar**

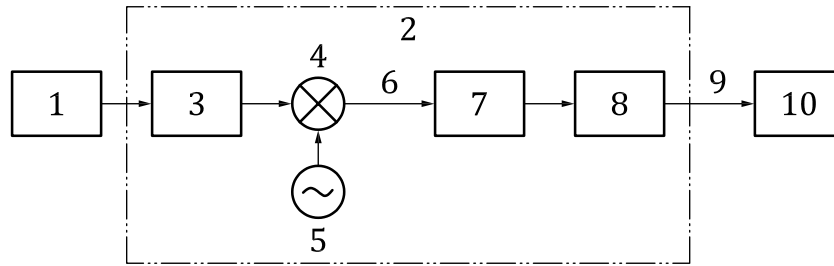
A.3.6.2.1 **Bandwidth measurement**

A.3.6.2.1.1 *Measurement diagram*

The measurement diagram is given in Figure A.10.

A.3.6.2.1.2 *Measurement device*

The measurement device is given in Table A.6.



Key:

- | | |
|-----------------------------|-------------------|
| 1 SG | 6 IF output |
| 2 Receiver/signal processor | 7 AD |
| 3 LNA | 8 BPF |
| 4 Mixer | 9 Received signal |
| 5 OSC | 10 PC |

Figure A.10. Bandwidth measurement diagram for non-pulse-compression radar

Table A.6. Measurement device of bandwidth for non-pulse-compression radar

No.	Name of device	Remarks
1	Signal generator	Radio frequency
2	Personal computer (PC)	Received power recording and display

A.3.6.2.1.3 Measurement method

Set the frequency of the SG to centre frequency f_0 used by the radar and set the suitable output power of the SG within the receiver input range, then record the received power P_0 with the PC.

Next, record the frequency f_+ of the SG when the received power goes 3 dB down from P_0 while increasing frequency of the SG from f_0 . Similarly, record the frequency f_- of the SG when received power goes 3 dB down from P_0 while decreasing frequency of the SG from f_0 . Thus, the bandwidth B is obtained by formula (A.9) (see also Figure A.11). The step size of the SG must be determined so that there is no significant gap in the frequency characteristics obtained.

$$B = f_+ - f_- \text{ (Hz)} \tag{A.9}$$

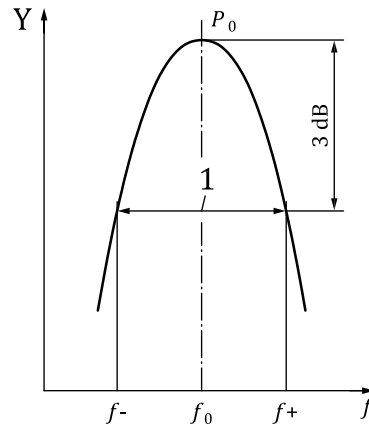
A.3.6.2.2 Noise-figure measurement

The ambient noise of a system is usually the lower limit of what a receiver can detect. As with any receiving system, the signal competes with the excess thermal noise generated by the receiver. Here, the amplifiers in the low noise front end are particularly a source for additional noise. A reduction of the amplifier noise would result in an enhancement of the minimum detectable signal (S_{\min}). The excess thermal noise generated in the receiver is characterized by a parameter called the "noise figure" (NF). NF is the ratio of the additional receiver noise to the thermal noise floor present at the receiver input. See formula (A.10) (in dB):

$$NF = 10 \log \left(\frac{SNR_{in}}{SNR_{out}} \right) \tag{A.10}$$

with $SNR = \frac{Signal_{level}}{Noise_{level}}$, in dB.

To determine the NF of the radar receiver, a calibrated noise source delivers a signal of known noise level, N_{on} , into the receiver front end. The output power of the receiver can be measured



Key:

1 Bandwidth

Y Power

Figure A.11. Measurement of bandwidth (non-pulse-compression radar)

corresponding to the noise source turned on and off, N_{on} and N_{off} . The two power values are used to calculate the Y-factor. The Y-factor is a ratio of the two noise power levels in terms of linear power, as shown by formula (A.11):

$$Y = \frac{N_{\text{on}}}{N_{\text{off}}} \quad (\text{A.11})$$

NF is expressed in dB. The Y-factor and the excess noise ratio (ENR) of the noise diode can be used to calculate NF , as shown by formula (A.12) (in dB):

$$NF = ENR - 10 \log(Y - 1) \quad (\text{A.12})$$

A.3.6.3 Pulse-compression radar

A.3.6.3.1 Bandwidth measurement

A.3.6.3.1.1 Measurement diagram

The measurement diagram is given in Figure A.12.

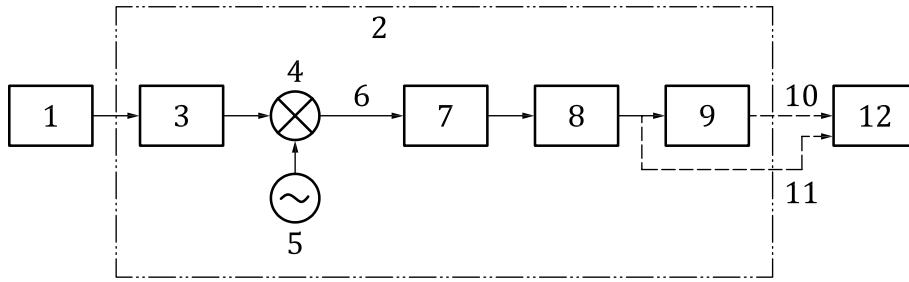
A.3.6.3.1.2 Measurement device

Refer to A.3.6.2.1.2.

A.3.6.3.1.3 Measurement method

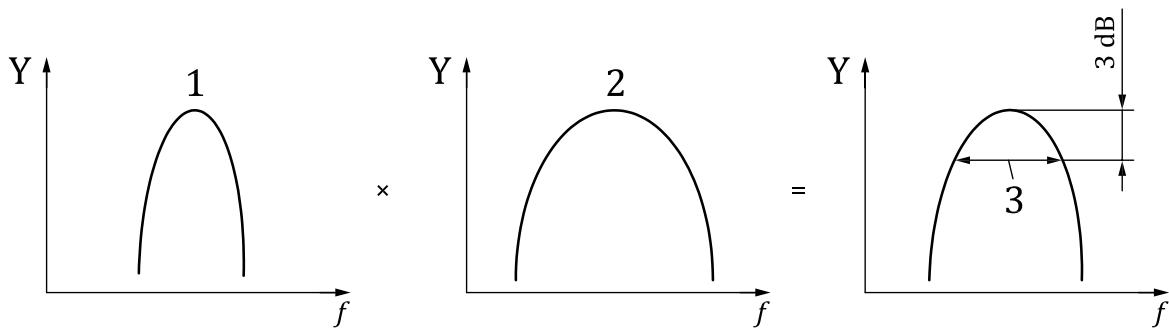
Pulse-compression processing functions as a matched filter and its performance depends on the frequency characteristic of the reference wave used for pulse compression. The frequency characteristic of the pulse-compression receiver is determined by the product of the BPF and the reference wave in the frequency domain.

Frequency characteristics of the BPF can be measured by the same method as the non-pulse-compression receiver using the SG as input and bypassing pulse-compression processing as shown in Figure A.12. Frequency characteristics of the reference wave is obtained by FFT of its time waveform.



- Key:
- | | |
|-----------------------------|--------------------------|
| 1 SG | 7 AD |
| 2 Receiver/signal processor | 8 BPF |
| 3 LNA | 9 Pulse compression |
| 4 Mixer | 10 FFT of reference wave |
| 5 OSC | 11 Bandwidth |
| 6 IF output | 12 PC |

Figure A.12. Bandwidth measurement diagram for pulse-compression radar



- Key:
- | | |
|------------------|---|
| 1 BPF | 3 Receiver bandwidth of pulse-compression radar |
| 2 Reference wave | Y Power |

Figure A.13. Measurement of bandwidth for pulse-compression radar

These frequency characteristics are multiplied offline. The bandwidth is defined as the width measured at the 3 dB down point from the peak at centre frequency f_0 (see Figure A.13, and also as in Figure A.11).

A.3.6.3.2 **Noise-figure measurement**

Same as A.3.6.2.2.

A.3.7 **Pulse-compression gain**

A.3.7.1 **General**

This measurement is applied only for pulse-compression radar.

A.3.7.2 **Measurement diagram**

The measurement diagram is given in Figure A.14.

A.3.7.3 Measurement device

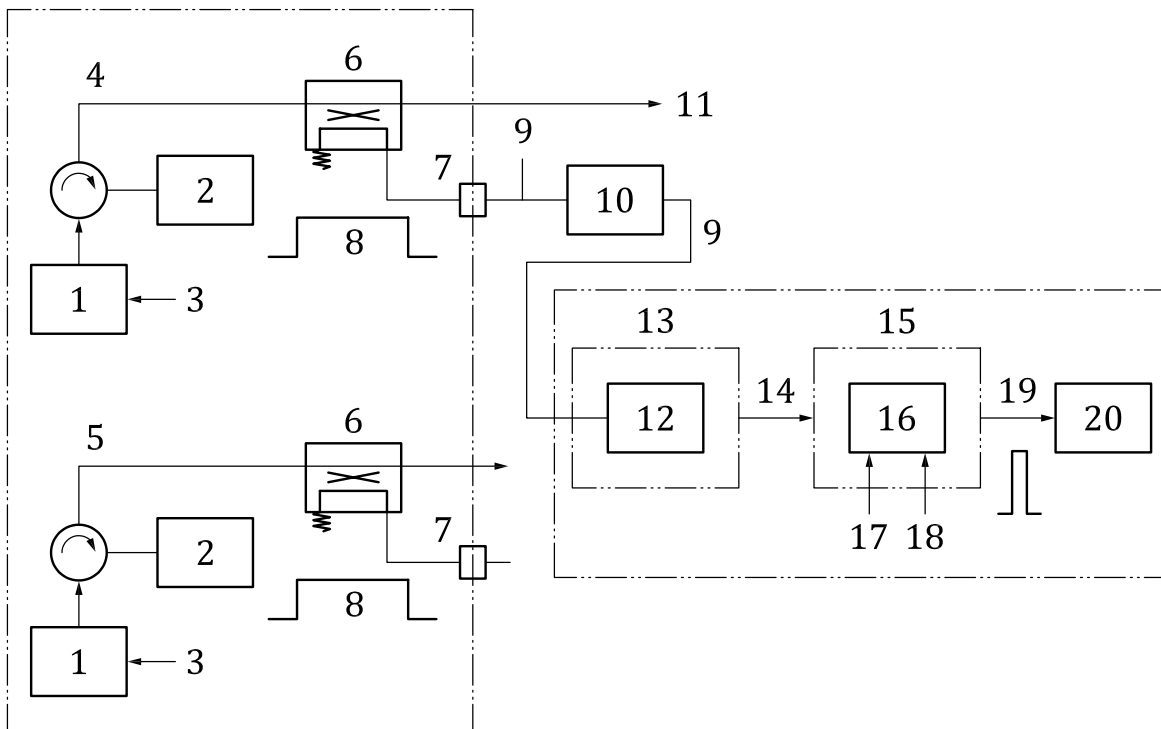
The measurement device is given in Table A.7.

Table A.7. Measurement device of pulse-compression gain (G_c)

No.	Name of device	Remarks
1	High power attenuator	For P_t attenuation to input to receiver
2	Power meter	For cable loss measurement
3	Signal generator	For cable loss measurement

A.3.7.4 Measurement method

Attenuate the transmit power monitoring output until it is within the received dynamic range, via an attenuator, and connect it to the first stage LNA of the receiver. The pulse width, pulse repetition frequency, and modulation method of input signals are set as same as when in operation.



Key:

- | | |
|---|----------------------------|
| 1 Transmitter | 11 To antenna pedestal |
| 2 Dummy load | 12 LNA |
| 3 Pulse modulation on/off | 13 Receiver |
| 4 Horizontal polarization (H) channel | 14 IF output |
| 5 Vertical polarization (V) channel | 15 Signal processor |
| 6 Directional coupler | 16 Pulse compression |
| 7 Monitoring point for transmitter output | 17 Reference signal on/off |
| 8 Transmission pulse | 18 Window function on/off |
| 9 Cable for measurement | 19 Received signal |
| 10 High power attenuator | 20 A-Scope |

Figure A.14. Measurement diagram of G_c (dual-polarization independent transmitter type)

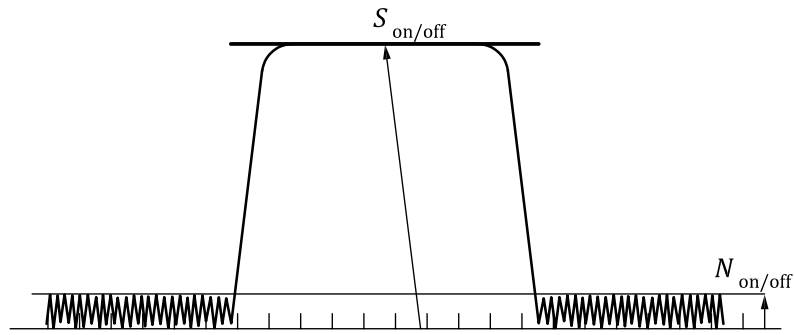


Figure A.15. Pulse-compression gain measurement

The pulse-compression gain is measured as SNR difference when the pulse compression is switched ON and OFF. Measure the signal and noise level when the pulse compression is OFF as S_{off} and N_{off} , respectively, and its ratio as SNR_{off} . Likewise, measure the signal and noise level when the pulse compression is ON as S_{on} and N_{on} , respectively, and its ratio as SNR_{on} . Then, SNR is expressed as $SNR_{off} = S_{off}/N_{off}$ and $SNR_{on} = S_{on}/N_{on}$, respectively. Pulse-compression gain G_c is expressed in dB. See formula (A.13):

$$G_c = 10 \log(SNR_{on} / SNR_{off}) \quad (A.13)$$

In the case of measurement with pulse compression OFF, the reference signal and window function are respectively OFF for the signal processor, as shown in Table A.8. In the case of the measurement with pulse compression ON, the reference signal and window function are respectively ON for the signal processor. Window function loss is included in this measurement. Regarding noise, measurement value in a non-input state is used. Refer to 6.2.1.5 and A.3.8.3 with respect to the sensitivity calculation for the pulse-compression radar. A diagram is given in Figure A.15.

Table A.8. Settings for measurement of pulse-compression gain

Measuring item	Setting				Remarks
	Pulse compression	Transmit power	Reference signal	Window function	
S_{off}	OFF	ON	OFF	OFF	
N_{off}	OFF	OFF	OFF	OFF	
S_{on}	ON	ON	ON	ON	
N_{on}	ON	OFF	ON	ON	

A.3.8 **Range resolution**

A.3.8.1 **Non-pulse-compression radar**

There are three parameters related to range resolution, as described in 6.2.2.3:

- Transmit pulse half width;
- Sampling interval of received signal;
- Bandwidth of receiver.

Range resolution (as the system performance) is estimated as a maximum of resolution values calculated from these bottleneck factors.

A.3.8.2 Transmit pulse half power width

A.3.8.2.1 *General*

Same as A.3.2.

A.3.8.2.2 *Sampling interval of received signal*

A.3.8.2.2.1 *General*

The sampling interval of received signal is the processing time interval t_s in the final stage of the signal processor.

Using a unit of t_s as a microsecond (μs), the value in unit of length, L_{si} , is calculated as formula (A.14):

$$L_{si} = 150t_s \text{ (m)} \quad (\text{A.14})$$

A.3.8.2.2.2 *Measurement diagram*

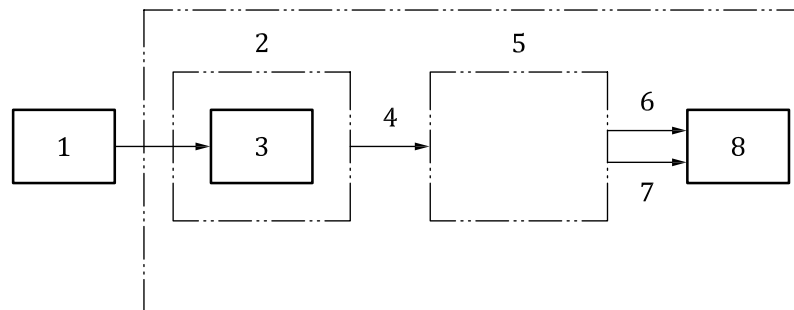
The measurement diagram is given in Figure A.16.

A.3.8.2.2.3 *Measurement method*

Input a sine AM modulation signal with the SG to the receiver. Check the received signal and sampling clock of the signal processor output on the monitor of the (software emulated) oscilloscope and measure the sampling interval of the sampling clock (see also Figure A.17).

A.3.8.2.3 *Bandwidth of receiver*

See A.3.6.2.



Key:

- | | | | |
|---|----------|---|------------------|
| 1 | SG | 5 | Signal processor |
| 2 | Receiver | 6 | Received signal |
| 3 | LNA | 7 | Sampling clock |
| 4 | IF input | 8 | Oscilloscope |

Figure A.16. Sampling interval measurement

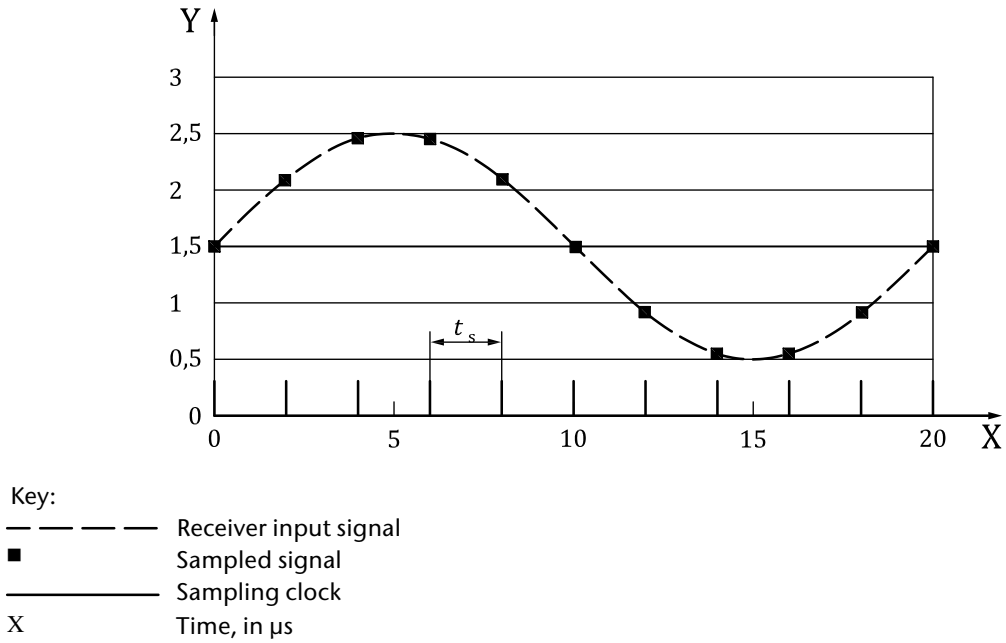


Figure A.17. Example of oscilloscope screen

A.3.8.3 Pulse-compression radar

A.3.8.3.1 Measurement diagram

The measurement diagram is given in Figure A.18.

A.3.8.3.2 Measurement device

The measurement device is given in Table A.9.

Table A.9. Measurement device of pulse width after pulse compression

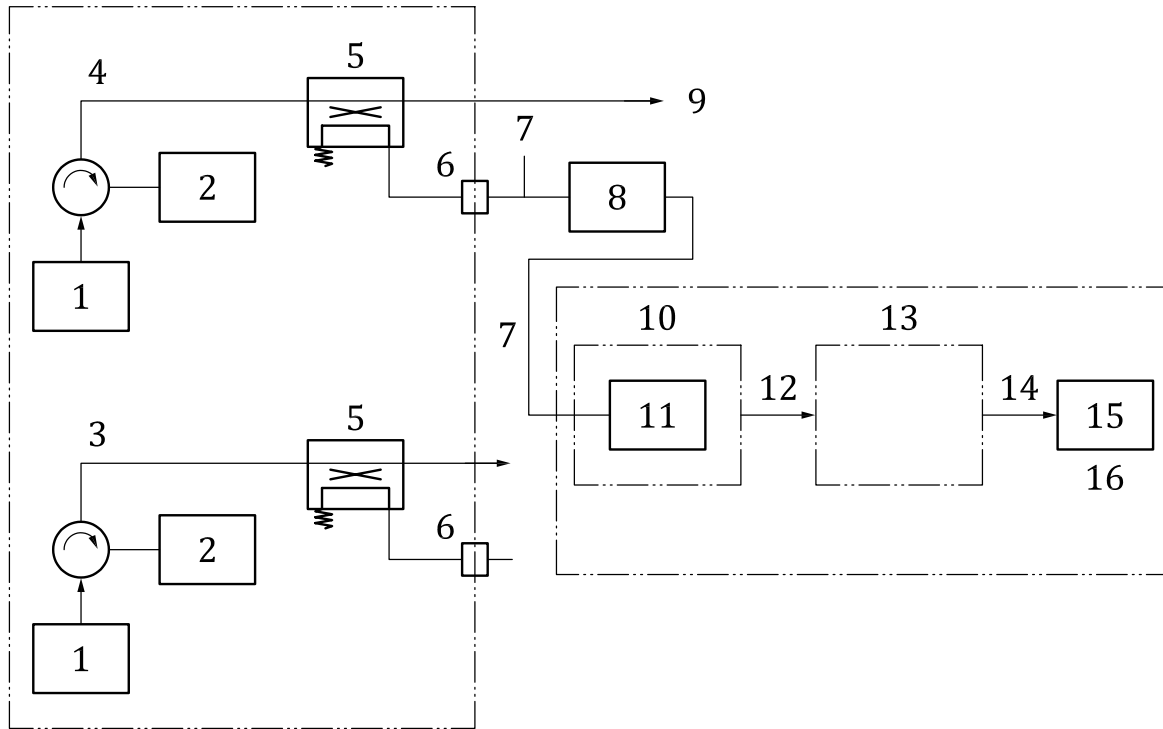
No.	Name of device	Remarks
1	High power attenuator	More than 80 dB
2	A-Scope	System component

A.3.8.3.3 Measurement method

For a pulse-compression radar, measure the received pulse width after pulse-compression processing, while the transmitted pulse is turned back to the receiver.

As in Figure A.18, connect a high-power attenuator to the transmit power monitoring point with a measurement cable, and connect its output to the first stage LNA of the receiver. A high-power attenuator is chosen that can attenuate transmit power sufficiently until it is at a level that is within the receiver’s dynamic range. The transmitter is set to long-pulse continuous-transmission mode.

Refer to 6.2.2.3 for the derivation of range resolution. An example of a calculation of received pulse width and a graph of received pulse shape are shown in Figure A.19. A calculation table is given in Table A.10.



Key:

- | | |
|---|------------------------|
| 1 Transmitter | 9 To antenna pedestal |
| 2 Dummy load | 10 Receiver |
| 3 Vertical polarization (V) channel | 11 LNA |
| 4 Horizontal polarization (H) channel | 12 IF output |
| 5 Directional coupler | 13 Signal processor |
| 6 Monitoring point for transmitter output | 14 Received signal |
| 7 Cable for measurement | 15 a-scope |
| 8 High power attenuator | 16 Measure pulse width |

Figure A.18. Measurement diagram of pulse width after pulse compression (dual-polarization independent transmitter type)

Table A.10. Calculation table of received pulse width

<i>Measured data (input)</i>	<i>Time μs</i>	<i>Normalized power</i>
	x_1	y_1
	-1	0.292 0
	x_2	y_2
	0	1.000 0
	x_3	y_3
	0.5	0.399 9
μ (see formula 7.A.28)		-0.198 7
σ^2 (see formula 7.A.29)		0.244 8
A (see formula 7.A.30)		1.084 0
τ (μs) (see formula 7.A.31)		1.16

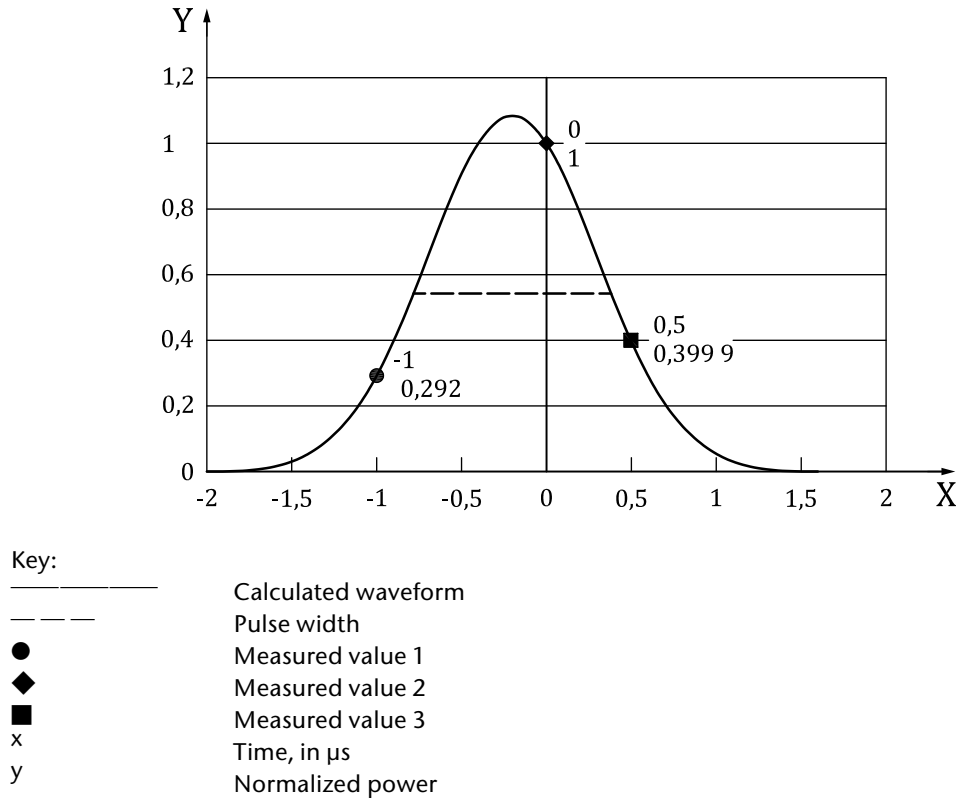


Figure A.19. Received pulse shape and pulse width calculated with measured values

This value is also used for sensitivity, where pulse-compression gain is added. Read 6.2.1.5 and A.3.7 to calculate sensitivity for pulse-compression radar.

A.3.9 **System loss, F**

A.3.9.1 **General**

The elements of system loss F include:

- Transmission system loss: F_{tx} (in dB);
- Reception system loss: F_{rx} (in dB);
- Matched filter losses: F_{mf} (in dB);
- Radome transmission loss: F_{rd} (in dB).

The system loss F is expressed as formula (A.15) (in dB):

$$F = F_{tx} + F_{rx} + F_{mf} + 2F_{rd} \tag{A.15}$$

As the radome is subject to loss during both transmission and reception, it is multiplied by two.

A.3.9.2 **Measurement of radome transmission loss**

A.3.9.2.1 **General**

While the attenuation of the radome material is quite constant in time, thin layers of water, snow or ice can cause a very significant but temporal increase in radome attenuation, which

is also known as “wet radome attenuation”. Up to now, there have been no operational and widely used methods to correct for wet radome attenuation due to its temporal and spatially variant nature. Usually the wetting is non-uniform, which leads to an inhomogeneous coverage of hydrometeors on the radome surface. Attenuation of the radome material (“dry radome attenuation”) is determined by the radome manufacturer by testing single radome panels.

A.3.9.2.2 *Measurement diagram*

The measurement diagrams are given in Figures A.20 and A.21.

A.3.9.2.3 *Measurement device*

Refer to A.3.4. (Plus a radome test piece.)

A.3.9.2.4 *Measurement method*

The radome loss can be measured by two methods. The first one is using a sufficiently large test piece of the radome at a test range. The second one is performed with a fully assembled radome.

As shown in Figure A.20, for the first method, a radome panel is installed between two antennas with an SG on one side and a power meter on the other side. The distance between the two antennas should be the far field distance of the bigger antenna. The first measurement is done without the radome panel and the second with the radome panel set-up in the measurement range. The difference between the received power equals the radome loss.

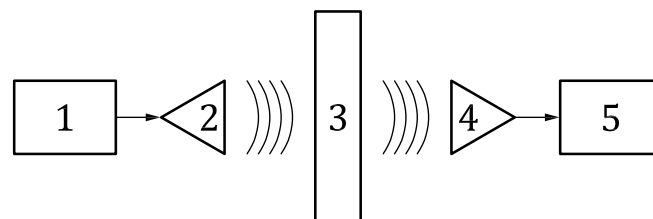
The second method (with and without radome) is shown in Figure A.21. The measurement is performed with the radome in a dry state.

Note: Measuring loss in a wet state using super-water-repellent material remains a future task.

If the gain (in dB) with the radome or radome panel is G and the gain (in dB) without radome or radome panel is G_0 , the transmit power loss of the radome F_{rd} is obtained as formula (A.16) (in dB):

$$F_{rd} = G_0 - G \quad (\text{A.16})$$

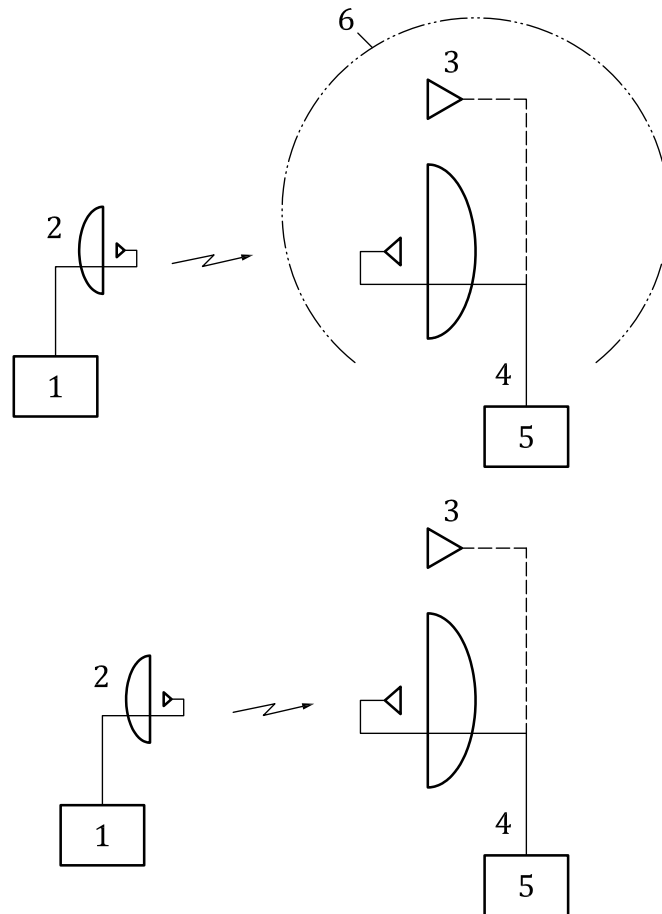
As this loss is generated during both transmission and reception, the value multiplied by two is applied to the system loss.



Key:

- | | | | |
|---|----------------------|---|-----------------|
| 1 | SG | 4 | Receive antenna |
| 2 | Transmission antenna | 5 | Power meter |
| 3 | Radome panel | | |

Figure A. 20. Measurement diagram of radome transmission loss at a test range



- Key:
- | | | | |
|---|-----------------------|---|-----------------------------|
| 1 | SG | 4 | Antenna to be measured |
| 2 | Transmission antenna | 5 | Receiver (pattern recorder) |
| 3 | Standard horn antenna | 6 | Radome |

Figure A.21. Measurement diagram of radome transmission loss at the radar site

A.3.9.3 Measurement of loss of transmit and receive paths

A.3.9.3.1 General

The loss related to transmit and receive paths depends on actual installation conditions. The value is known after the exact layout of the equipment at the site is determined. Even so, the standard measurement method described here provides a loss estimate that is objectively comparable among radar systems from different manufacturers.

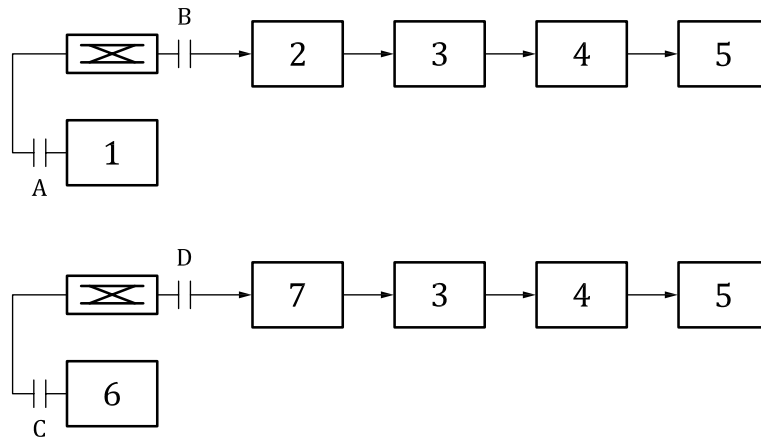
A.3.9.3.2 Measurement diagram

Three measurement diagrams are available in line with the different configurations as described in Figures 2 to 5.

The case of dual-polarization independent transmitter types is given in Figures A.22 and A.23.

A.3.9.3.3 Measurement device

The measurement device is given in Table A.11.



- Key:
- 1 Transmitter (H)
 - 2 LNA (H channel)
 - 3 Frequency conversion
 - 4 Signal processor
 - 5 PC
 - 6 Transmitter (V)
 - 7 LNA (V channel)
- A – B Transmit to receive return path (H pol.)
 C – D Transmit to receive return path (V pol.)

Figure A.22. Measurement diagram of loss of transmit and receive paths in case of the dual-polarization independent transmitter type

Table A.11. Measurement device of loss of transmit path and receive path

No.	Name of device	Remarks
1	Signal generator	
2	Power meter	

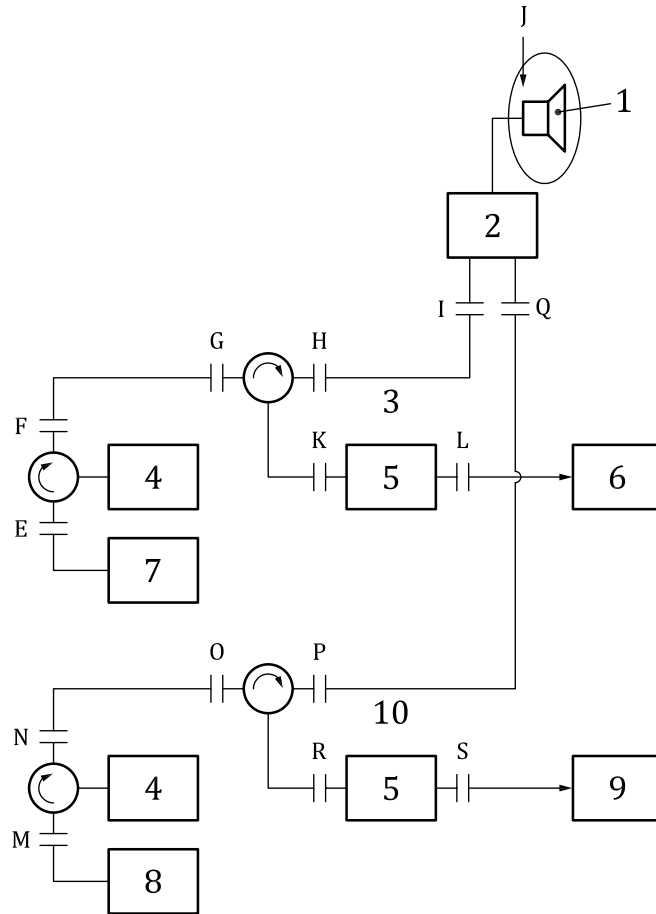
A.3.9.3.4 Measurement method

Measurement is divided into several parts and measured values are summed together. First, for the transmitter to receive return paths (H/V pol.): A – B and C – D, where the transmitter is directly connected to the receiver via a directional coupler (DC), the coupling loss of DC and cable loss are measured. Measurement of the loss of cables is the same as the method shown in Figure A.4.

Then, for the transmit path, the loss values of each circulator in the H/V channels are independently measured. (Connect an SG at one end and a power meter at the other end in each section of measurement points shown with alphabets in Figure A.23.) Also, for the receive path, the loss values of each TR limiter in the H/V channels are measured independently.

For the sections I - J, Q - J, where antenna-related loss exists resulting from rotary joints and OMT, cover the horn aperture with a steel plate. Reflect the radio wave fully at the horn and measure the loss between I and J for the H channel and Q and J for the V channel, respectively, and divide the value by two.

The waveguide length needs a common value used for calculation. In this document, 10 m is supposed to be the net length of the entire waveguide connecting all the equipment parts, under the assumption that the radar equipment will be installed right under the antenna. The waveguide loss for 10 m is then estimated from the specification of the waveguide model used.



- Key:
- | | | | |
|---------------------|-------------------------------------|----|-----------------------------------|
| 1 | Reflector (horn) | 6 | LNA (H channel) |
| 2 | Antenna pedestal | 7 | Transmitter (H) |
| 3 | Horizontal polarization (H channel) | 8 | Transmitter (V) |
| 4 | Dummy load | 9 | LNA (V channel) |
| 5 | TR limiter | 10 | Vertical polarization (V channel) |
| E - F, G - H, I - J | transmit path (H pol.) | | |
| M - N, O - P, Q - J | transmit path (V pol.) | | |
| J - I, H - K, K - L | receive path (H pol.) | | |
| J - Q, P - R, R - S | receive path (V pol.) | | |

Figure A.23. Diagram of measurement of transmit/receive system loss of dual-polarization independent transmitter type

However, when the distance between the antenna bottom and the transmit/receive is within 3 m (for example, for the antenna mounted receiver type) and this relation holds for the equipment regardless of radar site environments, such as a building or tower, a loss value measured in the past installations can be used.

A.3.9.4 Measurement of matched filter losses

A.3.9.4.1 General

The matched filter losses, F_{mf} are given by formula (A.17):

$$F_{mf} = E_{RX,on} / E_{RX,off} \tag{A.17}$$

where:

$E_{RX,on}$ is the received signal energy after the matched filter;

$E_{RX,off}$ is the received signal energy without matched filter.

Note: For pulse compression, matched filter losses are included in the pulse-compression gain.

A.3.9.4.2 *Measurement diagram*

The measurement diagram is given in Figure A.24.

A.3.9.4.3 *Measurement method*

A sample of the transmitter signal taken via a coupler is injected into the TR limiter. If the power exceeds the maximum input level of the receiver, LNA attenuators must be added. The energy of the signal is measured by a dedicated algorithm hosted by the signal processor. $E_{RX,off}$ is measured with the all-pass matched filter and de-activated pulse compression (in the case of a pulse-compression radar). $E_{RX,on}$ is measured with the filter matched to the transmitter pulse (including pulse compression in the case of a pulse-compression radar) and with activated pulse compression (in the case of a pulse-compression radar).

A.3.10 *Phase stability*

A.3.10.1 *General aspects*

Two alternative methods are described. One is only applicable for klystron and solid-state radars. The second can also be used for magnetron radars.

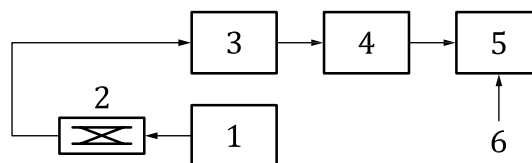
A.3.10.2 *Measurement for klystron and solid-state radar*

A.3.10.2.1 *Measurement diagram*

The measurement diagram is given in Figure A.25.

A.3.10.2.2 *Measurement device*

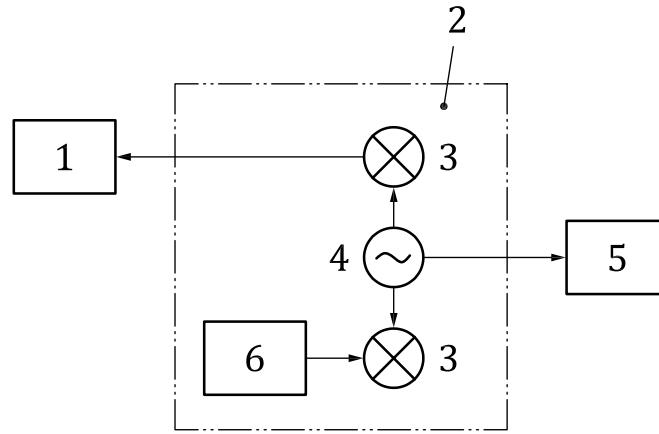
The measurement device is given in Table A.12.



Key:

1	Transmitter	4	Receiver
2	Coupler	5	Signal processor
3	TR limiter	6	Matched filter control

Figure A.24. Measurement diagram of matched filter losses



Key:

- | | | | |
|---|-------------|---|------------------|
| 1 | Transmitter | 4 | STALO |
| 2 | Receiver | 5 | Network analyser |
| 3 | Mixer | 6 | LNA |

Figure A.25. Measurement diagram of phase stability

Table A.12. Measurement device of phase stability

No.	Name of device	Remarks
1	Network analyser	

A.3.10.2.3 **Measurement method**

Connect a network analyser to the STALO monitoring port as in Figure A.25. Tune the analyser to the carrier frequency. Then, measure spectral power density at offsets from the carrier.

As in Figure A.26, when the measured values (in dBc/Hz) are obtained for each log scale, namely as 100 Hz, 1 kHz, 10 kHz and 1 MHz, calculate values for offset frequencies between them with log linear interpolation. Calculate $\int_a^b L(f) \mathbb{Q}f$, an integral value between $a = 100$ Hz and $b = 1$ MHz as antilogarithm.

Then, S/N due to phase noise of this interval of integration is calculated as formula (A.18):

$$S / N = -10 \log \left[2 \int_a^b L(f) \mathbb{Q}f \right] \tag{A.18}$$

where 2 is a factor of double side band.

Finally, convert this value into phase stability, θ_{ps} , in degrees, as formula (A.19):

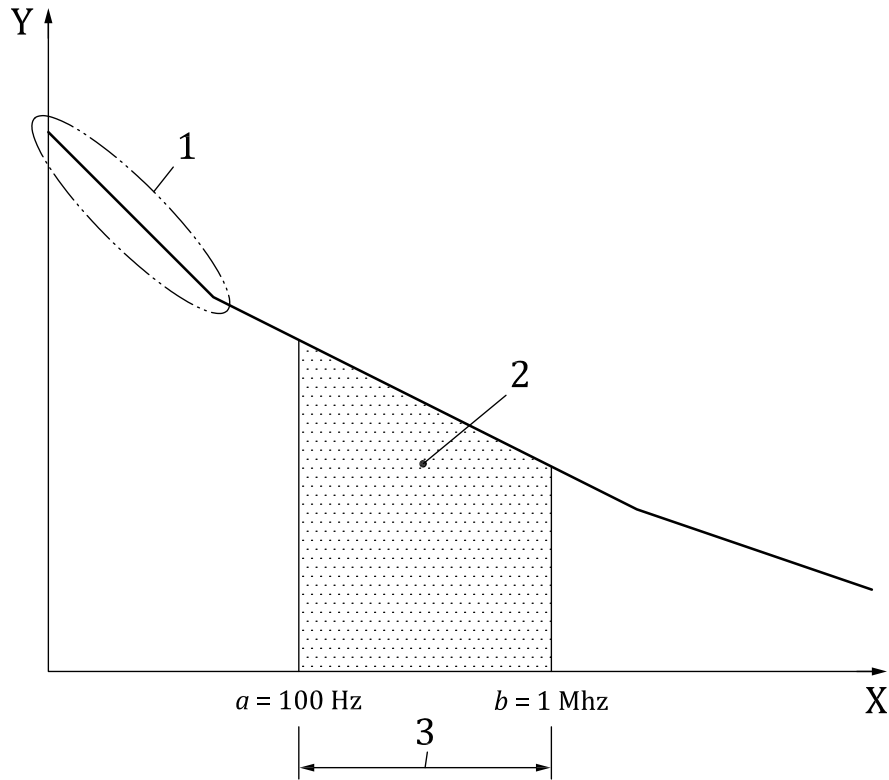
$$\theta_{ps} = \frac{180}{\pi} \left(10^{-\frac{S/N}{10}} \right)^{0.5} \tag{A.19}$$

When the network analyser has an integral calculation function within a user set period, this function can be used for direct calculation.

A.3.10.3 **Measurement for magnetron, klystron and solid-state radar**

A.3.10.3.1 **Measurement diagram**

The measurement diagram is given in Figure A.27. It applies for magnetron radar but is also applicable to klystron and solid-state radar.



Key:

- 1 Log linear interpolation
- 2 Phase stability within 100 Hz to 1 MHz
- 3 Interval of integration
- X Offset frequency, in Hz, log scale
- Y Phase noise, in dBc/Hz, as $L(f)$

Figure A.26. Method for calculating phase stability

A.3.10.3.2 **Measurement device**

The measurement device is given in Table A.13.

Table A.13. Measurement device of a dual-pol radar system

No.	Name of device	Remarks
1	Optical delay line including fibre optic reel	A fibre optic length of at least 6 km must be used.

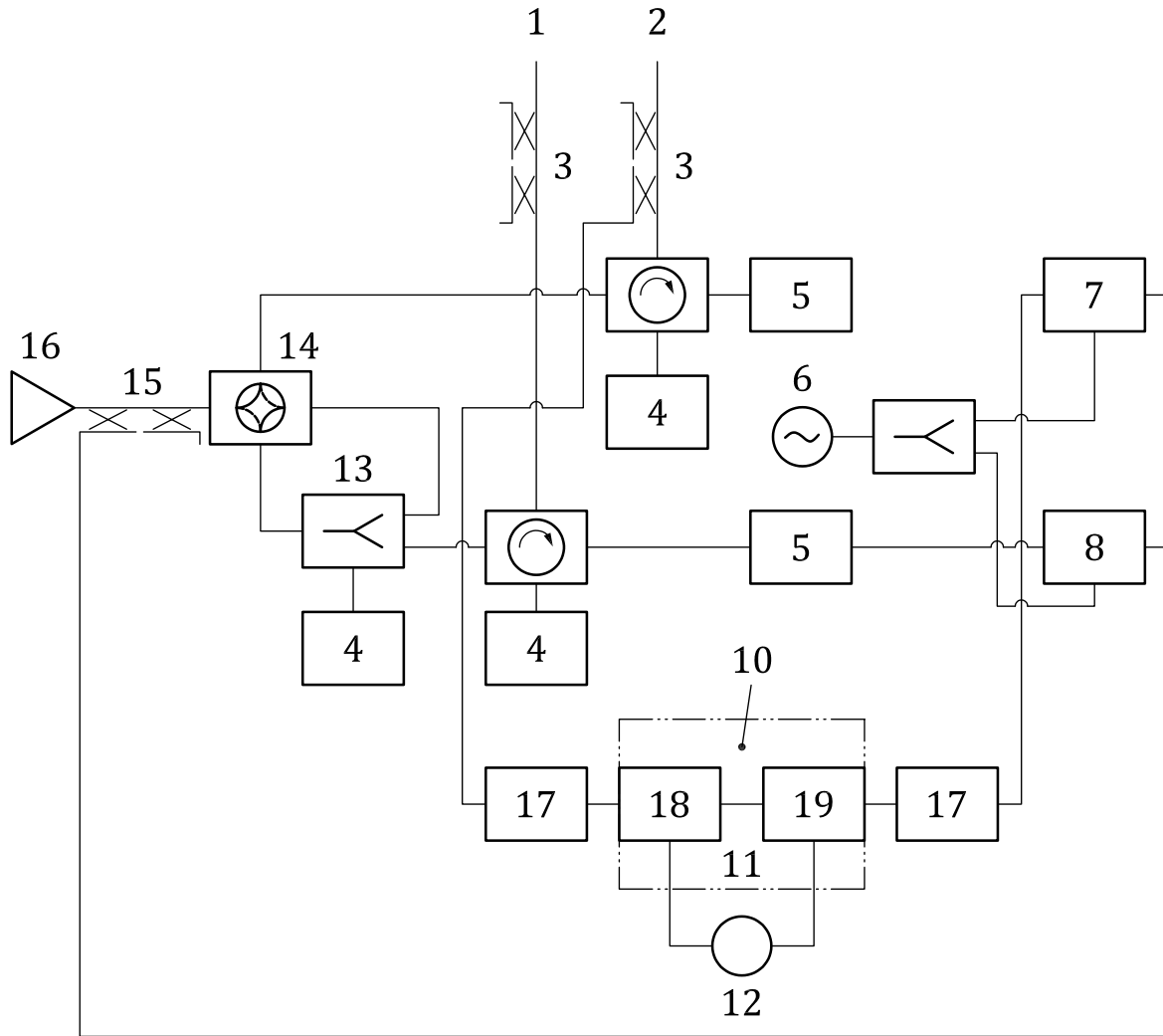
A.3.10.3.3 **Measurement method**

The fibre optic delay line will be inserted between the forward port of the system waveguide coupler and the input of the low noise front end. The system waveguide coupler is usually located directly behind the circulator. If needed, additional attenuators must be inserted at the input or output of the delay line. A general set-up for a dual pol radar system is given in Figure A.26. Solid state or single polarization radar systems can have different set-ups, but the general connections are usually the same.

The ratio FR between mechanical length of the fibre l and the radar distance r is given by formula (A.20):

$$FR = \frac{l}{r} = \frac{2}{n} = \frac{2}{1.467} = 1.363 \tag{A.20}$$

where n is the group index of refraction (group delay) of the fibre optic line used.



Key:

- | | |
|---|----------------------|
| 1 Vertical | 11 Optical interface |
| 2 Horizontal | 12 Fibre optic reel |
| 3 Coupler | 13 Divider |
| 4 Absorber | 14 RF switch |
| 5 TR limiter | 15 Transmit coupler |
| 6 STALO | 16 Transmitter |
| 7 Low noise front end + down converter (horizontal) | 17 Attenuator |
| 8 Low noise front end + down converter (vertical) | 18 RF in |
| 9 Signal processing | 19 RF out |
| 10 Fibre optic delay line | |

Figure A.27. Block measurement diagram of a dual-pol radar system

Using a fibre optic reel with a mechanical length of 6.12 km and $n = 1.467$ will result in an equivalent radar distance of 4.5 km in this example. Depending on the length of the fibre optic line length, the radar distance can be further extended.

The calculation of the phase stability is done by the signal-processing unit and will be displayed by the integrated software tools used to control the radar.

A.4 Other key parameters

A.4.1 General

Other key parameters shown in Table 3 are ordered, in Table A.14, by radar component and with or without pulse-compression method.

Table A.14. Measurement devices

<i>Component</i>	<i>Measurement parameter</i>	<i>Applicability</i>	<i>Remarks</i>	<i>Reference</i>
Transmitter	Unwanted emissions	Common		A.4.2
Antenna	Side lobe level	Common		A.4.3, A.3.4
	Beam direction co-alignment	Common		A.4.4, A.3.4
	Beam width matching	Common		A.4.5, A.3.4
	Maximum rotation speed	Common		A.4.6
	Acceleration	Common		A.4.7
	Antenna pointing accuracy	Common		A.4.8
Receiver	Dynamic range	Common		A.4.9
	Range side lobe	Pulse-compression radar		A.4.10

A.4.2 Unwanted emissions

A.4.2.1 Measurement diagram

The measurement diagram is given in Figure A.28.

A.4.2.2 Measurement device

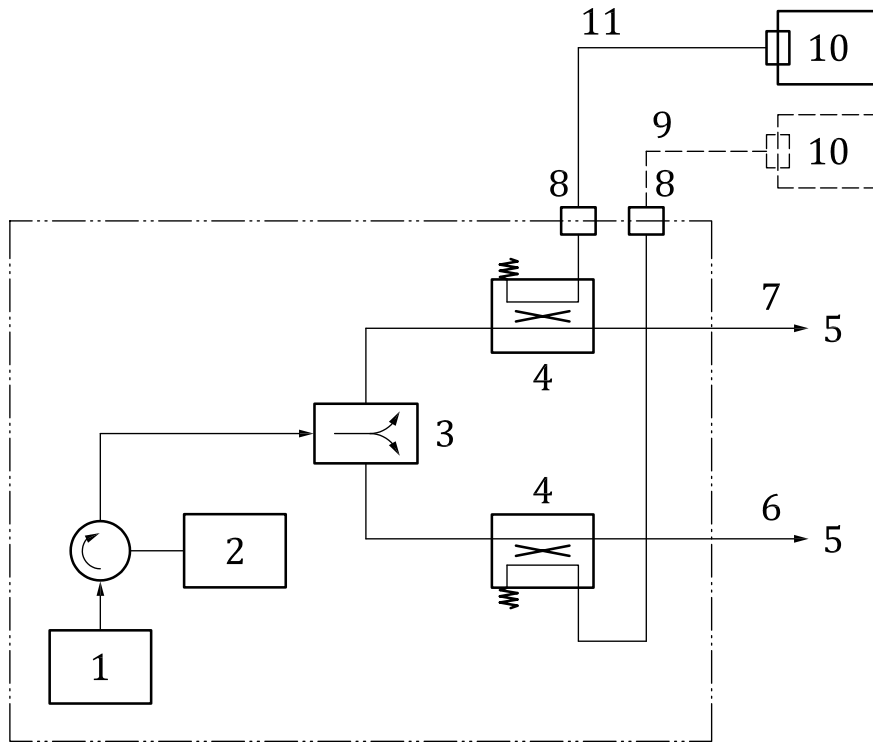
The measurement device is given in Table A.15.

Table A.15. Measurement device of unwanted emissions

<i>No.</i>	<i>Name of device</i>	<i>Remarks</i>
1	Signal generator	
2	Spectrum analyser	

A.4.2.3 Measurement method

Connect an SG to the LNA input and a spectrum analyser to the monitoring point of transmit power and measure the transmit frequency spectrum. Unwanted emissions are measured as attenuation from the centre frequency f_0 at $\pm A$ MHz away. Measurement must be done for



Key:

- | | |
|-------------------------------------|---|
| 1 Transmitter | 7 Horizontal polarization (H) channel |
| 2 Dummy load | 8 Monitoring point for transmission power |
| 3 3 dB power splitter | 9 Cable for measurement |
| 4 Directional coupler | 10 Spectrum analyser |
| 5 To antenna pedestal | 11 Cable for measurement |
| 6 Vertical polarization (V) channel | |

Figure A.28. Measurement diagram of unwanted emissions

both H/V polarizations. For pulse-compression radar, emission for both a long and a short pulse must be measured. It must be confirmed that also at frequencies much larger or smaller than the operating frequency, emission level is kept lower than the specified B dB.

Alternative methods can be found in, for example, ITU-R M.1177-4.

A.4.3 **Antenna side lobe**

A.4.3.1 **Measurement diagram**

Refer to A.3.4.

A.4.3.2 **Measurement device**

Refer to A.3.4.

A.4.3.3 **Measurement method**

As an antenna side lobe brings the mixing of reflected waves from directions other than the target spatial sampling volume, the definition and measurement of side lobe level are required.

Measurement is performed with the first side lobe, evaluating the difference of its peak and main lobe peak level. Measurement is performed in sufficiently wide angles where the first side lobe appears, both for the horizontal and vertical planes. See Figure A.29.

It is assumed that a classical antenna pattern has an axial symmetry with respect to the main beam axis. A cheap way to assess this hypothesis, at least partially, is to move the antenna 180° in EL (most modern antennas can do this) and compare if the meteorological echoes are more or less intense after the move.

A.4.4 **Beam direction co-alignment**

A.4.4.1 **Measurement diagram**

Refer to A.3.4.

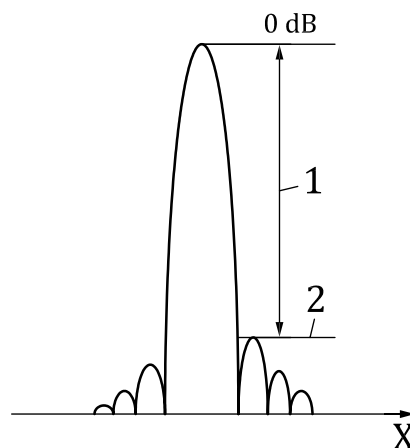
A.4.4.2 **Measurement device**

Refer to A.3.4.

A.4.4.3 **Measurement method**

To determine the beam direction co-alignment (*BDA*) the co-polar antenna diagrams as described in A.3.4 can be used. Estimate the AZ angle of the co-polar peak of the horizontal channel ($Peak_h$). Typically each peak deviates a little from 0° AZ. Do the same for the vertical channel ($Peak_v$). The beam direction co-alignment is then defined as formula (A.21) (in degrees):

$$BDA = Peak_h - Peak_v \quad (A.21)$$



Key:

- 1 Side lobe level ΔV_{pa}
- 2 First side lobe
- X Horizontal/vertical angle

Figure A.29. Measurement of antenna side lobe level

A.4.5. **Beam width matching**

A.4.5.1 **Measurement diagram**

Refer to A.3.4.

A.4.5.2 **Measurement device**

Refer to A.3.4.

A.4.5.3 **Measurement method**

To determine the beam width matching (*BWM*), the co-polar antenna diagrams as described in A.3.4 can be used. Estimate the antenna beam width for both polarizations as described in Figure A.8. In addition to the beam width at the -3 dB level, the beam width can also be determined at, for example, the -10 dB level. The beam width matching is then defined as formula (A.22):

$$BWM = \theta_h - \theta_v \quad (\text{A.22})$$

A.4.6 **Maximum rotation speed**

A.4.6.1 **Measurement diagram**

The antenna system must be set up in a room large enough for full rotation.

A.4.6.2 **Measurement device**

The measurement device is given in Table A.16.

Table A.16. Measurement device of maximum rotation speed

No.	Name of device	Remarks
1	Stop watch	

A.4.6.3 **Measurement method**

Rotate an antenna at maximum speed and measure with a stopwatch the time the antenna takes to rotate N times. Giving the measurement time as t seconds, the maximum rotation speed R_{\max} is calculated as formula (A.23). N is typically set as 10.

$$R_{\max} = 60 \frac{N}{t} \quad (\text{A.23})$$

A.4.7 **Acceleration**

A.4.7.1 **Measurement diagram**

Refer to A.4.6.

A.4.7.2 Measurement device

Refer to A.4.6.

A.4.7.3 Measurement method

For the EL acceleration, start with the antenna at the EL angle = 0 degrees. Then measure t_{aEL} , the time it takes for the antenna to be driven to the EL angle = 90 degrees. Likewise, measure t_{aAZ} , the time it takes to move from 90 degrees to 0 degrees. Take the worst value as a measurement.

For the AZ direction, rotate the antenna with the maximum velocity. Measure the time it takes for the antenna to stop completely.

Measurement is done with a stopwatch. Care should be taken to count in any overshoots.

A.4.8 Antenna pointing accuracy

A.4.8.1 Measurement diagram

Refer to A.4.6.

A.4.8.2 Measurement device

The measurement device is given in Table A.17.

Table A.17. Measurement device of antenna pointing accuracy

No.	Name of device	Remarks
1	Laser pointer	Beam diameter/spread as narrow as possible. It must be rigidly fixed on the antenna.

A.4.8.3 Measurement method

Set up a laser pointer that is small enough to not influence the weight of the antenna system rigidly on a horn or another component. The laser pointer should have a diameter and divergence as narrow as possible.

Direct the antenna directly towards the wall (see Figure A.30). First, fix an EL angle at 0 degrees. Then at the AZ angle = 0 degrees, project the laser beam on to the wall. This projected point, p_{orig} , must be marked on the wall. Because of the divergence of the laser beam, this point is actually a circle with a diameter of several millimetres. Therefore, draw parallel lines to determine the central point. Set the distance between the laser pointer and p_{orig} as h (in m). Then, rotate the antenna in the AZ direction by 360 degrees. Then, project the beam again on to the wall. Record the projected point as $p_{rot,a}$ in the same way as p_{orig} . Taking the difference between p_{orig} and $p_{rot,a}$ as d (in m), calculate angular error θ_{az} as given by formula (A.24):

$$\theta_{az} = \tan^{-1} \left(\frac{d}{h} \right) \quad (A.24)$$

Measure θ_{az} 10 times. Let the standard deviation of 10 samples be defined as the pointing accuracy for the AZ direction.

Fix an AZ angle at 0 degrees. At EL angle = 0 degrees, project the laser beam on to the wall. This projected point p_{orig} is again marked on the wall (the same way as before). Move the antenna in

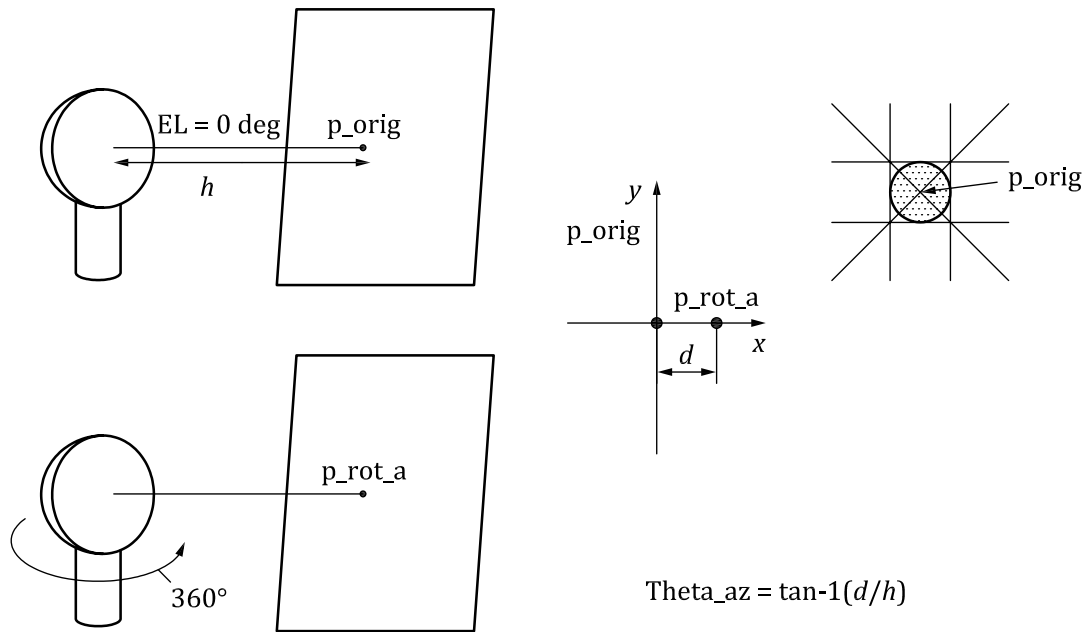


Figure A.30. Antenna pointing accuracy (AZ)

the EL direction by +90 degrees. Then, move it by -90 degrees and again project the beam onto the wall. Record the projected point as $p_{rot,e}$ in the same way as p_{orig} . Taking the difference between p_{orig} and $p_{rot,e}$ as d' (in m), calculate angular error θ_{EZ} as given by formula (A.25):

$$\theta_{EZ} = \tan^{-1}\left(\frac{d'}{h}\right) \tag{A.25}$$

Measure θ_{EZ} 10 times. Let the standard deviation of 10 samples be defined as the pointing accuracy for the EL direction. See Figure A.31.

A.4.9 Dynamic range

A.4.9.1 Measurement diagram

The measurement diagram is given in Figure A.32.

A.4.9.2 Measurement device

The measurement device is given in Table A.18.

Table A.18. Measurement device of dynamic range

No.	Name of device	Remarks
1	Signal generator	

A.4.9.3 Measurement method

Connect an external highly stable (amplitude) SG with a calibration line and wide dynamic range to the receiver. Inject a signal with the SG and read the equivalent power at the output given by the signal processor. Start with a value that is below the minimum detectable signal and then

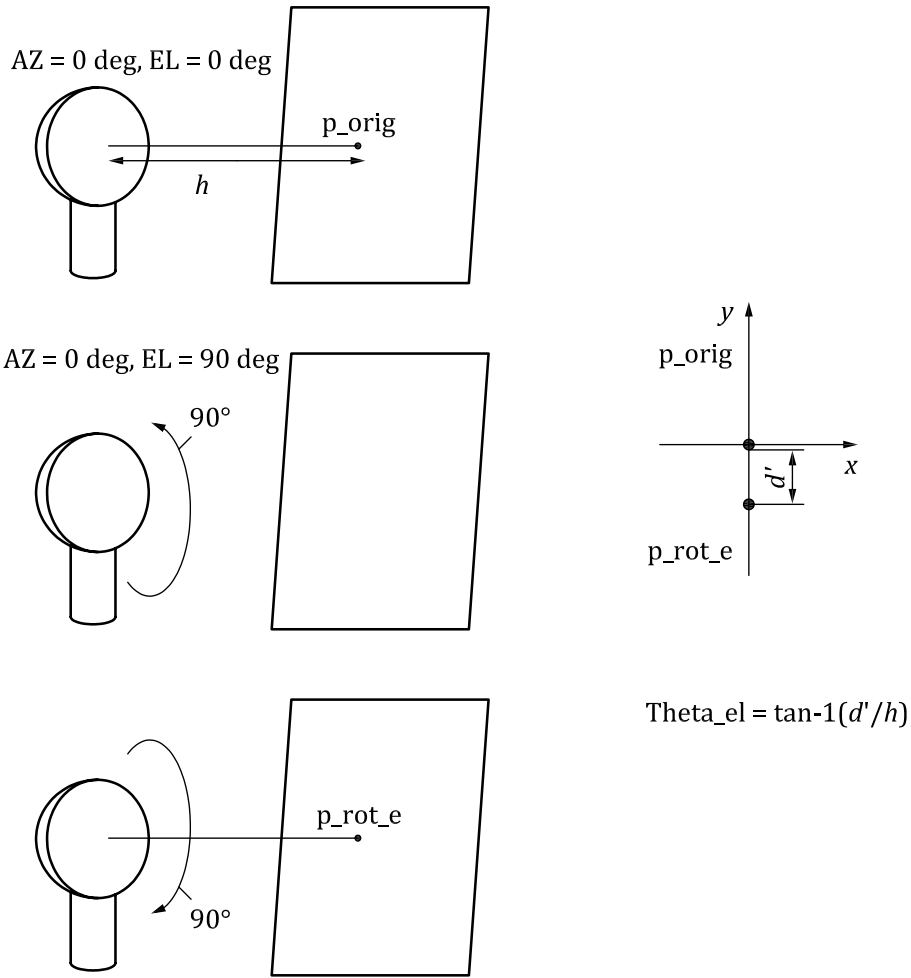
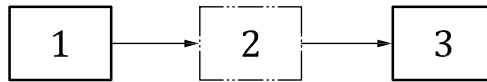


Figure A.31. Antenna pointing accuracy (EL)



- Key:
- 1 SG
 - 2 Analogue and digital receiver
 - 3 Signal processor

Figure A.32. Measurement diagram of dynamic range

increase the injected signal by equidistant steps of, for example, 1 dB or smaller. Stop when the power level of the SG is 2 dB to 3 dB larger than the 1 dB compression point of the receiver. See Figure A.33.

Measure $L_{V_{d'}}$ the level between the 1 dB compression point and S_{min} , in accordance with Figure A.32 (difference between points a and b).

A.4.10 **Range side lobe**

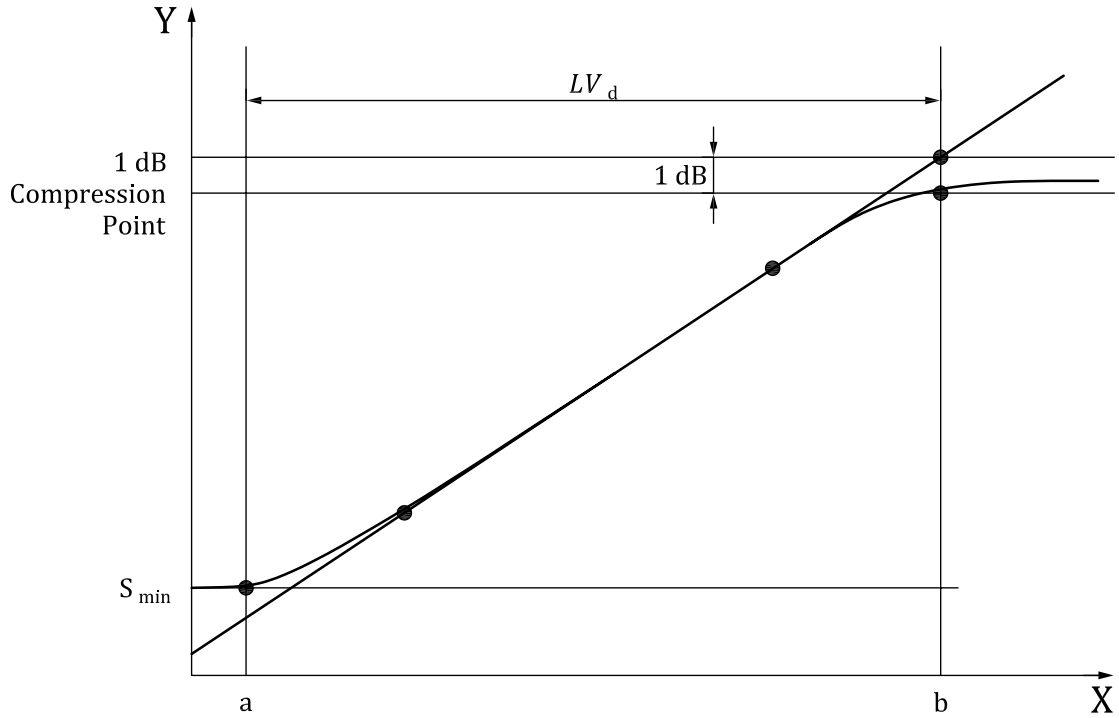
A.4.10.1 **Measurement method**

The range side lobe is measured using the same method as shown in A.4.3.

As range side lobes appear near the centre of the compressed main pulse, read V_m , the peak voltage value of the main pulse, and V_s , the peak voltage value of the range side lobe, on an A-scope. The range side lobe must be derived in a range wider than the pulse width after pulse compression, which is $\Delta t > \tau_{pc}$, using the maximum peak value as the reference. The range side lobe ΔV_p is calculated, in units of dB, as formula (A.26):

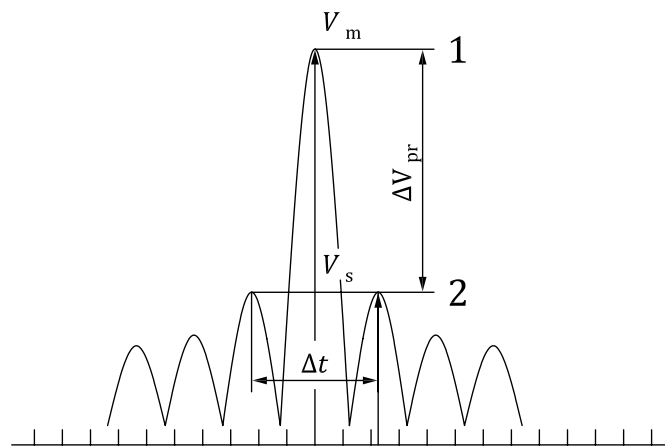
$$\Delta V_{pr} = 10 \log \left(\frac{V_m}{V_s} \right) \tag{A.26}$$

Figure A.34 shows an example of a pulse wave compressed at the receiver.



Key:
 LV_d Dynamic range
 X Input power, in dBm
 Y Output power, in dBm

Figure A.33. Dynamic range



Key:
 1 Peak pulse voltage
 2 Peak range side lobe voltage

Figure A.34. Measurement method of range side lobe

A.4.10.2 Measurement device

The measurement device is given in Table A.19.

Table A.19. Measurement device of range side lobe

<i>No.</i>	<i>Name of device</i>	<i>Remarks</i>
1	A-scope	

ATTACHMENT B. SAMPLE RADAR SPECIFICATIONS

(informative)

The table below gives examples of common specifications of weather radar in the current market (as of 2016).

Common specifications of weather radar

System performance requirements for weather radar		Radar operating frequency		
Fundamental parameters	Criteria	Radar 1 (S-band)	Radar 2 (C-band)	Radar 3 (X-band)
Sensitivity ^a	Minimum detectable reflectivity must be A dBz or less at a distance up to B km, where max unambiguous velocity of more than ± 48 m/s is attained with 2-stagger f_{PRF} of either 2:3 or 3:4 or 4:5	< 18; 240	< 13; 120	< 8; 60
Spatial resolution	Beam resolution must be θ_H and θ_V (in degrees) or less	< 1	< 1	< 1
	Range resolution must be ΔR (in m) or less	≤ 150	≤ 150	≤ 150
	Antenna side lobe must be ΔV_{pa} (in dB) or less	< -25	< -25	< -25
	Range side lobe must be ΔV_{pr} (in dB) or less for pulse-compression radar	< -50	< -50	< -50
Phase stability	Phase stability should be θ_{ps} (in degrees) or less	0.3	0.6	1.2
Accuracy of dual-polarization measurement	Cross polarization ratio must be XPD_{sys} (in dB) or less	< -30	< -30	< -30

<i>Other key parameters</i>	<i>Criteria</i>	<i>Radar 1 (S-band)</i>	<i>Radar 2 (C-band)</i>	<i>Radar (X-band)</i>
Maximum rotation speed	Antenna maximum rotation speed must be R_{\max} (in rpm) or more	≥ 6	≥ 6	≥ 6
Acceleration	As EL antenna acceleration, EL drive time from 0 to 90 (in degrees), and 90 to 0 (in degrees) must be less than t_{aEL} (in sec)	< 20	< 20	< 20
	As AZ antenna acceleration, time from maximum speed to complete stop must be less than t_{aAZ} (in sec)	< 5	< 5	< 5
Antenna pointing accuracy	Antenna pointing accuracy must be θ_{AZ} (in degrees) or less and θ_{EL} (in degrees) or less	< 0.1	< 0.1	< 0.1
Dynamic range	Dynamic range must be LV_d (in dB) or more	> 100	> 100	> 100
Unwanted emissions ^b	The level of unwanted emissions must be A dB or less at B MHz away from the central frequency f_0 (in MHz).	$< -60; 5$	$< -60; 5$	$< -60; 5$

^a For a typical pulse-compression radar the minimum detectable reflectivity at short ranges cannot be calculated from the given values.

^b National requirements might request different values.

ATTACHMENT C. RECORDING OF MEASUREMENT RESULTS

(informative)

Examples of recording measurement results are given in Tables C.1 to C.13.

Table C.1. Pulse width

<i>System</i>	<i>Pulse width τ μs</i>	<i>Accuracy</i>	<i>Remarks</i>
Horizontal polarization channel		$\pm 1/10 \mu$ s	
Vertical polarization channel		$\pm 1/10 \mu$ s	

Table C.2. Peak power

<i>System</i>	<i>P_t dBm</i>	<i>P_m dBm</i>	<i>P'_m dBm</i>	<i>L_c dBm</i>	<i>L_t dBm</i>	<i>Accuracy</i>	<i>Remarks</i>
Horizontal polarization channel						$\pm 1/10$ dB	
Vertical polarization channel						$\pm 1/10$ dB	Only in cases of dual polarization

Table C.3. Antenna gain

<i>System</i>	<i>Frequency MHz</i>	<i>Gain dB</i>	<i>Remarks</i>
Horizontal polarization channel			
Vertical polarization channel			Only in cases of dual polarization

Table C.4. Beam width

<i>System</i>		<i>Beam width degrees</i>	<i>Remarks</i>
Horizontal polarization channel	H plane		θ_H
	V plane		θ_V
Vertical polarization channel	H plane		Only in case of dual polarization
	V plane		

Table C.5. Cross polarization isolation

<i>Polarization</i>	<i>Pattern</i>	<i>Measured XPD dB</i>
Horizontal polarization transmission	XPD_h	
Vertical polarization transmission	XPD_v	

Table C.6. Recording of measurement of H/V isolation

<i>Port</i>	<i>Measurement</i>	<i>Measured level dB</i>
Horizontal	LV_{diff-h}	
Vertical	LV_{diff-v}	

Table C.7. Pulse compression

<i>System</i>	<i>Power level dB</i>		<i>SNR dB</i>		<i>Pulse-compression gain dB</i>	<i>Remarks</i>
Horizontal polarization channel	S_{off}		SNR_{off}			
	N_{off}					
	S_{on}		SNR_{on}			
	N_{on}					
Vertical polarization channel	S_{off}		SNR_{off}			Only in case of dual polarization
	N_{off}					
	S_{on}		SNR_{on}			
	N_{on}					

Table C.8. Sampling interval of received signal

<i>System</i>	<i>Sampling interval, ts μs</i>	<i>Sampling length, Lsi m</i>	<i>Remarks</i>
Horizontal polarization channel			
Vertical polarization channel			Only in case of dual polarization

Table C.9. Receive pulse width (pulse-compression radar)

<i>System</i>	<i>Pulse width μs</i>	<i>Remarks</i>
Horizontal polarization channel		
Vertical polarization channel		Only in case of dual polarization

Table C.10. Radome loss

<i>System</i>	<i>Radome transmission loss dB</i>	<i>Remarks</i>
Horizontal polarization channel		
Vertical polarization channel		Only in case of dual polarization

Table C.11. Transmit/receive path loss for dual-polarization independent transmitter type (refer to Figure A.22)

	<i>Item</i>	<i>Measurement method</i>	<i>Result</i>
1	Transmit to receive return path	(1) Measure the coupling loss of DC and cable loss between A and B.	(H): a = dB (V): b = dB
		(a) dB	
		(2) Measure the coupling loss of DC and cable loss between C and D.	
		(b) dB	

	<i>Item</i>	<i>Measurement method</i>	<i>Result</i>			
2	Transmit path	(1) Measure the loss between E and F. (c) dB	(H): c + d + e = dB (V): f + g + h = dB			
		(2) Measure the loss between G and H. (d) dB				
		(3) Cover the horn aperture with a steel plate. Reflect the radio wave fully at the horn and measure the loss between I and J and divide the value by 2. (e) dB				
		(4) Measure the loss between M and N. (f) dB				
		(5) Measure the loss between O and P. (g) dB				
		(6) Cover the horn aperture with a steel plate. Reflect the radio wave fully at the horn and measure the loss between Q and J and divide the value by 2. (h) dB				
		3		Receive path	(1) Measure the loss between H and K. (i) dB	(H): i + j = dB (V): k + l = dB
					(2) Measure the loss between K and L. (j) dB	
(3) Measure the loss between P and R. (k) dB						
(4) Measure the loss between R and S. (l) dB						
4	Total		Sum all the loss values for H/V (1 to 3 for each H/V).		(H): dB (V): dB	

Table C.12. Matched filter losses

<i>Matched filter losses dB</i>	<i>Remarks</i>
F_{mf}	For pulse-compression matched filter losses are included in the pulse compression gain.

Table C.13. Unwanted emissions

<i>Pulse</i>	<i>Polarization</i>	<i>Separation from f_0</i>	<i>Measurement</i>
Short pulse	H	+A MHz	
		-A MHz	
	V	+A MHz	
		-A MHz	
Long pulse (in case of pulse-compression radar)	H	+A MHz	
		-A MHz	
	V	+A MHz	
		-A MHz	

ATTACHMENT D. RECOMMENDED MAINTENANCE AND CALIBRATION ACTIONS

(informative)

Always follow the manufacturer's instructions for maintenance procedures and intervals for a given system. Recommended actions are given in the table below.

Recommended maintenance and calibration actions

Equipment	Item	Method	Recommended time interval	Procedure (calibration, monitoring, maintenance)		
				Cal	Mon	Main
System	Waveguide attenuation	Test the SG and power meter	During commissioning	X		
	System noise	Power measurement in a spatial region without backscattering (high EL, large distance)	Every volume scan	X	X	
	BITE check/status check	Check the alarm and status of respective equipment by BITE system window	Daily		X	
			Monthly (if not continuously monitored)			X
	Visual check	Check the visual appearance of all equipment	Half-yearly (or during each site visit)			X
	Site safety systems	Check the site safety interlock circuits, such as emergency shutdown switches	Half-yearly			X
	Cooling fan	Check the condition of cooling fan	Half-yearly (or during each site visit)			X
			Daily		X	
	DC voltage	Measure the DC voltage of power supply in the respective equipment	Half-yearly			X
			Daily		X	
	VSWR	Measure the VSWR using power meter	Yearly			X
			Daily		X	
Air filter cleaning	Cleaning of the air filter of respective equipment	Half-yearly or when necessary			X	

Equipment	Item	Method	Recommended time interval	Procedure (calibration, monitoring, maintenance)		
				Cal	Mon	Main
Antenna/ antenna controller	Antenna gain and dry radome attenuation	Far-field test rig, near-field test rig, sun, with radome where possible	At the manufacturer	X		
	Beam width	Far-field test rig, near-field test rig, sun, with radome where possible	At the manufacturer	X		
	Positioning accuracy	Measure the antenna positioning accuracy by means of the sun	Half-yearly (using a sun tracking tool)			X
			Daily (based on sun hits)		X	
	Sound check	Check the sound of mechanical gear and motor	During each site visit			X
	Rotation speed	Measure the antenna rotation speed	Half-yearly			X
			Daily		X	
	Lubricant quantity	Check the lubricant quantity	Half-yearly (or during each site visit)			X
	Lubricant colour	Check the lubricant colour	Half-yearly (or during each site visit)			X
	Slip-ring cleaning	Cleaning of the slip-ring and checking the condition of the brush	Every 1 to 5 years			X
	Lubricant replace	Replace the lubricant of pedestal	Yearly			X
Grease supply	Insert the grease of pedestal	Yearly			X	
Limit switch function check	Check the limit switch function	Yearly			X	
Dehydrator ³	Status check	Check the status of the dehydrator	Daily		X	

Equipment	Item	Method	Recommended time interval	Procedure (calibration, monitoring, maintenance)		
				Cal	Mon	Main
Transmitter	Pulse repetition frequency (f_{PRF})	Measure the f_{PRF} using detector and oscilloscope	Yearly			X
			Daily		X	
	Transmitted frequency	Measure the frequency using frequency counter or spectrum analyser In the case of solid state type, short pulse and chirp pulse should be measured using spectrum analyser	After installation and half-yearly	X		X
	Pulse width	Measure the pulse width using detector, 3 dB attenuator, and oscilloscope	Half-yearly	X		
	Transmitted power	Measure the transmit power using power meter	Half-yearly	X		
			Daily		X	
Major transmitter component replacement	Replace the electronic tube, such as magnetron or klystron In the case of solid state type, no item is required to replace	Typically every ~5 years (replace)			X	
Receiver/ signal processor	Receiver amplification (external measurement)	Test the SG and power meter	Half-yearly	X		
	Dynamic filter attenuation (matched filter loss)	Direct feeding of the emitted signal, power comparison with/without filter	During commissioning	X		
	Receiver single point calibration	Internal reference signal (if available)	Every volume scan (optional)	X	X	
			Half-yearly	X		
	Dynamic range	Measure the dynamic range using the SG	Yearly			X
Minimum detectable sensitivity	Measure the minimum detectable sensitivity using an SG	Yearly			X	
Radome	Rain leaking	Check that rain leaking does not occur	Half-yearly (or during each site visit)			X
	Radome condition	Check the condition of the radome (for example, coating)	Half-yearly			X
		Cleaning of radome	Every 5 years or more frequently, if required			X

^a If liquid water condenses inside the waveguide, electrical sparks can develop, which lead to radar malfunction and possible damage to the electronics. The dehydrator role is to keep the inside of the waveguide dry.

ATTACHMENT E. RADAR DATA EXCHANGE

(informative)

Weather radars are part of the Global Observing System and an exchange of volume-scan radar data will contribute to improved surveillance capability, longer lead times for nowcasts and severe weather warnings, and improved numerical weather prediction. Quality control and extensive data processing is required for hydrological and climate applications.

To facilitate the downstream processing and exchange of both radar volume scan data and derived surface precipitation products, the data must be properly described with respect to:

- How they were collected;
- How they were quality controlled;
- Their quality.

WMO is developing a weather radar data exchange format, an information model, a data model and (a) file format(s) that will include data quality metrics.

ATTACHMENT F. OTHER RADAR SYSTEMS

(informative)

F.1 Phased-array weather radar

Phased-array weather radars (PAWRs) are roughly classified into two categories. One category is the imaging radar type, which performs point-by-point rapid scanning within a limited observation area [20]. Although antenna rotation speed is important, its system performance can be measured with the same criteria (fundamental parameters and other key parameters) explained in section 6. The other category is the radar type that emits electronic beams covering multiple EL angles simultaneously and separates them by digital beam forming (DBF) techniques on the receiver side [21][22][23].

For the latter type of PAWR, a new item must be added to the fundamental parameters, namely a 3-dimensional volume observation speed, which can be expressed as the number of EL angles radar can process at the same time – see Table F.1. However, as this number increases, transmit power P_t and antenna gain G_t will decrease accordingly. Regarding this trade-off between improved rapidness and decreased sensitivity, a radar operator can adopt a scanning strategy such that, for high EL angles, beams are widened to put priority on rapidness, while, for low EL angles, beams are narrowed to put priority on sensitivity.

Table F.1. Fundamental parameter for PAWRs

<i>Parameter category</i>	<i>Purpose</i>	<i>Value</i>
3-dimensional volume observation speed	Determines how fast the entire 3-dimensional volume can be scanned.	The number of EL angles processed simultaneously: the higher the value is, the more rapid the 3-dimensional scanning

Also, for other key parameters, a new item must be added, namely DBF capability to suppress ground clutter – see Table F.2. In contrast to conventional ground clutter suppression with spectrum-based techniques, suppression with DBF techniques that insert null values into unwanted wave directions must be evaluated.

Table F.2. Other key parameter(s) for PAWRs

<i>Parameter category</i>	<i>Purpose</i>	<i>Value</i>
Ground clutter suppression level with DBF techniques	Determines how well DBF can distinguish weather echoes from ground clutter	The higher the value is, the greater ground clutter suppressed with DBF

F.2 Micro rain radar

The micro rain radar (MRR) is a vertically pointing Doppler radar that derives profiles of drop size distributions (DSDs) using the relation between terminal fall velocity and drop size [24]. DSDs can be used to reduce one of the major measurement uncertainties of the weather radar. Since the DSD in weather radar measuring volume can be retrieved, the MRR provides a basis for real-time adjustment of the Z-R-relation and of the weather radar's calibration [25]. Another typical MRR application is determining the melting layer height, which shows up not only as an increase in backscattered power but also (and often more clearly) as a jump in fall velocity.

The MRR, implemented as a solid state 24 GHz FM-CW radar, has a transmit power of a few milliwatts with a typical sensitivity of 3 dBz at $z = 1$ km, $\Delta z = 30$ m, $\Delta t = 10$ s with z , Δz , and

At measuring height, height and time resolution. A major retrieval error is caused by the vertical wind because of its impact on the terminal fall velocity. A favourable set-up consists of an MRR and a rain gauge for controlling the MRR calibration.

F.3 Terminal Doppler weather radar

A terminal Doppler weather radar (TDWR) is a kind of meteorological radar designed to detect microbursts and shear lines around airports and to issue the alert information to the ATC controller in real time. A downburst with its outburst wind zone extending 4 km or less in horizontal direction is called a “microburst” [26]. A microburst is a small but harmful phenomenon producing bursts of outward winds that are strongly divergent near the surface. The intense winds caused by a microburst often last only for 2 min to 5 min. Shear lines produced by gust fronts, the leading edge of the diverging airmass caused by a downdraft, or convergence lines, the interface of warm and cold air masses, are also hazardous. A shear line may be several kilometres or longer, lasts for dozens of minutes, and produces sudden changes of wind speed.

A TDWR is typically a C-band Doppler radar with large parabolic antenna of approximately 7 m or more in diameter. Generally speaking, TDWRs can observe wind direction and wind speed under only rainy weather conditions. In cases where the airport is located in a topography where turbulences are likely to occur, terminal Doppler lidars (TDLs, see F.4) are sometimes used as well as TDWR for clear air conditions.

F.4 Terminal Doppler lidar

TDL is a ground-based remote-sensing system using a laser beam instead of a radio/microwave. TDL radiates the pulse-modulated laser into the air and receives the backscattered light from aerosol. The moving speed of the aerosol or atmospheric wind speed can be calculated by the frequency analysis of the received signals, because the signals from moving object have Doppler speed components according to the object speed.

TDL measures the wind motion within a range of 7 km (at least) to 15 km (typical in horizontal) or to the atmospheric boundary layer (in vertical). Laser beam scanning with repeated pulse radiation can measure the range and direction to the object. TDL can measure the wind speed and direction under clear weather conditions. The observation range is reduced with the reduction of the visibility range, such as rainy conditions.

TDLs are used as a valuable supplement to TDWR observations, since they have complimentary performance with respect to precipitation. TDLs perform best in clear air conditions when TDWR receives no or less signals. On the other hand, when precipitation limits TDL observations, TDWR performs optimally.

F.5 Cloud radar

Cloud radar with a millimetre wave, such as Ka-band and W-band, is an excellent tool to observe cloud and fog for which the particle size is smaller than that associated with precipitation. Cloud radar can observe the formation process of a thundercloud that generates torrential rain, and is expected to forecast heavy rain just before its occurrence. The latest cloud radar has a high sensitivity of approximately -20 dBz or less at 20 km distance, Doppler observation and dual-polarization observation mode.

F.6 Small-size radar system

Generally speaking, a small type of radar besides the standard type (see the description of 1 degree beam width radar in section 5) is particularly used on the X-band because it can reduce the cost of equipment and construction fees, and is easy to carry.

Although X-band radar is more sensitive to radio attenuation by rainfall, the coverage area of a lower-frequency radar could be covered by two or more low-cost X-band radars. A dual radar system can observe 2-dimensional velocity precisely and triple radar system can observe 3-dimensional velocity.

The antenna rotation speed of both AZ and EL scans can ease restriction by using the light and small antenna. It is possible to increase f_{PRF} by focusing on short-range observation (for example, 30 km) to achieve as accurate observations with a high rotation speed as with a radar operating at lower frequency.

Furthermore, time resolution would be improved by a high-speed rotation that can shorten the data output interval. It would provide a high refresh rate to users to make it convenient for short-time phenomenon observation, such as for tornadoes and torrential rainfall.

BIBLIOGRAPHY

- [1] World Meteorological Organization, 2018: *Guide to Instruments and Methods of Observation* (WMO-No. 8), Volume III – Observing Systems. Chapter 7. Geneva.
- [2] Probert-Jones, J.R., 1962: The radar equation in meteorology. *Quarterly Journal of the Royal Meteorological Society*, 1962, 88(376):485–495.
- [3] Doviak, R.J. and D.S. Zrnić, 1993: *Doppler Radar and Weather Observations*. Second edition. San Diego, Academic Press.
- [4] Joe, P. and S. Lapczak, 2002: Evolution of the Canadian Operational Radar Network. In: *Proceedings of the 2nd European Conference on Radar in Meteorology and Hydrology*, Delft, Netherlands: 370–382.
- [5] Seliga, T.A. and V.N. Bringi, 1976: Potential use of radar differential reflectivity measurements at orthogonal polarizations for measuring precipitation. *Journal of Applied Meteorology*, 15:69–76.
- [6] Vollbracht, D., M. Sartori and M. Gabella M., 2014: Absolute dual-polarization radar calibration: Temperature dependence and stability with focus on antenna-mounted receivers and noise source-generated reference signal. In: *Proceedings of the 8th European Conference on Radar in Meteorology and Hydrology (ERAD 2014)*, Garmisch-Partenkirchen, Germany, 1–5 September:91–102.
- [7] Reimann, J., 2013: On Fast, Polarimetric Non-reciprocal Calibration and Multi-polarization Measurements on Weather Radars. PhD dissertation. Deutsches Zentrum für Luft und Raumfahrt and Technische Universität Chemnitz, ISRN DLR-FB-2013-36, ISSN 1434-8454.
- [8] Gabella, M., M. Sartori, O. Progin and U. Germann, 2013: Acceptance tests and monitoring of the next generation polarimetric weather radar network in Switzerland. In: *Proceedings of the Institute of Electrical and Electronics Engineers International Conference on Electromagnetics in Advanced Applications*, Torino, Italy, 9–13 September:211–214.
- [9] Kumagai, H., T. Kozu, M. Satake, H. Hanado and K. Okamoto, 1995: Development of an active radar calibrator for the TRMM Precipitation Radar. *IEEE Transactions on Geoscience and Remote Sensing*, 33:1316–1318.
- [10] Schmidt, K., M. Schwerdt, N.T. Ramon, G.C. Alfonzo, B. Döring, S. Raab, J. Reimann, D. Rudolf and J.W. Antony, 2015: Verification of the Sentinel-1A SAR Instrument Calibration using active and passive point targets. *Wave Propagation and Scattering in Communications, Microwave Systems and Navigation*, Chemnitz, Germany, 11–13 April.
- [11] Gabella, M., M. Sartori, O. Progin, U. Germann and M. Boscacci, 2010: An innovative instrumentation for checking electromagnetic performances of operational meteorological radar. In: *Proceedings of the 6th European Conference on Radar in Meteorology and Hydrology*, Sibiu, Romania, 6–10 September:263–269.
- [12] Gabella, M., M. Boscacci, M. Sartori and U. Germann, 2016: Calibration accuracy of the dual-polarization receivers of the C-band Swiss weather radar network. *Atmosphere*, 7(76).
- [13] Holleman, I., A. Huuskonen, M. Kurri and H. Beekhuis, 2010: Operational monitoring of weather radar receiving chain using the Sun. *Journal of Atmospheric and Oceanic Technology*, 27:159–166.
- [14] Holleman, I., A. Huuskonen, R. Gill and P. Tabary, 2010: Operational monitoring of radar differential reflectivity using the Sun. *Journal of Atmospheric and Oceanic Technology*, 27:881–887.
- [15] Gabella, M., M. Sartori, M. Boscacci and U. Germann, 2015: Vertical and horizontal polarization observations of slowly varying solar emissions from operational Swiss weather radars. *Atmosphere*, 6:50–59.
- [16] Huuskonen, A., M. Kurri and I. Holleman I., 2016: Improved analysis of solar signals for differential reflectivity monitoring. *Atmospheric Measurement Techniques*, 9:3183–3192.
- [17] Leone, D.A., R.M. Endlich, J. Petriceks, R.T.H. Collis and J.R. Porter, 1989: Meteorological considerations used in planning the NEXRAD network. *Bulletin of the American Meteorological Society*, 70:4–13.
- [18] Heiss, W.H., D.L. McGrew and D. Sirmans, 1990: NEXRAD: Next generation weather radar (WSR-88D). *Microwave Journal*, 33(1):79–98.
- [19] Skolnik, M.I. (ed.), 1979: *Radar Handbook*. New York, McGraw-Hill.
- [20] Isom, B., R. Palmer, R. Kelley, J. Meier, D. Bodine, M. Yeary, B. Cheong, Y. Zhang, T.-Y. Yu and M. Biggerstaff, 2015: The atmospheric imaging radar: Simultaneous volumetric observations using a phased array weather radar. *Journal of Atmospheric and Oceanic Technology*, 30(4):655–675.

- [21] Anraku, N., F. Mizutani, M. Wada, H. Handa, T. Ushio and S. Satoh, 2013: Development of phased-array weather radar system for 3D observation of cumulonimbus clouds. 36th Conference on Radar Meteorology, Breckenridge, Colorado, 16–20 September 2013. American Meteorological Society.
- [22] Wada, M., H. Goto, F. Mizutani, T. Ushio and S. Satoh, 2013: Development of dual polarization phased array radar. 36th Conference on Radar Meteorology, Breckenridge, Colorado, 16–20 September 2013. American Meteorological Society.
- [23] Wada, M., H. Yonekubo, T. Ushio, S. Satoh, A. Adachi and S. Tsuchiya, 2016: Keynote 2A: Development of phased-array weather radar: Field trial, dual-pol and how it reduces disaster. WMO Technical Conference on Meteorological and Environmental Instruments and Methods of Observation, Madrid, 27–30 September 2016.
- [24] Atlas, D., R.C.Srivastava and R.S. Sekhon, 1973: Doppler radar characteristics of precipitation at vertical incidence. *Reviews of Geophysics*, 11:1–35.
- [25] Gage, K.S., C.R. Williams, P.E. Johnston, W.L. Ecklund, R. Cifelli, A. Tokay and D.A. Carter, 2000: Doppler radar profilers as calibration tools for scanning radars. *Journal of Applied Meteorology*, 39:2209–2222.
- [26] Fujita, T.T., 1985: The Downburst, microburst and macroburst. SMRP Research Paper 210. University of Chicago.
-

ANNEX 7.B. WMO GUIDANCE STATEMENT ON WEATHER RADAR/RADIO FREQUENCY SHARED SPECTRUM USE

The World Meteorological Organization expresses concern over increasing pressure on weather radar-related radio-frequency bands and stresses the need for adequate efforts for mitigating the damage to data and enabling successful shared use of this spectrum. WMO addresses its concern to policymakers, to national radio-frequency administration agencies, to national hydrological and meteorological societies, to commercial vendors of telecommunication equipment and to the meteorological community.

Protection of traditional weather radar-related radio frequencies is critical to the continued function and improvement of weather sensing, monitoring, forecasting, and warning, and is therefore in the best interests of public safety and security. The meteorological community increasingly relies on remote-sensing technologies for both routine and experimental observations of weather and climate. These activities require global access to the radio-frequency spectrum by not only radars but also wind profilers, microwave radiometers, and telemetry systems, as well as satellite-based passive and active sensors. The progress in weather warning services and other meteorological predictions made in recent years is largely attributable to these technologies.

Weather prediction models and localized operational forecasts increasingly depend on national networks of ground-based Doppler radars for severe weather warnings such as tornadoes, flash flooding, land-falling hurricanes, precipitation (rain, snow, hail), aircraft icing and air traffic/ weather avoidance. Worldwide, Doppler radar networks are now contending with increasing pressures on shared spectrum usage with unlicensed broadband wireless applications. As already experienced in many parts of the world, the impacts of radio-frequency interference by wireless communications can render weather radars blind in particular directions or even over large portions of their coverage. The situation is exacerbated by the ubiquitous and unlicensed nature of these wireless applications that could lead to a total loss of the related spectrum for weather radars.

Development of new radar technologies, including adaptive scanning strategies, shorter pulses, polarization, pulse compression, frequency and phase agility is ongoing. Current and planned satellite radar systems measure clouds and precipitation, which is important for weather forecasting and global climate change research and assessment. Varieties of other space-based and ground-based radio technologies are currently in experimental use and may require future radio spectrum allocations.

WMO recommends that all weather radar users:

- (a) Seek cooperation with owners of nearby radars to avoid radar-to-radar interference;
- (b) Work closely with the national frequency authorities to ensure the proper use of mitigation methods such as dynamic frequency selection;
- (c) Encourage radar manufacturers to implement technologies to identify rogue transmitters and to identify opportunities for dynamic frequency access.

New communication applications make the radio-frequency spectrum an extremely valuable commodity, and so the frequency bands used for operational meteorology and research are in increasing jeopardy. WMO and the meteorological community rely on and support mandated international and national radio-frequency agencies and promote cooperation with the telecommunication authorities and industries to continue to protect or to appropriately share these radio frequencies. WMO is working with these agencies intensively, through the International Telecommunication Union (ITU), to establish appropriate mechanisms to protect meteorological uses of the radio-frequency spectrum. WMO encourages the development of a clear definition of interference, permissible or otherwise, and a remedial process or solution if shared use becomes a problem. WMO encourages funding and implementation of studies

to determine the impact of the total or partial loss of one or more frequency bands used by current operational observing systems and by planned systems. Further, WMO recommends that the results of these studies be made available to ITU radiocommunication groups and to national radio-frequency agencies and the telecommunications industry to encourage dialogue between active and passive users of the spectrum. Vigilance is necessary, as degradations of meteorological data due to intrusions or shared usage will evolve over time. Cooperation with national radio-frequency agencies, the telecommunications industry, and with other spectrum users is encouraged both to advocate support for critically important meteorological use of radio spectrum and to mitigate potential problems.

It is in all nations' best interests to protect radio frequencies essential for meteorological activities that are critical to the accurate forecasting of adverse weather. Global solutions are sought and should be advocated. WMO is actively participating in international frequency management activities, through a group of experts with global representation, to protect current frequency bands used in meteorology, climatology and Earth observations, as well as to obtain new bands required for research and operations.

Further information is available in a guide entitled *Use of Radio Spectrum for Meteorology: Weather, Water and Climate Monitoring and Prediction*, produced jointly by WMO and ITU.

ANNEX 7.C. WMO GUIDANCE STATEMENT ON WEATHER RADAR/ WIND TURBINE SITING

WMO expresses concern over increasing deployment of wind turbine farms and stresses the need for adequate consultation, protection and mitigation efforts. WMO addresses its concern to policymakers, to national radio administration agencies, to national hydrological and meteorological societies, to wind turbine farm developers, to commercial vendors of wind turbine equipment and to the meteorological community.

Protection of weather-radar data is critical to the continued function and improvement of weather sensing, monitoring, forecasting, and warning, and is therefore in the best interests of public safety and security. Weather prediction models and localized operational forecasts increasingly depend on national networks of ground-based Doppler weather radars and wind profilers for severe weather warnings such as tornadoes, flash flooding, land-falling hurricanes, precipitation (rain, snow, hail) forecasts, aircraft icing and air traffic/weather avoidance. Worldwide, Doppler radar and wind profile networks are contending with increasing pressures by wind farms.

Wind farms have already had an impact on operational weather-radar networks, creating confounding ground echoes that create a significant loss of data or create false precipitation for hydrological applications. The rotating blades can create velocities which could potentially be mistaken to be severe weather such as a tornado. While weather radars have been voluntarily moved by the wind farm developers, generally, the meteorological community has no direct jurisdiction on the location of the wind farms and relies on cooperative “good neighbour” policies for mitigation.

Development of new radar and wind profiler networks and wind farms will require strategic planning for mitigation by the meteorological and wind farm communities. WMO and the meteorological community rely on and support mandated international and national radio agencies and will proactively encourage and support these agencies’ efforts to promote and to protect the meteorological use of unobstructed space. WMO encourages national radio agencies to develop acceptable obstruction criteria and to provide tools to help the wind farm developer on site selection.

The World Meteorological Organization encourages wind farm developers to consult with local and national weather-radar programmes early in their planning to minimize operational conflicts with weather warning and forecasting. Each country has its own processes for avoiding or minimizing negative interference with weather-radar data. Frequently there are tools and evaluation processes to facilitate site selection and wind farm design. In some jurisdictions, operating protocols are put in place to mitigate interference only under specific dangerous weather conditions.

Most weather-radar operators and NMHSs can be contacted through their websites for further information and guidance regarding siting information and mitigation agreements.

The range between wind turbines and the weather radar can be used to generally describe the impact on radar quality and also used to provide a mitigation strategy for cooperative siting of weather radars and wind turbines. Below are the general guidelines for typical radars and flat terrain situations, which may require modifications for specific situations and for particular radars. Higher powered radars such as S band (10 cm wavelength) radars with less attenuation may necessitate increasing the range limits in the table.

The World Meteorological Organization encourages funding and implementation of studies to develop technologies to mitigate the impact. Weather radar signal-processing techniques or use of other materials to construct wind turbines may be able to mitigate clutter at long ranges. Further, WMO recommends that the results of these studies be made available to commercial weather radar and wind turbine manufacturers.

It is in all nations' best interests to protect unobstructed space for weather radars and wind profilers that are essential and critical to the accurate forecasting of adverse weather. Local, national and technological solutions are sought. WMO will support and provide guidance material and tools to protect unobstructed space for weather radars and wind profilers.

<i>Range</i>	<i>Potential impact</i>	<i>Guideline</i>
0–5 km	The wind turbine may completely or partially block the radar and can result in significant loss of data that cannot be recovered.	Definite impact zone: Wind turbines should not be installed in this zone.
5–20 km	Multiple reflection and multi-path scattering can create false echoes and multiple elevations. Doppler velocity measurements may be compromised by rotating blades.	Moderate impact zone: Terrain effects will be a factor. Analysis and consultation is recommended. Reorientation or re-siting of individual turbines may reduce or mitigate the impact.
20–45 km	Generally visible on the lowest elevation scan; ground-like echoes will be observed in reflectivity; Doppler velocities may be compromised by rotating blades.	Low impact zone: Notification is recommended.
> 45 km	Generally not observed in the data but can be visible due to propagation conditions.	Intermittent impact zone: Notification is recommended.

REFERENCES AND FURTHER READING

- Ahnert, P.R., M. Hudlow, E. Johnson, D. Greene and M. Dias, 1983: Proposed on-site processing system for NEXRAD. *Preprints of the Twenty-first Conference on Radar Meteorology* (Edmonton, Canada), American Meteorological Society, Boston, 378–385.
- Anagnostou, E.N., C.A. Morales and T. Dinku, 2001: The use of TRMM precipitation radar observations in determining ground radar calibration biases. *Journal of Atmospheric and Oceanic Technology*, 18(4):616–628.
- Aoyagi, J., 1983: A study on the MTI weather radar system for rejecting ground clutter. *Papers in Meteorology and Geophysics*, 33(4):187–243.
- Aoyagi, J. and N. Kodaira, 1995: The reflection mechanism of radar rain echoes. *Preprints of the Twenty-seventh Conference on Radar Meteorology* (Vail, Colorado), American Meteorological Society, Boston, 246–248.
- Atlas, D., 1964: Advances in radar meteorology. In: *Advances in Geophysics* (H.E. Landsberg and J. Van Meighem, eds.). Academic Press, New York, 10:317–479.
- (ed.), 1990: *Radar in Meteorology*. American Meteorological Society, Boston.
- Atlas, D., R.C. Srivastava and R.S. Sekhon, 1973: Doppler radar characteristics of precipitation at vertical incidence. *Reviews of Geophysics and Space Physics*, 11(1):1–35.
- Battan, L.J., 1973: *Radar Observation of the Atmosphere*. University of Chicago Press, Chicago.
- Baynton, H.W., 1979: The case for Doppler radars along our hurricane affected coasts. *Bulletin of the American Meteorological Society*, 60(9):1014–1023.
- Bean, B.R. and E.J. Dutton, 1966: *Radio Meteorology*. US Government Printing Office, Washington DC.
- Bebbington, D.H.O., 1992: Degree of polarization as a radar parameter and its susceptibility to coherent propagation effects. *Preprints from URSI Commission F Symposium on Wave Propagation and Remote Sensing* (Ravenscar, United Kingdom), 431–436.
- Bellon, A. and G.L. Austin, 1978: The evaluation of two years of real-time operation of a Short-Term Precipitation Forecasting Procedure (SHARP). *Journal of Applied Meteorology*, 17(12):1778–1787.
- Berenguer, M., S. Park, D. Sempere-Torres, J. Didszun, M. Pool and M. Pfeifer, 2012: RAINSCANNER@Barcelona: an experiment to assess the hydrological value of a portable X-band radar. Preprints, *Seventh European Conference on Radar in Meteorology and Hydrology* (ERAD 2012), Toulouse, France.
- Bringi, V.N. and V. Chandrasekar, 2001: *Polarimetric Doppler Weather Radar*, Cambridge University Press.
- Bringi, V.N. and A. Hendry, 1990: Technology of polarization diversity radars for meteorology. In: *Radar in Meteorology* (D. Atlas, ed.). American Meteorological Society, Boston, 153–190.
- Brown, R.A. and L.R. Lemon, 1976: Single Doppler radar vortex recognition: Part II – Tornadic vortex signatures. *Preprints of the Seventeenth Conference on Radar Meteorology* (Seattle, Washington), American Meteorological Society, Boston, 104–109.
- Brown, R.A., V.T. Wood, R.M. Steadham, R.R. Lee, B.A. Flickinger and D. Sirmans, 2005: New WSR-88D Volume Coverage Pattern 12: Results of field tests. *Weather and Forecasting*, 20:385–393.
- Browning, K.A. and C.G. Collier, 1982: An integrated radar-satellite nowcasting system in the United Kingdom. In: *Nowcasting* (K.A. Browning, ed.). Academic Press, London, 47–61.
- Browning, K.A., C.G. Collier, P.R. Larke, P. Menmuir, G.A. Monk and R.G. Owens, 1982: On the forecasting of frontal rain using a weather radar network. *Monthly Weather Review*, 110:534–552.
- Browning, K.A. and R. Wexler, 1968: The determination of kinematic properties of a wind field using Doppler radar. *Journal of Applied Meteorology*, 7:105–113.
- Brunkow, D., 2001: *Sphere Calibrations, The Most Hated Experiment in Radar Meteorology*, RADCAL 2000 Workshop, AMS Short Course, Albuquerque, NM.
- Burgess, D.W., 1976: Single Doppler radar vortex recognition: Part I – Mesocyclone signatures. *Preprints of the Seventeenth Conference on Radar Meteorology* (Seattle, Washington), American Meteorological Society, Boston, 97–103.
- Burgess, D.W. and L.R. Lemon, 1990: Severe thunderstorm detection by radar. In: *Radar in Meteorology* (D. Atlas, ed.). American Meteorological Society, Boston, 619–647.
- Burrows, C.R. and S.S. Attwood, 1949: *Radio Wave Propagation*. Academic Press, New York.
- Byers, H.R., 1948: The use of radar in determining the amount of rain falling over a small area. *Transactions of the American Geophysical Union*, 187–196.
- Chandrasekar, V. and L. Baldini, 2013: *RADCAL 2013*, AMS Short Course, Fort Collins, CO.
- Chandrasekar, V., R. Meneghini and I. Zawadzki, 2003: Global and local precipitation measurements by radar. *Meteorological Monographs*, 30(52):215–215.

- Cluckie, I.D. and M.E. Owens, 1987: Real-time rainfall run-off models and use of weather radar information. In: *Weather Radar and Flood Forecasting* (V.K. Collinge and C. Kirby, eds.). John Wiley and Sons, New York.
- Collier, C.G., 1989: *Applications of Weather Radar Systems: A Guide to Uses of Radar Data in Meteorology and Hydrology*. John Wiley and Sons, Chichester, England.
- Commission of the European Communities, 1990: *Une revue du programme ARAMIS* (J.L. Cheze). Seminar on Cost Project 73: Weather Radar Networking (Brussels, 5–8 September 1989), 80–85.
- Crook, N.A. and J. Sun, 2002: Assimilating radar, surface, and profiler data for the Sydney 2000 Forecast Demonstration Project. *Journal of Atmospheric and Oceanic Technology*, 19:888–898.
- Crozier, C.L., P. Joe, J. Scott, H. Herscovitch and T. Nichols, 1991: The King City operational Doppler radar: Development, all-season applications and forecasting. *Atmosphere-Ocean*, 29:479–516.
- Crum, T.D. and R.L. Alberty, 1993: The WSR-88D and the WSR-88D Operational Support Facility. *Bulletin of the American Meteorological Society*, 74(9):1669–1687.
- Dennis, A.S., C.A. Schock and A. Koscielski, 1970: Characteristics of hailstorms of western South Dakota. *Journal of Applied Meteorology*, 9:127–135.
- Dexter, P.E., M.L. Heron and J.F. Ward, 1982: Remote sensing of the sea-air interface using HF radars. *Australian Meteorological Magazine*, 30:31–41.
- Dixon, M. and G. Wiener, 1993: TITAN: Thunderstorm identification, tracking, analysis, and nowcasting – A radar-based methodology. *Journal of Atmospheric and Oceanic Technology*, 10(6):785–797.
- Donaldson, R.J., Jr., 1970: Vortex signature recognition by a Doppler radar. *Journal of Applied Meteorology*, 9:661–670.
- Doneaud, A.A., S. Ionescu-Niscov, D.L. Priegnitz and P.L. Smith, 1984: The area-time integral as an indicator for convective rain volumes. *Journal of Climate and Applied Meteorology*, 23:555–561.
- Doneaud, A.A., J.R. Miller Jr., L.R. Johnson, T.H. Vonder Haar and P. Laybe, 1987: The area-time integral technique to estimate convective rain volumes over areas applied to satellite data: A preliminary investigation. *Journal of Climate and Applied Meteorology*, 26:156–169.
- Doviak, R.J. and D.S. Zrnić, 1993: *Doppler Radar and Weather Observations*. Second edition, Academic Press, San Diego.
- Dupuy, P., S. Matthews, N. Gaussia, R. Scovel and A. Kergomard, 2010: Developing a European Radar Data Centre. Preprints, *Sixth European Conference on Radar in Meteorology and Hydrology* (ERAD 2010), Sibiu, Romania.
- Eccles, P.J. and D. Atlas, 1973: A dual-wavelength radar hail detector. *Journal of Applied Meteorology*, 12:847–854.
- Eilts, M.D. and S.D. Smith, 1990: Efficient dealiasing of Doppler velocities using local environment constraints. *Journal of Atmospheric and Oceanic Technology*, 7:118–128.
- English, M.E., B. Kochtubajda, F.D. Barlow, A.R. Holt and R. McGuinness, 1991: Radar measurement of rainfall by differential propagation phase: A pilot experiment. *Atmosphere-Ocean*, 29:357–380.
- Fabry, F., 2004: Meteorological value of ground target measurements by radar. *Journal of Atmospheric and Oceanic Technology*, 21:560–573.
- Fabry, F., C. Augros and A. Bellon, 2013: The case of sharp velocity transitions in high vertical wind shear when measuring Doppler velocities with narrow Nyquist intervals. *Journal of Atmospheric and Oceanic Technology*, 30:389–394.
- Federer, B., A. Waldvogel, W. Schmid, F. Hampel, Rosini, D. Vento and P. Admirat, 1978: Grossversuch IV: Design of a randomized hail suppression experiment using the Soviet method. *Pure and Applied Geophysics*, 117:548–571.
- Frush, C., R.J. Doviak, M. Sachidananda and D.S. Zrnić, 2002: Application of the SZ phase code to mitigate range – Velocity ambiguities in weather radars. *Journal of Atmospheric and Oceanic Technology*, 19:413–430.
- Germann, U., G. Galli, M. Boscacci and M. Bolliger, 2006a: Radar precipitation measurement in a mountainous region. *Quarterly Journal of the Royal Meteorological Society*, 132:1669–1692.
- Germann, U., I. Zawadzki and B. Turner, 2006b: Predictability of precipitation from continental radar images. Part IV: Limits to prediction. *Journal of the Atmospheric Sciences*, 63:2092–2108.
- Gossard, E.E. and R.G. Strauch, 1983: *Radar Observations of Clear Air and Clouds*. Elsevier Scientific Publication, Amsterdam.
- Harlan, J.A. and T.M. Georges, 1994: An empirical relation between ocean-surface wind direction and the Bragg line ratio of HF radar sea echo spectra. *Journal of Geophysical Research: Oceans*, 99(C4):7971–7978.
- Heiss, W.H., D.L. McGrew and D. Sirmans, 1990: NEXRAD: Next generation weather radar (WSR-88D). *Microwave Journal*, 33(1):79–98.

- Holleman, I., 2001: *Hail Detection Using Single-polarization Radar*. Scientific Report, Royal Netherlands Meteorological Institute (KNMI), WR-2001-01, De Bilt.
- Holleman, I., H.R.A. Wessels, J.R.A. Onvlee and S.J.M. Barlag, 2000: Development of a hail-detection product. *Physics and Chemistry of the Earth, Part B*, 25:1293–1297.
- Holt, A.R., M. Chandra and S.J. Wood, 1995: Polarisation diversity radar observations of storms at C-band. *Preprints of the Twenty-seventh Conference on Radar Meteorology* (Vail, Colorado), American Meteorological Society, Boston, 188–189.
- Holt, A.R., P.I. Joe, R. McGuinness and E. Torlaschi, 1993: Some examples of the use of degree of polarization in interpreting weather radar data. *Proceedings of the Twenty-sixth International Conference on Radar Meteorology*, American Meteorological Society, 748–750.
- Hubbert, J.C., M. Dixon, S.M. Ellis and G. Meymaris, 2009a: Weather radar ground clutter. Part I: Identification, modeling, and simulation. *Journal of Atmospheric and Oceanic Technology*, 26:1165–1180.
- Hubbert, J.C., M. Dixon and S.M. Ellis, 2009b: Weather radar ground clutter. Part II: Real-time identification and filtering. *Journal of Atmospheric and Oceanic Technology*, 26:1181–1197.
- Joe, P., 1999: Beamheight Statistics for Low Elevation Scans. Paper, *Twenty-ninth AMS Radar Conference*, Montreal, American Meteorological Society, Boston, 922–925.
- , 2001: RADCAL 2000 Workshop, AMS Short Course, Albuquerque, NM.
- , 2010: RADMON Workshop, *Sixth European Conference on Radar in Meteorology and Hydrology* (ERAD 2010), Sibiu, Romania.
- Joe, P., D. Burgess, R. Potts, T. Keenan, G. Stumpf and A. Treloar, 2004: The S2K severe weather detection algorithms and their performance. *Weather and Forecasting*, 19:43–63.
- Joe, P., S. Dance, V. Lakshmanan, D. Heizenrehder, P. James, P. Lang, T. Hengstebeck, Y. Feng, P.W. Li, H.Y. Yeung, O. Suzuki, K. Doi and J. Dai, 2012: Automated processing of Doppler radar data for severe weather forecasting. In: *Doppler Radar Observations, Weather Radar, Wind Profiler, Ionospheric Radar and other Advanced Applications* (J. Bech and J.L. Chau, eds.), Intech.
- Joe, P., M. Falla, P. Van Rijn, L. Stamadianos, T. Falla, D. Magosse, L. Ing and J. Dobson, 2002: Radar data processing for severe weather in the national radar project of Canada. *Preprints, Twenty-first Conference on Severe Local Storms*, San Antonio, 12–16 August 2002, 221–224.
- Joe, P. and P.T. May, 2003: Correction of dual PRF velocity errors for operational Doppler weather radars. *Journal of Atmospheric and Oceanic Technology*, 20(4):429–442.
- Joe, P., R.E. Passarelli and A.D. Siggia, 1995: Second trip unfolding by phase diversity processing. *Preprints of the Twenty-seventh Conference on Radar Meteorology* (Vail, Colorado), American Meteorological Society, Boston, 770–772.
- Joe, P., B. Scott, C. Doyle, G. Isaac, I. Gultepe, D. Forsyth, S. Cober, E. Campos, I. Heckman, N. Donaldson, D. Hudak, R. Rasmussen, R. Stewart, J.M. Thériault, H. Carmichael, M. Bailey and F. Boudala, 2014: The monitoring network of the Vancouver 2010 Olympics. *Pure and Applied Geophysics*, 171(1):25–58.
- Joint Doppler Operational Project (JDOP), 1979: *Final Report on the Joint Doppler Operational Project*. NOAA Technical Memorandum, ERL NSSL-86, Norman, Oklahoma, National Severe Storms Laboratory.
- Joss, J. and R.W. Lee, 1993: Scan strategy, clutter suppression calibration and vertical profile corrections. *Preprints of the Twenty-sixth Conference on Radar Meteorology* (Norman, Oklahoma), American Meteorological Society, Boston, 390–392.
- Joss, J. and A. Waldvogel, 1990: Precipitation measurement and hydrology. In: *Radar in Meteorology* (D. Atlas, ed.). American Meteorological Society, Boston, 577–606.
- Keeler, R.J., C.A. Hwang and E. Loew, 1995: Pulse compression weather radar waveforms. *Preprints of the Twenty-seventh Conference on Radar Meteorology* (Vail, Colorado), American Meteorological Society, Boston, 767–769.
- Keenan, T.D. and S.J. Anderson, 1987: Some examples of surface wind field analysis based on Jindalee skywave radar data. *Australian Meteorological Magazine*, 35:153–161.
- Lakshmanan, V., T. Smith, G. Stumpf and K. Hondl, 2007: The Warning Decision Support System–Integrated Information. *Weather and Forecasting*, 22:596–612.
- Leber, G.W., C.J. Merrit and J.P. Robertson, 1961: WSR-57 analysis of heavy rains. *Preprints of the Ninth Weather Radar Conference*, American Meteorological Society, Boston, 102–105.
- Lee, R., G. Della Bruna and J. Joss, 1995: Intensity of ground clutter and of echoes of anomalous propagation and its elimination. *Preprints of the Twenty-seventh Conference on Radar Meteorology* (Vail, Colorado), American Meteorological Society, Boston, 651–652.

- Lemon, L.R., 1978: *New Severe Thunderstorm Radar Identification Techniques and Warning Criteria: A Preliminary Report*. NOAA Technical Memorandum, NWS NSSFC-1, Kansas City, National Severe Storms Forecast Center.
- , 1998: The radar “three-body scatter spike”: An operational large-hail signature. *Weather and Forecasting*, 13:327–340.
- Lemon, L.R., D.W. Burgess and R.A. Brown, 1978: Tornadic storm airflow and morphology derived from single-Doppler radar measurements. *Monthly Weather Review*, 106:48–61.
- Leone, D.A., R.M. Endlich, J. Petriceks, R.T.H. Collis and J.R. Porter, 1989: Meteorological considerations used in planning the NEXRAD network. *Bulletin of the American Meteorological Society*, 70:4–13.
- Lhermitte, R. and D. Atlas, 1961: Precipitation motion by pulse Doppler radar. *Preprints of the Ninth Weather Radar Conference*, American Meteorological Society, Boston, 218–233.
- López, P., 2011: Direct 4D-Var assimilation of NCEP stage IV radar and gauge precipitation data at ECMWF. *Monthly Weather Review*, 139:2098–2116.
- Makihara, Y., 2000: Algorithms for precipitation nowcasting focused on detailed analysis using radar and raingauge data. *Technical Report of the Meteorological Research Institute*, Japan Meteorological Agency, 39:63–111.
- Markowski, P.M., 2002: Hook echoes and rear-flank downdrafts: A review. *Monthly Weather Review*, 130:852–876.
- Marshall, J.S. and E.H. Ballantyne, 1978: Weather Surveillance Radar. *Journal of Applied Meteorology*, 14(7):1317–1338.
- Marshall, J.S. and K.L.S. Gunn, 1952: Measurement of snow parameters by radar. *Journal of Meteorology*, 9:322–327.
- Marshall, J.S. and W.M. Palmer, 1948: The distribution of raindrops with size. *Journal of Meteorology*, 5:165–166.
- McLaughlin, D., D. Pepyne, B. Philips, J. Kurose, M. Zink, D. Westbrook, E. Lyons, E. Knapp, A. Hopf, A. Defonzo, R. Contreras, T. Djafaris, E. Insanic, S. Frasier, V. Chandrasekar, F. Junyent, N. Bharadwaj, Y. Wang, Y. Liu, B. Dolan, K. Droegemeier, J. Brotzge, M. Xue, K. Kloesel, K. Brewster, F. Carr, S. Cruz-Pol, K. Hondl and P. Kollias, 2009: Short-wavelength technology and the potential for distributed networks of small radar systems. *Bulletin of the American Meteorological Society*, 90(12):1797–1817.
- Meischner, P. (ed.), 2003: *Weather Radar: Principles and Advanced Applications*, Springer, Berlin.
- Melnikov, V., D.S. Zrnić, R.J. Doviak and J.K. Carter, 2002: Status of the dual polarization upgrade on the NOAA’s research and development WSR-88D. *Preprints of the Eighteenth International Conference on Interactive Information Processing Systems* (Orlando, Florida), American Meteorological Society, Boston, 124–126.
- Michelson, D., R. Gill, M. Peura and J. Szturc, 2010: Community-based weather radar networking with BALTRAD. *Preprints, Sixth European Conference on Radar in Meteorology and Hydrology (ERAD 2010)*, Sibiu, Romania.
- Michelson, D.B., P.I. Joe, D. Lockett, S. Goldstraw, L. Bai, A. Becker, K.P. Georgakakos, S. Foreman, E. Fucile, R. Giraud, N. Gaussiat, T. Hohmann, A. Kamilliddin, M. Kitchen, E. Kyte, J.F. Mahfouf, S. Matthews, J.M. de Rezende, O. Sireci, M.A. de Barros Teixeira and E. Wattlelot, 2013: WMO initiative for the global exchange of radar data. Manuscript, *Thirty-sixth AMS Radar Meteorology Conference*, Breckenridge, CO, American Meteorological Society.
- Michelson, M., W.W. Schrader and J.G. Wilson, 1990: Terminal Doppler weather radar. *Microwave Journal*, 33(2):139–148.
- Mie, G., 1908: Beiträge zur Optik trüber Medien, speziell kolloidaler Metallösungen. *Annalen der Physik*, 25:377–445.
- Mueller, C.K. and R.E. Carbone, 1987: Dynamics of a thunderstorm outflow. *Journal of the Atmospheric Sciences*, 44:1879–1898.
- Mueller, E.A., S.A. Rutledge, V.N. Bringi, D. Brunkow, P.C. Kennedy, K. Pattison, R. Bowie and V. Chandrasekar, 1995: CSU-CHILL radar upgrades. *Preprints of the Twenty-seventh Conference on Radar Meteorology* (Vail, Colorado), American Meteorological Society, Boston, 703–706.
- Neff, E.L., 1977: How much rain does a rain gauge gage? *Journal of Hydrology*, 35:213–220.
- Passarelli, R.E., Jr., P. Romanik, S.G. Geotis and A.D. Siggia, 1981: Ground clutter rejection in the frequency domain. *Preprints of the Twentieth Conference on Radar Meteorology* (Boston, Massachusetts), American Meteorological Society, Boston, 295–300.
- Probert-Jones, J.R., 1962: The radar equation in meteorology. *Quarterly Journal of the Royal Meteorological Society*, 88:485–495.
- Ray, P.S., C.L. Ziegler, W. Bumgarner and R.J. Serafin, 1980: Single- and multiple-Doppler radar observations of tornadic storms. *Monthly Weather Review*, 108:1607–1625.

- Rinehart, R.E., 2004: *Radar for Meteorologists*. 4th Edition, Rinehart Publishing.
- Ruggiero, F.H. and R.J. Donaldson, Jr., 1987: Wind field derivatives: A new diagnostic tool for analysis of hurricanes by a single Doppler radar. *Preprints of the Seventeenth Conference on Hurricanes and Tropical Meteorology* (Miami, Florida), American Meteorological Society, Boston, 178–181.
- Sauvageot, H., 1982: *Radarmétéorologie*. Eyrolles, Paris.
- , 1994: Rainfall measurement by radar: A review. *Atmospheric Research*, 35:27–54.
- Seed, A.W., 2003: A dynamic and spatial scaling approach to advection forecasting. *Journal of Applied Meteorology*, 42(3):381–388.
- Seliga, T.A. and V.N. Bringi, 1976: Potential use of radar differential reflectivity measurements at orthogonal polarizations for measuring precipitation. *Journal of Applied Meteorology*, 15:69–76.
- Seltmann, J.E.E., T. Hohmann, M. Frech and P. Tracksdorf, 2013: DWD's new operational scan strategy. *Thirty-sixth AMS Radar Meteorology Conference*, 16–20 September 2013, Breckenridge, CO, poster 329.
- Shearman, E.D.R., 1983: Radio science and oceanography. *Radio Science*, 18(3):299–320.
- Sireci, O., P. Joe, S. Eminoglu and K. Akyildiz, 2010: A comprehensive worldwide web-based weather radar database. *Preprints, Sixth European Conference on Radar in Meteorology and Hydrology (ERAD 2010)*, Sibiu, Romania.
- Skolnik, M.I. (ed.), 1970: *Radar Handbook*. McGraw-Hill, New York.
- (ed.), 1990: *Radar Handbook*. Second edition, McGraw-Hill, New York.
- Smith, P.L., 1990: Precipitation measurement and hydrology: Panel report. In: *Radar in Meteorology* (D. Atlas, ed.). American Meteorological Society, Boston, 607–618.
- , 1995: Dwell time considerations for weather radars. *Preprints of the Twenty-seventh Conference on Radar Meteorology* (Vail, Colorado), American Meteorological Society, Boston, 760–762.
- Smull, B.S. and R.A. Houze Jr., 1987: Rear inflow in squall lines with trailing stratiform precipitation. *Monthly Weather Review*, 115(12):2869–2889.
- Strauch, R.G., 1981: Comparison of meteorological Doppler radars with magnetron and klystron transmitters. *Preprints of the Twentieth Conference on Radar Meteorology* (Boston, Massachusetts), American Meteorological Society, Boston, 211–214.
- Sun, J., M. Xue, J.W. Wilson, I. Zawadzki, S.P. Ballard, J. Onvlee-Hooimeyer, P. Joe, D. Barker, P.W. Li, B. Golding, M. Xu and J. Pinto, 2013: [Use of NWP for nowcasting convective precipitation: Recent progress and challenges](#). *Bulletin of the American Meteorological Society*, 95:409–426.
- Tapping, K., 2001: Antenna Calibration using 10.7cm Solar Flux, RADCAL 2000, AMS Short Course, Albuquerque, NM.
- Treloar, A., 1998: Vertically integrated radar reflectivity as an indicator of hail size in the greater Sydney region of Australia. *Preprints of the Nineteenth Conference on Severe Local Storms*, Minneapolis, MN, American Meteorological Society, 48–51.
- Turner, B.J., I. Zawadzki and U. Germann, 2004: Predictability of precipitation from continental radar images. Part III: Operational nowcasting implementation (MAPLE). *Journal of Applied Meteorology*, 43:231–248.
- Ulbrich, C.W. and D. Atlas, 1984: Assessment of the contribution of differential polarization to improve rainfall measurements. *Radio Science*, 19(1):49–57.
- Weber, M.E., J.Y.N. Cho, J.S. Herd, J.M. Flavin, W.E. Benner and G.S. Torok, 2007: The next-generation multimission U.S. surveillance radar network. *Bulletin of the American Meteorological Society*, 88(11):1739–1751.
- Wiener, N., 1964: *Time Series*. M.I.T. Press, Cambridge, Massachusetts.
- Wilson, J.W. and E.A. Brandes, 1979: Radar measurement of rainfall – A summary. *Bulletin of the American Meteorological Society*, 60(9):1048–1058.
- Wilson, J.W., N.A. Crook, C.K. Mueller, J. Sun and M. Dixon, 1998: Nowcasting thunderstorms: A status report. *Bulletin of the American Meteorological Society*, 79(10):2079–2099.
- Wilson, J.W. and W.E. Schreiber, 1986: Initiation of convective storms at radar-observed boundary-layer convergence lines. *Monthly Weather Review*, 114:2516–2536.
- Wilson, J.W., T.M. Weckwerth, J. Vivekanandan, R.M. Wakimoto, R.W. Russell, 1994: Origin of echoes and accuracy of derived winds. *Journal of Atmospheric and Oceanic Technology*, 11(5):1184–1206.
- Witt, A., M. Eilts, G. Stumpf, J. Johnson, D. Mitchell and K. Thomas, 1998: An enhanced hail detection algorithm for the WSR-88D. *Weather and Forecasting*, 13:286–303.
- Wolff, D.B. and B.L. Kelley, 2009: [NASA's Radar Software Library \(RSL\) and RSL in IDL](#). Paper, *Thirty-fourth AMS Radar Conference*, Breckenridge, CO.
- Wood, V.T. and R.A. Brown, 1986: Single Doppler velocity signature interpretation of nondivergent environmental winds. *Journal of Atmospheric and Oceanic Technology*, 3:114–128.

- World Meteorological Organization, 1985: *Use of Radar in Meteorology* (G.A. Clift). Technical Note No. 181 (WMO-No. 625). Geneva.
- , 2012: Operational use of dual-polarisation: lessons learned at Météo France after 8 years of experience at all wavelengths (S/C/X) (P. Tabary). *Papers Presented at the WMO Technical Conference on Meteorological and Environmental Instruments and Methods of Observation (TECO-2012)*. Instruments and Observing Methods Report No. 109. Geneva.
- Wurman, J., M. Randall and C. Burghart, 1995: Real-time vector winds from a bistatic Doppler radar network. *Preprints of the Twenty-seventh Conference on Radar Meteorology* (Vail, Colorado), American Meteorological Society, Boston, 725–728.
- Wurman, J., J.M. Straka and E.N. Rasmussen, 1996 : Fine-scale Doppler radar observations of tornadoes. *Science*, 272:1774–1777.
- Xue, M., K. Kloesel, K. Brewster, F. Carr, S. Cruz-Pol, K. Hondl and P. Kollias, 2009: Short-wavelength technology and the potential for distributed networks of small radar systems. *Bulletin of the American Meteorological Society*, 90(12):1797–1817.
- Yamauchi, H., A. Adachi, O. Suzuki and T. Kobayashi, 2013: Precipitation estimate of a heavy rain event using a C-band solid-state polarimetric radar. *Preprints, Seventh European Conference on Radar in Meteorology and Hydrology (ERAD 2012)*, Toulouse, France.
- Zhang, J., K. Howard and J.J. Gourley, 2005: Constructing three-dimensional multiple-radar reflectivity mosaics: Examples of convective storms and stratiform rain echoes. *Journal of Atmospheric and Oceanic Technology*, 22:30–42.
- Zrnić, D.S. and S. Hamidi, 1981: *Considerations for the Design of Ground Clutter Cancelers for Weather Radar*. Report DOT/FAA/RD-81/72, NTIS.
- Zrnić, D.S. and A.V. Ryzhkov, 1995: Advantages of rain measurements using specific differential phase. *Preprints of the Twenty-seventh Conference on Radar Meteorology* (Vail, Colorado), American Meteorological Society, Boston, 35–37.
- Zrnić, D.S., A. Ryzhkov, J. Straka, Y. Liu and J. Vivekanandan, 2001: Testing a procedure for automatic classification of hydrometeor types. *Journal of Atmospheric and Oceanic Technology*, 18:892–913.
- Zrnić, D.S., G. Zhang, V. Melnikov and J. Andric, 2010: Three-body scattering and hail size. *Journal of Applied Meteorology and Climatology*, 49:687–700.
-

CHAPTER 8. BALLOON TECHNIQUES

8.1 BALLOONS

8.1.1 Main types of balloons

Two main categories of balloons are used in meteorology, as follows:

- (a) Pilot balloons, which are used for the visual measurement of upper wind, and ceiling balloons for the measurement of cloud-base height. Usually they do not carry an appreciable load and are therefore considerably smaller than radiosonde balloons. They are almost invariably of the spherical extensible type and their chief requirement, apart from the ability to reach satisfactory heights, is that they should keep a good spherical shape while rising;
- (b) Balloons which are used for carrying recording or transmitting instruments for routine upper-air observations are usually of the extensible type and spherical in shape. They are usually known as radiosonde or sounding balloons. They should be of sufficient size and quality to enable the required load (usually 200 g to 1 kg) to be carried up to heights as great as 35 km at a rate of ascent sufficiently rapid to enable reasonable ventilation of the measuring elements. For the measurement of upper winds by radar methods, large pilot balloons (100 g) or radiosonde balloons are used depending on the weight and drag of the airborne equipment.

Other types of balloons used for special purposes are not described in this chapter. Constant-level balloons that rise to, and float at, a predetermined level are made of inextensible material. Large constant-level balloons are partly filled at release. Super-pressure constant-level balloons are filled to extend fully the balloon at release. Tetroons are small super-pressure constant-level balloons, tetrahedral in shape, used for trajectory studies. The use of tethered balloons for profiling is discussed in the present volume, Chapter 5.

8.1.2 Balloon materials and properties

The best basic materials for extensible balloons are high-quality natural rubber latex and a synthetic latex based upon polychloroprene. Natural latex holds its shape better than polychloroprene – which is stronger and can be made with a thicker film for a given performance. It is less affected by temperature, but more affected by the ozone and ultraviolet radiation at high altitudes, and has a shorter storage life. Both materials may be compounded with various additives to improve their storage life, strength and performance at low temperatures both during storage and during flight, and to resist ozone and ultraviolet radiation. As one of the precautions against explosion, an antistatic agent may also be added during the manufacture of balloons intended to be filled with hydrogen.

There are two main processes for the production of extensible balloons. A balloon may be made by dipping a form into latex emulsion, or by forming it on the inner surface of a hollow mould. Moulded balloons can be made with more uniform thickness, which is desirable for achieving high altitudes as the balloon expands, and the neck can be made in one piece with the body, which avoids the formation of a possible weak point.

Polyethylene is the inextensible material used for constant-level balloons.

8.1.3 Balloon specifications

The finished balloons should be free from foreign matter, pinholes or other defects and must be homogeneous and of uniform thickness. They should be provided with necks of

between 1 and 5 cm in diameter and 10 to 20 cm long, depending on the size of the balloon. In the case of sounding balloons, the necks should be capable of withstanding a force of 200 N without damage. In order to reduce the possibility of the neck being pulled off, it is important that the thickness of the envelope should increase gradually towards the neck; a sudden discontinuity of thickness forms a weak spot.

Balloons are distinguished in size by their nominal weights in grams. The actual weight of individual balloons should not differ from the specified nominal weight by more than 10%, or preferably 5%. They should be capable of expanding to at least four times, and preferably five or six times, their unstretched diameter and of maintaining this expansion for at least 1 h. When inflated, balloons should be spherical or pear-shaped.

The question of specified shelf life of balloons is important, especially in tropical conditions. Artificial ageing tests exist but they are not reliable guides. One such test is to keep sample balloons in an oven at a temperature of 80 °C for four days, this being reckoned as roughly equivalent to four years in the tropics, after which the samples should still be capable of meeting the minimum expansion requirement. Careful packing of the balloons so that they are not exposed to light (especially sunlight), fresh air or extremes of temperature is essential if rapid deterioration is to be prevented.

Balloons manufactured from synthetic latex incorporate a plasticizer to resist the stiffening or freezing of the film at the low temperatures encountered near and above the tropopause. Some manufacturers offer alternative balloons for daytime and night-time use, the amount of plasticizer being different.

8.2 BALLOON BEHAVIOUR

8.2.1 Rate of ascent

From the principle of buoyancy, the total lift of a balloon is given by the buoyancy of the volume of gas in it, as follows:

$$T = V(\rho - \rho_g) = 0.523 D^3 (\rho - \rho_g) \quad (8.1)$$

where T is the total lift; V is the volume of the balloon; ρ is the density of the air; ρ_g is the density of the gas; and D is the diameter of the balloon, which is assumed to be spherical.

All units are in the International System of Units. For hydrogen at ground level, the buoyancy ($\rho - \rho_g$) is about 1.2 kg m⁻³. All the quantities in equation 8.1 change with height.

The free lift L of a balloon is the amount by which the total lift exceeds the combined weight W of the balloon and its load (if any):

$$L = T - W \quad (8.2)$$

namely, it is the net buoyancy or the additional weight which the balloon, with its attachments, will just support without rising or falling.

It can be shown by the principle of dynamic similarity that the rate of ascent V of a balloon in still air can be expressed by a general formula:

$$V = \frac{qL^n}{(L+W)^{1/3}} \quad (8.3)$$

in which q and n depend on the drag coefficient, and therefore on the Reynolds number, $v\rho D/\mu$ (μ being the viscosity of the air). Unfortunately, a large number of meteorological balloons, at some stages of flight, have Reynolds numbers within the critical region of $1 \cdot 10^5$ to $3 \cdot 10^5$, where a rapid change of drag coefficient occurs, and they may not be perfectly spherical. Therefore, it is impracticable to use a simple formula which is valid for balloons of different sizes and different free lifts. The values of q and n in the above equation must, therefore, be derived

by experiment; they are typically, very approximately, about 150 and about 0.5, respectively, if the ascent rate is expressed in m min^{-1} . Other factors, such as the change of air density and gas leakage, can also affect the rate of ascent and can cause appreciable variation with height.

In conducting soundings during precipitation or in icing conditions, a free lift increase of up to about 75%, depending on the severity of the conditions, may be required. An assumed rate of ascent should not be used in any conditions other than light precipitation. A precise knowledge of the rate of ascent is not usually necessary except in the case of pilot- and ceiling-balloon observations, where there is no other means of determining the height. The rate of ascent depends largely on the free lift and air resistance acting on the balloon and train. Drag can be more important, especially in the case of non-spherical balloons. Maximum height depends mainly on the total lift and on the size and quality of the balloon.

8.2.2 Balloon performance

The table in this section lists typical figures for the performance of various sizes of balloons. They are very approximate. If precise knowledge of the performance of a particular balloon and train is necessary, it must be obtained by analysing actual flights. Balloons can carry payloads greater than those listed in the table if the total lift is increased. This is achieved by using more gas and by increasing the volume of the balloon, which will affect the rate of ascent and the maximum height.

Typical balloon performance

Weight (g)	10	30	100	200	350	600	1 000	1 500	3 000
Diameter at release (cm)	30	50	90	120	130	140	160	180	210
Payload (g)	0	0	0	250	250	250	250	1 000	1 000
Free lift (g)	5	60	300	500	600	900	1 100	1 300	1 700
Rate of ascent (m min^{-1})	60	150	250	300	300	300	300	300	300
Maximum height (km)	12	13	20	21	26	31	34	34	38

The choice of a balloon for meteorological purposes is dictated by the load, if any, to be carried, the rate of ascent, the altitude required, whether the balloon is to be used for visual tracking, and by the cloud cover with regard to its colour. Usually, a rate of ascent between 300 and 400 m min^{-1} is desirable in order to minimize the time required for observation; it may also be necessary in order to provide sufficient ventilation for the radiosonde sensors. In choosing a balloon, it is also necessary to bear in mind that the altitude attained is usually less when the temperature at release is very low.

For balloons used in regular operations, it is beneficial to determine the free lift that produces optimum burst heights. For instance, it has been found that a reduction in the average rate of ascent from 390 to 310 m min^{-1} with some mid-size balloons by reducing the amount of gas for inflation may give an increase of 2 km, on average, in the burst height. Burst height records should be kept and reviewed to ensure that optimum practice is sustained.

Daytime visual observations are facilitated by using uncoloured balloons on clear sunny days, and dark-coloured ones on cloudy days.

The performance of a balloon is best gauged by the maximum linear extension it will withstand before bursting and is conveniently expressed as the ratio of the diameter (or circumference) at burst to that of the unstretched balloon. The performance of a balloon in flight, however, is not necessarily the same as that indicated by a bursting test on the ground. Performance can be affected by rough handling when the balloon is filled and by stresses induced during launches

in gale conditions. In flight, the extension of the balloon may be affected by the loss of elasticity at low temperatures, by the chemical action of oxygen, ozone and ultraviolet radiation, and by manufacture faults such as pinholes or weak spots. A balloon of satisfactory quality should, however, give at least a fourfold extension in an actual sounding. The thickness of the film at release is usually in the range of 0.1 to 0.2 mm.

There is always a small excess of pressure p_1 within the balloon during ascent, amounting to a few hPa, owing to the tension of the rubber. This sets a limit to the external pressure that can be reached. It can be shown that, if the temperature is the same inside and outside the balloon, this limiting pressure p is given by:

$$p = \left(\frac{1.07W}{L_0} + 0.075 \right) p_1 \cong \frac{Wp_1}{L_0} \quad (8.4)$$

where W is the weight of the balloon and apparatus; and L_0 is the free lift at the ground, both expressed in grams. If the balloon is capable of reaching the height corresponding with p , it will float at this height.

8.3 HANDLING BALLOONS

8.3.1 Storage

It is very important that radiosonde balloons should be correctly stored if their best performance is still to be obtained after several months. It is advisable to restrict balloon stocks to the safe minimum allowed by operational needs. Frequent deliveries, wherever possible, are preferable to purchasing in large quantities with consequent long periods of storage. To avoid the possibility of using balloons that have been in storage for a long period, balloons should always be used in the order of their date of manufacture.

It is generally possible to obtain the optimum performance up to about 18 months after manufacture, provided that the storage conditions are carefully chosen. Instructions are issued by many manufacturers for their own balloons and these should be observed meticulously. The following general instructions are applicable to most types of radiosondes balloons.

Balloons should be stored away from direct sunlight and, if possible, in the dark. At no time should they be stored adjacent to any source of heat or ozone. Balloons made of either polychloroprene or a mixture, or polychloroprene and natural rubber may deteriorate if exposed to the ozone emitted by large electric generators or motors. All balloons should be kept in their original packing until required for preflight preparations. Care should be taken to see that they do not come into contact with oil or any other substance that may penetrate the wrapping and damage the balloons.

Wherever possible, balloons should be stored in a room at temperatures of 15 to 25 °C; some manufacturers give specific guidance on this point and such instructions should always be followed.

8.3.2 Conditioning

Balloons made from natural rubber do not require special heat treatment before use, as natural rubber does not freeze at the temperatures normally experienced in buildings used for human occupation. It is, however, preferable for balloons that have been stored for a long period at temperatures below 10 °C to be brought to room temperature for some weeks before use.

Polychloroprene balloons suffer a partial loss of elasticity during prolonged storage at temperatures below 10 °C. For the best results, this loss should be restored prior to inflation by conditioning the balloon. The manufacturer's recommendations should be followed.

It is common practice to place the balloon in a thermally insulated chamber with forced air circulation, maintained at suitable temperature and humidity for some days before inflation, or alternatively to use a warm water bath.

At polar stations during periods of extremely low temperatures, the balloons to be used should have special characteristics that enable them to maintain strength and elasticity in such conditions.

8.3.3 Inflation

If a balloon launcher is not used, a special room, preferably isolated from other buildings, should be provided for filling balloons. It should be well ventilated (for example, NFPA, 1999). If hydrogen gas is to be used, special safety precautions are essential (see 8.6). The building should be free from any source of sparks, and all electric switches and fittings should be spark-proof; other necessary details are given in 8.6.2. If helium gas is to be used, provision may be made for heating the building during cold weather. The walls, doors and floor should have a smooth finish and should be kept free from dust and grit. Heating hydrogen-inflation areas can be accomplished by steam, hot water or any other indirect means; however, electric heating, if any, shall be in compliance with national electrical codes (e.g. NFPA 50A for Class I, Division 2, locations).

Protective clothing (see 8.6.4) should be worn during inflation. The operator should not stay in a closed room with a balloon containing hydrogen. The hydrogen supply should be controlled and the filling operation observed, from outside the filling room if the doors are shut, and the doors should be open when the operator is in the room with the balloon.

Balloons should be inflated slowly because sudden expansion may cause weak spots in the balloon film. It is desirable to provide a fine adjustment valve for regulating the gas flow. The desired amount of inflation (free lift) can be determined by using either a filling nozzle of the required weight or one which forms one arm of a balance on which the balloon lift can be weighed. The latter is less convenient, unless it is desirable to allow for variations in the weights of balloons, which is hardly necessary for routine work. It is useful to have a valve fitted to the weight type of the filler, and a further refinement, used in some services, is to have a valve that can be adjusted to close automatically at the required lift.

8.3.4 Launching

The balloon should be kept under a shelter until everything is ready for its launch. Prolonged exposure to bright sunshine should be avoided as this may cause a rapid deterioration of the balloon fabric and may even result in its bursting before leaving the ground. Protective clothing should be worn during manual launches.

No special difficulties arise when launching radiosonde balloons in light winds. Care should always be taken to see that there is no risk of the balloon and instruments striking obstructions before they rise clear of trees and buildings in the vicinity of the station. Release problems can be avoided to a large extent by carefully planning the release area. It should be selected to have a minimum of obstructions that may interfere with launching; the station buildings should be designed and sited considering the prevailing wind, likely gust effects on the release area and, in cold climates, drifting snow.

It is also advisable in high winds to keep the suspension of the instrument below the balloon as short as possible during launching, by using some form of suspension release or unwinder. A convenient device consists of a reel on which the suspension cord is wound and a spindle to which is attached an air brake or escapement mechanism that allows the suspension cord to unwind slowly after the balloon is released.

Mechanical balloon launchers have the great advantage that they can be designed to offer almost foolproof safety, by separating the operator from the balloon during filling and launching.

They can be automated to various degrees, even to the point where the whole radiosonde operation requires no operator to be present. They might not be effective at wind speeds above 20 m s^{-1} . Provision should be made for adequate ventilation of the radiosonde sensors before release, and the construction should desirably be such that the structure will not be damaged by fire or explosion.

8.4 ACCESSORIES FOR BALLOON ASCENTS

8.4.1 Illumination for night ascents

The light source in general use for night-time pilot-balloon ascents is a lamp powered by a small electric battery. A battery of two 1.5 V cells, or a water-activated type used with a 2.5 V 0.3 A bulb, is usually suitable. Alternatively, a device providing light by means of chemical fluorescence may be used. For high-altitude soundings, however, a more powerful system of 2 to 3 W, together with a simple reflector, is necessary.

If the rate of ascent is to remain unchanged when a lighting unit is to be used, a small increase in free lift is theoretically required; that is to say, the total lift must be increased by more than the extra weight carried (see equation 8.3). In practice, however, the increase required is probably less than that calculated since the load improves the aerodynamic shape and the stability of the balloon.

At one time, night ascents were carried with a small candle in a translucent paper lantern suspended some 2 m or so below the balloon. However, there is a risk of flash or explosion if the candle is brought near the balloon or the source of hydrogen, and there is a risk of starting a forest fire or other serious fires upon return to the Earth. Thus, the use of candles is strongly discouraged.

8.4.2 Parachutes

In order to reduce the risk of damage caused by a falling sounding instrument, it is usual practice to attach a simple type of parachute. The main requirements are that it should be reliable when opening and should reduce the speed of descent to a rate not exceeding about 5 m s^{-1} near the ground. It should also be water-resistant. For instruments weighing up to 2 kg, a parachute made from waterproof paper or plastic film of about 2 m diameter and with strings about 3 m long is satisfactory. In order to reduce the tendency for the strings to twist together in flight it is advisable to attach them to a light hoop of wood, plastic or metal of about 40 cm in diameter just above the point where they are joined together.

When a radar reflector for wind-finding is part of the train it can be incorporated into the parachute and can serve to keep the strings apart. The strings and attachments must be able to withstand the opening of the parachute. If light-weight radiosondes are used (less than about 250 g), the radar reflector alone may provide sufficient drag during descent.

8.5 GASES FOR INFLATION

8.5.1 General

The two gases most suitable for meteorological balloons are helium and hydrogen. The former is much to be preferred on account of the fact that it is free from risk of explosion and fire. However, since the use of helium is limited mainly to the few countries which have an abundant natural supply, hydrogen is more generally used (see WMO, 1982). The buoyancy (total lift) of helium is 1.115 kg m^{-3} , at a pressure of 1 013 hPa and a temperature of $15 \text{ }^\circ\text{C}$. The corresponding figure for pure hydrogen is 1.203 kg m^{-3} and for commercial hydrogen the figure is slightly lower than this.

It should be noted that the use of hydrogen aboard ships is no longer permitted under the general conditions imposed for marine insurance. The extra cost of using helium has to be reckoned against the life-threatening hazards to and the extra cost of insurance, if such insurance can be arranged.

Apart from the cost and trouble of transportation, the supply of compressed gas in cylinders affords the most convenient way of providing gas at meteorological stations. However, at places where the cost or difficulty of supplying cylinders is prohibitive, the use of an on-station hydrogen generator (see 8.5.3) should present no great difficulties.

8.5.2 Gas cylinders

For general use, steel gas cylinders, capable of holding 6 m³ of gas compressed to a pressure of 18 MPa (10 MPa in the tropics), are probably the most convenient size. However, where the consumption of gas is large, as at radiosonde stations, larger capacity cylinders or banks of standard cylinders all linked to the same outlet valve can be useful. Such arrangements will minimize handling by staff. In order to avoid the risk of confusion with other gases, hydrogen cylinders should be painted a distinctive colour (red is used in many countries) and otherwise marked according to national regulations. Their outlet valves should have left-handed threads to distinguish them from cylinders of non-combustible gases. Cylinders should be provided with a cap to protect the valves in transit.

Gas cylinders should be tested at regular intervals ranging from two to five years, depending on the national regulations in force. This should be performed by subjecting them to an internal pressure of at least 50% greater than their normal working pressure. Hydrogen cylinders should not be exposed to heat and, in tropical climates, they should be protected from direct sunshine. Preferably, they should be stored in a well-ventilated shed which allows any hydrogen leaks to escape to the open air.

8.5.3 Hydrogen generators

Hydrogen can be produced on site using various kinds of hydrogen generators. All generator plants and hydrogen storage facilities shall be legibly marked and with adequate warnings according to national regulations (for example, "This unit contains hydrogen"; "Hydrogen – Flammable gas – No smoking – No open flames"). The following have proven to be the most suitable processes for generating hydrogen for meteorological purposes:

- (a) Ferro-silicon and caustic soda with water;
- (b) Aluminium and caustic soda with water;
- (c) Calcium hydride and water;
- (d) Magnesium-iron pellets and water;
- (e) Liquid ammonia with hot platinum catalyst;
- (f) Methanol and water with a hot catalyst;
- (g) Electrolysis of water.

Most of the chemicals used in these methods are hazardous, and the relevant national standards and codes of practice should be scrupulously followed, including correct markings and warnings. They require special transportation, storage, handling and disposal. Many of them are corrosive, as is the residue after use. If the reactions are not carefully controlled, they may produce excess heat and pressure. Methanol, being a poisonous alcohol, can be deadly if ingested, as it may be by substance abusers.

In particular, caustic soda, which is widely used, requires considerable care on the part of the operator, who should have adequate protection, especially for the eyes, from contact not only with the solution, but also with the fine dust which is liable to arise when the solid material is being put into the generator. An eye-wash bottle and a neutralizing agent, such as vinegar, should be kept at hand in case of an accident.

Some of the chemical methods operate at high pressure, with a consequential greater risk of an accident. High-pressure generators should be tested every two years to a pressure at least twice that of the working pressure. They should be provided with a safety device to relieve excess pressure. This is usually a bursting disc, and it is very important that the operational instructions should be strictly followed with regard to the material, size and form of the discs, and the frequency of their replacement. Even if a safety device is efficient, its operation is very liable to be accompanied by the ejection of hot solution. High-pressure generators must be carefully cleaned out before recharging since remains of the previous charge may considerably reduce the available volume of the generator and, thus, increase the working pressure beyond the design limit.

Unfortunately, calcium hydride and magnesium-iron, which have the advantage of avoiding the use of caustic soda, are expensive to produce and are, therefore, likely to be acceptable only for special purposes. Since these two materials produce hydrogen from water, it is essential that they be stored in containers which are completely damp-proof. In the processes using catalysts, care must be taken to avoid catalyst contamination.

All systems produce gas at sufficient pressure for filling balloons. However, the production rates of some systems (electrolysis in particular) are too low, and the gas must be produced and stored before it is needed, either in compressed form or in a gasholder.

The processes using the electrolysis of water or the catalytic cracking of methanol are attractive because of their relative safety and moderate recurrent cost, and because of the non-corrosive nature of the materials used. These two processes, as well as the liquid ammonia process, require electric power. The equipment is rather complex and must be carefully maintained and subjected to detailed daily check procedures to ensure that the safety control systems are effective. Water for electrolysis must have low mineral content.

8.6 USE OF HYDROGEN AND SAFETY PRECAUTIONS

8.6.1 General

Hydrogen can easily be ignited by a small spark and burns with a nearly invisible flame. It can burn when mixed with air over a wide range of concentrations, from 4% to 74% by volume (NFPA, 1999), and can explode in concentrations between 18% and 59%. In either case, a nearby operator can receive severe burns over the entire surface of any exposed skin, and an explosion can throw the operator against a wall or the ground, causing serious injury.

It is possible to eliminate the risk of an accident by using very carefully designed procedures and equipment, provided that they are diligently observed and maintained (Gremia, 1977; Ludtke and Saraduke, 1992; NASA, 1968). The provision of adequate safety features for the buildings in which hydrogen is generated and stored, or for the areas in which balloons are filled or released, does not always receive adequate attention (see the following section). In particular, there must be comprehensive training and continual meticulous monitoring and inspection to ensure that operators follow the procedures.

The advantages of automatic balloon launchers (see 8.3.4) are that they can be made practically foolproof and operator injuries can be prevented by completely separating the operator from the hydrogen.

An essential starting point for the consideration of safety precautions is to follow the various national standards and codes of practice concerned with the risks presented by explosive

atmospheres in general. Additional information on the precautions that should be followed will be found in publications dealing with explosion hazards, such as in hospitals and other industrial situations where similar problems exist. The operator should never be in a closed room with an inflated balloon. Other advice on safety matters can be found throughout the chapter.

8.6.2 Building design

Provisions should be made to avoid the accumulation of free hydrogen and of static charges as well as the occurrence of sparks in any room where hydrogen is generated, stored or used. The accumulation of hydrogen must be avoided even when a balloon bursts within the shelter during the course of inflation (WMO, 1982).

Safety provisions must be part of the structural design of hydrogen buildings (NFPA, 1999; SAA, 1985). Climatic conditions and national standards and codes are constraints within which it is possible to adopt many designs and materials suitable for safe hydrogen buildings. Codes are advisory and are used as a basis of good practice. Standards are published in the form of specifications for materials, products and safe practices. They should deal with topics such as flame-proof electric-light fittings, electrical apparatus in explosive atmospheres, the ventilation of rooms with explosive atmospheres, and the use of plastic windows, bursting discs, and so on (WMO, 1982).

Both codes and standards should contain information that is helpful and relevant to the design of hydrogen buildings. Furthermore, it should be consistent with recommended national practice. Guidance should be sought from national standards authorities when hydrogen buildings are designed or when the safety of existing buildings is reviewed, in particular for aspects such as the following:

- (a) The preferred location for hydrogen systems;
- (b) The fire resistance of proposed materials, as related to the fire-resistance ratings that must be respected;
- (c) Ventilation requirements, including a roof of light construction to ensure that hydrogen and products of an explosion are vented from the highest point of the building;
- (d) Suitable electrical equipment and wiring;
- (e) Fire protection (extinguishers and alarms);
- (f) Provision for the operator to control the inflation of the balloon from outside the filling room.

Measures should be taken to minimize the possibility of sparks being produced in rooms where hydrogen is handled. Thus, any electrical system (switches, fittings, wiring) should be kept outside these rooms; otherwise, special spark-proof switches, pressurized to prevent the ingress of hydrogen, and similarly suitable wiring, should be provided. It is also advisable to illuminate the rooms using exterior lights which shine in through windows. For the same reasons, any tools used should not produce sparks. The observer's shoes should not be capable of emitting sparks, and adequate lightning protection should be provided.

If sprinkler systems are used in any part of the building, consideration should be given to the possible hazard of hydrogen escaping after the fire has been extinguished. Hydrogen detection systems exist and may be used, for instance, to switch off power to the hydrogen generator at 20% of the lower explosive limit and should activate an alarm, and then activate another alarm at 40% of the lower explosive limit.

A hazard zone should be designated around the generator, storage and balloon area into which entry is permitted only when protective clothing is worn (see 8.6.4).

Balloon launchers (see 8.3.4) typically avoid the need for a special balloon-filling room, and greatly simplify the design of hydrogen facilities.

8.6.3 Static charges

The hazards of balloon inflation and balloon release can be considerably reduced by preventing static charges in the balloon-filling room, on the observer's clothing, and on the balloon itself. Loeb (1958) provides information on the static electrification process. Static charge control is effected by good earthing provisions for hydrogen equipment and filling-room fittings. Static discharge grips for observers can remove charges generated on clothing (WMO, 1982).

Charges on balloons are more difficult to deal with. Balloon fabrics, especially pure latex, are very good insulators. Static charges are generated when two insulating materials in contact with each other are separated. A single brief contact with the observer's clothing or hair can generate a 20 kV charge, which is more than sufficient to ignite a mixture of air and hydrogen if it is discharged through an efficient spark. Charges on a balloon may take many hours to dissipate through the fabric to earth or naturally into the surrounding air. Also, it has been established that, when a balloon bursts, the separation of the film along a split in the fabric can generate sparks energetic enough to cause ignition.

Electrostatic charges can be prevented or removed by spraying water onto the balloon during inflation, by dipping balloons into antistatic solution (with or without drying them off before use), by using balloons with an antistatic additive in the latex, or by blowing ionized air over the balloon. Merely earthing the neck of the balloon is not sufficient.

The maximum electrostatic potential that can be generated or held on a balloon surface decreases with increasing humidity, but the magnitude of the effect is not well established. Some tests carried out on inflated 20 g balloons indicated that spark energies sufficient to ignite hydrogen-oxygen mixtures are unlikely to be reached when the relative humidity of the air is greater than 60%. Other studies have suggested relative humidities from 50% to 76% as safe limits, yet others indicate that energetic sparks may occur at even higher relative humidity. It may be said that static discharge is unlikely when the relative humidity exceeds 70%, but this should not be relied upon (see Cleves et al., 1971).

It is strongly recommended that fine water sprays be used on the balloon because the wetting and earthing of the balloon will remove most of the static charges from the wetted portions. The sprays should be designed to wet as large an area of the balloon as possible and to cause continuous streams of water to run from the balloon to the floor. If the doors are kept shut, the relative humidity inside the filling room can rise to 75% or higher, thus reducing the probability of sparks energetic enough to cause ignition. Balloon release should proceed promptly once the sprays are turned off and the filling-shed doors opened.

Other measures for reducing the build-up of static charge include the following (WMO, 1982):

- (a) The building should be provided with a complete earthing (grounding) system, with all fittings, hydrogen equipment and the lightning conductor separately connected to a single earth, which itself must comply with national specifications for earth electrodes. Provision should be made to drain electrical charges from the floor;
- (b) Static discharge points should be provided for the observers;
- (c) The windows should be regularly coated with an antistatic solution;
- (d) Operators should be encouraged not to wear synthetic clothing or insulating shoes. It is good practice to provide operators with partially conducting footwear;
- (e) Any contact between the observer and the balloon should be minimized; this can be facilitated by locating the balloon filler at a height of 1 m or more above the floor.

8.6.4 **Protective clothing and first-aid facilities**

Proper protective clothing should be worn whenever hydrogen is being used, during all parts of the operations, including generation procedures, when handling cylinders, and during balloon inflation and release. The clothing should include a light-weight flame-proof coat with a hood made of non-synthetic, antistatic material and a covering for the lower face, glasses or goggles, cotton gloves, and any locally recommended anti-flash clothing (see Hoschke et al., 1979).

First-aid facilities appropriate to the installation should be provided. These should include initial remedies for flash burns and broken limbs. When chemicals are used, suitable neutralizing solutions should be on hand, for example, citric acid for caustic soda burns. An eye-wash apparatus ready for instant use should be available (WMO, 1982).

REFERENCES AND FURTHER READING

- Atmospheric Environment Service (Canada), 1978: *The Use of Hydrogen for Meteorological Purposes in the Canadian Atmospheric Environment Service*, Toronto.
- Cleves, A.C., J.F. Sumner and R.M.H. Wyatt, 1971: The Effect of Temperature and Relative Humidity on the Accumulation of Electrostatic Charges on Fabrics and Primary Explosives. *Proceedings of the Third Conference on Static Electrification*, (London).
- Gremia, J.O., 1977: *A Safety Study of Hydrogen Balloon Inflation Operations and Facilities of the National Weather Service*. Trident Engineering Associates, Annapolis, Maryland.
- Hoschke, B.N. et al., 1979: *Report to the Bureau of Meteorology on Protection Against the Burn Hazard from Exploding Hydrogen-filled Meteorological Balloons*. CSIRO Division of Textile Physics and the Department of Housing and Construction, Australia.
- Loeb, L.B., 1958: *Static Electrification*, Springer-Verlag, Berlin.
- Ludtke, P. and G. Saraduke, 1992: *Hydrogen Gas Safety Study Conducted at the National Weather Service Forecast Office*. Norman, Oklahoma.
- National Aeronautics and Space Administration, 1968: *Hydrogen Safety Manual*. NASA Technical Memorandum TM-X-52454, NASA Lewis Research Center, United States.
- National Fire Protection Association, 1999: *NFPA 50A: Standard for Gaseous Hydrogen Systems at Consumer Sites*. National Fire Protection Association, Quincy, Maryland.
- , 2002: *NFPA 68: Guide for Venting of Deflagrations*. National Fire Protection Association, Batterymarch Park, Quincy, Maryland.
- , 2005: *NFPA 70, National Electrical Code*. National Fire Protection Association, Quincy, Maryland.
- , 2006: *NFPA 220, Standard on Types of Building Construction*. National Fire Protection Association, Quincy, Maryland.
- Rosen, B., V.H. Dayan and R.L. Proffit, 1970: *Hydrogen Leak and Fire Detection: A Survey*. NASA SP-5092.
- Standards Association of Australia, 1970: AS C99: *Electrical equipment for explosive atmospheres – Flameproof electric lightning fittings*.
- , 1980: AS 1829: *Intrinsically safe electrical apparatus for explosive atmospheres*.
- , 1985: AS 1482: *Electrical equipment for explosive atmospheres – Protection by ventilation – Type of protection V*.
- , 1995: ASNZS 1020: *The control of undesirable static electricity*.
- , 2004: AS 1358: *Bursting discs and bursting disc devices – Application selection and installation*.
- World Meteorological Organization, 1982: *Meteorological Balloons: The Use of Hydrogen for Inflation of Meteorological Balloons*. Instruments and Observing Methods Report No. 13. Geneva.
-

CHAPTER 9. URBAN OBSERVATIONS

9.1 GENERAL

There is a growing need for meteorological observations conducted in urban areas. Urban populations continue to expand, and Meteorological Services are increasingly required to supply meteorological data in support of detailed forecasts for citizens, building and urban design, energy conservation, transportation and communications, air quality and health, storm water and wind engineering, and insurance and emergency measures. At the same time, Meteorological Services have difficulty in making urban observations that are not severely compromised. This is because most developed sites make it impossible to conform to the standard guidelines for site selection and instrument exposure given in Volume I of the present Guide owing to obstruction of air-flow and radiation exchange by buildings and trees, unnatural surface cover and waste heat and water vapour from human activities.

This chapter provides information to enable the selection of sites, the installation of a meteorological station and the interpretation of data from an urban area. In particular, it deals with the case of what is commonly called a “standard” climate station. Despite the complexity and inhomogeneity of urban environments, useful and repeatable observations can be obtained. Every site presents a unique challenge. To ensure that meaningful observations are obtained requires careful attention to certain principles and concepts that are virtually unique to urban areas. It also requires the person establishing and running the station to apply those principles and concepts in an intelligent and flexible way that is sensitive to the realities of the specific environment involved. Rigid “rules” have little utility. The need for flexibility runs slightly counter to the general notion of standardization that is promoted as WMO observing practice. In urban areas, it is sometimes necessary to accept exposure over non-standard surfaces at non-standard heights, to split observations between two or more locations, or to be closer than usual to buildings or waste heat exhausts.

The units of measurement and the instruments used in urban areas are the same as those for other environments. Therefore, only those aspects that are unique to urban areas, or that are made difficult to handle because of the nature of cities, such as the choice of site, instrument exposure and the documentation of metadata, are covered in this chapter.

The timing and frequency of observations and the coding of reports should follow appropriate standards (WMO, 2006, 2011a, 2011b, 2015a, 2015b).

With regard to automated stations and the requirements for message coding and transmission, quality control, maintenance (noting any special demands of the urban environment) and calibration, the recommendations of Chapter 1 of the present volume should be followed.

9.1.1 Definitions and concepts

9.1.1.1 *Station rationale*

The clarity of the reason for establishing an urban station is essential to its success. Two of the most usual reasons are the wish to represent the meteorological environment at a place for general climatological purposes and the wish to provide data in support of the needs of a particular user. In both cases, the spatial and temporal scales of interest must be defined, and, as outlined below, the siting of the station and the exposure of the instruments in each case may have to be very different.

9.1.1.2 **Horizontal scales**

There is no more important an input to the success of an urban station than an appreciation of the concept of scale. There are three scales of interest (Oke, 1984; Figure 9.1):

- (a) **Microscale:** Every surface and object has its own microclimate on it and in its immediate vicinity. Surface and air temperatures may vary by several degrees in very short distances, even millimetres, and air-flow can be greatly perturbed by even small objects. Typical scales of urban microclimates relate to the dimensions of individual buildings, trees, roads, streets, courtyards, gardens, and so forth. Typical scales extend from less than 1 m to hundreds of metres. The formulation of the guidelines in Volume I of the present Guide specifically aims to avoid microclimatic effects. The climate station recommendations are designed to standardize all sites, as far as practical. This explains the use of a standard height of measurement, a single surface cover, minimum distances to obstacles and little horizon obstruction. The aim is to achieve climate observations that are free of extraneous microclimate signals and hence characterize local climates. With even more stringent standards, first order stations may be able to represent conditions at synoptic space and timescales. The data may be used to assess climate trends at even larger scales. Unless the objectives are very specialized, urban stations should also avoid microclimate influences; however, this is hard to achieve;
- (b) **Local scale:** This is the scale that standard climate stations are designed to monitor. It includes landscape features such as topography, but excludes microscale effects. In urban areas this translates to mean the climate of neighbourhoods with similar types of urban development (surface cover, size and spacing of buildings, activity). The signal is the integration of a characteristic mix of microclimatic effects arising from the source area in the vicinity of the site. The source area is the portion of the surface upstream that contributes the main properties of the flux or meteorological concentration being measured (Schmid, 2002). Typical scales are one to several kilometres;
- (c) **Mesoscale:** A city influences weather and climate at the scale of the whole city, typically tens of kilometres in extent. A single station is not able to represent this scale.

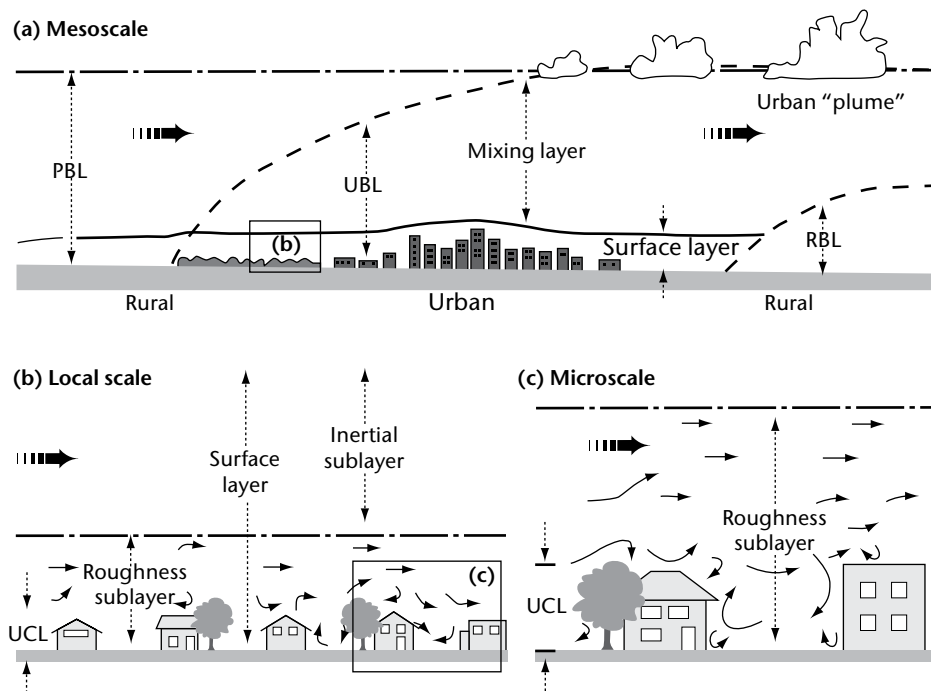


Figure 9.1. Schematic of climatic scales and vertical layers found in urban areas: planetary boundary layer (PBL), urban boundary layer (UBL), urban canopy layer (UCL), rural boundary layer (RBL) (modified from Oke, 1997).

9.1.1.3 **Vertical scales**

An essential difference between the climate of urban areas and that of rural or airport locations is that in cities the vertical exchanges of momentum, heat and moisture do not occur at a (nearly) plane surface, but in a layer of significant thickness, called the urban canopy layer (UCL) (Figure 9.1). The height of the UCL is approximately equivalent to that of the mean height of the main roughness elements (buildings and trees), z_H (see Figure 9.4 for parameter definitions). The microclimatic effects of individual surfaces and obstacles persist for a short distance away from their source and are then mixed and muted by the action of turbulent eddies. The distance required before the effect is obliterated depends on the magnitude of the effect, wind speed and stability (namely, stable, neutral or unstable). This blending occurs both in the horizontal and the vertical. As noted, horizontal effects may persist up to a few hundred metres. In the vertical, the effects of individual features are discernible in the roughness sublayer (RSL), which extends from ground level to the blending height z_r , where the blending action is complete. Rule-of-thumb estimates and field measurements indicate that z_r can be as low as $1.5 z_H$ at densely built (closely spaced) and homogeneous sites, but greater than $4 z_H$ in low density areas (Grimmond and Oke, 1999; Rotach, 1999; Christen, 2003). An instrument placed below z_r may register microclimate anomalies, but, above that, it “sees” a blended, spatially averaged signal that is representative of the local scale.

There is another height restriction to consider. This arises because each local scale surface type generates an internal boundary layer, in which the flow structure and thermodynamic properties are adapted to that surface type. The height of the layer grows with increasing fetch (the distance upwind to the edge where the transition to a distinctly different surface type occurs). The rate at which the internal boundary layer grows with fetch distance depends on the roughness and stability. In rural conditions, the height to fetch ratios might vary from as small as 1:10 in unstable conditions to as large as 1:500 in stable cases, and the ratio decreases as the roughness increases (Garratt, 1992; Wieringa, 1993). Urban areas tend towards neutral stability owing to the enhanced thermal and mechanical turbulence associated with the heat island and their large roughness. Therefore, a height to fetch ratio of about 1:100 is considered typical. The internal boundary layer height is taken above the displacement height z_d , which is the reference level for flow above the blending height. (For an explanation of z_d , see Figure 9.4 and Note b in Table 9.2.)

For example, take a hypothetical densely built district with z_H of 10 m. This means that z_r is at least 15 m. If this height is chosen to be the measurement level, the fetch requirement over similar urban terrain is likely to be at least 0.8 km, since $\text{fetch} = 100 (z_r - z_d)$, and z_d will be about 7 m. This can be a significant site restriction because the implication is that, if the urban terrain is not similar out to at least this distance around the station site, observations will not be representative of the local surface type. At less densely developed sites, where heat island and roughness effects are less, the fetch requirements are likely to be greater.

At heights above the blending height, but within the local internal boundary layer, measurements are within an inertial sublayer (Figure 9.1), where standard boundary layer theory applies. Such theory governs the form of the mean vertical profiles of meteorological variables (including air temperature, humidity and wind speed) and the behaviour of turbulent fluxes, spectra and statistics. This provides a basis for:

- (a) The calculation of the source area (or “footprint”, see below) from which the turbulent flux or the concentration of a meteorological variable originates; hence, this defines the distance upstream for the minimum acceptable fetch;
- (b) The extrapolation of a given flux or property through the inertial layer and also downwards into the RSL (and, although it is less reliable, into the UCL). In the inertial layer, fluxes are constant with height and the mean value of meteorological properties are invariant horizontally. Hence, observations of fluxes and standard variables possess significant utility and are able to characterize the underlying local scale environment. Extrapolation into the RSL is less prescribed.

9.1.1.4 Source areas ("footprints")

A sensor placed above a surface "sees" only a portion of its surroundings. This is called the "source area" of the instrument which depends on its height and the characteristics of the process transporting the surface property to the sensor. For upwelling radiation signals (short- and long-wave radiation and surface temperature viewed by an infrared thermometer) the field of view of the instrument and the geometry of the underlying surface set what is seen. By analogy, sensors such as thermometers, hygrometers, gas analysers and anemometers "see" properties such as temperature, humidity, atmospheric gases and wind speed and direction which are carried from the surface to the sensor by turbulent transport. A conceptual illustration of these source areas is given in Figure 9.2.

The source area of a down-facing radiometer with its sensing element parallel to the ground is a circular patch with the instrument at its centre (Figure 9.2). The radius (r) of the circular source area contributing to the radiometer signal at height (z_1) is given in Schmid et al. (1991):

$$r = z_1 \left(\frac{1}{F} - 1 \right)^{-0.5} \quad (9.1)$$

where F is the view factor, namely the proportion of the measured flux at the sensor for which that area is responsible. Depending on its field of view, a radiometer may see only a limited circle, or it may extend to the horizon. In the latter case, the instrument usually has a cosine response, so that towards the horizon it becomes increasingly difficult to define the actual source area seen. Hence, the use of the view factor which defines the area contributing a set proportion (often selected as 50%, 90%, 95%, 99% or 99.5%) of the instrument's signal.

The source area of a sensor that derives its signal via turbulent transport is not symmetrically distributed around the sensor location. It is elliptical in shape and is aligned in the upwind direction from the tower (Figure 9.2). If there is a wind, the effect of the surface area at the base of the mast is effectively zero, because turbulence cannot transport the influence up to the sensor level. At some distance in the upwind direction the source starts to affect the sensor; this effect rises to a peak, thereafter decaying at greater distances (for the shape in both the x and y directions see Kljun et al., 2002; Schmid, 2002). The distance upwind to the first surface

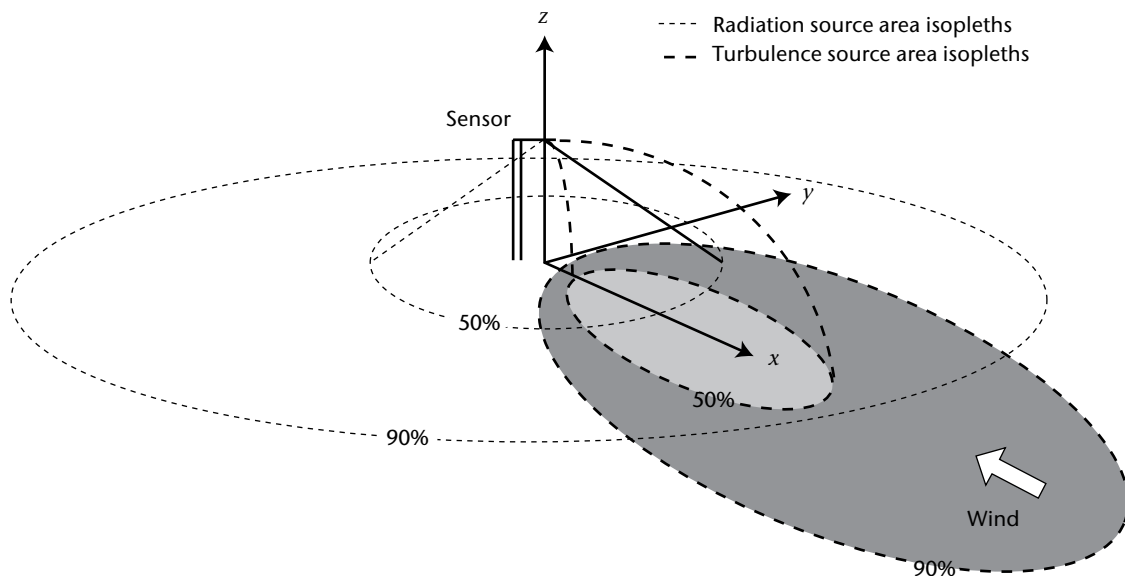


Figure 9.2. Conceptual representation of source areas contributing to sensors for radiation and turbulent fluxes of concentrations. If the sensor is a radiometer 50% or 90% of the flux originates from the area inside the perspective circle. If the sensor is responding to a property of turbulent transport, 50% or 90% of the signal comes from the area inside the respective ellipses. These are dynamic in the sense that they are oriented into the wind and hence move with wind direction and stability.

area contributing to the signal, to the point of peak influence, to the furthest upwind surface influencing the measurement, and the area of the so-called “footprint” vary considerably over time. They depend on the height of measurement (larger at greater heights), surface roughness, atmospheric stability (increasing from unstable to stable) and whether a turbulent flux or a meteorological concentration is being measured (larger for the concentration) (Kljun et al., 2002). Methods to calculate the dimensions of flux and concentration “footprints” are available (Schmid, 2002; Kljun et al., 2004).

Although the situation illustrated in Figure 9.2 is general, it applies best to instruments placed in the inertial sublayer, well above the complications of the RSL and the complex geometry of the three-dimensional urban surface. Within the UCL, the way in which the effects of radiation and turbulent source areas decay with distance has not yet been reliably evaluated. It can be surmised that they depend on the same properties and resemble the overall forms of those in Figure 9.2. However, obvious complications arise due to the complex radiation geometry, and the blockage and channelling of flow, which are characteristic of the UCL. Undoubtedly, the immediate environment of the station is by far the most critical and the extent of the source area of convective effects grows with stability and the height of the sensor. The distance influencing screen-level (~1.5 m) sensors may be a few tens of metres in neutral conditions, less when they are unstable and perhaps more than 100 m when they are stable. At a height of 3 m, the equivalent distances probably extend up to about 300 m in the stable case. The circle of influence on a screen-level temperature or humidity sensor is thought to have a radius of about 0.5 km typically, but this is likely to depend upon the building density.

9.1.1.5 **Measurement approaches**

It follows from the preceding discussion that, if the objective of an instrumented urban site is to monitor the local-scale climate near the surface, there are two viable approaches as follows:

- (a) Locate the site in the UCL at a location surrounded by average or “typical” conditions for the urban terrain, and place the sensors at heights similar to those used at non-urban sites. This assumes that the mixing induced by flow around obstacles is sufficient to blend properties to form a UCL average at the local scale;
- (b) Mount the sensors on a tall tower above the RSL and obtain blended values that can be extrapolated down into the UCL.

In general, approach (a) works best for air temperature and humidity, and approach (b) for wind speed and direction and precipitation. For radiation, the only significant requirement is for an unobstructed horizon. Urban stations, therefore, often consist of instruments deployed both below and above roof level; this requires that site assessment and description include the scales relevant to both contexts.

9.1.1.6 **Urban site description**

The magnitude of each urban scale does not agree precisely with those commonly given in textbooks. The scales are conferred by the dimensions of the morphometric features that make up an urban landscape. This places emphasis on the need to adequately describe properties of urban areas which affect the atmosphere. The most important basic features are the urban structure (dimensions of the buildings and the spaces between them, the street widths and street spacing), the urban cover (built-up, paved and vegetated areas, bare soil, water), the urban fabric (construction and natural materials) and the urban metabolism (heat, water and pollutants due to human activity). Hence, the characterization of the sites of urban climate stations must take account of these descriptors, use them in selecting potential sites, and incorporate them in metadata that accurately describe the setting of the station.

These four basic features of cities tend to cluster to form characteristic urban classes. For example, most central areas of cities have relatively tall buildings that are densely packed together, so the ground is largely covered with buildings or paved surfaces made of durable

materials such as stone, concrete, brick and asphalt and where there are large releases from furnaces, air conditioners, chimneys and vehicles. Near the other end of the spectrum there are districts with low density housing of one- or two-storey buildings of relatively light construction and considerable garden or vegetated areas with low heat releases, but perhaps large irrigation inputs.

No universally accepted scheme of urban classification for climatic purposes exists. A good approach to the built components is that of Ellefsen (1991) who developed a set of urban terrain zone (UTZ) types. He initially differentiates according to 3 types of building contiguity (attached (row), detached but close-set, detached and open-set). These are further divided into a total of 17 sub-types by function, location in the city, and building height, construction and age. Application of the scheme requires only aerial photography, which is generally available, and the scheme has been applied in several cities around the world and seems to possess generality.

Ellefsen's scheme can be used to describe urban structure for roughness, airflow, radiation access and screening. It can be argued that the scheme indirectly includes aspects of urban cover, fabric and metabolism because a given structure carries with it the type of cover, materials and degree of human activity. Ellefsen's scheme is less useful, however, when built features are scarce and there are large areas of vegetation (urban forest, low plant cover, grassland, scrub, crops), bare ground (soil or rock) and water (lakes, swamps, rivers). A simpler scheme of urban climate zones (UCZs) is illustrated in Table 9.1. It incorporates groups of Ellefsen's zones, plus a measure of the structure, z_H/W (see Table 9.1, Note c) shown to be closely related to both flow, solar shading and the heat island, and also a measure of the surface cover (% built) that is related to the degree of surface permeability.

The importance of UCZs is not their absolute accuracy to describe the site, but their ability to classify areas of a settlement into districts, which are similar in their capacity to modify the local climate, and to identify potential transitions to different UCZs. Such a classification is crucial when beginning to set up an urban station, so that the spatial homogeneity criteria are met approximately for a station in the UCL or above the RSL. In what follows, it is assumed that the morphometry of the urban area, or a portion of it, has been assessed using detailed maps, and/or aerial photographs, satellite imagery (visible and/or thermal), planning documents or at least a visual survey conducted from a vehicle and/or on foot. Although land-use maps can be helpful, it should be appreciated that they depict the *function* and not necessarily the *physical form* of the settlement. The task of urban description should result in a map with areas of UCZs delineated.

Herein, the UCZs as illustrated in Table 9.1 are used. The categories may have to be adapted to accommodate special urban forms characteristic of some ancient cities or of unplanned urban development found in some less-developed countries. For example, many towns and cities in Africa and Asia do not have as large a fraction of the surface covered by impervious materials and roads may not be paved.

9.2 CHOOSING A LOCATION AND SITE FOR AN URBAN STATION

9.2.1 Location

First, it is necessary to establish clearly the purpose of the station. If there is to be only one station inside the urban area it must be decided if the aim is to monitor the greatest impact of the city, or of a more representative or typical district, or if it is to characterize a particular site (where there may be perceived to be climate problems or where future development is planned). Areas where there is the highest probability of finding maximum effects can be judged initially by reference to the ranked list of UCZ types in Table 9.1. Similarly, the likelihood that a station will be typical can be assessed using the ideas behind Table 9.1 and choosing extensive areas of similar urban development for closer investigation.

Table 9.1. Simplified classification of distinct urban forms arranged in approximate decreasing order of their ability to have an impact on local climate (Oke, 2004 unpublished)

<i>Urban climate zone^a</i>	<i>Image</i>	<i>Roughness class^b</i>	<i>Aspect ratio^c</i>	<i>% built (impermeable)^d</i>
1. Intensely developed urban with detached close-set high-rise buildings with cladding, e.g. downtown towers		8	> 2	> 90
2. Intensely high density urban with 2–5 storey, attached or very-close set buildings often of bricks or stone, e.g. old city core		7	1.0–2.5	> 85
3. Highly developed, medium density urban with row or detached but close-set houses, stores and apartments, e.g. urban housing		7	0.5–1.5	70–85
4. Highly developed, low or medium density urban with large low buildings and paved parking, e.g. shopping malls, warehouses		5	0.05–0.2	70–95
5. Medium development, low density suburban with 1 or 2 storey houses, e.g. suburban houses		6	0.2–0.6, up to > 1 with trees	35–65
6. Mixed use with large buildings in open landscape, e.g. institutions such as hospitals, universities, airports		5	0.1–0.5, depends on trees	< 40
7. Semi-rural development, scattered houses in natural or agricultural areas, e.g. farms, estates		4	> 0.05, depends on trees	< 10

Buildings; Vegetation
 Impervious ground; Pervious ground

Notes:

- ^a A simplified set of classes that includes aspects of the schemes of Auer (1978) and Ellefsen (1991) plus physical measures relating to wind, and thermal and moisture control (columns on the right). Approximate correspondence between UCZ and Ellefsen's urban terrain zones is: 1 (Dc1, Dc8), 2 (A1–A4, Dc2), 3 (A5, Dc3–5, Do2), 4 (Do1, Do4, Do5), 5 (Do3), 6 (Do6), 7 (none).
- ^b Effective terrain roughness according to the Davenport classification (Davenport et al., 2000); see Table 9.2.
- ^c Aspect ratio = z_r/W is the average height of the main roughness elements (buildings, trees) divided by their average spacing; in the city centre this is the street canyon height/width. This measurement is known to be related to flow regime types (Oke, 1987) and thermal controls (solar shading and longwave screening) (Oke, 1981). Tall trees increase this measure significantly.
- ^d Average proportion of ground plan covered by built features (buildings, roads and paved and other impervious areas); the rest of the area is occupied by pervious cover (green space, water and other natural surfaces). Permeability affects the moisture status of the ground and hence humidification and evaporative cooling potential.

The search can be usefully refined in the case of air temperature and humidity by conducting spatial surveys, wherein the sensor is carried on foot, or mounted on a bicycle or a car and taken through areas of interest. After several repetitions, cross-sections or isoline maps may be drawn (see Figure 9.3), revealing where areas of thermal or moisture anomaly or interest lie. Usually, the best time to do this is a few hours after sunset or before sunrise on nights with relatively calm air-flow and cloudless skies. This maximizes the potential for the differentiation of microclimate and local climate differences. It is not advisable to conduct such surveys close to sunrise or sunset because weather variables change so rapidly at these times that meaningful spatial comparisons are difficult.

If the station is to be part of a network to characterize spatial features of the urban climate, a broader view is needed. This consideration should be informed by thinking about the typical spatial form of urban climate distributions. For example, the isolines of urban heat and moisture "islands" indeed look like the contours of their topographic namesakes (Figure 9.3). They have relatively sharp "cliffs", often a "plateau" over much of the urban area interspersed with localized "mounds" and "basins" of warmth/coolness and moistness/dryness. These features are co-located with patches of greater or lesser development such as clusters of apartments, shops, factories or parks, open areas or water. Therefore, a decision must be made: is the aim to make a representative sample of the UCZ diversity, or is it to faithfully reflect the spatial structure?

In most cases the latter is too ambitious with a fixed-station network in the UCL. This is because it will require many stations to depict the gradients near the periphery, the plateau region,

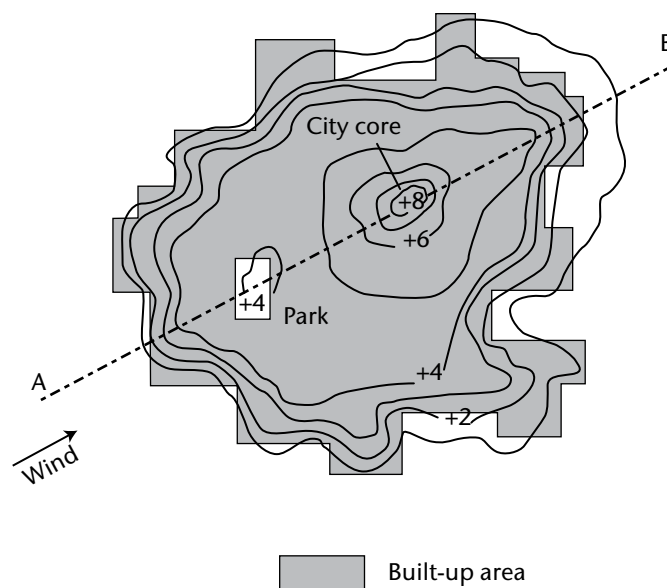


Figure 9.3. Typical spatial pattern of isotherms in a large city at night with calm, clear weather illustrating the heat island effect (after Oke, 1982)

and the highs and lows of the nodes of weaker and stronger than average urban development. If measurements are to be taken from a tower, with sensors above the RSL, the blending action produces more muted spatial patterns and the question of distance of fetch to the nearest border between UCZs, and the urban-rural fringe, becomes relevant. Whereas a distance to a change in UCZ of 0.5 to 1 km may be acceptable inside the UCL, for a tower-mounted sensor the requirement is likely to be more like a few kilometres of fetch.

Since the aim is to monitor local climate attributable to an urban area, it is necessary to avoid extraneous microclimatic influences or other local or mesoscale climatic phenomena that will complicate the urban record. Therefore, unless there is specific interest in topographically generated climate patterns, such as the effects of cold air drainage down valleys and slopes into the urban area, or the speed-up or sheltering of winds by hills and escarpments, or fog in river valleys or adjacent to water bodies, or geographically locked cloud patterns, and so on, it is sensible to avoid locations subject to such local and mesoscale effects. On the other hand, if a benefit or hazard is derived from such events, it may be relevant to design the network specifically to sample its effects on the urban climate, such as the amelioration of an overly hot city by sea or lake breezes.

9.2.2 Siting

Once a choice of UCZ type and its general location inside the urban area is made, the next step is to inspect the map, imagery and photographic evidence to narrow down candidate locations within a UCZ. Areas of reasonably homogeneous urban development without large patches of anomalous structure, cover or material are sought. The precise definition of “reasonably” however is not possible; almost every real urban district has its own idiosyncrasies that reduce its homogeneity at some scale. Although a complete list is therefore not possible, the following are examples of what to avoid: unusually wet patches in an otherwise dry area, individual buildings that jut up by more than half the average building height, a large paved car park in an area of irrigated gardens, a large, concentrated heat source like a heating plant or a tunnel exhaust vent. Proximity to transition zones between different UCZ types should be avoided, as should sites where there are plans for or the likelihood of major urban redevelopment. The level of concern about anomalous features decreases with distance away from the site itself, as discussed in relation to source areas.

In practice, for each candidate site a “footprint” should be estimated for radiation (for example, equation 9.1) and for turbulent properties. Then, key surface properties such as the mean height and density of the obstacles and characteristics of the surface cover and materials should be documented within these footprints. Their homogeneity should then be judged, either visually or using statistical methods. Once target areas of acceptable homogeneity for a screen-level or high-level (above-RSL) station are selected, it is helpful to identify potential “friendly” site owners who could host it. If a government agency is seeking a site, it may already own land in the area which is used for other purposes or have good relations with other agencies or businesses (offices, work yards, spare land, rights of way) including schools, universities, utility facilities (electricity, telephone, pipelines) and transport arteries (roads, railways). These are good sites, because access may be permitted and also because they also often have security against vandalism and may have electrical power connections.

Building roofs have often been used as the site for meteorological observations. This may often have been based on the mistaken belief that at this elevation the instrument shelter is free from the complications of the UCL. In fact, rooftops have their own very distinctly anomalous microclimates that lead to erroneous results. Airflow over a building creates strong perturbations in speed, direction and gustiness which are quite unlike the flow at the same elevation away from the building or near the ground (Figure 9.5). Flat-topped buildings may actually create flows on their roofs that are counter to the main external flow, and speeds vary from extreme jetting to a near calm. Roofs are also constructed of materials that are thermally rather extreme. In light winds and cloudless skies they can become very hot by day and cold by night. Hence, there is often a sharp gradient of air temperature near the roof. Furthermore, roofs are designed to be waterproof and to shed water rapidly. This, together with their openness to solar radiation and

the wind, makes them anomalously dry. In general, therefore, roofs are very poor locations for air temperature, humidity, wind and precipitation observations, unless the instruments are placed on very tall masts. They can, however, be good for observing incoming radiation components.

Once the site has been chosen, it is essential that the details of the site characteristics (metadata) be fully documented (see 9.4).

9.3 **INSTRUMENT EXPOSURE**

9.3.1 **Modifications to standard practice**

In many respects, the generally accepted standards for the exposure of meteorological instruments set out in Volume I of the present Guide apply to urban sites. However, there will be many occasions when it is impossible or makes no sense to conform. This section recommends some principles that will assist in such circumstances; however, all eventualities cannot be anticipated. The recommendations here remain in agreement with general objectives set out in Volume I, Chapter 1.

Many urban stations have been placed over short grass in open locations (parks, playing fields) and as a result they are actually monitoring modified rural-type conditions, not representative urban ones. This leads to the curious finding that some rural-urban pairs of stations show no urban effect on temperature (Peterson, 2003).

The guiding principle for the exposure of sensors in the UCL should be to locate them in such a manner that they monitor conditions that are representative of the environment of the selected UCZ. In cities and towns it is inappropriate to use sites similar to those which are standard in open rural areas. Instead, it is recommended that urban stations should be sited over surfaces that, within a microscale radius, are representative of the local scale urban environment. The % built category (Table 9.1) is a crude guide to the recommended underlying surface.

The requirement that most obviously cannot be met at many urban sites is the distance from obstacles — the site should be located well away from trees, buildings, walls or other obstructions (Volume I, Chapter 1). Rather, it is recommended that the urban station be centred in an open space where the surrounding aspect ratio (z_H/W) is approximately representative of the locality.

When installing instruments at urban sites it is especially important to use shielded cables because of the ubiquity of power lines and other sources of electrical noise at such locations.

9.3.2 **Temperature**

9.3.2.1 **Air temperature**

The sensors in general use to measure air temperature (including their accuracy and response characteristics) are appropriate in urban areas. Careful attention to radiation shielding and ventilation is especially recommended. In the UCL, a sensor assembly might be relatively close to warm surfaces, such as a sunlit wall, a road or a vehicle with a hot engine, or it might receive reflected heat from glassed surfaces. Therefore, the shields used should block radiation effectively. Similarly, because an assembly placed in the lower UCL might be too well sheltered, forced ventilation of the sensor is recommended. If a network includes a mixture of sensor assemblies with/without shields and ventilation, this might contribute to inter-site differences. Practices should therefore be uniform.

The surface over which air temperature is measured and the exposure of the sensor assembly should follow the recommendations given in the previous section, namely, the surface should be typical of the UCZ and the thermometer screen or shield should be centred in a space with approximately average z_H/W . In very densely built-up UCZ this might mean that it is located

only 5 to 10 m from buildings that are 20 to 30 m high. If the site is a street canyon, z_H/W only applies to the cross-section normal to the axis of the street. The orientation of the street axis may also be relevant because of systematic sun-shade patterns. If continuous monitoring is planned, north-south oriented streets are favoured over east-west ones because there is less phase distortion, although daytime course of temperature may be rather peaked.

At non-urban stations recommended screen height is between 1.25 and 2 m above ground level. While this is also acceptable for urban sites, it may be better to relax this requirement to allow greater heights. This should not lead to significant error in most cases, especially in densely built-up areas, because observations in canyons show very slight air temperature gradients through most of the UCL, provided that the location is more than 1 m from a surface (Nakamura and Oke, 1988). Measurements at heights of 3 or 5 m are not very different from those at the standard height, have slightly greater source areas and place the sensor beyond easy reach, thus preventing damage, and away from the path of vehicles. They also ensure greater dilution of vehicle exhaust heat and reduce contamination from dust.

Air temperatures measured above the UCL, using sensors mounted on a tower, are influenced by air exchanged with the UCL plus the effects of the roofs. Roofs have much more thermic variability than most surfaces within the UCL. Most roofs are designed to insulate and hence to minimize heat exchange with the interior of the building. As a result, roof-surface temperatures often become very hot by day, whereas the partially shaded and better conducting canyon walls and floor are cooler. At night circumstances are reversed with the roofs being relatively cold and canyon surfaces warmer as they release their daytime heat uptake. There may also be complications due to the release of heat from roof exhaust vents. Therefore, while there is little variation of temperature with height in the UCL, there is a discontinuity near roof level both horizontally and vertically. Hence, if a meaningful spatial average is sought, sensors should be well above mean roof level, $> 1.5 z_H$ if possible, so that the mixing of roof and canyon air is accomplished. In dealing with air temperature data from an elevated sensor, it is difficult to extrapolate these levels down towards screen level because currently no standard methods are available. Similarly, there is no simple, general scheme for extrapolating air temperatures horizontally inside the UCL. Statistical models work, but they require a large archive of existing observations over a dense network, which is not usually available.

9.3.2.2 **Surface temperature**

Surface temperature is not commonly measured at urban stations, but it can be a very useful variable to use as input in models to calculate fluxes. A representative surface temperature requires the averaging of an adequate sample of the many surfaces, vertical as well as horizontal, that make up an urban area. This is possible only using infrared remote sensing either from a scanner mounted on an aircraft or satellite, or a downward-facing pyrgeometer, or one or more radiation thermometers of which the combined field of view covers a representative sample of the urban district. Hence, to obtain accurate results, the target must be sampled appropriately and its average emissivity known.

9.3.2.3 **Soil and road temperature**

It is desirable to measure soil temperature in urban areas. The heat island effect extends down beneath a city and this may be of significance to engineering design for water pipes or road construction. In practice, the measurement of this variable may be difficult at more heavily developed urban sites. Bare ground may not be available, the soil profile is often highly disturbed, and at depth there may be obstructions or anomalously warm or cool artefacts (for example, empty, full or leaky water pipes, sewers, heat conduits). In urban areas, the measurement of grass minimum temperature has almost no practical utility.

Temperature sensors are often embedded in road pavements, especially in areas subject to freezing. They are usually part of a monitoring station for highway weather. It is often helpful to have sensors beneath both the tire track area and the centre of the lane.

9.3.3 Atmospheric pressure

At the scale of urban areas it will probably not be necessary to monitor atmospheric pressure if there is already a synoptic station in the region. If pressure sensors are included, the recommendations of Volume I, Chapter 3, apply. In rooms and elsewhere in the vicinity of buildings there is the probability of pressure "pumping" due to gusts. Also, interior-exterior pressure differences may exist if the sensor is located in an air-conditioned room. Both difficulties can be alleviated if a static pressure head is installed (see Volume I, Chapter 3, 3.1.4.3).

9.3.4 Humidity

The instruments normally used for humidity (Volume I, Chapter 4) are applicable to urban areas. The guidelines given in 9.3.2.1 for the siting and exposure of temperature sensors in the UCL, and above the RSL, apply equally to humidity sensors.

Urban environments are notoriously dirty (dust, oils, pollutants). Several hygrometers are subject to degradation or require increased maintenance in urban environments. Hence, if psychrometric methods are used, the wet-bulb sleeve must be replaced more frequently than normal and close attention should be given to ensuring that the distilled water remains uncontaminated. The hair strands of a hair hygrometer can be destroyed by polluted urban air; hence, their use is not recommended for extended periods. The mirror of dewpoint hygrometers and the windows of ultraviolet and infrared absorption hygrometers need to be cleaned frequently. Some instruments degrade to such an extent that the sensors have to be completely replaced fairly regularly. Because of shelter from wind in the UCL, forced ventilation at the rate recommended in Volume I, Chapter 4, 4.3 is essential, as is the provision of shielding from extraneous sources of solar and long-wave radiation.

9.3.5 Wind speed and direction

The measurement of wind speed and direction is highly sensitive to flow distortion by obstacles. Obstacles create alterations in the average wind flow and turbulence. Such effects apply at all scales of concern, including the effects of local relief due to hills, valleys and cliffs, sharp changes in roughness or in the effective surface elevation (z_0 , see below), perturbation of flow around clumps of trees and buildings, individual trees and buildings and even disturbance induced by the physical bulk of the tower or mounting arm to which the instruments are attached.

9.3.5.1 Mean wind profile

However, if a site is on reasonably level ground, has sufficient fetch downstream of major changes of roughness and is in a single UCZ without anomalously tall buildings, a mean wind profile such as that in Figure 9.4 should exist. The mean is both spatial and temporal. Within the UCL no one site can be expected to possess such a profile. Individual locations experience highly variable speed and direction shifts as the air-stream interacts with individual building arrangements, streets, courtyards and trees. In street canyons, the shape of the profile is different for along-canyon versus across-canyon flow (Christen et al., 2002) and depends on position across and along the street (DePaul and Shieh, 1986). Wind speed gradients in the UCL are small until quite close to the surface. As a first approximation the profile in the UCL can be described by an exponential form (Britter and Hanna, 2003) merging with the log profile near the roof level (Figure 9.4).

In the inertial sublayer, the Monin-Obukhov similarity theory applies, including the logarithmic law:

$$\bar{u}_z = (u_* / k) \left\{ \ln \left[(z - z_d) / z_0 \right] + \Psi_M \left(\frac{z}{L} \right) \right\} \quad (9.2)$$

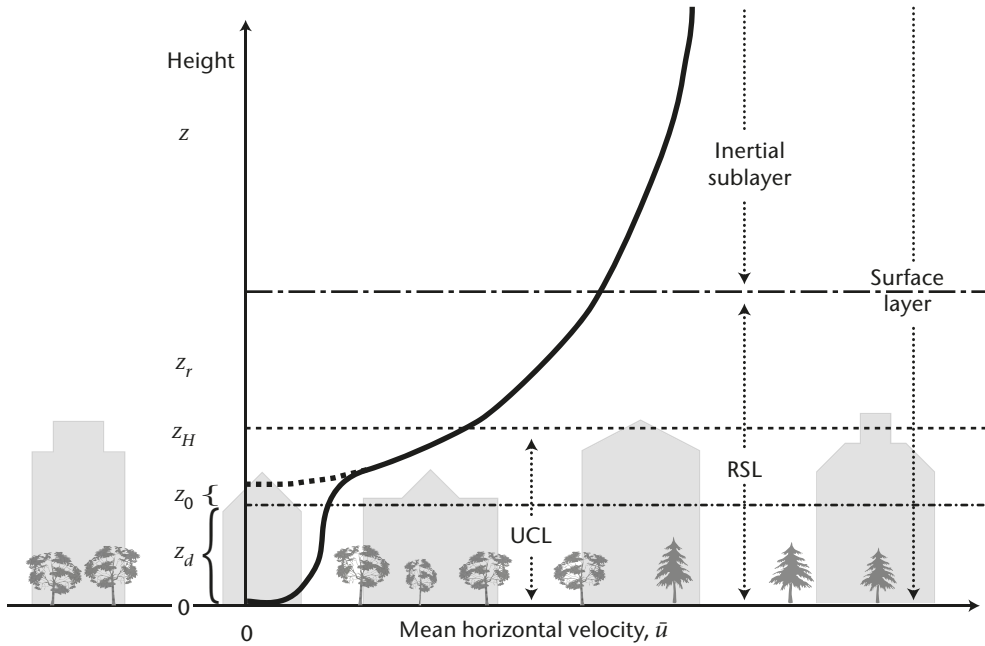


Figure 9.4. Generalized mean (spatial and temporal) wind velocity (\bar{u}) profile in a densely developed urban area including the location of sublayers of the surface layer. The measures on the height scale are the mean height of the roughness elements (z_H) the roughness sublayer (z_r , or the blending height), the roughness length (z_0) and zero-plane displacement length (z_d). The dashed line represents the profile extrapolated from the inertial sublayer, the solid line represents the actual profile.

where u_* is the friction velocity; k is von Karman’s constant (0.40); z_0 is the surface roughness length; z_d is the zero-plane displacement height (Figure 9.4); L is the Obukhov stability length ($= -u_*^3/[k(g/\theta_v)Q_H]$), where g is the gravitational acceleration, θ_v the virtual potential temperature and Q_H the turbulent sensible heat flux; and Ψ_M is a dimensionless function that accounts for the change in curvature of the wind profile away from the neutral profile with greater stability or instability.¹ In the neutral case (typically with strong winds and cloud) when Ψ_M is unity, equation 9.2 reduces to:

$$\bar{u}_z = (u_* / k) \ln [(z - z_d) / z_0] \tag{9.3}$$

The wind profile parameters can be measured using a vertical array of anemometers, or measurements of momentum flux or gustiness from fast-response anemometry in the inertial layer, but estimates vary with wind direction and are sensitive to errors (Wieringa, 1996; Verkaik, 2000). Methods to parameterize the wind profile parameters z_0 and z_d for urban terrain are also available (for reviews, see Grimmond and Oke, 1999; Britter and Hanna, 2003). The simplest methods involve general descriptions of the land use and obstacles (see Tables 9.1 and 9.2 as well as Davenport et al., 2000; Grimmond and Oke, 1999), or a detailed description of the roughness element heights and their spacing from either a geographic information system of the building and street dimensions, or maps and aerial oblique photographs, or airborne/satellite imagery and the application of one of several empirical formulae (for recommendations, see Grimmond and Oke, 1999).

It is important to incorporate the displacement height z_d into urban wind-profile assessments. Effectively, this is equivalent to setting a base for the logarithmic wind profile that recognizes the physical bulk of the urban canopy. It is like setting a new “ground surface” aloft, where the mean momentum sink for the flow is located (Figure 9.4).

¹ For more details on L and the form of the Ψ_M function, see a standard micrometeorology text, for example, Stull, 1988; Garratt, 1992; or Arya, 2001. Note that u_* and Q_H should be evaluated in the inertial layer above the RSL.

Table 9.2. Davenport classification of effective terrain roughness^a

Class	z_o (m)	Landscape description
4 Roughly open	0.10	Moderately open country with occasional obstacles (e.g. isolated low buildings or trees) at relative horizontal separations of at least 20 obstacle heights
5 Rough	0.25	Scattered obstacles (buildings) at relative distances of 8 to 12 obstacle heights for low solid objects (e.g. buildings) (analysis may need z_d) ^b
6 Very rough	0.5	Area moderately covered by low buildings at relative separations of 3 to 7 obstacle heights and no high trees (analysis requires z_d) ^b
7 Skimming	1.0	Densely built-up area without much building height variation (analysis requires z_d) ^b
8 Chaotic	2.0	City centres with mix of low and high-rise buildings (analysis by wind tunnel advised)

Notes:

^a Abridged version (revised 2000, for urban roughness only) of Davenport et al. (2000); for classes 1 to 3 and for rural classes 4 to 8, see Volume I, Chapter 5, Annex and WMO (2003).

^b First order values of z_d are given as fractions of average obstacle height, that is: $0.5 z_H$, $0.6 z_H$ and $0.7 z_H$ for Davenport classes 5, 6 and 7, respectively.

Depending on the building and tree density, this could set the base of the profile at a height of between 0.5 and $0.8 z_H$ (Grimmond and Oke, 1999). Hence, failure to incorporate it in calculations causes large errors. First estimates can be made using the fractions of z_H given in Table 9.2 (Note b).

9.3.5.2 **Height of measurement and exposure**

The choice of height at which wind measurements should be taken in urban areas is a challenge. However, if some basic principles are applied, meaningful results can be attained. The poor placement of wind sensors in cities is the source of considerable wasted resources and effort and leads to potentially erroneous calculations of pollutant dispersion. Of course, this is even a source of difficulty in open terrain due to obstacles and topographic effects. This is the reason why the standard height for rural wind observations is set at 10 m above ground, not at screen level, and why there the anemometer should not be at a horizontal distance from obstructions of less than 10 obstacle heights (Volume I, Chapter 5, 5.9.2 of the present Guide). In typical urban districts it is not possible to find such locations, for example, in a UCZ with 10 m high buildings and trees it would require a patch that is at least 100 m in radius. If such a site exists it is almost certainly not representative of the zone. It has already been noted that the roughness sublayer, in which the effects of individual roughness elements persist, extends to a height of about $1.5 z_H$ in a densely built-up area and perhaps higher in less densely developed sites. Hence, in the example district the minimum acceptable anemometer height is at least 15 m, not the standard 10 m. When buildings are much taller, an anemometer at the standard 10 m height would be well down in the UCL, and, given the heterogeneity of urban form and therefore of wind structure, there is little merit in placing a wind sensor beneath, or even at about, roof level.

It is well known from wind tunnel and field observations that flow over an isolated solid obstacle, like a tall building, is greatly perturbed both immediately over and around it. These perturbations include modifications to the streamlines, the presence of recirculation zones on the roof and in the so-called "bubble" or cavity behind it, and wake effects that persist in the downstream flow for tens of building height multiples that affect a large part of the neighbourhood (Figure 9.5).

There are many examples of poorly exposed anemometer-vane systems in cities. The data registered by such instruments are erroneous, misleading, potentially harmful if used to obtain wind input for wind load or dispersion applications, and wasteful of resources. The inappropriateness of placing anemometers and vanes on short masts on the top of buildings

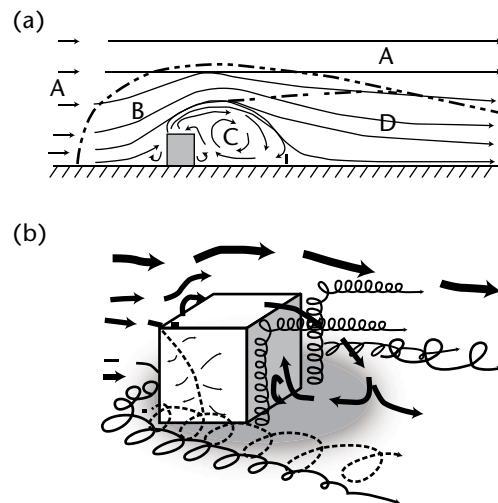


Figure 9.5. Typical two-dimensional flow around a building with flow normal to the upwind face (a): streamlines and flow zones; A represents undisturbed, B represents displacement, C represents cavity, D represents wake (after Halitsky, 1963), and (b): flow, and vortex structures (simplified after Hunt et al., 1978).

cannot be over-emphasized. Speed and directions vary hugely in short distances, both horizontally and vertically. Results from instruments deployed in this manner bear little resemblance to the general flow and are entirely dependent on the specific features of the building itself, the mast location on the structure, and the angle-of-attack of the flow to the building. The circulating and vortex flows seen in Figure 9.5 mean that, if the mast is placed ahead of, on top of, or in the cavity zone behind a building, direction measurements could well be counter to those prevailing in the flow outside the influence of the building's own wind climate (namely, in zone A of Figure 9.5(a)), and speeds are highly variable. To get outside the perturbed zone, wind instruments must be mounted at a considerable height. For example, it has been proposed that such sensors should be at a height greater than the maximum horizontal dimension of the major roof (Wieringa, 1996). This implies an expensive mast system, perhaps with guys that subtend a large area and perhaps difficulties in obtaining permission to install. Nevertheless, this is the only acceptable approach if meaningful data are to be measured.

Faced with such realities, sensors should be mounted so that their signal is not overly compromised by their support structure. The following recommendations are made:

- (a) In urban districts with low element height and density (UCZ 6 and 7), it may be possible to use a site where the "open country" standard exposure guidelines can be met. To use the 10 m height, the closest obstacles should be at least 10 times their height distant from the anemometer and not be more than about 6 m tall on average;
- (b) In more densely built-up districts, with relatively uniform element height and density (buildings and trees), wind speed and direction measurements should be taken with the anemometer mounted on a mast of open construction at a minimum height of 1.5 times the mean height of the elements;
- (c) In urban districts with scattered tall buildings the recommendations are as in (b), but with special attention to avoid the wake zone of the tall structures;
- (d) It is not recommended that measurements be taken of wind speed or direction in densely built areas with multiple high-rise structures unless a very tall tower is used.

Anemometers on towers with open construction should be mounted on booms (cross-arms) that are long enough to keep the sensors at least two (preferable three) tower diameters' distance from the side of the mast (Gill et al., 1967). Sensors should be mounted so that the least frequent

flow direction passes through the tower. If this is not possible, or if the tower construction is not very open, two or three booms with duplicate sensors may have to be installed to avoid wake effects and upwind stagnation produced by the tower itself.

If anemometer masts are to be mounted on tall or isolated buildings, the effects of the dimensions of that structure on the flow must be considered (see Chapter 5, 5.3.3, of the present volume). This is likely to require analysis using wind tunnel, water flume or computational fluid dynamics models specifically tailored to the building of interest, and including its surrounding terrain and structures.

The objective is to ensure that all wind measurements are taken at heights where they are representative of the upstream surface roughness at the local scale and are as free as possible of confounding influences from microscale or local scale surface anomalies. Hence the emphasis on gaining accurate measurements at whatever height is necessary to reduce error rather than measuring at a standard height. This may require splitting the wind site from the location of the other measurement systems. It may also result in wind observations at several different heights in the same settlement. That will necessitate extrapolation of the measured values to a common height, if spatial differences are sought or if the data are to form input to a mesoscale model. Such extrapolation is easily achieved by applying the logarithmic profile (equation 9.2) to two heights:

$$\bar{u}_1 / \bar{u}_{ref} = \ln(z_1 / z_0) / \ln(z_{ref} / z_0) \quad (9.4)$$

where z_{ref} is the chosen reference height; z_1 is the height of the site anemometer; and z_0 is the roughness length of the UCZ. In urban terrain it is correct to define the reference height to include the zero-plane displacement height, namely, both z_1 and z_{ref} have the form $(z_x - z_d)$, where the subscript x stands for "1" or "ref". A suitable reference height could be 50 m above displacement height.

Other exposure corrections for flow distortion, topography and roughness effects can be made as recommended in Volume I, Chapter 5 (see 5.9.4: Exposure correction) of the present Guide. It may well be that suitable wind observations cannot be arranged for a given urban site. In that case, it is still possible to calculate the wind at the reference height using wind observations at another urban station or the airport using the "logarithmic transformation" model of Wieringa (1986):

$$\bar{u}_{zA} = \bar{u}_{zB} \left[\frac{\ln(z_r / z_{0B}) \cdot \ln(z_A / z_{0A})}{\ln(z_B / z_{0B}) \cdot \ln(z_r / z_{0A})} \right] \quad (9.5)$$

where the subscripts A and B refer to the site of interest where winds are wanted and the site where standard wind measurements are available, respectively. The blending height z_r should either be taken as $4 z_H$ (see 9.1.1.3) or be given a standard value of 60 m; the method is not very sensitive to this term. Again, if either site has dense, tall roughness elements, the corresponding height scale should incorporate z_d .

9.3.5.3 **Wind sensor considerations**

Instruments used to measure wind speed and direction, gustiness and other characteristics of the flow in non-urban environments are applicable to urban areas. In cities, wind direction should always be measured, as well as speed, in order to allow azimuth-dependent corrections of tower influence to be made. If mechanical cup anemometers are used, because of the dirtiness of the atmosphere maintenance should be more frequent and close attention should be given to bearings and corrosion. If measurements are taken in the UCL, gustiness may increase the problem of cup over-speeding, and too much shelter may cause anemometers to operate near or below their threshold minimum speed. This must be dealt with through heightened maintenance and perhaps by using fast-response anemometers, propeller-type anemometers or sonic anemometers. Propeller anemometers are less prone to over-speeding, and sonic anemometers, having no moving parts, are practically maintenance-free. However, they are expensive and require sophisticated electronic logging and processing and not all models work when it is raining.

9.3.6 Precipitation

The instruments and methods for the measurement of precipitation given in Volume I, Chapter 6 of the present Guide are also relevant to urban areas. The measurement of precipitation as rain or snow is always susceptible to errors associated with the exposure of the gauge, especially in relation to the wind field in its vicinity. Given the urban context and the highly variable wind field in the UCL and the RSL, concerns arise from four main sources as follows:

- (a) The interception of precipitation during its trajectory to the ground by nearby collecting surfaces such as trees and buildings;
- (b) Hard surfaces near the gauge which may cause splash-in into the gauge, and over-hanging objects which may drip precipitation into the gauge;
- (c) The spatial complexity of the wind field around obstacles in the UCL causes very localized concentration or absence of rain- or snow-bearing airflow;
- (d) The gustiness of the wind in combination with the physical presence of the gauge itself causes anomalous turbulence around it which leads to under- or over-catch.

In open country, standard exposure requires that obstacles should be no closer than two times their height. In some ways, this is less restrictive than for temperature, humidity or wind measurements. However, in the UCL the turbulent activity created by flow around sharp-edged buildings is more severe than that around natural obstacles and may last for greater distances in their wake. Again, the highly variable wind speeds and directions encountered on the roof of a building make these sites to be avoided.

On the other hand, unlike temperature, humidity and wind measurements, the object of precipitation measurements is often not for the analysis of local effects, except perhaps in the case of rainfall rate. Some urban effects on precipitation may be initiated at the local scale (for example, by a major industrial facility), but may not show up until well downwind of the city. Distinct patterns within an urban area are more likely to be due to relief or coastal topographic effects.

Selecting an extensive open site in the city, where normal exposure standards can be met, may be acceptable, but it almost certainly will mean that the gauge will not be co-located with the air temperature, humidity and wind sensors. While the latter sensors need to be representative of the local scale urban structure, cover, fabric and metabolism of a specific UCZ, this is not the case for precipitation.

However, the local environment of the gauge is important if the station is to be used to investigate intra-urban patterns of precipitation type. For example, the urban heat island has an influence on the survival of different forms of precipitation, for example, snow or sleet at the cloud base may melt in the warmer urban atmosphere and fall as rain at the ground. This may result in snow at rural and suburban sites when the city centre registers rain.

With regard to precipitation gauges in urban areas, it is recommended that:

- (a) Gauges should be located in open sites within the city where the standard exposure criteria can be met (for example, playing fields, open parkland with a low density of trees, urban airports);
- (b) Gauges should be located in conjunction with wind instruments if a representative exposure for them is found. In other than low density built-up sites, this probably entails mounting the gauge above roof level on a mast. This means that the gauge will be subject to greater than normal wind speed and hence the error of estimation will be greater than near the surface, and the gauge output will have to be corrected. Such correction is feasible if wind is measured on the same mast. It also means that automatic recording is favoured, and the gauge must be checked regularly to ensure that it is level and that the orifice is free of debris;

- (c) Gauges should not be located on the roofs of buildings unless they are exposed at a sufficient height to avoid the wind envelope of the building;
- (d) The measurement of snowfall depth should be taken at an open site or, if made at developed sites, that a large spatial sample should be obtained to account for the inevitable drifting around obstacles. Such sampling should include streets oriented in different directions.

Urban hydrologists are interested in rainfall rates, especially during major storm events. Hence, tipping-bucket raingauges or weighing gauges have utility. The measurement of rain and snowfall in urban areas stands to benefit from the development of techniques such as optical raingauges and radar.

Dew, ice and fog precipitation also occurs in cities and can be of significance to the water budget, especially for certain surfaces, and may be relevant to applications such as plant diseases, insect activity, road safety and finding a supplementary source of water resources. The methods outlined in Volume I, Chapter 6 are appropriate for urban sites.

9.3.7 **Radiation**

At present, there is a paucity of radiation flux measurements conducted in urban areas. For example, there are almost none in the Global Energy Balance Archive of the World Climate Programme and the Atmospheric Radiation Measurement Program of the US Department of Energy. Radiation measurement sites are often located in rural or remote locations specifically to avoid the aerosol and gaseous pollutants of cities which “contaminate” their records. Even when a station has the name of a city, the metadata usually reveal they are actually located well outside the urban limits. If stations are located in the built-up area, only incoming solar (global) radiation is likely to be measured; neither incoming long-wave radiation nor any fluxes with outgoing components are monitored. For the most part, short-term experimental projects focusing specifically on urban effects measure both the receipt and loss of radiation in cities. All short- and long-wave fluxes are affected by the special properties of the atmosphere and surface of cities, and the same is true for the net all-wave radiation balance that effectively drives the urban energy balance (Oke, 1988a).

All of the instruments, calibrations and corrections, and most of the field methods outlined in relation to the measurement of radiation at open country sites in Volume I, Chapter 7 of the present Guide, apply to urban areas. Only differences, or specific urban needs or difficulties, are mentioned here.

9.3.7.1 ***Incoming fluxes***

Incoming solar radiation is such a fundamental forcing variable of urban climate that its measurement should be given a high priority when a station is established or upgraded. Knowledge of this term, together with standard observations of air temperature, humidity and wind speed, plus simple measures of the site structure and cover, allows a meteorological pre-processor scheme (namely, methods and algorithms used to convert standard observation fields into the variables required as input by models, but not measured, for example, fluxes, stability, mixing height, dispersion coefficients, and so on) such as the Hybrid Plume Dispersion Model (Hanna and Chang, 1992) or the Local-scale Urban Meteorological Parameterization Scheme (Grimmond and Oke, 2002) to be used to calculate much more sophisticated measurements such as atmospheric stability, turbulent statistics, the fluxes of momentum, heat and water vapour. These in turn make it possible to predict the mixing height and pollutant dispersion (COST 710, 1998; COST 715, 2001). Furthermore, solar radiation can be used as a surrogate for daytime cloud activity, and is the basis of applications in solar energy, daylight levels in buildings, pedestrian comfort, legislated rights to solar exposure and many other fields. At automatic stations, the addition of solar radiation measurement is simple and relatively inexpensive.

The exposure requirements for pyranometers and other incoming flux sensors are relatively easily met in cities. The fundamental needs are for the sensor to be level, free of vibration and free of any obstruction above the plane of the sensing element including both fixed features (buildings, masts, trees and hills) and ephemeral ones (clouds generated from exhaust vents or pollutant plumes). Therefore, a high, stable and accessible platform like the roof of a tall building is often ideal. It may be impossible to avoid the short-term obstruction of direct-beam solar radiation impinging on an up-facing radiometer by masts, antennas, flag poles and similar structures. If this occurs, the location of the obstruction and the typical duration of its impact on the sensing element should be fully documented (see 9.4). Methods to correct for such interference are mentioned in Volume I, Chapter 7. It is also important to ensure that there is no excessive reflection from very light-coloured walls that may extend above the local horizon. It is essential to clean the upper domes at regular intervals. In heavily polluted environments this may mean on a daily basis.

Other incoming radiation fluxes are also desirable but their inclusion depends on the nature of the city, the potential applications and the cost of the sensors. These radiation fluxes (and their instruments) are the following: incoming direct solar beam (pyrheliometer), diffuse sky solar (pyranometer fitted with a shade ring or a shade disc on an equatorial mount), solar ultraviolet (broadband and narrowband sensors, and spectrometers) and long-wave (pyrgeometer). All of these radiation fluxes have useful applications: beam (pollution extinction coefficients), diffuse (interior daylighting, solar panels), ultraviolet (depletion by ozone and damage to humans, plants and materials) and long-wave (monitoring nocturnal cloud and enhancement of the flux by pollutants and the heat island effect).

9.3.7.2 **Outgoing and net fluxes**

The reflection of solar radiation and the emission and reflection of long-wave radiation from the underlying surface, and the net result of short-, long- and all-wave radiant fluxes, are currently seldom monitored at urban stations. This means that significant properties of the urban climate system remain unexplored. The albedo, which decides if solar radiation is absorbed by the fabric or is lost back to the atmosphere and space, will remain unknown. The opportunity to invert the Stefan-Boltzmann relation and solve for the surface radiant temperature is lost. The critical net radiation that supports warming/cooling of the fabric, and the exchanges of water and heat between the surface and the urban boundary layer, is missing. Of these, net all-wave radiation data lack the most. Results from a well-maintained net radiometer are invaluable to drive a pre-processor scheme and as a surrogate measurement of cloud.

The main difficulty in measuring outgoing radiation terms accurately is the exposure of the down-facing radiometer to view a representative area of the underlying urban surface. The radiative source area (equation 9.1 and Figure 9.2) should ideally “see” a representative sample of the main surfaces contributing to the flux. In the standard exposure cases, defined in the relevant sections of Volume I, Chapter 7, a sensor height of 2 m is deemed appropriate over a short grass surface. At that height, 90% of the flux originates from a circle with a diameter of 12 m on the surface. Clearly, a much greater height is necessary over an urban area in order to sample an area that contains a sufficient population of surface facets to be representative of that UCZ. Considering the case of a radiometer at a height of 20 m (at the top of a 10 m high mast mounted on a 10 m high building) in a densely developed district, the 90% source area has a diameter of 120 m at ground level. This might seem sufficient to “see” several buildings and roads, but it must also be considered that the system is three-dimensional, not quasi-flat like grass. At the level of the roofs in the example, the source area is now only 60 m in diameter, and relatively few buildings may be viewed.

The question becomes whether the sensor can “see” an appropriate mix of climatically active surfaces. This means that the sensor must not only see an adequate set of plan-view surface types, but also sample appropriate fractions of roof, wall and ground surfaces, including the correct fractions of each that are in the sun or shade. This is a non-trivial task that depends on the surface structure and the positions of both the sensor and the sun in space above the array. Soux et al. (2004) developed a model to calculate these fractions for relatively simple urban-like geometric arrays. However, more work is needed before guidelines specific to individual UCZ

types are available. It seems likely that the sensor height has to be *greater* than that for turbulence measurements. The non-linear nature of radiative source area effects is clear from equation 9.1 (see Figure 9.2). The greater weighting of surfaces closer to the mast location means that the immediate surroundings are most significant. In the previous example of the radiometer at a height of 20 m on a 10 m high building, 50% of the signal at the roof-level comes from a circle of only 20 m in diameter (perhaps only a single building). If the roof of that building, or any other surface on which the mast is mounted, has anomalous radioactive properties (albedo, emissivity or temperature), it disproportionately affects the flux, which is supposed to be representative of a larger area. Hence, roofs with large areas of glass or metal, or with an unusually dark or light colour, or those designed to hold standing water, should be avoided.

The problems associated with down-facing radiometers at large heights include: (a) the difficulty of ensuring that the plane of the sensing element is level; (b) ensuring that at large zenith angles the sensing element does not "see" direct beam solar radiation or incoming long-wave radiation from the sky; (c) considering whether there is need to correct results to account for radiative flux divergence in the air layer between the instrument height and the surface of interest. To eliminate extraneous solar or long-wave radiation near the horizon, it may be necessary to install a narrow collar that restricts the field of view to a few degrees less than 2π . This will necessitate a small correction applied to readings to account for the missing diffuse solar input (see Volume I, Chapter 7, Annex 7.E for the case of a shading ring) or the extra long-wave input from the collar.

Inverted sensors may be subject to error because their back is exposed to solar heating. This should be avoided by using some form of shielding and insulation. Maintaining the cleanliness of the instrument domes and wiping away deposits of water or ice may also be more difficult. The inability to observe the rate and effectiveness of instrument ventilation at a certain height means that instruments that do not need aspiration should be preferred. The ability to lower the mast to attend to cleaning, the replacement of desiccant or polyethylene domes and levelling is an advantage.

It is recommended that:

- (a) Down-facing radiometers be placed at a height at least equal to that of a turbulence sensor (namely, a minimum of $2z_H$ is advisable) and preferably higher;
- (b) The radiative properties of the immediate surroundings of the radiation mast should be representative of the urban district of interest.

9.3.8 **Sunshine duration**

The polluted atmospheres of urban areas cause a reduction in sunshine hours compared with their surroundings or pre-urban values (Landsberg, 1981). The instruments, methods and exposure recommendations given in Volume I, Chapter 8 of the present Guide are applicable to an urban station.

9.3.9 **Visibility and meteorological optical range**

The effects of urban areas upon visibility and meteorological optical range (MOR) are complex because, while pollutants tend to reduce visibility and MOR through their impact on the attenuation of light and the enhancement of certain types of fog, urban heat and humidity island effects often act to diminish the frequency and severity of fog and low cloud. There is considerable practical value in having urban visibility and MOR information for fields such as aviation, road and river transportation and optical communications, and thus to include these observations at urban stations.

The visual perception of visibility is hampered in cities. While there are many objects and lights that can serve as range targets, it may be difficult to obtain a sufficiently uninterrupted line of sight at the recommended height of 1.5 m. The use of a raised platform or the upper level of

buildings is considered non-standard and is not recommended. Observations near roof level may also be affected by scintillation from heated roofs, or the “steaming” of water from wet roofs during drying, or pollutants and water clouds released from chimneys and other vents.

Instruments to measure MOR, such as transmissometers and scatter meters, generally work well in urban areas. They require relatively short paths and will give good results if the optics are maintained in a clean state. Naturally, the instrument must be exposed at a location that is representative of the atmosphere in the vicinity, but the requirements are no more stringent than for other instruments placed in the UCL. It may be that, for certain applications, knowledge of the height variation of MOR is valuable, for example, the position of the fog top or the cloud base.

9.3.10 **Evaporation and other fluxes**

Urban development usually leads to a reduction in evaporation primarily due to the fact that built features seal the surface and that vegetation has been removed. Nonetheless, in some naturally dry regions, an increase may occur if water is imported from elsewhere and used to irrigate urban vegetation.

Very few evaporation measurement stations exist in urban areas. This is understandable because it is almost impossible to interpret evaporation measurements conducted in the UCL using atmometers, evaporation pans or lysimeters. As detailed in Volume I, Chapter 10 of the present Guide, such measurements must be at a site that is representative of the area; not closer to obstacles than 5 times their height, or 10 times if they are clustered; not placed on concrete or asphalt; not unduly shaded; and free of hard surfaces that may cause splash-in. In addition to these concerns, the surfaces of the instruments are assumed to act as surrogates for vegetation or open water systems. Such surfaces are probably not representative of the surroundings at an urban site. Hence, they are in receipt of micro-advection that is likely to force evaporation at unrealistically high rates.

Consider the case of an evaporation pan installed over a long period which starts out at a semi-arid site that converts to irrigated agricultural uses and is then encroached upon by suburban development and is later in the core of a heavily developed urban area. Its record of evaporation starts out very high, because it is an open water surface in hot, dry surroundings. Therefore, although actual evaporation in the area is very low, advection forces the loss from the pan to be large. Because the introduction of irrigation makes conditions cooler and more humid, the pan readings drop, but actual evaporation is large. Inasmuch as urban development largely reverses the environmental changes and reduces the wind speed near the ground, pan losses increase but the actual evaporation probably drops. Hence, throughout this sequence pan evaporation and actual evaporation are probably in anti-phase. During the agricultural period a pan coefficient might have been applied to convert the pan readings to those typical of short grass or crops. No such coefficients are available to convert pan to urban evaporation, even if the readings are not corrupted by the complexity of the UCL environment. In summary, the use of standard evaporation instruments in the UCL is not recommended.

The dimensions and heterogeneity of urban areas renders the use of full-scale lysimeters impractical (for example, the requirement to be not less than 100 to 150 m from a change in surroundings). Micro-lysimeters can give the evaporation from individual surfaces, but they are still specific to their surroundings. Such lysimeters need careful attention, including soil monolith renewal to prevent drying out, and are not suitable for routine long-term observations.

Spatially averaged evaporation and other turbulent fluxes (momentum, sensible heat, carbon dioxide) information can be obtained from observations above the RSL. Several of these fluxes are of greater practical interest in urban areas than in many open country areas. For example, the vertical flux of horizontal momentum and the integral wind statistics and spectra are needed to determine wind loading on structures and the dispersion of air pollutants. The sensible heat flux is an essential input to calculate atmospheric stability (for example, the flux Richardson number and the Obukhov length) and the depth of the urban mixing layer. Fast response eddy covariance or standard deviation methods are recommended, rather than profile gradient

methods. Appropriate instruments include sonic anemometers, infrared hygrometers and gas analysers and scintillometers. The sensors should be exposed in the same manner as wind sensors: above the RSL but below the internal boundary layer of the UCZ of interest. Again, such measurements rely on the flux “footprint” being large enough to be representative of the local area of interest.

If such flux measurements are beyond the financial and technical resources available, a meteorological pre-processor scheme such as the Ozone Limiting Method, the Hybrid Plume Dispersion Method or the Local-scale Urban Meteorological Parameterization Scheme (see 9.3.7) can be an acceptable method to obtain aerielly representative values of urban evaporation and heat flux. Such schemes require only spatially representative observations of incoming solar radiation, air temperature, humidity and wind speed and general estimates of average surface properties such as albedo, emissivity, roughness length and the fractions of the urban district that are vegetated or built-up or irrigated. Clearly, the wind speed observations must conform to the recommendations in 9.3.5. Ideally air temperature and humidity should also be observed above the RSL; however, if only UCL values are available, this is usually acceptable because such schemes are not very sensitive to these variables.

9.3.11 **Soil moisture**

Knowledge of urban soil moisture can be useful, for example, to gardeners and in the calculation of evaporation. Its thermal significance in urban landscapes is demonstrated by the remarkably distinct patterns in remotely sensed thermal imagery. By day, any patch with active vegetation or irrigated land is noticeably cooler than land that is built on, paved or bare. However, the task of sampling to obtain representative values of soil moisture is daunting.

Some of the challenges presented include the fact that large fractions of urban surfaces are completely sealed over by paved and built features; much of the exposed soil has been highly disturbed in the past during construction activity or following abandonment after urban use; the “soil” may actually be largely formed from the rubble of old buildings and paving materials or have been imported as soil or fill material from distant sites; or the soil moisture may be affected by seepage from localized sources such as broken water pipes or sewers or be the result of irrigation. All of these elements lead to a very patchy urban soil moisture field that may have totally dry plots situated immediately adjacent to over-watered lawns. Hence, while some idea of local-scale soil moisture may be possible in areas with very low urban development, or where the semi-natural landscape has been preserved, it is almost impossible to characterize in most urban districts. Again, in this case it may be better to use rural values that give a regional background value rather than to have no estimate of soil moisture availability.

9.3.12 **Present weather**

If human observers or the usual instrumentation are available, the observation of present weather events and phenomena such as rime, surface ice, fog, dust and sand storms, funnel clouds and thunder and lightning can be valuable, especially those with practical implications for the efficiency or safety of urban activities, for example transportation. If archiving facilities are available, the images provided by webcams can provide very helpful evidence of clouds, short-term changes in cloud associated with fronts, fog banks that ebb and flow, low cloud that rises and falls, and the arrival of dust and sand storm fronts.

9.3.13 **Cloud**

Although cloud cover observation is rare in large urban areas, this information is very useful. All of the methods and instruments outlined in Volume I, Chapter 15 of the present Guide are applicable to urban areas. The large number and intensity of light sources in cities, combined with a hazy, sometimes polluted, atmosphere, make visual observation more difficult. Where possible, the observational site should avoid areas with particularly bright lighting.

9.3.14 **Atmospheric composition**

The monitoring of atmospheric pollution in the urban environment is increasingly important. However, this is another specialist discipline and will not be dealt with in this chapter. Volume I, Chapter 16 of the present Guide deals with the subject in the broader context of the Global Atmosphere Watch.

9.3.15 **Profiling techniques for the urban boundary layer**

Because urban influences extend throughout the planetary boundary layer (Figure 9.1), it is necessary to use towers and masts to obtain observations above the RSL to probe higher. Of special interest are effects on the wind field and the vertical temperature structure including the depth of the mixing layer and their combined role in affecting pollutant dispersion.

All of the special profiling techniques outlined in Chapter 5 of the present volume are relevant to urban areas. Acoustic sounders (sodars) are potentially very useful; nonetheless, it must be recognized that they suffer from two disadvantages: first, their signals are often interfered with by various urban sources of noise (traffic, aircraft, construction activity, and even lawnmowers); and second, they may not be allowed to operate if they cause annoyance to residents. Wind profiler radars, radio-acoustic sounding systems, microwave radiometers, microwave temperature profilers, laser radars (lidars) and modified ceilometers are all suitable systems to monitor the urban atmosphere if interference from ground clutter can be avoided. Similarly, balloons for wind tracking, boundary layer radiosondes (minisondes) and instrumented tethered balloons can all be used with good success rates as long as air traffic authorities grant permission for their use. Instrumented towers and masts can provide an excellent means of placing sensors above roof level and into the inertial sublayer, and very tall structures may permit measurements into the mixing layer above. However, it is necessary to emphasize the precautions given in Chapter 5, 5.3.3, of the present volume regarding the potential interference with atmospheric properties by the support structure. Although tall buildings may appear to provide a way to reach higher into the urban boundary layer, unless obstacle interference effects are fully assessed and measures instituted to avoid them, the deployment of sensors can be unfruitful and probably misleading.

9.3.16 **Satellite observations**

Remote sensing by satellite with adequate resolution in the infrared may be relevant to extended urban areas. A description of these techniques is available in Volume IV, and a review of their use in the study of urban climates is given in Voogt and Oke (2003).

9.4 **METADATA**

The full and accurate documentation of station metadata (see Volume I, Chapter 1 of the present Guide) is absolutely essential for any station “to ensure that the final data user has no doubt about the conditions in which data have been recorded, gathered and transmitted, in order to extract accurate conclusions from their analysis” (WMO, 2003). It can be argued that this is even more critical for an urban station, because urban sites possess both an unusually high degree of complexity and a greater propensity to change. The complexity makes every site truly unique, whereas good open country sites conform to a relatively standard template. Change means that site controls are dynamic, meaning that documentation must be updated frequently. In Figure 9.6 it is assumed that the minimum requirements for station metadata set by WMO (2003) are all met and that hopefully some or all of the best practices they recommend are implemented. Here, emphasis is placed on special urban characteristics that need to be included in the metadata, in particular under the categories of “local environment” and “historical events”.

9.4.1 Local environment

As explained in 9.1.1, urban stations involve the exposure of instruments both within and above the urban canopy. Hence, the description of the surroundings must include both the microscale and the local scale. Following WMO (2003), with adaptations to characterize the urban environment, it is recommended that the following descriptive information be recorded for the station:

- A map at the local scale to mesoscale ($\sim 1:50\,000$) as in Figure 9.6(a), updated as necessary to describe large-scale urban development changes (for example, conversion of open land to housing, construction of a shopping centre or airport, construction of new tall buildings, cutting of a forest patch, drainage of a lake, creation of a detention pond). Ideally, an aerial photograph of the area should also be provided and a simple sketch map (at $1:500\,000$ or $1:1\,000\,000$) to indicate the location of the station relative to the rest of the urbanized region (Figures 9.6(b) and (c)) and any major geographic features such as large water bodies, mountains and valleys or change in ecosystem type (desert, swamp, forest). An aerial oblique photograph can be especially illuminating because the height of buildings and trees can also be appreciated. If available, aerial or satellite infrared imagery may be instructive regarding important controls on microclimate. For example, relatively cool surfaces by day usually indicate the availability of moisture or materials with anomalous surface emissivity. Hotter than normal areas may be very dry, or have a low albedo or very good insulation. At night, relative coolness indicates good insulation, and relative warmth the opposite, or it could be a material with high thermal admittance that is releasing stored daytime heat or there could be an anomalous source of anthropogenic heat. UCZ and Davenport roughness classes can be judged using Tables 9.1 or 9.2;
- A microscale sketch map ($\sim 1:5\,000$), according to metadata guidelines, updated each year (Figure 9.7(a));

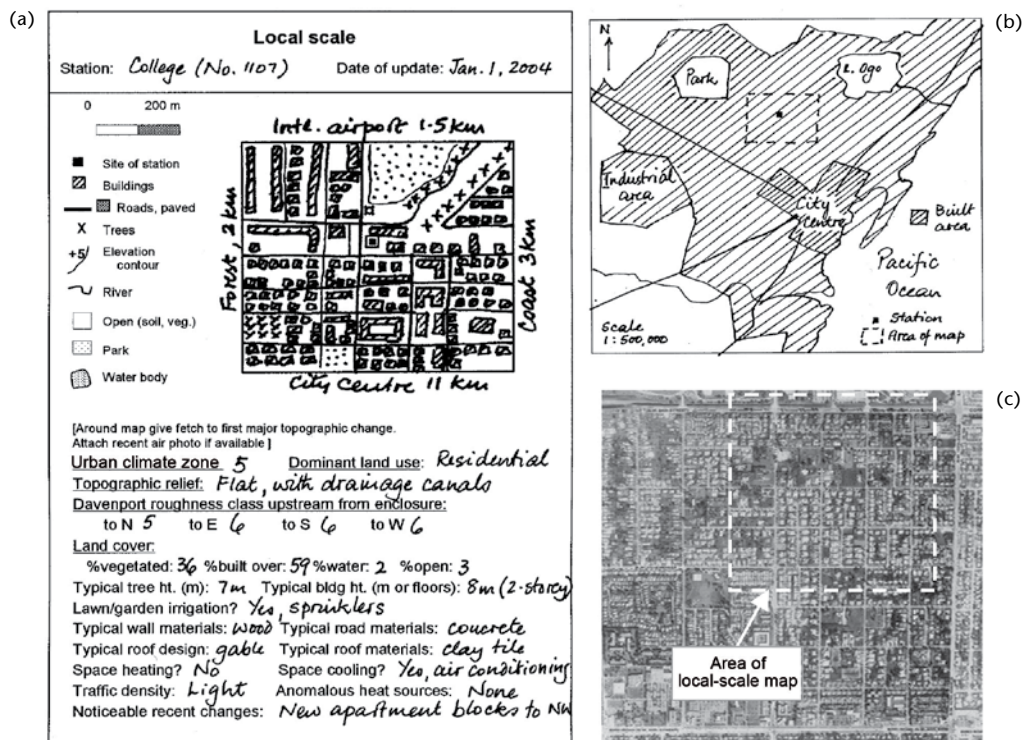


Figure 9.6. Minimum information necessary to describe the local-scale environment of an urban station, consisting of (a) a template to document the local setting; (b) a sketch map to situate the station in the larger urban region; and (c) an aerial photograph.

- (c) Horizon mapping using a clinometer and compass survey in a circle around the screen (as shown in the diagram at the base of the template, Figure 9.7(a), and a fisheye lens photograph taken looking vertically at the zenith with the camera's back placed on the ground near the screen, but not such that any of the sky is blocked by it (Figure 9.7(b)). If a fisheye lens is not available, a simpler approach is to take a photograph of a hemispheric reflector (Figure 9.7(c)). This should be updated every year or more frequently if there are marked changes in horizon obstruction, such as the construction or demolition of a new building nearby, or the removal of trees;
- (d) Photographs taken from cardinal directions of the instrument enclosure and of other instrument locations and towers;
- (e) A microscale sketch of the instrument enclosure, updated when instruments are relocated or other significant changes occur;
- (f) If some of the station's measurements (wind, radiation) are made away from the enclosure (on masts, rooftops, more open locations) repeat steps (b) to (d) above for each site.

9.4.2 Historical events

Urban districts are subject to many forces of change, including new municipal legislation that may change the types of land uses allowed in the area, or the height of buildings, or acceptable materials and construction techniques, or environmental, irrigation or traffic laws and regulations. Quite drastic alterations to an area may result from central planning initiatives

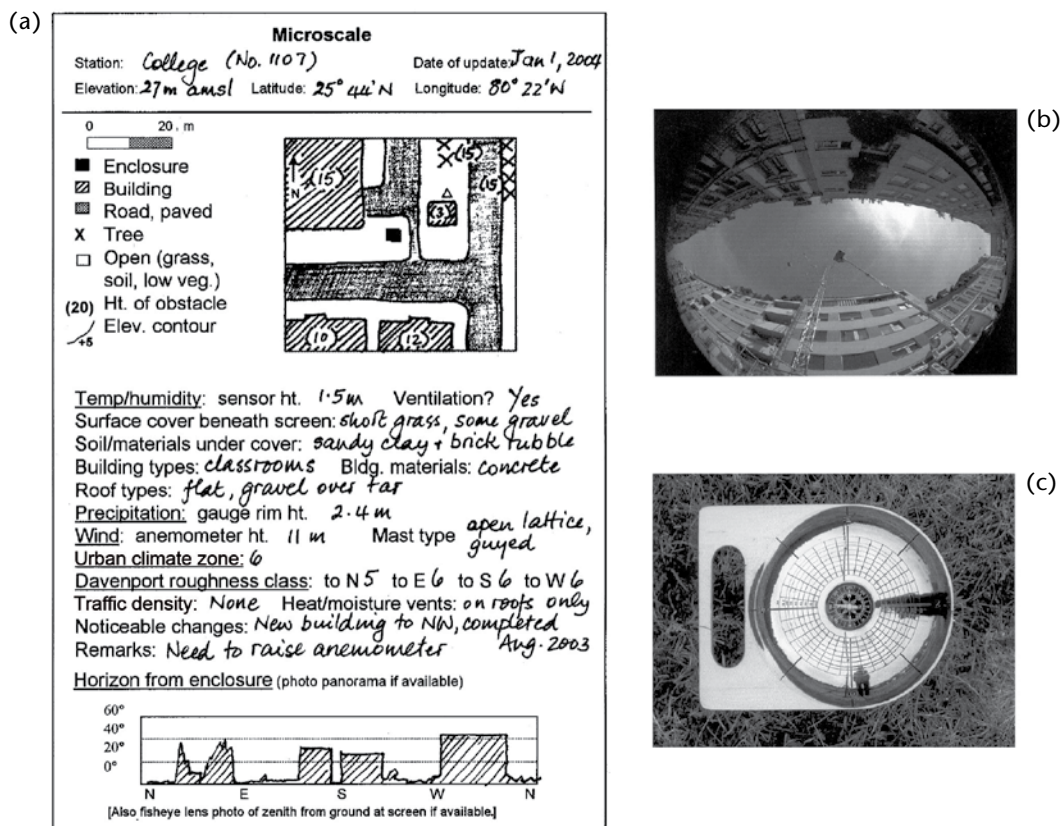


Figure 9.7. Information required to describe the microscale surroundings of an urban climate station; (a) a template for a metadata file; (b) an example of a fisheye lens photograph of a street canyon illustrating horizon obstruction; and (c) a UK Met Office hemispheric reflector placed on a raingauge.

for urban renewal. More organic alterations to the nature of a district also arise because of in- or out-migrations of groups of people, or when an area comes into, or goes out of, favour or style as a place to live or work. The urban area may be a centre of conflict and destruction. Such events should be documented so that later users of the data understand some of the context of changes that might appear in the urban climate.

9.4.3 **Observance of other WMO recommendations**

All other WMO recommendations regarding the documentation of metadata, including station identifiers, geographical data, instrument exposure, types of instruments, instrument mounting and sheltering, data recording and transmission, observing practices, metadata storage and access and data processing should be observed at urban stations.

9.5 **ASSESSMENT OF URBAN EFFECTS**

The study of urban weather and climate possesses a perspective that is almost unique. People are curious about the role of humans in modifying the urban atmosphere. Therefore, unlike other environments of interest, where it is sufficient to study the atmosphere for its own sake or value, in urban areas there is interest in knowing about urban effects. This means assessing possible changes to meteorological variables as an urban area develops over time, compared to what would have happened had the settlement not been built. This question that is essentially unanswerable when a settlement has been built, and, even if the settlement had not been built, the landscape may well have evolved into a different state compared with the pre-existing one (for example, owing to other human activity such as agriculture or forestry). The assessment of urban effects is therefore fraught with methodological difficulties and no "truth" is possible, only surrogate approximations. If an urban station is being established alone, or as part of a network, to assess urban effects on weather and climate, it is recommended that careful consideration be given to the analysis given in Lowry (1977), and Lowry and Lowry (2001).

9.6 **SUMMARY OF KEY POINTS FOR URBAN STATIONS**

9.6.1 **Working principles**

When establishing an urban station, the rigid guidelines for climate stations are often inappropriate. It is necessary to apply guiding principles rather than rules, and to retain a flexible approach. This often means different solutions for individual atmospheric properties and may mean that not all observations at a "site" are made at the same place.

Because the environment of urban stations changes often as development proceeds, frequently updated metadata are as important as the meteorological data gathered. Without good station descriptions it is impossible to link measurements to the surrounding terrain.

9.6.2 **Site selection**

An essential first step in selecting urban station sites is to evaluate the physical nature of the urban terrain, using a climate zone classification. This will reveal areas of homogeneity.

Several urban terrain types make up an urban area. In order to build a picture of the climate of a settlement, multiple stations are required. Sites should be selected that are likely to sample air drawn across relatively homogenous urban terrain and are thus representative of a single climate zone. Care must be taken to ensure that microclimatic effects do not interfere with the objective of measuring the local-scale climate.

9.6.3 Measurements

With regard to measurements, the following key points should be taken into account:

- (a) Air temperature and humidity measurements taken within the UCL can be locally representative if the site is carefully selected. If these variables are observed above roof level, including above the RSL, there is no established link between them and those within the UCL;
 - (b) Wind and turbulent flux measurements should be taken above the RSL but within the internal boundary layer of the selected UCZ. Such measurements must establish that the surface “footprint” contributing to the observations is representative of the climate zone. For wind, it is possible to link the flow at this level and that experienced within the canopy;
 - (c) Precipitation observations can be conducted either near the ground at an unobstructed site, or above the RSL, corrected according to parallel wind measurements;
 - (d) With the exception of incoming solar radiation measurements, rooftop sites are to be avoided, unless instruments are exposed on a tall mast;
 - (e) Measurements of the net and upwelling radiation fluxes must be taken at heights that make it possible to sample adequately the range of surface types and orientations typical of the terrain zone.
-

REFERENCES AND FURTHER READING

- Arya, P.S., 2001: *Introduction to Micrometeorology*. Academic Press, New York.
- Auer, A.H. Jr., 1978: Correlation of land use and cover with meteorological anomalies. *Journal of Applied Meteorology*, 17(5):636–643.
- Britter, R.E. and S.R. Hanna, 2003: Flow and dispersion in urban areas. *Annual Review of Fluid Mechanics*, 35:469–496.
- Christen, A., 2003: (personal communication). Institute of Meteorology, Climatology and Remote Sensing, University of Basel.
- Christen, A., R. Vogt, M.W. Rotach and E. Parlow, 2002: *First results from BUBBLE I: Profiles of fluxes in the urban roughness sublayer. Proceedings of the Fourth Symposium on Urban Environment*, (Norfolk, Virginia), American Meteorological Society, Boston, pp. 105–106.
- COST 710, 1998: *Final Report: Harmonisation of the Pre-processing of Meteorological Data for Atmospheric Dispersion Models*. European Commission. EUR 18195 EN.
- COST 715, 2001: *Preparation of Meteorological Input Data for Urban Site Studies*. European Commission, EUR 19446 EN.
- Davenport, A.G., C.S.B. Grimmond, T.R. Oke and J. Wieringa, 2000: *Estimating the roughness of cities and sheltered country. Proceedings of the Twelfth Conference on Applied Climatology* (Asheville, North Carolina), American Meteorological Society, Boston, pp. 96–99.
- DePaul, F.T. and C.M. Shieh, 1986: Measurements of wind velocity in a street canyon. *Atmospheric Environment*, 20:455–459.
- Ellefsen, R., 1991: Mapping and measuring buildings in the canopy boundary layer in ten US cities. *Energy and Buildings*, 16:1025–1049.
- Garratt, J.R., 1992: *The Atmospheric Boundary Layer*. Cambridge University Press, Cambridge.
- Gill, G.C., L.E. Olsson, J. Sela and M. Suda, 1967: Accuracy of wind measurements on towers or stacks. *Bulletin of the American Meteorological Society*, 48:665–674.
- Grimmond, C.S.B. and T.R. Oke, 1999: Aerodynamic properties of urban areas derived from analysis of surface form. *Journal of Applied Meteorology*, 38(9):1262–1292.
- , 2002: Turbulent heat fluxes in urban areas: Observations and a local-scale urban meteorological parameterization scheme (LUMPS). *Journal of Applied Meteorology*, 41(7):792–810.
- Halitsky, J., 1963: Gas diffusion near buildings. *Transactions of the American Society of Heating, Refrigerating and Air-conditioning Engineers*, 69:464–485.
- Hanna, S.R. and J. C. Chang, 1992: Boundary-layer parameterizations for applied dispersion modeling over urban areas. *Boundary-Layer Meteorology*, 58:229–259.
- Hunt, J.C.R., C.J. Abell, J.A. Peterka and H.Woo, 1978: Kinematical studies of the flow around free or surface-mounted obstacles: Applying topology to flow visualization. *Journal of Fluid Mechanics*, 86:179–200.
- Kljun, N., P. Calanca, M.W. Rotach, H.P. Schmid, 2004: A simple parameterization for flux footprint predictions. *Boundary-Layer Meteorology*, 112:503–523.
- Kljun, N., M. Rotach and H.P. Schmid, 2002: A three-dimensional backward Lagrangian footprint model for a wide range of boundary-layer stratifications. *Boundary-Layer Meteorology*, 103(2):205–226.
- Landsberg, H.E., 1981: *The Urban Climate*. Academic Press, New York.
- Lowry, W.P., 1977: Empirical estimation of urban effects on climate: A problem analysis. *Journal of Applied Meteorology*, 16(2):129–135.
- Lowry, W.P. and P.P. Lowry, 2001: *Fundamentals of Biometeorology: Volume 2 – The Biological Environment*. Chapter 17, Peavine Publications, St Louis, Missouri, pp. 496–575.
- Nakamura, Y. and T.R. Oke, 1988: Wind, temperature and stability conditions in an east-west oriented urban canyon. *Atmospheric Environment*, 22:2691–2700.
- Oke, T.R., 1981: Canyon geometry and the nocturnal heat island: Comparison of scale model and field observations. *Journal of Climatology*, 1(3):237–254.
- , 1982: The energetic basis of the urban heat island. *Quarterly Journal of the Royal Meteorological Society*, 108(455):1–24.
- , 1984: Methods in urban climatology. In: *Applied Climatology* (W. Kirchofer, A. Ohmura and W. Wanner, eds.). Zürcher Geographische Schriften, 14:19–29.
- , 1987: *Boundary Layer Climates*. Chapter 8, second edition, Routledge, pp. 262–303.
- , 1988a: The urban energy balance. *Progress in Physical Geography*, 12:471–508.
- , 1988b: Street design and urban canopy layer climate. *Energy and Buildings*, 11:103–113.
- , 1997: Urban environments. In: *The Surface Climates of Canada* (W.G. Bailey, T.R. Oke and W.R. Rouse, eds.). McGill-Queen's University Press, Montreal, pp. 303–327.

- Peterson, T.C., 2003: Assessment of urban versus rural in situ surface temperatures in the contiguous United States: No difference found. *Journal of Climate*, 16:2941–2959.
- Rotach, M.W., 1999: On the influence of the urban roughness sublayer on turbulence and dispersion. *Atmospheric Environment*, 33:4001–4008.
- Schmid, H.P., 2002: Footprint modeling for vegetation atmosphere exchange studies: A review and perspective. *Agricultural and Forest Meteorology*, 113(1):159–183.
- Schmid, H.P., H.A. Cleugh, C.S.B. Grimmond and T.R. Oke, 1991: Spatial variability of energy fluxes in suburban terrain. *Boundary-Layer Meteorology*, 54(3):249–276.
- Soux, A., J.A. Voogt and T.R. Oke, 2004: A model to calculate what a remote sensor ‘sees’ of an urban surface. *Boundary-Layer Meteorology*, 111:109–132.
- Stull, R.B., 1988: *An Introduction to Boundary Layer Meteorology*. Kluwer Academic Publishers, Dordrecht.
- Verkaik, J.W., 2000: Evaluation of two gustiness models for exposure correction calculations. *Journal of Applied Meteorology*, 39(9):1613–1626.
- Voogt, J.A. and T.R. Oke, 2003: Thermal remote sensing of urban climates. *Remote Sensing of Environment*, 86(3):370–384.
- Wieringa, J., 1986: Roughness-dependent geographical interpolation of surface wind speed averages. *Quarterly Journal of the Royal Meteorological Society*, 112(473):867–889.
- , 1993: Representative roughness parameters for homogeneous terrain. *Boundary-Layer Meteorology*, 63(4):323–363.
- , 1996: Does representative wind information exist? *Journal of Wind Engineering and Industrial Aerodynamics*, 65(1):1–12.
- World Meteorological Organization, 2003: *Guidelines on Climate Metadata and Homogenization* (E. Aguilar, I. Auer, M. Brunet, T.C. Peterson and J. Wieringa). World Climate Data and Monitoring Programme No. 53 (WMO/TD-No. 1186). Geneva.
- , 2006: *Initial Guidance to Obtain Representative Meteorological Observations at Urban Sites* (T.R. Oke). Instruments and Observing Methods Report No. 81 (WMO/TD-No. 1250). Geneva.
- , 2011a: *Guide to Climatological Practices* (WMO-No. 100). Geneva.
- , 2011b: *Manual on Codes* (WMO-No. 306), Volume I.1 and I.2. Geneva.
- , 2015a (updated in 2018): *Technical Regulations* (WMO-No. 49), Volume I. Geneva.
- , 2015b (updated in 2017): *Manual on the Global Observing System* (WMO-No. 544), Volume I. Geneva.
-

CHAPTER 10. ROAD METEOROLOGICAL MEASUREMENTS

10.1 GENERAL

10.1.1 Definition

Road meteorological measurements are of particular value in countries where the serviceability of the transport infrastructure in winter exerts a great influence on the national economy. In some countries there will be other road hazards such as dust storms or volcanic eruptions. Safe and efficient road transport is adversely affected by the following conditions which affect speed, following distance, tyre adhesion and braking efficiency: poor visibility (heavy precipitation, fog, smoke, sand storm), high winds, surface flooding, land subsidence, snow, freezing precipitation and ice.

10.1.2 Purpose

The role of a road network manager is to ensure the optimal, safe, free flow of traffic on arterial routes. Operational decisions on the issuing of road weather information and on initiating de-icing and snow clearing operations are dependent on road meteorological observations that are increasingly made by special-purpose automatic weather stations (AWSs). While these stations should conform as far as practicable to the sensor exposure and measurement standards of conventional AWSs (see the present volume, Chapter 1) they will have characteristics specific to their function, location and measurement requirements.

The reliability of road meteorological measurement stations which supply data to a transport decision support system is critical: Each station will relate to the immediate environment of important high-density transport routes and may be responsible for feeding data to road meteorology forecast routines and for generating automatic alarms. Thus, equipment reliability and maintenance, power supply, communications continuity and data integrity are all important elements in the selection, implementation and management of the weather measurement network. These concerns point to the benefits of an effective collaboration between road management services and the National Meteorological and Hydrological Service (NMHS).

10.1.3 Road meteorological requirements

This chapter should assist in standardizing road meteorological measurements with a method that adheres to WMO common standards as closely as possible. However, those users who may wish to employ road measurements in other meteorological applications will be advised of important deviations, in sensor exposure, for example.

The needs of road network managers focus in four main areas (WMO 1997, 2003):

- (a) *Real-time observation of road meteorology*: The practical objective, on the one hand, is to inform road users of the risks (forecast or real-time) that they are likely to face on designated routes; and on the other hand, to launch a series of actions aimed at increasing road safety, such as scraping snow or spreading chemical melting agents;
- (b) *Improvement of pavement surface temperature forecasting*: The measurements of road AWSs are the important input data for the temperature and pavement condition forecasting programmes which may be run by the NMHS. This authority has the capability of ensuring continuity and timeliness in the observations and in the forecast service. In practice, two tools are available to forecasters. The first tool is a computer model for the transposition of a weather forecast of atmospheric conditions to a pavement surface temperature

forecast, taking account of the physical characteristics of each station. The second tool is the application of an algorithm based on a specific climatological study of the pavement surface;

- (c) *Road climate database*: The establishment of a road climatological database is important because in many situations an assessment of current events at a well-instrumented location enables experienced road network managers to transpose the data using the climate model to other locations they know well. In some cases, thermal fingerprints can be taken in order to model this spatial relationship. The recording of road weather data will be useful for analysing previous winter disturbances and for carrying out specific road-dedicated climatology studies. National Meteorological and Hydrological Services can fill the data gaps and compare and provide quality assurance for measurements coming from different sources;
- (d) *Reliable data*: Road managers do not need exceedingly accurate measurements (with the exception of road-surface temperature). Rather, they want the data to be as reliable as possible. That is to say the data must be a consistent reflection of the real situation, and the measuring devices must be robust. Communication and power supply continuity are often of prime importance.

10.2 ESTABLISHMENT OF A ROAD METEOROLOGICAL STATION

10.2.1 Standardized representative measurements

The general requirements for meteorological stations, their siting and the type and frequency of measurements are defined in WMO (2003, 2015a). It is recommended that these standards and other relevant material in the present Guide should be adhered to closely when establishing road meteorological stations in order to make standardized, representative measurements that can be related to those from other road stations in the network and also to data from standard synoptic or climatological stations, except where the unique measurements for road meteorology demand other standards, for example, for the exposure of sensors. Advice on the optimum placement and density of stations may be obtained from the local branch office of the NHMS which will be able to access climatological data for the region.

A meteorological station site is chosen so that it will properly represent a particular geographic region. A road meteorological station will be sited to best represent part of the road network or a particular stretch of important roadway that is known to suffer from weather-related or other hazards. The station must therefore be adjacent to the roadway so that road-surface sensors may be installed, and therefore some compromise on “ideal” meteorological siting and exposure may occur. The sensors are installed so that their exposure enables the best representation in space and time of the variable being measured, without undue interference from secondary influences. In general, the immediate site adjacent to the roadway should be level, with short grass, and not shaded by buildings or trees.

10.2.2 Station metadata

In every case it is important that the location and characteristics of the site and the specification of equipment and sensors are fully documented, including site plans and photographs. These metadata (Volume I, Chapter 1 and Volume V, Chapter 1 of the present Guide) are invaluable for the management of the station and for comparing the quality of the measurements with those from other sites.

10.3 **OBSERVED VARIABLES**

10.3.1 **Road meteorological measurements**

The important measurements at road weather stations for forecasting roadway conditions include air temperature and humidity, wind speed and direction, precipitation amount and type, visibility, global and long-wave radiation, road-surface temperature and road-surface condition. Some of the measurements, for example, temperature and humidity, will be used to forecast conditions of concern to road users, while others (wind and visibility) may indicate impending or real-time hazards; yet others (meteorological radiation, road-surface temperature and condition) are specific to predicting the performance of the road surface.

The sensors will be selected for their accuracy, stability, ease of maintenance and calibration, and for having electrical outputs suitable for connecting with the automatic data-acquisition system. The choice of sensors and their exposure should conform to standard WMO practice and recommendations (see the relevant chapters in Volume I of the present Guide), except when these are incompatible with the specific requirements of road meteorology. Measurement accuracy should generally conform to the performances quoted in Volume I, Chapter 1, Annex 1.A. Note also the recommendations on the measurements at AWSs in the present volume, Chapter 1.

10.3.1.1 ***Air temperature***

The sensor may be an electrical resistance thermometer (platinum or stable thermistor). The air-temperature sensor, its radiation shield or screen and exposure should conform to the guidelines of Volume I, Chapter 2, with the shield mounted at a height of 1.25 to 2 m over short grass or natural soil.

Measurement issues: The sensor and screen should not be mounted above concrete or asphalt surfaces that could inflate the measured temperature. The placement of the shield should ensure that it is not subject to water spray from the wheels of passing traffic, which might cause significant sensing errors.

10.3.1.2 ***Relative humidity***

The hygrometric sensor may be one of the thin-film electrical conductive or capacitive types (Volume I, Chapter 4). A wet-bulb psychrometer is not recommended on account of the continual contamination of the wick by hydrocarbons. The sensor may be combined with or co-located with the air-temperature sensor in its radiation shield as long as the sensor thermal output (self-heating) is very low, so as not to influence the temperature measurement.

Measurement issues: Note the same water spray hazard as for the temperature sensor. Humidity-sensor performance is subject to the effects of contamination by atmospheric and vehicle pollution. Functional checks should be made regularly as part of the data-acquisition quality control, and calibration should be checked at least every six months, particularly before the winter season. A sensor that is not responding correctly must be replaced immediately.

10.3.1.3 ***Wind speed and direction***

These variables are usually measured by either a pair of cup and vane sensors or by a propeller anemometer (Volume I, Chapter 5 of the present Guide) with pulse or frequency output. The sensors must be mounted at the standard height of 10 m above the ground surface and in a representative open area in order to carry out measurements not influenced by air mass flow disturbances due to traffic and local obstacles.

Measurement issues: The freezing of moving parts, water ingress and corrosion and lightning strike are potential hazards.

10.3.1.4 **Precipitation**

- (a) *Accumulated precipitation:* The tipping-bucket recording gauge (Volume I, Chapter 6) where increments of usually 0.2 mm of precipitation are summed, is commonly used at automatic stations. Heated gauges may be employed to measure snow or other solid precipitation. A rate of precipitation may be estimated by registering the number of counts in a fixed time interval.

Measurement issues: The gauge must be kept level and the funnel and buckets clean and free from obstruction. The tipping-bucket gauge is not satisfactory for indicating the onset of very light rain, or in prolonged periods of freezing weather. Totals will be lower than the true values because of wind effects around the gauge orifice, evaporation from the buckets between showers, and loss between tips of the buckets in heavy rain;

- (b) *Precipitation occurrence and type:* Sensors are available which use electronic means (including heated grids, conductance and capacitance measurement) to estimate the character of precipitation (drizzle, rain or snow) falling on them. Optical sensors that determine the precipitation characteristic (size, density and motion of particles) by the scattering of a semiconductor laser beam offer better discrimination at much greater expense.

Measurement issues: These sensing functions are highly desirable at all stations, but existing types of sensors are lacking in discrimination and stable reproducibility. Provisions must be made (heating cycles) to remove accumulated snow from the surface. The regular cleaning of sensitive elements and optical surfaces is required.

Only sensors that are well documented and that can be calibrated against an appropriate reference should be installed. If any system uses an algorithm to derive a variable indirectly, the algorithm should also be documented.

10.3.1.5 **Meteorological radiation**

- (a) *Global radiation:* The solar radiation (direct and diffuse) received from a solid angle of 2π sr on a horizontal surface should be measured by a pyranometer using thermoelectric or photoelectric sensing elements (Volume I, Chapter 7 of the present Guide). The sensor should be located to have no significant nearby obstructions above the plane of the instrument and with no shadows or light reflections cast on the sensor. Although the location should be such as to avoid accidental damage to the sensor, it should be accessible for inspection and cleaning. Global radiation measured "on site" is particularly relevant to the road manager. It expresses the quantity of energy received by the road during the day. The relationship of incoming radiation to surface temperature and road inertia will depend on the constituent materials and dimensions of the pavement mass.

Measurement issues: Obstructed sensor horizon, sensor not level, surface dirt, snow or frost obscuring the glass dome or sensing surface, and water condensation inside the glass dome;

- (b) *Long-wave radiation:* A pyrgeometer may be used which measures radiation in the infrared by means of a thermopile, filtering out the visible spectrum. Mounted with the sensor facing upwards and a sufficiently unobstructed horizon, it determines the long-wave radiation received from the atmosphere, in particular at night, and gives an indication of cloud cover and therefore of roadway radiative cooling. A sensor sensitive to a spectrum from 5 to 50 μm , with a maximum sensitivity of $15\ \mu\text{V}/\text{Wm}^{-2}$ and a response time lower than 5 s is adequate for road weather forecasting purposes.

Measurement issues: See those for global radiation.

10.3.1.6 **Visibility**

Transmissometers and forward-scatter meters may be applicable (Volume I, Chapter 9 of the present Guide).

Measurement issues: Road managers are interested in visibilities below 200 m (the danger threshold). Maintaining sensor windows and lenses clean is important. Some systems will compensate for a degree of window contamination. An appropriate calibration procedure should be carried out during routine maintenance.

10.3.1.7 **Road-surface temperature**

Active sensors based on a 100 ohm platinum resistance and providing serial digital transmission are available, and may be imbedded in the road surface. The manufacturer's instructions for the installation of the sensor and cabling and bonding to the road surface should be followed. The sensor has to be positioned out of the line of tyre tracks, otherwise the sensor surface will be soiled and measurements affected by friction heating. The sensor must lie in the road surface plane with no depression where water could gather and affect the measurement. The sensor's correct position must be checked on a regular basis.

Measurement issues: The thermal lag (time constant) of the sensor and the imbedding material should match that of the road-surface composition. The sensor should have a surface finish with low absorptance in the infrared to minimize radiation error. For long connecting cable lengths (over 20 m), cable resistance compensation is recommended.

10.3.1.8 **Road-pavement temperature**

Temperatures of the pavement at 5, 10 and 20 cm below the road surface may be determined by sinking appropriately sheathed electrical resistance sensors at corresponding depths and using suitable bonding material.

Measurement issues: See those for road-surface temperature.

10.3.1.9 **Road-surface condition and freezing temperature**

This sensor estimates the road-surface condition (dry, wet, frost, ice) and the freezing temperature of residual surface water. The sensor control circuit heats the sensor before cooling it, using the Peltier effect. The rate of cooling is a function of the surface condition and freezing temperature. See also Volume I, Chapter 6, regarding ice on pavements. The sensor output should give road managers an indication of the chemical de-icing agent's persistence at the specific location and enable them to optimize chemical spreading operations.

Measurement issues: The sensor must not be covered by foreign matter or when road re-surfacing. The sensor requires regular cleaning. It is difficult to ensure a sensor response that is representative of the true road-surface condition because of the small sample size, the location on road surface and variable imbedding practices. Measurement depends on traffic density and is otherwise not very stable with time. This sensor, of which there are few alternative makes, may be difficult to obtain. The remote sensing of road-surface temperature by thermal infrared sensors is generally not practical because of the interference caused by water spray from vehicle tyres. Road-surface frost risk estimation may be improved through better measurement of temperature, air humidity and temperature in and on the road surface, namely, improved sensor exposure and reduction of systematic and random errors.

10.3.1.10 **Video surveillance**

Video surveillance is a component of what have come to be called intelligent transport systems. They are principally used for road-incident detection, but also give a useful indication of present weather for transport management. Image processing algorithms will aid the discrimination between different weather conditions.

10.4 **CHOOSING THE ROAD WEATHER STATION EQUIPMENT**

Chapter 1 of the present volume gives information that may be applied to road meteorological measurement applications. In what follows, attention is drawn to the particular issues and concerns from the experience of road network managers, in particular the need for high performance where public safety is a primary issue.

10.4.1 **The road environment**

A road weather station is subject to considerable stress due to the vicinity of the roadway: vibration, vehicle ignition interference, exhaust pollution, corrosion from salt spray, and unwelcome attention from members of the public. In some respects the station may be considered to operate in an industrial environment, with all that that implies for the robustness of the design and concern for data integrity. Frequently met problems are: lack of protection against over-voltage on sensor interface circuits; inadequate electrical isolation between sensors, sensor cables and the data-acquisition unit; variable connector contact resistance causing calibration drift; measurement failure; and extended maintenance attention.

10.4.2 **Remote-station processing capability**

There is a move in AWS design to include increased data-processing capacity and storage at the remote data-acquisition unit in order to employ processing algorithms that act on several sensor signals to give complex outputs; to provide for some level of quality assurance on the data; to provide two-way communications between the control centre and remote units for diagnostics of both the sensor and unit performance; and to provide for downloading new algorithms and software updates to the remote units. On the other hand, a network of remote stations which are not more complex than necessary for reliable data acquisition, and a central control and data-acquisition computer where the more complex algorithms, quality assurance and code translation is carried out as well as the higher level processing for road management decisions, may provide a more reliable and less costly overall system. Those planning for the implementation of a road meteorological measurement network are encouraged to consider flexible and extendable equipment solutions with powerful programming options for sensor data processing and system control.

The station data processing may include: control of the measurement cycle (initiation, frequency, time and date); complex sensor management (power on/off, sampling regime); sensor signal processing (filtering, conversion to scientific units, algorithms); data quality checks; alarm generation (variables outside pre-set limits, partial system failure, station integrity breached); data storage (short-term storage and archiving); output message generation (code form, communications protocol); communications management; and station housekeeping (power supply, sensor checks, communications).

10.4.3 **Network configuration and equipment options**

The selection of station equipment, communications and network control (the network infrastructure) should reflect the particular demands of road meteorology and the road network management decision-making. These choices will be materially affected by the relationship between the road network authority and the local NMHS. For example, the road network

authority might contract the NMHS to provide road meteorology forecasting services and specified road data, to which the road network managers apply their physical criteria to make operational decisions. In this case, it would be logical for the road network stations to be an extension of the NMHS AWS network employing common station hardware, communications and maintenance service, with particular attention to network reliability, and including the special sensors, algorithms and software for the road meteorological task. However, if such close integration is impractical, the road authority may still wish to adopt some commonality with NMHS systems to take advantage of operational experience and the supply of hardware and spare parts.

If an entirely new or separate network is required, the following guidelines are recommended for the choice of data-acquisition equipment and communications. Rather than develop new hardware and software for road meteorological measurement, it is wise to employ existing proven systems from reputable manufacturers and sources, with only necessary adaptation to the road network application, and taking advantage of the experience and advice of other road network administrations. The equipment and its software should be modular to allow for future added sensors and changes in sensor specifications. To facilitate the extension of the network after a few years it is most helpful if the hardware is sourced from standardized designs from a sound manufacturing base where later versions are likely to maintain technical compatibility with earlier generations.

10.4.4 **Design for reliability**

Data-processing modules should be of industry-standard architecture with robust standard operating systems with a well-managed upgrade process. Application software should be written in a standard language and well documented. To achieve the desired reliability, special industrialized components and modules may be selected. A cheaper alternative may be to use standard commercial designs with redundant parallel or back-up systems to ensure system reliability. The design of the remote-unit power supply needs particular attention. An uninterruptible power supply may be recommended, but it should be recognized that communications systems will also depend on a functioning local power supply.

Whatever the system design, housing the electronics in a robust, corrosion-resistant, secure, even temperature, dust- and moisture-free enclosure will add much to its reliability. Connectors carrying the sensor signals should be of high-quality industrial or military grade and well protected against cable strain, water ingress and corrosion. Sensor cabling should have an earth shield and a robust, waterproof insulating sheath and be laid in conduit.

Special attention should be given to obviating the effect of electrical noise or interference introduced into the data-acquisition system through sensor cables, the power supply or communications lines. These unwanted electrical signals may cause sensor signal errors and corrupt data, and cause electronic failure, particularly in sensitive interface circuits. Great care needs to be given to: the design of sensor and communication line isolation and over-voltage protection, including an appropriate level of protection from atmospheric electricity; the adequate earthing or grounding of sensors, power supplies, communications modems and equipment cabinets; and to earth shielding all parts of the measurement chain, avoiding earth current loops which will cause measurement errors.

Good standardized installation and maintenance practices will contribute much to system reliability. System reliability is also related to the "mean time to repair", which involves the call-out and travel time of maintenance staff to make equipment replacement from whole unit and module stock.

10.5 MESSAGE CODING

10.5.1 Coding functions

The message transmitted from the remote road meteorological station will contain a station identifier, the message time and date, sensor channel data, including channel identification, and some “housekeeping” data which may include information on station security, power supply, calibration and other data quality checks. This message will be contained in the code envelope relating to the communications channel with an address header, control information and redundancy check characters to provide for error detection. The road meteorological data part of the message may be coded in any efficient, unambiguous way that enables the central control and data-acquisition computer to decode and process before delivering intelligible guidance information to the network managers for their decision-making.

10.5.2 WMO standard coding

Designers of road meteorology measurement networks should also consider the value of WMO standard message coding (see WMO, 2011) which enables other users like NMHSs to receive the data by some arrangement and employ it in other meteorological applications. This message coding may be carried out at the remote AWS, which places demands on station software and processing, or, as is more likely, in the central control and data-acquisition computer after the completion of any quality assurance operations on the data.

10.6 CENTRAL CONTROL AND DATA-ACQUISITION COMPUTER

The functions of the central computer (or computers) have already been mentioned. The functions are to manage the network by controlling communications (see below), receive reports (road meteorological messages, AWS housekeeping messages and quality information), and process the road measurement data to give the road network managers the operational information and decision-making tools that they require. The network architecture may be designed to enable the central computer to act as an Intranet or Web server to enable ready access to this information by regional managers and other users of the meteorological data.

A separate computer will probably be allocated to manage the road network climate database and to produce and distribute analyses and statistical summaries. In a sophisticated network the central computer will manage certain maintenance and calibration operations, change AWS operating modes and update AWS software.

10.7 COMMUNICATIONS CONSIDERATIONS

A reliable telecommunications service that enables the network of stations to be effectively managed while it delivers the requisite data on time is vital. Since communications charges will make up a large proportion of the annual operating cost, the analysis of communications options is important, so that the cost per message can be optimized with respect to the level of service required. A detailed review of telecommunications options for the data collection and management of the road AWS is beyond the scope of this chapter (see the present volume, Chapter 1, for guidance on data transmission). The communications solution selected will depend on the management objectives of the road meteorological measurement network and the services offered by the telecommunications providers of the country, with their attendant tariffs.

10.8 SENSOR SIGNAL PROCESSING AND ALARM GENERATION

10.8.1 Signal processing algorithms

The raw signal data from sensors must be processed or filtered to produce representative average values. This is either done in some active sensors, in the sensor interface in the data-acquisition unit, or in the higher level data processing of the station. The specifications for averaging the sensor outputs may be found in Volume I, Chapter 1, Annex 1.A of the present Guide.

Algorithms which are applied to sensor outputs (or groups of outputs) either at the remote station or in the central computer should be from authoritative sources, rigorously tested and preferably published in the open literature. Any in-house algorithms adopted by the road network management should be well defined and recorded in the station metadata or network manuals.

10.8.2 Alarm generation

Alarm indications may be generated from sensor outputs when values exceed preset limits to initiate alarm messages from the AWS. The choice of alarms and limit tests will depend on national or regional practice. Some examples of alarms from road AWS follow. Note the use of the logical "and" and "or" combinations in the algorithms.

Examples of alarms include:

- Alarm 1: $t(\text{air})$ OR $t(\text{road surface}) \geq 3 \text{ } ^\circ\text{C}$
AND
 $t(\text{extrapolated road surface})^a \leq 1 \text{ } ^\circ\text{C}$
- Alarm 2: $t(\text{air}) \leq 0 \text{ } ^\circ\text{C}$
- Alarm 3: First condition
 $t(\text{road surface}) \leq 1 \text{ } ^\circ\text{C}$
OR $t(\text{extrapolated road surface}) \leq 0 \text{ } ^\circ\text{C}$
OR $t(\text{pavement at } -5 \text{ cm}) \leq 0 \text{ } ^\circ\text{C}$
OR $t(\text{pavement at } -10 \text{ cm}) \leq -1 \text{ } ^\circ\text{C}$
OR $t(\text{pavement at } -20 \text{ cm}) \leq -2 \text{ } ^\circ\text{C}$
AND
Second condition
Carriage-way is not dry
OR at least one precipitation count in the past hour
OR relative humidity $\geq 95\%$
OR $t(\text{road surface}) - t(\text{dewpoint}) \leq 1 \text{ } ^\circ\text{C}$
- Alarm 4: $t(\text{road surface}) \leq 0 \text{ } ^\circ\text{C}$
AND
detected state: frost or black ice
- Alarm 5: First condition
Detected precipitation = snow or hail
AND
Second condition
 $t(\text{air}) \leq 2 \text{ } ^\circ\text{C}$
OR $t(\text{road surface}) \leq 0 \text{ } ^\circ\text{C}$
- Alarm 6: Wind average $\geq 11 \text{ m s}^{-1}$
AND
Wind direction referred to road azimuth,
between 45° to 135° OR 225° to 315°
- Alarm 7: Visibility $\leq 200 \text{ m}$

^a Extrapolated road-surface temperature is calculated with an algorithm that takes account of the last measures and creates a quadratic equation. This can be used to calculate estimates of temperatures over the next 3 h.

Other alarms may be set if faults are detected in sensors, message formats, power supplies or communications.

10.9 MEASUREMENT QUALITY CONTROL

Good decision-making for road management is dependent on reliable measurements so that, when sensors, their cabling or their interfaces in the AWS develop a fault, the defective unit is detected and repaired without undue delay. It is very difficult for a road manager to detect erroneous measurements. Reference should be made to the guidance on quality control provided in the present volume, Chapter 1 and in Volume V, Chapter 1. Gross sensor faults may be detected by the AWS system software, which should then generate an alarm condition.

10.9.1 Checking for spurious values

Measurements that fall outside the expected operating range for the sensor may be rejected by setting limits for each variable. For example, wind directions may be confined to the range of 0° to 359° . Where there has been a faulty zero output, a rapid drift or step change in sensor response, invalid measurements may be rejected by software that performs statistical analysis of measurements over time, either in the AWS if it has sufficient processing power, or in the central data acquisition computer. In some of the examples that follow, the standard deviation of the last n values is compared with a parameterized threshold.

Examples of check algorithms (only for road meteorological measurements) include the following:

- (a) *Test for all temperatures:* Accept data only if standard deviation of the last 30 values is $\geq 0.2^\circ\text{C}$;
- (b) *Test for wind speed:* Accept data only if standard deviation of the last 20 values is $\geq 1\text{ km hr}^{-1}$;
- (c) *Test for wind direction:* Accept data only if standard deviation of the last 30 values is $\geq 10^\circ$;
- (d) *Test for liquid precipitation:* Check for consistency of amount with previous day's count;
- (e) *Test for snow precipitation:* Check data if $t(\text{air}) > 4^\circ\text{C}$;
- (f) *Test for atmospheric long-wave radiation (AR) (related to cloud cover):* Refuse data if $\text{AR} > 130\text{ W m}^{-2}$, if relative humidity $> 97\%$ and $\text{AR} > 10\text{ W m}^{-2}$, and if relative humidity $\geq 90\%$ and $\text{AR} > 10\text{ W m}^{-2}$, for four successive hours.

10.10 ROAD WEATHER STATION MAINTENANCE

10.10.1 The road environment

Reference should be made to Volume I, Chapter 1 and the present volume, Chapter 1 for the sections on inspection, maintenance and calibration. The chapters of Volume I include advice on the maintenance and calibration of specific sensors. Note, however, that the road AWS exists in an environment with peculiar problems: vulnerability of the AWS and its sensors to accidental or intentional damage; exposure to severe vehicle exhaust pollution; electrical interference from vehicle ignition and nearby high-tension power lines; corrosion from salt spray; and vibration (affecting connections between sensors and cables).

10.10.2 **Maintenance plans and documentation**

Because operational decisions affecting road safety may critically depend on reliable AWS data, there are stringent requirements for maintenance of specific stations at particular times of the year. These considerations are outlined in the maintenance management plan for the network, which should include scheduled routine preventive maintenance as well as effective response to known fault conditions.

The road network administration should have its own maintenance manual for its road meteorological stations, based on the manufacturer's recommendations, information gleaned from the present Guide and from its own experience. A good manual contains checklists to aid inspection and the performance of maintenance tasks. The administration may decide to contract out inspection and maintenance work to the local NMHS, which should have experience with this kind of instrumentation.

10.10.3 **Inspections and work programme**

Each station should undergo a complete maintenance programme twice a year, consisting of site maintenance (cutting grass and vegetation which could affect sensor exposure); checking enclosures for water ingress and replacing desiccants; treating and painting weathered and corroded enclosures, screens and supports; checking cable and connector integrity; cleaning and levelling sensors (noting the measurement issues referred to previously); and calibrating or replacing sensors and the AWS measurement chain.

Road managers should maintain a physical inspection programme to check for the integrity and proper operation of their stations once a month in winter and once every two months in the summer. When conducting any work on the road surface, the regulation warning signs must be set out and approved safety clothing must be worn.

10.11 **TRAINING**

To manage, operate and maintain a network of road meteorological stations in order to obtain a continuous flow of reliable data and to interpret that data to give fully meaningful information requires personnel with specific training in the necessary disciplines. Some of these areas of expertise are: the roadway environment and operational decision-making for the safe and efficient movement of traffic; remote data acquisition, telecommunications and computing; the selection, application and maintenance of meteorological sensors and their signal processing; and the interpretation of meteorological and other data for the operational context. The administration responsible for the road network should collaborate with other agencies as necessary in order to ensure that the optimum mix of knowledge and training is maintained to ensure the successful operation of the road meteorological measurement network.

REFERENCES AND FURTHER READING

World Road Association (PIARC), 2002: *Proceedings of the Eleventh PIARC International Winter Road Congress* (Sapporo, Japan).

World Meteorological Organization, 1997: *Road Meteorological Observations* (R.E.W. Pettifer and J. Terpstra). Instruments and Observing Methods Report No. 61 (WMO/TD-No. 842). Geneva.

———, 2003: *Road Managers and Meteorologists over Road Meteorological Observations: The Result of Questionnaires* (J.M. Terpstra and T. Ledent). Instruments and Observing Methods Report No. 77 (WMO/TD-No. 1159). Geneva.

———, 2011: *Manual on Codes* (WMO-No. 306), Volumes I.1 and I.2. Geneva.

———, 2015a (updated in 2018): *Technical Regulations* (WMO-No. 49), Volume I. Geneva.

———, 2015b (updated in 2017): *Manual on the Global Observing System* (WMO-No. 544), Volume I. Geneva.

For more information, please contact:

World Meteorological Organization

7 bis, avenue de la Paix – P.O. Box 2300 – CH 1211 Geneva 2 – Switzerland

Strategic Communications Office

Tel.: +41 (0) 22 730 83 14 – Fax: +41 (0) 22 730 80 27

Email: cpa@wmo.int

public.wmo.int